frontiers | Research Topics

Echinoderms: Biology, ecology and exploitation

Edited by
Libin Zhang, Annie Mercier, Jun Ding, Chenghua Li
and Marie Antonette Juinio-Meñez

Published in
Frontiers in Marine Science

ISSN 1664-8714
ISBN 978-2-8325-2585-2
DOI 10.3389/978-2-8325-2585-2

About Frontiers

Frontiers is more than just an open access publisher of scholarly articles: it is a pioneering approach to the world of academia, radically improving the way scholarly research is managed. The grand vision of Frontiers is a world where all people have an equal opportunity to seek, share and generate knowledge. Frontiers provides immediate and permanent online open access to all its publications, but this alone is not enough to realize our grand goals.

Frontiers journal series

The Frontiers journal series is a multi-tier and interdisciplinary set of open-access, online journals, promising a paradigm shift from the current review, selection and dissemination processes in academic publishing. All Frontiers journals are driven by researchers for researchers; therefore, they constitute a service to the scholarly community. At the same time, the *Frontiers journal series* operates on a revolutionary invention, the tiered publishing system, initially addressing specific communities of scholars, and gradually climbing up to broader public understanding, thus serving the interests of the lay society, too.

Dedication to quality

Each Frontiers article is a landmark of the highest quality, thanks to genuinely collaborative interactions between authors and review editors, who include some of the world's best academicians. Research must be certified by peers before entering a stream of knowledge that may eventually reach the public - and shape society; therefore, Frontiers only applies the most rigorous and unbiased reviews. Frontiers revolutionizes research publishing by freely delivering the most outstanding research, evaluated with no bias from both the academic and social point of view. By applying the most advanced information technologies, Frontiers is catapulting scholarly publishing into a new generation.

What are Frontiers Research Topics?

Frontiers Research Topics are very popular trademarks of the *Frontiers journals series*: they are collections of at least ten articles, all centered on a particular subject. With their unique mix of varied contributions from Original Research to Review Articles, Frontiers Research Topics unify the most influential researchers, the latest key findings and historical advances in a hot research area.

Find out more on how to host your own Frontiers Research Topic or contribute to one as an author by contacting the Frontiers editorial office: frontiersin.org/about/contact

Echinoderms: Biology, ecology and exploitation

Topic editors

Libin Zhang — Institute of Oceanology, Chinese Academy of Sciences (CAS), China
Annie Mercier — Memorial University of Newfoundland, Canada
Jun Ding — Dalian Ocean University, China
Chenghua Li — Ningbo University, China
Marie Antonette Juinio-Meñez — University of the Philippines Diliman, Philippines

Citation

Zhang, L., Mercier, A., Ding, J., Li, C., Juinio-Meñez, M. A., eds. (2023). *Echinoderms: Biology, ecology and exploitation*. Lausanne: Frontiers Media SA. doi: 10.3389/978-2-8325-2585-2

Table of contents

frontiers | Frontiers in Marine Science

ORIGINAL RESEARCH
published: 30 June 2022
doi: 10.3389/fmars.2022.930156

Sea Urchins in Acute High Temperature and Low Oxygen Environments: The Regulatory Role of microRNAs in Response to Environmental Stress

*Lingshu Han[1], Yanglei Wu[2], Pengfei Hao[2], Beichen Ding[2], Yuanxin Li[2], Wenpei Wang[2], Xianglei Zhang[2], Chuang Gao[2], Heng Wang[2], Luo Wang[2], Weijie Zhang[2], Yaqing Chang[2], Dewen Ding[1] and Jun Ding[2]**

[1] School of Marine Sciences, Ningbo University, Ningbo, China, [2] Key Laboratory of Mariculture and Stock Enhancement in North China's Sea, Ministry of Agriculture and Rural Affairs, Dalian Ocean University, Dalian, China

OPEN ACCESS

Edited by:
Mark Botton,
Fordham University, United States

Reviewed by:
Lusheng Xin,
Chinese Academy of Fishery Sciences (CAFS), China
Silvia Gomez-Jimenez,
Consejo Nacional de Ciencia y Tecnología (CONACYT), Mexico

***Correspondence:**
Jun Ding
dingjun19731119@hotmail.com

Specialty section:
This article was submitted to Marine Biology, a section of the journal Frontiers in Marine Science

Received: 27 April 2022
Accepted: 26 May 2022
Published: 30 June 2022

Citation:
Han L, Wu Y, Hao P, Ding B, Li Y, Wang W, Zhang X, Gao C, Wang H, Wang L, Zhang W, Chang Y, Ding D and Ding J (2022) Sea Urchins in Acute High Temperature and Low Oxygen Environments: The Regulatory Role of microRNAs in Response to Environmental Stress. Front. Mar. Sci. 9:930156. doi: 10.3389/fmars.2022.930156

Strongylocentrotus intermedius is an economically valuable sea urchin species in China. However, its growth and survival are severely constrained by ocean warming and the hypoxia that often accompanies high water temperatures. MicroRNAs (miRNAs) are important regulators of gene expression in response to environmental change. In this study, high-throughput RNA sequencing was used to investigate changes in miRNA expression in *S. intermedius* under heat (25°C), hypoxia (2 mg/L O_2), and combined heat and hypoxia stresses. Twelve small RNAs libraries were constructed and 17, 14, and 23 differentially expressed miRNAs (DEMs) were identified in the heat, hypoxia, and combined stress groups ($P<0.05$), respectively. Gene ontology and Kyoto Encyclopedia of Genes and Genomes pathway functional analyses of putative target genes of the DEMs suggested that these miRNAs were important in basal metabolism, apoptosis, oxidative stress, and immune-related pathways. By co-analysis with published transcriptome data, key DEMs (miR-193, miR-184, miR-133, miR-125, miR-2008) and their key target genes (*EGF3*, *ABCB4*, *CYCL*, *PAN2*, *CALN*) were identified. Quantitative real-time PCR analysis of the expression of 10 DEMs and their key target genes confirmed the RNA sequencing results. These results provide information on gene expression regulation of the molecular mechanisms underlying the response of *S. intermedius* to multi-cause environmental stresses.

Keywords: *strongylocentrotus intermedius*, microRNA, global climate change, high temperature stress, hypoxia

Abbreviations: MiRNA, MicroRNA; DEGs, Different expression genes; DEMs, Different expression microRNA; GO, Gene Ontology; BP, Biological processes; MF, Molecular functions; CC, Cellular components; KEGG, Kyoto Encyclopedia of Genes and Genomes; qRT-PCR; Quantitative Real-time PCR.

INTRODUCTION

Global warming has profoundly affected the nearshore and marine environments. The resulting environmental changes include increased seawater surface temperature, acidification, increased hypoxic zones, and extreme weather, which seriously threaten the reproduction of marine fishery species and the sustainable development of aquaculture (Blencowe, 2006; Xu et al., 2018; García Molinos, 2020). Among them, water temperature is the most fundamental and widespread ecological (environmental) factor that affects the survival of marine organisms (Pinsky et al., 2019). Increased seawater temperatures have been shown to impact the growth, metabolism, reproduction, and development of marine animals (García-Echauri et al., 2020; Gouda and Agatsuma, 2020; Strøm et al., 2020). Hypoxia caused by high temperatures, nutrient enrichment, water pollution, and high-density farming affects wild and farmed aquatic animals (Vaquer-Sunyer and Duarte, 2008; Breitburg et al., 2018). Dissolved oxygen levels of <2.8 mg/L (equivalent to 2 mL O_2/L or 91.4 mM) are considered hypoxic. Very high summer temperatures and depleting aquaculture resources lead to hypoxic conditions that can be fatal or sub-lethal for sea urchins and can cause mass mortality (Riedel et al., 2014). Under hypoxic stress, significant changes in the oxygen consumption rate (Tomi et al., 2011) and the expression of immune and metabolic-related genes were found to occur in sea urchins (Suh et al., 2014; Hao et al., 2022). Therefore, hypoxia is another important factor that limits the survival and growth of sea urchins.

Sea urchins are a model organism for embryological development and a globally crucial marine fishery resource species (Nesbit et al., 2019). Among them, *Strongylocentrotus intermedius*, which has fast growth and excellent qualities, is China's main sea urchin culture species, accounting for >90% of the total sea urchin culture in China (Chang et al., 2016). However, *S. intermedius* is a cold-water species that is sensitive to temperature changes. The high temperatures in the northern summers of 2017 and 2020 led to high mortality rates (up to 80%) of *S. intermedius* cultured in the Shandong and Liaoning provinces (Ding and Chang, 2020). Furthermore, between 1978 and 2014, the monthly average dissolved oxygen content in the Bohai Sea declined (Shi, 2016). These patterns suggest that environmental factors will seriously threaten the sustainable development of the aquaculture industry. Echinoderms have specific molecular biological mechanisms to respond to stress, such as histone modification, transcription, translation, and post-translational modification (Branco et al., 2013; Huo et al., 2018; Huo et al., 2021).

Various non-coding RNAs are known to be involved in post-transcriptional regulation. Among them, microRNAs (miRNAs) are small non-coding RNAs with about 18-25 nucleotides, which are endogenous regulatory RNAs found mainly in eukaryotes. Most miRNAs are transcribed from DNA sequences into primary miRNA, and processed into precursor RNAs by a series of nucleases to obtain mature miRNAs. The mature miRNAs are assembled into RNA-induced silencing complexes that recognize the target mRNAs through complementary base pairing and instruct the silencing complex to degrade or inhibit the translation of the target mRNAs according to the different degrees of complementation (Fabian et al., 2010; Fu, 2014; Zgheib et al., 2017). MiRNAs play irreplaceable roles in cell proliferation and differentiation, cell apoptosis, gene expression, restoration of homeostasis, and target recognition (Bartel, 2009; Leung and Sharp, 2010; Noman et al., 2017; Tian et al., 2019a; Tian et al., 2019b). Many studies have shown that miRNAs are activated in animals under environmental stress. For example, miR-210-5p and miR-92b-3p were highly activated in sea cucumber in response to the environmental pressures of hypoxia and high temperature (Huo et al., 2021). Sun et al. (2019) reported that miR-122, miR-15b-5p, miR-30b, miR-20a-5p, and miR-7b helped maintain the energy requirements of common carp (*Cyprinus carpio*) under high temperature stress by regulating glycolysis. In sea cucumbers under salinity stress, miR-2008 and miR-92a were shown to respond by regulating proteins and phospholipids (Tian et al., 2019b). In Chinese shrimp (*Fenneropenaeus chinensis*), novel-mir-76 and novel-mir-193 responded to high pH stress by regulating lipid metabolism, amino acid metabolism, and carbon metabolism pathways (Li et al., 2019). Multiple environmental factors can affect organisms in natural environments. In a previous study (Hao et al., 2022), we performed transcriptome-wide gene expression profiling by RNA sequencing (RNA-seq) of *S. intermedius* under short-term high temperature, hypoxia, and combined stresses. We found that exposure to the combined stresses resulted in a two-factor additive effect at the transcriptome level and had a broader effect on immune-related pathways in the *S. intermedius* than a single stress had (Hao et al., 2022). However, no reports on the involvement of miRNAs in the regulatory mechanism of sea urchins under acute environmental stresses have been published so far.

In this study, we used RNA-seq technology to screen and identify differentially expressed miRNAs (DEMs) under high temperature, low oxygen, and combined stresses. We analyzed the obtained DEMs jointly with published transcriptome data to further explore the molecular mechanisms of *S. intermedius* in response to multiple environmental stresses. The results provide information for selecting and breeding resistant sea urchins and provide a theoretical basis for healthy sea urchin culture.

METHOD

Experimental Animals and Treatment

Healthy 1-years-old *S. intermedius* (average test diameter: 35.74 ± 1.35 mm; average test height: 16.34 ± 1.27 mm; weight: 19.25 ± 0.37 g) were bought from Dalian Haibao Fishery Co., Ltd. (38°91′25′′N" 121°60′25′′E) in Dalian, Liaoning Province, China, then immediately transported to the Key Laboratory of Mariculture and Stock Enhancement in North China's Sea, Ministry of Agriculture and Rural Affairs, Dalian Ocean University. All the *S. intermedius* were temporarily raised in the same environment for 14 days before the experiment. The breeding conditions are as follows: temperature, 15 - 16 °C; salinity, 31.22 - 31.36 ppt; pH, 8.15 - 8.25; and oxygen content, 8 - 9 mg/L. Sea urchins were fasted for 48 h before the start of the experiment to expel the intestinal contents.

According to the changes in temperature and dissolved oxygen in the Yellow Sea and the Bohai Sea in the past ten years (Song et al., 2020) and previous experiments (Hao et al., 2022), this study selected 25°C and 2 mg/L oxygen as the conditions of temperature and hypoxia stress. Healthy *S. intermedius* were randomly cultured in high temperature (HT group, 25 °C, 8 mg/L O_2), low oxygen (LO group, 15 °C, 2 mg/L O_2), combined stress of heat and hypoxia (HL group, 25 °C, 2 mg/L O_2) and control group (NC group, 15 °C, 8 mg/L O_2), using 6 *S. intermedius* per group. The stress experiment was carried out in the automatic temperature control system and the dissolved oxygen control system (**Figure 1**). The temperature control system's temperature deviation was less than 0.5 °C, and the oxygen concentration deviation of the dissolved oxygen control system was less than 0.5 mg/L (Huo et al., 2018). Previous experiments showed that individuals died at 12 hours of combined stress, and transcriptome sequencing revealed significant changes in genes related to sea urchin immunity and metabolism at 12 hours of acute stress (Hao et al., 2022). Therefore, we selected 12 h as the time of stress. After 12 h, 6 sea urchins in each group were dissected on ice to absorb the coelomic fluid and centrifuged at 3000 rpm for 10 min at 4 °C. The coelomocyte of *S. intermedius* were collected and immediately stored in an -80 °C for further experiments.

RNA Extraction, Small RNA Library Construction, Sequencing, and Annotation

Three coelomocyte samples were selected from every group of sea urchins. The extraction, quality testing, and purification of total RNA were performed according to Wang's method (Wang et al., 2022). The experimental procedure was performed following the standard steps provided by Illumina, including library preparation and sequencing experiments. The Small RNA sequencing library was prepared using TruSeq Small RNA Sample Prep Kits (Illumina, San Diego, USA). The Illumina HiSeq 2500 (LC Sciences, Houston, Texas, USA) platform was used to sequence the constructed library, and the reading length was 1×50 bp on a single end. Data analysis was based on this literature (Huo et al., 2021). The obtained sequences with 18-25 nt were used to perform BLAST analysis in miR Base 22.0 database (http://microrna.sanger.ac.uk) to identify miRNAs and examine their variations.

Identification, Target Gene Prediction, and Functional Analysis of Differentially Expressed miRNAs (DEMs)

To identify DEMs between treatment group (HT, LO, and HL) and control group (NC), the expression levels of miRNAs in the whole library were normalized, and then DEMs were screened using Student's T-test. $P<0.05$ was considered significant. A heatmap was constructed using TBtools and clustered by row scale. Target genes of miRNAs were predicated by using Target Finder (http://www.targetfinder.org) and were subjected to the enrichment analysis of functions and pathways by GO and KEGG database (P-value<0.05).

Interaction Analysis of miRNA-mRNA

Association analysis of DEM and differentially expressed genes (DEGs) were based on published transcriptome data (Database

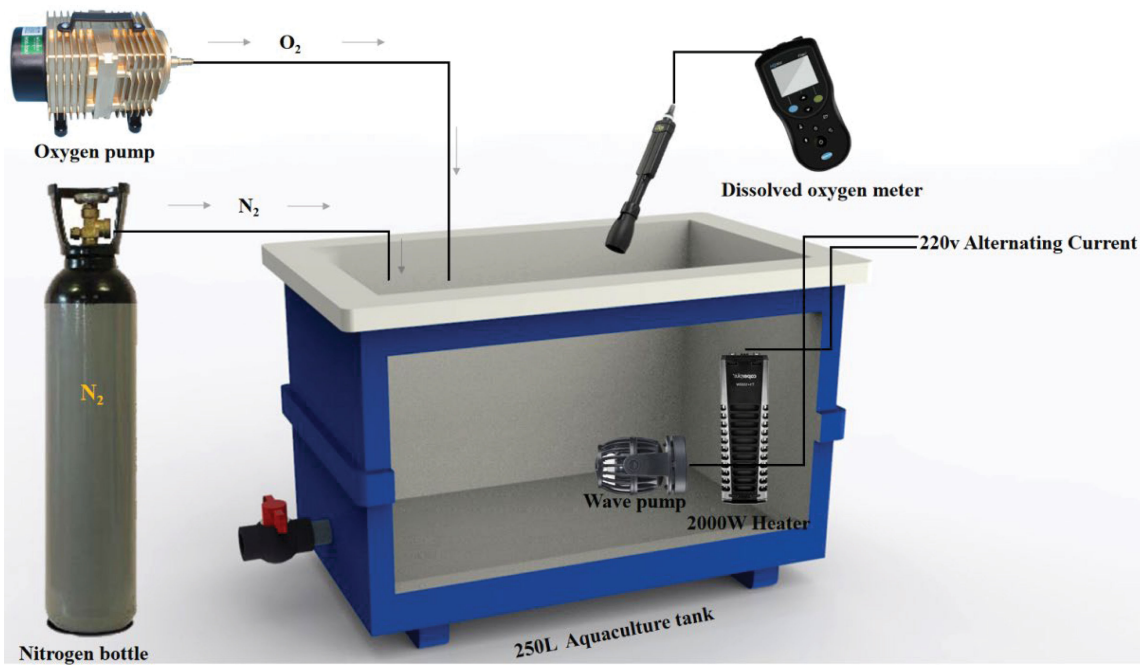

FIGURE 1 | Temperature dissolved oxygen control device.

number: PRJNA776993). All possible positively and negatively correlated miRNA-mRNA pairs were predicted using ACGT101-CORR1.1. Based on the comprehensive analysis of DEGs and DEMs, we screened the negatively associated miRNA-mRNA pairs and constructed interaction networks using Cytoscape 2.8.3 software (http://www.cytoscape.org/).

Verification of Differential Expression of miRNAs

To validate the results of RNA-seq, DEMs and target DEGs were randomly selected for real-time fluorescence quantitative PCR (qRT-PCR). Total RNA extraction and reverse transcription were performed by referring to Han et al. (Han et al., 2021). 18s rRNA and U6 RNA were used as internal reference gene for qRT-PCR, which was conducted with the LightCycler96 Real-time System (Roch, Switzerland) and followed by the manufacturer's instructions of the FastStart Essential DNA Green Master (Roch, Switzerland). The PCR primers were designed and synthesized by Shanghai Sangon Biotech and the primer sequences are shown in **Table 1**. The qRT-PCR was performed in a 20 μL reaction sample containing 2 μL of cDNA, 10 μL of FastStart Essential DNA Green Master, 6 μL of ddH2O water, and 1 μL (10 mM) of each primer. The reaction conditions were followed by 40 cycles of 95°C for 30 s, 95°C for 5 s, 60°C for 32 s, 95°C for 15 s, 60°C for 60 s, 95°C for 15 s and 60°C for 15 s. Compared with the control gene, fold-change of expression levers was determined using the $2^{-\Delta\Delta CT}$ method (Livak and Schmittgen, 2001), both in miRNA and mRNA PCR amplification. Statistical analysis was performed using SPSS software version 19.0 (IBM, Armonk, NY, USA). The data are expressed as the mean ± standard error of the mean (SEM) (n=3). In the results of gene expressions, significant differences ($P<0.05$) for each variable were first detected using the one-way ANOVA test between different groups, followed by Tukey's HSD test.

RESULTS

MiRNA Profiling of S. intermedius Exposed to Heat, Hypoxia, and Combined Stresses

We constructed small RNA libraries from *S. intermedius* and sequenced them on an Illumina HiSeq2500 platform to identify the miRNAs involved in heat, hypoxia, and combined stresses. Twelve libraries were established from the four experimental groups. A total of 12,049,632 ± 1,609,813 (NC), 9,169,509 ± 1,182,352 (HT), 12,077,449 ± 2,083,876 (LO), and 12,214,860 ± 1,271,035 (HL) raw reads were obtained. After removing low-

TABLE 1 | Primers used for DEMs and target DEGs verification.

Category	Name	Primers sequence (5'→3')
miRNA	lva-miR-125-5p	F: AACGGCTCCCTGAGACCCTA
	spu-miR-125-3p	F: ATCTGCACACAGGTTGGTATCTC
	lva-miR-133-3p	F: AACTTGATTTTGGTCCCCTTCAAC
	spu-miR-92e-1ss20TG	F: CGCTGCATTATTGCACTTACCC
	lva-miR-2003-3p_R-1	F: AACACGCCAGGTTATGCCCT
	spu-miR-9-3p	F: CTGCGCGAATAAAGCTAGGTTAC
	lva-miR-2012-5p	F: CCTCGAGCTAGTACTGGCATATG
	spu-miR-2008_R+1	F: AACCACTATCAGCCTCGCTGT
	lva-miR-4854-5p	F: AACTTGATTGTTGCAGTGACGAC
	spu-miR-2013	F: AAGAGCGTTGCAGCATGATGTA
Reference miRNA	U6	F: ACGCAAATTCGTGAAGCGTT
mRNA	*ABCB4*	F: GCTTCTCGCAGGCTACCATCTTC
		R: AGGCACCAAACATCAAGGCAGAG
	KIF4	F: AAGAGACGGAGTGGACGATAGCC
		R: TTTCCCAGTTGCCCCATTTCTTCC
	ZNFX1	F: AGGCACACATCATCTCGGCATTG
		R: CCAGGTAGTACACGTTCGGTTTCG
	EGF3	F: AATGGCGGTACGTGCGAAGATG
		R: GTCACTCATACAGGCGTCCACAAG
	DHX33	F: AGGCTTGTTCATGTATTCGGCTGAG
		R: AGAGACACGAGGAGGGATGGATTG
	PTRPF	F: TCTTCCGACCAGGAGAGCATCAC
		R: GTGGCACCAACATCATCCGTCTC
	CALN	F: CCGATGCAGAGAAACCAGACGAC
		R: GAGCCTTCCATTCGCCACATCC
	CUL4A	F: GAGGCTTGTGCATGAACGAGAGG
		R: GGCGATTAGAGGTTTCCGAGTAGTG
	PAN2	F: GGCGTCCTCTCACTCTACAACAATG
		R: TGATGACCTCCCAGCAGCAGAC
	CYCL	F: TAGGAGTGAGCAGGACAAGGAGAAC
		R: CGACTGACTGTCTGCGATGTAAGG
Reference gene	*18S rRNA*	F: TGAGCCGCAACAGTAATC
		R:AAGGGAAAAGGAAGTGAAAG

quality reads, we mapped the clean reads against the Rfam database, which contains rRNA, tRNA, snRNA, snoRNA families, and Repbase to filter unwanted sequences and obtain valid small RNA data. A total of 7,846,735 ± 1,822,577 (NC), 5,549,774 ± 3,009,597 (HT), 8,869,277 ± 1,415,005 (LO), and 9,613,111 ± 885,961 (HL) valid reads were obtained (**Table 2**). The length distribution statistics for the total number of filtered valid reads showed that most of the reads were 22-nt (**Supplementary Figure 1**).

The bioinformatic analysis identified 140 miRNAs in the four experimental groups; 70 known and 70 novel miRNAs (**Table 3**). By co-expression analysis of the four groups (three comparison groups), a total of 70 (55 co-expressed, HT 1, NC 14), 78 (61 co-expressed, LO 9, NC 8) and 82 (67 co-expressed, HL 13, NC 2) miRNAs were identified in the HT vs NC, LO vs NC, and HL vs NC comparisons, respectively (**Figure 2**).

Differentially Expressed miRNAs (DEMs) in Three Comparison Groups

We identified 17, 14, and 23 DEMs in the HT vs NC, LO vs NC, and HL vs NC comparisons, respectively, by analyzing the RNA-seq data. Among the 17 DEMs in the HT vs NC comparison, 7 were up-

TABLE 2 | Overview of reads from raw data to cleaned sequences.

Sample		Raw reads	3ADT&length filter	Junk reads	Rfam	Repeats	valid reads	rRNA	tRNA	snoRNA	snRNA	other Rfam RNA
NT1	Total	10243015	2605706	17509	1427085	69370	6190556	434776	925238	8042	12264	46765
	% of Total	100.00	25.44	0.17	13.93	0.68	60.44	4.24	9.03	0.08	0.12	0.46
	uniq	1461697	704280	5788	23737	489	727811	10184	10654	350	571	1978
	% of uniq	100.00	48.18	0.40	1.62	0.03	49.79	0.70	0.73	0.02	0.04	0.14
NT2	Total	12573998	3257425	23380	1739864	102857	7550284	663282	969640	10924	24813	71205
	% of Total	100.00	25.91	0.19	13.84	0.82	60.05	5.28	7.71	0.09	0.20	0.57
	uniq	1807890	910655	6569	27639	538	862934	12084	11638	479	916	2522
	% of uniq	100.00	50.37	0.36	1.53	0.03	47.73	0.67	0.64	0.03	0.05	0.14
NT3	Total	13331885	2220139	25179	1281716	68369	9799364	467576	695791	11079	30746	76524
	% of Total	100.00	16.65	0.19	9.61	0.51	73.50	3.51	5.22	0.08	0.23	0.57
	uniq	1644836	741590	7730	27300	757	868005	13359	10293	423	697	2528
	% of uniq	100.00	45.09	0.47	1.66	0.05	52.77	0.81	0.63	0.03	0.04	0.15
HT1	Total	8577093	1805181	26938	618997	19315	6122514	208024	367369	7720	6963	28921
	% of Total	100.00	21.05	0.31	7.22	0.23	71.38	2.43	4.28	0.09	0.08	0.34
	uniq	1305399	588644	8583	17730	416	690351	9160	6538	352	335	1345
	% of uniq	100.00	45.09	0.66	1.36	0.03	52.88	0.70	0.50	0.03	0.03	0.10
HT2	Total	10530958	1745541	27742	522899	14469	8231847	208230	276875	6876	5066	25852
	% of Total	100.00	16.58	0.26	4.97	0.14	78.17	1.98	2.63	0.07	0.05	0.25
	uniq	1326233	580640	8908	17655	372	718952	9379	6361	354	285	1276
	% of uniq	100.00	43.78	0.67	1.33	0.03	54.21	0.71	0.48	0.03	0.02	0.10
HT3	Total	8400476	5809150	10165	285059	6147	2294962	69102	201759	2146	2271	9781
	% of Total	100.00	69.15	0.12	3.39	0.07	27.32	0.82	2.40	0.03	0.03	0.12
	uniq	1289897	904019	4195	8924	216	372717	4346	3644	141	130	663
	% of uniq	100.00	70.08	0.33	0.69	0.02	28.90	0.34	0.28	0.01	0.01	0.05
LO1	Total	11247361	1550143	17851	897787	28924	8777912	223260	629471	10909	9322	24825
	% of Total	100.00	13.78	0.16	7.98	0.26	78.04	1.98	5.60	0.10	0.08	0.22
	uniq	1243041	562511	7384	17347	409	655710	8393	6794	401	363	1396
	% of uniq	100.00	45.25	0.59	1.40	0.03	52.75	0.68	0.55	0.03	0.03	0.11
LO2	Total	14448447	3232933	14158	872015	25638	10327751	207538	621207	9651	9950	23669
	% of Total	100.00	22.38	0.10	6.04	0.18	71.48	1.44	4.30	0.07	0.07	0.16
	uniq	1575774	847933	6686	16326	270	704773	7697	6721	384	327	1197
	% of uniq	100.00	53.81	0.42	1.04	0.02	44.73	0.49	0.43	0.02	0.02	0.08
LO3	Total	10536539	2202009	17808	811268	24484	7502169	185791	579121	13056	9991	23309
	% of Total	100.00	20.90	0.17	7.70	0.23	71.20	1.76	5.50	0.12	0.09	0.22
	uniq	1255042	646936	6667	16185	388	585162	7340	6838	431	330	1246
	% of uniq	100.00	51.55	0.53	1.29	0.03	46.62	0.58	0.54	0.03	0.03	0.10
HL1	Total	12959469	2435730	14469	531578	19186	9973246	211701	277533	6153	6048	30143
	% of Total	100.00	18.79	0.11	4.10	0.15	76.96	1.63	2.14	0.05	0.05	0.23
	uniq	1101567	657103	3343	11648	325	429398	6158	3314	294	241	1641
	% of uniq	100.00	59.65	0.30	1.06	0.03	38.98	0.56	0.30	0.03	0.02	0.15
HL2	Total	12937862	2080346	16434	572686	32073	10262292	274021	244267	6286	10411	37701
	% of Total	100.00	16.08	0.13	4.43	0.25	79.32	2.12	1.89	0.05	0.08	0.29
	uniq	950584	505095	3261	12367	364	429768	6608	3394	310	379	1676
	% of uniq	100.00	53.14	0.34	1.30	0.04	45.21	0.70	0.36	0.03	0.04	0.18
HL3	Total	10747248	1613140	11916	513863	22544	8603794	215763	261339	4950	6795	25016
	% of Total	100.00	15.01	0.11	4.78	0.21	80.06	2.01	2.43	0.05	0.06	0.23
	uniq	818902	424313	3156	10891	341	380460	5934	3038	250	253	1416
	% of uniq	100.00	51.81	0.39	1.33	0.04	46.46	0.72	0.37	0.03	0.03	0.17

TABLE 3 | Number of known and novel miRNA identified in each sample.

	NT libaray					
	NT1		NT2		NT3	
Groups:	**Pre-miRNA**	**Unique miRNA**	**Pre-miRNA**	**Unique miRNA**	**Pre-miRNA**	**Unique miRNA**
gp1	2	4	2	4	2	4
gp2a	1	1	1	1	2	2
gp2b	5	4	3	2	4	3
gp3	48	56	49	57	49	57
gp4	12	12	20	19	22	21
	HT libaray					
	HT1		**HT2**		**HT3**	
	Pre-miRNA	Unique miRNA	Pre-miRNA	Unique miRNA	Pre-miRNA	Unique miRNA
gp1	2	4	2	4	2	3
gp2a	1	1	1	1	1	1
gp2b	3	2	3	2	1	1
gp3	45	52	43	50	41	48
gp4	21	19	22	21	5	4
	LO libaray					
	LO1		**LO2**		**LO3**	
Groups:	Pre-miRNA	Unique miRNA	Pre-miRNA	Unique miRNA	Pre-miRNA	Unique miRNA
gp1	2	4	2	4	2	4
gp2a	1	1	1	1	1	1
gp2b	4	3	1	1	5	4
gp3	45	52	44	51	44	51
gp4	22	20	27	25	33	28
	HL libaray					
	HL1		**HL2**		**HL3**	
Groups:	Pre-miRNA	Unique miRNA	Pre-miRNA	Unique miRNA	Pre-miRNA	Unique miRNA
gp1	2	4	2	4	2	4
gp2a	2	2	1	1	2	2
gp2b	4	3	5	4	4	3
gp3	48	57	48	57	48	56
gp4	26	22	30	25	22	20

regulated and 10 were down-regulated. Among the 14 DEMs in the LO vs NC comparison, 8 were up-regulated and 6 were down-regulated. Among the 23 DEMS in the HL vs NC comparison, 14 were up-regulated and 9 were down-regulated (**Supplementary Table 1**). The heat map (**Figure 3**) shows that 42 of the DEMs in the three comparisons were significantly differentially expressed (P <0.05), and four of them (PC-3p-56283_77, lva-miR-2008-5p, lva-miR-219-5p_R-1, lva-miR-9-5p_R+1) were significantly different in all three comparison groups.

Identification and Functional Annotation of the Target Genes of the DEMs

The roles of the identified DEMs in regulating the expression and function of their target genes were predicted by gene ontology (GO) and Kyoto Encyclopedia of Genes and Genomes (KEGG) pathway functional enrichment analysis. A total of 69,912 target genes were predicted for the 17 DEMs identified in the HT vs NC comparison, and 12,825 of them were annotated to 9,879 GO terms under the three main GO categories: biological process (BP), cellular component (CC), and molecular function (MF). Under BP, biological process, signal transduction, and positive regulation of transcription by RNA polymerase II were the three most enriched terms (P <0.05). Under CC, integral component of membrane, membrane, and plasma membrane were the three most enriched terms. Under MF, calcium ion binding, serine-type endopeptidase activity, and GTP binding were the three most enriched terms (**Figure 4A** and **Supplementary Table 2**). In addition, 5,710 target genes were annotated to 388 KEGG pathways. Five of these pathways were significantly enriched, namely Glycosaminoglycan biosynthesis - chondroitin sulfate/dermatan sulfate (ko00532), Neuroactive ligand–receptor interaction (ko04080), mTOR signaling pathway (ko04150), FoxO signaling pathway (ko04068), and Drug metabolism - cytochrome P450 (ko00982) (**Figure 5A** and **Supplementary Table 3**).

A total of 56,715 target genes were predicted for the 14 DEMs identified in the LO vs NC comparison, and 12,217 of them were annotated to 9,592 GO terms. Under BP and CC, the three most enriched terms were the same as those for the HT vs NC comparison. Under MF, metal ion binding, transferase activity, and nucleic acid binding were the three most enriched terms (**Figure 4B**). A total of 5,471 target genes were annotated to 383 KEGG pathways. Four of these pathways were the most significantly enriched, namely Histidine metabolism, mTOR signaling pathway, ECM-receptor interaction, and FoxO signaling pathway (**Figure 5B**).

A total of 79,746 target genes were predicted for the 23 DEMs identified in the HL vs NC comparison, and 14,343 of them were annotated to 9,958 GO terms. Under BP, biological process, oxidation-reduction process, and signal transduction were the three most enriched terms (P <0.05). Under CC, integral

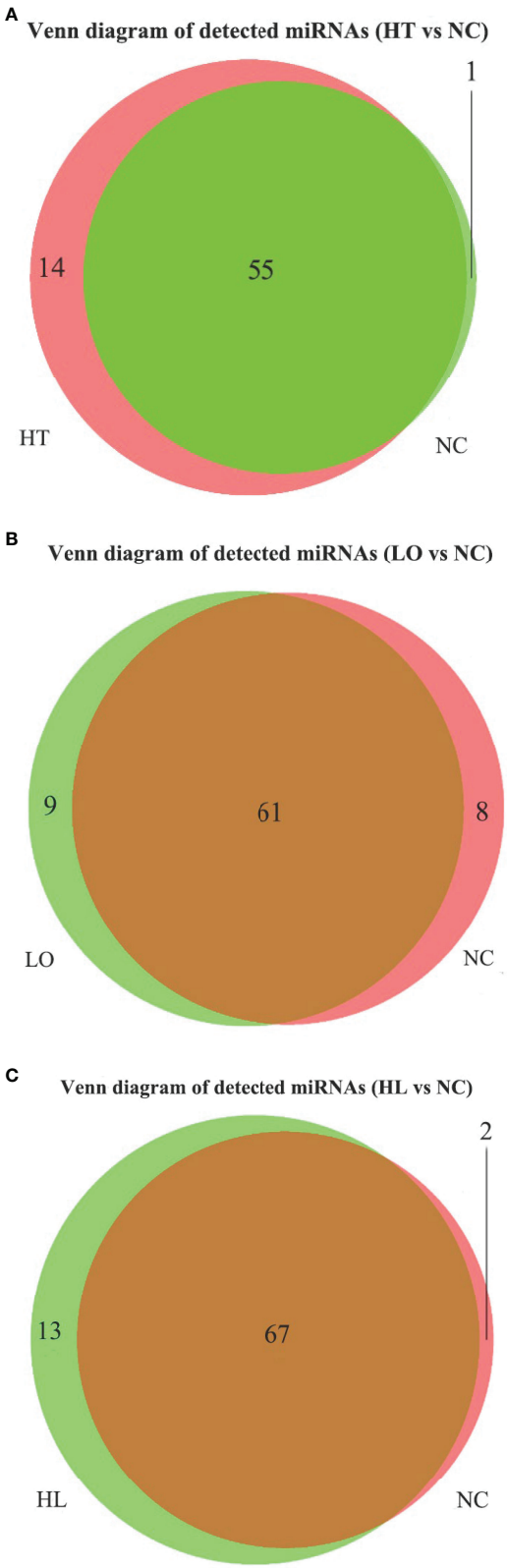

FIGURE 2 | Venn of detected miRNA in four groups. **(A)** HT vs NT, **(B)** LO vs NT, **(C)** HL vs NT.

component of membrane, plasma membrane, and mitochondrion were the three most enriched terms. Under MF, metal ion binding, zinc ion binding, and transferase activity were the three most enriched terms (P <0.05) (**Figure 4C**). Unlike the KEGG pathway annotations of the single stresses, the KEGG pathway annotations of the target genes of the 23 DEMs obtained for the combined stresses were mostly enriched in metabolic pathways, such as Glycosaminoglycan biosynthesis, Lysine degradation, Peroxisome, and Valine, leucine and isoleucine degradation and Fatty acid elongation (P <0.05) (**Figure 5C**).

Prediction of Interactions Between DEMs and Differentially Expressed Genes (DEGs)

The pre-constructed transcriptome library and previously identified DEGs (Hao et al., 2022) were used for co-analysis with the target genes of the DEMs. We identified 15 DEMs that interacted with 33 DEGs under high temperature stress by association analysis. Among them, the expression of 24 DEM–DEG pairs was negatively correlated and the expression of 32 DEM–DEG pairs was positively correlated. We also found 14 DEMs that interacted with 171 DEGs under hypoxia stress; 139 were negatively correlated DEM–DEG pairs and 108 were positively correlated DEM–DEG pairs. Under the combined stresses, 23 DEMs interacted with 102 DEGs; 69 were negatively correlated DEM–DEG pairs and 79 were positively correlated DEM–DEG pairs (**Supplementary Table 4**). The predicted DEM–DEG network map is shown in **Figure 6**. Meanwhile, we found that the key DEM in high-temperature stress was lva-miR-193-3p_R-2, whose predicted target genes were *DHX33* and *CSTF1*; the key DEM in hypoxic stress was spu-miR-92e_1ss20TG, with nine essential target genes predicted to be negatively regulated, namely *ZNFX1*, *Pola2*, *DDB_ G0276821*, *ACSM3*, *ctps1*, *PLOD1*, *GRID2IP*, *Pole*, and *FAU*; the key DEM was lva-miR-9- in combined stresses, whose had 28 key negatively regulated target genes, mainly *SOD*, *PAN2*, and *PRPF*.

Validation of DEMs and Their Target DEGs by qRT-PCR

A qRT-PCR analysis was performed to validate the RNA-seq results. A total of 10 DEGs (including *ABCB4*, *CYCL*, *EGF3*, *ZNFX1*, *CALN*) and 10 DEMs (such as miR-193, miR-184, miR-133, miR-125, miR-2008) were selected for the qRT-PCRs. The results of the qRT-PCR analysis were consistent with the results obtained by the RNA-seq analysis and showed similar expression trends (**Figure 7**). In addition, the relative expressions of *ABCB4*, *KIF4*, *ZNFX1*, *EGF3*, *DHX33*, and *PTRPF* were significantly increased in high-temperature stress, and *CALN*, *CUL4A*, and *PAN2* were up-regulated in hypoxic stress; *CYCL* genes showed a decreasing trend in high temperature and hypoxic stress, but their expressions were increased under combined stress.

DISCUSSION

Many aquatic organisms are located in environmentally sensitive coastal zones or estuaries, which are extremely vulnerable to climate change. Water temperature and dissolved oxygen are the

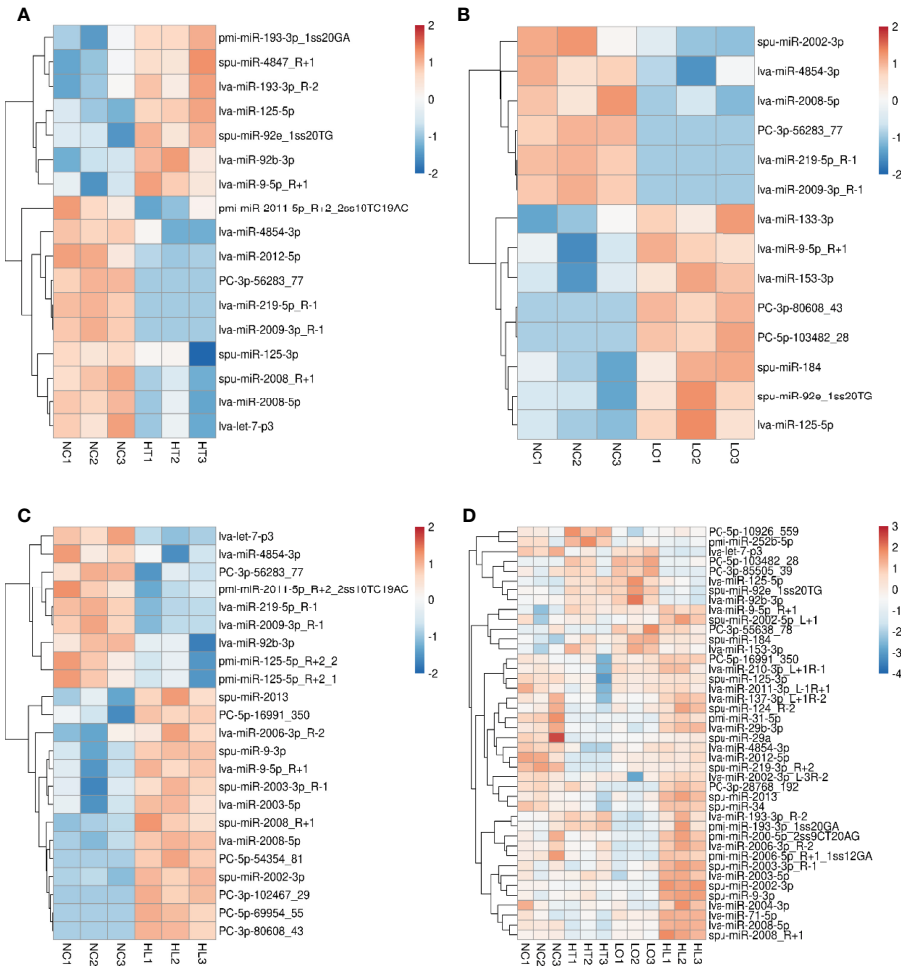

FIGURE 3 | Differentially expressed miRNAs (DEMs) in the four groups. **(A)** HT vs NT, **(B)** LO vs NT, **(C)** HL vs NT, **(D)** DEMs (non-repetitive) in the pairwise comparison among the three treatments ($P < 0.05$). All red rectangles indicate higher levels of miRNAs, and blue rectangles indicate lower levels of miRNAs. Color scale bar represents $\log_2$FoldChange.

most important environmental factors that affect the survival of *S. intermedius*. MiRNAs are known to modulate gene expression and have critical roles in many biological processes, including cell proliferation, apoptosis, differentiation, cell cycle progression, and organ development (Tse et al., 2016; Biggar and Storey, 2018). In this study, miRNA libraries of sea urchins under heat, hypoxia, and combined stresses were constructed, sequenced by RNA-seq, and analyzed together with published transcriptome data to investigate the molecular mechanisms of sea urchins in response to different environmental conditions. The miRNAs were mainly distributed at 22-nt long, which is consistent with a previous study of *S. intermedius* (Zhan et al., 2018). A total of 140 miRNAs were identified; 70 were known and 70 were newly identified miRNAs. We identified 17, 14, and 23 DEMs in the HT, LO, and HL comparisons with NC, respectively, and found that they were involved in multiple key biological processes related to biosynthesis, metabolism, immunity, and signaling transduction by functional enrichment analysis.

These biological processes may be associated with major changes in the predicted target genes. We found changes in lysosomal pathways related to translation that were similar to the results of Huo et al. (2018). Regarding signal transduction, for the DEMs in the HT vs NC comparison, the mTOR and Wnt signaling pathways were among the enriched pathways; for the DEMs in the LO vs NC comparison, the FoxO signaling and Fanconi anemia pathways were among the enriched pathways; and for the DEMs in the HL vs NC comparison, the Hippo signaling and TGF-β signaling pathways were among the enriched pathways. Interestingly, the KEGG pathway annotations Lysine degradation, Peroxisome, Glycerolipid metabolism, and TGF-β signaling pathway were assigned to targent genes of DEMs in all three comparisons. Small amounts of lysine ingested by animals have been shown to cause triglyceride accumulation and significantly inhibit growth and development (Forster and Ogata, 1998; Ahmed and Khan, 2004). Peroxisomes are involved in multiple metabolic processes, including fatty acid oxidation, ether lipid synthesis, and reactive oxygen

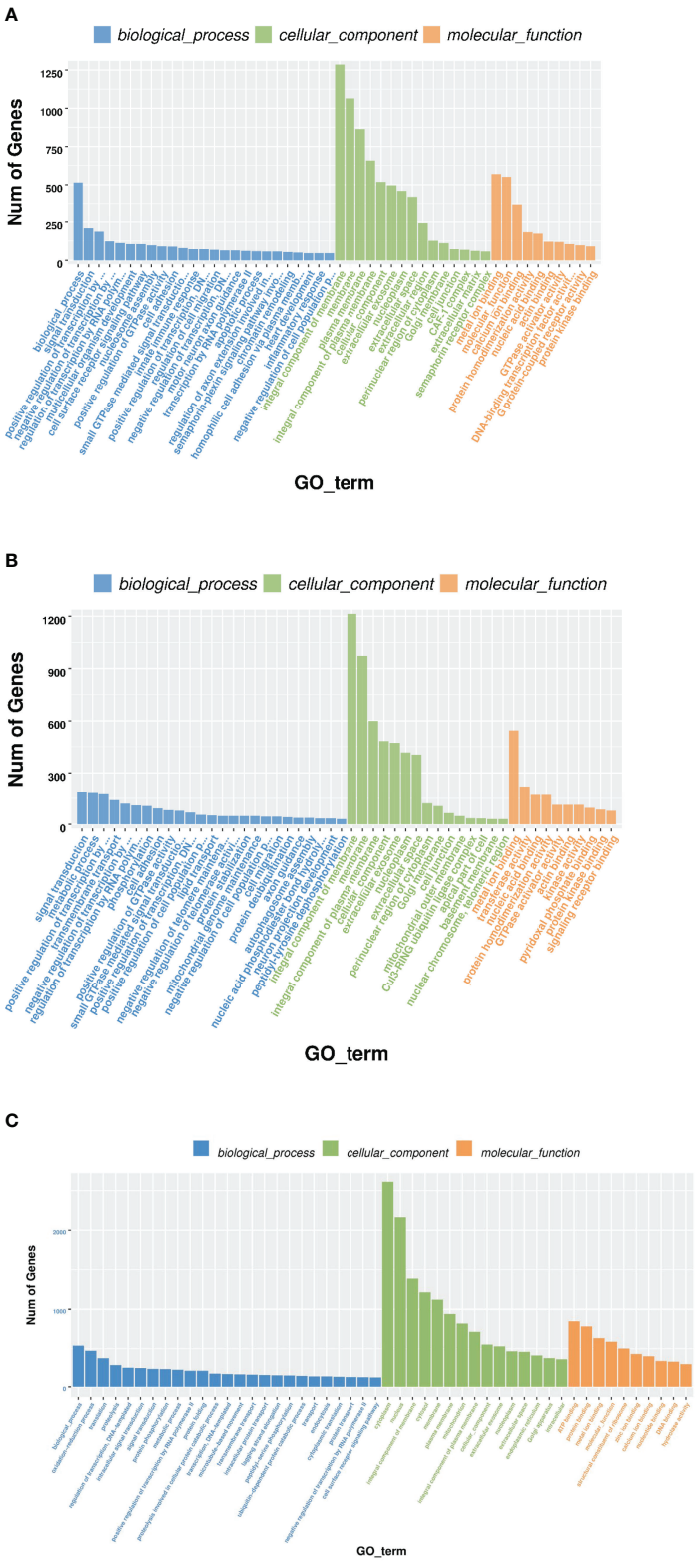

FIGURE 4 | GO enrichment of target genes of DEMs. The x-axis is the rich factor, which indicates the proportion of genes in total genes in a GO term. The y-axis is the gene functional classification of GO. Various colors of plots indicate different values of –log 10 (P-value). Plot diameter represents target gene numbers in a GO term. (For interpretation of the references to color in this figure legend, the reader is referred to the Web version of this article.). **(A)** HT VS NT, **(B)** LO vs NT, **(C)** HL vs NT.

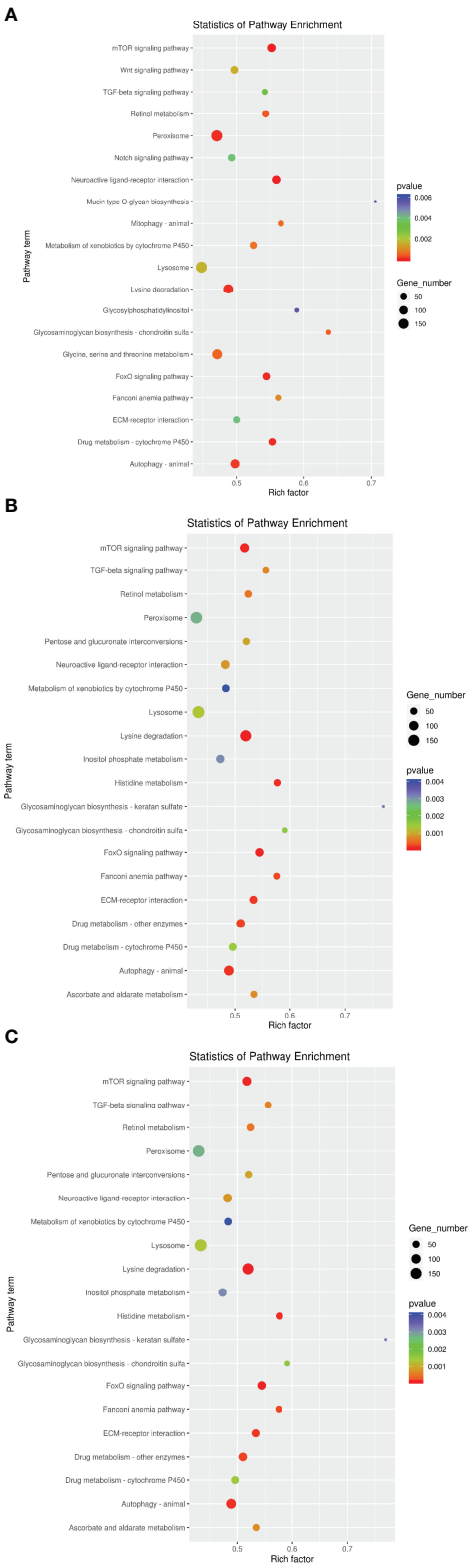

FIGURE 5 | KEGG enrichment of target genes of DEMs. The x-axis is the rich factor, which means that the proportion of target genes in total genes in a KEGG term. The y-axis is the gene functional classification of KEGG. Various colors of plots indicate different values of –log 10 (*P*-value). Plot diameter represents target gene numbers in a KEGG term. (For interpretation of the references to color in this figure legend, the reader is referred to the Web version of this article). **(A)** HT VS NT, **(B)** LO vs NT, **(C)** HL vs NT.

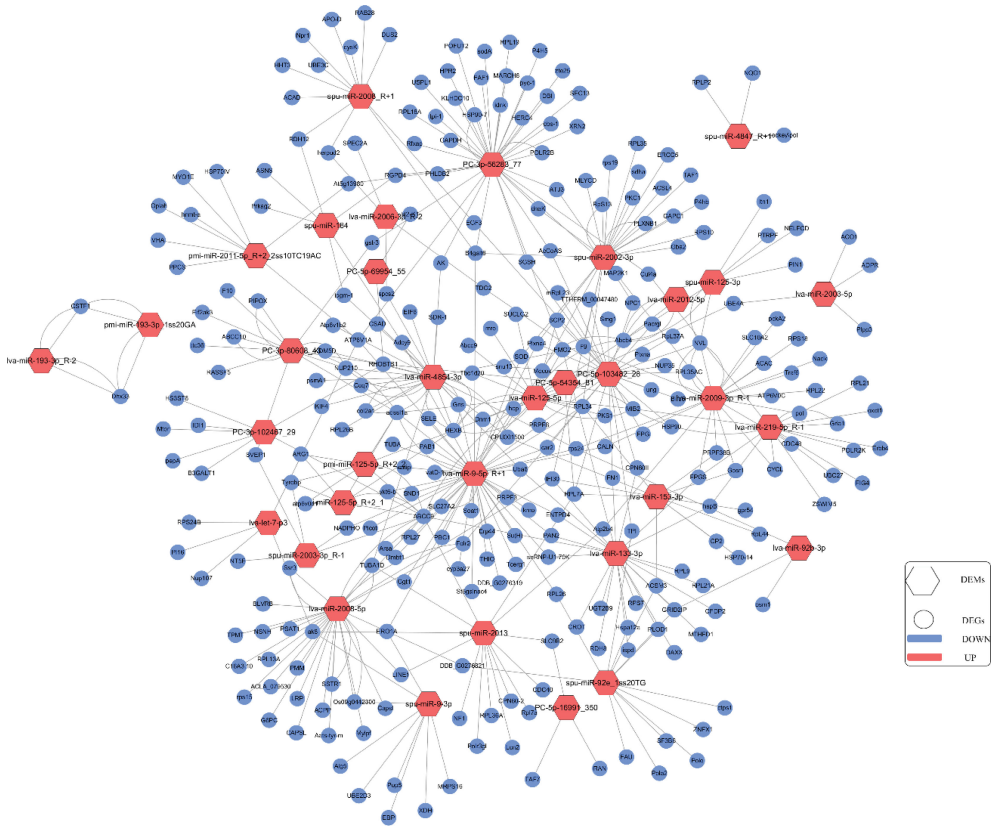

FIGURE 6 | The network of DEMs and their target DEGs was constructed using Cytoscape 3.3.0. Hexagon is miRNA, circle is target DEGs, red means up-regulated expression, blue means down-regulated expression.

species (ROS) metabolism. Recent studies suggest that peroxisomes are critical mediators of cellular responses to various forms of stress, including oxidative stress, hypoxia, starvation, cold exposure, and noise (He et al., 2021a). Jain et al. discovered regulators of cell fitness in high and low oxygen conditions which led to the identification of an essential role for peroxisomes in metabolic adaptation to hypoxic stress (Jain et al., 2020). TGF-β signaling is a multifunctional pathway that controls cell proliferation, cell differentiation and tissue homeostasis (Hata and Chen, 2016). A study has found that TGF-β sensu stricto signaling plays an essential role in the formation of the embryonic skeleton of this sea urchin (Sun and Ettensohn, 2017). This finding together with the changes in the multi-metabolic and apoptosis-multi-species pathways, suggest that the metabolic system of sea urchins will be affected and apoptosis will occur under environmental stresses, in addition, multiple signal transduction pathways may work together to activate the same defense response. The DEMs were also involved in biosynthesis and metabolism-related pathways such as "Glucose metabolism", "Serotonin metabolism", and "Galactose metabolism". These results indicates that sea urchins respond to the adverse effects of environmental stress through a variety of miRNA regulatory mechanisms.

MiRNA sequences are usually partially or totally matched with specific regions of the target genes. This interaction results in endonuclease digestion or translation inhibition, thereby negatively regulating the expression of the target gene. Therefore, identifying target genes that are differentially expressed is critical for understanding the biological functions of the encoded proteins.

Effects of Heat Stress on miRNA Regulation in *S. intermedius*

MiR-193 plays an important role in cell growth, proliferation, and apoptosis. MiR-193 down-regulates the insulin growth factor 2 gene (*IGF2*) to induce cell proliferation and migration, which affect the angiogenic process (Yi et al., 2017). We found that miR-193 expression was up-regulated and its target genes *DHX33* (putative ATP-dependent RNA helicase *DHX33*) and *CSTF1* (cleavage stimulation factor subunit 1) were down-regulated under high temperature stress. *DHX33* is a nucleoprotein involved in cell cycle regulation (Zhang et al., 2011), and *CSTF1* encodes a nuclear protein that contains a ribonucleoprotein (RNP)-type RNA binding domain at its N-terminal end, which is essential for mRNA cleavage and polyadenylation. When DNA-damaged cells undergo oxidative stress, *CSTF1* can bind to the BARD1/BRCA1 ubiquitin ligase heterodimer, thereby inhibiting 3′ end processing (Fontana et al., 2017). This finding and the regulation of alternative polyadenylation in development, differentiation, and neuronal

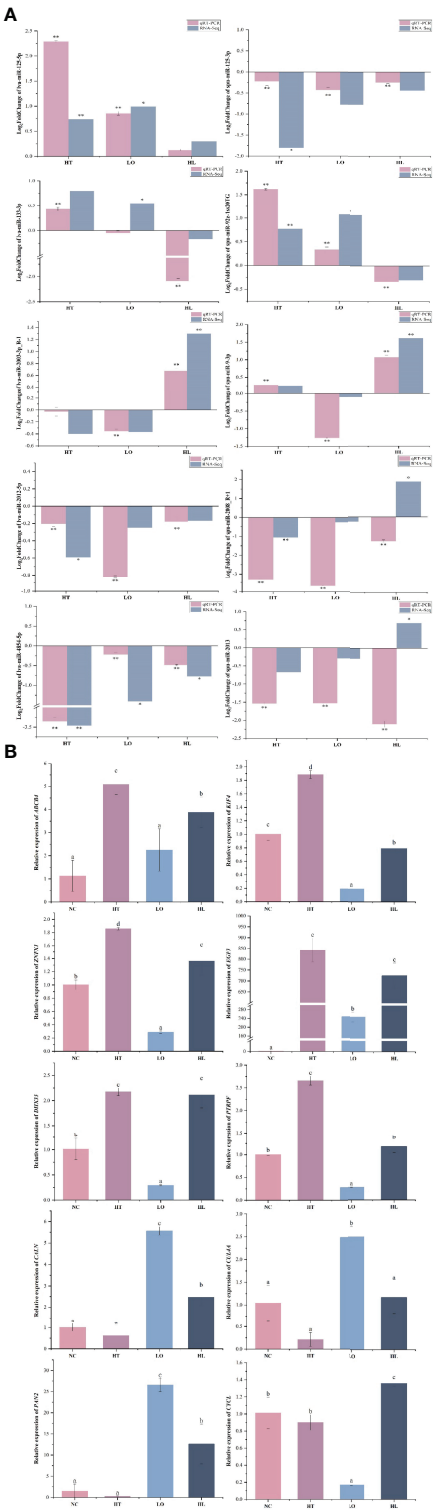

FIGURE 7 | qRT-PCR verification of DEMs **(A)** and target DEGs **(B)**. Each vertical bar represents the Mean ± SD (n=3), U6 and18s rRNA were used as a reference miRNA/gene. *Significant differences at $P<0.05$ vs control (NT). **Highly significant differences at $P<0.01$ vs control (NT). Letters above the bars indicate significant differences at $P<0.05$.

activation suggest that 3′ end processing can be regulated in response to physiological and pathological stimuli. Therefore, we hypothesized that DNA was damaged under high temperature stress and miR-193a negatively regulated *DHX33* and *CSTF1* to promote apoptosis.

The expression of miRNA let-7 was also found to be down-regulated under high temperature stress. Members of the let-7 family are significantly elevated under high temperature stimulation, and are involved in regulating cell growth, differentiation, apoptosis, and metabolism (Gibadulinova et al., 2020; Tristán-Ramos et al., 2020; Huo et al., 2021). In the current study, the expression of lva-let-7-p3 was significantly down-regulated under heat stress and combined heat and hypoxic stresses. Lva-let-7-p3 may regulate potential target genes, including *PI16* (peptidase inhibitor 16), *ATP6V1A* (V-type proton ATPase catalytic subunit A isoform X4), and *Nup107* (nuclear pore complex protein Nup107 isoform X2).

Effects of Hypoxia on miRNA Regulation in *S. intermedius*

MiR-184 was shown to be an important regulator of stem cell proliferation and growth (Liu et al., 2015), and its overexpression led to apoptosis and its suppression led to an increase in cell numbers (Foley et al., 2010; Liu et al., 2010). Previous studies have shown that miR-184 overexpression inhibited autophagy and exacerbated oxidative damage, and miR-184 also negatively regulated Wnt signaling *in vivo* and *in vitro* (Takahashi et al., 2015). MiR-184 was found to inhibit gene expression in human trabecular meshwork cell cytotoxicity, apoptosis, and the extracellular matrix by targeting the hypoxia-inducible factor *HIF-1αin vivo*, and it also exhibited angiostatic properties by regulating signaling pathways such as the Akt, TNF-α, and VEGF signaling pathways (Park et al., 2017). Furthermore, reduced expression of miR-184 was shown to inhibit cell growth through the CDC25A-dependent Notch signaling pathway (Cao et al., 2020).

MiR-133 is a key regulator of muscle proliferation and myocardial differentiation and is associated with cell proliferation and apoptosis (Chen et al., 2006; Uchida et al., 2013). The target of miR-133 was shown to be epidermal growth factor (*EGF*), and when *EGF* was down-regulated by miR-133, it inhibited its downstream signaling pathways, including the MAPK and AKT signaling pathways (Hernes et al., 2004; Dimauro et al., 2014). MiR-133 was also found to be an important component of the apoptotic pathway. In this study, we found that miR-133 expression was down-regulated under hypoxic stress and that its target genes *HSP70*, *EGF*, *PAN2*, and *ABCC9* were up-regulated. In addition, the functional enrichment analysis of miRNA target genes under hypoxic stress showed that most of the genes were related to basal metabolism. Therefore, we hypothesized that miR-133 inhibited apoptosis by regulating *HSP70*, *EGF*, and other genes when sea urchins were exposed to hypoxia stress, and that metabolism-related genes were mobilized to maintain vital metabolism processes.

We found that the expression of lva-miR-125-5p was remarkably up-regulated in sea urchins under hypoxic conditions. Previous studies of miR-125-5p focused mainly on its role in regulating cell migration, apoptosis, immunity, proliferation, and cancer (Fassan et al., 2013; Natalia et al.,

2018; Xu et al., 2019; Zheng et al., 2019; He et al., 2021b). In zebrafish (*Danio rerio*), the main target gene for hypoxia response was *HIF-1a*, which up-regulated the expression of miR-125 under hypoxic conditions (He et al., 2017). However, no up-regulation of *HIF* genes was detected in the present study. Previous studies have demonstrated that under hypoxic stress, the expression of *HIF* in the brain of the Wuchang bream (*Megalobrama amblycephala*) did not differ significantly from that of the control group (Shen et al., 2010). It is speculated that different species may have different hypoxia tolerance thresholds or species-specific differences in oxygen requirements. It might be duo to the short duration of the stress treatment in this study, we plan to further investigate the response of sea urchins under long-term hypoxic stress in future work. MiR-125 was shown to inhibit the expression of the mitofusin *Mfn1* and reduce the disordered growth of pulmonary arterial smooth muscle cells under hypoxic conditions, as well as protect pulmonary blood vessels from mitochondrial dysfunction and abnormal remodeling (Ma et al., 2017). These findings provided a theoretical foundation for successful lung organ care. In this study, the potential target genes that may be regulated by lva-miR-125-5p included *ZFP708* (zinc finger protein 708-like), *ALDH* (aldehyde dehydrogenase), *KMT2A* (lysine methyltransferase 2A), and *MAP3K7* (mitogen-activated protein kinase kinase kinase 7). In the Gene Expression Omnibus (GEO) Profiles database (Tanya et al., 2007), *ZFP708*, *ALDH*, and *MAP3K7* are recorded as being involved in the regulation of organisms in a hypoxic environment. These findings suggest that these genes may be involved in the response of sea urchins to low oxygen environments.

Effects of the Combined Stresses on miRNA Regulation in *S. intermedius*

Under the combined stresses, spu-miR-2002-3p, which was highly expressed under hypoxic stress, was significantly up-regulated. This miRNA has not been reported in this context in previous studies. We found that under hypoxic stress, 14, 30, 5, 25, 39, and 11 target genes of spu-miR-2002-3p were enriched in neuroactive ligand–receptor interaction, lysine degradation, biosynthesis of unsaturated fatty acids, valine, leucine and isoleucine degradation, lysosome, and tryptophan metabolism KEGG pathways, respectively. The neuroactive ligand–receptor interaction signaling pathway involves all the receptors and ligands on the plasma membrane associated with intracellular and extracellular signaling pathways (Lauss et al., 2007). Under hypoxic stress, the cells pass through the surface of the sea urchin, then the receptors interact with extracellular ligands to trigger a series of metabolic changes. These processes may support the response of sea urchins to high temperature and low oxygen stress to protect them from damage.

We also identified miR-2008 and miR-9, which were significantly expressed under all three conditions. MiR-2008 was identified as a regulator of sea cucumber skin ulcer syndrome outbreaks by deep sequencing, and its target gene is the toll like receptor *TLR3* (Li et al., 2012; Zhou et al., 2018). The expression of miR-2008 was also found to be up-regulated in sea cucumber under hypoxic stress. In the present study, miR-2008 expression was up-regulated under all three stress conditions, and the key target genes were *EGF3*, *ABCC9*, *TUBA*, and *ACAD*. We hypothesized that when *S. intermedius* is damaged by environmental stresses, the expression of genes related to apoptosis and immunity is significant. Our results support the view that miRNA–target gene interactions are complex, and a single miRNA can regulate multiple target genes simultaneously, and a gene can be regulated by multiple miRNAs simultaneously (Agarwal et al. 2015; Lan et al., 2016; Lai et al., 2022; Miao et al., 2022). The mechanism of the *S. intermedius* response to environmental stress is also complex. Compared with the effects of a single-factor stress, under multi-factor stress conditions, *S. intermedius* suffers an increased degree of organismal damage and responds comprehensively through metabolic and immune pathways. The qRT-PCR results further imply that there may be meaningful targeted regulatory interactions between the candidate DEMs and DEGs. In future research, the targeted regulatory interactions of the putative DEM–DEG pairs need to be confirmed by additional *in vivo* and *in vitro* experiments (e.g., dual luciferase reporter analysis, gain or loss of function analysis, and western blotting).

CONCLUSIONS

In this study, we report the miRNAs profiles of the sea urchin *S. intermedius* under high temperature, low oxygen, and combined stresses, and identified 17, 14, and 23 DEMs, respectively. By co-analysis with published transcriptome data, key DEMs (miR-193, miR-184, miR-133, miR-125, miR-2008) and their key target genes (*EGF3*, *ABCC9*, *TUBA*, *PAN2*, *CALN*) were identified. We found that the *S. intermedius* defense responses were activated by multiple miRNAs that regulate multiple signal transduction pathways in response to the adverse effects of environmental stress. Furthermore, under the combined heat and hypoxic stresses, the effects of both these factors were superimposed. The expression of target genes associated with apoptosis and oxidative stress was up-regulated, implying transcriptional regulation is a comprehensive response in sea urchins in the face of global climate change. Our results provide information on gene expression regulation of the molecular mechanisms underlying the response of *S. intermedius* to multi-cause environmental stress and provide a theoretical basis for healthy sea urchin reproduction.

DATA AVAILABILITY STATEMENT

The datasets presented in this study can be found in online repositories. The data presented in the study are deposited in the NCBI repository, accession number PRJNA828018.

AUTHOR CONTRIBUTIONS

JD, DD, and YC: conceptualization and resources. JD and BD: conceived and designed the experiment. BD, PH, and XZ: performed the experiment. PH, YL, and WW: data curation. LH, PH and YW: analyzed the data. WZ, HW, LW and CG: contributed reagents/materials/analysis tools. YW and LH: writing—original draft preparation. LH: writing—review and editing. JD: funding acquisition. All authors have read and agreed to the published version of the manuscript.

FUNDING

This work was financially supported by Liaoning Department of Natural Resources Promotion of Marine Economic Development Project No.84[2021], High-level Talent Support Grant for Innovation in Dalian [2020RD03], and Liaoning Province Higher Education Innovation Team and Innovative Talent Support Program Project [LT2019003].

ACKNOWLEDGMENTS

We thank Margaret Biswas, PhD, from Liwen Bianji (Edanz) (www.liwenbianji.cn/) for editing the English text of a draft of this manuscript.

SUPPLEMENTARY MATERIAL

The Supplementary Material for this article can be found online at: https://www.frontiersin.org/articles/10.3389/fmars.2022.930156/full#supplementary-material

REFERENCES

Agarwal, V., Bell, G. W., Nam, J. W., and Bartel, D. P. (2015). Predicting Effective microRNA Target Sites in Mammalian mRNAs. *Elife* 4, e05005. doi: 10.7554/eLife.05005

Ahmed, I., and Khan, M. A. (2004). Dietary Lysine Requirement of Fingerling Indian Major Carp, *Cirrhinus Mrigala* (Hamilton). *Aquaculture* 235, 499–511. doi: 10.1016/j.aquaculture.2003.12.009

Bartel, D. P. (2009). MicroRNAs: Target Recognition and Regulatory Functions. *Cell* 136, 215–233. doi: 10.1016/j.cell.2009.01.002

Biggar, K. K., and Storey, K. B. (2018). Functional Impact of microRNA Regulation in Models of Extreme Stress Adaptation. *J. Mol. Cell Biol.* 10, 93–101. doi: 10.1093/jmcb/mjx053

Blencowe, B. J. (2006). Alternative Splicing: New Insights From Global Analyses. *Cell* 126, 37–47. doi: 10.1016/j.cell.2006.06.023

Branco, P. C., Borges, J. C., Santos, M. F., Jensch Junior, B. E., and Da Silva, J. R. (2013). The Impact of Rising Sea Temperature on Innate Immune Parameters in the Tropical Subtidal Sea Urchin *Lytechinus Variegatus* and the Intertidal Sea Urchin *Echinometra Lucunter*. *Mar. Environ. Res.* 92, 95–101. doi: 10.1016/j.marenvres.2013.09.005

Breitburg, D., Levin, L. A., Oschlies, A., Grégoire, M., Chavez, F. P., Conley, D. J., et al. (2018). Declining Oxygen in the Global Ocean and Coastal Waters. *Science* 359, eaam7240. doi: 10.1126/science.aam7240

Cao, Q., Xu, W., Chen, W., Peng, D., Liu, Q., Dong, J., et al. (2020). MicroRNA-184 Negatively Regulates Corneal Epithelial Wound Healing *via* Targeting CDC25A, CARM1, and LASP1. *Eye Vis. (Lond)* 7, 35. doi: 10.1186/s40662-020-00202-6

Chang, Y., Tian, X., Zhang, W., Han, F., Chen, S., Zhou, M., et al. (2016). Family Growth and Survival Response to Two Simulated Water Temperature Environments in the Sea Urchin *Strongylocentrotus Intermedius*. *Int. J. Mol. Sci.* 17, 1356. doi: 10.3390/ijms17091356

Chen, J. F., Mandel, E. M., Thomson, J. M., Wu, Q., Callis, T. E., Hammond, S. M., et al. (2006). The Role of microRNA-1 and microRNA-133 in Skeletal Muscle Proliferation and Differentiation. *Nat. Genet.* 38, 228–233. doi: 10.1038/ng1725

Dimauro, I., Grasso, L., Fittipaldi, S., Fantini, C., Mercatelli, N., Racca, S., et al. (2014). Platelet-Rich Plasma and Skeletal Muscle Healing: A Molecular Analysis of the Early Phases of the Regeneration Process in an Experimental Animal Model. *PLoS One* 9, e102993. doi: 10.1371/journal.pone.0102993

Ding, J., and Chang, Y. Q. (2020). Research Progress in Conservation and Utilization of Economic Echinoderm: A Review. *J. Dalian Ocean Univ.* 35, 645–656. (in Chinese)

Fabian, M. R., Sonenberg, N., and Filipowicz, W. (2010). Regulation of mRNA Translation and Stability by microRNAs. *Annu. Rev. Biochem.* 79, 351–379. doi: 10.1146/annurev-biochem-060308-103103

Fassan, M., Pizzi, M., Realdon, S., Balistreri, M., Guzzardo, V., Zagonel, V., et al. (2013). The HER2-Mir125a5p/Mir125b Loop in Gastric and Esophageal Carcinogenesis. *Hum. Pathol.* 44, 1804–1810. doi: 10.1016/j.humpath.2013.01.023

Foley, N. H., Bray, I. M., Tivnan, A., Bryan, K., Murphy, D. M., Buckley, P. G., et al. (2010). MicroRNA-184 Inhibits Neuroblastoma Cell Survival Through Targeting the Serine/Threonine Kinase AKT2. *Mol. Cancer* 9, 83. doi: 10.1186/1476-4598-9-83

Fontana, G. A., Rigamonti, A., Lenzken, S. C., Filosa, G., Alvarez, R., Calogero, R., et al. (2017). Oxidative Stress Controls the Choice of Alternative Last Exons *via* a Brahma-BRCA1-CstF Pathway. *Nucleic Acids Res.* 45, 902–914. doi: 10.1093/nar/gkw780

Forster, I., and Ogata, H. Y. (1998). Lysine Requirement of Juvenile Japanese Flounder *Paralichthys Olivaceus* and Juvenile Red Sea Bream *Pagrus Major*. *Aquaculture* 161, 131–142. doi: 10.1016/S0044-8486(97)00263-9

Fu, X. D. (2014). Non-Coding RNA: A New Frontier in Regulatory Biology. *Natl. Sci. Rev.* 1, 190–204. doi: 10.1093/nsr/nwu008

García-Echauri, L. L., Liggins, G., Cetina-Heredia, P., Roughan, M., Coleman, M. A., and Jeffs, A. (2020). Future Ocean Temperature Impacting the Survival Prospects of Post-Larval Spiny Lobsters. *Mar. Environ. Res.* 156, 104918. doi: 10.1016/j.marenvres.2020.104918

García Molinos, J. (2020). Global Marine Warming in a New Dimension. *Nat. Ecol. Evol.* 4, 16–17. doi: 10.1038/s41559-019-1037-5

Gibadulinova, A., Bullova, P., Strnad, H., Pohlodek, K., Jurkovicova, D., Takacova, M., et al. (2020). CAIX-Mediated Control of LIN28/let-7 Axis Contributes to Metabolic Adaptation of Breast Cancer Cells to Hypoxia. *Int. J. Mol. Sci.* 21, 4299. doi: 10.3390/ijms21124299

Gouda, H., and Agatsuma, Y. (2020). Effect of High Temperature on Gametogenesis of the Sea Urchin *Strongylocentrotus Intermedius* in the Sea of Japan, Northern Hokkaido, Japan. *J. Exp. Mar. Biol. Ecol.* 525, 151324. doi: 10.1016/j.jembe.2020.151324

Han, L., Quan, Z., Han, B., Ding, B., and Ding, J. (2021). Molecular Characterization and Expression of the SiUCP2 Gene in Sea Urchin *Strongylocentrotus Intermedius*. *J. Oceanol. Limnol.* 39, 1523–1537. doi: 10.1007/s00343-020-0181-8

Hao, P., Ding, B., Han, L., Xie, J., Wu, Y., Jin, X., et al. (2022). Gene Expression Patterns of Sea Urchins (*Strongylocentrotus Intermedius*) Exposed to Different Combinations of Temperature and Hypoxia. *Comp. Biochem. Physiol. Part D Genomics Proteomics* 41, 100953. doi: 10.1016/j.cbd.2021.100953

Hata, A., and Chen, Y. G. (2016). TGF-β Signaling From Receptors to Smads. *Cold Spring Harb. Perspect. Biol.* 8, a022061. doi: 10.1101/cshperspect.a022061

He, A. Y., Dean, J. M., and Lodhi, I. J. (2021a). Peroxisomes as Cellular Adaptors to Metabolic and Environmental Stress. *Trends Cell Biol.* 31, 656–670. doi: 10.1016/j.tcb.2021.02.005

He, Y., Huang, C. X., Chen, N., Wu, M., Huang, Y., Liu, H., et al. (2017). The Zebrafish miR-125c is Induced Under Hypoxic Stress *via* Hypoxia-Inducible Factor 1α and Functions in Cellular Adaptations and Embryogenesis. *Oncotarget* 8, 73846–73859. doi: 10.18632/oncotarget.17994

Hernes, E., Fosså, S. D., Berner, A., Otnes, B., and Nesland, J. M. (2004). Expression of the Epidermal Growth Factor Receptor Family in Prostate Carcinoma Before and During Androgen-Independence. *Br. J. Cancer* 90, 449–454. doi: 10.1038/sj.bjc.6601536

He, W., Zhang, N., and Lin, Z. (2021b). MicroRNA-125a-5p Modulates Macrophage Polarization by Targeting E26 Transformation-Specific Variant 6 Gene During Orthodontic Tooth Movement. *Arch. Oral. Biol.* 124, 105060. doi: 10.1016/j.archoralbio.2021.105060

Huo, D., Sun, L., Ru, X., Zhang, L., Lin, C., Liu, S., et al. (2018). Impact of Hypoxia Stress on the Physiological Responses of Sea Cucumber *Apostichopus Japonicus*: Respiration, Digestion, Immunity and Oxidative Damage. *PeerJ* 6, e4651. doi: 10.7717/peerj.4651

Huo, D., Sun, L., Sun, J., Zhang, L., Liu, S., Su, F., et al. (2021). Sea Cucumbers in a High Temperature and Low Dissolved Oxygen World: Roles of miRNAs in the Regulation of Environmental Stresses. *Environ. Pollut.* 268, 115509. doi: 10.1016/j.envpol.2020.115509

Jain, I. H., Calvo, S. E., Markhard, A. L., Skinner, O. S., To, T. L., Ast, T., et al. (2020). Genetic Screen for Cell Fitness in High or Low Oxygen Highlights Mitochondrial and Lipid Metabolism. *CELL* 181, 716–727. doi: 10.1016/j.cell.2020.03.029

Lai, K. P., Tam, N. Y. K., Chen, Y., Leung, C. T., Lin, X., Tsang, C. F., et al. (2022). miRNA–mRNA Integrative Analysis Reveals the Roles of miRNAs in Hypoxia-Altered Embryonic Development- and Sex Determination-Related Genes of Medaka Fish. *Front. Mar. Sci.* 8. doi: 10.3389/fmars.2021.736362

Lan, C., Chen, Q., and Li, J. (2016). Grouping miRNAs of Similar Functions *via* Weighted Information Content of Gene Ontology. *BMC Bioinf.* 17, 507. doi: 10.1186/s12859-016-1367-0

Lauss, M., Kriegner, A., Vierlinger, K., and Noehammer, C. (2007). Characterization of the Drugged Human Genome. *Pharmacogenomics* 8, 1063–1073. doi: 10.2217/14622416.8.8.1063

Leung, A. K., and Sharp, P. A. (2010). MicroRNA Functions in Stress Responses. *Mol. Cell* 40, 205–215. doi: 10.1016/j.molcel.2010.09.027

Li, C., Feng, W., Qiu, L., Xia, C., Su, X., Jin, C., et al. (2012). Characterization of Skin Ulceration Syndrome Associated microRNAs in Sea Cucumber *Apostichopus Japonicus* by Deep Sequencing. *Fish Shellfish Immunol.* 33, 436–441. doi: 10.1016/j.fsi.2012.04.013

Liu, X., Fu, B., Chen, D., Hong, Q., Cui, J., Li, J., et al. (2015). miR-184 and miR-150 Promote Renal Glomerular Mesangial Cell Aging by Targeting Rab1a and Rab31. *Exp. Cell Res.* 336, 192–203. doi: 10.1016/j.yexcr.2015.07.006

Liu, C., Teng, Z. Q., Santistevan, N. J., Szulwach, K. E., Guo, W., Jin, P., et al. (2010). Epigenetic Regulation of miR-184 by MBD1 Governs Neural Stem Cell Proliferation and Differentiation. *Cell Stem Cell* 6, 433–444. doi: 10.1016/j.stem.2010.02.017

Livak, K. J., and Schmittgen, T. D. (2001). Analysis of Relative Gene Expression Data Using Real-Time Quantitative PCR and the 2(-Delta Delta C(T)) Method. *Methods* 25, 402–408. doi: 10.1006/meth.2001.1262

Li, Z., Wang, J., He, Y., Hu, S., and Li, J. (2019). Comprehensive Identification and Profiling of Chinese Shrimp (*Fenneropenaeus Chinensis*) microRNAs in Response to High pH Stress Using Hiseq2000 Sequencing. *Aquac. Res.* 50, 14269. doi: 10.1111/are.14269

Ma, C., Zhang, C., Ma, M., Zhang, L., Zhang, L., Zhang, F., et al. (2017). MiR-125a Regulates Mitochondrial Homeostasis Through Targeting Mitofusin 1 to Control Hypoxic Pulmonary Vascular Remodeling. *J. Mol. Med. (Berl)* 95, 977–993. doi: 10.1007/s00109-017-1541-5

Miao, B.-B., Niu, S.-F., Wu, R.-X., Liang, Z.-B., and Zhai, Y. (2022). The MicroRNAs-Transcription Factors-mRNA Regulatory Network Plays an Important Role in Resistance to Cold Stress in the Pearl Gentian Grouper. *Front. Mar. Sci.* 8. doi: 10.3389/fmars.2021.824533

Natalia, M. A., Alejandro, G. T., Virginia, T. J., and Alvarez-Salas, L. M. (2018). MARK1 is a Novel Target for miR-125a-5p: Implications for Cell Migration in Cervical Tumor Cells. *Microrna* 7, 54–61. doi: 10.2174/2211536606666171024160244

Nesbit, K. T., Fleming, T., Batzel, G., Pouv, A., Rosenblatt, H. D., Pace, D. A., et al. (2019). The Painted Sea Urchin, *Lytechinus Pictus*, as a Genetically-Enabled Developmental Model. *Methods Cell Biol.* 150, 105–123. doi: 10.1016/bs.mcb.2018.11.010

Noman, A., Fahad, S., Aqeel, M., Ali, U., Amanullah,, Anwar, S., et al. (2017). miRNAs: Major Modulators for Crop Growth and Development Under Abiotic Stresses. *Biotechnol. Lett.* 39, 685–700. doi: 10.1007/s10529-017-2302-9

Park, J. K., Peng, H., Yang, W., Katsnelson, J., Volpert, O., and Lavker, R. M. (2017). miR-184 Exhibits Angiostatic Properties *via* Regulation of Akt and VEGF Signaling Pathways. *FASEB J.* 31, 256–265. doi: 10.1096/fj.201600746R

Pinsky, M. L., Eikeset, A. M., Mccauley, D. J., Payne, J. L., and Sunday, J. M. (2019). Greater Vulnerability to Warming of Marine Versus Terrestrial Ectotherms. *Nature* 569, 108–111. doi: 10.1038/s41586-019-1132-4

Riedel, B., Pados, T., Pretterebner, K., Schiemer, L., Steckbauer, A., Haselmair, A., et al. (2014). Effect of Hypoxia and Anoxia on Invertebrate Behaviour: Ecological Perspectives From Species to Community Level. *Biogeosciences* 11, 1491–1518. doi: 10.5194/bg-11-1491-2014

Shen, R. J., Jiang, X. Y., Pu, J. W., and Zou, S. M. (2010). HIF-1alpha and -2alpha Genes in a Hypoxia-Sensitive Teleost Species *Megalobrama Amblycephala*: cDNA Cloning, Expression and Different Responses to Hypoxia. *Comp. Biochem. Physiol. Part B Biochem. Mol. Biol.* 157, 273–280. doi: 10.1016/j.cbpb.2010.06.013

Shi, Q. (2016). Spatio-Temporal Mode for Inter-Annual Change of Dissolved Oxygen and Apparent Oxygen Utilization in Summer Bohai Sea. *J. Appl. Oceanogr.* 35, 243–255. (in Chinese)

Song, G., Zhao, L., Chai, F., Liu, F., Li, M., and Xie, H. X. (2020). Summertime Oxygen Depletion and Acidification in Bohai Sea, China. *Front. Mar. Sci.* 7. doi: 10.3389/fmars.2020.00252

Strøm, J. F., Thorstad, E. B., and Rikardsen, A. H. (2020). Thermal Habitat of Adult Atlantic Salmon Salmo Salar in a Warming Ocean. *J. Fish Biol.* 96, 327–336. doi: 10.1111/jfb.14187

Suh, S. S., Hwang, J., Park, M., Park, S. Y., Ryu, T. K., Lee, S., et al. (2014). Hypoxia-Modulated Gene Expression Profiling in Sea Urchin (*Strongylocentrotus Nudus*) Immune Cells. *Ecotoxicol. Environ. Saf.* 109, 63–69. doi: 10.1016/j.ecoenv.2014.08.011

Sun, Z., and Ettensohn, C. A. (2017). TGF-β Sensu Stricto Signaling Regulates Skeletal Morphogenesis in the Sea Urchin Embryo. *Dev. Biol.* 421, 149–160. doi: 10.1016/j.ydbio.2016.12.007

Sun, J., Liu, Q., Zhao, L., Cui, C., Wu, H., Liao, L., et al. (2019). Potential Regulation by miRNAs on Glucose Metabolism in Liver of Common Carp (*Cyprinus Carpio*) at Different Temperatures. *Comp. Biochem. Physiol. Part D Genomics Proteomics* 32, 100628. doi: 10.1016/j.cbd.2019.100628

Takahashi, Y., Chen, Q., Rajala, R. V. S., and Ma, J. X. (2015). MicroRNA-184 Modulates Canonical Wnt Signaling Through the Regulation of Frizzled-7 Expression in the Retina With Ischemia-Induced Neovascularization. *FEBS Lett.* 589, 1143–1149. doi: 10.1016/j.febslet.2015.03.010

Tanya, B., Troup, D., Wilhite, S. E., Pierre, L., Dmitry, R., Carlos, E., et al. (2007). NCBI GEO: Mining Tens of Millions of Expression Profiles—Database and Tools Update. *Nucleic Acids Res.* 35, 760–765. doi: 10.1093/nar/gkl887

Tian, Y., Li, G., Bu, X., Shen, J., Tao, Z., Chen, L., et al. (2019a). Changes in Morphology and miRNAs Expression in Small Intestines of Shaoxing Ducks in Response to High Temperature. *Mol. Biol. Rep.* 46, 3843–3856. doi: 10.1007/s11033-019-04827-2

Tian, Y., Shang, Y., Guo, R., Chang, Y., and Jiang, Y. (2019b). Salinity Stress-Induced Differentially Expressed miRNAs and Target Genes in Sea Cucumbers *Apostichopus Japonicus*. *Cell Stress Chaperones* 24, 719–733. doi: 10.1007/s12192-019-00996-y

Tomi, S., Stankovi, S., and Lucu, Č. (2011). Oxygen Consumption Rate and Na+/K+-ATPase Activity in Early Developmental Stages of the Sea Urchin *Paracentrotus Lividus Lam*. *Helgoland Mar. Res.* 65, 431–434. doi: 10.1007/s10152-011-0261-4

Tristán-Ramos, P., Rubio-Roldan, A., Peris, G., Sánchez, L., Amador-Cubero, S., Viollet, S., et al. (2020). The Tumor Suppressor microRNA Let-7 Inhibits Human LINE-1 Retrotransposition. *Nat. Commun.* 11, 5712. doi: 10.1038/s41467-020-19430-4

Tse, A. C. K., Rubio-Roldan, A., Li, J. W., Wang, S. Y., Chan, T. F., Lai, K. P., et al. (2016). Hypoxia alters testicular functions of marine medaka through microRNAs regulation. *Aquatic Toxicology* 180, 266–273. doi: 10.1016/j.aquatox.2016.10.007

Uchida, Y., Chiyomaru, T., Enokida, H., Kawakami, K., Tatarano, S., Kawahara, K., et al. (2013). MiR-133a Induces Apoptosis Through Direct Regulation of GSTP1 in Bladder Cancer Cell Lines. *Urol. Oncol.* 31, 115–123. doi: 10.1016/j.urolonc.2010.09.017

Vaquer-Sunyer, R., and Duarte, C. M. (2008). Thresholds of Hypoxia for Marine Biodiversity. *Proc. Natl. Acad. Sci. U.S.A.* 105, 15452–15457. doi: 10.1073/pnas.0803833105

Wang, H., Zhao, W., Liu, X., Gang, D., Zuo, R., Han, L., et al. (2022). Comparative Lipidome and Transcriptome Provide Novel Insight Into Polyunsaturated Fatty Acids Metabolism of the Sea Urchin. *Front. Mar. Sci.* 9. doi: 10.3389/fmars.2022.777341

Xu, X., Lai, Y., Zhou, W., and Hua, Z. (2019). Lentiviral Delivery of a shRNA Sequence Analogous to miR-4319/miR-125-5p Induces Apoptosis in NSCLC Cells by Arresting G2/M Phase. *J. Cell Biochem.* 120, 14017–14027. doi: 10.1002/jcb.28676

Xu, Y., Ramanathan, V., and Victor, D. G. (2018). Global Warming Will Happen Faster Than We Think. *Nature* 564, 30–32. doi: 10.1038/d41586-018-07586-5

Yi, F., Shang, Y. G., Li, B., Dai, S. L., Wu, W., Cheng, L., et al. (2017). MicroRNA-193-5p Modulates Angiogenesis Through IGF2 in Type 2 Diabetic Cardiomyopathy. *Biochem. Biophys. Res. Commun.* 491, 876–882. doi: 10.1016/j.bbrc.2017.07.108

Zgheib, C., Hodges, M. M., Hu, J., Liechty, K. W., and Xu, J. (2017). Long non-Coding RNA Lethe Regulates Hyperglycemia-Induced Reactive Oxygen Species Production in Macrophages. *PLoS One* 12, e0177453. doi: 10.1371/journal.pone.0177453

Zhang, Y., Forys, J. T., Miceli, A. P., Gwinn, A. S., and Weber, J. D. (2011). Identification of DHX33 as a Mediator of rRNA Synthesis and Cell Growth. *Mol. Cell. Biol.* 31, 4676–4691. doi: 10.1128/MCB.05832-11

Zhan, Y., Li, Y., Cui, D., Pei, Q., Sun, J., Zhang, W., et al. (2018). Identification and Characterization of microRNAs From the Tube Foot in the Sea Urchin *Strongylocentrotus Intermedius*. *Heliyon* 4, e00668. doi: 10.1016/j.heliyon.2018.e00668

Zheng, X., Wu, Z., Xu, K., Qiu, Y., Su, X., Zhang, Z., et al. (2019). Interfering Histone Deacetylase 4 Inhibits the Proliferation of Vascular Smooth Muscle Cells *via* Regulating MEG3/miR-125a-5p/IRF1. *Cell Adh. Migr.* 13, 41–49. doi: 10.1080/19336918.2018.1506653

Zhou, X., Chang, Y., Zhan, Y., Wang, X., and Lin, K. (2018). Integrative mRNA-miRNA Interaction Analysis Associate With Immune Response of Sea Cucumber *Apostichopus Japonicus* Based on Transcriptome Database. *Fish Shellfish Immunol.* 72, 69–76. doi: 10.1016/j.fsi.2017.10.031

Conflict of Interest: The authors declare that the research was conducted in the absence of any commercial or financial relationships that could be construed as a potential conflict of interest.

Publisher's Note: All claims expressed in this article are solely those of the authors and do not necessarily represent those of their affiliated organizations, or those of the publisher, the editors and the reviewers. Any product that may be evaluated in this article, or claim that may be made by its manufacturer, is not guaranteed or endorsed by the publisher.

frontiers | Frontiers in Marine Science

TYPE Correction
PUBLISHED 15 September 2022
DOI 10.3389/fmars.2022.1027240

OPEN ACCESS

EDITED AND REVIEWED BY
Bronwyn M. Gillanders,
University of Adelaide, Australia

*CORRESPONDENCE
Jun Ding
dingjun19731119@hotmail.com

SPECIALTY SECTION
This article was submitted to Marine Biology, a section of the journal Frontiers in Marine Science

RECEIVED 24 August 2022
ACCEPTED 05 September 2022
PUBLISHED 15 September 2022

CITATION
Han L, Wu Y, Hao P, Ding B, Li Y, Wang W, Zhang X, Gao C, Wang H, Wang L, Zhang W, Chang Y, Ding D and Ding J (2022) Corrigendum: Sea urchins in acute high temperature and low oxygen environments: The regulatory role of microRNAs in response to environmental stress. *Front. Mar. Sci.* 9:1027240. doi: 10.3389/fmars.2022.1027240

Corrigendum: Sea urchins in acute high temperature and low oxygen environments: The regulatory role of microRNAs in response to environmental stress

Lingshu Han[1], Yanglei Wu[2], Pengfei Hao[2], Beichen Ding[2], Yuanxin Li[2], Wenpei Wang[2], Xianglei Zhang[2], Chuang Gao[2], Heng Wang[2], Luo Wang[2], Weijie Zhang[2], Yaqing Chang[2], Dewen Ding[1] and Jun Ding[2]*

[1]School of Marine Sciences, Ningbo University, Ningbo, China, [2]Key Laboratory of Mariculture and Stock Enhancement in North China's Sea, Ministry of Agriculture and Rural Affairs, Dalian Ocean University, Dalian, China

KEYWORDS

***strongylocentrotus intermedius*, microRNA, global climate change, high temperature stress, hypoxia**

A Corrigendum on:

Sea urchins in acute high temperature and low oxygen environments: The regulatory role of microRNAs in response to environmental stress.

by Han L, Wu Y, Hao P, Ding B, Li Y, Wang W, Zhang X, Gao C, Wang H, Wang L, Zhang W, Chang Y, Ding D and Ding J (2022) Front. Mar. Sci. 9:930156. doi: 10.3389/fmars.2022.930156

In the published article, the reference "Xu C., Lu Y., Pan Z., Chu W., Luo X., Lin H., et al. (2007). The Muscle-Specific microRNAs miR-1 and miR-133 Produce Opposing Effects on Apoptosis by Targeting HSP60, HSP70 and Caspase-9 in Cardiomyocytes. *J. Cell Sci.* 120, 3045–3052. doi: 10.1242/jcs.010728" should be removed as this manuscript was retracted in 2011.

In the Discussion, Effects of Hypoxia on miRNA Regulation in *S. intermedius*, paragraph two, the sentence "Xu et al. reported that miR-133 and miR-1 target *HSP60*, *HSP70*, and caspase-9 (*CASP9*) in cardiomyocytes and have opposite effects on apoptosis (Xu et al., 2007)." should be removed.

The authors apologize for these errors and state that this does not change the scientific conclusions of the article in any way. The original article has been updated.

Publisher's note

frontiers | Frontiers in Marine Science

ORIGINAL RESEARCH
published: 11 July 2022
doi: 10.3389/fmars.2022.931430

Influence of Water Temperature and Flow Velocity on Locomotion Behavior in Tropical Commercially Important Sea Cucumber *Stichopus monotuberculatus*

Mengling Chen[1,2], *Shuo Sun*[1,2], *Qiang Xu*[1,2], *Fei Gao*[1,2]*, *Haiqing Wang*[1,2] *and Aimin Wang*[1,2]

[1] State Key Laboratory of Marine Resource Utilization in South China Sea, Hainan University, Haikou, China, [2] Ocean College, Hainan University, Haikou, China

OPEN ACCESS

Edited by:
Chenghua Li,
Ningbo University, China

Reviewed by:
Yingbin Wang,
Zhejiang Ocean University, China
Xiutang Yuan,
Chinese Academy of Sciences (CAS), China

***Correspondence:**
Fei Gao
gaofeicas@126.com

Specialty section:
This article was submitted to Marine Fisheries, Aquaculture and Living Resources, a section of the journal Frontiers in Marine Science

Received: 29 April 2022
Accepted: 09 June 2022
Published: 11 July 2022

Citation:
Chen M, Sun S, Xu Q, Gao F, Wang H and Wang A (2022) Influence of Water Temperature and Flow Velocity on Locomotion Behavior in Tropical Commercially Important Sea Cucumber Stichopus monotuberculatus. Front. Mar. Sci. 9:931430. doi: 10.3389/fmars.2022.931430

Sea cucumber *Stichopus monotuberculatus* is one species of tropical sea cucumbers with high recognition and economic value. While advances have been made in the nursery rearing of the sea cucumber, influence of environmental factors on its locomotion behavior remains less understood, which restricts the establishment of mariculture technologies. In the present study, locomotion behavior of *S. monotuberculatus* under different temperatures and flow velocities were examined through controlled simulation experiments. Results showed that the creeping activities were obviously affected by temperature, and the most active movement and feeding behavior were recorded at relatively high temperatures. Diurnal variation of locomotion and feeding activities indicated that *S. monotuberculatus* displayed an evident nocturnal activity pattern, being the most active at night, exhibiting intermediate activity at dusk, and minimal activity during the daytime. The movement velocity decreased with the increasing flow speed and was only 1.65 ± 1.35cm·min^{-1} in the highest flow rate group (20.8 ± 3.4cm/s). Moreover, the sea cucumber *S. monotuberculatus* displayed positive rheotaxis behavior of moving downstream at all flow velocities. Overall, the sea cucumber *S. monotuberculatus* exhibited high locomotor and feeding activities at night of relatively high temperature, and its favoured flow regime was downstream and low water velocity area. These findings may assist the sea ranching and aquaculture development of the tropical commercial sea cucumber species.

Keywords: ***Stichopus monotuberculatus*, water temperature, flow velocity, locomotion, feeding**

1. INTRODUCTION

Sea cucumbers (Holothurians) are considered to be one of the most conspicuous marine invertebrates species belonging to class Holothuroidea of phylum Echinodermata. While resource managers struggle to address pandemic overfishing of tropical sea cucumber stocks, mariculture and sea ranching of some tropical species ascends as a viable prospect to subsidise waning captures (Bell et al., 2005; Yang et al., 2015). Tropical sea cucumber mariculture has potential to become a

profitable industry and contribute towards natural population replenishment.

Movement of holothurians is mainly related to feeding, reproduction and searching for optimal environmental conditions (Uthicke, 1999; Navarro et al., 2013; Sun et al., 2018a; Hamel et al., 2019). Knowledge about the behavioral features of sea cucumbers under different environmental conditions is beneficial not just to understand the species' behavior in wild but also to improve the rearing techniques for sea cucumbers. Sea cucumbers are mostly slow-moving or sedentary, and the feature makes their distribution and behavior susceptible to environmental drivers (Hair et al., 2020; Sun et al., 2020), such as substrate type (Woodby et al., 2000), salinity (Kashenko, 2002), light cycles (Dong et al., 2011) and so on. Temperature, as an essential environmental factor, can directly affect the locomotion (Sun et al., 2018b), circadian rhythm (Kato and Hirata, 1990), burying and feeding (Wolkenhauer, 2008; Purcell, 2010) behavior of sea cucumbers. Also, water flow is an important ecological factor for aquatic organisms, and researches on the effect of water flow on aquatic organisms mainly focuses on fishes (Pavlov et al., 2000; Liao and Cotel, 2013; Li et al., 2018). Water current can affect the movement, orientation, feeding, and growth of shellfish (Wildish and Kristmanson, 1988; Wildish and Saulnier, 1992; Pilditch, 1999; Sakurai and Seto, 2000). Movement pattern and feeding behavior in response to variable water currents have been observed in echinoderms, including sea urchin (Dumont et al., 2007), sea lily (Kitazawa and Oji, 2014), and numerous species of sea cucumbers. According to Lin (2014), *A japonicus* moved more distance at the slow flow (5 cm/s) than in the still water, but almost stationary in the riptide (30 cm/s); Qiu et al. (2014) considered that water current is a key factor that influences substrate selection by *A. japonicus*. In addition, water flow can elicit displacement and feeding behavior changes in suspension-feeding sea cucumber *Cucumaria frondosa* (Sun et al., 2018a).

Sea cucumber *Stichopus monotuberculatus* (previously named as *Stichopus variegatus*, Fan et al., 2012) is a tropical species that colonize benthic habitats in the Indian Ocean from the Red Sea and Madagascar to Easter Island, and in the Pacific Ocean from Japan to Australia (Massin, 1996; Purcell et al., 2012b). As a large edible sea cucumber with thick body wall and well mouthfeel, it is one of the species with high recognition and economic value among tropical economic sea cucumbers (Conand, 1993; Liao, 1997). Due to its nutritional and medicinal value, previous researches mainly focused on the nutritional components and biologically active components which have anticoagulant, lipid-lowering, anti-tumor, and other physiological pharmacological activities (Wang et al., 2010; Zhong et al., 2015; Huang et al., 2020). In recent years, the biological function of a series of immune related proteins such as ferritin, translationally controlled tumor protein, serine protease inhibitors, gamma-interferon-inducible lysosomal thiol reductase and poly-U-binding factor 60 kDa were characterized in sea cucumber *S. monotuberculatus* (Ren et al., 2014a; Ren et al., 2014b; Ren et al., 2015a; Ren et al., 2015b; Yan et al., 2016). Genetic structure of different populations of *S. montuberculatus* in the South China Sea were characterized (Yuan et al., 2013; Wen et al., 2018).As one widely accepted species in international bêche-de-mer markets, the artificial breeding of *S. monotuberculatus* has been successfully broken through in China (Hu et al., 2010; Wang et al., 2017; Cheng et al., 2021). Technology for culturing a few of the tropical species has advanced in recent years, but a number of diverse impediments currently undermine profitability and reliability of mariculture and present challenging research opportunities (Purcell et al., 2012a). However, the effect of important environmental factors, including water temperature and water flow, on the locomotor behaviors of *S. monotuberculatus* has received less attention.

Water temperature and flows represent the critical aspects of the environment affecting sea cucumbers. They are inextricably linked to the distribution (Pan et al, 2015), locomotion behavior, ingestion rate, and diel rhythm of sea cucumber (Sun et al., 2018b), which were closely related to the area selection of sea ranching and the setting of suitable breeding conditions. For example, an inappropriately high flow rate would lead to feed waste, and sea cucumbers had to consume more energy to increase the adsorption force of the tube feet in order to maintain body stability. Well-designed experiments and analyses are needed to fill critical knowledge gaps if its mariculture is to expand in the tropics as the temperate sea cucumber *A. japonicus* has presented in Asia. The current study was carried out under controlled laboratory conditions to ensure that the effects of temperature or flow velocity were separate from other environmental factors. We used video technology and behavior analysis software to investigate the behavior of *S. monotuberculatus* under different water temperatures or flow velocity. Quantitative indices were applied to analyze the experimental data. We examined locomotion behavior, diel feeding activity of *S. monotuberculatus* under different temperatures, and behavior responses of *S. monotuberculatus* to flow velocity variation. Such research may be helpful for understanding the distribution as well as the feeding and locomotor behaviors of *S. monotuberculatus* in response to various stimuli. We hope our study can provide a reference for stock management in identifying the most suitable sea ranching areas and assist in the eventual development of aquaculture programs.

2. MATERIALS AND METHODS

2.1 Specimen Collection and Maintenance

Sea cucumbers were collected from Dingda Breeding limited company, in Wenchang city of Hainan Province, China, and transported to the State Key Laboratory of Marine Resource Utilization in South China Sea. All individuals were acclimated in tanks (1000 L) at 26.0 ± 1.0°C, salinity 32-35, a Ph of 8.0-8.3. During the acclimation period, the light condition is natural without artificial light sources, and the sea cucumbers were fed using an artificial feed (sea mud: Sargasso algal powder =7:3, weight ratio) once at 09:00 h each day. Healthy

and undamaged sea cucumbers (about 10g) were selected for the experiments.

2.2 Experimental Design

2.2.1 Effect of Temperature

Four temperatures (22, 25, 28, and 31°C) were selected, approximately representing the overall temperature range (20-33° C) found in the natural habitat of *S. monotuberculatus*, to study their effects on the sea cucumber's behavior. After acclimation, a group of five sea cucumbers were introduced into each of the four opaque experimental tanks (100×100×150cm, height × width × depth). The water temperature was then adjusted to the desired temperature at a rate of 1°C day^{-1}, and the sea cucumbers were maintained at the experimental temperatures for 7 days. The water depth was maintained at 30 cm during the experiment. Each trial was run for 5 days in the experimental condition. The animals were fed once per day, and half of the water was exchanged at 09: 00 h. Charge-coupled device cameras (Hikvision, DS-2CC11A2P-IR3, China) with the infrared system and a video recorder were used to record the behaviors of sea cucumbers. Video images were analyzed using Tracker Video Analysis and Modeling Tool software (Open Source Physics Project, https://physlets.org/tracker/, Vasquez et al., 2018; Vasquez et al., 2020). The experimental indexes include movement distance, cumulative motion time and movement velocity of the sea cucumber. Moving distance means the distance the sea cucumber traveled in the experimental area. Cumulative motion time refers to the total time of sea cucumber moved during the day or night. Movement velocity means the average velocity of the sea cucumber crept in each day.

Feeding behavior was determined by the sea cucumber's position (if or not near the food), behavior (Sea cucumbers move their heads from side to side in order to scratch for food by their tentacles, rather than moving straight with their heads close to the ground) and the variation of feed on the aquarium bottom (Sun et al., 2018b). The proportion of feeding sea cucumbers were determined every 2 h based on the videos. The observation of locomotion is based on the analysis of the distance of sea cucumber every three minutes.

In the present study, 06:00 h to 18:00 h was defined as 'day', and 18:00 h to 06:00 h was defined as 'night'. The sea cucumbers were fed on the same diet as during the acclimation period for all studies.

2.2.2 Effect of Water Flow

The experiment was conducted in an annulus tank (1.2 m × 0.45 m) with a 0.2m wide region for water flow (**Figure 1**). A water pump was used to circulate water through the tank, and a frequency converter connected to the water pump was used to adjust water velocity. Water velocity was measured using a current meter (LS1206B, Xiangruide Inc., China).

The locomotion of *S. monotuberculatus* was investigated at four flow rates, 0 cm/s (S), 4.7 ± 1.2 cm/s (L), 10.5 ± 1.7 cm/s (M), and 20.8 ± 3.4 cm/s (H). Ten replicate trials were run for each of the four treatments, and each trial was conducted by different sea cucumber individuals. In each experiment, one sea cucumber was placed in the center of a rectangular arena (20 cm × 20 cm) in the straight section of the tank, so the arena was divided into two zones, the upstream area and the downstream area (**Figure 1**). Each trial was run until the experimented sea cucumber moved out of the arena or the time for the trial reached 0.5 h.

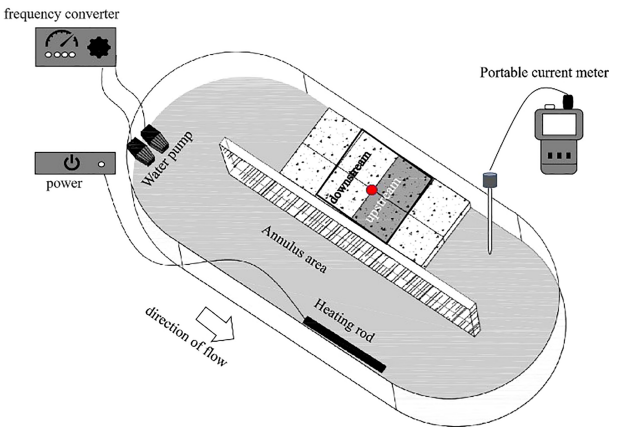

FIGURE 1 | The tank used in the water flow experiment. The red dot is the starting point of the sea cucumbers.

Charge-coupled device cameras (Hikvision, DS-2CC11A2P-IR3, China) were used to record the activities of *S. monotuberculatus* at 10s intervals. Video images were analyzed using Tracker software to record the tracks of *S. monotuberculatus* at four flow rates. The experimental indexes include movement distance, movement velocity, and cumulative residence time of the sea cucumber. The calculation of movement distance and movement velocity is the same with the index in part 2.2.1. Cumulative residence time means the time spent between the start of the experiment and the time the sea cucumber left the experimental area.

2.3 Statistical Analysis

All statistical analysis was performed with the SPSS 19.0 for Windows statistical package. One-way ANOVA followed by *post hoc* multiple comparisons with Tukey's test was performed to test the distance, time, and speed over environmental factors. The differences between day and night of the distance, time, and speed of sea cucumbers were compared using an independent sample t-test. The probability level of 0.05 was used to reject of the null hypothesis, and all data were presented as means ± s. d.

3. RESULTS

3.1 Effects of Temperature on Locomotion Behavior

3.1.1 Movement Distance

The movement distance of *S. monotuberculatus* was significantly affected by water temperature (ANOVA, F=15.39; $P<0.001$). At

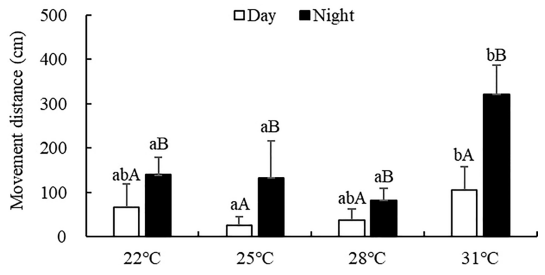

FIGURE 2 | Movement distance of *S. monotuberculatus* at four temperature conditions. Marks of lowercase letters indicate that there is a significant difference at different temperatures ($P < 0.05$); marks of uppercase letters indicate that there is a significant difference between day and night ($P < 0.05$).

every temperature tested, the movement distance at night (82.58-321.12 cm) was significantly higher than that in the daytime (25.47-105.17 cm) (**Figure 2**, $P<0.05$). The movement distance during the day decreased as the temperature increased from 22°C to 25°C, then increased from 25°C and reached a peak at 31°C. At night, the movement distance decreased as the temperature increased from 22°C to 28°C, then increased above 28°C. No significant difference was observed in the movement distance at night at water temperatures of 22, 25, or 28°C. However, at 31°C, the movement distance at night was significantly higher than in other treatment groups ($P<0.05$).

3.1.2 Cumulative Motion Time

The cumulative motion time of *S. monotuberculatus* was significantly affected by water temperature (ANOVA, F=12.87, $P<0.001$). At every temperature tested, the cumulative motion time was significantly higher at night (69.96-195.00 min) than that in the daytime (18.12-73.32 min) ($P<0.05$; **Figure 3**). During the day, *S. monotuberculatus* decreased its cumulative motion time as the temperature changed from 22 to 25°C, then increased above 25°C. The maximum movement distance in the day was observed at 31°C, which was significantly higher than the other groups ($P<0.05$). No significant differences in the cumulative motion time during the day were observed between 22, 25, and 28°C treatments ($P>0.05$). At night, the cumulative motion time decreased as the temperature increased from 22°C to 28°C, then increased above 28°C. At 31°C, the cumulative motion time at night was significantly higher with respect to other treatment groups ($P<0.05$ for all).

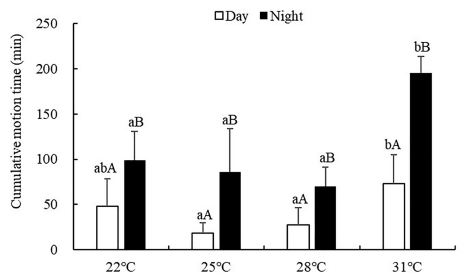

FIGURE 3 | Cumulative motion time of *S. monotuberculatus* at four temperature conditions. Marks of lowercase letters indicate that there is a significant difference at different temperatures ($P<0.05$); marks of uppercase letters indicate that there is a significant difference between day and night ($P<0.05$).

3.1.3 Movement Velocity

Movement velocity of *S. monotuberculatus* was 0.85-1.91 cm/min during the experiment period. The movement velocity was also significantly affected by water temperature (ANOVA, F=4.89, $P=0.01$) (**Figure 4**). Significant differences were observed between day and night at 25 and 31°C temperature treatments ($P<0.05$). During the day, no significant difference was observed among all treatment groups ($P>0.05$). However, at night, the movement velocity at 31°C treatment was significantly higher than the other treatments ($P<0.05$).

3.1.4 Diel Motor Rhythm

All temperature treatments displayed a similar locomotion pattern, sea cucumbers traveled more at night than during the day (**Figure 5**). The motion peak appeared from 20:00 to 06:00 of the next day, while the through period was from 12:00 to 18:00. While comparing between different temperature treat groups, the sea cucumbers at 31°C showed higher locomotion activity, especially at night, with the movement distances at 31°C were significantly higher than all the other groups from 20:00 to 04:00 ($P<0.05$).

3.2 Effects of Temperature on Diel Feeding Rhythm

Sea cucumbers showed a nocturnal feeding rhythm (**Figure 6**). The proportion of feeding sea cucumber did not change significantly within one day, but had a higher feeding proportion at night than during the day. The feeding proportion in the daytime was generally lower, then had an obvious rising trend after 18:00 under all temperature treatments, occurred peaks at 18:00 to 20:00 and 0:00 to 04:00. The feeding peak appeared at 00:00-02:00 at 31°C with an ingestion ratio of 60.00± 14.00%, and the lowest ingestion ratio appeared at 08:00-10:00 at 25°C (4.00 ± 2.20%). At 22°C and 28°C, sea cucumbers have a similar feeding rhythm. The 22°C and 25°C treatments showed a feeding peak at 18:00 to 20:00, whereas other treatments occurred during 0:00 to 02:00.

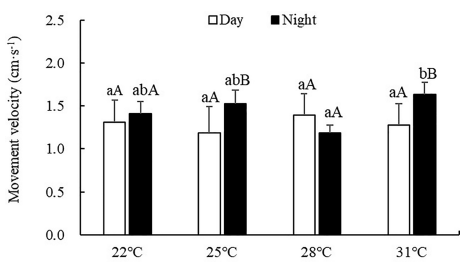

FIGURE 4 | Movement velocity of *S. monotuberculatus* at four temperature conditions. Marks of lowercase letters indicate that there is a significant difference at different temperatures ($P < 0.05$); marks of uppercase letters indicate that there is a significant difference between day and night ($P< 0.05$).

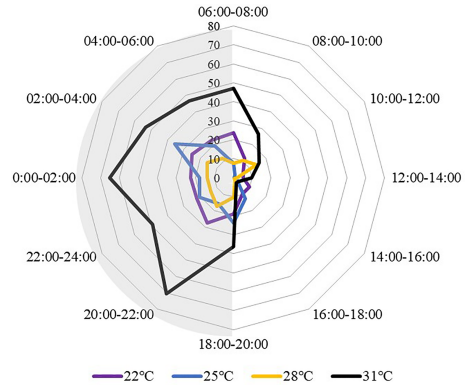

FIGURE 5 | Movement distance of *S. monotuberculatus* changed with time at four temperature conditions. Grey areas correspond to periods of night.

3.3 Effects of Flow on Locomotion Behavior

3.3.1 Movement Velocity

The flow rate had a significant influence on the movement velocity of sea cucumbers (F=9.486; $P<0.001$). The movement velocity of *S. monotuberculatus* was 4.33 ± 2.29 cm/min, 5.46 ± 3.41 cm/min, 4.17 ± 1.87 cm/min, and 1.63 ± 1.35 cm/min for the still, low, medium, and high flow rate respectively, which showed a trend of increasing first and then decreasing with the further increasing flow velocity. The sea cucumber's movement velocity was significantly lower at high flow rates (20.8 ± 3.4 cm/s) compared with that at the other three flow rates ($P<0.05$) (**Figure 7**).

3.3.2 Cumulative Residence Time

The flow rate had a significant influence on the cumulative residence time of sea cucumbers (F=45.186, $P<0.001$). The cumulative residence time of *S. monotuberculatus* was 4.88 ± 1.71 min, 7.58 ± 3.87 min, 10.28 ± 4.24 min and 26.6 ± 7.01 min

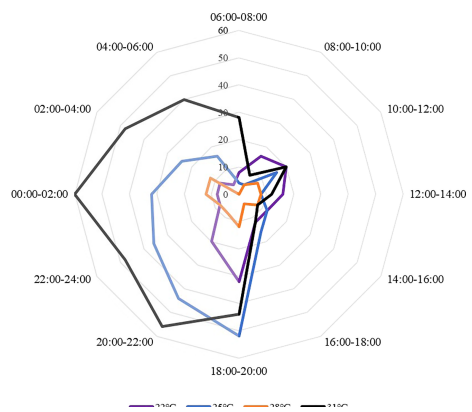

FIGURE 6 | The feeding proportions of *S. monotuberculatus* changed with time at four temperature conditions.

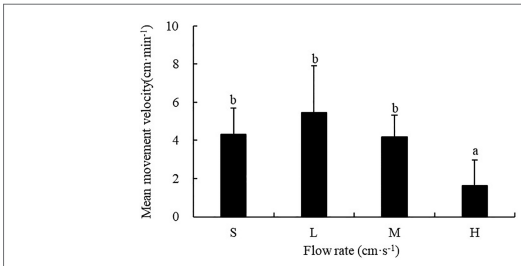

FIGURE 7 | Movement velocity of *S. monotuberculatus* at four different flow rates. S, L, M, and H represent the four flow rates: 0 cm/s, 4.7 ± 1.2 cm/s, 10.5 ± 1.7 cm/s, and 20.8 ± 3.4 cm/s respectively.

for the still, low, medium, and high flow rate respectively, which showed a sustained rising tendency with the augment of flow rate. The cumulative residence time at high flow rates of 20.8 ± 3.4cm/s was significantly higher than those at the other three flow rates ($P<0.05$) (**Figure 8**).

3.3.3 Cumulative Residence Time in the Downstream and Upstream Area

At every flow rate tested, the cumulative residence time of *S. monotuberculatus* was longer in the downstream area compared with the upstream area (**Figure 9**). At the low and fastest flow rate, 4.7 ± 1.2 cm/s and 20.8 ± 3.4 cm/s, the cumulative residence time in the downstream area was significantly longer than in the downstream area ($P<0.05$) (**Figure 3**). At the other two flow rates, there were no significant differences in cumulative residence time between the two zones ($P>0.05$) (**Figure 9**).

3.3.4 Movement Velocity in the Downstream and Upstream Area

Except for the low flow rate (4.7 ± 1.2 cm/s), at all other flow rates tested, the movement velocity of *S. monotuberculatus* was higher in the downstream area than in the upstream area (**Figure 10**). However, at every flow rate tested, there was no significant difference in the movement velocity of sea cucumber in the two zones ($P>0.05$).

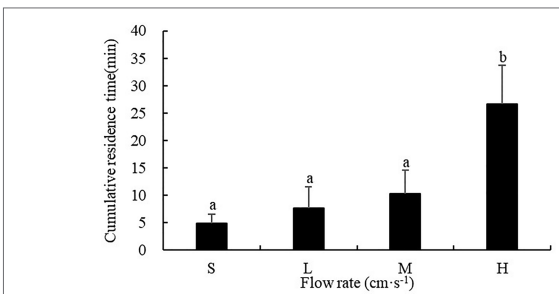

FIGURE 8 | Cumulative residence time of *S. monotuberculatus* at four different flow rates. S, L, M, and H represent the four flow rates: 0 cm/s, 4.7 ± 1.2 cm/s, 10.5 ± 1.7 cm/s, and 20.8 ± 3.4 cm/s respectively.

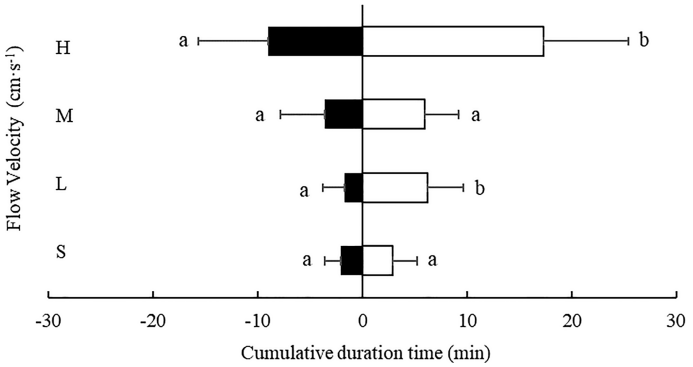

FIGURE 9 | Cumulative residence time of *S. monotuberculatus* at four water velocities in the downstream (white) and upstream zones (black) at four different flow. S, L, M, and H represent the four flow rates: 0 cm/s, 4.7 ± 1.2 cm/s, 10.5 ± 1.7 cm/s, and 20.8 ± 3.4 cm/s respectively.

4. DISCUSSION

The factors that influence aquatic animal distribution and behaviors have been studied in many respects to understand better habitat requirements, community dynamics, and species-specific aquaculture prerequisites (Lovatelli et al., 2004; Sun et al., 2018a). Researches on the locomotion behavior of sea cucumbers can be traced back to 1990, and an automatic apparatus was designed to quantitatively study the movement of sea cucumbers *Stichopus japonicus* (Kato and Hirata, 1990). In recent years, sea cucumber behavior studies mainly focus on the effects of substrate or artificial reefs on distribution (Zhang et al., 2014; Sun et al., 2020), the influence of light and phytoplankton on the behavior rhythm and feeding (Zhang et al., 2006; Dong et al., 2010; Dong et al., 2011; Sun et al., 2015; Sun et al., 2020), and the effects of water temperature and flow velocity on the feeding and locomotion behavior (Pan et al., 2015; Sun et al., 2018a; Sun et al., 2018b). The objects of previous researches mostly involved temperate deposit-feeding sea cucumber *A. japonicus* and suspension-feeding species *C. frondosa*. In the present study, the influences of environmental factors, including temperature and water flow, on the behavior of the tropical deposit-feeding sea cucumber *S. monotuberculatus* were studied under controlled laboratory conditions.

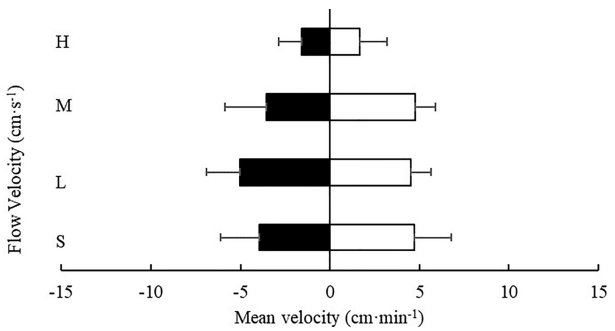

FIGURE 10 | Movement velocity of *S. monotuberculatus* at four water velocities in the downstream (white) and upstream zones (black) at four different flows. S, L, M, and H represent the four flow rates: 0 cm/s, 4.7 ± 1.2 cm/s, 10.5 ± 1.7 cm/s, and 20.8 ± 3.4 cm/s respectively.

4.1 Effects of Temperature on Behavior

Water temperature is a crucial factor in the living condition of aquatic organisms (Buentello et al., 2000). It is closely linked to the growth (Dong and Dong, 2006; Dong et al., 2006; Ji et al., 2008), metabolism (Dong et al., 2006; Wang et al., 2008; Gao et al., 2009), and behavior of sea cucumbers (Wolkenhauer, 2008; Sun et al., 2018b). *A. japonicus* is one species of most studied temperate holothurian. Under low temperatures in winter or high temperatures in summer, *A. japonicus* reduces movement, metabolism, and feeding activities, entering hibernation when temperatures are lower than 3°C, commencing estivation at high temperature >20°C (Bao et al., 2010). The creeping activity of the sea cucumber *A. japonicus* decreased with increasing temperature from peak 52.3 m day^{-1} at 16°C to 21.6 m day^{-1} at 18°C (Kato and Hirata, 1990), and its highest feeding proportion was also at 16°C (Sun et al., 2018b). Studies of tropical sea cucumber species have also shown the effect of temperature on their behavior. The buried periods of sea cucumber *H. scabra* increased with decreasing temperature from 6.7 h per day at 24°C to 14.5 h per day at 17°C, and feeding activity decreased from 9.8 h a day at 24°C to 0.8 h per day at 17°C (Wolkenhauer, 2008). Mercier et al. (2000) found that most adult *H. scabra* did not follow their usual burying cycle when the water temperature increased to more than 30°C.

The present results showed that the creeping activities of *S. monotuberculatus* were also obviously affected by temperature. However, it was different from *A. japonicus* and *H. scabra*, and the highest movement distance and the cumulative motion time were recorded at the temperature of 31°C. The evolution of regional behavior may explain the differences in locomotion behavior among different species in response to temperature changes. Previous studies supported this point by Buccheri et al. (2019), which considered that different tropical sea cucumber species responded differently to temperature fluctuations, even though the testing sea cucumber species were collected from the same sea area. For instance, they found *Holothuria atra* had faster righting times at warmer temperatures (29°C and 33°C) than

at 23°C, but *Stichopus chloronotus* had optimal righting times at 29°C and slower and more varied righting times at cooler and warmer temperatures (23°C and 33°C), while *Holothuria edulis* had righting times that were seemingly unaffected by the temperature changes. *S. monotuberculatus* is a tropical sea cucumber widely distributed from 1m to 30m depth in the coral reefs through the Indo-Pacific Ocean (Massin, 1996; Purcell et al., 2012b). In China, *S. monotuberculatus* has been recorded in the coastal shallow of the Xisha Islands, Hainan Island and the Leizhou Peninsula in the South China Sea (Liao, 1997). In Leizhou Peninsula sea area, *S. monotuberculatus* could survive in a temperature range of 14-32°C (Liang, 1987). Our results imply that this species of sea cucumber has the ability to live and feed at high water temperatures in the habitat. Additionally, one of the primary reasons for the movement of sea cucumbers is seeking for diets (Uthicke, 1999; Mercier et al., 1999), and high environmental temperatures resulted in an increased energetic cost and oxygen consumption (Dong and Dong, 2006; Dong et al., 2006). The sea cucumbers might augment movements to search for enough food meeting metabolic needs.

Recent studies of other large tropical holothuroids, *Stichopus herrmanni*, *B. argus* and *T. ananas*, showed that they moved 9-15, 2-8 and 5-9 m d^{-1}, respectively (Purcell et al., 2016; Wolfe and Byrne, 2017). These species exhibited site fidelity and long-term home ranging behaviour (Purcell et al., 2016; Wolfe and Byrne, 2017). The present results showed the movement distance of *S. monotuberculatus* was 1.19-4.26 m·d^{-1} in different temperature conditions. Thus, *S. monotuberculatus* may also display home range affinity. This behavior character highlights their vulnerability to overharvesting, with the potential risk of suffering significant declines, local extinctions and poor recovery (Uthicke et al., 2004). This finding has important implications for fisheries management regarding connectivity between recruitment and nearby adult habitats within the same area (Gillanders et al., 2003). In addition, artificial fishing reefs can be cast according to the movement distance of sea cucumbers or evoke reserve.

4.2 Diel Cycles

Many species of holothurians exhibited daily activity rhythms, with some ones having diurnal activity pattern (e.g., *Pearsonothuria graeffei*, Wheeling et al., 2007; *Holothuria whitmaei*, Shiell, 2006), some having nocturnal activity pattern (e.g., *H. edulis*, Wheeling et al., 2007; *A. japonicus*, Dong et al., 2011; *H. scabra*, Mercier et al., 1999; Mercier et al., 2000), or crepuscular activity pattern (e.g., *Actinopyga mauritiana*, Graham and Battaglene, 2004). In all the temperature treatments of the current study, the locomotion and feeding behavior of *S. monotuberculatus* displayed an evident diel cycle, being the most active at night, exhibiting intermediate activity at dusk, and minimal or no activity during the daytime, which showed a nocturnal activity pattern. Purcell et al. (2012b) also reported similar results that *S. monotuberculatus* hides during the day in crevices and under rubble, emerging at night on the reef flat, lagoons and reef slope. Nocturnal activity is thought to be a behavioral strategy that sea cucumbers evolved to increase their chances of survival in the nature, avoiding diurnal predation (Sun et al., 2018b). While water temperature significantly affected the movement activity of *S. monotuberculatus*, it did not alter diel locomotion rhythm. The observation of creeping activity at different temperatures showed that *S. monotuberculatus* exhibited a higher motor activity from 20:00 h to 04:00 h, and the minimum movement activity occurred at 12:00-18:00. Meanwhile, at all test temperatures, nocturnal feeding behavior of *S. monotuberculatus* was also evident. This suggests that the major factor influencing the diel locomotion rhythm of *S. monotuberculatus*, might be stress (Purcell et al., 2006), spring tides (Skewes et al., 2000), or predation (Dance et al., 2003), instead of temperature. Conversely, the high temperature (>24°C) may alter the diel locomotion rhythm of *A. japonicus* and became relatively inactive (Sun et al., 2018b); adult *H. scabra* did not follow their usual burying cycle when the water temperature was more than 30°C (Mercier et al., 2000). Future research would be required to aim specifically to exclude other variables to find a key factor be related to diel locomotion rhythm.

4.3 Effects of Flow on Behavior

As one of the most important environmental drivers, water flow can dramatically influence the locomotor behavior of marine organisms. Aquatic animals can adjust their activities with various strategies to adapt to the water flow. Like many other aquatic biotas, sea cucumbers also have distinct reactions to water flow. Qiu et al. (2014) found that water current is a key factor influencing sea cucumber distribution on the bare mud substrate, with 90% of juvenile sea cucumbers being unable to keep still in a current speed of 0.115 m·s^{-1} for 10 min. For suspension-feeding sea cucumber *C. frondosa* depending upon currents to bring food particles, the flow regime favoured by *C. frondosa* was proved to be between 21 and 40 cm s^{-1}, under which a balance aquired between energy expenditure for attachment to the bottom and efficient food capture, but individuals passively rolled at flows >40 cm s^{-1} (Sun et al., 2018a). The present study demonstrated that *S. monotuberculatus* had the lowest velocity and the highest residence time at the highest flow rate (20.8 ± 3.4 cm/s). Sea cucumber *A. japonicus* also showed the lowest movement velocity while the experimental flow rate was the highest (29.3 ± 3.7 cm s^{-1}, Pan et al., 2015). Pan et al. (2015) divided the holothurian's movement into three steps, 1) grasping and adhesion to the substrate at the present position, 2) the tube feet are lifted from the substrate and migrate to a new position and 3) grasping and adhesion to the substrate at a new position. If the water flow rate was too high, more energy and time would be needed to grasp the substrate at the present position, which might result in especially less or slower movements.

Water motion could influence the distribution and locomotion of benthic echinoderms (Fankboner, 1978; McKenzie, 1991; Liao, 1997; Zhao, 1998). Sea urchin *Echinometra oblonga* dominates where water flow is vigorous and *Echinometra mathaei* dominates in calmer water (Russo, 1977). Dense individuals of the dendrochirotid *Aslia lefevrei* were commonly found in areas of moderately strong water movement (Costelloe and Keegan, 1984). Pan et al. (2015) observed that the sea cucumber

A. japonicus did not show positive rheotaxis, but did move downstream at the fast current rates. In the present study, the sea cucumber *Stichopus monotuberculatus* displayed positive rheotaxis behavior of moving downstream at all flow velocities. The most obvious rheotaxis was observed at the highest water flow rates (20.8 ± 3.4cm·s^{-1}). Rheotaxis is a directed behavioral response to flow direction and velocity involving locomotion or muscular turning of body parts. This behavior change is intended to ensure that the body remains relatively stable during the feeding process, allowing for efficient filter-feeding (Kitazawa and Oji, 2014), and can save energy used to move against the flow. Sea cucumbers respire mainly by taking up oxygen across the general body surface and drawing and expelling water through the cloaca, in and out of the respiratory tree (Woodby et al., 2000). Perhaps, the authors suggest, rheotaxis can reduce the pressure of water flow on respiratory tree during relaxation. For the sea star *Asterias vulgaris*, macroscale flow is an essential condition for locating distant prey, and they oriented themselves upstream and 70% succeeded in finding the prey in a flume existed current and prey odors (Morissette and Himmelman, 2000). The sea urchins *Echinometra oblonga* and *E. mathaei* generally moved along the water flow, rarely in a perpendicular direction, because the tube feet are too weak to stretch across the flow (Russo, 1977). The sea cucumber *S. monotuberculatus* moved both across the flow, like the sea stars, and along the flow axis, like the sea urchins. This finding is in line with the previous study, which showed that *A. japonicus* could display a search pattern in their motor behavior, moving diagonally across the direction of flow, and curve the body, turning in a new direction across flow (Pan et al., 2015).

Overall, the sea cucumber *S. monotuberculatus* exhibited high locomotor and feeding activities at night of relatively high temperature, and its favored flow regime was downstream and low water velocity area. According to the present results, this species is suitable for being cultured in still or running water with a relatively low flow rate, and adequate feed should be supplied at night. The motion and feeding of *S. monotuberculatus* peaked at 31°C, yet the optimum growth temperature might not be determined as the lack of energy budget and growth rate data. While sea ranching, a reasonable releasing time and site is helpful to improve the survival rate, and juvenile *S. monotuberculatus* is recommended to be released in the high-temperature season and the slow flow region. Or, artificial reefs can be deployed to adjust water flow in sea areas with complex currents.

5. CONCLUSION

The behavioral reaction of tropical commercial sea cucumber *S. monotuberculatus* to different temperature and water flow were investigated using quantitative indices. *S. monotuberculatus* exhibited a comparatively higher locomotion and feeding activity at high test environmental temperature, and this is a converse behavioral feature with temperate sea cucumber, such as the most studied *A. japonicus*. Also, *S. monotuberculatus* showed a distinct nocturnal pattern at all temperature treatments, which may be a behavioral strategy, sea cucumbers have evolved in long history, in order to avoid diurnal predators. The movement velocity decreased with increasing flow current, which led to the increased staying time in the study area. Moreover, *S. monotuberculatus* displayed an "escape" behavior response to water flow, with higher levels of motor activity at all flow speeds tested than that in the experiment on the effect of temperature, while suspension-feeding sea cucumbers had their own favoured flow regime. Knowledge of the motor behavior habits of *S. monotuberculatus* at different water temperatures or flow rates would be conducive to optimize aquaculture environments and techniques of tropical commercial holothurian species.

DATA AVAILABILITY STATEMENT

The original contributions presented in the study are included in the article/**Supplementary Material**. Further inquiries can be directed to the corresponding authors.

AUTHOR CONTRIBUTIONS

FG, QX, and SS: conceptualization. FG, QX, and SS: methodology. FG, SS, and MC analyzed the data and wrote the original draft. All authors discussed the results and contributed to the writing the manuscript

FUNDING

This research was financially supported by the National Natural Science Foundation of China (Nos. 41766005, 42166005) and the National Key Research and Development Program of China (No. 2019YFD0901304).

ACKNOWLEDGMENTS

We thank all researchers and funding agencies.

SUPPLEMENTARY MATERIAL

The Supplementary Material for this article can be found online at: https://www.frontiersin.org/articles/10.3389/fmars.2022.931430/full#supplementary-material

REFERENCES

Bao, J., Dong, S. L., Tian, X. L., Wang, F., Gao, Q. F. and Dong, Y. W. (2010). Metabolic Rates and Biochemical Compositions of *Apostichopus japonicus* (Selenka) Tissue During Periods of Inactivity. *Chin. J. Oceanol. Limn.* 28 (2), 218–223. doi: 10.1007/s00343-010-9016-3

Bell, J. D., Rothlisberg, P. C., Munro, J. L., Loneragan, N. R., Nash, W. J., Ward, R. D., et al. (2005). Restocking and Stock Enhancement of Marine Invertebrate Fisheries. *Adv. Mar. Bio.* 49, 1–374. doi: 10.1016/S0065-2881(05)49010-0

Buentello, J. A., Gatlin, D. M. and Neill, W. H. (2000). Effects of Water Temperature and Dissolved Oxygen on Daily Feed Consumption, Feed Utilization and

Growth of Channel Catfish (*Ictalurus punctatus*). *Aquaculture* 182 (3-4), 339–352. doi: 10.1016/S0044-8486(99)00274-4

Buccheri, E., Foellmer, M. W., Christensen, B. A., Langis, P., Freeman, A. S. (2019). Variation in righting times of *Holothuria atra*, *Stichopus chloronotus* and *Holothuria edulis* in response to increased seawater temperatures on Heron Reef in the Southern GBR. *J. Mar. Biol.* 2019, 1-6. doi: 10.1155/2019/6179705

Cheng, C. H., Wu, F. F., Ren, C. H., Jiang, X., Zhang, X., Li, X. M., et al. (2021). Aquaculture of the Tropical Sea Cucumber, *Stichopus monotuberculatus*: Induced Spawning, Detailed Records of Gonadal and Embryonic Development, and Improvements in Larval Breeding by Digestive Enzyme Supply in Diet. *Aquaculture* 540, 736690. doi: 10.1016/j.aquaculture.2021.736690

Conand, C. (1993). Ecology and Reproductive Biology of *Stichopus Variegatus* an Indo-Pacific Coral Reef Sea Cucumber (Echinodermata: Holothuroidea). *B. Mar. Sci.* 52 (3), 970–981.

Costelloe, J. and Keegan, B. F. (1984). Feeding and Related Morphological Structures in the Dendrochirote *Aslia Lefevrei* (Holothuroidea: Echinodermata). *Mar. Biol.* 84, 135–142. doi: 10.1007/BF00392998

Dance, S. K., Lane, I. and Bell, J. D. (2003). Variation in Short-Term Survival of Cultured Sandfish (*Holothuria scabra*) Released in Mangrove-Seagrass and Coral Reef Flat Habitats in Solomon Islands. *Aquaculture* 220 (1-4), 495–505. doi: 10.1016/S0044-8486(02)00623-3

Dong, Y. W. and Dong, S. L. (2006). Growth and Oxygen Consumption of the Juvenile Sea Cucumber *Apostichopus japonicus* (Selenka) at Constant and Fluctuating Water Temperatures. *Aquac. Res.* 37 (13), 1327–1333. doi: 10.1111/j.1365-2109.2006.01570.x

Dong, G. C., Dong, S. L., Tian, X. L. and Wang, F. (2011). Effects of Photoperiod on Daily Activity Rhythm of Juvenile Sea Cucumber, *Apostichopus japonicus* (Selenka). *Chin. J. Oceanol. Limn.* 29, 1015. doi: 10.1007/s00343-011-0204-6

Dong, Y. W., Dong, S. L., Tian, X. L., Wang, F. and Zhang, M. Z. (2006). Effects of Diel Temperature Fluctuations on Growth, Oxygen Consumption and Proximate Body Composition in the Sea Cucumber *Apostichopus Japonicus* (Selenka). *Aquaculture* 255 (1-4), 514–521. doi: 10.1016/j.aquaculture.2005.12.013

Dong, G. C., Dong, S. L., Wang, F. and Tian, X. L. (2010). Effects of Light Intensity on Daily Activity Rhythm of Juvenile Sea Cucumber, *Apostichopus Japonicus* (Selenka). *Aquac. Res.* 41 (11), 1640–1647. doi: 10.1111/j.1365-2109.2010.02534.x

Dumont, C. P., Himmelman, J. H. and Robinson, S. M. C. (2007). Random Movement Pattern of the Sea Urchin *Strongylocentrotus droebachiensis*. *J. Exp. Mar. Biol. Ecol.* 340 (1), 80–89. doi: 10.1016/j.jembe.2006.08.013

Fan, S. G., Hu, C. Q., Zhang, L. P., Sun, H. Y., Wen, J. and Luo, P. (2012). Complete Mitochondrial Genome of the Sea Cucumber Stichopus Sp. And its Application in the Identification of This Species. *Aquac. Res.* 43 (9), 1306–1316. doi: 10.1111/j.1365-2109.2011.02934.x

Fankboner, P. V. (1978). Suspension-Feeding Mechanisms of the Armoured Sea Cucumber *Psolus chitinoides* Clark. *J. Exp. Mar. Biol. Ecol.* 31 (1), 11–25. doi: 10.1016/0022-0981(78)90133-8

Gao, F., Yang, H. S., Xu, Q., Wang, F. Y. and Liu, G. B. (2009). Effect of Water Temperature on Digestive Enzyme Activity and Gut Mass in Sea Cucumber *Apostichopus japonicus* (Selenka), With Special Reference to Aestivation. *Chin. J. Oceanol. Lim.* 27, 714–722. doi: 10.1007/s00343-009-9202-3

Gillanders, B. M., Able, K. W., Brown, J. A., Eggleston, D. B. and Sheridan, P. F. (2003). Evidence of Connectivity Between Juvenile and Adult Habitats for Mobile Marine Fauna: An Important Component of Nurseries. *Mar. Ecol. Prog. Ser.* 247, 281–295. doi: 10.3354/meps247281

Graham, J. C. H. and Battaglene, S. C. (2004). Periodic Movement and Sheltering Behavior of *Actinopyga mauritiana* (Holothuroidea: Aspidochirotidae) in Solomon Islands. *SPC Beche-de-mer Inf. Bull.* 19, 23–30.

Hair, C., Militz, T., Daniels, N. and Southgate, P. C. (2020). Comparison of Survival, Growth and Burying Behavior of Cultured and Wild Sandfish (*Holothuria scabra*) Juveniles: Implications for Ocean Mariculture. *Aquaculture* 526, 735355. doi: 10.1016/j.aquaculture.2020.735355

Hamel, J. F., Sun, J., Gianasi, B. L., Montgomery, E. M., Kenchington, E. L., Burel, B., et al. (2019). Active Buoyancy Adjustment Increases Dispersal Potential in Benthic Marine Animals. *J. Anim. Ecol.* 88 (6), 820–832. doi: 10.1111/1365-2656.12943

Huang, L. H., Pang, Q. J., Zhong, S. P., Liu, Y. H. and Pan, C. Y. (2020). Analysis on Morphological Character of Ossicles and Nutritive Content of *Holothuria leucospilota* and *Stichopus variegatus* in Beibu Gulf. *Guangxi Sci.* 27 (5), 578–584. doi: 10.13656/j.cnki.gxkx.20201214.018

Hu, C. Q., Xu, Y. H., Wen, J., Zhang, L. P., Fan, S. G. and Su, T. (2010). Larval Development and Juvenile Growth of the Sea Cucumber Stichopus Sp. (Curry Fish). *Aquaculture* 300, 73–79. doi: 10.1016/j.aquaculture.2009.09.033

Ji, T. T., Dong, Y. W. and Dong, S. L. (2008). Growth and Physiological Responses in the Sea Cucumber, *Apostichopus japonicus* Selenka: Aestivation and Temperature. *Aquaculture* 283 (1-4), 180–187. doi: 10.1016/j.aquaculture.2008.07.006

Kashenko, S. D. (2002). Reactions of the Larvae of the Sea Cucumber *Apostichopus japonicus* to Sharp Desalination of Surface Water: A Laboratory Study. *SPC Beche-de-Mer Inf. Bull.* 16, 15–21.

Kato, A. and Hirata, H. (1990). Effects of Water Temperature on the Circadian Rhythm of the Sea-Cucumber, *Stichopus japonicus* in Culture. *Aquaculture Science.* 38 (1), 75–80. doi: 10.11233/aquaculturesci1953.38.75

Kitazawa, K. and Oji, T. (2014). Active Feeding Behavior of and Current Modification by the Sea Lily *Metacrinus rotundus* (Echinodermata: Crinoidea). *J. Exp. Mar. Biol. Ecol.* 453, 13–21. doi: 10.1016/j.jembe.2013.12.017

Liang, G. Y. (1987). Preliminary Investigation of Three Sea Cucumber Resources in Guangxi Coastal Area. *J. Guangxi Agric. Sci.* 4, 54–56.

Liao, Y. L. (1997). *Fauna Sinica, Phylum Echinodermata, Class Holothuroidea* (Beijing: Science Press).

Liao, J. C. and Cotel, A. (2013). "Effects of Turbulence on Fish Swimming in Aquaculture," in *Swimming Physiology of Fish: Towards Using Exercise to Farm a Fit Fish in Sustainable Aquaculture*. Eds. Palstra, A. P. and Planas, J. V. (Berlin, Heidelberg: Springer Berlin Heidelberg), 109–127.

Lin, C. G. (2014). Effects of Four Physical Environment Factors on the Movement and Feeding Behavior of Sea Cucumber *Apostichopus japonicus* (Selenka). doctor's degree]. [Beijing]: University of Chinese Academy of Sciences. (in Chinese with English abstract)

Li, M. N., Zhu, H. F., Jin, Z. J., Luo, J., Xu, J. W., Li, , et al. (2018). The Effect of Accelerating Flow on Swimming Behavior of Juvenile *Aristichthys nobilis* and *Hypophthalmichthys molitrix* During Downstream Migration. *Acta Hydrobiologica Sinica*. 42 (3), 571–577. doi: 10.7541/2018.071

Lovatelli, A., Conand, C., Purcell, S., Uthicke, S., Hamel, J. F. and Mercier, A. (2004). "Advances in Sea Cucumber Aquaculture and Management," in *Fisheries and Aquaculture Technical Paper No. 516*, vol. 425. (Rome: FAO).

Massin, C. (1996). The Holothurians of Easter Island. *Bull. K. Belg. Inst. Nat. Wet.* 66, 151–178.

McKenzie, J. D. (1991). The Taxonomy and Natural History of North European Dendrochirote Holothurians (Echinodermata). *J. Nat. Hist.* 25, 123–171. doi: 10.1080/00222939100770091

Mercier, A., Battaglene, S. C. and Hamel, J. F. (1999). Daily Burrowing Cycle and Feeding Activity of Juvenile Sea Cucumbers *Holothuria scabra* in Response to Environmental Factors. *J. Exp. Mar. Biol. Ecol.* 239, 125–156. doi: 10.1016/S0022-0981(99)00034-9

Mercier, A., Battaglene, S. C. and Hamel, J. F. (2000). Periodic Movement, Recruitment and Size-Related Distribution of the Sea Cucumber *Holothuria scabra* in Solomon Islands. *Hydrobiologia* 440, 81–100. doi: 10.1023/A:1004121818691

Morissette, S. and Himmelman, J. H. (2000). Decision of the Asteroid *Leptasterias polaris* to Abandon its Prey When Confronted With its Predator, the Asteroid *Asterias Vulgaris*. *J. Exp. Mar. Biol. Ecol.* 252 (2), 151–157. doi: 10.1016/S0022-0981(00)00229-X

Navarro, P. G., Garcia-Sanz, S., Barrio, J. M. and Tuya, F. (2013). Feeding and Movement Patterns of the Sea Cucumber *Holothuria sanctori*. *Mar. Bio.* 160, 2957–2966. doi: 10.1007/s00227-013-2286-5

Pan, Y., Zhang, L. B., Lin, C. G., Sun, J. M., Kan, R. T. and Yang, H. S. (2015). Influence of Flow Velocity on Motor Behavior of Sea Cucumber *Apostichopus japonicus*. *Physiol. Behav.* 144, 52–59. doi: 10.1016/j.physbeh.2015.02.046

Pavlov, D. S., Lupandin, A. and Skorobogatov, M. A. (2000). The Effects of Flow Turbulence on the Behavior and Distribution of Fish. *J. Ichthyol.* 20, 232–261.

Pilditch, C. A. (1999). Effect of Variations in Flow Velocity and Phytoplankton Concentration on Sea Scallop (*Placopecten magellanicus*) Grazing Rates. *J. Exp. Mar. Biol. Ecol.* 240, 111–136. doi: 10.1016/S0022-0981(99)00052-0

Purcell, S. W. (2010). Diel Burying by the Tropical Sea Cucumber *Holothuria sabra*: Effects of Environmental Stimuli, Handling and Ontogeny. *Mar. Biol.* 157, 663–671. doi: 10.1007/s00227-009-1351-6

Purcell, S. W., Blockmans, B. F. and Agudo, N. N. S. (2006). Transportation Methods for Restocking of Juvenile Sea Cucumber, *Holothuria scabra*. *Aquaculture* 251, 238–244. doi: 10.1016/j.aquaculture.2005.04.078

Purcell, S. W., Conand, C., Uthicke, S. and Byrne, M. (2016). Ecological Roles of Exploited Sea Cucumbers. *Oceanogr. Mar. Biol.* 54, 367–386. doi: 10.1201/9781315368597-8

Purcell, S. W., Hair, C. A. and Mills, D. J. (2012a). Sea Cucumber Culture, Farming and Sea Ranching in the Tropics: Progress, Problems and Opportunities. *Aquaculture* 368-369, 68–81. doi: 10.1016/j.aquaculture.2012.08.053

Purcell, S. W., Samyn, Y. and Conand, C. (2012b). *Commercially Important Sea Cucumbers of the World* (Rome, Italy: FAO).

Qiu, T. L., Zhang, L. B., Zhang, T. and Yang, H. S. (2014). Effects of Mud Substrate and Water Current on the Behavioral Characteristics and Growth of the Sea Cucumber *Apostichopus japonicus* in the Yuehu Lagoon of Northern China. *Aquac. Int.* 22 (2), 423–433. doi: 10.1007/s10499-013-9650-9

Ren, C. H., Chen, T., Jiang, X., Luo, X., Wang, Y. H. and Hu, C. Q. (2015a). The First Echinoderm Gamma-Interferon-Inducible Lysosomal Thiol Reductase (GILT) Identified From Sea Cucumber (*Stichopus monotuberculatus*). *Fish. Shellfish. Immunol.* 42, 41–49. doi: 10.1016/j.fsi.2014.10.024

Ren, C. H., Chen, T., Jiang, X., Wang, Y. H. and Hu, C. Q. (2014a). Identification and Functional Characterization of a Novel Ferritin Subunit From the Tropical Sea Cucumber, *Stichopus monotuberculatus*. *Fish. Shellfish. Immunol.* 38, 265–274. doi: 10.1016/j.fsi.2014.03.022

Ren, C. H., Chen, T., Jiang, X., Wang, Y. and Hu, C. Q. (2014b). The First Characterization of Gene Structure and Biological Function for Echinoderm Translationally Controlled Tumor Protein (Tctp). *Fish. Shellfish. Immunol.* 41, 137–146. doi: 10.1016/j.fsi.2014.08.030

Ren, C. H., Chen, T., Sun, H. Y., Jiang, X., Hu, C. Q., Qian, J., et al. (2015b). The First Echinoderm Poly-U-Binding Factor 60 kDa (PUF60) From Sea Cucumber (*Stichopus monotuberculatus*): Molecular Characterization, Inducible Expression and Involvement of Apoptosis. *Fish. Shellfish. Immunol.* 47, 196–204. doi: 10.1016/j.fsi.2015.09.001

Russo, A. R. (1977). Water Flow and the Distribution and Abundance of Echinoids (Genus *echinometra*) on an Hawaiian Reef. *Mar. Freshw. Res.* 28 (6), 693–702. doi: 10.1071/MF9770693

Sakurai, I. and Seto, M. (2000). Movement and Orientation of the Japanese Scallop *Patinopecten Yessoensis* (Jay) in Response to Water Flow. *Aquaculture* 181, 269–279. doi: 10.1016/S0044-8486(99)00242-2

Shiell, G. R. (2006). Effect of Invasive Tagging on the Activity of *Holothuria Whitmaei* [Echinodermata: Holothuroidea]: A Suitable Mark-Recapture Method for Short-Term Weld Studies of Holothurian Behavior. *Mar. Fresh. Behav. Physiol.* 39, 153–162. doi: 10.1080/10236240600688789

Skewes, T., Dennis, D. and Burridge, C. M. (2000). Survey of *Holothuria scabra* (Sandfish) on Warrior Reef, Torres Strait. *CSIRO Marine Research Final Report*(Brisbane)

Sun, J., Hamel, J. F. and Mercier, A. (2018a). Influence of Flow on Locomotion, Feeding Behavior and Spatial Distribution of a Suspension-Feeding Sea Cucumber. *J. Exp. Biol.* 221 (20), jeb189597. doi: 10.1242/jeb.189597

Sun, J. M., Hamel, J. F., Stuckless, B., Small, T. J. and Mercier, A. (2020). Effect of Light, Phytoplankton, Substrate Types and Colour on Locomotion, Feeding Behaviour and Microhabitat Selection in the Sea Cucumber *Cucumaria frondosa*. *Aquaculture* 526, 735369. doi: 10.1016/j.aquaculture.2020.735369

Sun, J., Zhang, L. B., Pan, Y., Lin, C. G., Wang, F., Kan, R. T., et al. (2015). Feeding Behavior and Digestive Physiology in Sea Cucumber *Apostichopus japonicus*. *Physiol. Behav.* 139, 336–343. doi: 10.1016/j.physbeh.2014.11.051

Sun, J., Zhang, L. B., Pan, Y., Lin, C. G., Wang, F. and Yang, H. S. (2018b). Effect of Water Temperature on Diel Feeding, Locomotion Behaviour and Digestive Physiology in the Sea Cucumber *Apostichopus japonicus*. *J. Exp. Biol.* 221 (9), jeb177451. doi: 10.1242/jeb.177451

Uthicke, S. (1999). Sediment Bioturbation and Impact of Feeding Activity of Holothuria (Halodeima) Atra and Stichopus Chloronotus, Two Sediment Feeding Holothurians, at Lizard Island, Great Barrier Reef. Bull. Mar Sci. 64, 129–141.

Uthicke, S., Welch, D. and Benzie, J. A. H. (2004). Slow Growth and Lack of Recovery in Overfished Holothurians on the Great Barrier Reef: Evidence From DNA Fingerprints and Repeated Large-Scale Surveys. *Conserv. Biol.* 18, 1395–1404. doi: 10.1111/j.1523-1739.2004.00309.x

Vasquez, H. E., Zheng, X., Zhan, X., Gu, Z. F. and Wang, A. M. (2018). The Effect of Light on the Locomotion and Byssal Reattachment of Winged Pearl Oyster Pteria Penguin (Rding 1798) Juveniles. *J. Shellfish Res.* 37 (5), 1061–1066. doi: 10.2983/035.037.0517

Vasquez, H. E., Zheng, X., Zhan, X., Gu, Z. and Wang, A. M. (2020). Byssal Re-Attachment Behavior in the Winged Pearl Oyster *Apostichopus japonicus*. in Response to Low Salinity Levels. *J. World. Aquac. Soc* 52, 457–465. doi: 10.1111/jwas.12744

Wang, H. H., Yan, J. X., Feng, Y. Q., Fang, Z., Wang, S., Zhou, Y., et al. (2017). Embryonic and Larval Development of Sea Cucumber *Stichopus herrmanni*. *Fish. Sci.* 36 (05), 606–611. doi: 10.16378/j.cnki.1003-1111.2017.05.011

Wang, F. Y., Yang, H. S., Gao, F. and Liu, G. B. (2008). Effects of Acute Temperature or Salinity Stress on the Immune Response in Sea Cucumber, *Apostichopus japonicus*. *Comp. Biochem. Physiol. Part A: Mol. Integr. Physiol.* 151, 491–498. doi: 10.1016/j.cbpa.2008.06.024

Wang, Y. H., Yu, M. M., Wang, D. Y. and Lv, Z. (2010). Analysis of Nutritional Components of *Stichopus variegates*, *Thelenota ananas* and *Stichopus chloronotus* Boandt. *Acta Nutrimenta Sinica.* 32 (04), 397–398. doi: 10.13325/j.cnki.acta.nutr.sin.2010.04.016

Wen, J., Fan, S. G., Li, H. P. and Hu, C. Q. (2018). Genetic Diversity in Four Wild Populations of Sea Cucumber *Stichopus monotuberculatus* in South China Sea. *Fish. Sci.* 37 (3), 404–408. doi: 10.16378/j.cnki.1003-1111.2018.03.020

Wheeling, R. J., Verde, E. A. and Nestler, J. R. (2007). Diel Cycles of Activity, Metabolism, and Ammonium Concentration in Tropical Holothurians. *Mar. Biol.* 152, 297–305. doi: 10.1007/s00227-007-0683-3

Wildish, D. and Kristmanson, D. D. (1988). Growth Response of Giant Scallops to Periodicity of Flow. *Mar. Ecol. Prog. Ser.* 42, 163–169. doi: 10.3354/meps042163

Wildish, D. J. and Saulnier, A. M. (1992). The Effect of Velocity and Flow Direction on the Growth of Juvenile and Giant Scallops. *Exp. Mar. Biol. Ecol.* 133, 133–143. doi: 10.1016/0022-0981(92)90032-6

Wolfe, K. and Byrne, M. (2017). Biology and Ecology of the Vulnerable Holothuroid, *Stichopus herrmanni*, on a High-Latitude Coral Reef on the Great Barrier Reef. *Coral Reefs.*, 36: 1143- 1156. doi: 10.1007/s00338-017-1606-5

Wolkenhauer, S. M. (2008). Burying and Feeding Activity of Adult *Holothuria scabra* (Echinodermata: Holothuroidea) in a Controlled Environment. *SPC Beche Mer Inf. Bull.* 27, 25–28.

Woodby, D., Smiley, S. and Larson, R. (2000). Depth and Habitat Distribution of *Parastichopus californicus* Near Sitka, Alaska. *Alaska Fishery Res. Bull.* 7 (1), 22–32. http://146.63.61.200/static/home/library/PDFs/afrb/woodbyv7.pdf

Yang, H. S., Hamel, J-F. and Mercier, A. (2015). *The Sea Cucumber Apostichopus japonicus: History, Biology and Aquaculture* (Landon: Academic Press).

Yan, A. F., Ren, C. H., Chen, T., Jiang, X. and Sun, H. Y. (2016). Identification and Functional Characterization of a Novel Antistasin/WAP-Like Serine Protease Inhibitor From the Tropical Sea Cucumber, *Stichopus Monotuberculatus*. *Fish Shellfish Immunol.* 59, 203–212. doi: 10.1016/j.fsi.2016.10.038

Yuan, L. H., Hu, C. Q., Zhang, L. P. and Xia, J. J. (2013). Population Genetics of a Tropical Sea Cucumber Species (*Stichopus monotuberculatus*) in China. *Conserv. Biol.* 14, 1279–1284. doi: 10.1007/s10592-013-0506-7

Zhang, S., Chen, Y. and Sun, M. C. (2006). Effects of Light Intensity on the Behavior Characteristics of Sea Cucumbers and the Collection Effect of Artificial Reef Model. *Fishery Sci. China.* 1, 20–27.

Zhang, L. B., Zhang, T., Xu, Q. Z., Qiu, T. L., Yang, H. S. and Liu, S. L. (2014). An Artificial Oyster-Shell Reef for the Culture and Stock Enhancement of Sea Cucumber, *Apostichopus* japonicus, in Shallow Seawater. *Aquac. Res.* 46 (9), 2260–2269. doi: 10.1111/are.12383

Zhao, S. (1998). *Shallow-Water Sea Cucumbers of Taiwan* (Taipei: National Museum of Natural Science).

Zhong, M., Chen, T., Hu, C. Q. and Ren, C. H. (2015). Isolation and Characterization of Collagen From the Body Wall of Sea Cucumber *Stichopus monotuberculatus*. *J. Food. Sci.* 80 (4), C671–C679. doi: 10.1111/1750-3841.12826

Conflict of terest: The authors declare that the research was conducted in the absence of any commercial or financial relationships that could be construed as a potential conflict of interest.

evaluated in this article, or claim that may be made by its manufacturer, is not guaranteed or endorsed by the publisher.

frontiers | Frontiers in Marine Science

ORIGINAL RESEARCH
published: 12 July 2022
doi: 10.3389/fmars.2022.948882

Revealing Selection in Breeding and Genetic Characteristics of Economically Important Traits of New Species of *Apostichopus Japonicas* Based on Genome Resequencing and GWAS Analysis

Chao Guo[1], *Yuanxin Li*[1], *Jiahui Xie*[1], *Lingshu Han*[2], *Youquan Wang*[1], *Xianglei Zhang*[1], *Yanglei Wu*[1], *Jian Song*[1], *Yaqing Chang*[1]* *and Jun Ding*[1]*

[1] *Key Laboratory of Mariculture & Stock Enhancement in North China's Sea, Ministry of Agriculture and Rural Affairs, Dalian Ocean University, Dalian, China,* [2] *Ningbo University, Ningbo, China*

OPEN ACCESS

Edited by:
Bin Xia,
Qingdao Agricultural University, China

Reviewed by:
Lina Sun,
Chinese Academy of Sciences (CAS), China
Dongxue Xu,
Qingdao Agricultural University, China

***Correspondence:**
Jun Ding
dingjun19731119@hotmail.com
Yaqing Chang
yqchang@dlou.edu.cn

Specialty section:
This article was submitted to Marine Fisheries, Aquaculture and Living Resources, a section of the journal Frontiers in Marine Science

Received: *20 May 2022*
Accepted: *03 June 2022*
Published: *12 July 2022*

Citation:
Guo C, Li Y, Xie J, Han L, Wang Y, Zhang X, Wu Y, Song J, Chang Y and Ding J (2022) Revealing Selection in Breeding and Genetic Characteristics of Economically Important Traits of New Species of Apostichopus Japonicas Based on Genome Resequencing and GWAS Analysis. Front. Mar. Sci. 9:948882. 10.3389/fmars.2022.948882

Apostichopus japonicas is an economically important species with high nutritional value. However, our knowledge of its genetic diversity and the genetic changes that occurred during its domestication or trait selection is quite limited. In this study, the whole genomes of 254 A. *japonicas* samples were resequenced. Analyses of the population genetic structure revealed that the genetic diversity of *A. japonicas* in the north of China is generally high, there was no difference in the population structure among the six cultured populations, and they were divided into two subpopulations together with AY-1 (new species). The results also showed that the genetic diversity of the AY-1 population was relatively low, the degree of linkage of alleles was high, and this population had been subjected to more positive selection. Based on Tajima's D, F_{ST} analysis, and ROD analysis, the selected intervals and genes of the AY-1 population were identified, with some of the candidate intervals being related to an economically important trait and breeding target, namely, the number of parapodia. Gene Ontology analysis of the candidate genes revealed that the two subpopulations differed in their immune function, protein synthesis, decomposition, and transport, among others. Using GWAS, we identified 39 candidate genes for four economically important traits of *A. japonicas*, and we verified that those genes contained non-synonymous SNPs. Through this verification, BSL78_00022 and BSL78_00023 were found to be key genes for the number of parapodia in *A. japonicas*. Of these two genes, BSL78_00022 encodes a protein related to cell differentiation and proliferation, so it was assumed that three non-synonymous substitutions (Ser-Phe, Glu-Asp, and Ala-Val) in this gene are related to the changes in the number of parapodia. Meanwhile, the pleiotropic gene BSL78_04631, which is related to body weight and body wall weight, and promotes protein synthesis and cell growth, has a non-synonymous substitution (IIE-Val), which is assumed to be the reason for the difference in body weight and body wall weight of *A. japonicas*. These results provide a new perspective for explaining the genetic

structure characteristics of *A. japonicas* and analyzing the selection and economically important traits in the breeding of new species.

Keywords: *Apostichopus japonicas*, resequencing, genome-wide association analysis, population structure, population genetics

INTRODUCTION

Apostichopus japonicas, belonging to the class Holothuroidea within the Echinodermata, is an economically important species for aquaculture in China (Xu et al., 2015). In 2020, the output of *A. japonicas* in China reached 196,500 tons, with the coastal areas of Shandong and Liaoning being the main areas of production. To improve the yield and quality of cultured *A. japonicas*, genetic breeding of this species has been carried out in China since the early 1990s (Han et al., 2016). By 2021, six new species of *A. japonicas*, including "Shuiyuan No. 1" and "AY-1," had been approved by the National Appraisal Committee of Aquatic Protospecies and Improved Varieties. Before that, *A. japonicas* farms used wild or cultured *A. japonicas* without selection for breeding as the parents to carry out seedling breeding of this species (Ru et al., 2019). "AY-1" (GS-01-014-2017) is a new species of *A. japonicas* approved by the National Appraisal Committee of Aquatic Protospecies and Improved Varieties in 2018, which was cultured *via* four generations of breeding, with "Shuiyuan No. 1" (GS-02-005-2009) as the candidate parent. It features long parapodia (fleshy thorns) on the body surface that are arranged in six regular rows, with an average number in each individual of more than 45. Compared with "Shuiyuan No. 1," "AY-1" cultured under the same conditions had an average increase in the number of parapodia of 12.8%. At present, "AY-1" is widely cultured in Shandong and Liaoning provinces (Ding and Chang, 2020).

With the development of high-throughput sequencing technology and various omics technologies, basic studies on the application of breeding and population genetics of *A. japonicas* have been carried out. For example, Chen et al. (Chen et al., 2008) studied the genetic variation of wild and hatched *A. japonicas* populations in northern China using microsatellite markers. Their results showed that hatched populations typically differed significantly from wild populations. In addition, Chang et al. (Chang et al., 2009) studied the genetic structure of five natural *A. japonicas* populations [i.e., Aomori, Japan (JA and JR), Yosu, South Korea (KY), Dalian, China (CD), and Vladivostok, Russia (RV)], using 10 microsatellite markers. The results showed that the levels of genetic diversity of the five populations were similar. Moreover, Zhao et al. (Zhao et al., 2020) screened metabolic markers of *A. japonicas* populations in different regions of China (Jinzhou, Pikou, Dalian, and Rushan) through metabolomic methods. Furthermore, Gao et al. (Gao et al., 2019) carried out transcriptome analysis on the body wall of *A. japonicas* and revealed the differences in growth between the largest and smallest individuals in the purebred population and hybrid population. However, owing to technical constraints, the population genetic structure of the main cultured populations of *A. japonicas* in China is still largely unknown. In 2017, the Institute of Oceanography, Chinese Academy of Sciences, Ocean University of China, Dalian Ocean University, and other institutions in China successively completed the whole-genome sequencing of *A. japonicas*, laying a foundation for subsequent studies on the population structure and economically important traits of this species (Zhang et al., 2017; Li et al., 2018).

Genome-wide association study (GWAS) can mine sites and genes related to trait variation by obtaining a large number of single-nucleotide polymorphism (SNP) sites across the whole genome. Its results have the advantages of high resolution, providing a wide source of research materials, capturing abundant variation, high accuracy, and is relatively quick to obtain (Tam et al., 2019). To date, GWAS has been widely applied in the systematic screening of sites or genes related to economically important traits of aquatic animals such as fish, shellfish, and crustaceans (Abdelrahman et al., 2017). For example, Zhou et al. (Zhou et al., 2022) obtained genome regions and candidate genes related to various growth traits of mandarinfish through GWAS. In addition, Yang et al. (Yang et al., 2020) identified candidate SNPs and genes related to growth traits of *Epinephelus fuscoguttatus* using GWAS. Moreover, Wang et al. (Wang et al., 2022) identified genes related to carotenoid accumulation in scallops by GWAS, and He et al. (He et al., 2022) used this approach to reveal single-nucleotide polymorphism sites related to the shell shape of *Crassostrea Gigas*. Lyu et al. (Lyu et al., 2021) also identified candidate genes for growth traits in *Litopenaeus vannamei* by GWAS. Finally, Cui et al. (Cui et al., 2015) obtained sex-linked markers of *Eriocheir sinensis* by the same approach. However, no study on the trait-associated sites and genes of *A. japonicas* as determined using GWAS have been reported.

To summarize the current study, 254 *A. japonicas* individuals were resequenced based on their genomes, including "AY-1" and six major *A. japonicas* cultured populations in northern China. By population structure analysis, LD attenuation analysis, population group selection analysis, and genome-wide association study, we finally revealed the population structure and genetic diversity of this species, identified areas and candidate genes for artificial selection of "AY-1," and revealed four candidate genes related to economically important traits. This study provides important information for germplasm conservation and genetic breeding of *Apostichopus japonicas*.

Abbreviations: SNP, Single nucleotide polymorphism; LD, Linkage disequilibrium; GWAS, Genome-Wide Association Studies; GO, Gene Ontology; BP, Biological processes; qRT-PCR, Quantitative Real-time PCR.

MATERIALS AND METHODS

Sample Collection and Trait Measurement

From July 2020, The samples were distributed as the new variety "AY-1" (J) (n=49), the cultured *A. japonicas* in Yantai, Shandong province (Y) (n=40), Mouping, Shandong Province (SZ) (n=25), South Huangcheng Island, Yantai, Shandong Province (SY) (n=28), Xixiakou, Weihai, Shandong Province (YS) (n=26), Ant Island, Jinzhou District, Dalian, Liaoning Province (M) (n=28) and Xinyulong, Pingdao, Dalian, Liaoning Province (X) (n=58), Based on our traits of interest, we sampled from a total sample of 505 sea cucumbers based on a normal distribution, and finally obtained 254 sea cucumbers for resequencing (**Figure 1**).

All the samples were of the second age. The sea cucumber used in the experiment was harvested in July 2020 and transferred to the Key Laboratory of Marine Aquaculture of the Ministry of Agriculture and Rural Affairs for cultivation. All *A.japonicas* are reared in the same environment. The healthy non-destructive body surface of *A.japonicas* was selected from each population, and small pieces of the body wall and longitudinal muscle tissue were cut. After being frozen by liquid nitrogen, the samples were divided into centrifugal tubes and stored in a fresh freezer at -80°C. When measuring the number of parapodia, repeat counting three times and take the average value. Before weight measurement, dry the water on the surface of *A.japonicas* and let stand for 2-5min repeat weighing three times and take the average value. Similarly, the body wall weight was the average value after the visceral tissue was removed and repeatedly weighed three times. The body wall production rate was calculated by dividing the body wall weight by body weight.

DNA Extraction and Sequencing

Due to the particularity of Marine organisms' tissues, it is necessary to remove proteins, fats, and other organic compound impurities. In this experiment, The total genome DNA was extracted by the SDS method. TIANGEN amp Marine Animals DNA Kit (TIANGEN, Beijing, China) was used to extract the muscle tissue of *A.japonicas*. The purity and integrity of nucleic acid were preliminarily detected by 1% agarose gel electrophoresis. The main band of qualified DNA samples was clear without degradation or slight degradation. The mass concentration of the tested DNA samples was adjusted to about 100ng/ul and stored.

The qualified samples were randomly broken into 350bp fragments by Bioruptor Pico ultrasonic fragmentation instrument, and then the genomic DNA library construction kit was used for library preparation. The library's construction includes the process of DNA fragment end complementing, 3' end adding 'A', DNA end linking adaptor, and PCR amplification. Quality control was carried out for the constructed libraries, and high-throughput sequencing was performed on the Illumina HiSeq2500 sequencing platform for qualified libraries.

Sequence Alignment and Mutation Detection

Clean Reads are obtained by filtering Raw Reads of the original off-machine data. We adopt BWA (v0.7.12) software will clean reads and *A.japonicas* reference gene (https://ftp.ncbi.nlm.nih.gov/genomes/all/GCA/002/754/855/Gca_002754855.1_asm275485v1/). The initial comparison results were in Sam format, and then SamTools (1.9) was used to convert the results into BAM format and sort them. Suppose the result of a sample contains multiple libraries. In that case, the BAM results of multiple libraries are combined with SamTools. Then Picard is used to mark and remove repeated sequences, and then basic data information statistics and map comparison statistics are performed.

GATK (V3.8) was used for population SNPs detection of samples, and the obtained results were filtered to obtain credible SNPs, and the population SNPs results were saved in VCF

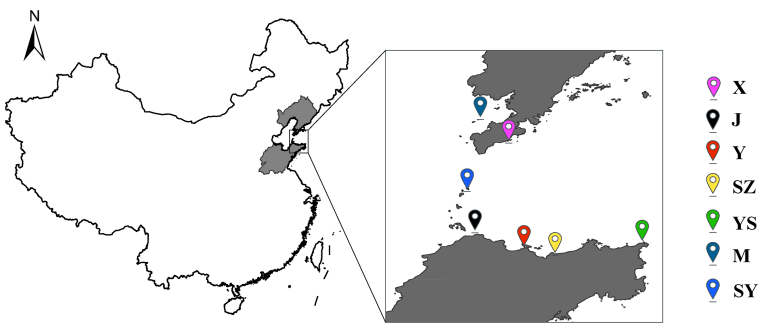

FIGURE 1 | Geographical distribution of 254 *Apostichopus japonicas*.

format. ANNOVAR (V0.35) annotated SNPs based on the given chromosome, origin site, termination site, reference nucleotide, and mutant nucleotide. According to the genome annotation results, these SNPs were divided into exon, intron, intergene, upstream and downstream, and splicing sites. SNPs located in coding exons are further divided into synonymous SNPs (which do not cause amino acid changes) and non-synonymous SNPs (which cause amino acid changes).

Population Structure and Phylogenetic Analysis

To determine that SNPs used for phylogenetic tree construction and structural analysis were independent, we extracted a subset of 607,714 SNPs from the SNP dataset of all samples using LD thresholds (r^2<0.05). The population structure analysis was carried out in Admixture (V1.3.0) with K value set from 1 to 9, and the minimum CV error value appeared at K = 2. Phylogenetic tree (NJ tree) analysis was constructed by VCF2Dis (V1.45).

PCA and LD Decay

The data analyzed by PCA and LD decay also used independent SNPs filtered by LD threshold(r^2<0.05), and Plink (V1.90b6.21) software was used for PCA analysis, and the analysis was specified to PC10. PopLDdecay software (V3.41) was used to analyze LDdecay.

Group Selection Analysis

In population selection analysis, VCFtools (V0.1.16) was used to calculate inter-population F_{ST} analysis and intra-population nucleotide diversity (Pi) with a sliding window of 100KB and a sliding step of 10KB. Tajima's D test in the population was performed by VCFtools using 100KB and 10KB non-overlapping sliding Windows, respectively. Use Perl scripts to calculate inter-group ROD values based on the formula ROD=1-(Pi pop1)/(Pi pop2).

Gene Ontology Analysis

Eggnog-mapper (V5.0) was used to carry out homology annotation according to the genome protein sequence file of *A.japonicas* to obtain the corresponding relationship between genes and GO term. R package AnnotationForge was used to construct the background file of GO analysis. R package clusterProfile (V4.2.0) was used for enrichment analysis.

GWAS Analysis and Candidate Gene Identification

Genome-wide association analysis was conducted by GEMMA (0.98.3), and generalized linear model (GLM) and mixed linear model (LMM) were used to analyze four economic traits, including the number of feet, body weight, body wall weight, and body wall production rate, respectively. Meanwhile, To avoid the influence of subgroup differentiation on GWAS results, When GEMMA was used for GLM association model analysis, we added the relatedness matrix as a covariable. The significance screening threshold of relevant SNPs was set as $-\log_{10P} > 6$, and the following strategies were adopted to analyze SNPs: Firstly, based on the screening of significantly correlated SNPs ($-\log_{10P} > 6$), the SNPs associated with both models were selected for further analysis; Secondly, LD block analysis was performed on the upstream and downstream of the genome of these SNPs, focusing on non-synonymous SNPs. Third, search for genes corresponding to non-synonymous SNPs and find out their functions; Fourth, to more accurately analyze the functions of these candidate genes, eggNOG annotation was used, and the homologous gene functions were searched.

qRT-PCR for Gene Expression Analysis

qRT-PCR was used for gene expression analysis. The primers were designed by Primer 5.0 (Primer sequences are shown in **Supplementary Table 1**), and two genes related to the number of parapodia and one gene related to growth traits were selected for qRT-PCR detection. For the verification of the number of parapodia, the number of parapodia was 25 (less parapodia), 30 (control), and 46 (more parapodia), with three parallel samples in each group. The body wall tissues with the weight of 50g (large weight), 100g (control), and 170g (lightweight) were selected for growth traits, with three parallel samples in each group. Total RNA was extracted by the Tiangen kit and verified by qRT-PCR. The gene expression level was calculated by the comparative -ΔΔt method.

RESULTS

Phenotypic Statistics and Sequencing Results

To study the population structure of "AY-1" and the *A. japonicas* populations in representative regions of northern China, we collected seven *A. japonicas* populations in the main production areas of Shandong and Liaoning. In the GWAS, the traits that we focused on were growth traits (body weight, body wall weight, and body wall production rate) and the number of parapodia. The distribution of each trait of the total sample is shown in **Supplementary Figure 1**. Under the condition that the characters conform to the normal distribution roughly, the parapodium number was 23-49, the body weight was 14-238 g, the body wall weight was 9.8-149 g, and the body wall production rate was 0.33%-0.95%. With consideration of the GWAS requirements, 25 to 60 sea cucumbers per population were selected for whole-genome resequencing. The high-throughput sequencing was performed through the sequencing platform Illumina HiSeq2500, and the reads between the sequencing data and the unique position of the reference genome were 92.57%-93.80%, and the average sequencing depth was 10.58x (see **Supplementary Table 2**). SNPs were unevenly distributed across the genome, with 53.74% in intergenic regions, 25.51% in introns, 3.51% in exons, and the rest scattered in other regions (see **Supplementary Table 3**). Indels had a distribution similar to SNPs, with 53.30% in intergenic regions, 24.55% in introns, only 0.89% in exons, and the rest scattered in other

regions (see **Supplementary Table 4**). Finally, 11,736,971 high-quality SNP sites were obtained by filtering (with MAF <0.05 and max-missing 0.8 as the standard), which could meet the requirements of subsequent analysis.

Population Structure and Domestication Analysis

To avoid the effect of long LD fragments on the population structure, single SNP sites filtered by a linkage disequilibrium threshold (LD $r^2 < 0.05$) were used for the population structure analysis, phylogenetic tree construction, and PCA of *A. japonicas*. The admixture population structure analysis showed that the seven *A. japonicas* populations could be divided into two subpopulations according to the minimum CV error value (when k=2), namely, the AY-1 subpopulation and the CN subpopulation (**Figure 2B**). When k=3 or 4, the AY-1 subpopulation also showed a population structure different from that of other *A. japonicas* populations.

The phylogenetic tree divided all individuals into two main groups of populations (**Figure 2A**), which was consistent with the results of the population structure analysis, in which most AY-1 *A. japonicas* clustered individually, while other *A. japonicas* populations clustered in a mixed way, showing clusters of individuals rather than populations.

In the PCA analysis, PC1 to PC10 were analyzed, and the proportions of variation explained by PC1, PC2, and PC3 were 11.7%, 10.9%, and 10.5%, respectively (**Figure 2C**). The PCA chart showed that the AY-1 subpopulation was clearly separated from the CN subpopulation, but it had a large internal degree of dispersion, and there were still a small number of individuals overlapping with the CN subpopulation, which was consistent with the phylogenetic tree and results of population structure analysis.

By calculating the nucleotide diversity (π) within the two subpopulations, we further characterized their genetic diversity and differences. The statistical results of the nucleotide diversity analysis of the two subpopulations are shown in **Figure 2D**. The nucleotide diversity of the *A. japonicas* subpopulation in northern China was significantly higher than that of the AY-1 subpopulation. With the windows whose π values corresponded to the top 5% of thresholds as the comparison node, the nucleotide diversity of the AY-1 subpopulation was 7.92×10^{-3}, and the nucleotide diversity of the CN subpopulation was 8.09×10^{-3}. This result was consistent with expectations, namely, the genetic diversity of artificially selected populations is lower than that of natural populations.

LD attenuation is often associated with genetic diversity and the history of domestication, so we further examined the linkage disequilibrium attenuation values of the two *A. japonicas* subpopulations. The results of this statistical analysis are shown in **Figure 2E**. The maximum value of the LD coefficient (r^2) of the AY-1 subpopulation was 0.39 and that of the CN subpopulation was 0.36. The corresponding physical distance when the LD coefficient (r^2) was reduced to 0.1 was taken as the LD attenuation distance of the subpopulations. The attenuation distance of the AY-1 subpopulation was 823 bp and that of the CN subpopulation was 598 bp. The LD attenuation rate of the AY-1 *A. japonicas* subpopulation was relatively low, indicating that the linkage between markers in this subpopulation was higher and its genetic diversity was lower. This conclusion is in line with the LD attenuation characteristics of domesticated

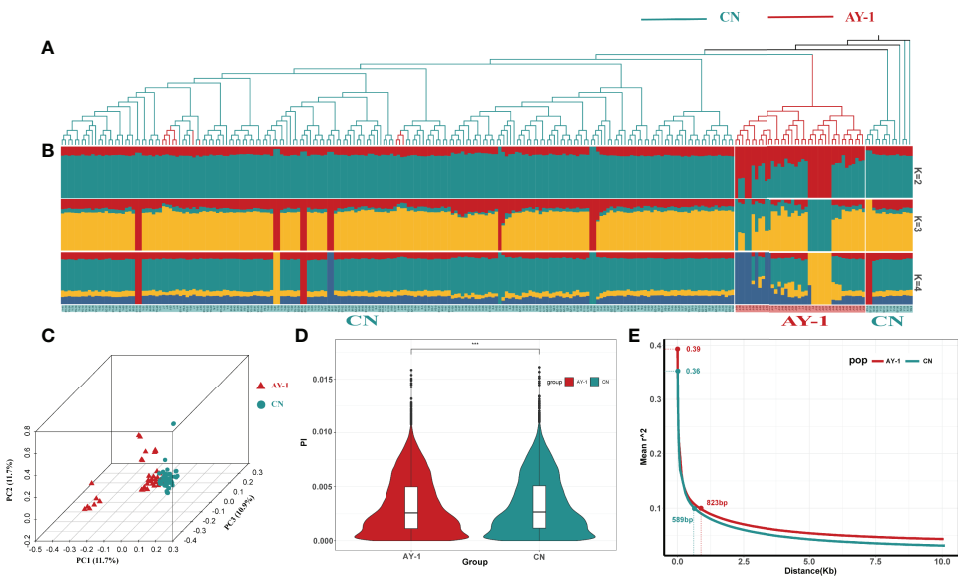

FIGURE 2 | Population structure analysis of *Apostichopus japonicas*. **(A)** phylogenetic tree, The blue branch represents the CN subgroup, and the red branch represents the AY-1 subgroup. **(B)** Population structure of *Apostichopus japonicas*, Each column represents an individual, and the individual is matched with the phylogenetic tree branches in Figure A in turn. The color in the structure plot indicates the component state in each sample. **(C)** PCA figure. **(D)** Nucleotide polymorphisms (Pi) in two subpopulations. **(E)** Linkage disequilibrium for two subgroups. *** means p<0.001 in significance test

populations, and consistent with the conclusion of the above nucleotide diversity (π) analysis.

Analysis of Population Selection

To examine the internal positive selection effect of the two *A. japonicas* subpopulations, we used Tajima's D test (Tajima, 1989) to analyze the differences in the number of nucleotide segregating sites (θw) and nucleotide diversity (π) within the two subpopulations. The results of Tajima's D test are shown in **Figure 3A** (calculated using a 100 kb non-overlapping sliding window). In most of the same genomically regions, Tajima's D value of the AY-1 subpopulation was lower than that of the CN subpopulation, and there were a large number of regions with Tajima's D values of less than 0. The AY-1 subpopulation had 164 windows with Tajima's D value less than 0, while the CN subpopulation had only 22. This indicated that the AY-1 subpopulation had lower genetic diversity and more rare alleles, and had been subjected to more positive selection. A 10 kb non-overlapping sliding window was used to calculate Tajima's D value of the AY-1 subpopulation, the top 5% of windows with the small to large Tajima's D value (Tajima's D < -0.167) were selected, and a total of 3871 candidate regions were obtained. These regions covered a total of 1842 genes in the genome annotation file. The Gene Ontology analysis showed that candidate genes were mainly enriched in biological process (BP) and the main functions involved were immune response (e.g., regulation of wound healing, regulation of response to effectiveness, positive regulation of wound healing, and others), morphological development (e.g., fin morphogenesis, embryonic Pectoral fin Morphogenesis, fin development, and others), and Signal transduction (positive regulation of Wnt signaling pathway). (**Supplementary Figure 2**).

Fixation statistic (F_{ST}) (Nei and Chesser, 1983) can be used to estimate the difference between the average amount of polymorphism in two subpopulations and the average amount of polymorphism in the whole subpopulation; the change in its value reflects the differentiation level of the population. To identify the regions where the domesticated population ("AY-1" subpopulation) was quite different from the natural population (subpopulations in northern China), we selected the regions with F_{ST} thresholds in the top 5% as candidate intervals (100 kb sliding window, sliding step size of 10 kb), and a total of 982 candidate intervals were screened (**Figure 3B**). These selected intervals

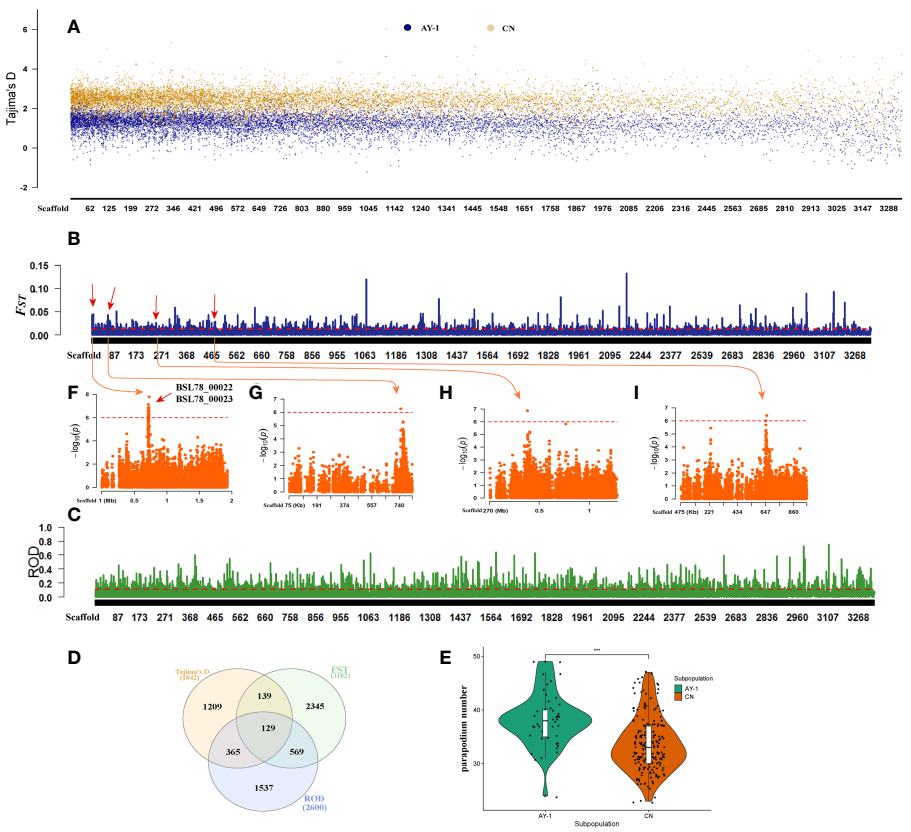

FIGURE 3 | Group selection analysis. **(A)** Tajima's D analysis, 1000kb non-overlapping sliding window. **(B)** Based on the F_{ST} analysis of the inter-population divergence test, the threshold line is the value corresponding to the top 95% of F_{ST}. **(C)** ROD analysis based on inter-group divergence test. **(D)** Tajima's D, F_{ST}, and ROD analyzed the intersection of selected genes. **(E)** Statistical analysis of quantitative characters of two subpopulations. **(F–I)** parapodium number GWAS analysis of local Manhattan map. The Scaffold starting with "MRZV" was replaced for the convenience of showing. The replacement method is Scaffold MRZV01000001.1-MRZV01003278.1 corresponding to Scaffold 1-Scaffold 3394 (**Supplementary Table 12**).

covered a total of 3182 genes in the genome annotation file. The results of Gene Ontology analysis of candidate genes showed that these genes were mainly enriched in biological process (BP) terms, such as regulation of inflammatory response; regulation of wound healing; negative regulation of inflammatory response; negative regulation of defense response; muscle cell cellular homeostasis; and inflammatory response (**Supplementary Figure 3**). Generally, the F_{ST} value was greater than 0.05 indicating that there was moderate or higher genetic differentiation among populations. In this study, 16 intervals with F_{ST} values greater than 0.05 were obtained, of which 7 intervals covered a total of 10 genes, such as BSL78_21603, BSL78_22159, and BSL78_27475. These genes are related to GTPase activity, GTP binding, ATP binding, DNA binding, and ATP-dependent microtubule motor activity, among others (**Supplementary Table 5**).

The reduction of diversity (ROD) index can measure the loss of polymorphism in a domesticated population relative to the corresponding wild population based on the difference in nucleic acid polymorphism π between these populations. Therefore, we adopted this index to evaluate the loss of nucleic acid polymorphisms in "AY-1" relative to the *A. japonicas* subpopulations in northern China (**Figure 3C**). After the π values of the two subpopulations were calculated using a 100 kb sliding window (with a sliding step size of 10 kb), the ROD value between the subpopulations was deduced, and the regions with ROD threshold values in the top 5% were selected as candidate intervals (ROD > 0.103), and a total of 1321 candidate intervals were obtained by screening. These selected intervals covered a total of 2600 genes in the genome annotation file. The results of Gene Ontology analysis showed that Candidate genes were mainly enriched in biological processes (BP) such as Proteasomal protein catabolic process, purine nucleoside catabolic process, and regulation of transcription by RNA polymerase III, etc. (**Supplementary Figure 4**). To improve the reliability of the selected regions and candidate genes of "AY-1" *A. japonicas*, we further selected Tajima's D, F_{ST}, ROD selected regions, and the overlapping genes obtained above, and finally obtained 255 regions and 129 genes (**Figure 3D**), which should be valuable for further study.

Through the phenotypic data analysis, it was found that the two subpopulations had a significant difference in the number of parapodia (**Figure 3E**). To explore whether the selected regions of "AY-1" were associated with this trait, we matched the parapodium number-associated sites obtained from the GWAS with the regions with F_{ST} and ROD thresholds in the top 5%. We found that 41 sites were located within the above-mentioned regions, of which 36 were located in the matching regions with F_{ST} thresholds within the top 5% (31 sites were located in Scaffold MRZV01000001.1: 710,001 bp-810,000 bp and the other 5 sites were in Scaffolds MRZV01000075.1, MRZV01000474.1, and MRZV01000269.1) (**Figures 3F–I**). The distribution of the other five loci matching the selected region of the ROD analysis was as follows, three SNP loci were located in Scaffold MRZV01000163.1, and the other two loci were located in Scaffold MRZV01000306.1 and Scaffold MRZV01000888.1, respectively (**Supplementary Table 6**).

Candidate Genes Associated With the Number of *A. Japonicas* Parapodia

The parapodia on the back of *A. japonicas* are hollow, cone-shaped, fleshy, thorn-like tissues, which function in breathing and exchanging information with the outside world. The number of parapodia has always been one of the most economically important traits of *A. japonicas*. In this study, the generalized linear model (GLM) and the linear mixed model (LMM) were used to perform a genome-wide association analysis on the number of parapodia. By using the threshold $-\log_{10P} > 6$, a total of 73 SNPs that were significantly associated with the number of parapodia were identified in the GLM association model (**Figure 4A**; **Supplementary Table 6**), QQ-plot shows that the fitting model is reasonable (**Supplementary Figure 5**). Using the same threshold, 16 significant loci were identified by the LMM model (**Supplementary Table 7**). Through mutual validation of the results of the two association models, we focused on the SNPs obtained in Scaffolds MRZV01000001.1, MRZV01000029.1, MRZV01000070.1, and MRZV01001092.1. These SNPs were associated with eight genes in the *A. japonicas* genome (**Figure 4A**; **Table 1**). Notably, the 31 SNPs located at MRZV01000001.1 were in genomic regions with selection signals (**Figure 3F**).

Linkage analysis of the upstream and downstream regions of the genome was performed with the above SNPs, and two LD blocks were identified in Scaffolds MRZV01000001.1 (711.7-723.7 kb) and MRZV01000070.1 (529-530 kb) (**Figures 4B, C**), of which the haplotype block located in Scaffold MRZV01000070.1 529-530 kb was located in the spacer region between the BSL78_03155 gene and the BSL78_03156 gene. Two related signal genes, namely, BSL78_00022 and BSL78_00023, were found in the haplotype block located at Scaffold MRZV01000070.1 711.7-723.7 kb. There were three non-synonymous significantly associated SNPs ($-\log_{10P} > 6$) in the BSL78_00022 gene as follows: SNP1 (G/A) located at Scaffold MRZV01000001.1 716,989 bp, which caused the amino acid to change from serine to phenylalanine; SNP2 (T/G) located at Scaffold MRZV01000001.1 714,882 bp, which caused the amino acid to change from glutamic acid to aspartic acid; and SNP3 (A/G) located at Scaffold MRZV01000001.1 713,704 bp, which caused the amino acid to change from alanine to valine (**Figure 4D**). The *A. japonicas* genome annotation file indicated that the BSL78_00022 gene encodes an enhancer-binding protein, and the eggNOG homology annotation indicated that its homologous gene is CTCF. CTCF is expressed in various structures of other species, and its function is mainly related to gene expression regulation and transcriptional regulation (Phillips and Corces, 2009). The qRT-PCR results showed that the expression levels of BSL78_00022 and BSL78_00023 were significantly higher in *A. japonicas* with multiple parapodia than in those with few parapodia (**Figure 4E**).

Candidate Genes Related to Growth Traits of *A. Japonicas*

The growth traits of *A. japonicas* are essential research topics in aquaculture breeding, and body weight, body wall weight, and

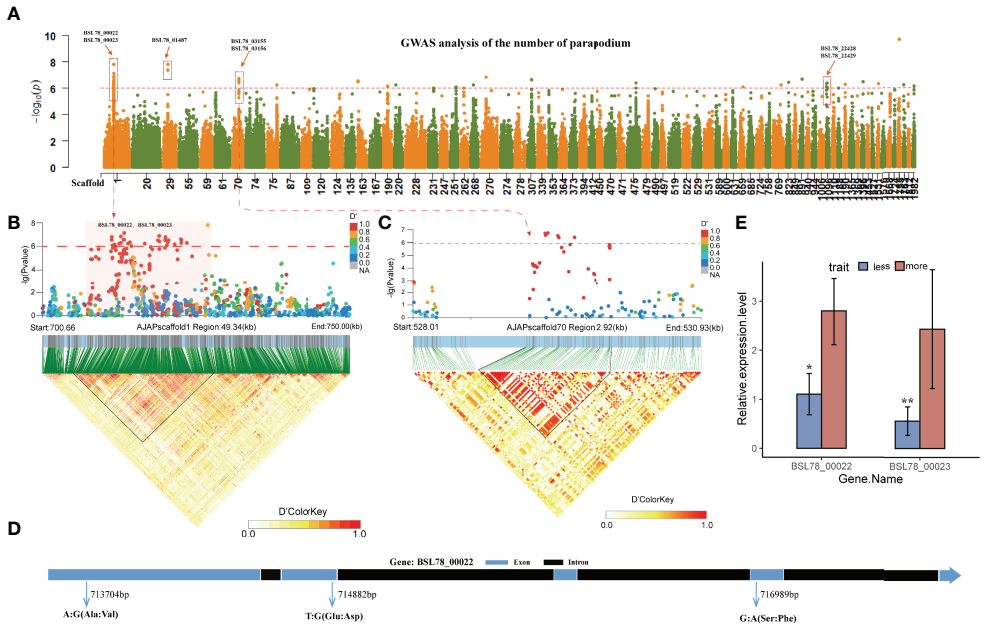

FIGURE 4 | GWAS analysis of the number of parapodium. **(A)** GWAS analysis of the number of parapodium, Only the scaffolds of the 200 SNPs with the maximum -$\log_{10P}$ values are shown (GLM model results). **(B)** A LD block on Scaffold 1 related to the number of parapodium. **(C)** A LD block on Scaffold 70 related to the number of parapodium. **(D)** Structure of gene BSL78_00022. **(E)** qRT-PCR results of gene BSL78_00022 and gene BSL78_00022. The Scaffold starting with "MRZV" was replaced for the convenience of showing. The replacement method is Scaffold MRZV01000001.1-MRZV01003278.1 corresponding to Scaffold 1-Scaffold 3394 (**Supplementary Table 12**). ** means p<0.01 in significance test. * means p<0.05 in significance test.

body wall production rate are important indicators to measure its growth. Pearson's correlation analysis showed that the body weight and body wall weight of *A. japonicas* were significantly positively correlated, but they were not correlated with the body wall production rate (**Supplementary Figure 6**).

Genome-wide association study on three traits was performed in this study with a generalized linear model (GLM) and linear mixed model (LMM), using a threshold of -$\log_{10P}$ > 6. Overall, 51 significantly associated SNPs were identified for body weight (**Figure 5A**; **Supplementary Table 8**) and 45 for body wall weight in the GLM association model (**Figure 5B**; **Supplementary Table 10**), QQ-plot shows that the fitting model is reasonable (**Supplementary Figures 7**, **8**). Using the same threshold, a total of 17 significant loci were identified in the LMM model related to body weight and 19 significant loci related to body wall weight (**Supplementary Tables 9**, **11**). After mutual verification of the association results, we focused on the genes corresponding to the SNPs associated with both models. A total of 21 associated genes were identified for body weight (**Table 1**), and a total of 16 were identified for body wall weight (**Table 1**). In addition, by comparison, we found six SNPs in Scaffold MRZV01000113.1 that were pleiotropically associated with body weight and body wall weight (**Figure 5B**), which provided a genetic explanation for the positive correlation between body wall weight and bodyweight of *A. japonicas*. These SNPs corresponded to the BSL78_04631 gene in the genome annotation file. Further analysis of the BSL78_04631 gene showed that there was a non-synonymous SNP (-$\log_{10P}$ > 6) significantly correlated with body weight and body wall weight in this gene, which was located at A/G of Scaffold MRZV01000113.1 278,613 bp, causing the amino acid to change from isoleucine to valine (**Figure 5C**). The qRT-PCR results showed that the expression level of BSL78_04631 in *A. japonicas* with large body weight and body wall was significantly higher than that in those with small body weight and body wall (**Figure 5D**).

In the association analysis of the body wall production rate of *A. japonicas*, a total of 13 significantly associated SNPs were identified by using the threshold -$\log_{10P}$ > 6 in the GLM association model (**Figure 5E**, **Supplementary Table 12**), QQ-plot shows that the fitting model is reasonable (**Supplementary Figure 9**). Using the same threshold, 10 significant loci were identified by the LMM model (**Supplementary Table 13**). The association results were mutually verified, and the two models were associated with two genes in the genome annotation file (**Table 1**). The LD linkage analysis was performed upstream and downstream of the significantly associated SNPs, and it was identified that there was one LD block in Scaffold MRZV01000033.1 771-773 kb (**Figure 5F**), which was completely located within the region of the BSL78_01694 gene.

DISCUSSION

Genetic Structure Analysis of the Cultured *Apostichopus Japonicas* in Northern China

Although the *Apostichopus japonicas* genome was published as early as 2017 (Zhang et al., 2017), no in-depth population-based

TABLE 1 | Candidate genes of 4 traits.

Traits	Scaffold	Position(bp)	SNPs number	Gene	Annotation
Parapodium number	MRZV01000001.1	711712-716998	16	BSL78_00022	Enhancer-binding protein
Parapodium number	MRZV01000001.1	719102-727071	15	BSL78_00023	Uncharacterized protein
Parapodium number	MRZV01000001.1	722766-727071	5	BSL78_00024	putative zinc finger protein
Parapodium number	MRZV01000029.1	333934-333944	2	BSL78_01487	putative sushi, von Willebrand factor type A
Parapodium number	MRZV01000070.1	529336-529636	6	BSL78_03155	putative coiled-coil domain-containing protein, partial
Parapodium number	MRZV01000070.1	529336-529637	6	BSL78_03156	putative short transient receptor potential channel 4 isoform X1
Parapodium number	MRZV01001092.1	10864-10894	5	BSL78_22428	putative dual-specificity protein phosphatase 3, partial
Parapodium number	MRZV01001092.1	10864-10894	6	BSL78_22429	Uncharacterized protein
weight&bodywall weight	MRZV01000113.1	277943-368824	6	BSL78_04631	putative pre-mRNA-splicing regulator WTAP
weight&bodywall weight	MRZV01000501.1	88015	1	BSL78_14328	Uncharacterized protein
weight&bodywall weight	MRZV01001374.1	209475	1	BSL78_24852	Putative peptide chain release factor 1-like, mitochondrial
weight&bodywall weight	MRZV01002271.1	20687	1	BSL78_29038	Putative galactosylceramide sulfotransferase-like
weight&bodywall weight	MRZV01002271.1	20687	1	BSL78_29039	Complement factor B
weight&bodywall weight	MRZV01000404.1	402599	1	BSL78_12322	Uncharacterized protein
weight&bodywall weight	MRZV01000404.1	402599	1	BSL78_12323	Uncharacterized protein
weight	MRZV01000114.1	683899	1	BSL78_04701	Fibrinogen-like protein A
weight	MRZV01000018.1	1068526-1068532	3	BSL78_00955	Uncharacterized protein
weight	MRZV01000209.1	121195	1	BSL78_07488	Uncharacterized protein
weight	MRZV01000209.1	121195	1	BSL78_07489	Proteasome subunit beta
weight	MRZV01000443.1	218169	1	BSL78_13248	Putative PAS domain-containing serine/threonine-protein kinase-like
weight	MRZV01000114.1	683899	1	BSL78_04699	Fibrinogen C-terminal domain-containing protein
weight	MRZV01000068.1	393713-395179	6	BSL78_03070	Putative egl nine-like 3
weight	MRZV01000068.1	393713-395179	6	BSL78_03071	Uncharacterized protein
weight	MRZV01000716.1	199987	1	BSL78_17759	Putative sister chromatid cohesion protein PDS5-like A
weight	MRZV01000938.1	46869-46892	2	BSL78_20744	Uncharacterized protein
weight	MRZV01000938.1	46869-46892	2	BSL78_20745	Uncharacterized protein
weight	MRZV01001525.1	300512	1	BSL78_25886	Putative ADP-ribosylation factor GTPase-activating protein 1
weight	MRZV01001525.1	300512	1	BSL78_25887	Uncharacterized protein
bodywall weight	MRZV01001303.1	11421	1	BSL78_24255	Complement factor B-2
bodywall weight	MRZV01001303.1	11421	1	BSL78_24256	Complement factor B-2
bodywall weight	MRZV01000545.1	42650	1	BSL78_15108	Uncharacterized protein
bodywall weight	MRZV01000062.1	545777	1	BSL78_02823	ZP domain-containing protein
bodywall weight	MRZV01000626.1	391978	1	BSL78_16429	Putative membrane metallo-endopeptidase-like 1 isoform X3
bodywall weight	MRZV01000626.1	391978	1	BSL78_16430	Putative neuronal acetylcholine receptor subunit alpha-7-like
bodywall weight	MRZV01001810.1	87273	1	BSL78_27366	Endonuclease-reverse transcriptase
bodywall weight	MRZV01001810.1	87273	1	BSL78_27367	Retrovirus-related Pol polyprotein from transposon
bodywall weight	MRZV01000645.1	110512	1	BSL78_16708	Putative alpha-1A adrenergic receptor-like
body wall production rate	MRZV01000033.1	77202-772969	3	BSL78_01694	Putative 28S ribosomal protein S36, mitochondrial-like isoform X2
body wall production rate	MRZV01000367.1	27665	1	BSL78_11556	Putative E3 ubiquitin-protein ligase HERC1-like

studies of population-wide selection and economically important traits have been reported on this species. In this study, whole-genome resequencing analysis was conducted on a total of 254 A. *japonicas* individuals collected from seven cultured populations including a new species of *A. japonicas*, "AY-1," which was used as the major research object, by the genetic resources of the major *A. japonicas* breeding areas in China. From the population structure analysis based on high-density SNP markers, we found that there was no difference in the population structure of *A. japonicas* cultured populations in different regions of northern China, while most individuals in the AY-1 population showed a different population structure from the CN population. This was associated with the AY-1 population being subjected to intentional artificial selection and having Russian *A. japonicas* ancestry, which was also confirmed by the phylogenetic tree and PCA results.

Genetic Diversity Analysis of the Cultured *Apostichopus Japonicas* in Northern China

In the comparative analysis of the two populations, we found that the genetic diversity (π) of the AY-1 population was lower than that of the CN population, which is in line with the genetic characteristics of domesticated populations, namely, the lower genetic diversity of populations subjected to artificial selection and domestication (Sonnante et al., 1994; Reif et al., 2005; Flint-Garcia, 2013; Smýkal et al., 2018). The linkage disequilibrium

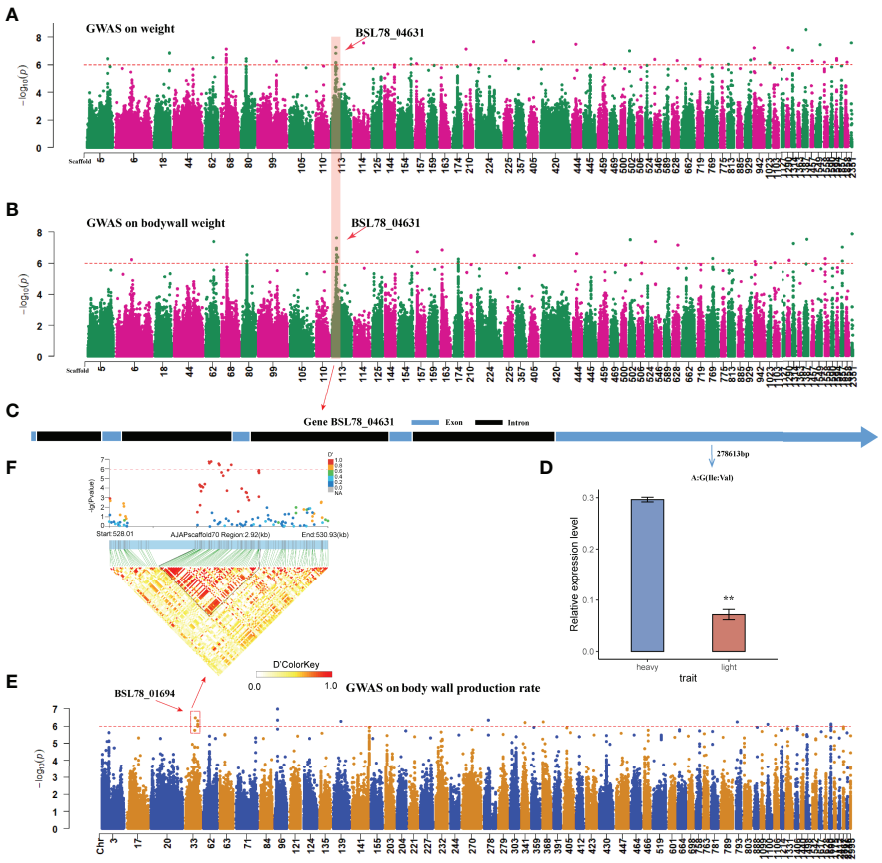

FIGURE 5 | Genome-wide association analysis of growth traits in Apostichopus japonicus. **(A)** Body weight GWAS analysis, Only the scaffolds of the 200 SNPs with the maximum -$\log_{10}P$ values are shown (GLM model results). **(B)** Body wall weight GWAS analysis, Only the scaffolds of the 200 SNPs with the maximum -$\log_{10}P$ values are shown (GLM model results). **(C)** Structure of gene BSL78_04631. **(D)** qRT-PCR results of gene BSL78_04631. **(E)** Genome-wide association analysis of body wall production rate in Apostichopus japonicus, Only the scaffolds of the 200 SNPs with the maximum -$\log_{10}P$ values are shown. **(F)** A LD block on Scaffold 33 related to body wall production rate. The Scaffold starting with "MRZV" was replaced for the convenience of showing. The replacement method is Scaffold MRZV01000001.1-MRZV01003278.1 corresponding to Scaffold 1-Scaffold 3394 (**Supplementary Table 12**). ** means p<0.01 in significance test.

(LD) analysis indicated that the LD attenuation distance of the AY-1 population was smaller than that of the CN population. The LD attenuation distance usually reflects the domestication relationship of a population to a certain extent: the LD attenuation distance of domesticated populations is longer. For example, the attenuation distance of wild oyster populations is 0.13 kb, while that of domesticated oyster populations is 0.35 kb (r^2 threshold = 0.2) (Hu et al., 2021); meanwhile, the LD attenuation distance of domesticated goldfish is significantly larger than that of common crucian carps (Chen et al., 2020). It is worth noting that, strictly speaking, the CN population is not a wild population, but has been subjected to unintentional artificial selection. Therefore, irrespective of whether we are referring to the AY-1 population or the CN population, the LD attenuation distance is shorter than that of other domesticated aquatic animals (For example, Crassostrea Gigas, Nile Tilapia, Large Yellow Croaker, scallop) (Cádiz et al., 2020; Hu et al., 2022; Kon et al., 2021; Wang et al., 2021). Therefore, we speculate that the gene recombination frequency and genetic diversity of the current cultured *A. japonicas* populations in China are generally high. Tajima's D is an important indicator to test the effect of positive selection within a population (Tajima, 1989; Prezeworski et al., 2005). In the AY-1 population, there were many regions where Tajima's D value was less than zero, and the values at most positions were smaller than those of the CN population. This indicated that AY-1 has more low-frequency allele sites, lower genetic diversity, and has been subjected to more positive selection.

Population Selection Analysis of the Cultured *Apostichopus Japonicas* in Northern China

For group selection candidate gene function analysis, we found that a large number of genes in the 982 candidate intervals obtained by F_{ST} analysis were enriched in pathways related to inflammation, inflammation regulation, and regulation of wound healing. Selected genes obtained by Tajima's D analysis in the AY-1 population were also enriched in the similar immune reaction-related term. These results indicated that the

immune function of the AY-1 population was different from that of the CN population. The genes' function in regions with F_{ST} values greater than 0.05 is mainly related to the biological processes involved in GTP and ATP. GTPase plays important role in energy supply (Sahlin et al., 1998), signal transduction (Narumiya, 1996), and protein biosynthesis (Hershey and Monro, 1966; Schimmel, 1993), and transport (Jones et al., 1995) *in vivo*. Therefore, we further speculate that the two subgroups may be different in these functions. Both F_{ST} analysis and ROD analysis were associated with the regulation of transcription by the RNA polymerase III pathway, RNA polymerase III plays a key functional role in the synthesis of a variety of small and stable RNAs and protein synthesis (Turowski and Tollervey, 2016). It is noteworthy that all three analyses are directly related to protein-related GO terms, such as secretory granule localization, proteasomal protein catabolic process, and negative regulation of protein homooligomerization. These results indicate that there are differences in protein synthesis, activation, and decomposition between the two subgroups, which is worthy of further investigation.

Genome-Wide Association Analysis of the Economic Traits in *Apostichopus Japonicas*

In the GWAS, we focused on the number of parapodia and growth traits (body weight, body wall weight, and meat yield) of *A. japonicas*. The parapodia of *A. japonicas* function in breathing and exchanging information with the outside world. The number of parapodia is an important indicator of the economic value of *A. japonicas*. In this study, 31 SNPs located in Scaffold MRZV01000001.1 were identified to be significantly correlated with the number of parapodia, and these sites were also in the top 5% of the candidate intervals in the F_{ST} analysis. This provides a genetic explanation for the positive selection to which the number of parapodia in *A. japonicas* was subjected in artificial breeding. The LD block analysis showed that these SNPs had a block in MRZV01000070.1 711.7–723.7 kb. In this block, we determined that the key genes for the number of parapodia in *A. japonicas* were BSL78_00022 and BSL78_00023. Of these two genes, BSL78_00022 encodes an enhancer-binding protein. One study showed that the enhancer-binding protein plays a key role in cell differentiation and cell proliferation (Umek Robert et al., 1991). In addition, a homolog of BSL78_00022, CTCF, is a highly conserved zinc finger protein, and it is involved in various regulatory functions including transcriptional activation/repression, insulation, and imprinting (Phillips and Corces, 2009; Ong and Corces, 2014). Therefore, we speculate that the BSL78_00022 gene plays a key role in the formation of *A. japonicas* parapodia. However, owing to the lack of experimental data to establish the link between this gene and the number of *A. japonicas* parapodia, its specific regulatory mechanism is still unclear.

In the association analysis of growth traits, six SNPs related to body weight and body wall weight pleiotropy were found in Scaffold MRZV01000113.1. The BSL78_04631 gene corresponding to these sites encodes the pre-mRNA-splicing regulator WTAP. WTAP has functions involving mRNA methylation, the spliceosome, and regulation of alternative mRNA splicing (Yang et al., 2015; Selberg et al., 2019), which also plays a role in promoting protein synthesis and cell growth (Villa et al., 2021). Therefore, we speculate that the BSL78_04631 gene plays a role in regulating the growth of *A. japonicas*. Meanwhile, we identified one LD block in Scaffold MRZV01000033.1 that was associated with the rate of body wall production rate. This block was completely contained in the BSL78_01694 gene, which was predicted to encode 28S ribosomal protein S36 and mitochondrial-like isoform X2. Ribosomal proteins are key proteins involved in the formation of ribosomes and are closely related to protein synthesis (Wilson and Nierhaus, 2005). Studies have shown that the body wall of *A. japonicas*. contains a large amount of collagen (Senadheera et al., 2020), and the gene BSL78_04694 is significantly correlated with the skin extraction rate of *A. japonicas*., which may indicate that it indirectly affects the collagen synthesis of the body wall of *A. japonicas*. by affecting the formation of ribosomes. In this study, other candidate genes associated with significantly related SNPs were also identified. However, because no gene transformation system has yet been established for *A. japonicas*, and some candidate genes have not been characterized, we could not determine the direct relationship between traits and gene functions within a short time. The data from this study provide a genetic basis for future gene function research and breeding of *A. japonicas*.

CONCLUSION

In this study, 254 *Apostichopus japonicas* individuals including the new species "AY-1" and six *A. japonicas* populations from major breeding areas of northern China were resequenced using high-throughput sequencing methods. The population structure analysis showed that the genetic diversity of *A. japonicas* was generally high and there was no difference in the population structure among the six cultured *A. japonicas* populations; they were divided into two subpopulations together with AY-1. The degree of linkage of alleles of the AY-1 population was high and this population was subject to more positive selection. In the population selection analysis, the selected intervals and genes of the AY-1 population were obtained, in which some of the candidate intervals were shown to be related to their economically important traits targeted by breeding, such as the number of parapodia. Functional analysis of the candidate genes showed that the two subpopulations had differences in terms of immune function, signal transduction, as well as protein synthesis, decomposition, activation, and transport. In the GWAS, 39 candidate genes for four economically important traits were obtained. Besides, we also verified the genes with non-synonymous SNPs; as a result, it was found that BSL78_00022 and BSL78_00023 are key genes for the number of parapodia in *A. japonicas*, and BSL78_04631 is a key gene associated with the growth traits of this species. This study provides new

insights into the genetic structure of *A. japonicas* in northern China and important information for the subsequent genetic analysis and breeding of this species.

DATA AVAILABILITY STATEMENT

The original contributions presented in the study are included in the article/**Supplementary Material**. Further inquiries can be directed to the corresponding authors.

ETHICS STATEMENT

The animal study was reviewed and approved by Ethics Committee of Dalian Ocean University. Written informed consent was obtained from the owners for the participation of their animals in this study.

AUTHOR CONTRIBUTIONS

JD and YC conceived and designed the experiments. CG, YL, XZ, JX, JS, YW, and LH performed the experiments. CG analyzed the data. CG wrote the paper. All authors read and approved the manuscript. All authors contributed to the article and approved the submitted version.

FUNDING

This work was supported by The National Key Research and Development Program of China (SY2018YD0901600), The National Natural Science Foundation of China (31772849), Liaoning Higher School Innovation Team Support Program (LT2019003), Dalian High-level Talent Innovation Support Program Project in 2020 (2020RD03).

ACKNOWLEDGMENTS

This work was supported by The National Key Research and Development Program of China (SY2018YD0901600), The National Natural Science Foundation of China (31772849), Liaoning Higher School Innovation Team Support Program (LT2019003), Dalian High-level Talent Innovation Support Program Project in 2020 (2020RD03). We thank Liwen Bianji (Edanz) (www.liwenbianji.cn) for editing the language of a draft of this manuscript.

SUPPLEMENTARY MATERIAL

The Supplementary Material for this article can be found online at: https://www.frontiersin.org/articles/10.3389/fmars.2022.948882/full#supplementary-material

REFERENCES

Abdelrahman, H., ElHady, M., Alcivar-Warren, A., Allen, S., Al-Tobasei, R., Bao, L., et al. (2017). Aquaculture Genomics, Genetics and Breeding in the United States: Current Status, Challenges, and Priorities for Future Research. *BMC Genomics* 18 (1), 191. doi: 10.1186/s12864-017-3557-1

Cádiz, M. I., López, M. E., Díaz-Domínguez, D., Cáceres, G., Yoshida, G. M., Gomez-Uchida, D., et al. (2020). Whole Genome Re-Sequencing Reveals Recent Signatures of Selection in Three Strains of Farmed Nile Tilapia (Oreochromis Niloticus). *Sci. Rep.* 10 (1), 11514. doi: 10.1038/s41598-020-68064-5

Chang, Y., Feng, Z., Yu, J. and Ding, J. (2009). Genetic Variability Analysis in Five Populations of the Sea Cucumber Stichopus (Apostichopus) Japonicus From China, Russia, South Korea and Japan as Revealed by Microsatellite Markers. *Mar. Ecol.* 30 (4), 455–461. doi: 10.1111/j.1439-0485.2009.00292.x

Chen, L., Li, Q. and Yang, J. (2008). Microsatellite Genetic Variation in Wild and Hatchery Populations of the Sea Cucumber (Apostichopus Japonicus Selenka) From Northern China. *Aquaculture. Res.* 39 (14), 1541–1549. doi: 10.1111/j.1365-2109.2008.02027.x

Chen, D., Zhang, Q., Tang, W., Huang, Z., Wang, G., Wang, Y., et al. (2020). The Evolutionary Origin and Domestication History of Goldfish (Carassius Auratus). *Proc. Natl. Acad. Sci.* 117 (47), 29775. doi: 10.1073/pnas.2005545117

Cui, Z., Hui, M., Liu, Y., Song, C., Li, X., Li, Y., et al. (2015). High-Density Linkage Mapping Aided by Transcriptomics Documents ZW Sex Determination System in the Chinese Mitten Crab Eriocheir Sinensis. *Heredity* 115 (3), 206–215. doi: 10.1038/hdy.2015.26

Ding, J. and Chang, Y. (2020). Advances in Conservation and Utilization of Echinodermata Germplasm Resources. *J. Dalian. Ocean. Univ.* 35 (5), 12. doi: 10.16535/j.cnki.dlhyxb.2020-157

Flint-Garcia, S. A. (2013). Genetics and Consequences of Crop Domestication. *J. Agric. Food Chem.* 61 (35), 8267–8276. doi: 10.1021/jf305511d

Gao, K., Wang, Z., Qiu, X., Song, J., Wang, H., Zhao, C., et al. (2019). Transcriptome Analysis of Body Wall Reveals Growth Difference Between the Largest and Smallest Individuals in the Pure and Hybrid Populations of Apostichopus Japonicus. *Comp. Biochem. Physiol. Part D: Genomics Proteomics* 31, 100591. doi: 10.1016/j.cbd.2019.05.001

Han, Q., Keesing, J. K. and Liu, D. (2016). A Review of Sea Cucumber Aquaculture, Ranching, and Stock Enhancement in China. *Rev. Fisheries. Sci. Aquaculture.* 24 (4), 326–341. doi: 10.1080/23308249.2016.1193472

Hershey, J. W. B. and Monro, R. E. (1966). A Competitive Inhibitor of the GTP Reaction in Protein Synthesis. *J. Mol. Biol.* 18 (1), 68–76. doi: 10.1016/S0022-2836(66)80077-3

He, X., Wu, F., Qi, H., Meng, J., Wang, W., Liu, M., et al. (2022). Whole-Genome Resequencing Reveals the Single Nucleotide Polymorphisms Associated With Shell Shape in Crassostrea Gigas. *Aquaculture* 547, 737502. doi: 10.1016/j.aquaculture.2021.737502

Hu, B., Tian, Y., Li, Q. and Liu, S. (2022). Genomic Signatures of Artificial Selection in the Pacific Oyster, Crassostrea Gigas. *Evolutionary. Appl.* 15, 618–630. doi: 10.1111/eva.13286

Jones, S., Litt, R. J., Richardson, C. J. and Segev, N. (1995). Requirement of Nucleotide Exchange Factor for Ypt1 GTPase Mediated Protein Transport. *J. Cell Biol.* 130 (5), 1051–1061. doi: 10.1083/jcb.130.5.1051

Kon, T., Pei, L., Ichikawa, R., Chen, C., Wang, P., Takemura, I., et al. (2021). Whole-Genome Resequencing of Large Yellow Croaker (Larimichthys Crocea) Reveals the Population Structure and Signatures of Environmental Adaptation. *Sci. Rep.* 11 (1), 11235. doi: 10.1038/s41598-021-90645-1

Li, Y., Wang, R., Xun, X., Wang, J., Bao, L., Thimmappa, R., et al. (2018). Sea Cucumber Genome Provides Insights Into Saponin Biosynthesis and Aestivation Regulation. *Cell Discov.* 4 (1), 29. doi: 10.1038/s41421-018-0030-5

Lyu, D., Yu, Y., Wang, Q., Luo, Z., Zhang, Q., Zhang, X., et al. (2021). Identification of Growth-Associated Genes by Genome-Wide Association Study (GWAS) and Their Potential Application in the Breeding of Pacific White Shrimp (Litopenaeus Vannamei). *Front. Genet.* 12, 465. doi: 10.3389/fgene.2021.611570

Narumiya, S. (1996). The Small GTPase Rho: Cellular Functions and Signal Transduction. *J. Biochem.* 120 (2), 215–228. doi: 10.1093/oxfordjournals.jbchem.a021401

Nei, M. and Chesser, R. K. (1983). Estimation of Fixation Indices and Gene Diversities. *Ann. Hum. Genet.* 47 (3), 253–259. doi: 10.1111/j.1469-1809.1983.tb00993.x

Ong, C.-T. and Corces, V. G. (2014). CTCF: An Architectural Protein Bridging Genome Topology and Function. *Nat. Rev. Genet.* 15 (4), 234–246. doi: 10.1038/nrg3663

Phillips, J. E. and Corces, V. G. (2009). CTCF: Master Weaver of the Genome. *Cell* 137 (7), 1194–1211. doi: 10.1016/j.cell.2009.06.001

Prezeworski, M., Coop, G. and Wall, J. D. (2005). The Signature Of Positive Selection On Standing Genetic Variation. *Evolution* 59 (11), 2312–2323. doi: 10.1111/j.0014-3820.2005.tb00941.x

Reif, J. C., Zhang, P., Dreisigacker, S., Warburton, M. L., van Ginkel, M., Hoisington, D., et al. (2005). Wheat Genetic Diversity Trends During Domestication and Breeding. *Theor. Appl. Genet.* 110 (5), 859–864. doi: 10.1007/s00122-004-1881-8

Ru, X., Zhang, L., Li, X., Liu, S. and Yang, H. (2019). Development Strategies for the Sea Cucumber Industry in China. *J. Oceanology. Limnology.* 37 (1), 300–312. doi: 10.1007/s00343-019-7344-5

Sahlin, K., Tonkonogi, M. and Söderlund, K. (1998). Energy Supply and Muscle Fatigue in Humans. *Acta Physiological Scandinavical* 162 (3), 261–266. doi: 10.1046/j.1365-201X.1998.0298f.x

Schimmel, P. (1993). GTP Hydrolysis in Protein Synthesis: Two for Tu? *Science* 259, 1264. doi: 10.1126/science.8446896

Selberg, S., Blokhina, D., Aatonen, M., Koivisto, P., Siltanen, A., Mervaala, E., et al. (2019). Discovery of Small Molecules That Activate RNA Methylation Through Cooperative Binding to the METTL3-14-WTAP Complex Active Site. *Cell Rep.* 26 (13), 3762–3771.e3765. doi: 10.1016/j.celrep.2019.02.100

Senadheera, T. R. L., Dave, D. and Shahidi, F. (2020). Sea Cucumber Derived Type I Collagen: A Comprehensive Review. *Mar. Drugs* 18 (9), 471. doi: 10.3390/md18090471

Smýkal, P., Nelson, M. N., Berger, J. D. and Von Wettberg, E. J. B. (2018). The Impact of Genetic Changes During Crop Domestication. *Agronomy* 8 (7). doi: 10.3390/agronomy8070119

Sonnante, G., Stockton, T., Nodari, R. O., Becerra Velásquez, V. L. and Gepts, P. (1994). Evolution of Genetic Diversity During the Domestication of Common-Bean (Phaseolus Vulgaris L.). *Theor. Appl. Genet.* 89 (5), 629–635. doi: 10.1007/BF00222458

Tajima, F. (1989). Statistical Method for Testing the Neutral Mutation Hypothesis by DNA Polymorphism. *Genetics* 123 (3), 585–595. doi: 10.1093/genetics/123.3.585

Tam, V., Patel, N., Turcotte, M., Bossé, Y., Paré, G. and Meyre, D. (2019). Benefits and Limitations of Genome-Wide Association Studies. *Nat. Rev. Genet.* 20 (8), 467–484. doi: 10.1038/s41576-019-0127-1

Turowski, T. W. and Tollervey, D. (2016). Transcription by RNA Polymerase III: Insights Into Mechanism and Regulation. *Biochem. Soc. Trans.* 44 (5), 1367–1375. doi: 10.1042/BST20160062

Umek Robert, M., Friedman Alan, D. and McKnight Steven, L. (1991). CCAAT-Enhancer Binding Protein: A Component of a Differentiation Switch. *Science* 251 (4991), 288–292. doi: 10.1126/science.1987644

Villa, E., Sahu, U., O'Hara, B. P., Ali, E. S., Helmin, K. A., Asara, J. M., et al. (2021). Mtorc1 Stimulates Cell Growth Through SAM Synthesis and M6a mRNA-Dependent Control of Protein Synthesis. *Mol. Cell* 81 (10), 2076–2093.e2079. doi: 10.1016/j.molcel.2021.03.009

Wang, H., Lv, J., Zeng, Q., Liu, Y., Xing, Q., Wang, S., et al. (2021). Genetic Differentiation and Selection Signatures in Two Bay Scallop (Argopecten Irradians) Breeds Revealed by Whole-Genome Resequencing Analysis. *Aquaculture* 543, 736944. doi: 10.1016/j.aquaculture.2021.736944

Wang, S., Wang, H., Zhao, L., Zhang, Y., Li, T., Liu, S., et al. (2022). Identification of Genes Associated With Carotenoids Accumulation in Scallop (Patinopecten Yessoensis). *Aquaculture* 550, 737850. doi: 10.1016/j.aquaculture.2021.737850

Wilson, D. N. and Nierhaus, K. H. (2005). Ribosomal Proteins in the Spotlight. *Crit. Rev. Biochem. Mol. Biol.* 40 (5), 243–267. doi: 10.1080/10409230500256523

Xu, D., Su, L. and Zhao, P. (2015). Apostichopus Japonicus in the Worldwide Production and Trade of Sea Cucumbers. *Developments. Aquaculture. Fisheries. Sci.* 2015 (39), 383–398.

Yang, Y., Sun, B.-F., Xiao, W., Yang, X., Sun, H.-Y., Zhao, Y.-L., et al. (2015). Dynamic M6a Modification and its Emerging Regulatory Role in mRNA Splicing. *Sci. Bull.* 60 (1), 21–32. doi: 10.1007/s11434-014-0695-6

Yang, Y., Wu, L., Wu, X., Li, B., Huang, W., Weng, Z., et al. (2020). Identification of Candidate Growth-Related SNPs and Genes Using GWAS in Brown-Marbled Grouper (Epinephelus Fuscoguttatus). *Mar. Biotechnol.* 22 (2), 153–166. doi: 10.1007/s10126-019-09940-8

Zhang, X., Sun, L., Yuan, J., Sun, Y., Gao, Y., Zhang, L., et al. (2017). The Sea Cucumber Genome Provides Insights Into Morphological Evolution and Visceral Regeneration. *PloS Biol.* 15 (10), e2003790. doi: 10.1371/journal.pbio.2003790

Zhao, G., Zhao, W., Han, L., Ding, J. and Chang, Y. (2020). Metabolomics Analysis of Sea Cucumber (Apostichopus Japonicus) in Different Geographical Origins Using UPLC–Q-TOF/MS. *Food Chem.* 333, 127453. doi: 10.1016/j.foodchem.2020.127453

Zhou, Y., Fu, H.-C., Wang, Y.-Y. and Huang, H.-Z. (2022). Genome-Wide Association Study Reveals Growth-Related SNPs and Candidate Genes in Mandarin Fish (Siniperca Chuatsi). *Aquaculture* 550, 737879. doi: 10.1016/j.aquaculture.2021.737879

Conflict of Interest: The authors declare that the research was conducted in the absence of any commercial or financial relationships that could be construed as a potential conflict of interest.

Publisher's Note: All claims expressed in this article are solely those of the authors and do not necessarily represent those of their affiliated organizations, or those of the publisher, the editors and the reviewers. Any product that may be evaluated in this article, or claim that may be made by its manufacturer, is not guaranteed or endorsed by the publisher.

frontiers | Frontiers in Marine Science

ORIGINAL RESEARCH
published: 22 July 2022
doi: 10.3389/fmars.2022.918158

Sea Ranching Feasibility of the Hatchery-Reared Tropical Sea Cucumber *Stichopus monotuberculatus* in an Inshore Coral Reef Island Area in South China Sea (Sanya, China)

OPEN ACCESS

Edited by:
Marie Antonette Juinio-Meñez, University of the Philippines Diliman, Philippines

Reviewed by:
Anselmo Miranda-Baeza, State University of Sonora, Mexico
Luis R. Martinez-Cordova, University of Sonora, Mexico
Nadia Palomar Abesamis, Silliman University, Philippines

***Correspondence:**
Fei Gao
gaofeicas@126.com

Specialty section:
This article was submitted to Marine Fisheries, Aquaculture and Living Resources, a section of the journal Frontiers in Marine Science

Received: *12 April 2022*
Accepted: *06 June 2022*
Published: *22 July 2022*

Citation:
Xu Q, Wu P, Huang D, Xiao Y, Wang X, Xia J, Ma W, Gao F and Wang A (2022) Sea Ranching Feasibility of the Hatchery-Reared Tropical Sea Cucumber Stichopus monotuberculatus in an Inshore Coral Reef Island Area in South China Sea (Sanya, China). Front. Mar. Sci. 9:918158. doi: 10.3389/fmars.2022.918158

Qiang Xu, Peilin Wu, Duanjie Huang, Yulin Xiao, Xinyuan Wang, Jingquan Xia, Wengang Ma, Fei Gao* and Aimin Wang

State Key Laboratory of Marine Resource Utilization in South China Sea, College of Marine Sciences, Hainan University, Haikou, China

Sea ranching of tropical edible sea cucumbers is an effective way to relieve the overfishing stress on their natural resources and protect the coral reef ecosystem, yet only a few species have been applied in the sea ranching practice based on hatchery-reared juveniles around the world. In this study, an 8-month (April to December) sea ranching study for hatchery-reared edible sea cucumber *Stichopus monotuberculatus* juveniles was carried out at a tropical coral reef island area in Sanya, China. Several growth performance indexes and basal nutritional components were monitored. Results revealed that the sea cucumbers had a growth rate of 0.35~0.78 mm day^{-1} during the experimental period, reaching 15.9 cm long before winter. The weight gain reached 491.13% at the end, and most sea cucumbers were able to grow to the commercial size (over 150 g WW) in the first year of sea ranching. The overall specific growth rate (SGR) and survival rates were 0.73 and 27.5%. Most of the death occurred in the first month after release (25.0%–37.5%), and this is probably due to inadaptation to the sudden change of the environment from the hatchery to the wild, which is proved by the remarkable decrease in nutritional indexes (amino acids, total lipid, and crude protein). Stable isotope and lipid biomarkers revealed that the food source mainly comes from water deposits (with microbes), *Sargassum sanyaense* seaweed debris, phytoplankton, and coral mucus-derived organics. The study proved the feasibility of the sea ranching of the hatchery-reared *S. monotuberculatus* juveniles in the tropical coral reef island area. Also, it is highly recommended that appropriate acclimation operation before release should be carried out to improve the survival rate of this species.

Keywords: *Stichopus monotuberculatus*, growth performance, nutritional quality, food source composition, sea ranching

1 INTRODUCTION

In recent years, the market demand for sea cucumbers is increasing due to their high nutritional and medicinal value (Eriksson and Clarke, 2015). Meanwhile, wild sea cucumber resource has shown continuous depletion because of overfishing (Pakoa and Bertram, 2013). Therefore, the sea ranching of high-value sea cucumbers developed rapidly since the early 21st century, especially in China (Chen, 2004; Eriksson and Clarke, 2015). In addition to the temperate species of *Stichopus japonicus*, which is widely cultured in North China, most of the high-valued tropical sea cucumber species exploitation relies on wild catching around the world, such as *Stichopus monotuberculatus*, *Stichopus horrens*, *Thelenota ananas*, and *Holothuria fuscogilva* (Purcell et al., 2018). Only *Holothuria scabra* is widely cultured in the pond or the coastal area. The development of tropical sea cucumber sea ranching is mostly restricted by the lack of techniques (Purcell et al., 2012; Zamora et al., 2018). There is an urgent need to develop sea ranching techniques for new sea cucumber species to promote the production of artificial released tropical sea cucumber population and subsequently relieve the fishery stress on other depleted wild species.

S. monotuberculatus is a tropical detritus-feeding sea cucumber species with high economic value. It prefers sandy sediment, fragmented coral, coral rubble, and seagrass bed between the depth of 0 and 30 m (Conand, 1993; Desurmont, 2003). The hatchery technique has been developed for years (Hu et al., 2010). Pond culture mode used to be tested on a small scale, but the risk of mass mortality caused by extremely low water temperature (below 16°C) was encountered during occasional cold waves in winter. Sea ranching is the most feasible way to solve the problem, yet many theoretical and practical aspects are still not clear, such as appropriate density, juvenile size, and release procedure.

S. monotuberculatus is a native species in the coral reef area in the southern part of Hainan Island and the Sansha area, China (Hu et al., 2010). However, since 2000, the natural resource depleted remarkably due to overfishing. Aiming to recover the sea cucumber resource and develop sea ranching technique, we carried out an 8-month study at Wuzhizhou Island, an inshore coral reef island in the southern part of Hainan Island. More than 3,000 hatchery-reared *S. monotuberculatus* juveniles were released, and the growth index, survival rate (SR), and nutrition accumulation were evaluated. Seasonal diet composition was also quantified to understand the food availability in the habitat, using a lipid biomarker and stable isotope method. The sea ranching feasibility of the hatchery-reared juveniles in the tropical coral reef area was verified based on these results.

2 MATERIALS AND METHODS

2.1 Study Area

Wuzhizhou Island is located in the southern part of Hainan Island (the South China Sea, 18°18′30″N–109°45′40″E) (**Figure 1**) with an area of 1.48 km^2. It has a tropical monsoon climate, with the dry season from November to April and the rainy season from May to October (Huang et al., 2020). It is affected by seasonal wind and waves, especially the upwelling event on the eastern coast of Hainan Island during summer, which brings cool water to keep the corals away from a high-temperature threat (Huang et al., 2003; Li et al., 2015). The island is also a famous tourism site with site-seeing and scuba diving projects. The sea area is well protected by the tourism company, and the collection of all the marine creatures is banned except for scientific research purposes.

2.2 Juvenile Acquisition, Transportation, and Release

The experimental area was set in the northern part of Wuzhizhou Island, which is covered with fine sand, coral reef, and volcanic rocky artificial reefs (**Figures 1**, **2A**). A total of over 3,000 sea cucumber juveniles (wet weight 17.36 ± 4.20 g, body length 5.6 ± 1.3 cm) were acquired from a hatchery in Wenchang (Hainan Province) in April 2019 (**Figure 2B**). The water temperature and salinity in the hatchery were 25.2°C and 32–33 ppt, respectively, and those in the sea ranching area were 26.7°C and 33 ppt, respectively. All the juveniles were carefully packed in plastic bags with water and oxygen, put in cool boxes with ice, and transported from the hatchery to the sea ranching area within 5 h. On the boat, the sea cucumbers were put into soft chinlon mesh bags (20 × 30 cm, 120 ind. each) and taken to the sea bottom by scuba divers. A stone was placed on each bag (mouth opened), and the juveniles crawled out by themselves in 2 days (**Figure 2C**).

2.3 Growth Performance and Survival Rate Monitor

The growth index was monitored periodically (May, June, July, September, October, and December 2019). The water temperature and salinity at a depth of 1 m were also measured by a multi-parameter sonder (YSI—Model 6600 V2, Xylem, USA) from January to December 2019 (**Figure 3**). At each month, samples (n = 4–6) were collected from the released population by scuba divers and immediately taken in water to the laboratory on the island to measure the wet weight (including total and body wall) and the body length. The total length (TL) from mouth to anus was measured to the nearest 0.1 cm. Before being weighted, gentle pressure was applied to the sea cucumber body to enable the expulsion of the maximum amount of water from the respiratory tree. The body surface was blotted dry with a paper towel, and the total weight (TW) was recorded (Sánchez-Tapia et al., 2018). Then the sea cucumber was dissected, and the body wall was also weighted.

For the SR evaluation, eighty sea cucumber juveniles were selected from the total released population in April 2019 and placed into two steel-frame bottom culture cages set on the same sea area (2.0 × 2.0 × 0.6 m, area 4 m^2; 40 ind·. each, density 10 ind· m^{-2}). The cages are covered with a plastic net (mesh size 0.5 cm) except for the bottom so that sea cucumbers

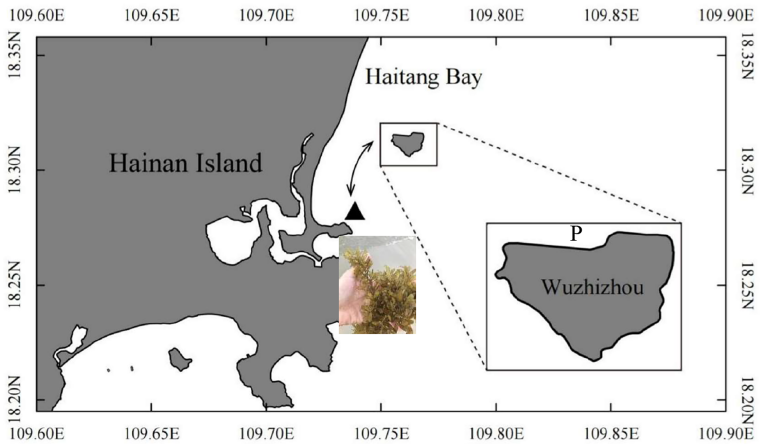

FIGURE 1 | Sea cucumber *Stichopus monotuberculatus* sea ranching area at Wuzhizhou Island, Hainan Province, China. P, juvenile release site; ▲, the *Sargassum sanyaense* seaweed bed (photographed by Qiang Xu). The arrow shows the tidal current direction.

can live directly on the seafloor. To prevent escape, a circle of soft nylon net curtain (mesh size 0.5 cm, 20 cm high) was fixed on the lower part of the cage, folded inside, and then buried into the sediment. Several coral rocks were placed into the cage as the shelter. The cages were anchored on the seafloor with nylon ropes. In May, July, and October 2019, the SR was calculated by counting sea cucumbers observed in the cages. During the counting process, all the rocky substrates in the cages were not moved and checked so as to avoid the destruction of the habitat and possibly hurting the sea cucumbers. Unfortunately, one of the cages was destroyed in a storm in late October. At the end of the experiment in December, all the rocks in the remaining cages were moved out, the surviving ones were counted, and the cage was also carefully checked, so the data reflect the overall SR of the 8-month study.

2.4 Sample Collection for Nutrition and Food Source Analyses

The initial sea cucumber samples (n = 5) were collected from the hatchery prior to mass release in April 2019. During the field

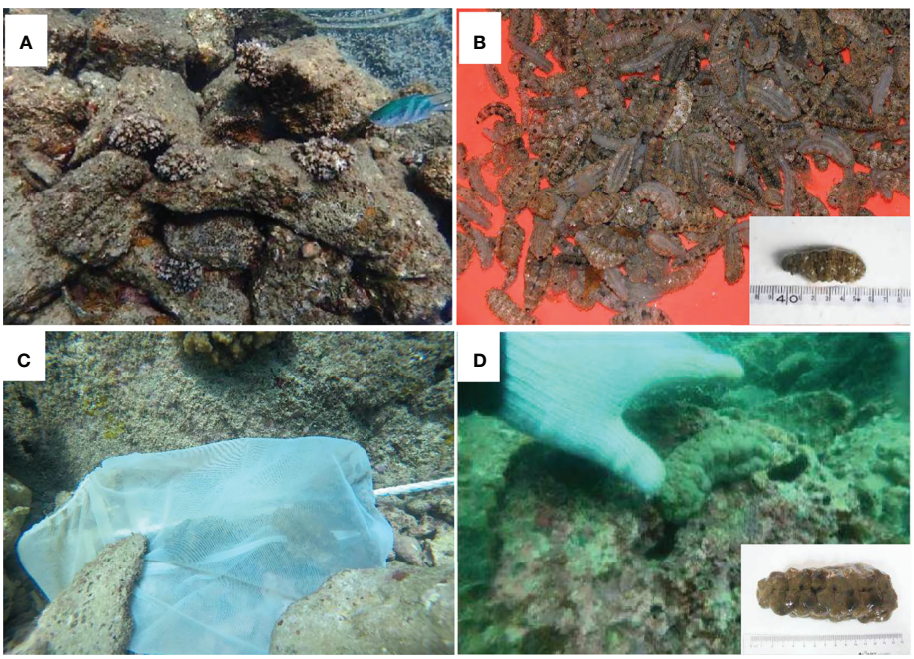

FIGURE 2 | The deployed volcano rocky artificial reefs with settled corals **(A)**. Sea cucumber *Stichopus monotuberculatus* juveniles in the hatchery **(B)**. The self-release mesh bag with juveniles in it **(C)**. A sea-ranched individual 8 months after release **(D)**. (photographed by Qiang Xu).

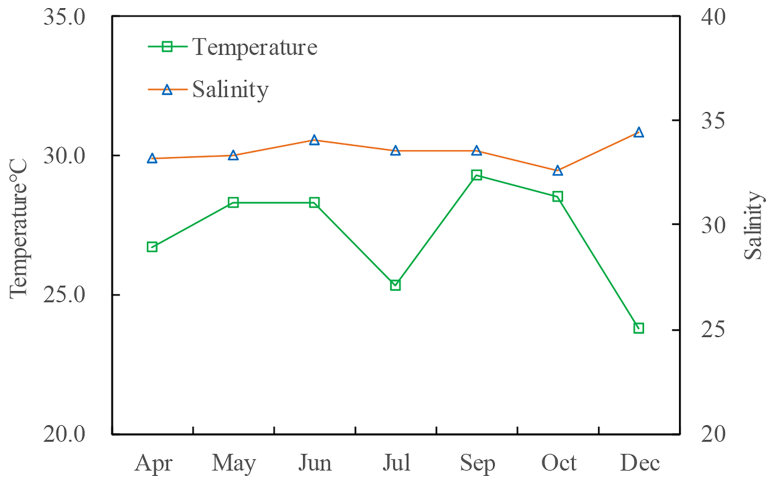

FIGURE 3 | Mean values of the temperature and salinity of the sea ranching area in 2019.

study, samples (n = 3–5) were collected by divers in May, July, October, and December. In the laboratory, sea cucumbers were dissected, and the body wall was washed with ultrapure water and then frozen and freeze-dried for 48 h. The samples were pulverized using a glass mortar and pestle and stored under the dry condition at −20°C for further analysis.

After referring to previous studies on other sea cucumber species (*Apostichopus japonicus*, Sun et al., 2013) and the character of the coral reef habitat (Coffroth, 1984; Wild et al., 2004; Wild et al., 2005), five potential food sources were selected from the pelagic and benthic habitats: phytoplankton, benthic microalgae, water deposit, *Sargassum sanyaense*, and coral mucus. Net-towed phytoplankton samples (mesh size 76 μm) were obtained by hauling them horizontally in the water. Benthic microalgae were collected using an *in situ* cultivation method: a polythene net was placed on a coral rock at a shallow area (3–5-m depth) with sufficient sunlight. After 5–10 days, the net was taken back and cleaned with filtered seawater. The cleaning water was filtered, and the microalgae sample was collected on Whatman GF/F glass-fiber filters (pre-combusted under 450°C for 4 h). Water deposit samples (n = 3) were acquired with three polythene cylinder trappers (Φ = 30 cm, 30-cm height), which were deployed for 5 days on the bottom. After the samples were taken back to the lab, the deposit was resuspended and filtered on pre-combusted Whatman GF/F glass-fiber filters for further analysis. Preliminary fatty acid biomarker results indicated brown algae organic source in the sea cucumber's diet, but field investigation only found two small Phaeophyta species, *Padina* sp. and *Turbinaria ornata*, with tough blades and sporadic distribution. Considering their extremely low biomass and difficulty in detritus release, they are unlikely to be the diet source for the sea cucumbers. It is reported that there is a seasonal *Sargassum* sp. seaweed bed at the opposite coastal area 3~4 km from the island (Li et al., 2020), and a supplemental investigation on this area in April 2021 was performed, revealing a *Sargassum* seaweed bed of about 30 ha with *S. sanyaense* as the dominant species in high biomass (3.7 kg m^{-2}, **Figure 1**, site ▲). The algae were sampled and added to the potential food sources. The specific isotope values of coral mucus come from the reference (Naumann et al., 2010).

2.5 Nutrition Composition Analysis

2.5.1 Crude Protein and Total Lipid

The content of crude protein was determined by the Kjeldahl method (AOAC, 1990). Lipids were extracted using a modified Folch extraction procedure (Folch et al., 1957; Parrish, 1999).

2.5.2 Amino Acid Analysis

Amino acid analysis was carried out based on literature methods (Block et al., 2016): the sample was hydrolyzed at 110°C for 22 h with 6 mol/L of HCl; following hydrolysis, 1 ml of hydrolyzate was withdrawn and evaporated to dryness under vacuum at 45°C to remove HCl. The hydrolyzate was dissolved in 5 ml of 0.02 mol/L of HCl, then centrifuged at 5,000 rpm, and filtered. Supernatant measuring 1 μl was used for amino acid analysis. Detection wavelengths were set at UV 570 and 440 nm. The amino acids' identity and quantity were assessed by comparison with retention times and peak areas of standard amino acids. The amino acid score was calculated using the following formula: amino acid score = amount of amino acid per test protein (mg/g)/amount of amino acid per protein in reference pattern (mg/g) × 100.

2.5.3 Fatty Acid Composition Analysis

Extracted total lipid was evaporated to near dryness under a gentle nitrogen stream. Fatty acid methyl esters (FAMEs) were prepared by esterification using 2% sulfuric acid methanol as described by (Xu, 2007). Gas chromatography (GC) was performed with Agilent Technologies (Santa Clara, CA, USA) 6890N GC equipped with a DB-FFAP capillary column (30 m × 0.25 mm × 0.25 μm). Helium was the carrier gas (99.999%, purity). The heating program consisted of an initial

temperature of 100°C, holding at 100°C for 5 min, a temperature increase to 240°C at a rate of 4°C/min, and then holding at 240°C for 15 min. The inlet temperature was 250°C, and the detector temperature was 250°C. Individual components were identified using mass spectral data and by comparing retention time data with those obtained for authentic and laboratory standards (Cod liver oil FAMEs (C2294-5G), Sigma-Aldrich, Germany). The peak area was quantified and expressed as a percentage of total fatty acids.

2.6 Stable C and N Isotope Analysis

The water deposit and benthic microalgae samples were acidified by exposing the filters to HCl vapor for 12 h to remove inorganic carbonates before analysis. $\delta^{15}N$ and $\delta^{13}C$ values of the sea cucumber and potential food sources were determined by a stable isotope ratio mass spectrometry (IRMS; Delta V Advantage, Thermo Fisher, Waltham, MA, USA) combined with an element analyzer (HT2000, Thermo, USA). About 5 mg of powdered samples was measured by the Millionth Scale (P6, Mettler, Schwerzenbach, Switzerland) and wrapped in a tin capsule. Then the capsule was closed with tweezers and placed into the automatic sampler of the elemental analyzer. The encapsulated samples were combusted and reduced at 1,020°C, and the flow rate of He (99.999%, purity) was 50 ml/min in a reactor and converted into CO_2 and N_2. Water was subsequently removed by anhydrous $Mg(ClO_4)_2$. The resulting gas was separated on a carbon sieve GC column (70°C) and then gradually entered into the ion source of the IRMS.

Results of the isotope ratios were expressed in standard δ-unit notation, as follows:

$$\delta X = \left[\left(R_{sample} / R_{standard}\right) - 1\right] \times 1{,}000‰$$

where *X* is ^{13}C or ^{15}N and *R* is ^{13}C:^{12}C ratio for C or ^{15}N:^{14}N ratio for N. The values were reported relative to the Vienna Pee Dee Belemnite (PDB) standard for C and air N_2 for N.

2.7 Statistical Analysis

2.7.1 Growth Index Estimation

The calculation of size growth rate (GR; mm day^{-1}), specific GR (SGR; % day^{-1}), and weight gain (WG; %) are based on samples from the released population, whereas the SR (%) was quantified by counting the individuals in the cages. The growth index was calculated at four months (May, July, October, and December). Growth estimations are determined using the following expressions (Sánchez-Tapia et al., 2018):

$$\text{Size growth rate}: GR(\text{mm day}^{-1}) = (L_i - L_1) / T_i,$$

$$\text{Specific growth rate}: SGR(\%\,\text{day}^{-1}) = 100 \times (\ln W_i - \ln W_1) / T_i, \text{ and}$$

$$\text{Weight gain}: WG(\%) = 100 \times (W_i - W_1) / W_1,$$

where L_1 and L_i are the average body lengths at the beginning (April 2019) and the course of the evaluation, respectively; W_1 and W_i are the TW of juveniles at the beginning and the course of the experiment, respectively; and T_i is the length of the experiment in days.

The SR was expressed as follows:

$$SR(\%) = (N_i \times 100) / N_1,$$

where N_i is the number of juveniles observed in the cages and N_1 is the number of juveniles at the beginning of the experiment ($N_1 = 40$).

The result was presented as mean values ± SD. The difference in the months of the content of $\delta^{13}C$, $\delta^{15}N$, amino acids, crude protein, total lipid, and relative percentages of the total pool of fatty acids was tested with one-way ANOVA. Significant differences ($p < 0.05$) were determined by using Tukey's honestly significant difference (HSD) post-hoc test.

2.7.2 Food Composition Calculation

The Bayesian mixed-model SIMMR of R (version 4.1.2) was used for the evaluation of the relative contribution of each food source to the sea cucumber (Parnell et al., 2013). Compared with the software "Isosource," SIMMR can incorporate supplementary features such as uncertainties, concentration dependence, and a greater quantity of sources (Lionel et al., 2018). For stable C and N isotopes, the average fractionation effects of 1‰ for ^{13}C (McClelland and Valiela, 1998; McCutchan Jr. et al., 2003; Sun et al., 2013) and 3.4‰ for ^{15}N (Sherwood & Rose, 2005; Carlier et al., 2007) were used to correct stable isotope shifts for each trophic level. By using the Markov chain Monte Carlo (MCMC) method, the model was run for 10,000 iterations with a burn rate of 1,000 to obtain the posterior distribution (Jiménez-Arias et al., 2020). SIMMR package checks whether the model works normally through the Gelman–Rubin diagnosis (Saccò et al., 2019). The results show that the model converges and runs normally. The average standard error of the mean for replicates was 0.11‰ for $\delta^{13}C$ and 0.15‰ for $\delta^{15}N$ (Sherwood & Rose, 2005).

3 RESULTS

3.1 Growth and Survival Rate of *Stichopus monotuberculatus*

During the study period, the salinity and water temperature varied at 32.58°C–34.44°C and 23.76°C–29.31°C, respectively (**Figure 3**). A temperature drop of 3°C (28.31°C to 25.33°C) was observed from June to July due to the impact of the upwelling event on the east coast of Hainan Island.

During the routine investigation, the sea cucumbers' activity showed a remarkable diurnal rhythm. Using an underwater time-lapse camera, we found that most of them hide in the reef during the daytime and come out to feed at night. The SR of juveniles in cage 1 over 8 months was 27.5%

(**Table 1**). The SR of cage 2 in December was not available because it was destroyed by a typhoon storm in late October, so the SR in cage 2 over 6 months was 52.5%. The death rate of juveniles was 25.0%–37.5% in the first month after release (April to May), which is much higher than in other months.

The juvenile's mean length increased from 5.6 ± 1.3 to 15.9 ± 2.2 cm at the end, and the total body weight was from 17.36 ± 4.20 to 102.62 ± 50.76 g (**Figures 2D**, **4**). After 8 months' growth, the maximum length and weight of adult individuals were 177.86 g and 19.0 cm, respectively. The final wet weight was about 4.9 times its initial value (WG 491.13%, **Table 1**). The highest WG occurred between October and December, but the GR showed an individual variation. The body wall wet weight grew from 12.94 ± 2.24 to 96.11 ± 20.91 g, 7.43 times the initial (**Figures 4A, B**). The juveniles grew faster from April to July (GR 0.78–0.73 mm day^{-1}; SGR 1.08–0.94% day^{-1}) compared to other months (GR 0.35–0.42 mm day^{-1}; SGR 0.48–0.73% day^{-1}), whereas a slight weight loss occurred from July to October (**Table 1**). SGR reached its lowest level in October (0.48% day^{-1}) but recovered in December (0.73% day^{-1}).

TABLE 1 | Survival rate and growth performance of sea ranched *Stichopus monotuberculatus* in 2019 (n = 4–6 for GR, WG, and SGR).

	May	Jul	Oct	Dec
SR_1 (%)	62.5	45.0*	57.5	27.5
SR_2 (%)	75.0	57.5	52.5	–
GR (mm day^{-1})	0.78	0.73	0.35	0.42
WG (%)	54.03	166.88	155.93	491.13
SGR (% day^{-1})	1.08	0.94	0.48	0.73

GR, WG, and SGR were based on samples outside of the cages.
$SR_{1,2}$, the survival rate of sea cucumbers in cages 1 and 2; GR, daily length growth rate; WG, weight gain based on the initial sample; SGR, specific growth rate; –, SR_2 in Dec was not available because cage 2 was destroyed by a storm in late October.
**SR_1 in July was lower than in Oct because some of the sea cucumbers hid deep in the reef and could not be observed.*

3.2 Nutritional Composition

3.2.1 Crude Protein and Total Lipid

The crude protein content in the body wall of *S. monotuberculatus* ranged from 18.13 ± 1.19 to 28.87 ± 1.82 g/100 g, and total lipid content was from 1.98 ± 0.04 to 2.95 ± 0.10 g/100 g (**Table 2**). During the first month after release, both the protein and lipid contents decreased significantly ($p< 0.05$). After that, the crude protein and lipid accumulated gradually, with the highest value reached in December and July, respectively.

3.2.2 Amino Acid Profiles

There were 16 amino acids detected in the body wall (**Table 3**). The total content of amino acids was 22.3 ± 0.97~29.19 ± 1.77 g/100 g throughout the experimental period, with the essential amino acid content varying from 4.67 ± 0.24 to 5.94 ± 0.36 g/100 g. Of all the amino acids, Gly and Glu are the most abundant, which accounted for 16.40%~18.10% and 16.30%~16.80% of the content, respectively. As for the eight essential amino acids for humans, seven of them were detected in the sea cucumber body, including Thr, Val, Ile, Leu, Phe, Lys, and Arg, whereas Trp was absent. Thr was the dominant essential amino acid, with the content ranging from 1.18 ± 0.09 to 1.53 ± 0.08 g/100 g. Surprisingly, all amino acid levels decreased during the first month after release, which is in line with the results of crude protein and total lipid content. From May to December, total and essential amino acid contents increased gradually, which is in accordance with the crude protein dynamic.

3.2.3 FATTY ACID COMPOSITION

In this study, 33 fatty acids from 14 to 22 carbons were detected in the sea cucumber's body wall (**Table 4**). Polyunsaturated fatty acids (PUFAs) were the dominant lipid class in all months, followed by monounsaturated fatty acids (MUFAs) and saturated fatty acids (SFAs). Branched-chain fatty acids (BFAs) were the lowest. SFAs were mainly composed of C16:0 and C18:0 and accounted for more than half of the total SFAs (**Table 4**). In December, the content of C16:0 was significantly lower than that in other months ($p< 0.05$), and the C18:0 percentage increased gradually after April ($p< 0.05$). The dominant MUFA was C20:1(n−9), which accounted for over 40% of the total MUFAs, and was followed by C22:1(n−9); both dropped to the lowest level in July (**Table 4**). The percent of C18:1(n−9) dropped remarkably after the release of the juveniles (from 4.87% to 0.66%). C20:4(n−6) was always the dominant PUFA throughout the experimental period, which accounted for over 40% of total PUFA. The percent of C20:4(n−6) reached the lowest in July and then increased gradually. EPA [C20:5(n−3)] content increased from 0.93% before release to 3.44% in the end, whereas DHA [C22:6(n−3)] content varied from 2.68% to 3.62% and peaked in May (**Table 4**).

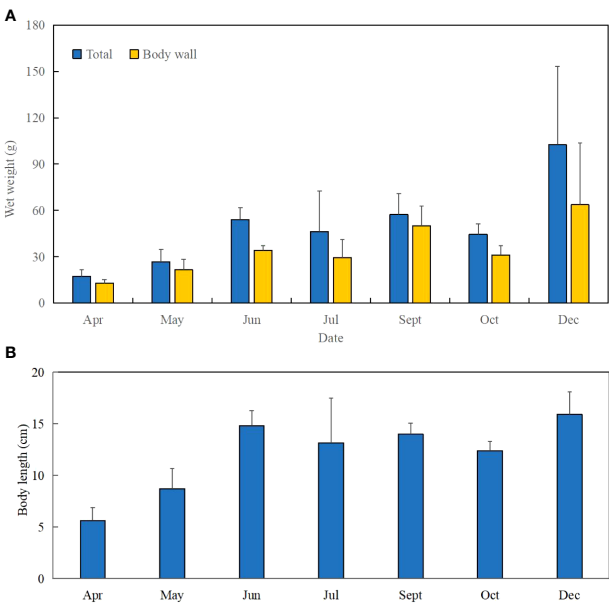

FIGURE 4 | Increase of wet weight and body length of *S. monotuberculatus* from April to December 2019. **(A)** Change of wet weight of *S. monotuberculatus* from April to December 2019. **(B)** Change of body length of *S. monotuberculatus* from April to December 2019.

TABLE 2 | Crude protein and total lipid of *Stichopus monotuberculatus* body wall from April to December 2019.

	Apr.	May	Jul.	Oct.	Dec.
Crude protein (g/100 g)	27.97 ± 0.81^{a}	18.13 ± 1.19^{b}	21.67 ± 3.04^{bc}	25.2 ± 2.95^{ac}	28.87 ± 1.82^{a}
Total lipid (g/100 g)	2.95 ± 0.10^{a}	1.98 ± 0.04^{bc}	2.42 ± 0.11^{bc}	2.32 ± 0.13^{bc}	2.20 ± 0.35^{ac}

Values in the same row not sharing the same letter are significantly different ($p < 0.05$), whereas values without letters indicate no significant differences.

3.3 Fatty Acid Biomarkers

In this study, seven fatty acid biomarkers were selected to indicate 6 potential food sources (**Table 5**; **Figure 5**). As for the two traditional diatom biomarkers C16:1(*n*−7)/C16:0 ratio and EPA content, the former was especially lower than 1.0 (0.15~0.42), whereas the latter was also very low from April to October (0.93%−1.90%), which only slightly raised to 3.44% in winter (**Figures 5A, B**). It indicates that diatoms may not be the prominent food source of the sea cucumber. The flagellate algae and protozoan's biomarker DHA content fluctuated from 2.68% to 3.62% in different months, showing a varied contribution to the diet (**Figure 5C**). The high level of C20:4 (*n*−6) throughout the study (14.02% to 19.30%) indicates the important contribution of brown algae-derived food sources (**Figure 5D**).

The biomarker C18:1(*n*−7)/C18:1(*n*−9) > 1 can indicate the green algae and bacterial organic matter (OM) together; hence, the data may give an ambiguous result. Considering the low level of another green alga biomarker 18:3(*n*−3) (below 1%, **Figure 5E**), it can be inferred that the increase of the C18:1(*n*−7)/C18:1(*n*−9) ratio indicates the bacterial food source to the sea cucumber (**Figure 5F**). After juveniles were released into the wild, the C18:1(*n*−7)/C18:1(*n*−9) ratio increased gradually, which indicates the elevated contribution of bacteria-derived OM (**Figure 5F**, $p< 0.05$). The bacterial odd and branched FA biomarker levels were abundant and stable from spring to winter, which coincides with the C18:1(*n*−7)/C18:1(*n*−9) biomarker (**Figure 5G**). ΣC18:2(*n*−6) + C18:3(*n*−3) > 2.5 indicates the terrestrial OM, and it stays at a low level (below 1%) except for a slightly high value of 1.79% in December (**Figure 5H**, $p< 0.05$), which indicates the less importance of the terrestrial organics to the sea cucumber.

3.4 Stable Isotope Values of Sea Cucumber and Potential Food Sources

The stable C and N isotopic values of the sea cucumber from May to December showed different variations (**Table 6**). The $\delta^{13}C$ value had no remarkable seasonal change (−13.08‰ to −12.01‰, $p > 0.05$), whereas the $\delta^{15}N$ varied from 8.04‰ to 10.98‰, with the lowest value appearing in December ($p< 0.05$). Both the carbon and nitrogen contents of the sea cucumber decreased remarkably in the first month after release, yet they were relatively stable during the field study (**Table 6**). The stable isotope values of the five potential food sources are shown in **Table 7**. The ^{13}C and ^{15}N isotopic dual plot clearly shows that the isotopic value of the sea cucumber gradually moved toward the center part of the closed region bounded by values of different potential food sources from May to December, which indicates that the diet shifted during the sea ranching period (**Figure 6**).

TABLE 3 | Amino acid content in body wall of *Stichopus monotuberculatus* in different months (g/100 g).

Amino	Apr	May	Jul	Oct	Dec
Asp	3.08 ± 0.15^{a}	2.38 ± 0.10^{b}	2.54 ± 0.23^{b}	2.43 ± 0.22^{b}	2.87 ± 0.19^{ab}
Thr*	1.53 ± 0.08^{a}	1.18 ± 0.09^{c}	1.25 ± 0.09^{bc}	1.25 ± 0.1^{bc}	1.46 ± 0.09^{ab}
Ser	1.23 ± 0.06^{a}	0.97 ± 0.06^{b}	1.04 ± 0.07^{ab}	1.03 ± 0.07^{ab}	1.17 ± 0.13^{ab}
Glu	4.81 ± 0.29^{a}	3.71 ± 0.20^{b}	3.99 ± 0.39^{ab}	4.02 ± 0.38^{ab}	4.56 ± 0.22^{a}
Gly	5.29 ± 0.32^{a}	3.88 ± 0.14^{b}	3.89 ± 0.47^{b}	3.99 ± 0.45^{b}	4.96 ± 0.31^{a}
Ala	2.30 ± 0.13^{ab}	1.69 ± 0.06^{b}	1.87 ± 0.37^{ab}	2.28 ± 0.24^{ab}	2.56 ± 0.41^{a}
Val*	1.00 ± 0.07^{ab}	0.78 ± 0.03^{b}	1.03 ± 0.28^{ab}	1.25 ± 0.09^{ab}	1.23 ± 0.17^{a}
Ile*	0.79 ± 0.04	0.63 ± 0.02	0.67 ± 0.06	0.63 ± 0.07	0.73 ± 0.12
Leu*	1.20 ± 0.07	0.94 ± 0.04	1.00 ± 0.14	0.89 ± 0.10	1.03 ± 0.18
Tyr	0.66 ± 0.05	0.53 ± 0.03	0.59 ± 0.05	0.52 ± 0.06	0.54 ± 0.21
Phe*	0.65 ± 0.06^{a}	0.52 ± 0.02^{b}	0.63 ± 0.04^{ab}	0.67 ± 0.04^{a}	0.68 ± 0.06^{a}
Lys*	0.77 ± 0.04	0.62 ± 0.04	0.76 ± 0.06	0.77 ± 0.07	0.79 ± 0.10
His	0.39 ± 0.02	0.33 ± 0.02	0.36 ± 0.04	0.32 ± 0.04	0.38 ± 0.06
Arg*	2.44 ± 0.16^{a}	1.87 ± 0.09^{ab}	1.89 ± 0.21^{ab}	1.81 ± 0.19^{ab}	2.23 ± 0.24^{a}
Pro	2.61 ± 0.23^{a}	1.90 ± 0.13^{b}	1.84 ± 0.19^{b}	1.81 ± 0.20^{b}	2.33 ± 0.24^{ab}
Met	0.45 ± 0.02	0.38 ± 0.03	0.41 ± 0.02	0.40 ± 0.03	0.42 ± 0.05
Total amino acid	29.19 ± 1.77^{a}	22.3 ± 0.97^{b}	23.77 ± 2.12^{b}	24.07 ± 2.28^{b}	27.96 ± 1.4^{ab}
Essential amino acid	5.94 ± 0.36^{a}	4.67 ± 0.24^{b}	5.34 ± 0.67^{ab}	5.46 ± 0.47^{ab}	5.92 ± 0.72^{a}

Values in the same row bearing different letters are significantly different ($p< 0.05$).
**Essential amino acid.*

TABLE 4 | Fatty acid composition of the body wall of *Stichopus monotuberculatus* in different months, 2019 (%).

Fatty acid	Apr	May	Jul	Oct	Dec
C14:0	2.35 ± 0.59^{a}	0.77 ± 0.08^{b}	1.17 ± 0.10^{b}	0.64 ± 0.19^{b}	0.93 ± 0.32^{b}
C14-isobr	0.30 ± 0.06	0.48 ± 0.03	0.73 ± 0.29	0.38 ± 0.13	0.61 ± 0.53
C14-antiso	0.18 ± 0.05	0.12 ± 0.06	0.21 ± 0.08	0.18 ± 0.02	–
C15:0	0.20 ± 0.07	0.17 ± 0.03	0.24 ± 0.09	0.20 ± 0.05	0.17 ± 0.18
C15-isobr	0.20 ± 0.04	0.24 ± 0.02	0.31 ± 0.14	0.32 ± 0.03	0.29 ± 0.08
C16:0	3.33 ± 0.48^{b}	3.54 ± 0.43^{b}	5.43 ± 0.28^{a}	3.94 ± 1.17^{ab}	2.66 ± 0.46^{b}
C16:1(*n*−7)	0.55 ± 0.04^{c}	1.22 ± 0.16^{b}	2.25 ± 0.06^{a}	1.01 ± 0.31^{b}	0.38 ± 0.10^{c}
C16-isobr	0.20 ± 0.06	0.27 ± 0.03	0.26 ± 0.10	0.20 ± 0.07	0.34 ± 0.20
C16-antiso	0.19 ± 0.04	0.18 ± 0.04	0.30 ± 0.10	0.34 ± 0.08	0.18 ± 0.06
C17:0	0.65 ± 0.18	0.69 ± 0.17	0.47 ± 0.13	0.55 ± 0.07	0.46 ± 0.04
C17:1(*n*−9)	0.44 ± 0.02^{a}	0.19 ± 0.10^{b}	0.53 ± 0.07^{a}	0.52 ± 0.04^{a}	0.49 ± 0.03^{a}
C16:4(*n*−3)	9.76 ± 0.91	10.74 ± 0.66	9.66 ± 1.45	8.50 ± 3.35	9.94 ± 0.37
C18:0	3.49 ± 0.74^{b}	6.15 ± 0.61^{a}	5.26 ± 0.54^{ab}	5.37 ± 0.89^{ab}	7.07 ± 0.90^{a}
C18:1(*n*−9)	4.87 ± 0.03^{a}	1.46 ± 0.21^{b}	0.85 ± 0.15^{c}	0.75 ± 0.06^{c}	0.66 ± 0.15^{c}
C18:1(*n*−7)	2.22 ± 0.39	1.64 ± 0.16	1.34 ± 0.44	1.34 ± 0.55	2.51 ± 0.83
C18:2(*n*−6)	0.39 ± 0.04^{b}	0.28 ± 0.00^{b}	0.24 ± 0.05^{b}	0.37 ± 0.09^{b}	0.94 ± 0.27^{a}
C18:2(*n*−4)	7.69 ± 6.01	5.54 ± 1.89	10.25 ± 3.02	10.55 ± 2.27	2.19 ± 0.20
C18:3(*n*−3)	0.73 ± 0.11^{a}	0.39 ± 0.03^{b}	0.27 ± 0.05^{b}	0.29 ± 0.03^{b}	0.85 ± 0.15^{a}
C18:4(*n*−3)	0.47 ± 0.09^{ab}	0.30 ± 0.21^{b}	0.32 ± 0.14^{b}	0.35 ± 0.09^{b}	0.58 ± 0.07^{a}
C20:0	1.50 ± 1.22^{b}	3.33 ± 0.15^{ab}	3.07 ± 0.16^{ab}	3.77 ± 0.77^{a}	4.18 ± 0.47^{a}
C20:1(*n*−9)	12.84 ± 1.63	12.96 ± 0.46	10.10 ± 1.96	13.48 ± 1.84	13.00 ± 0.17
C20:2(*n*−6)	0.36 ± 0.02^{b}	0.90 ± 0.10^{ab}	0.73 ± 0.06^{ab}	0.63 ± 0.29^{ab}	0.99 ± 0.39^{a}
C20:4(*n*−6)	18.57 ± 1.18	18.65 ± 0.88	14.10 ± 1.39	14.02 ± 4.91	19.30 ± 1.19
C20:4(*n*−3)	1.30 ± 0.30^{c}	4.21 ± 0.73^{a}	5.26 ± 0.57^{a}	2.79 ± 0.14^{b}	–
C20:5(*n*−3)	0.93 ± 0.13^{c}	1.21 ± 0.43^{bc}	1.55 ± 0.11^{bc}	1.90 ± 0.17^{b}	3.44 ± 0.58^{a}
C22:1(*n*−11)	0.86 ± 0.17^{c}	1.07 ± 0.17^{bc}	1.46 ± 0.31^{bc}	1.53 ± 0.22^{b}	3.23 ± 0.29^{a}
C22:1(*n*−1)	0.35 ± 0.14^{b}	0.22 ± 0.09^{b}	0.29 ± 0.06^{b}	0.29 ± 0.12^{b}	1.44 ± 0.30^{a}
C22:3(*n*−9)	0.29 ± 0.04	0.40 ± 0.05	0.32 ± 0.03	0.34 ± 0.12	–
C22:1(*n*−9)	7.90 ± 1.48^{a}	5.80 ± 0.26^{ab}	3.87 ± 1.13^{b}	5.18 ± 0.40^{b}	8.24 ± 0.57^{a}
C22:3(*n*−6)	0.38 ± 0.13^{b}	0.34 ± 0.03^{b}	0.31 ± 0.14^{b}	0.34 ± 0.04^{b}	0.66 ± 0.05^{a}
C22:4(*n*−6)	0.14 ± 0.13^{b}	0.74 ± 0.10^{a}	0.75 ± 0.18^{a}	0.64 ± 0.27^{a}	0.63 ± 0.07^{a}
C22:5(*n*−3)	0.14 ± 0.14^{bc}	0.25 ± 0.01	0.34 ± 0.05	0.27 ± 0.01	–
C22:6(*n*−3)	2.88 ± 0.50	3.62 ± 0.06	2.68 ± 0.34	3.34 ± 0.85	3.21 ± 0.35
SFA	11.53 ± 2.36	14.65 ± 1.09	15.64 ± 0.5	14.48 ± 2.81	15.47 ± 1.00
MUFA	30.02 ± 2.85^{a}	24.56 ± 0.16^{bc}	20.69 ± 3.46^{c}	24.11 ± 2.39^{bc}	29.95 ± 0.71^{ab}
PUFA	44.03 ± 4.99	47.69 ± 0.73	46.78 ± 1.53	44.35 ± 5.9	42.72 ± 0.37
BFA	1.07 ± 0.23	1.28 ± 0.13	1.81 ± 0.64	1.42 ± 0.23	1.47 ± 0.85
TFA	86.65 ± 1.07^{b}	88.18 ± 0.59^{ab}	84.93 ± 1.44^{b}	84.36 ± 1.02^{b}	89.62 ± 1.20^{a}

Data presented as mean ± SD, n = 3. Values in the same row bearing different letters are significantly different (p < 0.05).
–, content below 0.1% or not detected; SFA, saturated fatty acid; MUFA, monounsaturated fatty acid; PUFA, polyunsaturated fatty acid; BFA, branched-chain fatty acid; TFA, trans-fatty acid.

3.5 Food Composition Evaluation

The food source mixing model gave a result of the food composition of the sea cucumber in the four sampling months (**Figure 7**). Water deposit OM was the predominant diet part, which accounted for 33.4%–44.3% of the total. The organic proportion from Phaeophyta *S. sanyaense* peaked in May (41.4%) and then dropped gradually (11.3% to 6.0%) from July to December. The coral mucus-derived OM contribution was 13.1%–15.9% in July and October and peaked in December

TABLE 5 | Fatty acids and fatty acid ratios were used as biomarkers for food sources.

Fatty acids	Indicated sources	References
C20:5(*n*−3)	Diatoms or red algae	(Ackman et al., 1968)
C22:6(*n*−3)	Flagellate algae and protozoans	(Sargent et al., 1987)
C20:4(*n*−6)	Brown algae	(Cook et al., 2000; Li et al., 2002)
Odd FAs and BFAs	Bacteria	(Volkman et al., 1980; Findlay et al., 1990; Bachok et al., 2003)
∑C18:2(*n*−6)+C18:3(*n*−3) > 2.5	Terrestrial organic matter	(Findlay et al., 1990; Budge et al., 2001)
Ratio	Indicated sources	References
C16:1/C16:0 (>1.6)	Diatoms	(Ackman et al., 1968)
C18:1(*n*−7)/C18:1(*n*−9) (>1)	Bacteria or green algae	(Khotimchenko et al., 2002)

BFAs, branched-chain fatty acids.

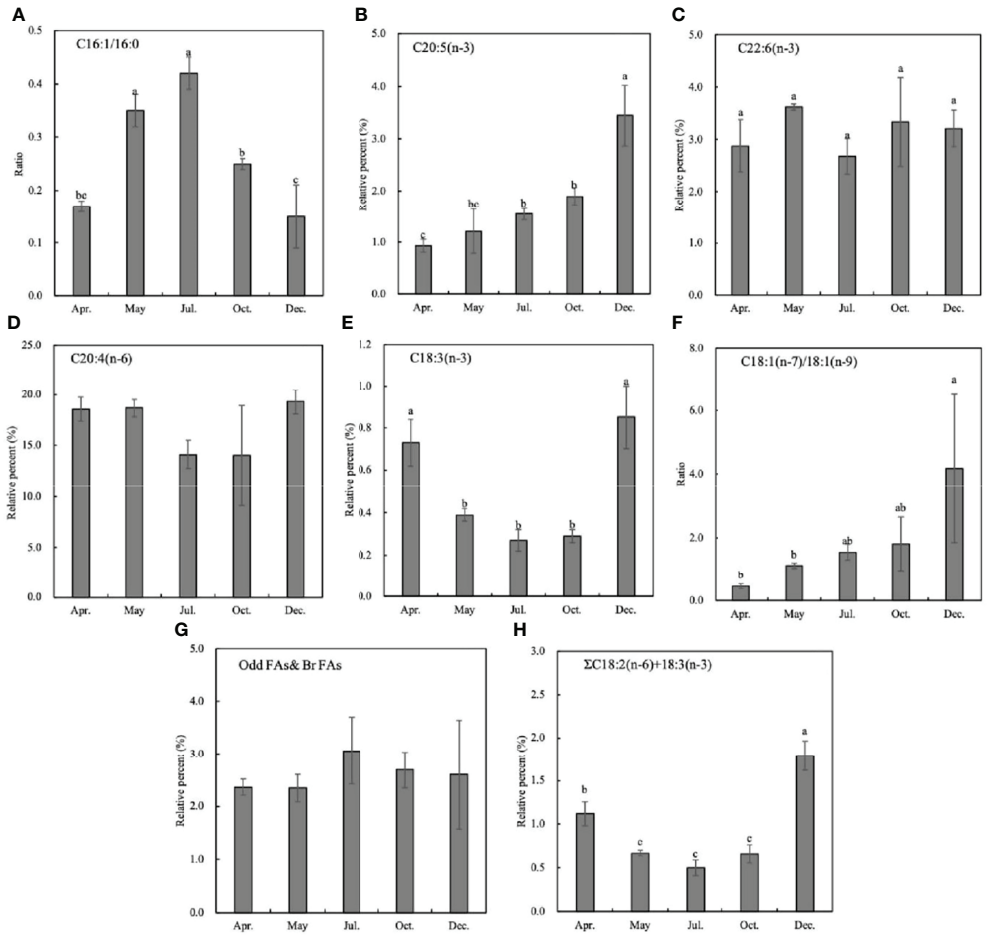

FIGURE 5 | Fatty acid biomarkers of *Stichopus monotuberculatus* at different months. Food sources are indicated by different fatty acid markers: **(A, B)** diatoms; **(C)** flagellate algae or protozoan; **(D)** brown algae; **(E, F)** green algae; **(G)** heterotrophic bacteria; **(H)** terrestrial organic matter. No letters indicate that there is no significant difference between different months.

(37.2%), but in May, the contribution was only 2.7%. Benthic microalgae had a contribution in July and October (18.6%–23.2%) to the diet, but in May and December, the contribution was only 4.5% and 10.3%, respectively. Phytoplankton-derived organic sources had the same contribution of 11.2% to the diet in July and October, but in May and December, the contribution was only 5.1%–5.9%.

TABLE 6 | The isotopic composition of *Stichopus monotuberculatus* body wall from April to December 2019.

Time	δ^{13}C (‰)	δ^{15}N (‰)	C%	N%
Apr	−12.01 ± 1.11	10.73 ± 0.66^{a}	23.88 ± 0.65^{a}	6.51 ± 0.32^{a}
May	−12.04 ± 0.67	10.98 ± 0.69^{a}	15.03 ± 2.15^{b}	4.26 ± 0.81^{b}
Jul	−12.46 ± 0.19	9.47 ± 0.85^{a}	14.63 ± 1.37^{b}	3.83 ± 0.45^{b}
Oct	−13.08 ± 0.83	9.31 ± 0.36^{b}	16.50 ± 2.05^{b}	4.59 ± 0.68^{b}
Dec	−12.37 ± 0.16	8.04 ± 0.39^{b}	16.20 ± 2.20^{b}	4.54 ± 0.80^{b}

Data presented as mean ± SD, n = 3. Values in the same column bearing different letters are significantly different ($p < 0.05$).

4 DISCUSSION

4.1 The Growth and Survival of *Stichopus monotuberculatus*

This study provides the evaluation results on the growth performance of the sea-ranched *S. monotuberculatus* juveniles in the coral reef area. Our study found that the overall GR of the sea cucumber was 0.42 mm day^{-1} and SGR was 0.73% day^{-1} throughout the year. The sea cucumber grew fast in May–July and November–December, although there was a slowdown from August to October, which may be caused by the frequent influence of typhoons during this period (**Table 1**). It is reported that the widely cultured tropical species *H. scabra* showed an SR of 14% with an SGR of 0.66% day^{-1} during a 6-month experiment in the New Caledonia Népoui region (Purcell and Simutoga, 2008). The growth and survival of *S. monotuberculatus*, compared with *H. scabra*, are much better. Bottom cultured temperate *A. japonicus* juveniles (WW 40.35 g) achieved an average SGR of 0.15%~0.54% day^{-1} over a 5-month culture period under a fish farm in the northern part

TABLE 7 | The isotopic composition of potential food sources of *Stichopus monotuberculatus* (n = 3).

Food sources	δ^{13}C (‰)	δ^{15}N (‰)
Phytoplankton	−20.70 ± 0.56	7.83 ± 0.16
Benthic microalgae	−15.98 ± 0.78	5.55 ± 0.18
Water deposit	−7.80 ± 1.11	6.25 ± 0.02
Sargassum sanyaense	−17.88 ± 0.13	9.36 ± 0.32
Coral mucus*	−16.20 ± 0.40	1.50 ± 0.70

**The δ^{13}C and δ^{15}N values are from the reference (Naumann et al., 2010).*

of the South China Sea (Yu et al., 2014), which is also lower than our result. Under pond culture conditions, sea cucumber juveniles tend to acquire a higher GR. Another tropical sea cucumber, *Stichopus* sp. (curry fish) juveniles (body length 4 cm), cultured in a pond showed a GR of 0.76 mm day^{-1} during 210 days, which is similar to our study (Hu et al., 2010). The individual growth variation (especially in December) of the *S. monotuberculatus* may result from the difference in the foraging efficiency and assimilation ability.

The final SR of *S. monotuberculatus* was 27.5%, which is lower than that of the pond cultured curry fish *Stichopus* sp. (30%~50%) (Hu et al., 2010) but higher than the bottom cultured *H. scabra* (less than 20%) (Purcell and Simutoga, 2008). There were 25%–37% of juveniles who died in the first month after being released, and this probably relates to the inability of the sea cucumber to adapt to the sudden change of living conditions from the indoor tank to the wild. Environmental factors such as water current and temperature variation together with natural food availability have been proved to affect the feeding behavior, metabolism, growth, and survival of sea cucumber juveniles (Zamora and Jeffs, 2012; Wang et al., 2015) (Zhou et al., 2013; Yu et al., 2016a; Montgomery et al., 2017; Montgomery et al., 2018; Sun et al., 2020). Considering the relatively low SR, necessary acclimation rearing should be carried out before samples are deployed into the wild. The sea ranching area should also be carefully selected for optimal physical and food conditions (such as mild wave and current, sufficient reefs for hiding, and abundant detritus food) to ensure better adaptation of the juveniles.

4.2 The Nutritional Composition

Protein and lipid nutrition is essential for the living of animals. Fatty acids and amino acids are crucial for the growth of sea cucumbers, as they are needed for energy conversion and body health (Wen et al., 2010; Omran, 2013; Rasyid, 2018). The dynamic change of the nutritional composition also gives insight into the growth performance. In the early stage of sea ranching, the contents of crude protein, total lipid, and total amino acids decreased significantly from April to May (**Tables 2**, **3**). Total C and N contents also dropped remarkably in this period (**Table 6**). These indicated the large energy consumption of the sea cucumber and related closely with the acclimation process after release. Two months later, the nutrition required for growth began to accumulate, such as glutamic acid and essential amino acids. Meanwhile, the SR also remained stable, showing that the sea cucumber has adapted to the wild.

The amino acid composition of *S. monotuberculatus*, especially the predominant Gly and Glu (**Table 3**), is similar to that of other sea cucumber species such as *Thelenota anax*, *H. fuscogilva*, *Holothuria fuscopunctata*, *Actinopyga mauritiana*, *Bohadschia argus*, and *Actinopyga caerulea* (Wen et al., 2010). The fatty acid profile of the *S. monotuberculatus* mostly consists of PUFAs, and this is consistent with other sea cucumber species (Yu et al., 2015; Gianasi et al., 2017). The arachidonic acid [ARA, 20:4(*n*−6)], which is the predominant PUFA in *S. monotuberculatus*, plays a significant role in the growth and development of sea cucumbers (Yu et al., 2016b; King and Smith, 2018). Previous studies also proved that ARA accounts for a large proportion of unsaturated fatty acids in almost all tropical sea cucumbers (Wen et al., 2010; Rasyid, 2018).

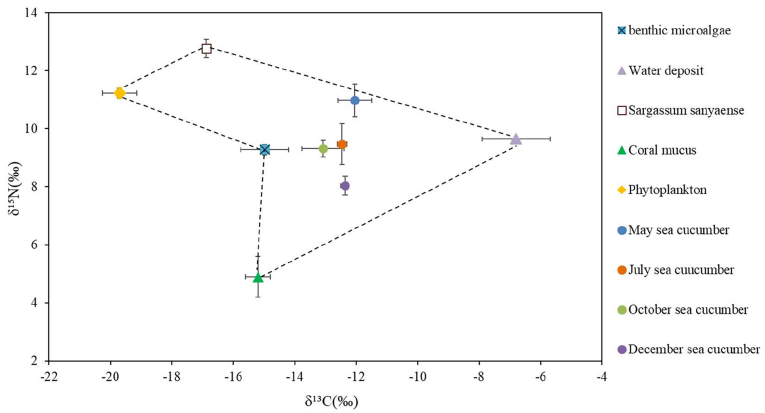

FIGURE 6 | Dual stable isotope plots of δ^{13}C and δ^{15}N for the sea cucumber *Stichopus monotuberculatus* and its potential food sources in two sampling seasons, from May to December 2019. The stable isotope ratios of sea cucumber were corrected with the average fractionation effects of 1.0‰ and 3.4‰ for C and N, respectively. Note: the values of δ^{13}C and δ^{15}N for coral mucus are −16.2 ± 0.4 and 1.5 ± 0.7 (Naumann et al., 2010).

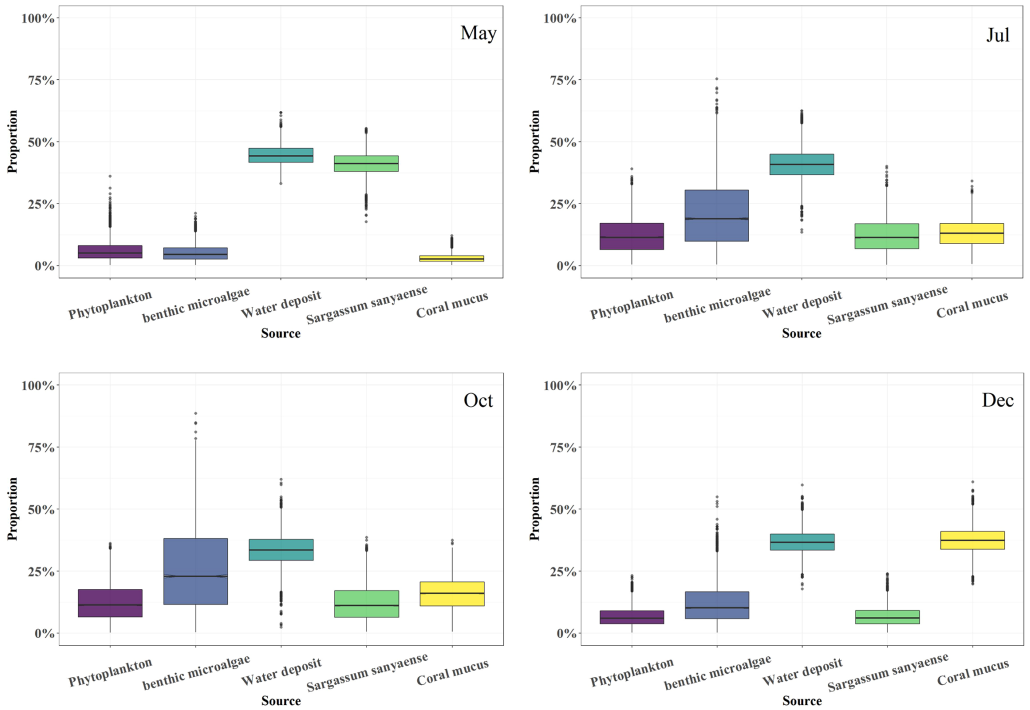

FIGURE 7 | Food composition of the cultured sea cucumber *Stichopus monotuberculatus* from May to December 2019.

4.3 The Potential Food Sources

The results of the lipid biomarker and stable isotope mixing model indicate that the diet of the sea cucumber changed gradually after release. Water deposits occupied the maximum part of the diet (33.4%–44.3%) throughout the year, proving its importance for the deposit feeder in the coral reef ecosystem. The organic composition of the water deposit may be complex, which includes debris and various kinds of microbes such as bacteria and protozoa (Lange et al., 2018). The considerable part of the microbial food source of the sea cucumber indicated by the flagellate/protozoa and bacterial fatty acid biomarkers may have a close relation to the organic debris from the water deposit.

Both the isotope model and lipid biomarker proved the importance of the adjacent *S. sanyaense* seaweed bed OM to the sea cucumber's diet (41.4% at most). Although the seaweed bed is on the opposite side to the island, algal derived detritus may probably be transported to the sea ranching area by the strong tidal current in the bay (current direction marked in **Figure 1**), and this can be confirmed by the seaweed branches frequently found at the beach around the island in spring and early summer. It means that protecting the coastal seaweed bed can bring supplemental food sources to the sea ranching sea cucumber. Previous research proved that the temperate (*A. japonicus*) and tropical (*S. horrens*) sea cucumber species prefer *Sargassum* sp. as a habitat and food source (Wen et al., 2016; Palomar-Abesamis et al., 2017). Seaweed-derived food source for other sea cucumber species (*A. japonicus*) was also confirmed in the pond culture mode, which is as high as 54.4% in spring (Sun et al., 2013). Furthermore, the food contributions of benthic microalgae and phytoplankton to *S. monotuberculatus* are higher than the pond-cultured *A. japonicus* (2.8%–4.2% and 2.8%–6.5% for benthic microalgae and particulate OM (POM), respectively; Sun et al., 2013).

Coral mucus OM also has a varied contribution to the diet. Its contribution was high in December (37.2%), and it proved the importance of coral productivity to the sea cucumber in the coral reef ecosystem, especially in winter. Coral mucus can act as an important energy and nutrient carrier *via* particle trapping in benthic–pelagic coupling processes while serving as a food source for various reef-dwelling benthic organisms including deposit-feeding sea cucumbers (Coffroth, 1984; Wild et al., 2004; Wild et al., 2005).

5 CONCLUSION

This study proved the feasibility of sea ranching for the hatchery-reared *S. monotuberculatus* juveniles in the tropical coral reef area in China. Compared with other cultured tropical sea cucumber species, *S. monotuberculatus* had a higher growth performance (SGR 0.73) and SR (27.5%). The death rate of the juveniles was much higher in the first month after release, mostly because of the inadaptation to the environment transition from the indoor tank to the wild. The food source of the sea cucumber mostly comes from the OM of water deposits and brown algae debris combined with various microbes. Coral mucus-derived organics, benthic microalgae, and

phytoplankton also showed their contribution in some seasons. Considering the high death rate in the first month after release, suitable acclimation operation such as pond domestication rearing is highly recommended before sea ranching. Meanwhile, more research is needed to optimize the release strategy so as to support a higher survival and GR of the species in tropical sea ranching areas.

DATA AVAILABILITY STATEMENT

The original contributions presented in the study are included in the article/supplementary material. Further inquiries can be directed to the corresponding author.

AUTHOR CONTRIBUTIONS

QX: Study design and paper writing; PW: Field experiment, sample analysis and paper writing; DH: Field experiment; YX: Food source quantification; XW: Field experiment; JX: Field experiment; WM: Field experiment; FG: Project raising, paper revise and sponsor; AW: Field study adviser. All authors contributed to the article and approved the submitted version.

FUNDING

The research was sponsored by the National Key R&D Project of China (No. 2019YFD0901304), National Natural Science Foundation of China (No. 42076097, 31760757), and National Natural Science Foundation of Hainan Province, China (No. 2019RC070).

ACKNOWLEDGMENTS

The authors are grateful to Wang Fengguo and Zhou Zhigang for their help in the fieldwork.

REFERENCES

Ackman, R. G., Tocher, C. S. and McLachlan, (1968). Marine Phytoplankton Fatty Acids. *J. Fisheries. Board. Canada.* 25, 1603–1620. doi: 10.1139/f68-145

AOAC (1990). *Official Methods of Analysis* (Washington DC: Association of official analytical chemists).

Bachok, Z., Mfilinge, P. L. and Tsuchiya, M. (2003). The Diet of the Mud Clam *Geloina Coaxans* (Mollusca, Bivalvia) as Indicated by Fatty Acid Markers in a Subtropical Mangrove Forest of Okinawa, Japan. *J. Exp. Mar. Biol. Ecology.* 292, 187–197. doi: 10.1016/S0022-0981(03)00160-6

Block, R. J., Durrum, E. L. and Zweig, G. (2016). *A Manual of Paper Chromatography and Paper Electrophoresis* (Elsevier: New York).

Budge, S. M., Parrish, C. C. and McKenzie, C. H. (2001). Fatty Acid Composition of Phytoplankton, Settling Particulate Matter and Sediments at a Sheltered Bivalve Aquaculture Site. *Mar. Chem.* 76, 285–303. doi: 10.1016/S0304-4203(01)00068-8

Carlier, A., Riera, P., Amouroux, J. M., Bodiou, J. Y. and Grémare, A. (2007). Benthic Trophic Network in the Bay of Banyuls-Sur-Mer (Northwest Mediterranean, France): An Assessment Based on Stable Carbon and Nitrogen Isotopes Analysis. *Estuarine. Coast. Shelf. Science.* 72, 1–15. doi: 10.1016/j.ecss.2006.10.001

Chen, J. X. (2004). ""Present Status and Prospects of Sea Cucumber Industry in China,"" in *Advances in Sea Cucumber Aquaculture and Management*. Eds. Lovatelli, A., Conand, C., Purcell, S., Uthicke, S., Hamel, J. F. and Mercie, A. (Rome: FAO), 25–38.

Coffroth, M. A. (1984). Ingestion and Incorporation of Coral Mucus Aggregates by a Gorgonian Soft Coral. *Mar. Ecol. Prog. series.* 17, 193–199. doi: 10.3354/meps017193

Conand, C. (1993). Ecology and Reproductive Biology of *Stichopus Variegatus* an Indo-Pacific Coral Reef Sea Cucumber (Echinodermata: Holothuroidea). *Bull. Mar. Science.* 52, 970–981.

Cook, E. J., Bell, M. V., Black, K. D. and Kelly, M. S. (2000). Fatty Acid Compositions of Gonadal Material and Diets of the Sea Urchin, *Psammechinus Miliaris*: Trophic and Nutritional Implications. *J. Exp. Mar. Biol. Ecology.* 255, 261–274. doi: 10.1016/S0022-0981(00)00301-4

Desurmont, A. (2003). Papua New Guinea Sea Cucumber and Beche-De-Mer Identification Cards. *SPC. Beche-de-mer. Inf. Bulletin.* 9, 12–15.

Eriksson, H. and Clarke, S. (2015). Chinese Market Responses to Overexploitation of Sharks and Sea Cucumbers. *Biol. Conserv.* 184, 163–173. doi: 10.1016/j.biocon.2015.01.018

Findlay, R. H., Trexler, M. B., Guckert, J. B. and White, D. C. (1990). Laboratory Study of Disturbance in Marine Sediments: Response of a Microbial Community. *Mar. Ecol. Prog. series.* 62, 121–133. doi: 10.3354/meps062121

Folch, J., Less, M. and Stanley, G. H. (1957). A Simple Method for the Isolation and Purification of Total Lipids From Animal Tissues. *Biol. Chem.* 226, 497–509. doi: 10.1016/s0021-9258(18)64849-5

Gianasi, B. L., Parrish, C. C., Hamel, J. F. and Mercier, A. (2017). Influence of Diet on Growth, Reproduction and Lipid and Fatty Acid Composition in the Sea Cucumber Cucumaria Frondosa. *Aquaculture. Res.* 48, 3413–3432. doi: 10.1111/are.13168

Huang, L. M., Tan, Y. H., Song, X. Y., Huang, X. P., Wang, H. K., Zhang, S., et al. (2003). The Status of the Ecological Environment and a Proposed Protection Strategy in Sanya Bay, Hainan Island, China. *Mar. pollut. Bull.* 47, 180–186. doi: 10.1016/S0025-326X(03)00070-5

Huang, J. Z., Wang, F. X., Zhao, H. W., Xu, H. L., Li, S., Xu, Q., et al. (2020). Reef Benthic Composition and Coral Communities at the Wuzhizhou Island in the South China Sea: The Impacts of Anthropogenic Disturbance. *Estuarine. Coast. Shelf. Sci.* 243, 106863. doi: 10.1016/j.ecss.2020.106863

Hu, C. Q., Xu, Y. H., Wen, J., Zhang, L. P., Fan, S. G. and Su, T. (2010). Larval Development and Juvenile Growth of the Sea Cucumber Stichopus Sp. (Curry Fish). *Aquaculture.* 300, 73–79. doi: 10.1016/j.aquaculture.2009.09.033

Jiménez-Arias, J. L., Morris, E., Rubio-de-Inglés, M. J., Peralta, G., Robledo, E. G., Corzo, A., et al. (2020). Tidal Elevation is the Key Factor Modulating Burial Rates and Composition of Organic Matter in a Coastal Wetland With Multiple Habitats. *Sci. Total. Environment.* 724, 1–15. doi: 10.1016/j.scitotenv.2020.138205

Khotimchenko, S. V., Vaskovsky, V. E. and Titlyanova, T. V. (2002). Fatty Acids of Marine Algae From the Pacific Coast of North California. *Botanica Marina.* 45, 17–22. doi: 10.1515/BOT.2002.003

King, J. and Smith, S. (2018). Arachidonic Acid Content in the Feed on the Growth Performance, Antioxidant Capacity and Fatty Acid Generation of Sea Cucumber. *CCAMLR. Science.* 25, 121–133.

Lange, G., Haynert, K., Dinter, T., Scheu, S. and Kröncke, I. (2018). Adaptation of Benthic Invertebrates to Food Sources Along Marine-Terrestrial Boundaries as Indicated by Carbon and Nitrogen Stable Isotopes. *J. Sea. Res.* 131, 12–21. doi: 10.1016/j.seares.2017.10.002

Li, X. C., Fan, X., Han, L. J., Yan, X. J. and Lou, Q. X. (2002). Fatty Acids of Common Marine Macrophytes From the Yellow and Bohai Seas. *Oceanologia. Limnologia. Sinica.* 33, 215–224. doi: 10.1016/S0031-9422(01)00437-X

Lionel, M., Max, G., Modou, M., Katrin, M., Arsenio, T., Christian, R., et al. (2018). Novel Application of Compound Specific Stable Isotope (CSSI) Techniques to Investigate on-Site Sediment Origins Across Arable Fields. *Geoderma.* 316, 19–26. doi: 10.1016/j.geoderma.2017.12.008

Li, X. B., Titlyanov, E. A., Titlyanova, T. V., Belous, O. S., Xia, J. Q. and Huang, H. (2020). An Inventory and Seasonal Changes in the Recent Benthic Flora of Coral Reefs of Wuzhizhou Island, Haitang Bay, South China Sea (China). *Russian J. Mar. Biol.* 46, 485–492. doi: 10.1134/S1063074020310028

Li, X. B., Wang, D. R., Huang, H., Zhang, J., Lian, J. S., Yuan, X. C., et al. (2015). Linking Benthic Community Structure to Terrestrial Runoff and Upwelling in the Coral Reefs of Northeastern Hainan Island. *Estuarine. Coast. Shelf. Science.* 156, 92–102. doi: 10.1016/j.ecss.2014.09.021

McClelland, J. W. and Valiela, I. (1998). Changes in Food Web Structure Under the Influence of Increased Anthropogenic Nitrogen Inputs to Estuaries. *Mar. Ecol. Prog. Series.* 168, 259–271. doi: 10.3354/meps168259

McCutchan, J. H., Jr., Lewis, W. M., Jr., Kendall, C. and McGrath, C. C. (2003). Variation in Trophic Shift for Stable Isotope Ratios of Carbon, Nitrogen, and Sulfur. *OIKOS.* 102, 378–390. doi: 10.1034/j.1600-0706.2003.12098.x

Montgomery, E. M., Hamel, J. F. and Mercier, A. (2017). Ontogenetic Shifts in Swimming Capacity of Echinoderm Propagules: A Comparison of Species With Planktotrophic and Lecithotrophic Larvae. *Mar. Biol.* 164, 43. doi: 10.1007/s00227-017-3072-6

Montgomery, E. M., Hamel, J. F. and Mercier, A. (2018). Ontogenetic Variation in Photosensitivity of Developing Echinoderm Propagules. *J. Exp. Mar. Biol. Ecology.* 500, 63–72. doi: 10.1016/j.jembe.2017.12.003

Naumann, M. S., Mayr, C., Struck, U. and Wild, C. (2010). Coral Mucus Stable Isotope Composition and Labeling: Experimental Evidence for Mucus Uptake by Epizoic Acoelomorph Worms. *Mar. Biol.* 157, 2521–2531. doi: 10.1007/s00227-010-1516-3

Omran, N.E.S.E.S. (2013). Nutritional Value of Some Egyptian Sea Cucumbers. *Afr. J. Biotechnol.* 12, 5466–5472. doi: 10.5897/AJB2013.13020

Pakoa, K. and Bertram, I. (2013). BECHE-DE-MER Information Bulletin. Australia, France and New Zealand: *Secretariat of the Pacific Community*. 33, 49–52.

Palomar-Abesamis, N., Abesamis, R. A. and Juinio-Meñez, M. A. (2017). Distribution and Microhabitat Associations of the Juveniles of a High-Value Sea Cucumber, *Stichopus* Cf. *Horrens*, in Northern Philippines. *Aquat. Ecol.* 51 (1), 17–31. doi: 10.1007/s10452-016-9591-2

Parnell, A. C., Phillips, D. L., Bearhop, S., Semmens, B. X., Ward, E. J., Moore, J. W., et al. (2013). Bayesian Stable Isotope Mixing Models. *Environmetrics* 24, 387–399. doi: 10.1002/env.2221

Parrish, C. C. (1999). ""Determination of Total Lipid, Lipid Classes, and Fatty Acids in Aquatic Samples,"" in *Lipids in Freshwater Ecosystems*. Eds. Arts, M. and Wainman, B. C. (New York: Springer), 4–20. doi: 10.1007/978-1-4612-0547-0_2

Purcell, S. W., Hair, C. A. and Mills, D. J. (2012). Sea Cucumber Culture, Farming and Sea Ranching in the Tropics: Progress, Problems and Opportunities. *Aquaculture.* 368, 68–81. doi: 10.1016/j.aquaculture.2012.08.053

Purcell, S. W. and Simutoga, M. (2008). Spatio-Temporal and Size-Dependent Variation in the Success of Releasing Cultured Sea Cucumbers in the Wild. *Rev. Fisheries. Sci.* 16, 204–214. doi: 10.1080/10641260701686895

Purcell, S. W., Williamson, D. H. and Ngaluafe, P. (2018). Chinese Market Prices of Beche-De-Mer: Implications for Fisheries and Aquaculture. *Mar. Policy.* 91, 58–65. doi: 10.1016/j.marpol.2018.02.005

Rasyid, A. (2018). Amino Acid and Fatty Acid Compositions of Sea Cucumber Stichopus Vastus From Salemo Island Waters, Indonesia. *Squalen. Bull. Mar. Fisheries. Postharvest. Biotechnol.* 13, 9–15. doi: 10.15578/squalen.v13i1.285

Saccò, M., Blyth, A. J., Humphreys, W. F., Kuhl, A., Mazumder, D., Smith, C., et al. (2019). Elucidating Stygofaunal Trophic Web Interactions *via* Isotopic Ecology. *PloS One* 14, e0223982. doi: 10.1371/journal.pone.0223982

Sánchez-Tapia, I. A., Slater, M. and Miguel A. Olvera-Novoa, M. A. (2018). Evaluation of the Growth and Survival Rate of the Caribbean Sea Cucumber, *Isostichopus Badionotus* (Selenk), Early Juveniles Produced in Captivity. *J. World Aquaculture. Soc.* 50, 763–773. doi: 10.1111/jwas.12568

Sargent, J. R., Parkes, R. J., Mueller-Harvey, I., Henderson, R. J. and Parkes, J. R. (1987). Lipid Biomarkers in Marine Ecology. (Ellis Horwood, Chichester, UK: *Microbes in the Sea*). 1987, 119–138.

Sherwood, G. D. and Rose, G. A. (2005). Stable Isotope Analysis of Some Representative Fish and Invertebrates of the Newfoundland and Labrador Continental Shelf Food Web. *Estuarine. Coast. Shelf. Science.* 63, 537–549. doi: 10.1016/j.ecss.2004.12.010

Sun, Z. L., Gao, Q. F., Dong, S. L., Shin, P. K. and Wang, F. (2013). Seasonal Changes in Food Uptake by the Sea Cucumber *Apostichopus Japonicus* in a Farm Pond: Evidence From C and N Stable Isotopes. *J. Ocean. Univ. China.* 12, 160–168. doi: 10.1007/s11802-012-1952-z

Sun, J. M., Hamel, J. F., Stuckless, B., Small, T. J. and Mercier, A. (2020). Effect of Light, Phytoplankton, Substrate Types and Colour on Locomotion, Feeding Behaviour and Microhabitat Selection in the Sea Cucumber *Cucumaria Frondosa*. *Aquaculture.* 526, 735369. doi: 10.1016/j.aquaculture.2020.735369

Volkman, J. K., Johns, R. B., Gillan, F. T., Perry, G. J. and Bavor, H. J. (1980). Microbial Lipids of an Intertidal Sediment—I. Fatty Acids and Hydrocarbons. *Geochimica. Cosmochimica. Acta* 44, 1133–1143. doi: 10.1016/0016-7037(80)90067-8

Wang, Q. L., Yu, S. S. and Dong, Y. W. (2015). Parental Effect of Long Acclimatization on Thermal Tolerance of Juvenile Sea Cucumber *Apostichopus Japonicus*. *PloS One* 10, e0143372. doi: 10.1371/journal.pone.0143372

Wen, B., Gao, Q. F., Dong, S. L., Hou, Y. R., Yu, H. B. and Li, W. D. (2016). Uptake of Benthic Matter by Sea Cucumber *Apostichopus Japonicus* (Selenka): Insights From Carbon Stable Isotopes and Fatty Acid Profiles. *J. Exp. Mar. Biol. Ecol.* 474, 46–53. doi: 10.1016/j.jembe.2015.10.003

Wen, J., Hu, C. Q. and Fan, S. (2010). Chemical Composition and Nutritional Quality of Sea Cucumbers. *J. Sci. Food Agriculture.* 90, 2469–2474. doi: 10.1002/jsfa.4108

Wild, C., Rasheed, M., Jantzen, C., Cook, P., Struck, U., Huettel, M., et al. (2005). Benthic Metabolism and Degradation of Natural Particulate Organic Matter in Carbonate and Silicate Reef Sands of the Northern Red Sea. *Mar. Ecol. Prog. Series.* 298, 69–78. 3354/meps298069. doi: 10.3354/meps298069

Wild, C., Rasheed, M., Werner, U., Franke, U., Johnstone, R. and Huettel, M. (2004). Degradation and Mineralization of Coral Mucus in Reef Environments. *Mar. Ecol. Prog. Series.* 267, 159–171. doi: 10.3354/meps267159

Xu, Q. (2007). Food sources composition of the bivalves in the seaweed-bivalve polyculture system. Ph D. thesis, Postgraduate school of Chinese Academy of Sciences (Institute of Oceanology), Qingdao, China. (in Chinese with English abstract).

Yu, H. B., Gao, Q. F., Dong, S. L. and Wen, B. (2015). Changes in Fatty Acid Profiles of Sea Cucumber *Apostichopus Japonicus* (Selenka) Induced by Terrestrial Plants in Diets. *Aquaculture.* 442, 119–124. doi: 10.1016/j.aquaculture.2015.03.002

Yu, H. B., Zhang, C., Gao, Q. F., Dong, S. L., Ye, Z. and Tian, X. L. (2016a). Impact of Water Temperature on the Growth and Fatty Acid Profiles of Juvenile Sea Cucumber *Apostichopus Japonicus* (Selenka). *J. Thermal. Biol.* 60, 155–161. doi: 10.1016/j.jtherbio.2016.07.011

Yu, H. B., Gao, Q. F., Dong, S. L., Zhou, J. S., Ye, Z. and Lan, Y. (2016b). Effects of Dietary N-3 Highly Unsaturated Fatty Acids (HUFAs) on Growth, Fatty Acid Profiles, Antioxidant Capacity and Immunity of Sea Cucumber *Apostichopus Japonicus* (Selenka). *Fish. Shellfish. Immunol.* 54, 211–219. doi: 10.1016/j.fsi.2016.04.013

Yu, Z. H., Zhou, Y., Yang, H. S. and Hu, C. Q. (2014). Survival, Growth, Food Availability and Assimilation Efficiency of the Sea Cucumber *Apostichopus Japonicus* Bottom-Cultured Under a Fish Farm in Southern China. *Aquaculture.* 426-427, 238–248. doi: 10.1016/j.aquaculture.2014.02.013

Zamora, L. N. and Jeffs, A. G. (2012). Feeding, Metabolism and Growth in Response to Temperature in Juveniles of the Australasian Sea Cucumber, *Australostichopus Mollis*. *Aquaculture.* 358-359, 92–97. doi: 10.1016/j.aquaculture.2012.06.024

Zamora, L. N., Yuan, X. T., Carton, A. G. and Slater, M. J. (2018). Role of Deposit-Feeding Sea Cucumbers in Integrated Multitrophic Aquaculture: Progress, Problems, Potential and Future Challenges. *Rev. Aquaculture.* 10, 57–74. doi: 10.1111/raq.12147

Zhou, Z., Jiang, Q. F., Wang, M. Q., Yue, F., Wang, L. L., Wang, L. L., et al. (2013). Modulation of Haemocyte Phagocytic and Antibacterial Activity by Alpha-Adrenergic Receptor in Scallop *Chlamys Farreri*. *Fish. Shellfish. Immunol.* 35, 825–832. doi: 10.1016/j.fsi.2013.06.020

Conflict of Interest: The authors declare that the research was conducted in the absence of any commercial or financial relationships that could be construed as a potential conflict of interest.

frontiers | Frontiers in Marine Science

TYPE Original Research
PUBLISHED 01 August 2022
DOI 10.3389/fmars.2022.917045

OPEN ACCESS

EDITED BY
Mercedes González-Wangüemert,
University of Algarve, Portugal

REVIEWED BY
Nathalie Rose Le François,
Espace pour la vie, Canada
Susana Galante-Oliveira,
University of Aveiro, Portugal

*CORRESPONDENCE
Hongsheng Yang
hshyang@ms.qdio.ac.cn

SPECIALTY SECTION
This article was submitted to Marine Fisheries, Aquaculture and Living Resources, a section of the journal Frontiers in Marine Science

RECEIVED 10 April 2022
ACCEPTED 01 July 2022
PUBLISHED 01 August 2022

CITATION
Xu S, Liu S, Sun J, Zhang L, Lin C, Sun L, Xing L, Jiang C and Yang H (2022) Optimizing cryopreservation of sea cucumber (*Apostichopus japonicus*) sperm using a programmable freezer and computer-assisted sperm analysis. *Front. Mar. Sci.* 9:917045. doi: 10.3389/fmars.2022.917045

Optimizing cryopreservation of sea cucumber (*Apostichopus japonicus*) sperm using a programmable freezer and computer-assisted sperm analysis

Shuai Xu[1,2,3,4,5,6], Shilin Liu[1,2,3,4,5,6], Jingchun Sun[1,2,3,4,6], Libin Zhang[1,2,3,4,5,6], Chenggang Lin[1,2,3,4,5,6], Lina Sun[1,2,3,4,5,6], Lili Xing[1,2,3,4,5,6], Chunxi Jiang[1,2,3,4,5,6] and Hongsheng Yang[1,2,3,4,5,6,7]*

[1]Chinese Academy of Sciences (CAS) Key Laboratory of Marine Ecology and Environmental Sciences, Institute of Oceanology, Chinese Academy of Sciences, Qingdao, China, [2]Laboratory for Marine Ecology and Environmental Science, Qingdao National Laboratory for Marine Science and Technology, Qingdao, China, [3]Center for Ocean Mega-Science, Chinese Academy of Sciences, Qingdao, China, [4]Chinese Academy of Sciences (CAS) Engineering Laboratory for Marine Ranching, Institute of Oceanology, Chinese Academy of Sciences, Qingdao, China, [5]University of Chinese Academy of Sciences, Beijing, China, [6]Shandong Province Key Laboratory of Experimental Marine Biology, Qingdao, China, [7]The Innovation of Seed Design, Chinese Academy of Sciences, Wuhan, China

The sea cucumber *Apostichopus japonicus* has high nutritional, medicinal, and economic value. However, factors such as overexploitation, climate change, and environmental pollution have resulted in serious germplasm degradation in both farmed and wild *A. japonicus*, and it has been listed as endangered on the IUCN (International Union for Conservation of Nature) Red List of Threatened Species. Cryopreservation is an important method to protect germplasm resources and solve the problem of germplasm degradation. Using a programmable freezer and computer-aided sperm analysis, we comprehensively studied and screened the factors that affect the post-thaw motility of *A. japonicus* sperm during cryopreservation. Based on our results, we propose the following optimal cryopreservation procedure for *A. japonicus* sperm: cryo-diluent composition of 12.5% dimethyl sulfoxide and 0.1 mol/L glucose, with filter-sterilized (the filter mesh size: 0.45μm) natural seawater (NSW) as the extender; 1:5 mixing ratio of sperm and cryo-diluent; cooling rate and thawing temperatures of 10°C/min and 20°C, respectively. The post-thaw motility of sperm treated using the optimal procedure was > 65%, the fertilization rate (in the blastocyst stage) was nearly 80%, and the hatching rate (in the early auricularia larva stage) was > 65%. Additionally, frozen sperm that had been cryopreserved for 1 year retained a considerable post-thaw motility and fertilization rate compared to recently cryopreserved sperm. We detected obvious differences in sperm freezability among individual *A. japonicus*, and cryopreservation caused some damage to the sperm structure. In conclusion, our optimized procedure make large-scale

cryopreservation of *A. japonicus* sperm possible, and our results provide valuable information that could be applied to research and conservation of *A. japonicus*.

KEYWORDS

***Apostichopus japonicus*, sperm, cryopreservation, motility, CASA, programmable freezer**

1 Introduction

Sea cucumbers are important marine species with an annual net global production of nearly 220,000 tons, yielding a gross value of over $7 billion US dollars (Liu et al., 2020). The sea cucumber *Apostichopus japonicus* is considered to be the most nutritious edible sea cucumber with a high nutrional and medicinal value (Bordbar et al., 2011; Ru et al., 2019; Xing et al., 2021). *A. japonicus* is widely cultivated in China and has gradually become one of the most important fishery resources in Asia (Yang et al., 2015). However, factors such as overexploitation, climate change, and environmental pollution have resulted in serious germplasm degradation in both farmed and wild *A. japonicus*, and it has been listed as endangered on the IUCN (International Union for Conservation of Nature) Red List of Threatened Species. Germplasm degradation in farmed *A. japonicus* mainly causes problems such as slow growth, frequent disease outbreaks, and low survival rates, which result in billions in economic losses in China every year (Xia et al., 2012; Wang et al., 2014b). Therefore, preservation of *A. japonicus* germplasm resources has become an urgent task.

The development of cryopreservation protocols is important for protecting germplasm resources and solving the problem of germplasm degradation. Cryopreservation has many advantages, such as establishment of biobanks; providing year-round access to high quality material; breaking through geographic isolation; realizing remote hybridization; and protecting endangered species (Paredes, 2015; Paredes, 2016; Paredes et al., 2019). Compared with germplasm resources such as eggs and embryos, spermatozoa are easier to use in cryopreservation research due to their simpler structure (Tsai and Lin, 2012; Paredes et al., 2019; Campos et al., 2021). Generally, the sperm cryopreservation process includes sperm collection, quality evaluation, cryo-diluent (extender and cryoprotectant agent (CPA)) preparation, mixing of cryo-diluent with semen, cooling, storage, thawing, and sperm quality evaluation after thawing. Among these steps, the type and concentration of CPAs (cryoprotectant agents), the type of extenders, the mixing ratio of sperm and cryo-diluent, the cooling procedure, and the thawing procedure greatly impact the quality of the sperm after thawing, and the most suitable conditions for these factors vary by species (Dunn and Mclachlan, 1973; Akarasanon et al., 2004; Paredes, 2015).

In contrast to the abundance of cryopreservation studies focused on mammals, fish, and plants, few studies of marine invertebrates have been reported (Paredes, 2015). Of the exiting studies, mollusks (mainly oysters) and echinoids (mainly sea urchins) together account for 72% of the research subjects (Liu et al., 2015; Paredes, 2015; Paredes, 2016; Paredes et al., 2019). At present, only two studies of cryopreservation of sea cucumber sperm have been published (Shao et al., 2006; Mizuno et al., 2019). Shao et al. (2006) reported that the optimal freezing rate, sperm motility, and fertilization rate after thawing were 35°C/min, 76.7 ± 2.9%, and 60.2 ± 5.4% respectively, whereas Mizuno et al. (2019) reported 10.4°C/min, 19.3 ± 1.1%, and 89.8 ± 1.7%, respectively.

These significantly different results may be related to their experimental facilities and experimental methods, which are subject to more subjective factors. To date, most studies of cryopreservation of echinoderm sperm have controlled the freezing rate by adjusting the distance of the sample from the liquid nitrogen surface, and assessment of sperm motility has been conducted visually using an optical microscope. These methods have too many subjective factors and potential procedural errors to accurately assess the quality of frozen sperm (Dunn and Mclachlan, 1973; Asahina and Takahashi, 1978; Adams et al., 2004; Shao et al., 2006; Jalali and Crawford, 2012; Fabbrocini et al., 2014; Paredes, 2015; Paredes, 2016; Mizuno et al., 2019; Paredes et al., 2019).

To eliminate the influence of subjective factors and errors as much as possible, we used a programmable control rate freezer to control the freezing rate of sperm and computer-assisted sperm analysis (CASA) to quantify sperm motility (Paredes, 2015; Wu et al., 2019). We evaluated key parameters in the cryopreservation of sea cucumber sperm to identify the optimal cryopreservation method for *A. japonicus* sperm. Fertilization rate and hatching rate of frozen sperm with different post-thawing motility were examined, and the application value of frozen sperm that had been cryopreserved for one year was tested. Our results can be used to establish a standardized protocol for *A. japonicus* sperm cryopreservation technology and a dedicated cryobank for *A. japonicus* sperm.

2 Materials and methods

2.1 Materials

Sexually mature *A. japonicus* with a weight of 300–450 g were collected from the sea area of Yantai, China during the spawning season (May–July). About 40 sea cucumber (about 10 ind/m^3) were maintained in two 2,000 L tanks (2×1×1 m^3) filled with circulating seawater at 10-15°C in our laboratory. Continuous aeration was provided to ensure adequate oxygen and 40% of the seawater in each container was changed daily to guarantee good water quality. The culture water quality parameters were: temperature

10-15°C, salinity 30 ± 2 ppt, pH 7.8-8.2, and dissolved oxygen > 8mg·L^{-1}. Sea cucumber was fed at 10 a.m. and 22 p.m. every day. The sea cucumbers feces were collected by siphon before changing the water. The uneaten food was also removed by siphoning.

2.2 Sperm collection and motility test

We removed sea cucumbers from the maintenance tanks for gamete collection and placed them individually in 20 L buckets connected to an air pump. For each spawning session, we injected 500 μL of 5 mg/L of a peptide (NGIWYamide, Wuhan Dangang Biotechnology Co., Ltd, Hubei, China) into the abdomen of three to five sea cucumbers. About 40 minutes after the injection, the sea cucumbers expelled gametes from the genital pore; females ejected granular eggs, and males ejected white, smoke-like semen (Kato et al., 2009). As soon as white semen was visible, which identified the specimen as male, the animal was immediately selected and dissected to obtain the testis. We used a sterile scalpel to dissect the sea cucumber, removed the complete testis, and dried its surface. We then cut the testis into pieces with scissors, placed the pieces into a sterile 50 mL centrifuge tube and filtered them through a 0.048 mm mesh in the tube, and placed the obtained semen in a 4°C constant temperature incubator until use. The whole process was conducted on crushed ice (Shao et al., 2006).

Sperm were activated by a 1:1000 dilution with activator. The composition of the activator was filter-sterilized (the filter mesh size: 0.45μm) NSW containing 5 wt% albumin (EVERY GREEN, Zhejiang, China) (Paredes et al., 2013; Mizuno et al., 2019). After the sperm were activated for about 30 s, we added 10 μL of the mixed solution to the sperm counting plate and placed it in the CASA system (ML-500JZ, Nanning Songjintianlun Biotechnology Co., Ltd, Nanning, China) to quantify sperm motility. Each sample was measured three times, and data from at least two fields of view were recorded each time. The CASA system was equipped with MAILANG sperm automatic analytical software (Nanning Songjintianlun Biotechnology Co., Ltd, Nanning, China), a high contrast sperm optical imaging lighting device, and a MAILANG computer sperm scanning counting board (Wu et al., 2019). The acquisition parameters were set as follows: frame rate = 60/s; total captured images = 60; microscope 100x magnification. We analyzed the following semen characteristics using the CASA system: a) sperm density (SD): the number of spermatozoid(spz) per unit volume in semen (spz/mL); b) sperm motility rate (SMR): motile sperm count as a percentage of total sperm count; c) sperm curvilinear velocity (VCL-tm, μm/sec): the ratio of the distance traveled by the sperm along the two-dimensional movement curve seen in the microscope to time; d) straight line velocity (VSL-tm, μm/sec): the average of the straight-line distance traveled by the sperm in the tested time range versus the time value; and e) beat cross frequency (BCF): whips per second) (Fabbrocini et al., 2016; Van Der Horst et al., 2018).

2.3 Protocol for sperm cryopreservation experiment

According to previous relevant experimental results (Adams et al., 2004; Shao et al., 2006; Jalali and Crawford, 2012; Fabbrocini et al., 2014; Liu et al., 2015; Paredes, 2015; Paredes, 2016; Mizuno et al., 2019; Paredes et al., 2019), we first established the general procedure for the sea cucumber sperm cryopreservation experiment using a programmable control rate freezer (CBS Micro-Digitcool, IMV Technologies (Shanghai) Co., Ltd) (http://www.cryobiosystem.cn). The steps were as follows:

(1) We prepared the cryo-diluent in advance and stored it in a 4°C constant temperature incubator until use. We made the cryo-diluent by mixing the extender and cryoprotectant in a certain volume ratio. For example, mix 45ml NSW and 5ml DMSO to make 50ml of 15% DMSO as cryo-diluent.

(2) Using fresh semen with sperm motility > 85%, we mixed fresh semen and cryo-diluent according to a certain dilution ratio into 2 mL cryotubes. The process was conducted on crushed ice. For example, mix 80ml fresh semen and 400ml cryo-diluent into 2 mL cryotubes at a dilution ratio of 1:5.

(3) We mixed the sample in the cryotube, immediately placed it in the programmable cooling instrument, and ran the cooling program. The cooling procedure was as follows: sample equilibration at 0°C for 5 min, cooling to -80° at a specific cooling rate, equilibration at -80°C for 5 min, cooling to -150°C at a cooling rate of 20°C/min, equilibration at -150°C for 5 min, and storage in liquid nitrogen (-196°C) for medium and long-term storage.

(4) The cryotube was removed from the liquid nitrogen after at least 2 h, and the sample was thawed in a water bath at 20°C, shaken gently, removed immediately when only a small amount of solids remained, and shaken in

air until completely thawed. Sperm vitality then was checked immediately. A certain volume of thawed frozen semen was evenly mixed with the activator so that the total dilution reached 600 times. For example, mix 10ul thawed frozen semen and 990ul activator at a dilution ratio of 1:5. After the sperm were diluted and activated for about 30 s, 10 μL of the activated frozen semen was added to the sperm counting plate, and the sperm motility analysis was performed with CASA.

2.4 Screening of the optimal parameters for sperm cryopreservation

Based on the basic protocol of sea cucumber sperm mother liquor cryopreservation described above, we screened each key part to select the optimal parameters for sperm cryopreservation. Each screening experiment was carried out in sequence, and the next experiment was performed after analyzing the results of the previous experiment. The semen used in each screening experiment came from only one sea cucumber.

2.4.1 Screening for the optimal extender

We tested seven different extenders [D15, Cortland, MPRS, artificial seawater (ASW), filter-sterilized (the filter mesh size: 0.45μm) NSW, Hank's Balanced Salt Solution (HBSS), and calcium-free Hank's (D-Hank's)], all of which are commonly used extenders in the cryopreservation of fish and invertebrate sperm (Adams et al., 2004; Shao et al., 2006; Fan et al., 2014; Figueroa et al., 2018; Vuthiphandchai et al., 2021) (Table 1). In this experiment, we used dimethyl sulfoxide (DMSO) as the cryoprotectant; cryo-diluent was prepared with a concentration of 10%; the mixing ratio of semen and cryo-diluent was 1:5; the cooling rate was 15°C/min; and the thawing temperature was 20°C. There were six replicates in each experimental group. Table 1 shows the formulas of the six extenders.

2.4.2 Screening for optimal cooling rate

In this experiment, we tested five cooling rates: 10°C/min, 15°C/min, 20°C/min, 25°C/min, and 30°C/min (Paredes, 2015; Paredes, 2016; Paredes et al., 2019). We used NSW and DMSO as extender and cryoprotectant to prepare cryo-diluent with a concentration of 10%, and the mixing ratio of semen and cryo-diluent was 1:5. The thawing temperature was 20°C. There were four replicates in each experimental group.

2.4.3 Screening for optimal dilution ratio

The dilution ratio is the mixing ratio of sperm and cryo-diluent. In this experiment, we tested six dilution ratios: 1:1, 1:3, 1:5, 1:7, 1:9, and 1:19. We used NSW and DMSO as extender and cryoprotectant to prepare cryo-diluent with a concentration of 10%, the cooling rate was 10°C/min, and the thawing temperature was 20°C. There were four replicates in each experimental group.

2.4.4 Screening for optimal thawing temperature

In this experiment, we tested three thawing temperatures: 20°C, 37°C, and 50°C. We used NSW and DMSO as extender and cryoprotectant to prepare cryo-diluent with a concentration of 10%, the cooling rate was 10°C/min, and the mixing ratio of semen and cryo-diluent was 1:5. There were six replicates in each experimental group.

2.4.5 Screening for optimal cryoprotectant type and concentration

We tested six commonly used CPAs: DMSO, propylene glycol (PG), ethylene glycol (EG), glycerol (GLY), methanol (MeOH), and dimethylacetamide (DMA) (Paredes, 2015; Paredes, 2016; Paredes et al., 2019). We used NSW as the extender to prepare cryo-diluent

TABLE 1 Composition of the six extenders used in this study.

Item (g/L)	D15	Cortland	MPRS	ASW	Hank's	D-Hank's
NaCl	8	7.25	3.53	26.52	8	8
KCl	1	0.38	0.24	0.73	0.4	0.4
$CaCl_2$	–	0.18	0.17	1.14	0.14	–
$NaHCO_3$	–	1	0.25	0.2	0.35	0.35
KH_2PO_4	–	–	–	–	0.06	0.06
$MgCl_2{\cdot}6H_2O$	–	–	0.19	2.45	–	–
$MgSO_4{\cdot}7H_2O$	–	0.23	–	3.31	0.2	–
$Na2HPO_4{\cdot}12H_2O$	–	–	–	–	0.126	0.126
$NaH2PO_4{\cdot}H_2O$	–	0.41	0.22	–	–	–
NaBr	–	–	–	0.08	–	–
D-Glu	15	1	11	–	1	1
Penicillin-streptomycin	1%	1%	1%	1%	1%	1%
pH	6.50	7.00	6.68	8.00	6.80	6.80

with concentrations of 5%, 10%, 15%, and 20% for each CPA. The mixing ratio of semen and cryo-diluent was 1:5, the cooling rate was 10°C/min, and the thawing temperature was 20°C. There were four replicates in each experimental group, and further screening will be carried out if necessary.

2.4.6 Screening for optimal co-CPAs

We tested three co-CPAs (non-permeable CPAs: sucrose, glucose (Glu), trehalose) at 0.025 mol/L, 0.05 mol/L, 0.1 mol/L, and 0.2 mol/L, and egg yolk powder at 10%, 20% (W/V). We used NSW and DMSO as the extender and cryoprotectant to prepare cryo-diluent with a concentration of 12.5%, the cooling rate was 10°C/min, the dilution ratio was 1:5, and the thawing temperature was 20°C. There were four replicates in each experimental group. The control group did not add co-CPAs and other conditions remained unchanged.

2.4.7 Screening for optimal frozen storage volume and type of cryotube

We tested 0.5 mL of cryo-diluent in a 0.5 mL cryotube and 0.5 mL, 1 mL, and 2 mL of cryo-diluent in a 2 mL cryotube. We used NSW and DMSO as the extender and cryoprotectant and prepared cryo-diluent with a concentration of 12.5%. The cooling rate was 10°C/min, the dilution ratio was 1:5, and the thawing temperature was 20°C. There were four replicates in each experimental group.

2.5 Fertilization experiment using frozen sperm with different cryopreservation formulas

Based on the results of the screening experiments described above, we conducted fertilization rate and hatching rate experiments using sperm from eight different groups of sperm: groups of sperm from five frozen formulas with different frozen sperm motility (A: 12.5% DMSO+ 0.1 mol/L Glu; B: 12.5% DMSO; C: 20% PG; D: 10% EG; and E: 20% DMA); sperm from formulas A and B that were cryopreserved for 1 year (A-1yr, B-1yr); and fresh unfrozen sperm (control group). There were three replicates in each experimental group.

After female sea cucumbers described in section 2.2 released eggs, we collected and rinsed fresh eggs to prepare the mother solution and calculate the egg concentration. Fertilization experiments were carried out within 2 h after eggs were released. We prepared fresh unfrozen sperm in advance and we thawed the frozen sperm, and then we calculated the concentration of sperm using CASA. Finally, fresh semen and frozen semen were separately mixed with eggs in 2 L beakers at a sperm-to-egg ratio of 10,000:1 (Shao et al., 2006). The beakers were filled with 2 L of filtered NSW and continuously aerated, and a heating rod was used to keep the water temperature at a constant temperature of 20°C. The fertilization rate and the hatching rate were calculated at 10 h and 52 h after fertilization, and random samples were taken from each beaker for measurement at each time point. The fertilization rate was calculated as the percentage of embryos in the blastocyst stage to the total number of cells in the field of view. The hatching rate was calculated as the percentage of the number of early auricularia larva to the total number of cells in the field of view.

2.6 Ultrastructure of fresh and cryopreserved sperm

Samples from fresh and thawed cryopreserved sperm treated with frozen formula A described above were sent to Wuhan Service Biotechnology Co., Ltd. for examination of ultrastructure using scanning electron microscopy (SEM) and transmission electron microscopy (TEM). Please refer to the website for the related operation steps (https://www.servicebio.cn/data-detail?id=4301&code=DJSYBG).

2.7 Statistical analysis

All data are presented as the mean ± standard error (SE). Statistical analysis was performed using IBM SPSS software 23.0 (Armonk, NY, USA). The percentage data for various treatment and control groups, such as SMR, fertilization rate, and hatching rate, were arcsine-square root transformed, and the normality of the distribution of the data was evaluated using the Shapiro-Wilk test. The equality of the groups was assessed using the F test or Bartlett's test. The Tukey multiple comparison test and Student's *t*-test were conducted to examine differences among the groups. For cases in which the data did not pass the normality test or the equality test, the statistical significance of the differences among the groups was calculated using the non-parametric Kruskal-Wallis H test. All significance levels were set at $P < 0.05$.

3 Results

3.1 Information about different sea cucumber individuals

Table 2 lists relevant information about seven sea cucumber individuals and their sperm before and after cryopreservation. Gross weight (GW) showed a correlation with body wall weight (BWW) and testis weight (TW) (R = 0.63; R = 0.70, respectively), and TW had the strongest correlation with semen volume (SV). Therefore, we initially assessed the relationship between SV and GW of sea cucumbers (y = 0.19x – 51.82, R =0.71, y = SV, x = GW) so that we could use the gross weight of sea cucumbers at the mature stage to estimate the amount of semen excreted. Fresh sperm motility (FSM) and fresh sperm density (FSD) were not

strongly correlated with GW (R=0.39, R=0.32). Additionally, there was no correlation between FSM and FSD or between FSM and post-thawing sperm motility (TSM). We found that the cryopreservation process significantly reduced sperm density ($P < 0.05$): the density in fresh samples was 2.0–5.0×10^{10} Pcs/mL compared to 1.0–2.0×10^{10} Pcs/mL in thawed samples. The fresh sperm velocity was significantly higher than that of post-thawing sperm. The curvilinear velocity and straight-line velocity of *A. japonicus* fresh sperm were generally in the range of 80-100 μm/s and 50-70 μm/s respectively. The curvilinear velocity and straight-line velocity of *A. japonicus* frozen sperm were generally in the range of 40-90 μm/s and 30-60 μm/s respectively.

3.2 Optimal extender

Table 2 and Figure 1 show the composition of the six extenders tested and the results of the screening experiment, respectively. The post-thaw motility was highest when the extender was NSW (45.97% ± 2.30%), followed by ASW (40.97% ± 1.32%) and D15 (32.05% ± 2.23%). Cryopreserved spermatozoa showed lower motilities (< 15%) when the other three extenders were used.

3.3 Optimal cooling rate

Figure 2 shows the post-thaw motility of sperm that were cryopreserved using five different cooling rates. As the cooling rate increases, the sperm motility significantly decreased gradually ($P < 0.05$). The post-thaw motility was highest at the cooling rate of 10°C/min (49.43% ± 3.63%), followed by 15°C/min (45.66% ± 3.98%), and these motility values did not differ significantly ($P > 0.05$).

3.4 Optimal dilution ratio

When we tested six different dilution ratios, we found that post-thaw motility was highest when the mixing ratio of sperm and cryo-diluent was 1:5 (29.79% ± 1.70%), followed by 1:7 (27.84% ± 1.48%), 1:9 (26.23% ± 1.21%), and 1:3 (24.54% ± 1.60%), and there was no significant difference in motility among these groups ($P > 0.05$) (Figure 3). When the dilution ratio was too small (1:19) or too large (1:1), lower sperm motilities were recorded (13.51% ± 2.04% and 15.60% ± 0.58%, respectively). Therefore, we used 1:5 as the dilution ratio in subsequent screening experiments.

3.5 Optimal thawing temperature

We found that higher thawing temperature resulted in lower post-thaw sperm motility (Figure 4). The post-thaw motility was highest when the thawing temperature was 20°C (27.23% ± 1.83%), which was significantly higher than that at 37°C (18.84% ± 1.79%) and 50°C (14.59% ± 1.19%) ($P < 0.05$).

3.6 Optimal cryoprotectant type and concentration

Figure 5A shows the post-thaw motility of spermatozoa that were cryopreserved with diluents containing one of six kinds of CPAs at one of four concentrations. The motility was highest when using 10% DMSO as the CPA (16.17% ± 0.50%), followed by 15% DMSO (14.91% ± 0.60%), and these motility values did not differ significantly ($P > 0.05$). Among the other CPAs, the 20% PG (7.84% ± 0.61%), 10% EG (4.98% ± 0.98%), and 20% DMA (6.52% ± 0.84%) treatment groups had relatively high

TABLE 2 Information about different sea cucumber individuals and their sperm before and after cryopreservation.

Number	GW/BWW(g)	TW(g)	SV(ml)	FSM/TSM(%)	FSD/TSD(10^{10} Pcs/ml)	FVCL/TVCL(μm/sec)	FVSL/TVSL (μm/sec)
1	367.5/ 220.8	48.8	33.5	89.28 ± 4.32/ 61.98 ± 0.99	2.5 ± 0.2/ 1.7 ± 0.1	103.73 ± 3.29/ 88.18 ± 6.14	69.84 ± 1.66/ 64.64 ± 5.36
2	334.0/ 223.8	24.0	17.0	96.79 ± 1.21/ 30.43 ± 2.23	4.8 ± 0.1/ 2.1 ± 0.1	98.33 ± 2.45/ 41.3 ± 2.73	54.44 ± 1.59/ 25.31 ± 3.68
3	334.2/ 196.8	15.0	7.5	93.24 ± 2.32/ 26.46 ± 0.56	4.3 ± 0.3/ 1.5 ± 0.1	93.56 ± 1.77/ 65.22 ± 6.24	52.64 ± 1.29/ 43.6 ± 4.46
4	444.5/ 244.1	49.9	34.5	93.70 ± 2.34/ 39.23 ± 2.83	4.8 ± 0.2/ 1.6 ± 0.1	87.19 ± 0.88/ 73.79 ± 6.58	49.22 ± 0.53/ 33.6 ± 4.46
5	365.6/ 249.0	14.7	8.1	77.84 ± 3.95/ –	2.0 ± 0.1/ –	93.15 ± 7.13/ –	62.74 ± 4.52/ –
6	314.8/ 217.2	23.8	13.1	68.81 ± 6.56/ –	2.4 ± 0.2/ –	78.44 ± 4.35/ –	54.42 ± 3.56/ –
7	341.2/ 226.0	21.6	9.8	65.53 ± 3.46/ –	2.7 ± 0.2/ –	60.78 ± 1.14/ –	29.97 ± 1.25/ –

All using the optimal cryopreservation procedure for A. japonicus sperm screened in this study. GW, gross weight; BWW, body wall weight; TW, testis weight; SV, semen volume; FSM, fresh sperm motility; FSD, fresh sperm density; TSM, post-thawing sperm motility; TSD, post-thawing sperm density; FVCL, fresh sperm curvilinear velocity; TVCL, post-thawing sperm curvilinear velocity; FVSL, fresh sperm straight-line velocity; TVSL, post-thawing sperm straight-line velocity. Data are the means ± SE (n = 6).

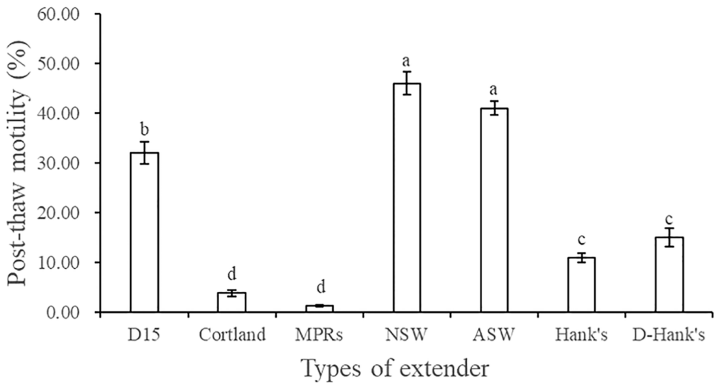

FIGURE 1
Effect of extender type on the post-thaw motility of *A. japonicus* spermatozoa. Data are presented as means ± SE (n = 6). Different letters indicate significant differences (P < 0.05). Data were not transformed when performing one-way ANOVA.

post-thaw sperm motility. Although the sea cucumber sperm used in this experiment had poor freezing resistance such that post-thaw sperm motility was not > 20%, we could still infer from the trend of the results that DMSO was the most suitable of the six antifreeze agents. Therefore, we conducted another screening experiment to identify the optimal concentration of DMSO and found that 12.5% DMSO yielded higher sperm motility than 10% DMSO and 15% DMSO (Figure 5B).

3.7 Optimal co-CPAs

Compared with the post-thaw sperm motility of the control group (38.34% ± 2.69%), the non-permeable co-CPA and concentration that achieved the highest post-thaw sperm motility was 0.1 mol/L Glu (65.07% ± 3.67%, P < 0.001), followed by 0.05 mol/L Glu (50.78% ± 1.98%, P < 0.05) (Figure 6). The post-thaw sperm motility of the other treatment groups was not significantly different from that of the control group (P > 0.05). The two concentrations of yolk (10% and 20%, W/V) did not achieve the expected effect as co-CPAs, and the post-thaw sperm was basically non-viable (< 2%).

3.8 Optimal frozen storage volume and type of cryotube

Figure 7 shows the post-thaw motility of sperm that were cryopreserved with different frozen storage volumes and types of cryotube. No significant difference in the cryopreservation effect was detected between the 0.5 mL and the 2 mL cryotubes (P > 0.05), for which the post-thaw motility values of sperm were

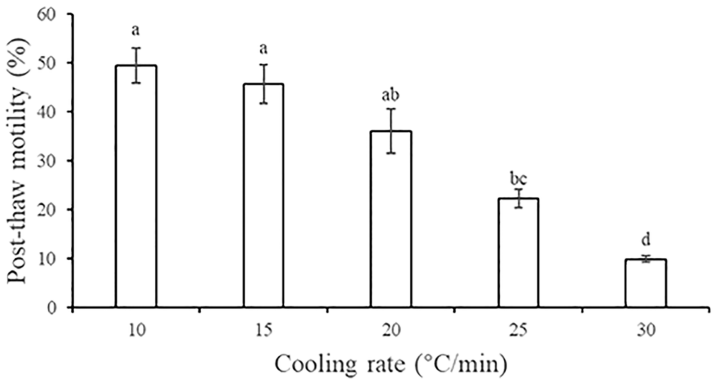

FIGURE 2
Effect of five cooling rates on the post-thaw motility of *A. japonicus* spermatozoa. Data are presented as the means ± SE (n = 4). Different letters indicate significant differences (P < 0.05). Data were not transformed when performing one-way ANOVA.

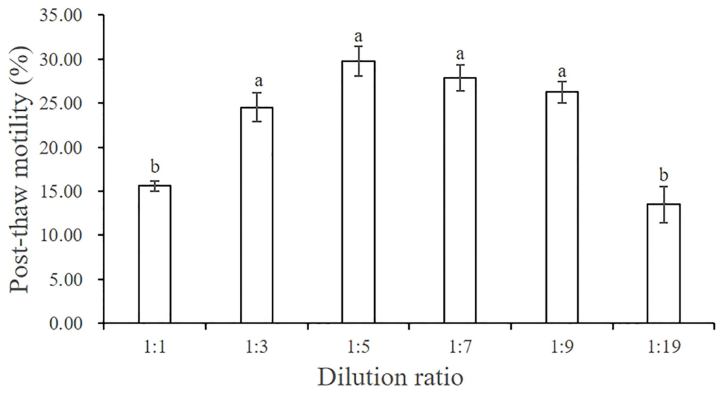

FIGURE 3
Effect of six dilution ratios on the post-thaw motility of *A. japonicus* spermatozoa. Data are presented as the means ± SE (n = 4). Different letters indicate significant differences (P < 0.05). Data were not transformed when performing one-way ANOVA.

57.44% ± 2.52% and 56.27% ± 6.41%, respectively, when filled with 0.5 mL of cryo-diluent. Additionally, post-thaw sperm motility did not differ significantly when the 2 mL cryotube was filled with different volumes of cryo-diluent.

3.9 Fertilization experiment using sperm frozen with different cryopreservation formulas

Based on the experiments described in sections 3.2–3.8, the optimal procedures for cryopreservation of *A. japonicus* sperm is as follows: cryo-diluent composition of 12.5% DMSO and 0.1 mol/L Glu using filter-sterilized (the filter mesh size: 0.45μm) NSW as the extender; 1:5 mixing ratio of sperm and cryo-diluent; cooling rate and thawing temperatures of 10°C/min and 20°C, respectively.

Sperm treated with the five different cryopreservation formulas had different post-thaw motility (Figure 8A). The motility was highest when using formula A (68.92% ± 0.97%), followed by formula B (63.04% ± 1.17%), and there was no significant difference between them (P > 0.05). Sperm treated with formulas C and E also achieved relatively high post-thaw motility (40.43% ± 7.33% and 34.45% ± 1.48%, respectively), but the values were significantly lower than those of formulas A and B (P < 0.05). The post-thaw motility of the sperm treated with formula D was extremely low (5.24% ± 1.43%), and the value was significantly different from those of the other formulas (P < 0.05). We also found that frozen sperm maintained a certain degree of vitality after one year of storage, and the corresponding

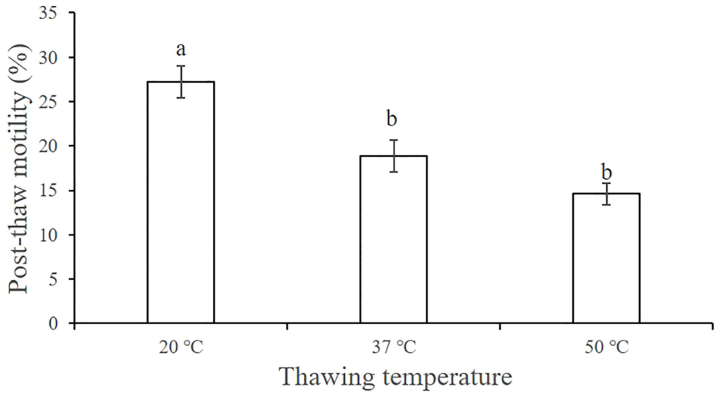

FIGURE 4
Effect of the thawing temperature on the post-thaw motility of *A. japonicus* spermatozoa. Data are presented as the means ± SE (n = 6). Different letters indicate significant differences (P < 0.05). Data were not transformed when performing one-way ANOVA.

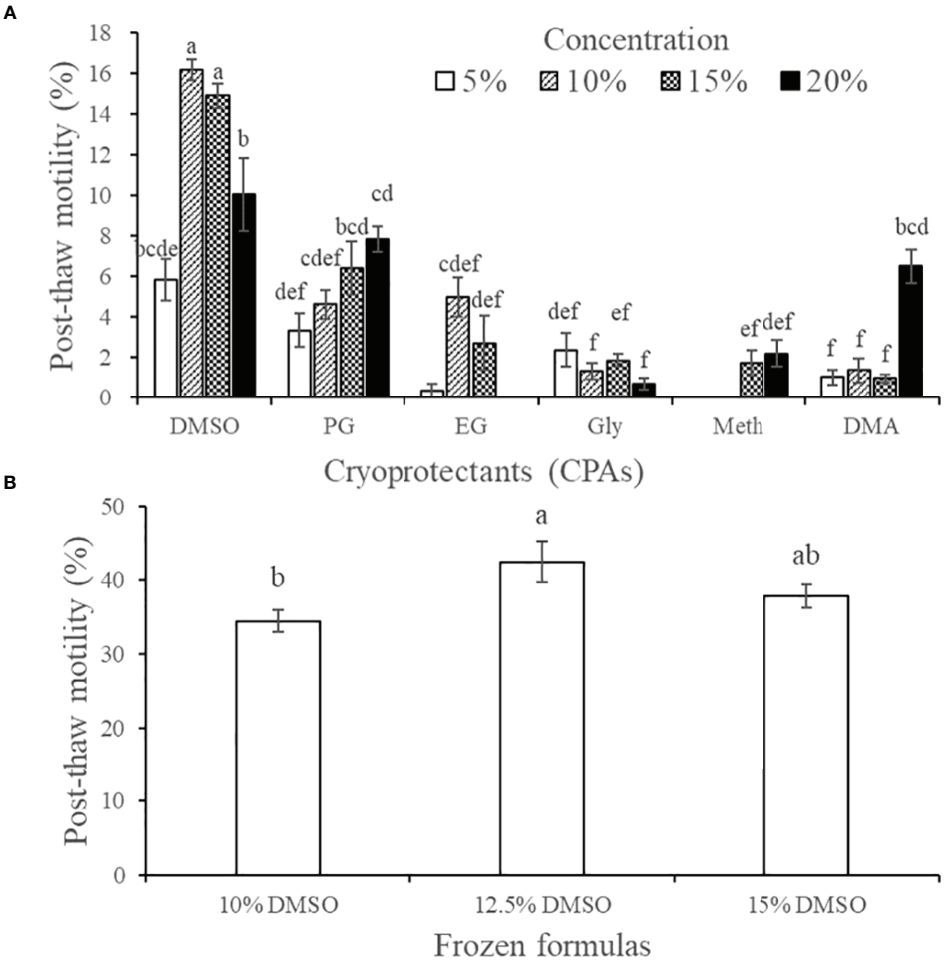

FIGURE 5
Effect of cryoprotective agents on the post-thaw motility of *A. japonicus* spermatozoa. **(A)** Preliminary screening results of six CPAs at four concentrations; **(B)** Further screening results of the optimal concentration of DMSO. Data are presented as the means ± SE (n = 4). Different letters indicate significant differences ($P < 0.05$). Data were not transformed when performing one-way ANOVA. Note: One-way ANOVA was performed on all treatment groups in A with a normal distribution, and discarding obviously invalid treatment group data.

post-thaw sperm motility values for formula A-1yr and formula B-1yr were 40.65% ± 1.08% and 36.08% ± 1.79%, respectively. The post-thaw motility of sperm cryopreserved with formula B after 1 year was not significantly different from its motility value a year earlier (38.34% ± 2.67%) (Figure 6).

After thawing, the fertilization rate of the cryopreserved sperm treated with formula A (79.03% ± 3.22%) was almost the same as that of fresh sperm (80.22% ± 1.90%), even though the motility of the fresh sperm was 99.00% ± 1.90% (Figure 8A). The fertilization rates of frozen sperm treated with formula B (73.34% ± 3.01%), formula C (72.86% ± 1.69%), formula A-1yr (66.67% ± 2.85%), and formula B-1yr (65.69% ± 1.04%) did not differ significantly from one another ($P > 0.05$). Although the post-thaw motility of the sperm treated with formula E was not significantly different from that of formula C, its fertilization rate was significantly lower than that of the other three formulas ($P > 0.05$), and a large number of deformed embryos appeared in this group. Formula D had the lowest fertilization rate due to the lowest post-thaw motility, and a large number of eggs were observed to be unfertilized and necrotic.

We measured the hatching rate 52 h after fertilization, so we observed both early auricularia larvae as well as some gastrula embryos. We counted both and used the sum of the two as the embryo survival rate (Figure 8B). The low post-thaw sperm motility and low fertilization rate of the formula D treatment group resulted in a low hatching rate, so we did not include the data in further analyses. Cryopreserved sperm treated with formula A had the highest hatching rate (66.74% ± 5.61%) and embryo survival rate (84.85% ± 2.70%), and the values were significantly higher than those of the other treatment groups ($P < 0.05$). Unexpectedly, the fresh sperm control group had a significantly lower hatching rate (43.03% ± 2.33%) than the formula A group ($P < 0.05$) and a significantly lower gastrula ratio (18.46% ± 3.19%) than the other

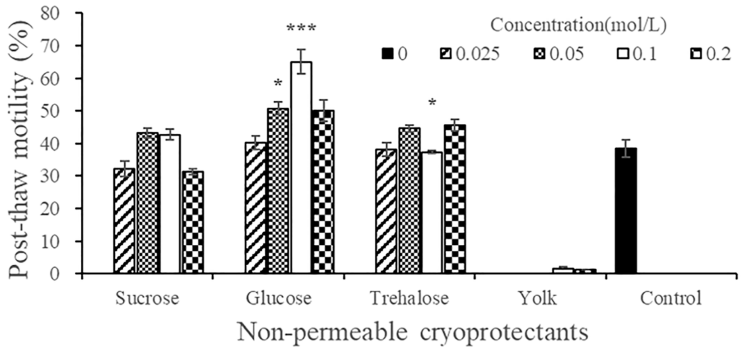

FIGURE 6
Effect of the types and concentrations of four non-permeable cryoprotectant agents on the post-thaw motility of *A. japonicus* spermatozoa. Note: The egg yolk powder uses the mass concentration (W/V), 0.1 represents 10% (0.1 kg/L), and 0.2 represents 20% (0.2 kg/L). Data are presented as the means ± SE (n = 4). Asterisks indicate significant differences between each experimental group and the control group (*P < 0.05, ***P < 0.001). One-way ANOVA was performed between the four concentration treatment groups of the three carbohydrates and the control group respectively, and data were not transformed.

treatment groups ($P < 0.05$). The water in the control group was turbid, with a lot of foam, and we speculate that this may be associated with the addition of an excessive number of sperm. Although the hatching rates of the formula B (44.06% ± 1.58%), formula C (37.51% ± 1.90%), and formula E (31.43% ± 1.30%) groups were significantly lower than those of formula A ($P < 0.05$), they had a relatively high proportion of gastrulae, resulting in a higher embryo survival rate, which means that the larvae had the potential to continue to develop.

3.10 Ultrastructure of fresh and cryopreserved sperm

Figure 9 shows the ultrastructure of fresh and cryopreserved *A. japonicus* sperm. SEM results showed that the head, middle, and tail of fresh sperm were intact and continuous (Figure 9A), whereas the head and middle of frozen sperm were ruptured and the tail was broken (Figure 9B). The proportions of morphologically normal sperm and morphologically deformed sperm in fresh semen were 89.0% and 11.0%, respectively. While those in cryopreserved sperm were 58.0% and 42.0%, respectively. TEM micrographs showed that the sperm membrane of fresh sperm was complete, the head and neck were continuous, the nucleus chromatin had high electron density, the proximal centriole structure was normal, the number of double microtubules was normal, all of them were symmetrically distributed in nine pairs, and there was no obvious separation between the central microtubules and the double microtubules (Figures 9C, E). In cryopreserved sperm, the sperm membrane was largely damaged, the organelles were free, the head was irregular, the nucleus was irregular in shape, the chromatin was condensed, the sub-acrosomal space was visible between nuclei, the

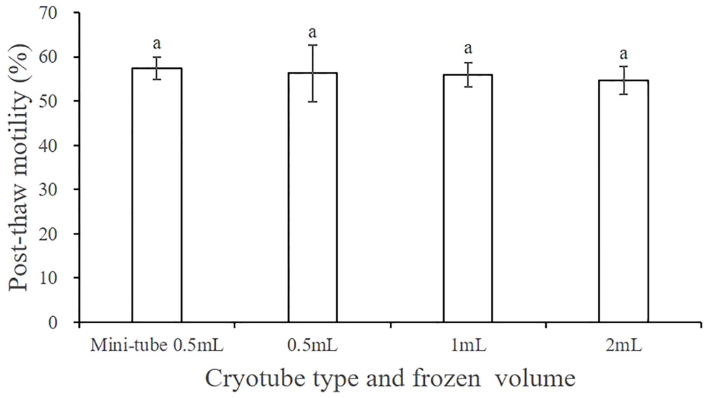

FIGURE 7
Effect of the cryotube types and frozen storage volume on the post-thaw motility of *A. japonicus* spermatozoa. Data are presented as the means ± SE (n = 4). Different letters indicate significant differences ($P < 0.05$). Data were not transformed when performing one-way ANOVA.

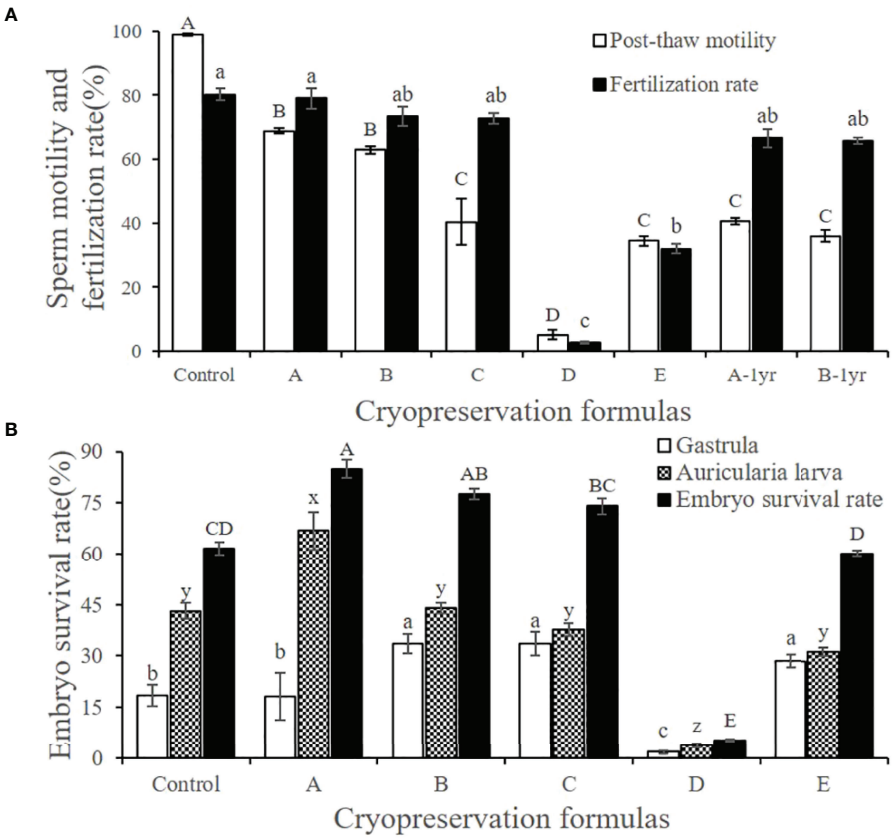

FIGURE 8
Effect of cryopreservation formulas with different post-thaw sperm motility on fertilization rate and hatching rate. (A) Post-thaw sperm motility and fertilization rate under different cryopreservation formulas. (B) Hatching rate of frozen spermatozoa under different cryopreservation formulas. Different cryopreservation formulas were (Control) Fresh unfrozen sperm; (A) 12.5% DMSO + 0.1 mol/L Glu; (B) 12.5% DMSO; (C) 20% DMA; (D) 10% EG; (E) 20% PG; (A-1yr) One-year cryopreservation of sea cucumber sperm with formula A; (B-1yr) One-year cryopreservation of sea cucumber sperm with formula **(B)** The rest of the freezing procedure was the same and was the optimum procedure. The fertilization rate and the hatching rate were calculated at 10 h (blastocyst stage) and 52 h (early auricularia larva stage) after fertilization. Data are presented as the means ± SE (n = 6). Different letters indicate significant differences ($P < 0.05$). Data were not transformed when performing one-way ANOVA.

sperm tail structure was swollen and the membrane was discontinuous, mitochondria were obviously swollen, the mitochondrial membrane was dissolved, cristae disappeared, most of the doublet microtubules were separated, and the sub-microtubule structure was absent (Figures 9D, F). These results showed that the cryopreservation process caused structural damage to *A. japonicus* sperm.

4 Discussion

4.1 The cryopreservation procedure for *A. japonicus* sperm

4.1.1 Extender

It is generally believed that an extender used for semen cryopreservation must be able to inhibit sperm motility and maintain the balance of cell electrolytes and osmotic pressure (Dong et al., 2005a; Liu et al., 2015). In cryopreservation studies of marine fish and mollusk sperm, Hank's balanced salt solution without Ca^{2+} is often used as the extender (Dong et al., 2005a). However, ASW or filtered NSW has been widely used as extender in echinoderm sperm cryopreservation research, but little is known about the effects of other potential extenders (Dunn and Mclachlan, 1973; Adams et al., 2004; Shao et al., 2006; Jalali and Crawford, 2012; Fabbrocini et al., 2014). It is worth noting that echinoderm sperm can be activated by ASW or filtered NSW, which is obviously contrary to the need for the extender to inhibit sperm motility (Shao et al., 2006).

In this study, we tested the effects of seven kinds of extenders on the motility of cryopreserved *A. japonicus* sperm and still found that using NSW as the extender resulted in the highest post-thaw motility (%), followed by ASW. NSW or ASW was suitable as the extender for echinoderm sperm cryopreservation

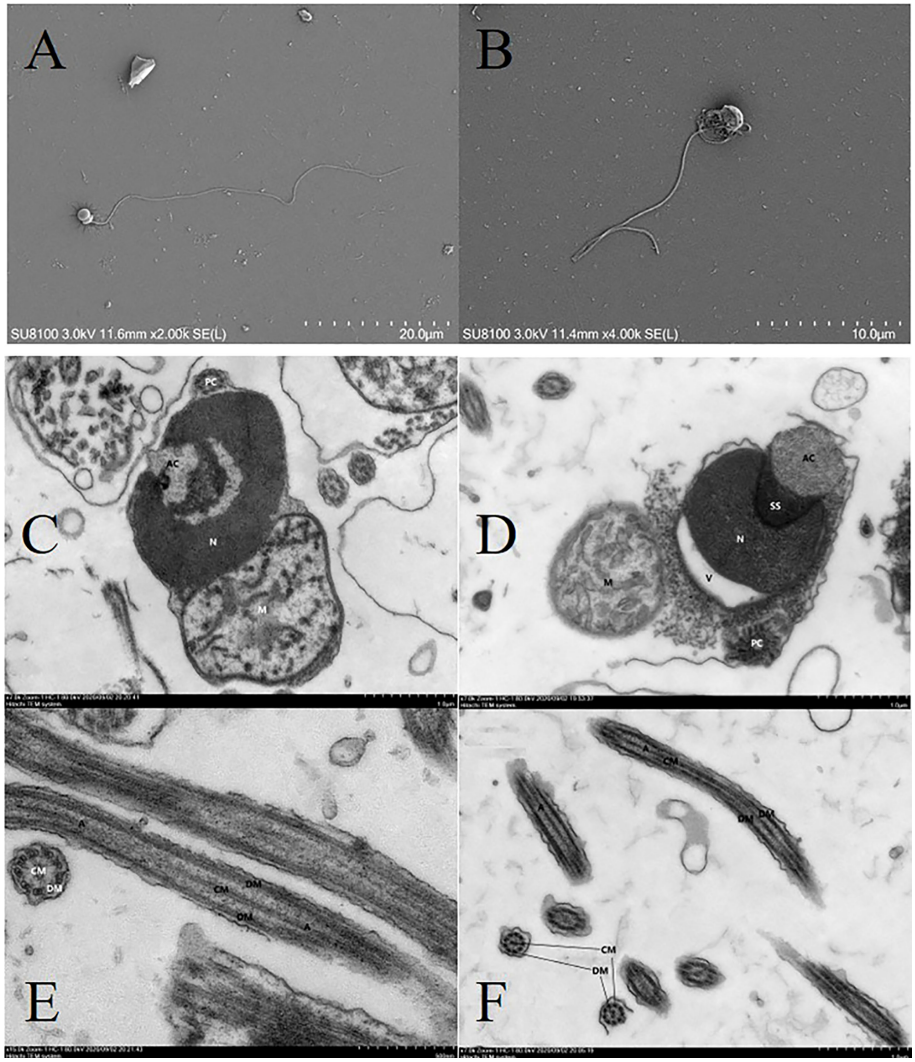

FIGURE 9
Electron micrographs showing structures of fresh and cryopreserved sperm of *A. japonicus*. SEM results: **(A)** fresh sperm; **(B)** cryopreserved sperm. TEM results: **(C)** head of fresh sperm; **(D)** head of cryopreserved sperm; **(E)** tail of fresh sperm; **(F)** tail of cryopreserved sperm. AC, acrosome; N, nucleus; M, mitochondrion; PC, proximal centriole; SS, subacrosome space; V, vesicle; A, axoneme; CM, central microtubules; DM, double microtubules; SEM, scanning electron microscopy.

may because the low amount of seawater used in the experiment that it did not activate all of the sperm and the longer survival time of the sperm after activation (Shao et al., 2006; Gallego et al., 2014; Fabbrocini et al., 2016). Shao et al. (2006) found that ASW concentration < 30% cannot activate *A. japonicus* sperm. Gallego et al. (2014) found that the sperm motilities and velocities of the sessile species (sea urchin and ascidian) were able to maintain at its initial value for a long time (about 45 min) after activation. Fabbrocini et al. (2016) found that sea urchin sperm could maintain high motility for 1 h after activation and maintain relative motility for 24 h. Although NSW is currently the most commonly used extender for cryopreservation of echinoderm sperm, we believe that we should continue to study the activation mechanism of sperm and develop new diluents to reduce the energy consumption of sperm (Liu et al., 2015).

4.1.2 Freezing techniques and cooling rate

Techniques to freeze sperm can be categorized as non-programmable (liquid nitrogen vapor) and programmable. Non-programmable freezing technique usually control the cooling rate by adjusting the distance of the sample from the liquid nitrogen (LN). Programmable freezing requires special equipment to control the cooling rate(s) precisely (Liu et al., 2015; Paredes, 2015). Programmable freezing offers more precise temperature control

and more accurate results than non-programmable freezing. To date, programmable freezing has been used frequently in studies of fish and mollusks, but it has rarely been used in cryopreservation research of echinoderm sperm.

In this study, we used a programmable control rate freezer to control the entire process of equilibrium and cooling, and found that frozen sperm had better post-thaw motility when the cooling rate was 10°C/min and 15°C/min and that post-thaw motility decreased as the cooling rate increased (Figure 2). Mizuno et al. (2019) reported that the post-thaw motility of frozen sperm was highest when the height of the sample from the liquid nitrogen level was 15 cm and the cooling rate was 10.4° C/min, which is basically consistent with our findings. In many previous echinoderm sperm cryopreservation studies, the optimal cooling rates ranged from 5°C/min to 50°C/min (Dunn and Mclachlan, 1973; Adams et al., 2004; Shao et al., 2006; Jalali and Crawford, 2012). However, these values were all based on non-programmable freezing techniques and different freezing devices, so the results are not comparable. Excessively rapid cooling may increase osmotic shock, cause more ice crystal damage, have irreversible effects on cells, and result in a sharp decline in sperm motility. In contrast, a cooling rate that is too slow will increase the toxicity of CPAs (Mazur, 1990; Gao and Critser, 2000; Pegg, 2002). Therefore, we will conduct further experiments to fully consider CPA toxicity, control the equilibration time, and combine different cooling rates to further optimize the cryopreservation technology for sea cucumber sperm. Our results can also be used to guide non-programmable freezing techniques of *A. japonicus* sperm.

4.1.3 Dilution and Thawing

Low levels of sperm dilution may lead to detrimental agglutination of sperm after thawing, whereas high levels of sperm dilution may result in rapid depletion of sperm energy, changes in physiology, and reduced protective components in semen (Paniagua-Chavez et al., 1998; Dong et al., 2005a). Studies have shown that the optimal dilution ratio for cryopreservation of echinoderm sperm ranges from 1:3 to 1:20 (Dunn and Mclachlan, 1973; Asahina and Takahashi, 1978; Adams et al., 2004; Shao et al., 2006; Fabbrocini et al., 2014). In this study, we found that dilution ratio in the range of 1:3 to 1:9 resulted in better post-thaw motility of frozen sperm compared to other ratios (Figure 3). Because sperm densities in fresh semen taken from individual gonads vary, it is reasonable to assume that the optimal cryopreservation dilution ratio for a species is actually a range (Asahina and Takahashi, 1978; Adams et al., 2004). To more effectively compare and optimize experimental protocols for sperm cryopreservation in future studies, we plan to dilute the sperm to a specific concentration and then carry out related optimization experiments.

Liu et al. (2015) divided the thawing temperature for cryopreservation of marine mollusk sperm into three ranges: low temperature (< 29°C), medium temperature (30°C–49°C), and high temperature (> 50°C). According to this standard, the thawing temperature of previous studies of cryopreservation of echinoderm sperm were low and medium temperatures, ranging from room temperature and 15°C to 45°C in a water bath (Dunn and Mclachlan, 1973; Adams et al., 2004; Shao et al., 2006; Jalali and Crawford, 2012; Fabbrocini et al., 2014; Mizuno et al., 2019). In this study, we found that the post-thaw motility of cryopreserved sperm from *A. japonicus* was highest at thawing temperature of 20°C (Figure 4). This result was similar to that previous studies (Anchordoguy et al., 1988; Mizuno et al., 2019). In contrast, Shao et al. (2006) reported that 37°C was the appropriate thawing temperature for cryopreservation of *A. japonicus* sperm. We believe that it may be more appropriate to use 20°C as the thawing temperature for cryopreservation of *A. japonicus* sperm because this temperature is the optimum temperature for sperm-egg union, and sperm thawed at this temperature are less stimulated (Ru et al., 2019). Thawing is the inverse process of freezing, and it may result in cryo-damage such as devitrification and recrystallization (He et al., 2004; Liu et al., 2015; Paredes, 2016; Guo and Weng, 2020). To date, little is known about proper thawing temperature selection for sperm cryopreservation in echinoderms, so the thawing process should be the focus of future research (Paredes, 2015).

4.1.4 CPAs and co-CPAs

In general, DMSO is the most used CPA for sperm cryopreservation. The addition methodology is highly variable, but the concentration range is usually 1–2 M (or 5%– 20%) (Liu et al., 2015; Paredes, 2015; Paredes, 2016). However, different sperm have specific optimal cryoprotectant and concentration ranges (Guo and Weng, 2020). For example, GLY has been used more successfully in the cryopreservation of shrimp and crab sperm, and it provides a better cryoprotective effect than DMSO on the semen of the horseshoe crab *Limulus polyphermus* (Behlmer and Brown, 1984) and the prawn *Macrobrachium rosenbergii* (Akarasanon et al., 2004). In invertebrates such as sea urchins and oysters, DMSO is the main permeating cryoprotectant used to preserve sperm, although EG and PG are also commonly used (Liu et al., 2015; Paredes, 2015; Paredes et al., 2019). However, DMSO can also be toxic, and its toxicity increases with increasing concentration (Nascimento et al., 2005; Paredes and Bellas, 2009; Tsai and Lin, 2012). The combination of permeating and non-permeating CPAs can improve sperm motility (Hassan et al., 2015).

In this study, we found that 12.5% DMSO + 0.1 mol/L Glu was the most suitable cryoprotectant formula for cryopreservation of sea cucumber sperm, which was in accordance with previously published reports (Paredes, 2015; Paredes, 2016; Tsai et al., 2018). Shao et al. (2006) reported that the optimal CPA for cryopreservation of *A. japonicus* sperm was 15% DMSO, but they only compared the concentrations of 15% and 20%. Mizuno et al.

(2019) reported that the optimal CPA for cryopreservation of *A. japonicus* sperm was 20% DMSO. However, the composition of their extender was 20% fetal bovine serum and 80% ASW, which may have affected the cryoprotectant osmolality, thus requiring a higher concentration of DMSO for freezing-dehydration. Sugar molecules typically interact with the lipid bilayer during the freezing phase to maintain plasma membrane integrity when cells undergo dehydration. When combined with other permeable cryoprotectants, sugar prolonged and enhanced cellular post-thaw viability, but the type and concentration of sugar should be optimized according to the species (Thurston et al., 2002; Dong et al., 2005b; Liu et al., 2014; Tsai et al., 2018). Future studies should assess the toxic effects and toxicity thresholds of different types and concentrations of CPAs on *A. japonicus* sperm in order to further improve the cryopreservation procedure.

4.1.5 Cryopreservation container

Straws (0.25–0.5 μL) and tubes (0.5–2 mL) are commonly used containers for sperm cryopreservation, and both have advantages (Liu et al., 2015; Paredes, 2015; Guo and Weng, 2020). Straws occupy less space and allow higher cooling and thawing rates, but they can only store small amounts of samples and are a bit cumbersome to handle.

Cryotubes have greater storage volume and can hold cryopreserved tissue or tissue fragments, which can be useful in aquaculture production. However, they have lower cooling and thawing rates (He et al., 2004; Paredes, 2016; Paredes et al., 2019). In this study, we found that the type of cryotube (0.5 mL or 2 mL) and cryopreservation volume (0.5-2 mL) had no significant effect on post-thaw motility, which makes it possible to obtain large quantities of frozen sea cucumber sperm and to improve production practice. In future research, we will study cryopreservation of sea cucumber embryos and the effect of freezing containers (cryotubes or straws) on the survival rate of embryos after thawing (Paredes, 2016; Paredes et al., 2019).

4.2 Quality of fresh and frozen *A. japonicus* sperm

4.2.1 Individual differences in sperm freezability

In this study, we found significant individual differences in sperm quality and sperm freezability of *A. japonicus*. Mature sea cucumbers with a heavy weight did not necessarily have higher sperm motility and sperm density than those with a lighter weight (Table 2). Similarly, different *A. japonicus* individuals with high fresh sperm motility would not necessarily have high post-thaw sperm motility (Table 2). It is normal for different individuals of the same species to have differences (Adams et al., 2004; Dere et al., 2016; Hussain et al., 2016). In this study, the semen used in each screening experiment came from only one sea cucumber to study the individual differences in sea cucumber sperm freezability. However, the current findings of this study are not sufficient to explain what factors determine the sperm freezability. In future studies, we will fully evaluate various factors such as nutrients in the seminal plasma, enzyme activity, transcriptome and proteomics of different sea cucumber individual sperm, and combine them with the quality of the thawed sperm to find out what are the factors that determine the freezability of *A. japonicus* sperm (Wang et al., 2014a).

4.2.2 Fertilization rate and hatching rate

Fertilization rate and hatching rate experiments are key steps to test the quality of frozen sperm (Liu et al., 2015; Paredes, 2015). Most previous studies of cryopreservation of echinoderm sperm have provided data on the fertilization rate (50%–95%) of frozen sperm, but few data on hatching rate are available (Liu et al., 2015; Paredes, 2015; Paredes, 2016; Paredes et al., 2019). Dunn and Mclachlan (1973) reported that the sperm motility of *Strongylocentrotus drobachiensis* was obviously compromised after cryopreservation, but could achieve 95% fertilization by increasing the sperm-oocyte ratio. Asahina and Takahashi (1978) also observed a significant decrease in post-thawing sperm motility and a 75% fertilization rate in *Strongylocentrotus intermedius*, *Hemicentrotus pulcherrimus*, and *Strongylocentrotus nudus*. Mizuno et al. (2019) reported that the maximum post-thaw motility of *A. japonicus* sperm after cryopreservation was 19.3%, and the fertilization rate was 89.8% (compared to 92.7% for fresh sperm). In our study, the maximum post-thaw motility of *A. japonicus* sperm treated with the optimal cryopreservation procedures was 68.92% ± 0.97%, the fertilization rate was 79.03% ± 3.22%, and the hatching rate was 66.74% ± 5.61% (Figure 8). Although our fertilization rate did not reach 90%, we think that related to the time point we assessed it. Dunn and Mclachlan (1973) calculated the fertilization rate based on whether or not the fertilization membrane was formed, and Shao et al. (2006) calculated it 1 h post-fertilization based on whether or not the second polar body was extruded. Mizuno et al. (2019) calculated the fertilization rate 3 h post-fertilization based on whether or not the fertilized egg was cleaved. In our study, we calculated the fertilization rate and hatching rate at 10 h (in the blastocyst stage) and 52 h (in the early auricularia larva stage) after fertilization, which is significantly later than other studies. As the duration of the artificial incubation time increased, the risk to embryo survival increased, and if the incubation conditions were unfavorable, the embryo may experience growth arrest (Asahina and Takahashi, 1978). In addition, when we counted the hatching rate, we observed both early auricularia larvae and some embryos in the gastrula stage. These factors may explain why our values are small and conservative.

It is worth noting that the fertilization rate and hatching rate of fresh sperm (control group) in our study were relatively low, as they should be > 90%. We believe that these results were due

to the addition of too many sperm and too sub-optimal egg quality. Because the motility of sperm is affected by cryopreservation, a large volume of sperm generally is added to ensure fertilization. However, too much semen can negatively impact water quality, so the proper sperm-egg ratio is very important (Dunn and Mclachlan, 1973; Adams et al., 2004; Fabbrocini et al., 2014; Paredes et al., 2019). Generally speaking, the concentration of cryopreserved sperm required to fertilize eggs has been estimated to be 30 times higher than that of unfrozen sperm (Paredes, 2015). Shao et al. (2006) reported that the fertilization rate and hatching rate of the 10,000:1 sperm-to-egg ratio achieved better results than the 1000:1 ratio for cryopreserved sperm of *A. japonicus*. In our study, we used the same 10,000:1 sperm-to-egg ratio for fresh semen and frozen semen in the fertilization rate experiment. Because the sperm concentration of fresh semen was nearly double that of frozen semen (Table 2), the fresh sperm control group may have contained too much sperm, resulting in poor water quality and affecting embryo growth. This may explain the suboptimal fertilization and hatchability results in the fresh sperm treatment group (Adams et al., 2004; Fabbrocini and D'adamo, 2017). In future studies, we will optimize the sperm-egg ratio for fresh sperm and frozen sperm and determine how to prolong and maintain the quality of sea cucumber eggs. We believe that if the egg quality is good and the sperm-to-egg ratio is suitable, the fertilization rate and hatching rate of the frozen sperm cryopreserved using our optimized procedure will improve.

In this study, we also examined the fertilization and hatchability of frozen sperm with different post-thaw motility values that were cryopreserved using non-optimal formulas (20% DMA or 20% PG). Based on the results, we propose that frozen sperm with post-thaw motility > 40% can be used in production practice, which lays the foundation for further studies of the protection mechanism of different types of CPAs. We also considered preservation time and found that cryopreservation for 1 year had no significant effect on the post-thaw motility of frozen sperm. This part of our research is ongoing, and future steps will including studying the effects of cryopreservation process and time on the transcriptome and proteome of *A. japonicus* sperm and exploring the effect of cryopreservation technology on *A. japonicus* sperm from a molecular perspective (Figure 8).

4.2.3 Ultrastructure

We attribute the observed decline in sperm motility and fertilization rate to the structural damage to sperm caused by the cryopreservation process (Diaz et al., 2019; Cerdeira et al., 2020). Our comparison of the ultrastructure of fresh sperm and cryopreserved sperm showed that the main damage occurred in the head, mitochondria, and membranes of *A. japonicus* sperm (Figure 9). In future studies, we will assess the damage ratio, enzyme activity changes, and DNA integrity of *A. japonicus* sperm after cryopreservation to comprehensively describe the effect of cryopreservation on *A. japonicus* sperm.

5 Conclusion

In this study, we used a programmable control rate freezer and CASA to comprehensively screen and evaluate for optimal values of key parameters involved in the cryopreservation of *A. japonicus* sperm. When we applied our established optimal method for cryopreservation of *A. japonicus* sperm, the post-thaw motility of sperm was > 65%, the fertilization rate (in the blastocyst stage) was nearly 80%, and the hatching rate (in the early auricularia larva stage) was > 65%. These results showed that our method had practical value for production. We also found that *A. japonicus* sperm that had been cryopreserved for 1 year retained a considerable post-thaw motility and fertilization rate compared to recently cryopreserved sperm. However, the cryopreservation process caused damage to the ultrastructure of *A. japonicus* sperm. Herein we have fully discussed individual differences in freezability of *A. japonicus* sperm, the direction of future development of *A. japonicus* sperm cryopreservation technology, and the problems that still need to be solved. Our results provide valuable information for future research and conservation of *A. japonicus*.

Data availability statement

The raw data supporting the conclusions of this article will be made available by the authors, without undue reservation.

Author contributions

SX, SLL, LBZ, CGL, LNS, JCS, LLX, and HSY conceived and designed the experiments. SX, SLL, JCS, and CXJ performed the experiments. SX, CXJ, and HSY analyzed the data and drafted the manuscript. SX, SLL, JCS, and HSY contributed to writing, review, and editing. SLL and HSY contributed to securing the funding. All authors contributed to the article and approved the submitted version.

Funding

This work was supported by National Key Research and Development Project (2018YFD0901602), the Agricultural Seed Project of Shandong Province (2020LZGC015), Marine S&T Fund of Shandong Province for Pilot National Laboratory for Marine Science and Technology (Qingdao) (2018SDKJ0502),

Chinese Academy of Sciences "Modern Marine Ranching Construction Principles and Engineering Technology Innovation Cross Team" Project (Y82327101L), the Strategic Priority Research Program of the Chinese Academy of Sciences (XDA24030304) and International Partners Program of Chinese Academy of Sciences (133137KYSB20180069). The funders had no role in experiment design, data processing and analysis, and decision to publish or preparation of the manuscript.

Acknowledgments

We thank Qinghua Liu, Xueying Wang, Xiaoshang Ru, and Da Huo for their help and advice on experimental design.

Conflict of interest

The authors declare that the research was conducted in the absence of any commercial or financial relationships that could be construed as a potential conflict of interest.

Publisher's note

References

Adams, S. L., Hessian, P. A., and Mladenov, P. V. (2004). Cryopreservation of sea urchin (*Evechinus chloroticus*) sperm. *Cryoletters* 25, 287–299. doi: 10.1201/9780849380549.ch41

Akarasanon, K., Damrongphol, P., and Poolsanguan, W. (2004). Long-term cryopreservation of spermatophore of the giant freshwater prawn, *Macrobrachium rosenbergii* (de man). *Aquacult. Res.* 35, 1415–1420. doi: 10.1111/j.1365-2109.2004.01163.x

Anchordoguy, T., Crowe, J. H., Griffin, F. J., and Clark, W. H. (1988). Cryopreservation of sperm from the marine shrimp *sicyonia-ingentis*. *Cryobiology* 25, 238–243. doi: 10.1016/0011-2240(88)90031-4

Asahina, E., and Takahashi, T. (1978). Freezing tolerance in embryos and spermatozoa of sea-urchin. *Cryobiology* 15, 122–127. doi: 10.1016/0011-2240(78)90016-0

Behlmer, S. D., and Brown, G. (1984). Viability of cryopreserved spermatozoa of the horseshoe-crab, *limulus-polyphemus*-L. *Int. J. Invertebr. Reprod. Dev.* 7, 193–199. doi: 10.1080/01688170.1984.10510089

Bordbar, S., Anwar, F., and Saari, N. (2011). High-value components and bioactives from Sea cucumbers for functional foods-a review. *Mar. Drugs* 9, 1761–1805. doi: 10.3390/md9101761

Campos, S., Troncoso, J., and Paredes, E. (2021). Major challenges in cryopreservation of sea urchin eggs. *Cryobiology* 98, 1–4. doi: 10.1016/j.cryobiol.2020.11.008

Cerdeira, J., Sanchez-Calabuig, M. J., Perez-Gutierrez, J. F., Hijon, M., Castano, C., and Santiago-Moreno, J. (2020). Cryopreservation effects on canine sperm morphometric variables and ultrastructure: Comparison between vitrification and conventional freezing. *Cryobiology* 95, 164–170. doi: 10.1016/j.cryobiol.2020.03.007

Dere, E., Huse, S., Hwang, K., Sigman, M., and Boekelheide, K. (2016). Intra- and inter-individual differences in human sperm DNA methylation. *Andrology* 4, 832–842. doi: 10.1111/andr.12170

Diaz, R., Lee-Estevez, M., Quinones, J., Dumorne, K., Short, S., Ulloa-Rodriguez, P., et al. (2019). Changes in *Atlantic salmon* (Salmo salar) sperm morphology and membrane lipid composition related to cold storage and cryopreservation. *Anim. Reprod. Sci.* 204, 50–59. doi: 10.1016/j.anireprosci.2019.03.004

Dong, Q. X., Eudeline, B., Huang, C. J., Allen, S. K., and Tiersch, T. R. (2005b). Commercial-scale sperm cryopreservation of diploid and tetraploid pacific oysters, *Crassostrea gigas*. *Cryobiology* 50, 1–16. doi: 10.1016/j.cryobiol.2004.09.003

Dong, Q. X., Huang, C. J., Eudeline, B., and Tiersch, T. R. (2005a). Systematic factor optimization for cryopreservation of shipped sperm samples of diploid pacific oysters, *Crassostrea gigas*. *Cryobiology* 51, 176–197. doi: 10.1016/j.cryobiol.2005.06.007

Dunn, R. S., and Mclachlan, J. (1973). Cryopreservation of echinoderm sperm. *Can. J. Zool.* 51, 666–669. doi: 10.1139/z73-100

Fabbrocini, A., and D'adamo, R. (2017). Motility of sea urchin *Paracentrotus lividus* spermatozoa in the post-activation phase. *Aquacult. Res.* 48, 5526–5532. doi: 10.1111/are.13373

Fabbrocini, A., D'adamo, R., Pelosi, S., Oliveira, L. F. J., Silvestri, F., and Sansone, G. (2014). Gamete cryobanks for laboratory research: Developing a rapid and easy-to-perform protocol for the cryopreservation of the sea urchin *Paracentrotus lividus* (Lmk 1816) spermatozoa. *Cryobiology* 69, 149–156. doi: 10.1016/j.cryobiol.2014.06.009

Fabbrocini, A., Maurizio, D., and D'adamo, R. (2016). Sperm motility patterns as a tool for evaluating differences in sperm quality across gonad development stages in the sea urchin *Paracentrotus lividus* (Lmk 1816). *Aquaculture* 452, 115–119. doi: 10.1016/j.aquaculture.2015.10.033

Fan, B., Liu, X. C., Meng, Z. N., Tan, B. H., Wang, L., Zhang, H. F., et al. (2014). Cryopreservation of giant grouper *Epinephelus lanceolatus* (Bloch 1790) sperm. *J. Appl. Ichthyol.* 30, 334–339. doi: 10.1111/jai.12321

Figueroa, E., Farias, J. G., Lee-Estevez, M., Valdebenito, I., Risopatron, J., Magnotti, C., et al. (2018). Sperm cryopreservation with supplementation of alpha-tocopherol and ascorbic acid in freezing media increase sperm function and fertility rate in Atlantic salmon (*Salmo salar*). *Aquaculture* 493, 1–8. doi: 10.1016/j.aquaculture.2018.04.046

Gallego, V., Perez, L., Asturiano, J. F., and Yoshida, M. (2014). Sperm motility parameters and spermatozoa morphometric characterization in marine species: A study of swimmer and sessile species. *Theriogenology* 82, 668–676. doi: 10.1016/j.theriogenology.2014.05.026

Gao, D., and Critser, J. K. (2000). Mechanisms of cryoinjury in living cells. *ILAR J.* 41, 187–196. doi: 10.1093/ilar.41.4.187

Guo, J. H., and Weng, C. F. (2020). Current status and prospects of cryopreservation in aquatic crustaceans and other invertebrates. *J. Crust. Biol.* 40, 343–350. doi: 10.1093/jcbiol/ruaa034

Hassan, M. M., Qin, J. G., and Li, X. (2015). Sperm cryopreservation in oysters: A review of its current status and potentials for future application in aquaculture. *Aquaculture* 438, 24–32. doi: 10.1016/j.aquaculture.2014.12.037

He, Y. M., Dong, Q. X., Tiersch, T. R., and Devireddy, R. V. (2004). Variation in the membrane transport properties and predicted optimal rates of freezing for spermatozoa of diploid and tetraploid pacific oyster, *Crassostrea gigas*. *Biol. Reprod.* 70, 1428–1437. doi: 10.1095/biolreprod.103.025296

Hussain, Y. H., Guasto, J. S., Zimmer, R. K., Stocker, R., and Riffell, J. A. (2016). Sperm chemotaxis promotes individual fertilization success in sea urchins. *J. Exp. Biol.* 219, 1458–1466. doi: 10.1242/jeb.134924

Jalali, A., and Crawford, B. (2012). A freezing technique that maintains viability of sperm from the starfish *Pisaster ochraceus*. *Invertebr. Reprod. Dev.* 56, 242–248. doi: 10.1080/07924259.2011.601125

Kato, S., Tsurumaru, S., Taga, M., Yamane, T., Shibata, Y., Ohno, K., et al. (2009). Neuronal peptides induce oocyte maturation and gamete spawning of sea cucumber, *Apostichopus japonicus*. *Dev. Biol.* 326, 169–176. doi: 10.1016/j.ydbio.2008.11.003

Liu, Y., Li, X., Robinson, N., and Qin, J. (2015). Sperm cryopreservation in marine mollusk: a review. *Aquacult. Int.* 23, 1505–1524. doi: 10.1007/s10499-015-9900-0

Liu, Z., Li, D., Song, L., Liu, Y., Yu, M., Zhang, M., et al. (2020). Effects of proteolysis and oxidation on mechanical properties of sea cucumber (*Stichopus japonicus*) during thermal processing and storage and their control. *Food Chem.* 330, 127248. doi: 10.1016/j.foodchem.2020.127248

Liu, Y. B., Xu, T., Robinson, N., Qin, J. G., and Li, X. X. (2014). Cryopreservation of sperm in farmed Australian greenlip abalone *Haliotis laevigata*. *Cryobiology* 68, 185–193. doi: 10.1016/j.cryobiol.2014.01.002

Mazur, P. (1990). Equilibrium, quasi-equilibrium, and nonequilibrium freezing of mammalian embryos. *Cell Biophysics* 17, 53–92. doi: 10.1007/bf02989804

Mizuno, Y., Fujiwara, A., Yamano, K., and Ohta, H. (2019). Motility and fertility of cryopreserved spermatozoa of the Japanese sea cucumber *Apostichopus japonicus*. *Aquacult. Res.* 50, 106–115. doi: 10.1111/are.13872

Nascimento, I. A., Leite, M., De Araujo, M. M. S., Sansone, G., Pereira, S. A., and Santo, M. D. (2005). Selection of cryoprotectants based on their toxic effects on oyster gametes and embryos. *Cryobiology* 51, 113–117. doi: 10.1016/j.cryobiol.2005.04.006

Paniagua-Chavez, C. G., Buchanan, J. T., and Tiersch, T. R. (1998). Effect of extender solutions and dilution on motility and fertilizing ability of Eastern oyster sperm. *J. Shellfish Res.* 17, 231–237.

Paredes, E. (2015). Exploring the evolution of marine invertebrate cryopreservation - landmarks, state of the art and future lines of research. *Cryobiology* 71, 198–209. doi: 10.1016/j.cryobiol.2015.08.011

Paredes, E. (2016). Biobanking of a marine invertebrate model organism: The Sea urchin. *J. Mar. Sci. Eng.* 4(1), 7. doi: 10.3390/jmse4010007

Paredes, E., Adams, S. L., and Vignier, J. (2019). "Cryopreservation of sea urchin sperm and early life stages," in *Echinoderms, pt a*. Methods in Cell Biology Eds. K. R. Foltz and A. Hamdoun, 47–69. doi: 10.1016/bs.mcb.2018.11.008

Paredes, E., and Bellas, J. (2009). Cryopreservation of sea urchin embryos (*Paracentrotus lividus*) applied to marine ecotoxicological studies. *Cryobiology* 59, 344–350. doi: 10.1016/j.cryobiol.2009.09.010

Paredes, E., Bellas, J., and Adams, S. L. (2013). Comparative cryopreservation study of trochophore larvae from two species of bivalves: Pacific oyster (*Crassostrea gigas*) and blue mussel (*Mytilus galloproviricialis*). *Cryobiology* 67, 274–279. doi: 10.1016/j.cryobiol.2013.08.007

Pegg, D. E. (2002). The history and principles of cryopreservation. *Semin. Reprod. Med.* 20, 5–13. doi: 10.1055/s-2002-23515

Ru, X., Zhang, L., Li, X., Liu, S., and Yang, H. (2019). Development strategies for the sea cucumber industry in China. *J. Oceanol. Limnol.* 37, 300–312. doi: 10.1007/s00343-019-7344-5

Shao, M. Y., Zhang, Z. F., Yu, L., Hu, J. J., and Kang, K. H. (2006). Cryopreservation of sea cucumber *Apostichopus japonicus* (Selenka) sperm. *Aquacult. Res.* 37, 1450–1457. doi: 10.1111/j.1365-2109.2006.01581.x

Thurston, L. M., Watson, P. F., and Holt, W. V. (2002). Semen cryopreservation: A genetic explanation for species and individual variation? *Cryoletters* 23, 255–262.

Tsai, S., Chong, G., Meng, P. J., and Lin, C. (2018). Sugars as supplemental cryoprotectants for marine organisms. *Rev. Aquac.* 10, 703–715. doi: 10.1111/raq.12195

Tsai, S., and Lin, C. (2012). Advantages and applications of cryopreservation in fisheries science. *Braz. Arch. Biol. Technol.* 55, 425–433. doi: 10.1590/s1516-89132012000300014

Van Der Horst, G., Bennett, M., and Bishop, J. D. D. (2018). CASA in invertebrates. *Reprod. Fertil. Dev.* 30, 907–918. doi: 10.1071/rd17470

Vuthiphandchai, V., Boonthai, T., and Nimrat, S. (2021). Chilled storage of Asian seabass, lates calcarifer Bloch semen: Effects of ions, extenders and storage periods on sperm quality and fertilization ability. *J. Appl. Ichthyol.* 37, 593–600. doi: 10.1111/jai.14218

Wang, Y., Rong, X., and Liao, M. (2014b). *Technical monograph for health culture and disease control of sea cucumber* (Beijing: China Agriculture Press).

Wang, P., Wang, Y. F., Wang, H., Wang, C. W., Zan, L. S., Hu, J. H., et al. (2014a). HSP90 expression correlation with the freezing resistance of bull sperm. *Zygote* 22, 239–245. doi: 10.1017/s096719941300004x

Wu, Y., Guo, L., Liu, Z., Wei, H., Zhou, Y., Tan, J., et al. (2019). Microelements in seminal and serum plasma are associated with fresh semen quality in Yorkshire boars. *Theriogenology* 132, 88–94. doi: 10.1016/j.theriogenology.2019.04.002

Xia, S., Yang, H., Li, Y., Liu, S., Zhou, Y., and Zhang, L. (2012). Effects of different seaweed diets on growth, digestibility, and ammonia-nitrogen production of the sea cucumber *Apostichopus japonicus* (Selenka). *Aquaculture* 338-341, 304–308. doi: 10.1016/j.aquaculture.2012.01.010

Xing, L., Sun, L., Liu, S., Zhang, L., and Yang, H. (2021). Comparative metabolomic analysis of the body wall from four varieties of the sea cucumber *Apostichopus japonicus*. *Food Chem.* 352, 129339. doi: 10.1016/j.foodchem.2021.129339

Yang, H., Hamel, J. F., and Mercier, A. (2015). *The Sea cucumber apostichopus japonicus: History, biology and aquaculture*. Academic Press.

frontiers | Frontiers in Marine Science

TYPE Original Research
PUBLISHED 08 August 2022
DOI 10.3389/fmars.2022.980221

OPEN ACCESS

EDITED BY
Jun Ding,
Dalian Ocean University, China

REVIEWED BY
Huan Wang,
Ningbo University, China
Chunlin Wang,
Ningbo University, China

*CORRESPONDENCE
Ye Zhao
zyzy19872006@163.com
Muyan Chen
chenmuyan@ouc.edu.cn

SPECIALTY SECTION
This article was submitted to Marine Biology, a section of the journal Frontiers in Marine Science

RECEIVED 28 June 2022
ACCEPTED 19 July 2022
PUBLISHED 08 August 2022

CITATION
Zhao Y, Wang H, Wang H, Pi Y and Chen M (2022) Metabolic response of the sea cucumber *Apostichopus japonicus* during the estivation-arousal cycles. *Front. Mar. Sci.* 9:980221. doi: 10.3389/fmars.2022.980221

Metabolic response of the sea cucumber *Apostichopus japonicus* during the estivation-arousal cycles

Ye Zhao[1]*, Haona Wang[1], Han Wang[1], Yongrui Pi[1] and Muyan Chen[2]*

[1]Ocean school, Yantai University, Yantai, China, [2]The Key Laboratory of Mariculture, Ministry of Education, Ocean University of China, Qingdao, China

Estivation is a widespread survival strategy for dealing with adverse environmental conditions such as high temperature, low oxygen and lack of water or food, which has been reported across multiple vertebrate and invertebrate species. The sea cucumber *Apostichopus japonicus* is an excellent model organism to investigate the adaptive mechanism of estivation in marine invertebrates. In this study, a metabolomics approach based on ultraperformance liquid chromatography coupled with electrospray ionization time-of-flight mass spectrometry (UPLC-ESI-Q-TOF/MS) was performed to reveal the metabolic response of intestines from adult *A. japonicus* over the annual estivation-arousal cycle: nonestivation (NA), deep-estivation (DA) and arousal from estivation (AA). A total of 424 metabolites were identified, and among them, 243, 238 and 37 significant differentially metabolites (DMs) were further screened in the comparisons of DA vs. NA, AA vs. DA, and AA vs. NA. Specifically, the levels of metabolites involved in glycolysis and the tricarboxylic acid cycle were significantly decreased, while higher amounts of long-chain fatty acids, phospholipids and free amino acids were found in *A. japonicus* during estivation, implying that sea cucumbers might reorganize metabolic priorities for ATP production by depressing carbohydrate metabolism and promoting lipid and amino acid catabolism. Interestingly, elevated relative carbon flow entry into the pentose phosphate pathway and accumulation of various nonenzymatic antioxidant molecules (e.g., tocotrienols, folic acid, catechin, genistein and resveratrol) were observed in estivating sea cucumbers, which suggested that enhancement of the reactive oxygen species defense system might promote long-term viability in the hypometabolic state in an energy-efficient manner. Thus, this research provides new insights into the adaptation mechanisms of marine invertebrates to estivation at the metabolic level.

KEYWORDS

Apostichopus japonicus, estivation, metabolomics, differential metabolites, oxidative stress, echinoderm

1 Introduction

Changing environmental conditions are always a major challenge to living creatures, yet global environmental change in recent years has made it even more intractable. Entering a hypometabolic state (e.g., hibernation, estivation, diapause and anaerobiosis) is an important survival strategy for many species when challenged by environmental stress (Storey and Storey, 2007). Interestingly, a number of previous studies have revealed that these environment-induced hypometabolism phenomena coincidentally shared several common metabolic regulation strategies highly conserved across phylogenic lines, including global metabolic rate depression, altered energy use strategies of fuel sources and metabolic priorities, transcriptional changes, enhancement of defense systems and cellular homeostasis (Heldmaier et al., 2004; Storey and Storey, 2012).

Estivation, as a state of aerobic hypometabolism, is a widespread survival strategy dealing with adverse environmental conditions such as high temperature, low oxygen and lack of water or food, which has been reported across multiple terrestrial and freshwater vertebrate and invertebrate species (Storey and Storey, 2012). However, estivation also occurs in marine organisms, which have not been well studied thus far. The sea cucumber *Apostichopus japonicus*, as an excellent model organism of marine invertebrate estivator, retreats into dormancy in summer annually when the ambient water temperature is above approximately 25 °C without feeding or locomotion in a period that lasts up to 100 days (Li et al., 1996). During this torpor period, sea cucumbers endure profound metabolic rate suppression, immune system modification and severe atrophy of the digestive tract, along with a loss of over one-third of their initial body mass. Since *A. japonicus* is one of the most important economic species that is widely cultured in Asia, mainly due to its high nutritional and pharmaceutical value, estivation obviously shortens the growth cycle and drives down the production efficiency in the sea cucumber aquaculture industry (Yuan et al., 2007a). Recently, accumulating studies have focused on the physiological and biochemical strategies of sea cucumber in dealing with estivation, including metabolic rate depression (Yang et al., 2006; Xiang et al., 2016), energetic reorganization (Yuan et al., 2007b), and degeneration of intestinal structure and function (Gao et al., 2008). With the rapid development of omics technology, the molecular regulation mechanisms underpinning estivation have been further elucidated, mainly focusing on global transcriptional and translational regulation (Zhao et al., 2014; Chen et al., 2016a; Li et al., 2018), miRNA-targeted posttranscriptional modifications (Chen et al., 2013; Chen et al., 2018), reversible protein phosphorylation (Chen et al., 2016b) and epigenetic modifications (Zhao et al., 2015; Yang et al., 2020).

Metabolites drive essential cellular functions in interactions between organisms and the environment. Metabolomics, as an important omics technique in systems biology, permits the identification and quantification of multiple metabolic compounds, which could provide deep insight into the adaptive regulatory mechanisms of biochemical pathways in response to environmental changes and autophysiological state shifts (Weckwerth, 2003; Johnson et al., 2016). Currently, the main methodologies that are widely applied in metabolomics analysis include high-performance liquid chromatography (HPLC), nuclear magnetic resonance (NMR), gas chromatography–mass spectrometry (GC–MS) and liquid chromatography–mass spectrometry (LC–MS). Among these analytical techniques, ultraperformance liquid chromatography coupled with electrospray ionization time-of-flight mass spectrometry (UPLC-ESI-Q-TOF/MS) has become an important means for metabolomics studies in multiple areas of sea cucumber research because of its high sensitivity, high separation efficiency, good repeatability and high universality (Li et al., 2019; Zhao et al., 2020; Xing et al., 2021; Guo et al., 2022). However, little is known about the metabolic response in adult *A. japonicus* across complete natural torpor-arousal cycles. In the present study, UPLC-ESI-Q-TOF/MS was performed to reveal the metabolic profile of the sea cucumber *A. japonicus* across the estivation period. This work aimed to (1) investigate the physiological metabolic transition during the estivation cycle, (2) identify the key differential metabolites and pathways during estivation, and (3) provide new insight into the potential molecular mechanisms of estivation and assist in guiding the aquaculture management of sea cucumbers.

2 Materials and methods

2.1 Animals

Adult *A. japonicus* (80-120 g body wet weight) were obtained from the coast of Yantai (Yantai, China) in May, August and

Abbreviations: NA, nonestivation; DA, deep-estivation; AA, arousal from estivation; DMs, differentially metabolites.

October 2021. These three phases of sea cucumbers were sampled across the active-estivation-arousal cycle: (1) nonestivating sea cucumbers (NA) as the control group from seawater temperature approximately 17°C with normal feeding and activity; (2) deep-estivation sea cucumbers (DA) from seawater at a temperature of approximately 26°C, as indicated by no signs of feeding or locomotion and the degeneration and atrophy of the intestine into a very tiny string; and (3) arousal from estivation sea cucumbers (AA) from seawater at a temperature of approximately 20°C with obvious feeding and movement and recovery of the intestinal structure and contents, the pictures of the intestinal tissues in three stages of the active-estivation-arousal cycle were shown in Figure S1. A total of 17 individuals were sacrificed and the intestinal tissue and contents were rapidly dissected out and frozen in liquid nitrogen for later analysis.

2.2 Metabolite extraction

Six individuals for NA group, six individuals for AA group and five individuals for DA group were used for metabolomics analysis. Each sample (~100 mg) was accurately weighed, and 0.6 mL precooled 2-chlorophenylalanine (4 ppm) methanol (± 1%) was added to a 2 mL EP tube. After vortexing for 30 seconds, 100 mg glass beads were added to the samples and ground for 90 s at 55 Hz by a tissue grinder. Then, the samples were ultrasonicated at room temperature for 10 minutes and centrifuged at 12000 rpm at 4 °C for 10 min to obtain 200 μL supernatant, which was then filtered through a 0.22 μm membrane for LC–MS analysis. Of note, 20 μL filtrates from each sample were pooled as the quality control (QC) to monitor deviations of the analytical results.

2.3 LC–MS analysis

The metabolic profiling analysis was conducted on a Thermo Vanquish system equipped with an ACQUITY UPLC® HSS T3 (150×2.1 mm, 1.8 μm, Waters) column maintained at 40°C. The temperature of the auto sampler was 8 °C. Gradient elution of analytes was carried out with 0.1% formic acid in water (A2) and 0.1% formic acid in acetonitrile (B2) in positive mode or 5 mM ammonium formate in water (A3) and acetonitrile (B3) in negative mode at a flow rate of 0.25 mL/min. Injection of 2 μL of each sample was performed after equilibration. An increasing linear gradient of solvent B2/B3 (v/v) was used as follows: 0~1 min, 2% B2/B3; 1~9 min, 2%~50% B2/B3; 9~12 min, 50%~98% B2/B3; 12~13.5 min, 98% B2/B3; 13.5~14 min, 98%~2% B2/B3; 14~20 min, 2% B2-positive model (or 14~17 min, 2% B3-negative model).

The ESI-MSn experiments were executed on a Thermo Q Exactive HF-X mass spectrometer with spray voltages of 3.5 kV and -2.5 kV in positive and negative modes, respectively. The sheath gas and auxiliary gas were set at 30 and 10 arbitrary units, respectively. The capillary temperature was 325 °C. The analyzer scanned over a mass range of m/z 81-1 000 for full scan at a mass resolution of 60000. Data-dependent acquisition (DDA) MS/MS experiments were performed with an HCD scan. The normalized collision energy was 30 eV. Dynamic exclusion was implemented to remove some unnecessary information from the MS/MS spectra.

2.4 Data processing

The raw MS data were converted into extensible markup language (mzXML) format by using the software ProteoWizard, and then the cryptographic message syntax (XCMS) program of the R language package was used for peak alignment, retention time correction, and peak area extraction to obtain the data matrix, including mass to charge ratio (m/z), retention time and intensity. The structure of metabolites was further identified by accurate mass matching (molecular weight error ≤30 ppm) and MS/MS data matching based on the online Human Metabolome Database (HMDB) (http://www.hmdb.ca), METLIN (http://metlin.scripps.edu), Massbank (http://www.massbank.jp/), LipidMaps (http://www.lipidmaps.org) and mzClound (https://www.mzcloud.org).

To clarify the relationships of the identified metabolites of sea cucumbers among different groups, principal component analysis (PCA) was applied using the R language package Phyloseq to reduce the data dimensionality. Supervised orthogonal projections for latent structures-discriminant analysis (OPLS-DA) were further performed by the R language package MetaboAnalystR (v1.0.1), and 200 permutation tests were performed to verify the reliability of the model.

2.5 Statistical analysis

For the metabolomics analysis, differential metabolites (DMs) between groups were determined by Student's t test based on p value ≤0.05, combined with absolute Log_2FC (fold change) ≥1 and variable importance in projection (VIP) values ≥1 from the OPLS-DA model. Venn plot was further constructed by jvenn online tool (http://jvenn.toulouse.inra.fr/app/example.html). The DMs were further annotated and mapped to the KEGG compound and pathway databases (http://www.kegg.jp/kegg/compound/ and http://www.kegg.jp/kegg/pathway.html) using a hypergeometric distribution test using the R language package MetaboAnalystR to identify the significantly enriched pathways, where $p < 0.05$ was considered to be significant.

3 Results and discussion

3.1 LC–MS metabolomic profiles

In this study, we employed UPLC-ESI-Q-TOF/MS-based metabolomics analysis to explore the potential biochemical

regulatory mechanism of estivation. Quality control samples were used to evaluate the signal drift of the entire mass spectrometry data during the acquisition process. In the present study, five QC samples showed dense distribution, suggesting the good correction effectiveness of the PCA model, and no obvious outliers were found in the two-dimensional PCA score plot (Figure S2). A total of 424 metabolites were identified in the intestines of *A. japonicus*. Figure 1A represents the relative abundances of the top 20 metabolites in each sample between the different groups. Since some metabolites play specific roles in an organism, the identified metabolites were further classified into eight categories based on KEGG analysis, including peptides, lipids, organic acids, carbohydrates, nucleic acids, vitamins and cofactors, steroids, and hormones and transmitters (Figure 1B). The results indicated that higher amounts of peptides, steroids, vitamins and cofactors were identified at the DA stage in comparison with the NA and AA stages, while lipids, carbohydrates and organic acids all showed smaller percentages at the DA stage than at the other stages. The increases in vitamins and cofactors might be helpful for the regulation of substance and energy metabolism since many vitamins act as critical cofactors for enzymatic reactions in metabolic processes (Huskisson et al., 2007). As reported previously, strong depression of the metabolic rate is a vital adaptive strategy targeting the energy budget during hypometabolism; hence, a decline in catabolism usually occurs during estivation (Storey and Storey, 1990; Storey and Storey, 2010). In this study, obvious decreases in the contents of carbohydrates and lipids were found in the DA group, consistent with previous results in *A. japonicus* during estivation (Xiang et al., 2016; Yang et al., 2021), suggesting that some necessary controls might be implemented for energy reorganization during dormancy.

PCA was applied to determine the metabolic variations in all groups (NA, DA, and AA), and the score plot is shown in Figure 2A. As indicated in the figure, the metabolites in each group had relatively good aggregation. Furthermore, the first principal axis (PC1) showed 53.7% variability, and the metabolites of *A. japonicus* in the dormant physiological state (DA) showed clear separation from those in the normal physiological state (NA and AA), suggesting that hypometabolism, such as estivation, could cause obvious metabolic phenotype alterations in the intestine of *A. japonicus*. Since PCA is an unsupervised algorithm without eliminating random and intragroup errors (Saccenti et al., 2014), a supervised model of OPLS-DA was further conducted to analyze the differences in metabolites between the three groups. As shown in Figure 2B, the OPLS-DA score plot revealed that the three groups (NA, DA, and AA) each clustered according to their physiological state with no overlap, indicating that sea cucumbers showed diverse metabolomic profiles under their various physiological conditions. The permutation tests have provided good model validation and accuracy of OPLS-DA analysis (Figure S3).

3.2 Differential metabolite analysis

In this study, significant differential metabolites (DMs) were screened by thresholds with VIP ≥1 (from the OPLS-DA model), Log_2FC ≥1 (fold change) and p value ≤0.05 (based on Student's t test). As shown in Figure 3A, 243 DMs (129 upregulated DMs

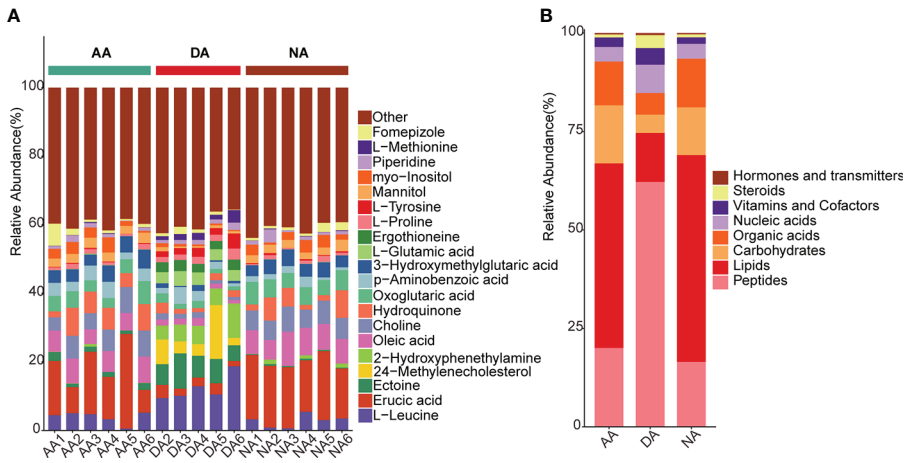

FIGURE 1
The annotated metabolites in *A. japonicus* during estivation cycles. **(A)** the relative abundance of top 20 metabolites in each group, **(B)** the relative abundance of the annotated metabolites in KEGG database in distribution of eight categories.

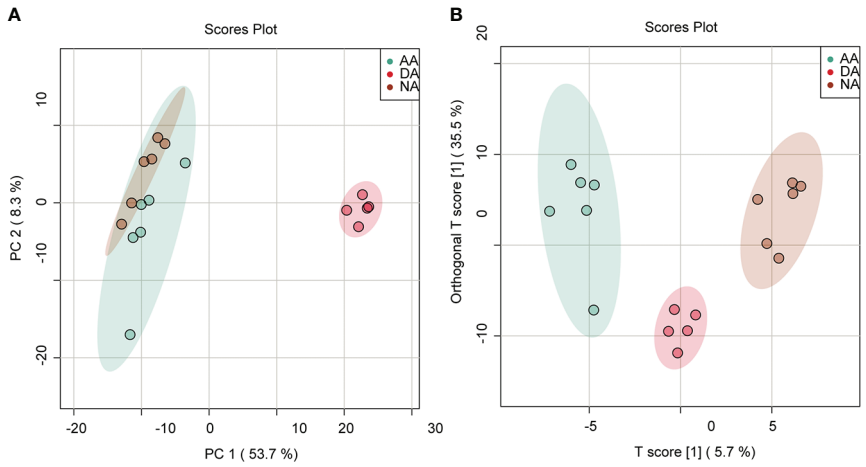

FIGURE 2
PCA and OPLS-DA score plot from the LC–MS intestinal metabolite profiles in *A. japonicus* during estivation cycles. **(A)** PCA score plot, **(B)** OPLS-DA score plot.

and 114 downregulated DMs) were identified in DA vs. NA, 238 DMs (100 upregulated DMs and 138 downregulated DMs) were identified in AA vs. DA, and 37 DMs (21 upregulated DMs and 16 downregulated DMs) were identified in AA vs. NA. These differential metabolites are listed in Supplementary Tables S1-S3. Among these differentially abundant metabolites, there were 13 overlapping DMs in three pairwise comparisons, while 63 (25.93%), 54 (22.69%), and 10 (27.03%) DMs were exclusively screened in DA vs. NA, AA vs. DA, and AA vs. NA, respectively (Figure 3B). To reveal the physiological response and metabolomic adaptation mechanisms during estivation-arousal cycles of *A. japonicus*, we listed the important differential metabolites in DA vs. NA and AA vs. DA in Table 1, including a wide range of carbohydrates, lipids, amino acids, nucleic acids and vitamins. To illustrate the possible metabolomic adaptation mechanism of *A. japonicus* during estivation, the relationships among the important DMs are summarized in Figure 4.

3.2.1 Glycolysis, TCA cycle and pentose phosphate pathway

For estivators, dormancy is characterized by metabolic rates lowered to at least 30% compared with those in active animals (Pedler et al., 1996), which requires a complex metabolic ordination of reactions involving both ATP-utilizing and ATP-generating pathways. Since glycolysis is an essential energy-yielding pathway by all cells in animals, regulation of glycolysis is an important part of metabolic depression during

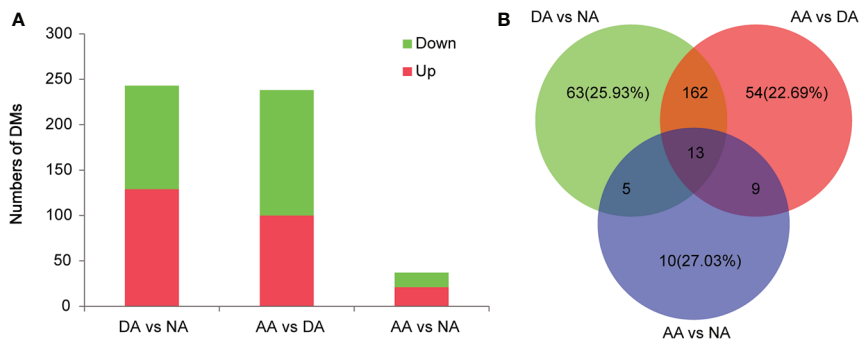

FIGURE 3
Differential metabolites identified in *A. japonicus* during estivation cycles. **(A)** The numbers of differential metabolites in the comparisons of DA vs. NA, AA vs. DA, and AA vs. NA, **(B)** Venn diagram of differential metabolites pairwise comparison.

estivation (Brooks and Storey, 1997). A previous study of the estivating land snail *Otala lactea* showed the reduced activity levels of key enzymes in glycolysis pathways, including hexokinase, phosphofructokinase, phosphoglycerate kinase and lactate dehydrogenase (Brooks and Storey, 1990). For *A. japonicus*, similar depression of glycolytic rates also occurs in the hypometabolic state. Xiang et al. (2016) found significant decreases in glucose and pyruvic acid concentrations in the intestines of estivating *A. japonicus*, along with reduced enzymatic activity and transcription levels of the rate-limiting enzyme hexokinase. In our study, the levels of the glycolysis precursor or the intermediate metabolites D-galactose, fructose 1,6-bisphosphate, and D-glyceraldehyde 3-phosphate were all significantly decreased in the DA group in comparison with the NA and AA groups, verifying that profound glycolytic suppression occurred in estivating *A. japonicus*. In addition, the current study showed that the levels of characteristic intermediate metabolites in the citric acid cycle (TCA cycle), such as succinic acid and malate, were also decreased in the DA group in comparison with the other groups, which was

TABLE 1 Important differential metabolites in *A. japonicus* during estivation cycles.

Metabolites	NA	DA	AA	DA vs NA			AA vs DA		
				Change	VIP	*p*	Change	VIP	*p*
Carbohydrates									
Glycolysis and TCA cycle									
Maltol	65.12	13.26	83.02	-2.30↓	1.11	0.00	2.65	0.77	0.05
D-Galactose	2.14	0.29	2.21	-2.88↓	1.07	0.00	2.92↑	1.10	0.00
6-Phosphogluconic acid	2.14	0.15	0.92	-3.87↓	1.20	0.00	2.66↑	1.23	0.00
D-Glyceraldehyde 3-phosphate	4.97	0.38	7.24	-3.70↓	1.23	0.00	4.24↑	1.22	0.00
Fructose 1,6-bisphosphate	32.39	5.72	24.32	-2.50↓	1.25	0.00	2.09↑	1.21	0.00
Succinic acid	11.65	3.91	2.49	-2.97	0.81	0.04	-0.65	0.71	0.08
Lactate	5.63	1.28	5.07	-2.13↓	1.19	0.00	1.98	0.91	0.01
Malate	1.50	0.42	1.80	-1.83↓	1.08	0.01	2.09↑	1.01	0.01
Pentose phosphate pathway									
D-Ribulose -5-phosphate	0.00	0.08	0.00	7.77↑	1.25	0.00	-7.96↓	1.28	0.00
Ribose 1-phosphate	0.01	1.23	0.01	7.76↑	1.28	0.00	-6.79↓	1.28	0.00
Sedoheptulose 7-phosphate	0.01	0.43	0.02	6.27↑	1.13	0.00	-4.58↓	1.11	0.00
meso-2,6-Diaminoheptanedioate	0.83	34.67	1.63	5.38↑	1.25	0.00	-4.41↓	1.22	0.00
Lipids									
long chain fatty acid									
Arachidic acid	18.12	4.38	10.90	-2.05↓	1.24	0.00	1.31	0.20	0.67
Eicosadienoic acid	0.37	0.10	0.49	-1.84↓	1.17	0.00	2.22↑	1.15	0.00
8,11,14-Eicosatrienoic acid	2.54	0.50	3.83	-2.34↓	1.15	0.00	2.93↑	1.20	0.00
16-Hydroxy hexadecanoic acid	1.01	0.04	0.28	-4.71↓	1.14	0.00	2.84↑	1.01	0.01
Oleic acid	615.25	91.44	536.22	-2.75↓	1.26	0.00	2.55↑	1.24	0.00
(6Z)-Octadecenoic acid	14.05	2.68	12.53	-2.39↓	1.24	0.00	2.23↑	1.22	0.00
Alpha-dimorphecolic acid	3.63	0.72	5.22	-2.34↓	1.23	0.00	2.86↑	1.21	0.00
13-L-Hydroperoxylinoleic acid	0.61	0.13	0.44	-2.23↓	1.15	0.00	1.75↑	1.12	0.00
Linoleic acid	0.31	0.10	0.41	-1.64↓	1.07	0.01	2.03↑	1.06	0.00
8(S)-HETE	1.36	0.64	1.38	-1.09↓	1.03	0.01	1.12↑	1.04	0.01
Stearidonic acid	0.60	0.05	0.18	-3.59↓	1.04	0.00	1.90	0.90	0.04
Hexadecanedioate	1.18	0.11	0.36	-3.41↓	1.03	0.00	1.69↑	1.01	0.01
Palmitoyl-L-carnitine	0.11	20.07	0.16	7.53↑	1.28	0.00	-6.98↓	1.28	0.00
Propionylcarnitine	0.35	30.56	1.16	6.43↑	1.26	0.00	-4.72↓	1.19	0.00
Butyryl-L-carnitine	0.08	2.83	0.16	5.09↑	1.11	0.00	-4.12↓	1.06	0.00
Oxidized lipids									
5(S)-HpETE	0.06	0.56	0.09	3.27↑	1.09	0.00	-2.72↓	1.08	0.00

(Continued)

TABLE 1 Continued

Metabolites	NA	DA	AA	DA vs NA			AA vs DA		
				Change	VIP	*p*	Change	VIP	*p*
Docosahexaenoic acid	0.03	1.71	0.02	5.94↑	1.23	0.00	-6.42↓	1.20	0.00
12-Keto-tetrahydro-leukotriene B4	2.62	15.09	3.31	2.53↑	1.14	0.00	-2.19↓	1.05	0.00
Maslinic acid	0.00	0.24	0.00	8.78↑	1.13	0.00	-11.43↓	1.21	0.00
Ergothioneine	0.43	157.90	0.99	8.51↑	1.27	0.00	-7.32↓	1.25	0.00
Membrane homeostasis									
LysoSM(d18:1)	0.03	3.68	0.01	7.07↑	1.29	0.00	-8.47↓	1.28	0.00
Phosphorylcholine	0.81	4.92	1.33	2.60↑	1.17	0.00	-1.89↓	1.08	0.01
Beta-Glycerophosphoric acid	0.03	2.46	0.01	6.57↑	1.25	0.00	-7.91↓	1.28	0.00
Galactosylsphingosine	0.01	8.60	0.01	9.67↑	1.17	0.00	-9.61↓	1.17	0.00
Sphinganine	3.73	59.82	1.89	4.00↑	1.23	0.00	-4.99↓	1.20	0.00
Sphingosine 1-phosphate	0.00	0.08	0.00	3.95↑	1.03	0.01	-4.53↓	1.09	0.00
N,N-Dimethylsphingosine	1.38	15.85	0.26	3.52↑	1.13	0.00	-5.93↓	1.27	0.00
Sphingosine	0.24	1.78	0.10	2.87↑	1.16	0.00	-4.13↓	1.27	0.00
3-Ketosphingosine	1.85	9.30	1.00	2.33↑	1.13	0.00	-3.22↓	1.12	0.00
Phytosphingosine	8.31	40.15	5.34	2.27↑	1.23	0.00	-2.91↓	1.22	0.00
3-Dehydrosphinganine	3.92	14.60	3.26	1.90↑	1.03	0.01	-2.16↓	1.16	0.00
Oleoylethanolamide	0.54	5.25	0.24	3.29↑	1.14	0.00	-4.45↓	1.25	0.00
24-Methylenecholesterol	0.96	392.59	1.60	8.68↑	1.26	0.00	-7.94↓	1.24	0.00
7-Dehydrocholesterol	0.22	67.53	0.34	8.26↑	1.24	0.00	-7.62↓	1.25	0.00
Amino acids and nucleic acids									
L-Glutamic acid	3.81	195.97	7.86	5.68↑	1.26	0.00	-4.64↓	1.27	0.00
(5-L-Glutamyl)-L-glutamate	0.00	1.10	0.00	15.04↑	1.29	0.00	-9.07↓	1.22	0.00
N-Acetylglutamic acid	0.14	0.45	0.14	1.68↑	1.26	0.00	-1.67↓	1.23	0.00
Phenylacetylglutamine	0.02	0.33	0.00	3.77↑	1.07	0.01	-5.22↓	1.23	0.00
L-Cystine	0.00	0.27	0.00	13.00↑	1.27	0.00	-10.88↓	1.26	0.00
L-Histidine	0.06	4.92	0.08	6.48↑	1.29	0.00	-5.86↓	1.28	0.00
L-Lysine	0.23	18.90	0.22	6.38↑	1.27	0.00	-6.44↓	1.28	0.00
L-Arginine	1.60	16.74	2.54	3.38↑	1.22	0.00	-2.72↓	1.13	0.00
L-Methionine	11.13	110.15	11.52	3.31↑	1.12	0.00	-3.26↓	1.09	0.00
Beta-Tyrosine	0.70	4.12	1.70	2.55↑	1.05	0.01	-1.28	0.71	0.09
L-Aspartic acid	0.29	1.87	0.38	2.70↑	1.22	0.00	-2.29↓	1.21	0.00
L-glycine	0.28	1.38	0.30	2.30↑	1.27	0.00	-2.22↓	1.24	0.00
Ectoine	29.00	385.01	135.31	3.73↑	1.26	0.00	-1.51↓	1.14	0.00
Hypoxanthine	1.31	10.09	0.85	2.95↑	1.09	0.00	-3.57↓	1.16	0.00
Thioguanine	0.15	1.14	0.24	2.93↑	1.27	0.00	-2.26↓	1.23	0.00
Uridine	0.76	4.68	1.17	2.62↑	1.07	0.00	-2.00	0.94	0.01
Deoxyuridine	10.99	67.55	14.16	2.62↑	1.24	0.00	-2.25↓	1.22	0.00
GMP	0.00	0.08	0.00	11.20↑	1.27	0.00	-9.75↓	1.25	0.00
UMP	0.00	0.55	0.04	9.19↑	1.24	0.00	-3.78↓	1.14	0.00
dTMP	0.00	0.13	0.01	7.18↑	1.18	0.00	-3.61↓	1.05	0.01
CMP	0.01	0.52	0.00	6.35↑	1.09	0.00	-7.70↓	1.20	0.00
3-AMP	0.01	0.93	0.01	6.25↑	1.10	0.00	-7.35↓	1.21	0.00
Vitamins and other notable metabolites									
epsilon-Tocopherol	0.34	11.67	0.23	5.10↑	1.27	0.00	-5.69↓	1.28	0.00
delta-Tocotrienol	0.00	12.83	0.01	11.44↑	1.20	0.00	-11.12↓	1.24	0.00
alpha-Tocotrienol	0.11	14.92	0.03	7.08↑	1.29	0.00	-9.02↓	1.27	0.00
Folic acid	0.00	0.37	0.00	10.35↑	1.25	0.00	-7.94↓	1.23	0.00

(Continued)

TABLE 1 Continued

Metabolites	NA	DA	AA	DA vs NA			AA vs DA		
				Change	VIP	*p*	Change	VIP	*p*
Niacinamide	1.53	84.21	11.17	5.79↑	1.29	0.00	-2.91↓	1.14	0.00
Dethiobiotin	0.42	4.12	0.32	3.29↑	1.19	0.00	-3.70↓	1.26	0.00
2-Hydroxybutyric acid	0.59	4.35	2.21	2.89↑	1.19	0.00	-0.98↓	0.82	0.03
Indolebutyric acid	0.20	1.19	0.21	2.55↑	1.27	0.00	-2.53↓	1.24	0.00
Resveratrol	0.08	2.01	0.15	4.70↑	1.28	0.00	-3.73↓	1.25	0.00
Genistein	0.03	0.19	0.04	2.89	1.20	0.00	-2.35↓	1.17	0.00
Epicatechin	0.01	1.41	0.03	7.25↑	1.28	0.00	-5.72↓	1.12	0.00
Catechin	0.02	0.48	0.01	4.98↑	1.26	0.00	-5.22↓	1.22	0.00
Spermidine	0.00	6.96	0.00	14.65↑	1.27	0.00	-14.32↓	1.27	0.00
N1-Acetylspermidine	0.02	61.24	0.02	11.52↑	1.28	0.00	-11.57↓	1.28	0.00
Resolvin D2	0.00	0.29	0.03	6.33↑	1.09	0.00	-3.19	0.98	0.01
Resolvin D1	0.02	0.53	0.03	4.72↑	1.02	0.01	-4.01↓	1.13	0.00

*The numeric values in "NA, DA and AA" represent the mean of normalized metabolite content value in each group. Change means Log_2Fold Change, ↑represents up-regulated differential metabolite, ↓represents down-regulated differential metabolite.

consistent with previous results of Chen et al. (2016a) and Yang et al. (2021), indicating decelerations in the rates of TCA cycle turnover and oxidative phosphorylation in the hypometabolic state.

Interestingly, the content levels of several metabolites involved in the pentose phosphate pathway (including ribulose-5-phosphate, ribose 1-phosphate, sedoheptulose 7-phosphate and meso-2,6-diaminoheptanedioate) were significantly increased in the intestines of the DA group in comparison with the NA and AA groups, indicating an elevated relative carbon flow entry into the pentose phosphate pathway in estivating *A. japonicus*. Likewise, Ramnanan and Storey (2006) reported that estivation could induce a highly phosphorylated glucose-6-phosphate dehydrogenase with greater structural enzymatic stability in *O. lactea*, which further enhanced carbohydrate flow through the pentose phosphate cycle. Indeed, the pentose phosphate pathway has an essential role in the production of reducing power in the form of NADPH for various antioxidant defense and detoxification reactions (DiGiulio et al., 1989; Das and White, 2002). Hence, preferential carbohydrate flow through the pentose phosphate cycle might favor NADPH

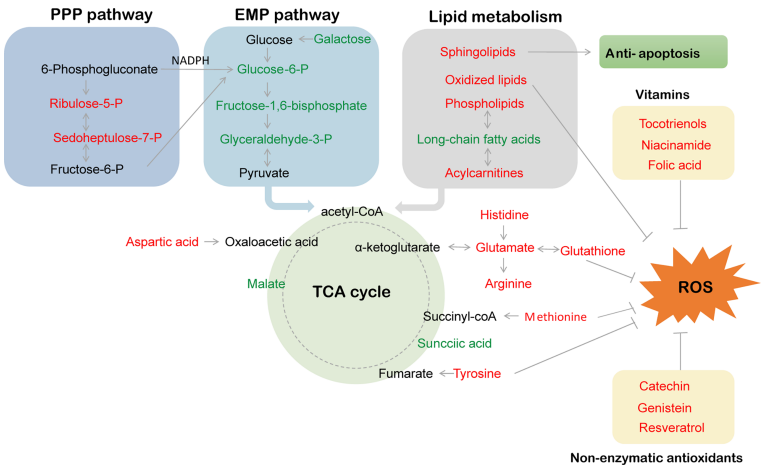

FIGURE 4
The hypothetical metabolic response map during estivation cycles. PPP pathway, EMP pathway and ROS respectively represent pentose-phosphate pathway, embden meyerhof pathway and reactive oxide species.

production, supplying reduction equivalents for the antioxidant system in response to high oxidative stress induced by estivation (Ramnanan and Storey, 2006).

3.2.2 Lipid metabolism

Many mammals typically rely on the oxidation of prestored lipids for energy production during hibernation (Storey, 2002), and there is accumulating evidence indicating that many estivators also utilize lipids as an important fuel source during dormancy Jones, 1980; Frick et al., 2008). For the sea cucumber *A. japonicus*, a wide array of long-chain fatty acids (e.g., arachidic acid, eicosadienoic acid, oleic acid and linoleic acid) showed decreased amounts, yet significant increases in some acylcarnitines (e.g., palmitoyl-L-carnitine, propionylcarnitine and butyryl-L-carnitine) during estivation, suggesting an increased reliance on fatty acid oxidation to support the energy need during hypometabolism, which is consistent with the results of the estivating African lungfish *Protopterus dolloi*, where both 3-hydroxyacyl CoA dehydrogenase (HOAD) and carnitine palmitoyl CoA transferase (CPT) activities were still sustained in the liver despite the 42% reduction in CCO activity during estivation (Frick et al., 2008).

Phospholipids are an essential component of the cell membrane and function in membrane dynamics, protein regulation, signal transduction and secretion. Research shows that phospholipids predominate in the composition of lipids in sea cucumber, accounting for 90% percent of the total fat content (Fan, 2001). In our present study, some kinds of phospholipids and their derivatives (e.g., LysoSM(d18:1), phosphorylcholine and beta-glycerophosphoric acid) were significantly elevated in sea cucumber intestine during deep estivation, which further confirms previous findings reported by Chen et al. (2016a) and Zhao et al. (2014) that upregulations in gene transcription and protein translation were involved in phospholipid catabolic processes in *A. japonicus* intestines during estivation (e.g., phospholipase, proactivator polypeptide, glycerol kinase, and group XV phospholipase A2), implying that membrane lipid catabolism may also be a major fuel source of energy. Moreover, the increases in phospholipids and cholesterols might enhance the stability of the basic structure of the cell membrane during the dormant period, which is an important adaptive strategy for marine invertebrates in resilience to environmental stress, such as high temperature and hypoxia (Li et al., 2019; Hu et al., 2022).

Remarkably, increased levels of several sphingolipid derivatives (e.g., sphingosine 1-phosphate, N,N-dimethylsphingosine, sphingosine, 3-ketosphingosine and phytosphingosine) were found in estivating sea cucumbers. Sphingolipids play integral roles in membrane domains and signaling, cell proliferation and apoptosis, inflammation and central nervous system development (Quinville et al., 2021). For instance, sphingosine 1-phosphate is a well-known anti-apoptotic regulator that can suppress caspase-3 activity and prevent apoptosis (Rutherford et al., 2013), which suggests that the increased level of sphingosine 1-phosphate during estivation in our present study may perform a protective function by reducing excessive tissue apoptosis. Indeed, inhibition of apoptosis is a key strategy for maintaining long-term viability in a low metabolic state, where the energy expenditure of cell replacement processes must be minimized to prolong survival (Biggar and Storey, 2010). Similar interactions have been described by Chen et al. (2016a) at the protein level, in which mediators of apoptosis were downregulated during deep estivation in sea cucumber. There is growing evidence that sphingolipids also play a role in the cellular response to oxidative stress (Van Brocklyn and Williams, 2012). Other lipids, such as 12-keto-tetrahydro-leukotriene B4 and docosahexaenoic acid, also showed elevated levels in sea cucumbers during estivation. Since leukotriene is an endogenous lipid mediator of inflammation (Le Bel et al., 2014) and docosahexaenoic acid is an antioxidant that can reinforce the antioxidative defense system (Hossain et al., 1999), higher amounts of these metabolites indicate that sea cucumbers were subjected to oxidative and inflammatory stress during estivation. However, the precise roles of these estivation-specific metabolites need to be explored further.

3.2.3 Amino acid and nucleic acid metabolism

Free amino acids are not only directly utilized as fuels by the immune system and energy metabolism but can also be converted to other amino acids or molecules that exert protective effects in organisms under various stresses (Calder, 2006; Chen et al., 2016a; Xu et al., 2017; Huo et al., 2019). In our study, higher amounts of amino acids, namely, L-glutamic acid, beta-tyrosine, L-glycine, L-histidine, L-arginine, L-methionine, L-cystine, L-lysine and L-aspartic acid, were observed at the DA stage than at the NA stage. Among these amino acids, some can also be converted into intermediate metabolites in the TCA cycle and used by cells to produce energy (e.g., tyrosine into fumarate, histidine, arginine and glutamic acid into alpha-ketoglutarate, aspartic acid into oxaloacetic acid, and methionine into succinyl-CoA). In addition, several amino acids are involved in the antioxidant defense system to prevent and repair the deleterious effects from free radicals; for example, tyrosine is an excellent antioxidant inside lipid bilayers and protects cells from oxidative destruction (Moosmann and Behl, 2000); glycine and glutamic acid are integral components of glutathione, which is the major antioxidant molecule of the cell and can effectively scavenge free radicals and other reactive oxygen species and

maintain the cellular redox balance (Hensley et al., 2000; Fang et al., 2002); and methionine is easily oxidized to methionine sulfoxide by many reactive species, thus serving to protect other functionally essential residues from oxidative damage (Levine et al., 2010). Furthermore, another investigation of estivating *Chilo partellus* larvae reported increased amounts of glycine, histidine, arginine, proline, tyrosine, and methionine, which may be constituents of heat-shock proteins to enhance stress tolerance and maintain development (Tanwar et al., 2021). Hence, the elevated levels of the above amino acids in estivating *A. japonicus* intestines could meet the greater energy requirements for dealing with oxidative stress and heat-shock proteins during torpor.

Additionally, various metabolites associated with nucleotide metabolism, such as pyrimidine ectoine, hypoxanthine, thioguanine and uridine, were significantly changed at the DA stage, as well as a series of mononucleotides (e.g., adenosine monophosphate (AMP), guanosine monophosphate (GMP), uridine monophosphate (UMP), cytidine monophosphate (CMP) and deoxythymoadenylate (dTMP)), reflecting that *A. japonicus* was facing a real energy crisis during estivation.

3.2.4 Vitamins and other physiological responses

Vitamin E is an essential nutrient for organisms that exerts an antioxidant response to reactive oxygen species (ROS) -induced oxidative stress by inhibiting membrane lipid peroxidation and damage to proteins and DNA (Miyazawa et al., 2019). Folic acid is an important, potent antioxidant that is involved in the trans-sulfuration pathway as a coenzyme, increasing glutathione synthesis and acetaldehyde oxidation and preventing glutathione inactivation (Ebaid et al., 2013). Nicotinamide (NAM) is a form of vitamin B3 that can suppress oxidative stress (Wei et al., 2018). In our study, the significantly increased levels of three isomers of the vitamin E family (alpha-tocotrienol, delta-tocotrienol and epsilon-tocopherol), nicotinamide and folic acid in estivating sea cucumbers implied their enhanced antioxidant effect to protect the body from oxidative damage. In addition, several flavanol and isoflavone antioxidants also increased during estivation, such as catechin, genistein and resveratrol (Simioni et al., 2018). In general, aerobic organisms develop antioxidant systems consisting of antioxidant enzymes (e.g., SOD, CAT and glutathione peroxidase) and low-molecular weight compounds (e.g., glutathione, α-tocopherol, and ascorbic acid) to maintain redox balance from ROS-induced oxidative stress. Our unpublished data and previous studies revealed the reduced activities of several antioxidant enzymes, such as catalase, in estivating *A. japonicus*, the freshwater snail *Biomphalaria tenagophila* and *Helix pomatia* (Ferreira et al., 2003; Nowakowska et al., 2009; Liu et al., 2016; Chen et al., 2016a), while the present study indicated that significantly elevated levels of nonenzymatic antioxidant molecules were observed at the DA stage compared to other stages, suggesting that an adjustment strategy of antioxidant defense might be adapted during hypometabolism in an energy-efficient manner.

Spermidine has a variety of effects, including anti-inflammatory, antioxidant, enhanced mitochondrial metabolic and respiration functions, and improved protein stability and chaperone activity (Madeo et al., 2018). Resolvins D1 and D2 are docosahexaenoic acid (DHA)-derived lipoxygenase metabolites that can exhibit anti-inflammatory effects by modulating the activation of T lymphocytes (Chiurchiu et al., 2016). Hence, changes in the contents of the above metabolites during estivation indicated that anti-inflammatory biological protective effects might be exerted in estivating sea cucumbers.

3.3 KEGG pathway enrichment analysis

To further assess the metabolic profiles of *A. japonicus* intestines during estivation cycles, pathway enrichment analysis was performed based on the identified metabolites that were significantly differentially expressed. In our present study, 58 and 61 pathways were enriched in the DA vs. NA and AA vs. DA groups, respectively. The top 25 pathways are shown in Figure 5. Furthermore, 6 (sphingolipid metabolism, linoleic acid metabolism, pyrimidine metabolism, D-glutamine and D-glutamate metabolism, lysine biosynthesis and pentose phosphate pathway) and 4 (sphingolipid metabolism, phenylalanine metabolism, pyrimidine metabolism, and lysine biosynthesis) pathways were significantly enriched in the DA vs. NA and AA vs. DA comparisons, respectively ($p < 0.05$). There were 17 key common increased metabolites involved in these significantly enriched pathways, including sphingosine-1-P, sphingosine, phyto-sphingosine, psychosine, 3-dehydro-sphingosine, L-aspartate, L-lysine, L-saccharopine, UMP, CMP, dTMP, uridine, and deoxyuridine. As previously mentioned, sphingolipid metabolism, D-glutamine and D-glutamate metabolism and pentose phosphate pathway were involved with anti-apoptosis and antioxidant defense, while linoleic acid metabolism and pyrimidine metabolism were involved with energy metabolism, suggesting that sea cucumbers might reorganize metabolic priorities for ATP production and enhance defense mechanisms by these key pathways to promote long-term viability in a hypometabolic state. However, further studies are required to elucidate the specific functions of these pathways in echinoderms during estivation.

In conclusion, our present metabolomics analysis demonstrated that sea cucumbers may meet the challenge of summer estivation by reorganizing metabolic priorities for ATP production (e.g., depressing carbohydrate metabolism and promoting lipid and amino acid catabolism) and enhancing antioxidant defenses in an

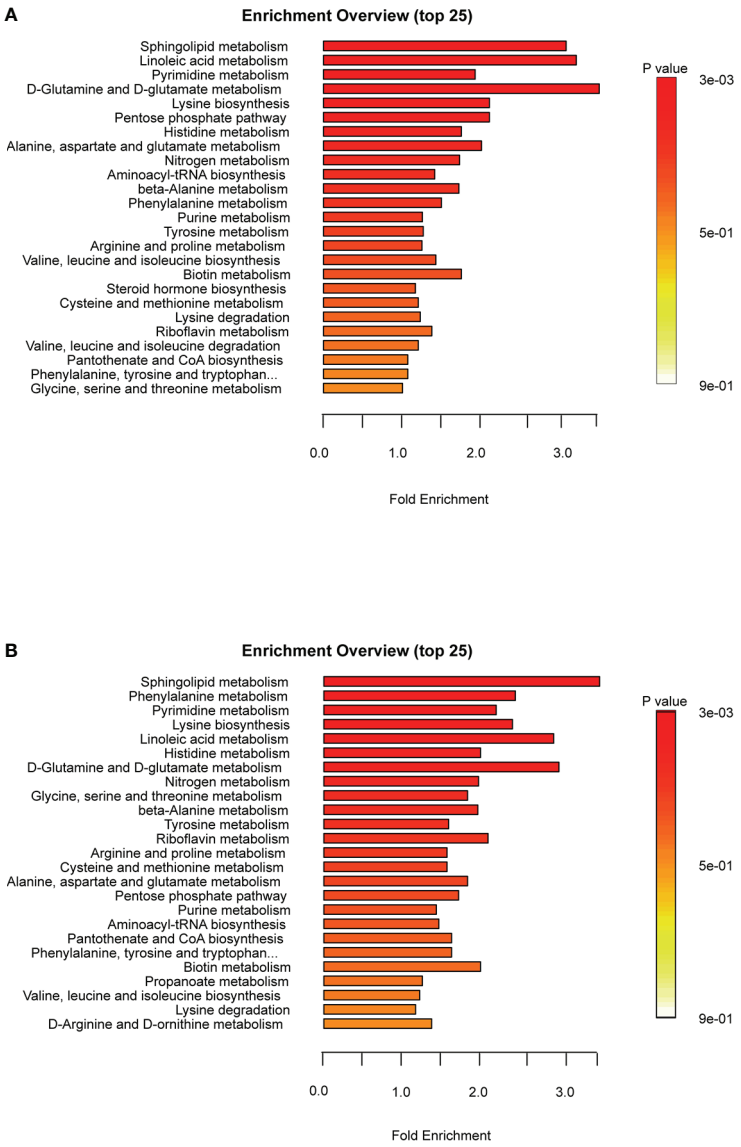

FIGURE 5
Metabolic pathways analysis of *A. japonicus* intestines in the comparisons of DA vs. NA **(A)** and AA vs. DA **(B)**.

energy-efficient manner to promote long-term viability. The present study identified a series of key differential metabolites and pathways and explored the potential metabolic strategies of *A. japonicus* during estivation, which will provide new insights into the adaptation mechanisms of estivation in marine invertebrates.

Data availability statement

The original contributions presented in the study are included in the article/Supplementary Material. Further inquiries can be directed to the corresponding author.

Author contributions

YZ: Conceptualization, Methodology, Writing- Original draft preparation. HaoW: Investigation, Data Curation. HanW: Visualization, Formal analysis. YP: Writing- Reviewing and Editing. MC: Writing- Reviewing and Editing. All authors contributed to the article and approved the submitted version.

Funding

This work was funded by the National Natural Science Foundation of China (No. 41906098 and 31972767).

Acknowledgments

We are grateful to Wekemo Tech Group Co., Ltd. for assisting in bioinformatic analysis.

Conflict of interest

The authors declare that the research was conducted in the absence of any commercial or financial relationships that could be construed as a potential conflict of interest.

Publisher's note

All claims expressed in this article are solely those of the authors and do not necessarily represent those of their affiliated organizations, or those of the publisher, the editors and the reviewers. Any product that may be evaluated in this article, or claim that may be made by its manufacturer, is not guaranteed or endorsed by the publisher.

Supplementary material

The Supplementary Material for this article can be found online at: https://www.frontiersin.org/articles/10.3389/fmars.2022.980221/full#supplementary-material

SUPPLEMENTARY FIGURE 1
The intestine tissue of *A. japonicus* during estivation cycles. **(A)** NA stage, **(B)** DA stage, **(C)** AA stage.

SUPPLEMENTARY FIGURE 2
PCA diagram of quality control analysis.

SUPPLEMENTARY FIGURE 3
The permutation tests of OPLS-DA analysis.

References

Biggar, K. K., and Storey, K. B. (2010). The emerging roles of microRNAs in the molecular responses of metabolic rate depression. *J. Mol. Cell. Biol* 3(3)167–75. doi: 10.1093/jmcb/mjq045

Brooks, S., and Storey, K. B. (1990). Glycolytic enzyme binding and metabolic control in estivation and anoxia in the land snail *Otala lactea*. *J. Exp. Biol.* 151, 193–204. doi: 10.1242/jeb.151.1.193

Brooks, S., and Storey, K. B. (1997). Glycolytic controls in estivation and anoxia: a comparison of metabolic arrest in land and marine molluscs. *Comp. Biochem. Phys. A.* 118, 1103–1114. doi: 10.1016/S0300-9629(97)00237-5

Calder, P. C. (2006). Branched chain amino acids and immunity. *J. Nutr.* 136, 288S–293S. doi: 10.1093/jn/136.1.288S

Chen, M., Li, X., Zhu, A., Storey, K. B., Sun, L., Gao, T., et al. (2016a). Understanding mechanism of sea cucumber *Apostichopus japonicus* aestivation: insights from TMT-based proteomic study. *Comp. Biochem. Physiol. D. Genom. Proteom.* 19, 78–89. doi: 10.1016/j.cbd.2016.06.005

Chen, M., Wang, S., Li, X., Storey, K. B., and Zhang, X. (2018). The potential contribution of miRNA-200-3p to the fatty acid metabolism by regulating *AjEHHADH* during aestivation in sea cucumber. *PeerJ* 6, e5703. doi: 10.7717/peerj.5703

Chen, M., Zhang, X., Liu, J., and Storey, K. B. (2013). High-throughput sequencing reveals differential expression of miRNAs in intestine from sea cucumber during aestivation. *PloS One* 8, e76120. doi: 10.1371/journal.pone.0076120

Chen, M., Zhu, A., and Storey, K. B. (2016b). Comparative phosphoproteomic analysis of intestinal phosphorylated proteins in active versus aestivating sea cucumbers. *J. Proteom.* 135, 141–150. doi: 10.1016/j.jprot.2015.09.016

Chiurchiu, V., Leuti, A., Dalli, J., Jacobsson, A., Battistini, L., Maccarrone, M., et al. (2016). Proresolving lipid mediators resolvin D1, resolvin D2, and maresin 1 are critical in modulating T cell responses. *Sci. Transl. Med.* 8 (353), 353ra111. doi: 10.1126/scitranslmed.aaf7483

Das, K. C., and White, C. W. (2002). Redox systems of the cell: possible links and implications. *Proc. Natl. Acad. Sci. U.S.A.* 99 (15), 9617–9618. doi: 10.1073/pnas.162369199

DiGiulio, R. T., Washburn, P. C., Wenning, R. J., Winston, G. W., and Jewell, C. S. (1989). Biochemical responses in aquatic animals: a review of determinants of oxidative stress. *Environ. Toxicol. Chem.* 8, 1103–1123. doi: 10.1002/etc.5620081203

Ebaid, H., Bashandy, S. A., Alhazza, I. M., Rady, A., and El-Shehry, S. (2013). Folic acid and melatonin ameliorate carbon tetrachloride-induced hepatic injury, oxidative stress and inflammation in rats. *Nutr. Metab. (Lond)* 10, 20. doi: 10.1186/1743-7075-10-20

Fan, H. (2001). Sea Cucumber: ginseng in the sea - a review about the research and exploration of the medical care function of sea cucumber and its ingredient. *Chin. J. Mar. Drugs* 82, 37–44.

Fang, Y. Z., Yang, S., and Wu, G. (2002). Free radicals, antioxidants, and nutrition. *Nutrition* 18, 872–879. doi: 10.1016/S0899-9007(02)00916-4

Ferreira, M. V. R., Alencastro, A. C. R., and Hermes-Lima, M. (2003). Role of antioxidant defenses during estivation and anoxia exposure in the freshwater snail *Biomphalaria tenagophila* (Orbigny 1835). *Can. J. Zool.* 81, 1239–1248. doi: 10.1139/z03-104

Frick, N. T., Bystriansky, J. S., Ip, Y. K., Chew, S. F., and Ballantyne, J. S. (2008). Lipid, ketone body and oxidative metabolism in the African lungfish, *Protopterus dolloi* following 60 days of fasting and aestivation. *Comp. Biochem. Physiol. A Mol. Integr. Physiol.* 151, 93–101. doi: 10.1016/j.cbpa.2008.06.004

Gao, F., Yang, H. S., Xu, Q., Wang, F. Y., Liu, G. B., and German, D. P. (2008). Phenotypic plasticity of gut structure and function during periods of inactivity in *Apostichopus japonicus*. *Comp. Biochem. Physiol. B* 150, 255–262. doi: 10.1016/j.cbpb.2008.03.011

Guo, C., Wang, Y., Wu, Y., Han, L., Gao, C., Chang, Y., et al. (2022). UPLC-Q-TOF/MS-based metabonomics study on *Apostichopus japonicus* in various aquaculture models. *Aquac. Res.* 53 (5), 2004–2014. doi: 10.1111/are.15729

Heldmaier, G., Ortmann, S., and Elvert, R. (2004). Natural hypometabolism during hibernation and daily torpor in mammals. *Respir. Physiol. Neurobiol.* 141, 317–329. doi: 10.1016/j.resp.2004.03.014

Hensley, K., Robinson, K. A., Gabbita, S. P., Salsman, S., and Floyd, R. A. (2000). Reactive oxygen species, cell signaling, and cell injury. *Free. Radic. Biol. Med.* 28 (10), 1456–1462. doi: 10.1016/S0891-5849(00)00252-5

Hossain, M. S., Hashimoto, M., Gamoh, S., and Masumura, S. (1999). Antioxidative effects of docosahexaenoic acid in the cerebrum versus cerebellum and brainstem of aged hypercholesterolemic rats. *J. Neurochem.* 72, 1133–1138. doi: 10.1046/j.1471-4159.1999.0721133.x

Hu, Z., Feng, J., Song, H., Zhou, C., Yang, M. J., Shi, P., et al. (2022). Metabolic response of *Mercenaria mercenaria* under heat and hypoxia stress by widely targeted metabolomic approach. *Sci. Total. Environ.* 809, 151172. doi: 10.1016/j.scitotenv.2021.151172

Huo, D., Sun, L., Zhang, L., Ru, X., Liu, S., and Yang, H. (2019). Metabolome responses of the sea cucumber *Apostichopus japonicus* to multiple environmental stresses: heat and hypoxia. *Mar. pollut. Bull.* 138, 407–420. doi: 10.1016/j.marpolbul.2018.11.063

Huskisson, E., Maggini, S., and Ruf, M. (2007). The role of vitamins and minerals in energy metabolism and well-being. *J. Int. Med. Res.* 35, 277–289. doi: 10.1177/147323000703500301

Johnson, C., Ivanisevic, J., and Siuzdak, G. (2016). Metabolomics: beyond biomarkers and towards mechanisms. *Nat. Rev. Mol. Cell. Biol.* 17, 451–459. doi: 10.1038/nrm.2016.25

Jones, R. M. (1980). Metabolic consequences of accelerated urea synthesis during seasonal dormancy of spadefoot toads, *Scaphiopus couchii* and *Scaphiopus multiplicatus*. *J. Exp. Zool.* 212, 255–267. doi: 10.1002/jez.1402120212

Le Bel, M., Brunet, A., and Gosselin, J. (2014). Leukotriene B4, an endogenous stimulator of the innate immune response against pathogens. *J. Innate. Immun.* 6 (2), 159–168. doi: 10.1159/000353694

Levine, R. L., Moskovitz, J., and Stadtman, E. R. (2010). Oxidation of methionine in proteins: roles in antioxidant defense and cellular regulation. *Iubmb. Life.* 50, 301–307. doi: 10.1080/713803735

Li, L., Chen, M., and Storey, K. B. (2019). Metabolic response of longitudinal muscles to acute hypoxia in sea cucumber *Apostichopus japonicus* (Selenka): a metabolome integrated analysis. *Comp. Biochem. Physiol. D.* 29, 235–244. doi: 10.1016/j.cbd.2018.12.007

Li, F., Liu, Y., Song, B., Sun, H., Gu, B., and Zhang, X. (1996). Study on aestivating habit of sea cucumber (*Apostichopus japonicus* selenka): 2. the factors relating to aestivation. *J. Fish. China.* 3, 49–57.

Liu, S., Zhou, Y., Ru, X., Zhang, M., Cao, X., and Yang, H. (2016). Differences in immune function and metabolites between aestivating and non-aestivating *Apostichopus japonicus*. *Aquaculture* 459, 36–42. doi: 10.1016/j.aquaculture.2016.03.029

Li, Y., Wang, R., Xun, X., Wang, J., Bao, L., Thimmappa, R., et al. (2018). Sea Cucumber genome provides insights into saponin biosynthesis and aestivation regulation. *Cell. Discovery* 4, 1–17. doi: 10.1038/s41421-018-0030-5

Madeo, F., Eisenberg, T., Pietrocola, F., and Kroemer, G. (2018). Spermidine in health and disease. *Science* 359 (6374), eaan2788. doi: 10.1126/science.aan2788

Miyazawa, T., Burdeos, G. C., Itaya, M., Nakagawa, K., and Miyazawa, T. (2019). Vitamin e: Regulatory redox interactions. *IUBMB Life* 71 (4), 430–441. doi: 10.1002/iub.2008

Moosmann, B., and Behl, C. (2020). Cytoprotective antioxidant function of tyrosine and tryptophan residues in transmembrane proteins. *Eur. J. Biochem.* 267 (18), 5687–92. doi: 10.1046/j.1432-1327.2000.01658.x

Nowakowska, A., Świderska-Kołacz, G., Rogalska, J., and Caputa, M. (2009). Antioxidants and oxidative stress in *Helix pomatia* snails during estivation. *Comp. Biochem. Phys. C.* 150 (4), 481–486. doi: 10.1016/j.cbpc.2009.07.005

Pedler, S., Fuery, C. J., Withers, P. C., Flanigan, J., and Guppy, M. (1996). Effectors of metabolic depression in an estivating pulmonate snail (*Helix aspersa*): whole animal and *in vitro* tissue studies. *J. Comp. Physiol. B.* 166, 375–381. doi: 10.1007/BF02336920

Quinville, B. M., Deschenes, N. M., Ryckman, A. E., and Walia, J. S. (2021). A comprehensive review: sphingolipid metabolism and implications of disruption in sphingolipid homeostasis. *Int. J. Mol. Sci.* 22 (11), 5793. doi: 10.3390/ijms22115793

Ramnanan, C. J., and Storey, K. B. (2006). Glucose-6-phosphate dehydrogenase regulation during hypometabolism. *Biochem. Biophys. Res. Commun.* 339, 7–16. doi: 10.1016/j.bbrc.2005.10.036

Rutherford, C., Childs, S., Ohotski, J., McGlynn, L., Riddick, M., MacFarlane, S., et al. (2013). Regulation of cell survival by sphingosine-1-phosphate receptor $S1P_1$ *via* reciprocal ERK-dependent suppression of bim and PI-3-kinase/protein kinase c-mediated upregulation of mcl-1. *Cell. Death. Dis.* 4, e927. doi: 10.1038/cddis.2013.455

Saccenti, E., Hoefsloot, H. C. J., Smilde, A. K., Westerhuis, J. A., and Hendriks, M. M. (2014). Reflections on univariate and multivariate analysis of metabolomics data. *Metabolomics* 10 (3), 361–374. doi: 10.1007/s11306-013-0598-6

Simioni, C., Zauli, G., Martelli, A. M., Vitale, M., Sacchetti, G., Gonelli, A., et al. (2018). Oxidative stress: role of physical exercise and antioxidant nutraceuticals in adulthood and aging. *Oncotarget* 9, 17181–17198. doi: 10.18632/oncotarget.24729

Storey, K. B. (2002). Life in the slow lane: molecular mechanisms of estivation. *Comp. Biochem. Physiol. A.* 133, 733–754. doi: 10.1016/S1095-6433(02)00206-4

Storey, K. B., and Storey, J. M. (1990). Facultative metabolic rate depression: molecular regulation and biochemical adaptation in anaerobiosis, hibernation, and estivation. *Q. Rev. Biol.* 65, 145–174. doi: 10.1086/416717

Storey, K. B., and Storey, J. M. (2007). Putting life on 'pause' - molecular regulation of hypometabolism. *J. Exp. Biol.* 210, 1700–1714. doi: 10.1242/jeb.02716

Storey, K. B., and Storey, J. M. (2010). Metabolic regulation and gene expression during aestivation. *Prog. Mol. Subcell. Biol.* 49, 25–45. doi: 10.1007/978-3-642-02421-4_2

Storey, K. B., and Storey, J. M. (2012). Aestivation: Signaling and hypometabolism. *J. Exp. Biol.* 215, 1425–1433. doi: 10.1242/jeb.054403

Tanwar, A. K., Kirti, J. S., Kumar, S., and Dhillon, M. K. (2021). The amino acid and lipophilic profiles of *Chilo partellus* (swinhoe) larvae fluctuate with diapause. *J. Exp. Zool. A. Ecol. Genet. Physiol.* 335 (7), 595–601. doi: 10.1002/jez.2502

Van Brocklyn, J. R., and Williams, J. B. (2012). The control of the balance between ceramide and sphingosine-1-phosphate by sphingosine kinase: oxidative stress and the seesaw of cell survival and death. comp. biochem. *Physiol. B. Biochem. Mol. Biol.* 163 (1), 26–36. doi: 10.1016/j.cbpb.2012.05.006

Weckwerth, W. (2003). Metaboomics in systems biology. *Annu. Rev. Plant Biol.* 54, 669–689. doi: 10.1146/annurev.arplant.54.031902.135014

Wei, X., Yin, Q., Zhao, H., Cao, Y., Cai, C., and Yao, J. (2018). Metabolomics for the effect of biotin and nicotinamide on transition dairy cows. *J. Agric. Food. Chem.* 66 (22), 5723–5732. doi: 10.1021/acs.jafc.8b00421

Xiang, X., Chen, M., Wu, C., Zhu, A., Yang, J., Lv, Z., et al. (2016). Glycolytic regulation in aestivation of the sea cucumber *Apostichopus japonicus*: evidence from metabolite quantification and rate-limiting enzyme analyses. *Mar. Biol.* 163 (8), 167. doi: 10.1007/s00227-016-2936-5

Xing, L., Sun, L., Liu, S., Zhang, L., and Yang, H. (2021). Comparative metabolomic analysis of the body wall from four varieties of the sea cucumber *Apostichopus japonicus*. *Food. Chem.* 352, 129339. doi: 10.1016/j.foodchem.2021.129339

Xu, D., Zhou, S., and Yang, H. (2017). Carbohydrate and amino acids metabolic response to heat stress in the intestine of the sea cucumber *Apostichopus japonicus*. *Aquac. Res.*, 00:1–9. doi: 10.1111/are.13411

Yang, Q., Zhang, X., Zhen, L. U., Huang, R., Tuan, T. N., Wu, J. S., et al. (2021). Transcriptome and metabolome analyses of sea cucumbers *Apostichopus japonicus* in southern china during the summer aestivation period. *J. Ocean Univ. China.* 20 (1), 198–212. doi: 10.1007/s11802-021-4482-0

Yang, Y., Zheng, Y., Sun, L., and Chen, M. (2020). Genome-wide DNA methylation signatures of sea cucumber *Apostichopus japonicus* during environmental induced aestivation. *Genes* 11 (9), 1020. doi: 10.3390/genes11091020

Yang, H., Zhou, Y., Zhang, T., Yuan, X., Li, X., Liu, Y., et al. (2006). Metabolic characteristics of sea cucumber *Apostichopus japonicus* (Selenka) during aestivation. *J. Exp. Mar. Biol. Ecol.* 330, 505–510. doi: 10.1016/j.jembe.2005.09.010

Yuan, X., Yang, H., Chen, M., and Gao, F. (2007a). Research advances in aestivation of sea cucumber *Apostichopus japonicus* (Selenka): A review. *Mar. Sci.* 31, 88–90.

Yuan, X., Yang, H., Wang, L., Zhou, Y., Zhang, T., and Liu, Y. (2007b). Effects of aestivation on the energy budget of sea cucumber *Apostichopus japonicus* (Selenka) (Echinodermata: Holothuroidea). *Acta Ecol. Sin.* 27, 3155–3161. doi: 10.1016/s1872-2032(07)60070-5

Zhao, Y., Chen, M., Storey, K. B., Sun, L., and Yang, H. (2015). DNA Methylation levels analysis in four tissues of sea cucumber *Apostichopus japonicus* based on fluorescence-labeled methylation-sensitive amplified polymorphism (F-MSAP) during aestivation. *Comp. Biochem. Phys. B.* 181, 26–32. doi: 10.1016/j.cbpb.2014.11.001

Zhao, Y., Yang, H. S., Storey, K. B., and Chen, M. Y. (2014). RNA-Seq dependent transcriptional analysis unveils gene expression profile in the intestine of sea cucumber *Apostichopus japonicus* during aestivation. *Comp. Biochem. Phys. D.* 10, 30–43. doi: 10.1016/j.cbd.2014.02.002

Zhao, G., Zhao, W., Han, L., Ding, J., and Chang, Y. (2020). Metabolomics analysis of sea cucumber (*Apostichopus japonicus*) in different geographical origins using UPLC-Q-TOF/MS. *Food. Chem.* 333, 127453. doi: 10.1016/j.foodchem.2020.127453

frontiers | Frontiers in Marine Science

TYPE Review
PUBLISHED 24 August 2022
DOI 10.3389/fmars.2022.931903

OPEN ACCESS

EDITED BY
Libin Zhang,
Institute of Oceanology (CAS), China

REVIEWED BY
Lina Sun,
Institute of Oceanology (CAS), China
Zhuang Xue,
Dalian Ocean University, China
Dongxue Xu,
Qingdao Agricultural University, China

*CORRESPONDENCE
Ming Guo
guoming@nbu.edu.cn

SPECIALTY SECTION
This article was submitted to Marine Fisheries, Aquaculture and Living Resources, a section of the journal Frontiers in Marine Science

RECEIVED 29 April 2022
ACCEPTED 02 August 2022
PUBLISHED 24 August 2022

CITATION
Chen J, Lv Z and Guo M (2022) Research advancement of *Apostichopus japonicus* from 2000 to 2021. *Front. Mar. Sci.* 9:931903. doi: 10.3389/fmars.2022.931903

Research advancement of *Apostichopus japonicus* from 2000 to 2021

Jiting Chen[1], Zhimeng Lv[1] and Ming Guo[1,2]*

[1]State Key Laboratory for Quality and Safety of Agro-Products, Ningbo University, Ningbo, China, [2]Shandong Key Laboratory of Disease Control in Mariculture, Qingdao, China

This study aims to establish a quantitative and qualitative evaluation model of sea cucumber *Apostichopus japonicus* research. Data from 2000 to 2021 were obtained from the Web of Science Core Collection (WoSCC) of Thomson Reuters. Bibliometrics and CiteSpace software were used to analyze authors, exporting countries, journals, influential articles, research areas, institutions, research hot spots, and trends. A total of 1,358 research papers on *A. japonicus* research were identified from 2000 to 2021. The number of papers published in this field is rapidly increasing, and the research phase can be divided into initial, developmental, and stabilization phases. Research on *A. japonicus* is mostly conducted in China, followed by Japan and the United States. Hongsheng Yang, Chenghua Li, and Shuanglin Dong are the lead authors. Research activities are focused on genetics and breeding, growth and development, immunology and disease, aestivation, regeneration, and food processing. Gut microbiota, activation, and collagen are potential research hot spots. The project highlights differences in the level of research between countries and teams, and regions with more developed industries or richer resources need further support. Governments or organizations are encouraged to 1) promote the development of the *A. japonicus* industry through the development or implementation of policies; 2) further participate in the research, production, and processing of *A. japonicus*; and 3) strengthen international exchange and cooperation to bring economic benefits to farmers in suitable breeding areas through technology sharing.

KEYWORDS

***Apostichopus japonicus*, co-citation analysis, research hot spots, frontier prediction, bibliometrics**

Introduction

More than 1,500 species of sea cucumbers have been recorded in the world (Liao, 1997). Sea cucumber *Apostichopus japonicus* (Echinodermata, Holothuroidea) was first described and reported by Selenka (1867). Considering its richness in bioactive substances such as triterpene glycosides, polysaccharides, and neuropeptides, it has

been a valuable traditional food and nutraceutical, especially in East Asian countries (Bordbar et al., 2011; Ramírez-González et al., 2020). Only approximately 60 species have exploitation value, among which *A. japonicus* is the most economically important species (Kinch et al., 2008). In 2021, China's total production of *A. japonicus* will be 350 million pounds, about 1.6 billion pieces, and the value of the whole industry chain will be about $9 billion (Sea Cucumber Industry Branch of China Fisheries Association, 2022). Wild *A. japonicus* is mainly found in the temperate waters of the western Pacific Ocean, including Japan, Korea, the Russian Far East, and Northeast China (Cui and Zhao, 2000). China is a major producer and consumer of *A. japonicus*. The economic growth and increased consumption of the Chinese society provide a good environment for the development of the *A. japonicus* industry (Ru et al., 2019). In addition to seabed seeding, three well-established aquaculture models, namely, shrimp pool coculture, floating raft culture, and bottom net culture, are being developed in China (Chang, 2002).

In the late 19th century, the Japanese scholar Kakichi Mitsukuri first studied the morphology and ecological habits of *A. japonicus* (Mitsukuri, 1897; Mitsukuri, 1905). The early research on *A. japonicus* was also conducted in Japan by a group of technical application talents who studied the growth and reproduction of *A. japonicus*. In 1938, Densaburo Inaba first tried to breed sea cucumbers in captivity (Midori and Kenichiro, 1981). In 1950, he worked with Takeshi Imai and Ryuhei Sato to develop the use of colorless flagellates as bait for sea cucumber larvae (Imai et al., 1950). Scholars Kinoshita and Tanaka reported on the short aestivation time of sea cucumbers from Hokkaido (Tanaka, 1958; Furukawa et al., 2016). A few years later, they sampled and analyzed the *A. japonicus* digestive tract and found that it mainly consisted of gravel, sediment, and shell fragments, providing a research basis for the culture of the species. Choe (1963) studied the genetics and regeneration of sea cucumbers. Over the next 60 years, Russia, South Korea, United States, and China will work together to improve *A. japonicus* breeding, disease control, and growth performance.

Zoology, agriculture, and other disciplines have begun using knowledge analysis and visualization tools, such as the CiteSpace software, to investigate and analyze water pollution (Hu et al., 2019; Liu et al., 2019), soil erosion (Liu et al., 2020; Huang X. et al., 2021), and marine conservation (Picone et al., 2021; Wang Z. Q. et al., 2021). In the case of *A. japonicus*, although we have a lot of basic research published in journals, access to cutting-edge data in the industry still relies on regular review articles, technical summits, and especially the support of government agencies in charge of fisheries. Scholars have not attempted to systematize and visualize the knowledge about *A. japonicus* developed from basic or industrial research. In the present study, we used bibliometrics and CiteSpace software to qualitatively or quantitatively analyze and visualize literature from 2000 to 2021, estimate the global scientific outputs of *A. japonicus* research, and analyze the hot spots and trends, which aims to provide fundamental data for further research on *A. japonicus* and encourage governments and organizations to promote the development of the *A. japonicus* industry through the development or implementation of policies.

Data and methods

Data sources

The data retrieval process was completed on 1 April 2022. This study is based on the Web of Science Core Collection (WoSCC) database, including Science Citation Index Expanded, Social Sciences Citation Index, Current Chemical Reactions, and Index Chemicus. Both *A. japonicus* and *Stichopus japonicus* were used in research papers because of the different usage habits of scholars or other factors. Therefore, the terms "*Apostichopus japonicus*" and "*Stichopus japonicus*" were used as keywords to retrieve titles, author information, abstracts, and references from 2000 to 2021, respectively. On this basis, we used the Boolean Operator "OR" to combine the two search formulas and obtained 1,358 research papers on *A. japonicus*. The bibliographies of 1,358 papers were downloaded and exported as "plain text files," and the records were set to "full records and cited references." The three downloaded text files were imported into the CiteSpace analysis software to perform taxonomy and visual analysis of the research literature.

Research method

To present the research hot spot and development trend of this subject intuitively, objectively, quantitatively, and authentically, we used bibliometrics theory and CiteSpace 5.8.R3 as research tools. As proposed by Allen Pritchard in 1969, bibliometrics is defined as "the assembling and interpretation of statistics relating to books and periodicals … to demonstrate historical movements, to determine the national or universal research use of books and journals, and to ascertain in many local situations the general use of books and journals" and is commonly used to analyze published literature and organize knowledge (Pritchard, 1969; Khalil and Crawford, 2015). CiteSpace is an excellent scientific mapping tool based on bibliometrics, and it was developed by Dr. Chaomei Chen, a tenured professor at Drexel University (Chen, 2006). It provides researchers with a powerful tool for the analysis of historical literature and creating a summary of the characteristics of the discipline through time-sharing and dynamic citation analysis visualization techniques (Chen et al., 2015). CiteSpace allows the identification of emerging trends while reducing our reliance on

domain experts or prior knowledge base. This approach makes the analysis repeatable with new data and can be validated by different analysts. The evolution of the research field can be shown centrally on citation network maps. Based on the citation nodes and co-citation clusters on the map, the research frontiers and hot spots in the field can be analyzed.

Results

Analysis of publication quantity

There is a positive correlation between the research heat and the number of articles published. Comparing the number of publications per year is an easy way to get an idea of how hot a particular research area is. Based on the search results, annual trends in *A. japonicus* research publications from 2000 to 2021 are presented, as shown in Figure 1. In this period, studies on *A. japonicus* have increased rapidly. We divided the development of *A. japonicus* research into three stages. Prior to 2009, the research was at a preliminary stage, in which fewer than 20 articles were published per year. The range of studies is relatively narrow. During this period, researchers focused primarily on growth performance and immune response, accounting for 20.22% and 24.72% of 93 papers, respectively. Common keywords include temperature, salinity, oxygen consumption, arginine kinase, and microsatellite. During the development period from 2009 to 2016, *A. japonicus* research rapidly became a research hot spot with an average annual growth rate of 22.91%. The research direction of this period has the characteristics of diversification and refinement. It has been in a stable phase since 2017, in which the number of *A. japonicus*-related publications exceeded 130. The rapid rise in the number of publications signifies that *A. japonicus* is becoming an increasingly important vector for scientific research.

Analysis of the research teams

Research teams led by high-yielding writers are the main force behind scientific work (Wuchty et al., 2007). The core team and highly productive group of authors for the *A. japonicus* study were therefore identified as being necessary. Table 1 lists the top 10 authors in the field of *A. japonicus*. According to Price's law of bibliometrics, which states that "On the same topic, half of all articles are written by highly effective authors" (Wei et al., 2020), we set N_{max} as the number of publications of the most productive authors and (1, N_{max}) is the total number of publications. The mathematical expression is as follows:

$$\frac{1}{2}(1,\ N_{max}) = x(m, N_{max}) = x(1, m) \tag{1}$$

where m is a positive integer set by Price, and the total number of articles published by author groups with publications greater than m is approximately half of all articles (Price et al., 1984). The formula can be derived by further calculation as follows:

$$m \approx 0.749 \times \sqrt{N_{max}} \tag{2}$$

The positive integer m is approximately 9 when N_{max}=$N_{Y,HS}$=123 . In other words, authors who have published nine or more papers in the field of *A. japonicus* can be considered highly productive, with a total of 134 authors, or only 4.43% of the total number of authors. Therefore, a stable core group of authors has not been formed in the field of *A. japonicus* research, and the concentration of authors is low. Every year, a large number of talents are absorbed into the field of *A. japonicus*. As shown in Table 1, the authors in the field of *A. japonicus* are mainly distributed in the Institute of Oceanology, Chinese Academy of Sciences (IOCAS), Ningbo University (NBU), and Ocean University of China (OUC). Team Hongsheng Yang from

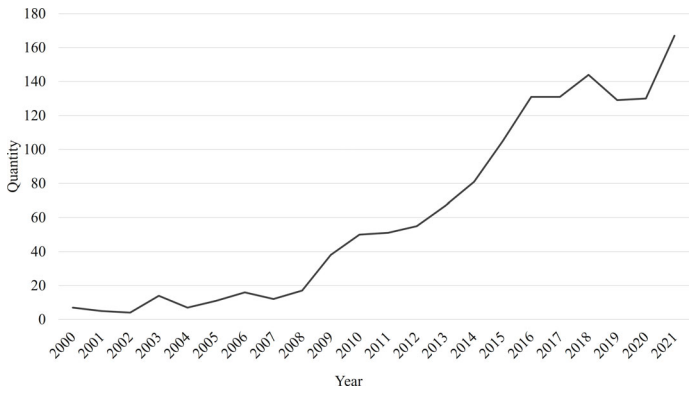

FIGURE 1
Trends of publications on *Apostichopus japonicus*-related research from 2000 to 2021.

TABLE 1 Top 10 authors in the field of *Apostichopus japonicus* from 2000 to 2021.

Ranking	Author	Count
1	Yang, Hongsheng (IOCAS)	123
2	Li, Chenghua (NBU)	113
3	Dong, Shuanglin (OUC)	86
4	Zhang, Weiwei (NBU)	82
5	Zhang, Libin (IOCAS)	80
6	Shao, Yina (NBU)	67
7	Liu, Shilin (IOCAS)	61
8	Chang, Yaqing (Dalian Ocean University)	59
9	Sun, Lina (IOCAS)	58
10	Gao, Qinfeng (OUC)	52

IOCAS, Institute of Oceanology, Chinese Academy of Sciences; NBU, Ningbo University; OUC, Ocean University of China.

IOCAS, Team Chenghua Li from NBU, and Team Shuanglin Dong from OUC are top teams in the field of *A. japonicus*. Identifying the central research team allows us then to have a timeline of the development of each research direction through its articles.

Analysis of source countries

The country-level analysis also deserves our consideration. The count of independent studies and the frequency of inter-country cooperation can reflect the status and problems of *A. japonicus* research. An analysis of the main source countries for the *A. japonicus* study is presented in Table 2. China contributed 1,026 articles, accounting for 75.55% of the total number of articles on *A. japonicus*, followed by Japan with 113 published articles (8.32%). Notably, Japan is not only a pioneer in research

TABLE 2 List of five main source countries of *Apostichopus japonicus* research papers from 2000 to 2021.

Ranking	Country	Count	Percentage
1	China	1,026	75.55%
2	Japan	113	8.32%
3	USA	74	5.45%
4	South Korea	73	5.38%
5	Russia	54	3.98%

but also the type locality of *A. japonicus* (Liao, 1997). Graphs indicating international comparisons of *A. japonicus* literature numbers and cooperative relationships were plotted (Figure 2). A total of 58 countries worldwide have been involved in *A. japonicus* research. However, only 115 international collaborations in the form of literature have been recorded, which is only 8.47% of the total literature. These data indicate that there is a huge scope for international collaboration in *A. japonicus* research.

Analysis of participating journals

The Journal Citation Reports (JCR) Quartile and Impact Factor (IF) of journals often represent the quality of the research output (Law and Leung, 2020). The top 10 journals published in the field of *A. japonicus* are listed in Table 3 based on the database and comparison with the JCR 2020. More than 297 academic journals have published articles on *A. japonicus* research. *Fish and Shellfish Immunology* (Q1; IF2020, 4.581) published the most articles on the study of *A. japonicus* (119 articles, 8.76%), followed by *Aquaculture* (Q1; IF2020, 4.242; 113

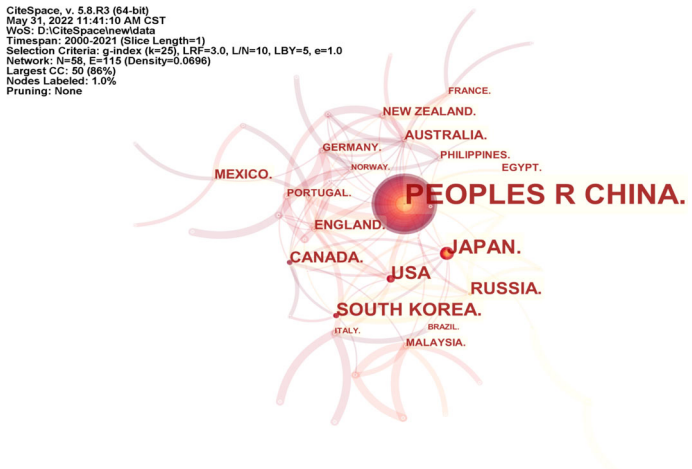

FIGURE 2
The map representing the international comparison of the number of *Apostichopus japonicus* literature and cooperative relationships.

TABLE 3 The most active journals with publication volume on *Apostichopus japonicus* search from 2000 to 2021.

Ranking	Journal abbreviation	Country	Count	JIF quartile	IF2020
1	*Fish Shellfish Immunol.*	England	119	Q1	4.581
2	*Aquaculture*	Netherlands	113	Q1	4.242
3	*Aquac. Res.*	England	98	Q2	2.082
4	*J. Oceanol. Limnol.*	China	40	Q4	1.265
5	*J. Ocean Univ. China*	China	31	Q4	0.913
6	*Dev. Comp. Immunol.*	England	30	Q1	3.636
7	*Fish. Sci.*	Japan	29	Q3	1.617
8	*Comp. Biochem. Physiol., Part D: Genomics Proteomics*	USA	28	Q3	2.674
9	*Food Chem.*	England	28	Q1	7.514
10	*Aquac. Int.*	Netherlands	27	Q2	2.235

articles, 8.32%) and *Aquaculture Research* (Q2; IF2020, 2.082; 98 articles, 7.22%). Notably, in 2019, JCR imposed a short penalty on the Q1 regional journal *Fish and Shellfish Immunology* for self-citing rate issues. As a result, the level of publications and research in the area of *A. japonicus* has declined in the short term. In comparison with other journals, articles on *A. japonicus* were more likely to be accepted by these active journals.

Analysis of the influence of the literature

Highly cited articles in the field represent the existence of more interest and affirmation by practitioners in the current state of research in a particular direction. We counted the papers published in the field of *A. japonicus* in the past 21 years. The 10 most influential academic papers were selected based on the number of citations as of 1 April 2022 (Table 4). The research directions of these 10 papers were briefly classified, and the general research directions were sea cucumber bioactive, fucosylated chondroitin sulfates (FCSs), diseases, growth performance, probiotics, aestivation, body wall collagen, and transcriptome sequencing.

Analysis of research directions

In the analysis of research directions, *A. japonicus* research is more focused on biology, marine science, and aquaculture. Based on the Web of Science subject classification method, the related literature of *A. japonicus* was classified (Table 5). Nearly 97% of these studies involved life sciences and biomedical research, with almost no research related to industry or

TABLE 4 The 10 most influential papers in the field of *Apostichopus japonicus* from 2000 to 2021.

Author	Title	Frequency	Year
Bordbar, Sara; Anwar, Farooq; Saari, Nazamid	High-value components and bioactives from sea cucumbers for functional foods-a review	404	2011
Duarte, MER; Cardoso, MA; Noseda, MD; Cerezo, AS	Structural studies on fucoidans from the brown seaweed *Sargassum stenophyllum*	234	2001
Chen, Shiguo; Xue, Changhu; Yin, Li'ang; et al.	Comparison of structures and anticoagulant activities of fucosylated chondroitin sulfates from different sea cucumbers	213	2011
Deng, Huan; He, Chongbo; Zhou, Zunchun; et al.	Isolation and pathogenicity of pathogens from skin ulceration disease and viscera ejection syndrome of the sea cucumber *Apostichopus japonicuss*	195	2009
Dong, YW; Dong, SL; Tian, XL; Wang, F; Zhang, MZ	Effects of diel temperature fluctuations on growth, oxygen consumption and proximate body composition in the sea cucumber *Apostichopus japonicus* Selenka	165	2006
Zhang, Qin; Ma, Hongming; Mai, Kangsen; et al.	Interaction of dietary *Bacillus subtilis* and fructooligosaccharide on the growth performance, non-specific immunity of sea cucumber, *Apostichopus japonicus*	161	2010
Yang, HS; Yuan, XT; Zhou, Y; Mao, YZ; Zhang, T; Liu, Y	Effects of body size and water temperature on food consumption and growth in the sea cucumber *Apostichopus japonicus* (Selenka) with special reference to aestivation	178	2005
Zhao, Yancui; Zhang, Wenbing; Xu, Wei; et al.	Effects of potential probiotic *Bacillus subtilis* T13 on growth, immunity and disease resistance against *Vibrio splendidus* infection in juvenile sea cucumber *Apostichopus japonicus*	151	2012
Saito, M; Kunisaki, N; Urano, N; Kimura, S	Collagen as the major edible component of sea cucumber (*Stichopus japonicus*)	153	2002
Du, Huixia; Bao, Zhenmin; Hou, Rui; Wang, Shan; et al.	Transcriptome sequencing and characterization for the sea cucumber *Apostichopus japonicus* (Selenka, 1867)	132	2012

TABLE 5 Classification of the main research areas of *Apostichopus japonicus* based on the subject classification method of Web of Science (WoS) from 2000 to 2021.

Ranking	Research areas	Count	Proportion
1	Fisheries	512	37.70%
2	Marine Freshwater Biology	339	24.96%
3	Immunology	179	13.18%
4	Food Science Technology	175	12.89%
5	Biochemistry Molecular Biology	166	12.22%

economy. It will be helpful for us to follow up on the subdivision of the research direction of *A. japonicus* and no longer consider the research on industrial economy, history and culture, and diet.

Analysis of main keywords

In the keyword set of a large number of professional papers in the same discipline, hidden clues can be found about the current status of research, research hot spots, and development trends (Yin et al., 2009). Therefore, quantitative and visual analysis of keywords in *A. japonicus* research literature is helpful in mining knowledge in this field.

The term frequency–inverse document frequency weighted algorithm was used to calculate the importance of a keyword in a set of all keywords, highlighting key nodes and important connections, and form keyword clusters (Chen et al., 2015). The bibliography was imported into CiteSpace software, and synonym merging and keyword nonsense deletion were performed to achieve a symbiotic map of 682 keywords consisting of nodes and 1,393 links (Figure 3). One of the nodes represents a keyword. The larger the circle of nodes, the more frequently the keyword is cited, and the more frequently it can be considered a research hot spot in the *A. japonicus* field. As shown in Figure 3, the largest keyword node is *A. japonicus*, while the other nodes are more widely distributed mainly along the three branches of the distribution. In combination with the keyword frequency ranking data (Table 6), *A. japonicus* hot spots can be identified. The main keywords that appear in three directions are growth, protein, body wall, immune response, temperature, gene expression, and purification.

Clustering graphs can accurately reflect the knowledge structure of different research directions (Rodriguez and Laio, 2014). We used the logarithmic likelihood ratio algorithm for keyword clustering. This algorithm can accurately reflect the contribution of low-frequency keywords to clustering and overcome the inaccuracy of the classical feature vector selection algorithm in low-frequency word estimation (Lin and Tang, 2009). By adjusting the contrast of the color blocks, a keyword network clustering map was formed (Figure 4). The hot spots in *A. japonicus* research over the past two decades can be briefly classified into the following categories: 1) growth, including keywords such as temperature, energy budget, and organic matter; 2) FCS, including body wall, *in vitro*, and glycosaminoglycan; 3) *Apostichopus japonicus*, including

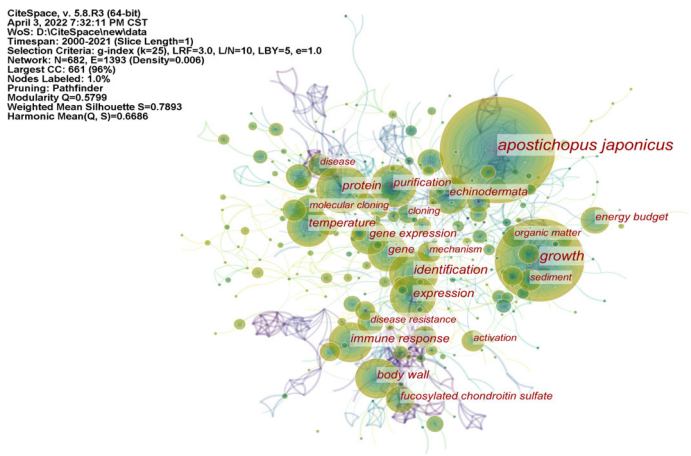

FIGURE 3
The map of keyword co-occurrence in articles related to the research of *Apostichopus japonicus* published from 2000 to 2021.

TABLE 6 The 20 most frequently used keywords in articles related to *Apostichopus japonicus* research published from 2000 to 2021.

Ranking	Keyword	Frequency	Centrality	Ranking	Keyword	Frequency	Centrality
1	*Apostichopus japonicus*	502	0.08	11	purification	74	0.11
2	growth	224	0.03	12	gene	72	0.04
3	identification	124	0.05	13	energy budget	53	0.04
4	protein	104	0.07	14	fucosylated chondroitin sulfate	53	0.05
5	expression	93	0.09	15	mechanism	44	0.05
6	body wall	89	0.1	16	cloning	43	0.07
7	immune response	88	0.01	17	activation	41	0.05
8	temperature	79	0.06	18	disease	41	0.02
9	gene expression	75	0.02	19	disease resistance	40	0.01
10	Echinodermata	74	0.13	20	sediment	40	0.03

identification, protein, expression, and gene; 4) arginine kinase, including purification, mechanism, binding, phosphagen kinase, and inactivation; 5) *Vibrio splendidus*, including collagen, bacteria, triterpene glycoside, and resistance; 6) sea cucumber, including anticoagulant activity, NF-kappa B (NF-κB), peptide, and fucoidan. Some clusters generated by software analysis do not cover the entire content of the knowledge structure, and these clusters need to be properly integrated or renamed.

In terms of keyword emergence time, CiteSpace uses Kleinberg's burst word monitoring algorithm, which is based on the vending machine model, to model keyword frequency over different periods (Kleinberg, 2003). The duration of the main keyword emergence varies, as shown in Figure 5. The emergence lasted from 2000 to 2010 for brown algae, 2003 to 2011 for arginine kinase, 2010 to 2015 for consumption, 2015 to 2017 for NF-κB, and 2018 to the present for identification. These keywords have strong intensity and long duration and are all important in any research period. Recently emerging keywords included gut microbiota, activation, and collagen, which may be the main direction and technical methods of current or future research.

Conclusion

As a condensation of literature knowledge, keywords deserve to be further classified and studied. The results of the software analysis can provide us with some assistance and evidence, but they do not fully represent the actual research status. Therefore, it is necessary to integrate all of the analyses and own experience to reach a final conclusion. Based on the network clustering map of keywords in Figure 4, the research direction in the *A. japonicus* domain was gradually clarified after integrating the citation frequency (Figure 3 and Table 6), occurrence time, and intensity (Figure 5) of keywords and the progress of large research teams. It was divided into six departments: genetics and breeding, growth

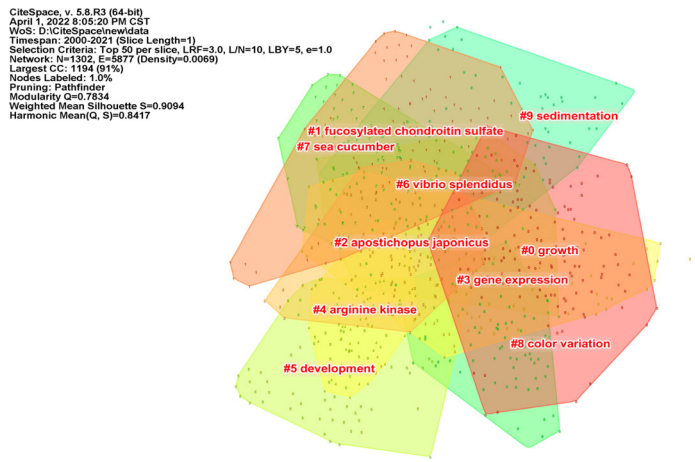

FIGURE 4
A network clustering map of keywords in the field of *Apostichopus japonicus* from 2000 to 2021.

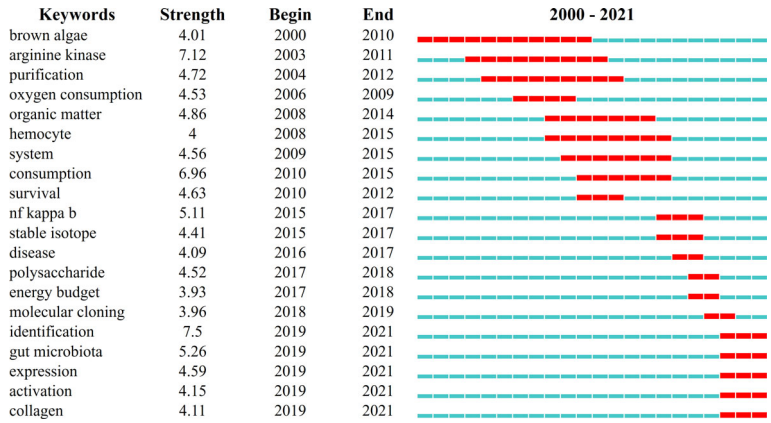

FIGURE 5
The emergence map of the top 20 keywords in the field of *Apostichopus japonicus* from 2000 to 2021.

and development, immunology and disease, aestivation, regeneration, and food processing.

Research on the genetics and breeding of *Apostichopus japonicus*

High-quality seedlings are important for the survival and development of the aquaculture industry. Research into the genetics and breeding of *A. japonicus* should also be the most concerning work in the *A. japonicus* industry. Genetics and breeding include but are not limited to genetic marker development, genetic linkage map construction, and genetic mechanism analysis of economic traits. 1) Studies on the genetic marker development of *A. japonicus*. The molecular genetics of *A. japonicus* concentrates on the development of microsatellite markers and single-nucleotide polymorphisms (SNPs). Microsatellite labeling technology is used for sifting through microsatellite locations and detecting them after PCR amplification. Kanno et al. (2005) have used magnetic bead enrichment methods by hybridization to develop 20 polymorphic microsatellite markers for sea cucumbers, which will be helpful for further research on the genetic structure and reproductive isolation of sea cucumbers. SNPs are the most common type of genetic variation among people. Each SNP represents a difference in a single DNA building block, called a nucleotide (National Library of Medicine, 2022). Based on the assembly transcriptome, Zhou et al. (2014) identified 142,511 high-quality SNPs. Attempts were made by Kang et al. (2011) to identify SNPs and to analyze differences associated with SNP genotypes between green and red color variants using heat shock protein (HSP)70 as the target gene. 2) Studies on the genetic linkage map construction of *A. japonicus*. Most of our earlier knowledge on echinoderm genomics came from the sea urchin *Strongylocentrotus purpuratus* and sea star *Acanthaster planci*; the need for the complete genome of *A. japonicus* is becoming increasingly urgent. The whole genome of *A. japonicus* released by team Hongsheng Yang in 2017 is a more complete one in recent years (Zhang X. J. et al., 2017). Li et al. (2018b) then updated the whole-genome landscape, perfecting the development of the whole genome of *A. japonicus*. 3) Studies on the genetic mechanism analysis of economic traits of *A. japonicus*. Growth rate, body wall thickness and flesh yield, and stress resistance are the most important economic traits of *A. japonicus*. Chen et al. (2020) tried to identify and screen potential molecular markers associated with the quantitative traits of "Anyuan No. 1" by miRNA-mRNA integrated analysis for future selective breeding and new seed creation in sea cucumbers. "Anyuan No. 1" is exactly the new generation breed of the Chinese, with weight, number of parapodium, and dressing-out percentage as the main target traits. The stress resistance includes indicators of a low-salt tolerance, high-temperature tolerance, and antibacterial infection. Song et al. (2012) compared the growth traits of different pedigrees under low-salt environment by means of line selection, and finally, nine low salt-tolerant pedigrees were obtained. Zhao H. et al. (2014) analyzed the survival rate and HSP gene expression characteristics under high-temperature stress in the offspring of a high temperature-oriented selection population of Sargassum and preliminarily validated the heritability of heat tolerance traits in the selection population.

Research on the growth and development of *Apostichopus japonicus*

Researchers have focused on the growth performance of *A. japonicus*. The research direction of growth performance mainly includes feed formulation, temperature, salinity, and

cocultivation environment. 1) Studies on the effect of feed formulation on the growth and development of *A. japonicus*. Qin Zhang and Yancui Zhao provided evidence that the addition of probiotic *Bacillus subtilis* T13 and prebiotic fructooligosaccharides to the feed has a synergistic effect on improving immunity and disease resistance of *A. japonicus* (Zhang et al., 2010; Zhao et al., 2012). According to the specific growth rate of sea cucumber, the formula of 75% bivalve feces and 25% powdered algae was the best diet for sea cucumber culture (Yuan et al., 2006). 2) Studies on the effect of temperature and salinity on the growth performance of *A. japonicus*. Dong et al. (2006) studied the effects of constant or variable temperature on the growth, proximate body composition, and oxygen consumption of juvenile sea cucumbers. Moreover, the appropriate temperature for *A. japonicus* growth is between 12°C and 21°C, the optimum temperature is 16°C–18°C, and the diel fluctuating temperature model promotes the growth of juvenile sea cucumbers and can be applied to the large-scale culture of *A. japonicus*. A temperature range of 21°C–24°C and a salinity of 30 are considered optimal for the early development of the red *A. japonicus* (Li and Li, 2010). 3) Studies on the effect of coculture environment on the growth performance of *A. japonicus*. The coculture of juvenile charm abalone *Haliotis discus hannai* and sea cucumber can reduce the content of inorganic nitrogen in water and promote synergistic growth (Kang et al., 2003). It can be used as an alternative culture method during the overwintering period of abalone farms.

Research on the immunology and disease of *Apostichopus japonicus*

The immunological research of *A. japonicus* mainly covers the epidemiology of pathogenic microorganisms, immunology and pathology of aquatic organisms, aquatic disease prevention, and control technology. 1) Pathogenic microorganism epidemiology mainly studies the epidemiological characteristics of diseases of farmed species, clarifies the regulatory effect of key environmental factors on pathogenic infection, reveals the molecular mechanism of epidemic outbreak and epidemic, and provides an analysis of the pathogenic principle of the main pathogens and the immune escape mechanism of the pathogens in the host. *V. splendidus* is the main causative agent of skin ulceration syndrome (SUS), which is the most common and serious disease in sea cucumber culture (Zhang et al., 2014). In the early stage of SUS, *A. japonicus* has the phenomenon of shaking its head, slow response, swelling of the mouth cannot be contracted; in the middle stage, the body of *A. japonicus* shrinks, the flesh spines turn white, small ulcers appear on the epidermis, and drainage of dirt; in the end stage, the epidermis ulcerates widely until death and autolysis (Li et al., 2013; Yang et al., 2016). The main causative factors identified at present of *V. splendidus* include adhesion molecules, iron absorption systems, and some extracellular products with toxicity (Zhang et al., 2016). Adhesion molecules in charge of contacting and binding to receptors include flagella, lipopolysaccharide, and outer membrane proteins (Dai et al., 2022). To cover the iron requirements for growth and reproduction, iron absorption systems have developed, including iron carriers and ferritin (Huang B. W. et al., 2021). Extracellular products can help defend the host immune killings, such as extracellular proteases and hemolysins (Binesse et al., 2008). 2) Immunology and pathology of aquatic organisms provide information about the changes in morphological structure, function, and metabolism of immune organs and immune cells in response to pathogenic microbial infection, revealing the occurrence and development of diseases. The immune system of *A. japonicus* in response to *V. splendidus* infection mainly consists of coelomocytes, immune factors, and gut microbiota. The defense means adopted by the coelomocytes when facing the invasion of pathogenic microorganisms are abundant, including chemotaxis (damaged cells release information to attract a large number of inflammatory cells, triggering inflammation) (Lv et al., 2022) and programmed cell death (apoptosis, autophagy, and pyroptosis may exist in *A. japonicus*) (Shao et al., 2016; Shao et al., 2019; Shao et al., 2020). The immune factors in *A. japonicus* mainly include Toll-like receptor (Sun H. J. et al., 2013), myeloid differentiation factor (Lv et al., 2019), interleukin-1 receptor-associated kinase (IRAK)-1 and IRAK-4 (Lu et al., 2015; Cui et al., 2018), NF-κB subunit (Wang et al., 2013), and signal transduction and activator of transcription-5 (Shao et al., 2015). Research on gut microbiota has been a hot topic in recent years, and we have mentioned above that the timing of their heat emergence may continue. Gut microbiota forms a biological barrier that restricts pathogen colonization in the intestine and enhances the original nonspecific immune function of *A. japonicus* (Li et al., 2012; Chi et al., 2014). *A. japonicus* gut microbiota provides a timely and accurate response to the occurrence of disease, which is directly reflected in the change of flora structure after the disease (Zhang Z. et al., 2018; Zhang et al., 2019). 3) Aquatic disease prevention and control technology aim to solve the root cause of disease problems in aquaculture, which requires the full management of all aspects such as disease-resistant seedlings, immune enhancers, symptomatic medication, and daily monitoring of the water environment (Li, 2021). "Anyuan No. 1" and "Shenyou No. 1" are new *A. japonicus* breeds with better economic performance and disease resistance that have been cultivated in China in recent years, and the development of new breeds can effectively improve breeding efficiency (Chen et al., 2020; Wang Z. P. et al., 2021). Immune enhancers improve nonspecific immunity and suppress invading pathogens in cultured animals to improve survival and growth rates. Numerous known substances can be used as immune

enhancers for *A. japonicus*, mainly classified as Chinese herbal preparations (Sun et al., 2015), polysaccharides (Gu et al., 2011), and probiotics (Zhao et al., 2012). The overuse of antibiotics in animal farming is costly and undesirable and has threatened the human living environment (Harikrishnan et al., 2011). The use of antibiotic alternatives for pathogen suppression is imperative, such as the use of antivirulence biologics (Zhang S. S. et al., 2017), phages (Katharios et al., 2017), and probiotics.

Research on the aestivation of *Apostichopus japonicus*

Aestivation of *A. japonicus* has also been widely studied. Metabolic rate depression is a very common mechanism for animals to escape from environmental stress (Brooks and Storey, 1997). For *A. japonicus*, the temperature is the principal environmental factor that determines its growth rate (Yang et al., 2005). Moreover, aestivation is the main strategy for *A. japonicus* to reduce its metabolic rate to resist high temperatures (Du et al., 2013). Studies on aestivation in *A. japonicus* have focused on histomorphology, physiobiology, and molecular biology (Yuan et al., 2007). 1) Studies on the histomorphology of *A. japonicus* during aestivation. According to the changes in the gut and respiratory trees of *A. japonicus*, the aestivation process can be roughly divided into four stages: active period, aestivation period, deep aestivation period, and recovery period (Cheo, 1963). The most obvious physiological manifestation of *A. japonicus* during aestivation is the cessation of feeding and activity (Chen et al., 2016), which causes degradation of the digestive system (Gao et al., 2009) and negative body mass growth to maintain minimum metabolic requirements (Zhao Y. et al., 2014). Wang et al. (2007) showed that the ratio of the digestive tract length to body length was only 0.8–1.1 during the aestivation from August to October, while the ratio was 2.7–5.9 for the normal growth period from January to May. Gao (2008) reported that the relative digestive mass of the intestine during aestivation was only 8.2%–35.8% of the annual maximum. Therefore, shortening the aestivation period can effectively improve the benefits of the cultivation process. 2) Studies on the physiobiology of *A. japonicus* during aestivation. Depending on the daily food intake of individuals, Yang et al. (2005) reported that the starting temperature at which medium and large *A. japonicus* (72.3–139.3 g) entered aestivation was 24.5°C–25.5°C and that of the small individual (28.9–40.7 g) was 25.5°C–30.5°C. They continued to determine the effect of water temperature on oxygen consumption rate (OCR) and ammonia-N excretion rate (AER) of aestivated *A. japonicus* using the Winkler and Hypobromite methods. Both OCR and AER of mature (large, 148.5 ± 15.4 g; medium, 69.3 ± 6.9 g) individuals peaked at 20.8° C, while the OCR of immature (small, 21.2 ± 4.7 g) individuals continued to increase with temperature and even beyond the aestivation temperature, while their AER peaked at 25.8°C (Yang et al., 2006). The results of previous studies have shown that both coelomocytes and immune enzymes of *A. japonicus* underwent significant changes during aestivation (Wang et al., 2008). Liu et al. (2016a) reported a significant effect of temperature on both immuno-enzyme activities [Superoxide dismutase, catalase, total antioxidant capacity (T-AOC)] and metabolic enzyme activities (pyruvate kinase (PK), hexokinase, malate dehydrogenase, lactate dehydrogenase (LDH)) in the non-aestivating group of *A. japonicus*, while the effects on T-AOC, PK, and LDH activities in the aestivating group were not significant. 3) Studies on the molecular biology of *A. japonicus* aestivation. At present, the molecular biology research on aestivation is still in its infancy, and the research content is mostly distributed in a dot-like distribution without systematization. Li et al.(2018b) reported that transcriptional factors Klf2 and Egr1 were identified as key regulators of aestivation, probably exerting their effects through a clock gene-controlled process. Yang (2017) investigated the changing pattern of *A. japonicus* 5-hydroxytryptamine (5-HT) receptor (Aj5-HTR) in the aestivation cycle and its function in metabolic regulation and, based on the results, elucidated the relationship between 5-HT and its receptor 5-HTR and the existence of metabolic regulation of aestivation in *A. japonicus*. Chen and Storey (2014) used high-throughput sequencing technology to detect and analyze the miRNA expression patterns in the intestine and respiratory tree before and after aestivation and screened out the differentially expressed miRNAs. They found that miR-124, miR-124-3p, miR-79, miR-9, and miR-2010 were significantly overexpressed during deep aestivation, and these miRNAs may play an important role in inhibiting the metabolic rate of *A. japonicus* during aestivation (Chen et al., 2013. In the follow-up study, they used tandem mass tag labeling followed by an immobilized metal-chelate affinity chromatography enrichment method to map aestivation sponsive changes in the *A. japonicus* intestinal phosphoproteome (Chen et al., 2016). The current research, including the above parts, has not clarified the molecular regulation mechanism of *A. japonicus* aestivation, which needs to be further broadened and deepened.

Research on the regeneration of *Apostichopus japonicus*

A growing number of scientists are attempting to demystify the organ regeneration process in invertebrates and lower vertebrates and determine whether the methods that trigger such regeneration can be applied to vertebrates (Tanaka and Reddien, 2011; Marques et al., 2019). The echinoderms to which sea cucumbers belong are grouped in the Duteromata evolutionary branch of animals and are therefore closely related to vertebrates in terms of phylogeny. Adult sea cucumbers are a useful model for organ regeneration (Garcia-Arraras et al., 2019). Current research on the regeneration of *A.*

japonicus is mainly focused on digestive tract regeneration (Garcia-Arraras and Greenberg, 2001), and a few of them involve coelomocyte and longitudinal muscle band (LMB) regeneration. 1) Studies on digestive tract regeneration in *A. japonicus*. The regeneration process of the digestive tract can be divided into the rudiment formation stage, intestinal lumen formation stage, differentiation stage, and growth stage (Nie and Li, 2006). Only the calcareous ring and the stump of the pharynx-esophagus and cloaca remained in the body cavity after gutting, and two rudiments are formed by the stump of the pharynx-esophagus and cloaca in the anterior and posterior parts of the body, respectively. They grow along the free edge of the thickened mesentery toward the middle of the body, penetrate the mesenchyme, and form a fine digestive tract (Leibson, 1992). The thickened mesentery allows *A. japonicus* to regenerate the missing part of the intestine between the two ends much faster in order to feed earlier (Mashanov and Garcia-Arraras, 2011). Garcia-Arraras et al. (1998) described the spatial and temporal patterns of cellular events that occur during intestinal regeneration after chemically induced evisceration. It is also essential to investigate the molecular mechanism of the digestive tract regeneration in *A. japonicus*. The first signs of somatic epithelial cell activation on the molecular level were detected as early as 24 h after organ culling, with increased the transcription of genes involved in transcription, translation, and protein transport (Quispe-Parra et al., 2021). Data obtained by metabolomic analysis showed that the accumulation of nutrients in the residual esophageal tissue occurred after 3 days post-evisceration (dpe) (Sun et al., 2017a). The accumulation of energy reserves and their further utilization during regeneration are regulated by deacetylation (Sun et al., 2018). The expression of Hox1 and Hox3 was recorded as increased during this period, which proves that the formation site of the anterior part of the intestine is determined (Sun et al., 2017b). While *Hox*9/10 started to be expressed after 7 dpe, the site of formation of the posterior part of the intestine was marked (Sun et al., 2013b). Yuan et al. (2019) reported that the Wnt signaling pathway is the only pathway under positive selection in regenerating echinoderms and the only pathway enriched by differentially expressed genes during intestinal regenerating. An increase in the number of Wnt4 and Wnt6 transcripts was recorded after 7 dpe (Sun et al., 2013a). At 14–21 dpe, the main feature of this phase is the redifferentiation of enterocytes. Expression of *Hox*9/10 and *Hox*11/13 continued to increase, and marking of the anterior–posterior axis continues. The main processes occurring in *A. japonicus* during intestinal tube formation are extracellular matrix (ECM) remodeling, cell dedifferentiation, cell migration, cell proliferation, and apoptosis (Dolmatov, 2021). Two matrix metalloproteinase (MMP) genes, *MMP-2* and *MMP-16*, may regulate the interaction between ECM components and growth factors by performing targeted proteolysis of ECM proteins and other biomolecules (Miao et al., 2017). The regeneration process requires a regulation between cell proliferation and cell death. Apoptotic cells greatly influence the behavior of the surrounding cells through phagocytosis and proliferation, as well as by activating the Wnt signaling (Kawamoto et al., 2016). The Wnt signaling pathway was activated during intestinal regeneration in sea cucumbers. The expression of Wnt7 and Wnt8 peaked after 1–3 dpe, while the number of Wnt6 transcripts was highest at 7 dpe and was maintained for a long time (Sun et al., 2013). 2) Studies on coelomocyte and LMB regeneration in *A. japonicus*. *A. japonicus* required depletion and regeneration of coelomocytes for effective innate immune mechanisms (Smith et al., 2010; Li et al., 2019). Available studies have shown that coelomic fluid and coelomocyte regenerate rapidly after the removal of viscera from sea cucumbers, returning to normal levels after 2 and 6 h, respectively (Li et al., 2018; Shi et al., 2020). Dolmatov et al. (1996) demonstrated that new muscle bundles were derived from coelomic epithelial cells covering LMBs. The migration of coelomic epithelial cells to damaged LMBs and their myogenic transformation are the basic mechanisms of muscle regeneration. Ginanova (2007) reported that the coelomic epithelium of the body wall and the coelomic epithelium of the muscle of *A. japonicus* are involved in the regeneration of muscle tissue at the same time and have an important role in the recruitment of myogenic cell pools. The work by Qin et al. (2015) illustrates that the S7 subunit of the 19S gene or the S7-based assembled 26S proteasome may be involved in the regulation of cell migration and cell cycle during the regeneration of the *A. japonicus* body wall.

Research on the food processing of *Apostichopus japonicus*

Sea cucumber is delicious and nutritious. They are highly edible and have medicinal value. The medical value of sea cucumbers still has enormous scope for development and is not yet widespread. As an important part of the entire industrial chain of sea cucumbers, food engineering is also a hot spot in the field of *A. japonicus* research. Sea cucumber derivatives have many types, including polysaccharides, saponins, sea cucumber bioactive peptides, and many other biologically active compounds. At first, sea cucumber polysaccharides extracted from the body wall of sea cucumbers are unique to sea cucumber species, which are composed mainly of holothurian glycosaminoglycan and holothurian fucan (Jin et al., 2019). Current research is mainly focused on anticoagulation, antitumor, antiviral, and other directions (Pomin, 2014). 1) Study on the anticoagulation mechanism of sea cucumber polysaccharides. FCSs have stronger anticoagulant activity than sulfated fucan (Chen et al., 2011; Luo et al., 2013). The difference in the anticoagulant properties of FCSs is mainly attributed to their different sulfation patterns. 2) Study on the antitumor effect of sea

cucumber polysaccharides. Low-molecular-weight FCSs could significantly inhibit the growth and metastasis of Lewis lung carcinoma in mice in a dose-dependent manner (Liu X. X. et al., 2016). *A. japonicus* acid mucopolysaccharide (AJAMP) has an effective inhibitory effect on experimental hepatocellular carcinoma in rats, and the antitumor mechanism of AJAMP can protect immune organs, promote the proliferation of immune organs and tissues, and enhance cellular immunity (Song et al., 2013). 3) Study on the antiviral activity of sea cucumber polysaccharides. Through screening, the Academician of the Chinese Academy of Engineering Zhu Beiwei obtained three polysaccharides, namely, sea cucumber sulfated polysaccharide, fucoidan from brown algae, and iota-carrageenan from red algae, which have significant antiviral activities. The three antiviral polysaccharides could be employed for the treatment and prevention of coronavirus disease 2019 (COVID-19) (Song et al., 2020). Secondly, as the most important and abundant secondary metabolites in sea cucumbers, the research on saponins is also one of the hot topics (Bahrami and Franco, 2015; Bahrami and Franco, 2016). Due to their numerous and positive bioactivities, sea cucumber saponins are now high-economic value natural compounds with great market potential in the fields of medicine (Aminin et al., 2015; Dai et al., 2020), healthcare (Li et al., 2020), and cosmetics (Osbourn et al., 2011). In addition, studies on bioactive peptides and other biologically active compounds of sea cucumber have shown that they have lots of functions beneficial to the human body (Zhu et al., 2012; Pangestuti and Arifin, 2018; Zhang L. Y. et al., 2018).

Discussion

This report reviews the history of *A. japonicus* research and the available scientific data from 2000 to 2021. Clearly, sea cucumbers should be considered a key component of aquaculture in terms of either economic or scientific value. We have divided the direction of *A. japonicus* research into six departments, namely, genetics and breeding, growth and development, immunology and disease, aestivation, regeneration, and food processing, which have independent and interlinked characteristics. These six research departments cover most of the problems that occurred during the production and processing of *A. japonicus*.

The five other research departments all serve the sea cucumber industry, and only the research on regeneration serves humans directly. Many tools and references can help improve the knowledge of regeneration phenomena in sea cucumbers and contribute to knowledge sharing. Biologically, regeneration is the process of displacing or restoring damaged or lost cells, tissues, organs, or even entire parts to respond resiliently to environmental fluctuations (Birbrair et al., 2013; National Institute of General Medical Sciences, 2021). Regeneration of tissues and organs depends on obtaining the cells required to form the new structure. These cells usually originate from two origins: 1) resident stem cells or 2) mature cells close to the injury site that lose their phenotype and dedifferentiate (Garcia-Arraras, 2017). Each metazoan species has the ability to regenerate and differs greatly (Carlson, 2007; Lindsay, 2010). In Echinodermata, tissue regeneration is well represented in Asteroidea, Holothuroidea, and Echinoidea to a higher degree (Carnevali et al., 1998). Among them, sea cucumbers show superb regenerative ability and can quickly regenerate various new functional internal organs when the environmental conditions are suitable, which is much greater than the ability of sea stars and sea urchins (Zhang et al., 2017). Therefore, they believe that studying the regeneration of sea cucumbers could inspire humans to find the key to initiating tissue regeneration *in vivo*. In contrast to other species, such as zebrafish (Yan and Gu, 2013; Marques et al., 2019), where various models of damage have been developed for the study, *Schmidtea mediterranea* (Lewallen and Burggren, 2022), where the metabolic cost of regeneration has been further investigated, and *Eublepharis macularius* (Austin et al., 2021), which has been found to regenerate spontaneous neurons in damaged brains, the road to regeneration research of sea cucumbers is long and difficult.

In summary, differences were observed based on the comparison of research power between regions and teams, and more extensive support is needed in regions with more developed industries or greater resource abundance. Governments or organizations are encouraged to 1) promote the development of the *A. japonicus* industry through the development or implementation of policies; 2) further participate in the whole process of research, production, and processing of *A. japonicus*; and 3) strengthen international exchange and cooperation to bring economic benefits to farmers in suitable breeding areas through technology sharing.

Author contributions

All authors contributed to the study conception and design. Material preparation, data collection and analysis were performed by JC, MG, ZL. The first draft of the manuscript was written by JC and all authors commented on previous versions of the manuscript. All authors read and approved the final manuscript.

Funding

This work was supported by Key Project from Science Technology Department of Zhejiang Province (2019R52016), National Natural Science Foundation of China (31902399), Natural Science Foundation of Zhejiang Province (LY22C190004), Ningbo Natural Science Foundation (2021J113), the Open Fund of Shandong Key Laboratory of Disease Control in

Mariculture (KF202002), and the K.C. Wong Magna Fund in Ningbo University.

Conflict of interest

The authors declare that the research was conducted in the absence of any commercial or financial relationships that could be construed as a potential conflict of interest.

Publisher's note

References

Aminin, D. L., Menchinskaya, E. S., Pisliagin, E. A., Silchenko, A. S., Avilov, S. A., and Kalinin, V. I. (2015). Anticancer activity of sea cucumber triterpene glycosides. *Mar. Drugs* 13, 1202–1223. doi: 10.3390/md13031202

Austin, L., Graham, C., and Vickaryous, M. (2021). Spontaneous neuronal regeneration following lesioning in the brain of the leopard gecko (Eublepharis macularius). *FASEB J.* 35, 1. doi: 10.1096/fasebj.2021.35.S1.04331

Bahrami, Y., and Franco, C. M. M. (2015). Structure elucidation of new acetylated saponins, lessoniosides a, b, c, d, and e, and non-acetylated saponins, lessoniosides f and G, from the viscera of the sea cucumber holothuria lessoni. *Mar. Drugs* 13, 597–617. doi: 10.3390/md13010597

Bahrami, Y., and Franco, C. M. M. (2016). Acetylated triterpene glycosides and their biological activity from holothuroidea reported in the past six decades. *Mar. Drugs* 14, 147. doi: 10.3390/md14080147

Binesse, J., Delsert, C., Saulnier, D., Champomier-Verges, M. C., Zagorec, M., Munier-Lehmann, H., et al. (2008). Metalloprotease vsm is the major determinant of toxicity for extracellular products of vibrio splendidus. *Appl. Environ. Microbiol.* 74, 7108–7117. doi: 10.1128/aem.01261-08

Birbrair, A., Zhang, T., Wang, Z. M., Messi, M. L., Enikolopov, G. N., Mintz, A., et al. (2013). Role of pericytes in skeletal muscle regeneration and fat accumulation. *Stem Cells Dev.* 22, 2298–2314. doi: 10.1089/scd.2012.0647

Bordbar, S., Anwar, F., and Saari, N. (2011). High-value components and bioactives from sea cucumbers for functional foods- a review. *Mar. Drugs* 9, 1761–1805. doi: 10.3390/md9101761

Brooks, S. P. J., and Storey, K. B. (1997). Glycolytic controls in estivation and anoxia: A comparison of metabolic arrest in land and marine molluscs. *Comp. Biochem. Physiol. A-Mol. Integr. Physiol.* 118, 1103–1114. doi: 10.1016/s0300-9629(97)00237-5

Carlson, B. M. (2007). "Chapter 1 - an introduction to regeneration," in *Principles of regenerative biology*. Ed. B. M. Carlson. (Burlington: Academic Press), 1–29.

Carnevali, M. D. C., Bonasoro, F., Patruno, M., and Thorndyke, M. C. (1998). Cellular and molecular mechanisms of arm regeneration in crinoid echinoderms: The potential of arm explants. *Dev. Genes Evol.* 208, 421–430. doi: 10.1007/s004270050199

Chang, Z. Y. (2002). Study on the mode and key points of sea cucumber culture. *China Fisheries* 06, 55.

Chen, C. M. (2006). CiteSpace II: Detecting and visualizing emerging trends and transient patterns in scientific literature. *J. Am. Soc Inf. Sci. Technol.* 57, 359–377. doi: 10.1002/asi.20317

Chen, Y., Chen, C. M., Liu, Z. Y., Hu, Z. G., and Wang, X. W. (2015). The methodological function of CiteSpace knowledge graph. *Sci. Res.* 33, 242–253. doi: 10.16192/j.cnki.1003-2053.2015.02.009

Chen, Y., Li, Y. Y., Zhan, Y. Y., Hu, W. B., Sun, J. X., Zhang, W. J., et al. (2020). Identification of molecular markers for superior quantitative traits in a novel sea cucumber strain by comparative microRNA-mRNA expression profiling. *Comp. Biochem. Physiol. Part D: Genomics Proteomics* 35, 100686. doi: 10.1016/j.cbd.2020.100686

Chen, M. Y., Li, X. K., Zhu, A. J., Storey, K. B., Sun, L. N., Gao, T. X., et al. (2016). Understanding mechanism of sea cucumber apostichopus japonicus aestivation: Insights from TMT-based proteomic study. *Comp. Biochem. Physiol. Part D: Genomics Proteomics* 19, 78–89. doi: 10.1016/j.cbd.2016.06.005

Chen, M. Y., and Storey, K. B. (2014). Large-Scale identification and comparative analysis of miRNA expression profile in the respiratory tree of the sea cucumber apostichopus japonicus during aestivation. *Mar. Genomics* 13, 39–44. doi: 10.1016/j.margen.2014.01.002

Chen, S. G., Xue, C. H., Yin, L. A., Tang, Q. J., Yu, G. L., and Chai, W. G. (2011). Comparison of structures and anticoagulant activities of fucosylated chondroitin sulfates from different sea cucumbers. *Carbohydr. Polym.* 83, 688–696. doi: 10.1016/j.carbpol.2010.08.040

Chen, M. Y., Zhang, X. M., Liu, J. N., and Storey, K. B. (2013). High-throughput sequencing reveals differential expression of miRNAs in intestine from sea cucumber during aestivation. *PLoS One* 8, e76120. doi: 10.1371/journal.pone.0076120

Cheo (1963). "Study of sea cucumber: morphology, ecology, and propagation of sea cucumber," in *Sea Cucumber research: reproduction of sea cucumbers* (Tokyo: Kaibundou publisher), 32–40.

Chi, C., Liu, J. Y., Fei, S. Z., Zhang, C., Chang, Y. Q., Liu, X. L., et al. (2014). Effect of intestinal autochthonous probiotics isolated from the gut of sea cucumber (Apostichopus japonicus) on immune response and growth of a. japonicus. *Fish Shellfish Immunol.* 38, 367–373. doi: 10.1016/j.fsi.2014.04.001

Cui, Y., Jiang, L. T., Xing, R. L., Wang, Z. D., Wang, Z. H., Shao, Y. N., et al. (2018). Cloning, expression analysis and functional characterization of an interleukin-1 receptor-associated kinase 4 from apostichopus japonicus. *Mol. Immunol.* 101, 479–487. doi: 10.1016/j.molimm.2018.08.006

Cui, G. Y., and Zhao, L. (2000). Identification of names and species of edible sea cucumbers. *Cuisine Journal of Yangzhou University* 3, 13–18.

Dai, F., Guo, M., Shao, Y. N., and Li, C. H. (2022). Vibrio splendidus flagellin c binds tropomodulin to induce p38 MAPK-mediated p53-dependent coelomocyte apoptosis in Echinodermata. *J. Biol. Chem.* 298, 102091. doi: 10.1016/j.jbc.2022.102091

Dai, Y. L., Kim, E. A., Luo, H. M., Jiang, Y. F., Oh, J. Y., Heo, S. J., et al. (2020). Characterization and anti-tumor activity of saponin-rich fractions of south Korean sea cucumbers (Apostichopus japonicus). *J. Food Sci. Technol.-Mysore* 57, 2283–2292. doi: 10.1007/s13197-020-04266-z

Dolmatov, I. Y. (2021). Molecular aspects of regeneration mechanisms in holothurians. *Genes* 12, 250. doi: 10.3390/genes12020250

Dolmatov, I. Y., Eliseikina, M. G., Bulgakov, A. A., Ginanova, T. T., Lamash, N. E., and Korchagin, V. P. (1996). Muscle regeneration in the holothurian stichopus japonicus. *Rouxs Arch. Dev. Biol.* 205, 486–493. doi: 10.1007/bf00377230

Dong, Y. W., Dong, S. L., Tian, X. L., Wang, F., and Zhang, M. Z. (2006). Effects of diel temperature fluctuations on growth, oxygen consumption and proximate body composition in the sea cucumber apostichopus japonicus selenka. *Aquaculture* 255, 514–521. doi: 10.1016/j.aquaculture.2005.12.013

Du, R. B., Zang, Y. Q., Tian, X. L., and Dong, S. L. (2013). Growth, metabolism and physiological response of the sea cucumber, apostichopus japonicus selenka during periods of inactivity. *J. Ocean Univ. China* 12, 146–154. doi: 10.1007/s11802-013-2076-1

Furukawa, N., Furukawa, Y., Yamana, Y., Kashiwao, S., Uekusa, R., and Goshima, S. (2016) 66, 39–46. Growth and survival of juvenile sea cucumbers released on artificial reefs. Hokkaido University Marine Studies Department Bulletin.

Gao, F. (2008). Seasonal variations of nutritional composition, food resources, and digestive physiology in sea cucumber apostichopus japonicus. *Doctoral thesis. Qingdao: Institute of Oceanology, Chinese Academy of Sciences.*

Gao, F., Yang, H. S., Xu, Q., Wang, F. Y., and Liu, G. B. (2009). Effect of water temperature on digestive enzyme activity and gut mass in sea cucumber apostichopus japonicus (Selenka), with special reference to aestivation. *Chin. J. Oceanol. Limnol.* 27, 714–722. doi: 10.1007/s00343-009-9202-3

Garcia-Arraras, J. E. (2017). "Dedifferentiation as a cell source for organ regeneration," in *Regenerative engineering and developmental biology*. Ed. D. Gardiner. (Florida: CRC Press), 373–394.

Garcia-Arraras, J. E., Bello, S. A., and Malavez, S. (2019). The mesentery as the epicenter for intestinal regeneration. *Semin. Cell Dev. Biol.* 92, 45–54. doi: 10.1016/j.semcdb.2018.09.001

Garcia-Arraras, J. E., Estrada-Rodgers, L., Santiago, R., Torres, I. I., Diaz-Miranda, L., and Torres-Avillan, I. (1998). Cellular mechanisms of intestine regeneration in the sea cucumber, holothuria glaberrima selenka (Holothuroidea: Echinodermata). *J. Exp. Zool.* 281, 288–304. doi: 10.1002/(sici)1097-010x(19980701)281:4<288::Aid-jez5>3.0.Co;2-k

Garcia-Arraras, J. E., and Greenberg, M. J. (2001). Visceral regeneration in holothurians. *Microsc. Res. Tech.* 55, 438–451. doi: 10.1002/jemt.1189

Ginanova, T. T. (2007). Participation of the coelomic epithelium of the body wall in muscle regeneration in apostichopus japonicus (Holothuroidea: Aspidochirota). *Russ. J. Mar. Biol.* 33, 411–416. doi: 10.1134/s1063074007060089

Gu, M., Ma, H. M., Mai, K. S., Zhang, W. B., Bai, N., and Wang, X. J. (2011). Effects of dietary beta-glucan, mannan oligosaccharide and their combinations on growth performance, immunity and resistance against vibrio splendidus of sea cucumber, apostichopus japonicus. *Fish Shellfish Immunol.* 31, 303–309. doi: 10.1016/j.fsi.2011.05.018

Harikrishnan, R., Balasundaram, C., and Heo, M. S. (2011). Impact of plant products on innate and adaptive immune system of cultured finfish and shellfish. *Aquaculture* 317, 1–15. doi: 10.1016/j.aquaculture.2011.03.039

Huang, B. W., Lv, Z. M., Li, Y. N., and Li, C. H. (2021). Identification and functional characterization of natural resistance-associated macrophage protein 2 from sea cucumber apostichopus japonicus. *Dev. Comp. Immunol.* 114, 12. doi: 10.1016/j.dci.2020.103835

Huang, X., Wang, K. R., Zou, Y. W., and Cao, X. C. (2021). Development of global soil erosion research at the watershed scale: a bibliometric analysis of the past decade. *Environ. Sci. Pollut. Res.* 28, 12232–12244. doi: 10.1007/s11356-020-11888-5

Hu, W., Li, C. H., Ye, C., Wang, J., Wei, W. W., and Deng, Y. (2019). Research progress on ecological models in the field of water eutrophication: CiteSpace analysis based on data from the ISI web of science database. *Ecol. Modell.* 410, 108779. doi: 10.1016/j.ecolmodel.2019.108779

Imai, T., Inaba, D., Sato, R., and Hatanaka, M. (1950). Artificial breeding of sea cucumbers in colorless flagellates. *Report of institute of agronomy*, (Northeastern University) 2, 269–278.

Jin, Q., Teng, Y., Hu, X. Q., and Zhang, C. H. (2019). Research progress on anti-tumor mechanism of sea cucumber polysaccharides. *Zhejiang Med.* 41, 300–303. doi: 10.12056/ j.issn.1006-2785.2019.41.3.2018-2412

Kang, K. H., Kwon, J. Y., and Kim, Y. M. (2003). A beneficial coculture: charm abalone haliotis discus hannai and sea cucumber stichopus japonicus. *Aquaculture* 216, 87–93. doi: 10.1016/s0044-8486(02)00203-x

Kang, J. H., Yu, K. H., Park, J. Y., An, C. M., Jun, J. C., and Lee, S. J. (2011). Allele-specific PCR genotyping of the HSP70 gene polymorphism discriminating the green and red color variants sea cucumber (Apostichopus japonicus). *J. Genet. Genomics* 38, 351–355. doi: 10.1016/j.jgg.2011.06.002

Kanno, M., Li, Q., and Kijima, A. (2005). Isolation and characterization of twenty microsatellite loci in Japanese sea cucumber (Stichopus japonicus). *Mar. Biotechnol.* 7, 179–183. doi: 10.1007/s10126-004-0006-3

Katharios, P., Kalatzis, P. G., Kokkari, C., Sarropoulou, E., and Middelboe, M. (2017). Isolation and characterization of a N4-like lytic bacteriophage infecting vibrio splendidus, a pathogen of fish and bivalves. *PLoS One* 12, e0190083. doi: 10.1371/journal.pone.0190083

Kawamoto, Y., Nakajima, Y., and Kuranaga, E. (2016). Apoptosis in cellular society: Communication between apoptotic cells and their neighbors. *Int. J. Mol. Sci.* 17, 2144. doi: 10.3390/ijms17122144

Khalil, G. M., and Crawford, C. A. G. (2015). A bibliometric analysis of US-based research on the behavioral risk factor surveillance system. *Am. J. Prev. Med.* 48, 50–57. doi: 10.1016/j.amepre.2014.08.021

Kinch, J., Purcell, S., Uthicke, S., and Friedman, K. (2008). "Population status, fisheries and trade of sea cucumbers in the Western central pacific" inM.V. Toral-Granda, A. Lovatelli and M. Vasconcellos Eds. *Sea cucumbers: a global review of fisheries and trade* (Rome: Food and Agriculture Organization of the United Nations), 7–55.

Kleinberg, J. (2003). Bursty and hierarchical structure in streams. *Data. Min. Knowl. Disc.* 7, 373–397. doi: 10.1023/a:1024940629314

Law, R., and Leung, D. (2020). Journal impact factor: A valid symbol of journal quality? *Tour. Econ.* 26, 734–742. doi: 10.1177/1354816619845590

Leibson, N. L. (1992). Regeneration of digestive tube in holothurians stichopus japonicus and eupentacta fraudatrix. *Monogr. Dev. Biol.* 23, 51–61.

Lewallen, M., and Burggren, W. (2022). Metabolic cost of development, regeneration, and reproduction in the planarian schmidtea mediterranea. *Comp. Biochem. Physiol. Part A: Mol. Integr. Physiol.* 265, 8. doi: 10.1016/j.cbpa.2021.111127

Li, C. H. (2021). Research progress on molecular regulation mechanism of skin ulcer syndrome in sea cucumber apostichopus japonicus: A review. *J. Dalian Ocean Univ.* 3, 355–373. doi: 10.16535/j.cnki.dlhyxb.2021-086

Liao, Y. L. (1997). *Fauna of China, phylum Echinodermata: Class holothuroidea* (Beijing: Science Press), 147–158.

Li, L., and Li, Q. (2010). Effects of stocking density, temperature, and salinity on larval survival and growth of the red race of the sea cucumber apostichopus japonicus (Selenka). *Aquacult. Int.* 18, 447–460. doi: 10.1007/s10499-009-9256-4

Lindsay, S. M. (2010). Frequency of injury and the ecology of regeneration in marine benthic invertebrates. *Integr. Comp. Biol.* 50, 479–493. doi: 10.1093/icb/icq099

Lin, S., and Tang, F. G. (2009). Feature selection algorithm based on log-likelihood ratio. *Comput. Eng.* 35, 56–58. doi: 10.3969/j.issn.1000-3428.2009.19.018

Li, Q., Ren, Y., Liang, C. L., Qiao, G., Wang, Y. N., Ye, S. G., et al. (2018a). Regeneration of coelomocytes after evisceration in the sea cucumber, apostichopus japonicus. *Fish Shellfish Immunol.* 76, 266–271. doi: 10.1016/j.fsi.2018.03.013

Li, Q., Ren, Y., Luan, L. L., Zhang, J. L., Qiao, G., Wang, Y. N., et al. (2019). Localization and characterization of hematopoietic tissues in adult sea cucumber, apostichopus japonicus. *Fish Shellfish Immunol.* 84, 1–7. doi: 10.1016/j.fsi.2018.09.058

Li, Q., Sun, K. T., and Zhang, X. Y. (2013). Research progress on "skin ulceration syndrome" of apostichopus japonicas. *J. Agric. Sci. Technol.* 15, 40–45. doi: 10.3969/j.issn.1008-0864.2013.06.07

Liu, X. X., Liu, Y., Hao, J. J., Zhao, X. L., Lang, Y. Z., Fan, F., et al. (2016b). In anti-cancer mechanism of low-molecular-weight fucosylated chondroitin sulfate (LFCS) from sea cucumber cucumaria frondosa. *Molecules* 21, 12. doi: 10.3390/molecules21050625

Liu, Y. N., Wu, K. N., and Zhao, R. (2020). Bibliometric analysis of research on soil health from 1999 to 2018. *J. Soils Sediments* 20, 1513–1525. doi: 10.1007/s11368-019-02519-9

Liu, Z. Q., Yang, J. Y., Zhang, J. E., Xiang, H. M., and Wei, H. (2019). A bibliometric analysis of research on acid rain. *Sustainability* 11, 3077. doi: 10.3390/su11113077

Liu, S. L., Zhou, Y., Ru, X. S., Zhang, M. Z., Cao, X. B., and Yang, H. S. (2016a). Differences in immune function and metabolites between aestivating and non-aestivating apostichopus japonicus. *Aquaculture* 459, 36–42. doi: 10.1016/j.aquaculture.2016.03.029

Li, Y. L., Wang, R. J., Xun, X. G., Wang, J., Bao, L. S., Thimmappa, R., et al. (2018b). Sea Cucumber genome provides insights into saponin biosynthesis and aestivation regulation. *Cell Discov* 4, 17. doi: 10.1038/s41421-018-0030-5

Li, H. Y., Zhang, G. L., Hou, H. M., Ge, J. H., and Sun, M. Y. (2012). Study on inhibitory ability and mechanism of apostichopus japonicus-related microbes against vibrio splendidus. *Food Industry* 33, 117–120.

Li, R., Zhang, L. Y., Li, Z. J., Xue, C. H., Dong, P., Huang, Q. R., et al. (2020). Characterization and absorption kinetics of a novel multifunctional nanoliposome stabilized by sea cucumber saponins instead of cholesterol. *J. Agric. Food Chem.* 68, 642–651. doi: 10.1021/acs.jafc.9b06460

Luo, L., Wu, M. Y., Xu, L., Lian, W., Xiang, J. Y., Lu, F., et al. (2013). Comparison of physicochemical characteristics and anticoagulant activities of polysaccharides from three sea cucumbers. *Mar. Drugs* 11, 399–417. doi: 10.3390/md11020399

Lu, M., Zhang, P. J., Li, C. H., Lv, Z. M., Zhang, W. W., and Jin, C. H. (2015). miRNA-133 augments coelomocyte phagocytosis in bacteria-challenged apostichopus japonicus *via* targeting the TLR component of IRAK-1 *in vitro* and *in vivo*. *Sci. Rep.* 5 1–14. doi: 10.1038/srep12608

Lv, Z. M., Guo, M., Zhao, X. L., Shao, Y. N., Zhang, W. W., and Li, C. H. (2022). IL-17/IL-17 receptor pathway-mediated inflammatory response in apostichopus japonicus supports the conserved functions of cytokines in invertebrates. *J. Immunol.* 208, 464–479. doi: 10.4049/jimmunol.2100047

Lv, Z. M., Li, C. H., Guo, M., Shao, Y. N., Zhang, W. W., and Zhao, X. L. (2019). Major yolk protein and HSC70 are essential for the activation of the TLR pathway *via* interacting with MyD88 in apostichopus japonicus. *Arch. Biochem. Biophys.* 665, 57–68. doi: 10.1016/j.abb.2019.02.019

Marques, I. J., Lupi, E., and Mercader, N. (2019). Mode systems for regeneration: zebrafish. *Development* 146, 13. doi: 10.1242/dev.167692

Mashanov, V. S., and Garcia-Arraras, J. E. (2011). Gut regeneration in holothurians: A snapshot of recent developments. *Biol. Bull.* 221, 93–109. doi: 10.1086/BBLv221n1p93

Miao, T., Wan, Z. X., Sun, L. N., Li, X. N., Xing, L. L., Bai, Y. C., et al. (2017). Extracellular matrix remodeling and matrix metalloproteinases (ajMMP-2 like and ajMMP-16 like) characterization during intestine regeneration of sea cucumber apostichopus japonicus. *Comp. Biochem. Physiol. Part B: Biochem. Mol. Biol.* 212, 12–23. doi: 10.1016/j.cbpb.2017.06.011

Midori, Y., and Kenichiro, W. (1981) 8, 51–62. About the initial breeding of sea cucumber larvae. Report of Yamaguchi Prefectural Sea Fisheries Experiment Station.

Mitsukuri, K. (1897). The growth of sea cucumber causes changes in bone pieces. *J. Zoology* 9, 41–47.

Mitsukuri, K. (1905). Bone fragment of sea cucumber. *J. Zoology* 17, 137–140.

National Institute of General Medical Sciences (2021) *What are regeneration and regenerative medicine*. Available at: https://www.nigms.nih.gov/education/fact-sheets/Pages/regeneration (Accessed April 3, 2022).

National Library of Medicine (2022) *What are single nucleotide polymorphisms (SNPs)*. Available at: https://medlineplus.gov/genetics/understanding/genomicresearch/snp/ (Accessed June 1, 2022).

Nie, Z. L., and Li, X. (2006). Study on the regeneration of sea cucumber. *Mar. Sci.* 5, 78–82. doi: 10.3969/j.issn.1000-3096.2006.05.016

Osbourn, A., Goss, R. J. M., and Field, R. A. (2011). The saponins - polar isoprenoids with important and diverse biological activities. *Nat. Prod. Rep.* 28, 1261–1268. doi: 10.1039/c1np00015b

Pangestuti, R., and Arifin, Z. (2018). Medicinal and health benefit effects of functional sea cucumbers. *J. Tradit. Complement. Med.* 8, 341–351. doi: 10.1016/j.jtcme.2017.06.007

Picone, F., Buonocore, E., Chemello, R., Russo, G. F., and Franzese, P. P. (2021). Exploring the development of scientific research on marine protected areas: From conservation to global ocean sustainability. *Ecol. Inform.* 61, 101200. doi: 10.1016/j.ecoinf.2020.101200

Pomin, V. H. (2014). Holothurian fucosylated chondroitin sulfate. *Mar. Drugs* 12, 232–254. doi: 10.3390/md12010232

Price, D. J., d., S., and Zhang, J. (1984). Lotka's law and price's law. *Sci. Sci. Manage. S. T.* 9, 17–22.

Pritchard, A. (1969). Statistical bibliography or bibliometrics. *J. Documentation* 25, 348–349.

Qin, Y. J., Zhao, X. J., Li, X., Wang, Y. F., and Liu, Y. (2015). Characterization of the 26S proteasome S7 subunit gene and its expression during regeneration in apostichopus japonicus. *J. World Aquacult. Soc* 46, 159–170. doi: 10.1111/jwas.12176

Quispe-Parra, D. J., Medina-Feliciano, J. G., Cruz-Gonzalez, S., Ortiz-Zuazaga, H., and Garcia-Arraras, J. E. (2021). Transcriptomic analysis of early stages of intestinal regeneration in holothuria glaberrima. *Sci. Rep.* 11, 1–14. doi: 10.1038/s41598-020-79436-2

Ramírez-González, J., Moity, N., Andrade-Vera, S., and Reyes, H. (2020). Overexploitation and more than a decade of failed management leads to no recovery of the galápagos sea cucumber fishery. *Front. Mar. Sci.* 7. doi: 10.3389/fmars.2020.554314

Rodriguez, A., and Laio, A. (2014). Clustering by fast search and find of density peaks. *Science* 344, 1492–1496. doi: 10.1126/science.1242072

Ru, X. S., Zhang, L. B., Li, X. N., Liu, S. L., and Yang, H. S. (2019). Development strategies for the sea cucumber industry in China. *J. Oceanol. Limnol.* 37, 300–312. doi: 10.1007/s00343-019-7344-5

Sea Cucumber Industry Branch of China Fisheries Association (2022) *Review of china's sea cucumber industry development in 2021*. Available at: http://www.haishenren.org.cn/industry_service/show-23.html (Accessed June 1, 2022).

Selenka, E. (1867). *Beiträge zur anatomie und systematik der holothurien* (Leipzig: W. Engelmann), 291–382.

Shao, Y. N., Che, Z. J., Chen, K. Y., Li, C. H., and Zhao, X. D. (2020). Target of rapamycin signaling inhibits autophagy in sea cucumber apostichopus japonicus. *Fish Shellfish Immunol.* 102, 480–488. doi: 10.1016/j.fsi.2020.05.013

Shao, Y. N., Che, Z. J., Li, C. H., Zhang, W. W., Zhao, X. L., and Guo, M. (2019). A novel caspase-1 mediates inflammatory responses and pyroptosis in sea cucumber apostichopus japonicus. *Aquaculture* 513, 11. doi: 10.1016/j.aquaculture.2019.734399

Shao, Y. N., Li, C. H., Zhang, W. W., Duan, X. M., Li, Y., Han, Q. X., et al. (2015). Three members in JAK/STAT signal pathway from the sea cucumber apostichopus japonicus: Molecular cloning, characterization and function analysis. *Fish Shellfish Immunol.* 46, 523–536. doi: 10.1016/j.fsi.2015.07.019

Shao, Y. N., Li, C. H., Zhang, W. W., Duan, X. M., Li, Y., Jin, C. H., et al. (2016). Molecular cloning and characterization of four caspases members in apostichopus japonicus. *Fish Shellfish Immunol.* 55, 203–211. doi: 10.1016/j.fsi.2016.05.039

Shi, W. B., Zhang, J. L., Wang, Y. N., Ji, J. L., Guo, L. Y., Ren, Y., et al. (2020). Transcriptome analysis of sea cucumber (Apostichopus japonicus) polian vesicles in response to evisceration. *Fish Shellfish Immunol.* 97, 108–113. doi: 10.1016/j.fsi.2019.12.016

Smith, L. C., Ghosh, J., Buckley, K. M., Clow, L. A., Dheilly, N. M., Haug, T., et al. (2010). "Echinoderm immunity," in *Invertebrate immunity*. Ed. K. Soderhall. (Cham: Springer), 260–301.

Song, J., and Chen, X. K. (2012). Establishment of low-salinity sea cucumber apostichopus japonicus family and comparison of their growth traits. *Hebei Fisheries* 11, 15–18+62. doi: 10.3969/j.issn.1004-6755.2012.11.005

Song, Y., Jin, S. J., Cui, L. H., Ji, X. J., and Yang, F. G. (2013). Immunomodulatory effect of stichopus japonicus acid mucopolysaccharide on experimental hepatocellular carcinoma in rats. *Molecules* 18, 7179–7193. doi: 10.3390/molecules18067179

Song, S., Peng, H. R., Wang, Q. L., Liu, Z. Q., Dong, X. P., Wen, C. R., et al. (2020). Inhibitory activities of marine sulfated polysaccharides against SARS-CoV-2. *Food Funct.* 11, 7415–7420. doi: 10.1039/d0fo02017f

Sun, Y. X., Du, X. F., Li, S. Y., Wen, Z. X., Li, Y. J., Li, X. J., et al. (2015). Dietary cordyceps militaris protects against vibrio splendidus infection in sea cucumber apostichopus japonicus. *Fish Shellfish Immunol.* 45, 964–971. doi: 10.1016/j.fsi.2015.05.053

Sun, L. N., Lin, C. G., Li, X. N., Xing, L., Huo, D. C., Sun, J. C., et al. (2018). Comparative phospho- and acetyl proteomics analysis of posttranslational modifications regulating intestine regeneration in sea cucumbers. *Front. Physiol.* 9. doi: 10.3389/fphys.2018.00836

Sun, L. N., Sun, J. C., Li, X. N., Zhang, L. B., Yang, H. S., and Wang, Q. (2017a). Understanding regulation of microRNAs on intestine regeneration in the sea cucumber apostichopus japonicus using high-throughput sequencing. *Comp. Biochem. Physiol. Part D: Genomics Proteomics* 22, 1–9. doi: 10.1016/j.cbd.2017.01.001

Sun, L. N., Xu, D. X., Xu, Q. Z., Sun, J. C., Xing, L. L., Zhang, L. B., et al. (2017b). iTRAQ reveals proteomic changes during intestine regeneration in the sea cucumber apostichopus japonicus. *Comp. Biochem. Physiol. Part D: Genomics Proteomics* 22, 39–49. doi: 10.1016/j.cbd.2017.02.004

Sun, L. N., Yang, H. S., Chen, M. Y., Ma, D. Y., and Lin, C. G. (2013b). RNA-Seq reveals dynamic changes of gene expression in key stages of intestine regeneration in the sea cucumber apostichopus japonicas. *PLoS One* 8, 18. doi: 10.1371/journal.pone.0069441

Sun, L. N., Yang, H. S., Chen, M. Y., and Xu, D. X. (2013a). Cloning and expression analysis of Wnt6 and Hox6 during intestinal regeneration in the sea cucumber apostichopus japonicus. *Genet. Mol. Res.* 12, 5321–5334. doi: 10.4238/2013.November.7.7

Sun, H. J., Zhou, Z. C., Dong, Y., Yang, A. F., Jiang, B., Gao, S., et al. (2013). Identification and expression analysis of two toll-like receptor genes from sea cucumber (Apostichopus japonicus). *Fish Shellfish Immunol.* 34, 147–158. doi: 10.1016/j.fsi.2012.10.014

Tanaka, Y. (1958). Feeding and digestive processes of stichopus japonicus *Bulletin of faculty of fisheries* (Hokkaido University), 14–28.

Tanaka, E. M., and Reddien, P. W. (2011). The cellular basis for animal regeneration. *Dev. Cell* 21, 172–185. doi: 10.1016/j.devcel.2011.06.016

Wang, Z. P., Li, B., Qin, L., Wang, Y. G., Liao, M. J., Rong, X. J., et al. (2021). Metabolic characteristics and adaptability of a new variety of sea cucumber "Shenyou No.1" under different salinities. *Prog. Fishery Sci.* 42, 108–115. doi: 10.19663/j.issn2095-9869.20200331002

Wang, T. T., Sun, Y. X., Jin, L. J., Thacker, P., Li, S. Y., and Xu, Y. P. (2013). Aj-rel and aj-p105, two evolutionary conserved NF-kappa b homologues in sea cucumber (Apostichopus japonicus) and their involvement in LPS induced immunity. *Fish Shellfish Immunol.* 34, 17–22. doi: 10.1016/j.fsi.2012.09.006

Wang, J. Q., Tang, L., Xu, C., and cheng, J. C. (2007). Histological observation of alimentary tract and annual changes of four digestive enzymes in sea cucumber (Apostichopus japonicus). *Fisheries Sci.* 09, 481–484. doi: 10.16378/j.cnki.1003-1111.2007.09.014

Wang, F. Y., Yang, H. S., Gabr, H. R., and Gao, F. (2008). Immune condition of apostichopus japonicus during aestivation. *Aquaculture* 285, 238–243. doi: 10.1016/j.aquaculture.2008.08.033

Wang, Z. Q., Zhou, Z. Y., Xu, W. C., Yang, D., Xu, Y., Yang, L. H., et al. (2021). Research status and development trends in the field of marine environment corrosion: A new perspective. *Environ. Sci. Pollut. Res* 28, 54403–54408. doi: 10.1007/s11356-021-15974-0

Wei, J. P., Liang, G. F., Alex, J., Zhang, T. C., and Ma, C. B. (2020). Research progress of energy utilization of agricultural waste in China: Bibliometric analysis by citespace. *Sustainability* 12, 812. doi: 10.3390/su12030812

Wuchty, S., Jones, B. F., and Uzzi, B. (2007). The increasing dominance of teams in production of knowledge. *Science* 316, 1036–1039. doi: 10.1126/science.1136099

Yang, Z. (2017). Characteristics and potential functions of 5-HT4R in sea cucumber (Apostichopus japonicus). *Master's thesis* Zhoushan:Zhejiang Ocean University. doi: 10.7666/d.Y3236272

Yan, L. F., and Gu, A. H. (2013). Progress and application of zebrafish in regenerative medicine. *Yi Chuan = Hereditas* 35, 856–866. doi: 10.3724/SP.J.1005.2013.00856

Yang, H. S., Yuan, X. T., Zhou, Y., Mao, Y. Z., Zhang, T., and Liu, Y. (2005). Effects of body size and water temperature on food consumption and growth in the sea cucumber apostichopus japonicus (Selenka) with special reference to aestivation. *Aquacult. Res.* 36, 1085–1092. doi: 10.1111/j.1365-2109.2005.01325.x

Yang, A. F., Zhou, Z. C., Pan, Y. J., Jiang, J. W., Dong, Y., Guan, X. Y., et al. (2016). RNA Sequencing analysis to capture the transcriptome landscape during skin ulceration syndrome progression in sea cucumber apostichopus japonicus. *BMC Genomics* 17, 1–16. doi: 10.1186/s12864-016-2810-3

Yang, H. S., Zhou, Y., Zhang, T., Yuan, X. T., Li, X. X., Liu, Y., et al. (2006). Metabolic characteristics of sea cucumber apostichopus japonicus (Selenka) during aestivation. *J. Exp. Mar. Biol. Ecol.* 330, 505–510. doi: 10.1016/j.jembe.2005.09.010

Yin, X. X., Zhang, G. P., and Li, X. F. (2009). Analysis of information science research status based on keyword statistics. *J. Inf.* 11, 5–8. doi: 10.3969/j.issn.1002-1965.2009.11.001

Yuan, J. B., Gao, Y., Sun, L. N., Jin, S. J., Zhang, X. J., Liu, C. Z., et al. (2019). Wnt signaling pathway linked to intestinal regeneration *via* evolutionary patterns and gene expression in the sea cucumber apostichopus japonicus. *Front. Genet.* 10. doi: 10.3389/fgene.2019.00112

Yuan, X. T., Yang, H. S., Chen, M. Y., and Gao, F. (2007). Research advances in aestivation of sea cucumber apostichopus japonicas (Selenka): A review. *Mar. Sci.* 31, 88–90. doi: 10.3969/j.issn.1000-3096.2007.08.018

Yuan, X. T., Yang, H. S., Zhou, Y., Mao, Y. Z., Zhang, T., and Liu, Y. (2006). The influence of diets containing dried bivalve feces and/or powdered algae on growth and energy distribution in sea cucumber apostichopus japonicus (Selenka) (Echinodermata: Holothuroidea). *Aquaculture* 256, 457–467. doi: 10.1016/j.aquaculture.2006.01.029

Zhang, W. W., Liang, W. K., and Li, C. H. (2016). Inhibition of marine vibrio sp. by pyoverdine from pseudomonas aeruginosa PA1. *J. Hazard. Mater.* 302, 217–224. doi: 10.1016/j.jhazmat.2015.10.003

Zhang, P., Li, C. H., Li, Y., Zhang, P. J., Shao, Y. N., Jin, C. H., et al. (2014). Proteomic identification of differentially expressed proteins in sea cucumber apostichopus japonicus coelomocytes after vibrio splendidus infection. *Dev. Comp. Immunol.* 44, 370–377. doi: 10.1016/j.dci.2014.01.013

Zhang, S. S., Liu, N. N., Liang, W. K., Han, Q. X., Zhang, W. W., and Li, C. H. (2017). Quorum sensing-disrupting coumarin suppressing virulence phenotypes in vibrio splendidus. *Appl. Microbiol. Biotechnol.* 101, 3371–3378. doi: 10.1007/s00253-016-8009-3

Zhang, Z., Lv, Z. M., Zhang, W. W., Shao, Y. N., Zhao, X. L., Guo, M., et al. (2019). Comparative analysis of midgut bacterial community under vibrio splendidus infection in apostichopus japonicus with hindgut as a reference. *Aquaculture* 513, 11. doi: 10.1016/j.aquaculture.2019.734427

Zhang, Q., Ma, H. M., Mai, K. S., Zhang, W. B., Liufu, Z. G., and Xu, W. (2010). Interaction of dietary bacillus subtilis and fructooligosaccharide on the growth performance, non-specific immunity of sea cucumber, apostichopus japonicus. *Fish Shellfish Immunol.* 29, 204–211. doi: 10.1016/j.fsi.2010.03.009

Zhang, X. J., Sun, L. N., Yuan, J. B., Sun, Y. M., Gao, Y., Zhang, L. B., et al. (2017). The sea cucumber genome provides insights into morphological evolution and visceral regeneration. *PLoS Biol.* 15, e2003790. doi: 10.1371/journal.pbio.2003790

Zhang, Z., Xing, R. L., Lv, Z. M., Shao, Y. N., Zhang, W. W., Zhao, X. L., et al. (2018). Analysis of gut microbiota revealed lactococcus garviaeae could be an indicative of skin ulceration syndrome in farmed sea cucumber apostichopus japonicus. *Fish Shellfish Immunol.* 80, 148–154. doi: 10.1016/j.fsi.2018.06.001

Zhang, L. Y., Zhang, T. T., Ding, L., Xu, J., Xue, C. H., Yanagita, T., et al. (2018). The protective activities of dietary sea cucumber cerebrosides against atherosclerosis through regulating inflammation and cholesterol metabolism in male mice. *Mol. Nutr. Food Res.* 62, 1800315. doi: 10.1002/mnfr.201800315

Zhao, H., Liu, S. L., Yang, H. S., Zhao, H. L., and Liu, C. G. (2014). The study on thermo tolerance of juvenile offspring apostichopus japonicus (Selenka) with directive breeding. *Mar. Sci.* 38, 1–6. doi: 10.11759/hykx20121105001

Zhao, Y., Yang, H. S., Storey, K. B., and Chen, M. Y. (2014). Differential gene expression in the respiratory tree of the sea cucumber apostichopus japonicus during aestivation. *Mar. Genom.* 18, 173–183. doi: 10.1016/j.margen.2014.07.001

Zhao, Y. C., Zhang, W. B., Xu, W., Mai, K. S., Zhang, Y. J., and Liufu, Z. G. (2012). Effects of potential probiotic bacillus subtilis T13 on growth, immunity and disease resistance against vibrio splendidus infection in juvenile sea cucumber apostichopus japonicus. *Fish Shellfish Immunol.* 32, 750–755. doi: 10.1016/j.fsi.2012.01.027

Zhou, Z. C., Dong, Y., Sun, H. J., Yang, A. F., Chen, Z., Gao, S., et al. (2014). Transcriptome sequencing of sea cucumber (Apostichopus japonicus) and the identification of gene-associated markers. *Mol. Ecol. Resour.* 14, 127–138.doi: 10.1111/1755-0998.12147

Zhu, B. W., Dong, X. P., Zhou, D. Y., Gao, Y., Yang, J. F., Li, D. M., et al. (2012). Physicochemical properties and radical scavenging capacities of pepsin-solubilized collagen from sea cucumber stichopus japonicus. *Food Hydrocolloids* 28, 182–188. doi: 10.1016/j.foodhyd.2011.12.010

frontiers | Frontiers in Marine Science

TYPE Original Research
PUBLISHED 26 August 2022
DOI 10.3389/fmars.2022.967452

OPEN ACCESS

EDITED BY
Chenghua Li,
Ningbo University, China

REVIEWED BY
Yanbo Wang,
Zhejiang Gongshang University, China
Zonghe Yu,
South China Agricultural University, China

*CORRESPONDENCE
Chong Zhao
chongzhao@dlou.edu.cn

SPECIALTY SECTION
This article was submitted to Marine Fisheries, Aquaculture and Living Resources, a section of the journal Frontiers in Marine Science

RECEIVED 12 June 2022
ACCEPTED 25 July 2022
PUBLISHED 26 August 2022

CITATION
Yu Y, Qiao Y, Ding P, Tian R, Sun J, Hu F, Wu G, Chang Y and Zhao C (2022) Effects of sea urchin feces on behaviors, digestion ability, growth, and resistance of the sea cucumber *Apostichopus japonicus*. *Front. Mar. Sci.* 9:967452. doi: 10.3389/fmars.2022.967452

Effects of sea urchin feces on behaviors, digestion ability, growth, and resistance of the sea cucumber *Apostichopus japonicus*

Yushi Yu, Yihai Qiao, Peng Ding, Ruihuan Tian, Jiangnan Sun, Fangyuan Hu, Guo Wu, Yaqing Chang and Chong Zhao*

Key Laboratory of Mariculture & Stock Enhancement in North China's Sea, Ministry of Agriculture and Rural Affairs, Dalian Ocean University, Dalian, China

Improving the aquaculture production efficiency by appropriate diets is an essential approach to meeting the increasing market demand for sea cucumbers. The feces of sea urchins, which contains various enzymes and microorganisms, is a potentially cost-effective food for sea cucumbers. To assess the usability of the fecal diet, a five-week laboratory simulation is conducted to investigate behaviors, digestion ability, growth and resistance ability of the sea cucumber *Apostichopus japonicus* fed with fecal diet at water temperatures of 15°C and 5°C. In the present study, *A. japonicus* fed with fecal diet shows an obvious preference to fecal diet rather than prepared feed at water temperatures of both 15°C and 5°C, which suggests that the feces is an applicable diet for *A. japonicus*. Furthermore, small *A. japonicus* fed with feces (group F) shows significant advantages in intestinal community richness, community diversity and intestine protease activity to *A. japonicus* fed with prepared feed (group S) at 15°C. These results indicate that the fecal diet provides benefits to digestion ability of small *A. japonicus* at 15°C. Weight gaining rate is significantly higher in the *A. japonicus* fed with feces than that in *A. japonicus* that were fed with feed or not fed with food (group C), which suggests that the direct improvement of the production efficiency at 15°C. The advantages in intestinal bacteria, protease activity, and growth are consistently found in group F compared with group S at 5°C. In addition, the composition of intestinal bacteria indicates that sea cucumbers may inherit the intestinal bacteria of sea urchins through fecal consumption. This suggests that the fecal diet enhances the digestion ability and enzyme activity at low water temperature and thus improves the growth of sea cucumbers. Furthermore, sea cucumbers fed with sea urchin feces have the highest survival rate among the three groups in exposure to an acute salinity decrease at both 5 and 15°C, indicating a better resistance to low salinity. This provides a new insight into the

geographical expansion to low-salinity areas in sea cucumber aquaculture. In conclusion, the present study suggests that sea urchin feces have a great potential for the application in improving the production efficiency of sea cucumber aquaculture.

KEYWORDS

Apostichopus japonicus, sea urchin feces, intestinal bacterial community, protease activity, resistance

Introduction

The sea cucumber *Apostichopus japonicus* is one of the primarily commercialized marine species with high output value and profit in China (Hair et al., 2012; Han et al., 2016). However, the production of *A. japonicus* does not meet the increasing market demand (Zhang et al., 2015). Therefore, it is essential to increase the production efficiency of *A. japonicus* aquaculture (An et al., 2007; Yuan et al., 2010).

Seed culture is one of the most important stages in aquaculture of *A. japonicus* (Chen, 2003; Yang et al., 2004). Small *A. japonicus* normally stops feeding when water temperature drops to ~5°C in winter (Chen, 2004). The fasting period lasts two months each year, which causes long-term growth retardation in winters in Northern China (Gao et al., 2009; Liu, 2015). Aqua-farmers thus raise the water temperature by burning coal. The method, however, is neither economically nor environmentally friendly. Therefore, it is valuable to develop a diet for overwintering without the need to raise water temperature. Furthermore, *A. japonicus* generally feed and grow most efficiently at the optimum temperature of 15°C (Yang et al., 2005). Meanwhile, prepared feeds are very expensive (Jiang et al., 2017), accounting for 50% of the total culture cost (Wang, 2015). Therefore, a cost-effective diet is essential for improving the production efficiency of sea cucumber aquaculture.

The feces of sea urchins is an inexpensive natural food source for deposit-feeders (e.g., *A. japonicus*) (Newell, 1965) Frankenberg & Smith, 1967; Sauchyn & Scheibling, 2009). It is mainly the aggregation of relatively unprocessed vegetative material (e.g., algae) coated in mucus (Peduzzi & Herndl, 1986; Yoon et al., 1996; Povero et al., 2003). The key nutritional values are even higher than the original algal tissues (Dethier et al., 2019). Thus, the feces of sea urchins probably meets the nutritive needs of small *A. japonicus* (Sui, 1988; Yang et al., 2004). Furthermore, the digestion ability of *A. japonicus* greatly depends on intestinal microorganisms and digestive enzymes (Jiang et al., 2007; Liu et al., 2013; Wang, 2015; Wang et al., 2016) because of the simple intestinal structure (Yang et al., 2004). The feces is rich in bacteria, protozoa, and enzymes (Robertson, 1982; González & Biddanda, 1990; Thor et al., 2003). Therefore, it probably has the advantage in improving the digestion ability of *A. japonicus*. Since digestion greatly affects growth (Yang et al., 2004), fecal diet has the great potential to be an alternative food for *A. japonicus* aquaculture at a water temperature of 15°C. Furthermore, sea cucumbers probably ingest live microorganisms, which enhances enzymatic activity and provides extra benefits (e.g., digestive and resistance benefits) during the feeding process (Moss et al., 2001; Liu et al., 2009; Dethier et al., 2019). The enzyme-rich and microbial-rich feces is even more crucial for improving the digestion ability of sea cucumbers in winter when *A. japonicus* have poor enzyme activity (Fu, 2004; Gao et al., 2009; Liu et al., 2013).

The present study aims to assess the usability of the fecal diet at water temperatures of 15°C and 5°C in order to improve the production efficiency of *A. japonicus* aquaculture. We ask: 1) whether the feces of sea urchins is an appreciated diet for *A. japonicus*, 2) whether the fecal diet improves the growth efficiency of *A. japonicus*, 3) whether the fecal diet enriches the intestine microbiota and enhances the intestine protease activity of *A. japonicus*, 4) whether the fecal diet provides resistance benefits to *A. japonicus* in low salinity at water temperatures of 15°C and 5°C.

Materials and methods

Animals

Small *A. japonicus* of two sizes (~0.15 g and ~0.5 g) were transported from Dalian Zhuang Yuanhai Ecological Seedling Industry Co., Ltd to the Key Laboratory of Mariculture & Stock Enhancement in the North China' s Sea, Ministry of Agriculture and Rural Affairs, Dalian Ocean University (121°37′ E, 38°87′ N) and separately cultured at 10°C in two circulating water temperature-control tanks, respectively (length × width × height: 75 × 45 × 40 cm; HXSWT-101, Huixin Co., Dalian, China). Water temperature was increased by 1°C every two days from 10°C to 15°C for the *A. japonicus* (body weight = 0.16 ±

0.03 g), while water temperature was decreased by 1°C every two days from 10°C to 5°C for *A. japonicus* (body weight = 0.53 ± 0.12 g). Sea cucumbers were fed with the commercial feed (Anyuan Industrial Co., Ltd) with sea mud (1: 6) for two weeks prior to the feeding trial to make the animals acclimate to the experimental diet and environment.

The sea urchin *Strongylocentrotus intermedius* were transported from a local aqua-farm to the laboratory (test diameter = 1.38 ± 0.47 cm). To provide fresh feces for sea cucumbers at 15°C and 5°C, sea urchins were randomly collected and cultured in six cylindrical plastic cages (20 cm of diameter, 0.5 cm of mesh size) in two circulating water temperature-control tanks of 15°C and 5°C, respectively (length × width × height: 75 × 45 × 40 cm; HXSWT-101, Huixin Co., Dalian, China). Sea urchins were fed with prepared feed *ad libitum* . The mesh size of 0.5 cm allowed the feces, while not sea urchins and un-ingested food, to fall to the bottom of the tanks for collection.

There was no major variation in water temperature (5.0 ± 0.5°C, 15.0 ± 0.5°C), salinity (32.5 ± 0.41‰) and pH (8.10 ± 0.11, mean ± SD) during the acclimation period, according to the daily measurement with a YSI probe (YSI Incorporated, OH, USA). The photoperiod was 12D: 12L. The seawater was renewed daily.

Experimental design

Diet was the experimental factor in the following groups: *A. japonicus* that were not fed (group C), *A. japonicus* that were fed with the feces of sea urchins (group F), and *A. japonicus* that were fed with the artificial feed (Anyuan Industrial Co., Ltd, the common food in *A. japonicus* aquaculture) (group S). Sea cucumbers (body weight = 0.56 ± 0.04 g) were randomly distributed into 18 plastic boxes (length × width × height: 20 × 20 × 15 cm, with fixed shelters on the bottom, Figure 1A). Each box (6 L/tank) was stocked with 20 sea cucumbers. Each diet had six boxes as replicates (N = 6). The water temperature was set at 5 ± 0.5°C using the method of water bath in temperature-controlled tanks (length × width × height: 75 × 45 × 35 cm, HXSWT-101, Huixin Co., Dalian, China). In the seawater at 5°C, the salinity was 32.2–32.5‰, the pH was 8.03–8.26, and dissolved oxygen was 6.2–7.0 mg L^{-1}.

Similarly, 20 sea cucumbers (body weight = 0.16 ± 0.01 g) were put into each experimental plastic box as one replicate, and cultured for five weeks at a water temperature of 15°C. Each group had six boxes as replicates fed with the three different diets (N = 6). The experiment lasted for 5 weeks from December 8, 2020 to January 12, 2021. The seawater in the boxes was aerated and changed every three days. In the seawater at 15°C, the salinity was 31.9–32.2‰, the pH was 7.98–8.42, and dissolved oxygen was 7.0–7.4 mg L^{-1}. The light intensity was 0–5 lx for seawater at both temperatures.

Survival rate

The number of survived sea cucumbers was recorded for all the three groups during the five weeks. Survival rate was calculated as the number of survived individuals divided by the number of all involved sea cucumbers.

Food preference

Food preference was a behavioral experiment to determine which food the sea cucumber prefers after the five-week culture with different diet in seawater at both 15°C and 5°C. Individual sea cucumber was placed in a plastic box with feed at the right side and feces at left side (length × width × height: 17 × 14 × 10 cm, Figure 1B). Each group had six replicates using different sea cucumbers for both 15°C and 5°C (N = 6). We recorded the experiment for an hour using a digital camera (Legria HF20; Canon, Tokyo, Japan). We subsequently calculated the number of grasping times and the staying time in both the feces side and the feed side to determine the food preference of sea cucumbers according to our previous method (Yu et al., 2022).

Growth performance

Sea cucumbers were all weighted after one-minute drying time in net using an electric balance (G & G Co., USA) for all the groups at the end of the experiment (N = 6). Weight gain rate

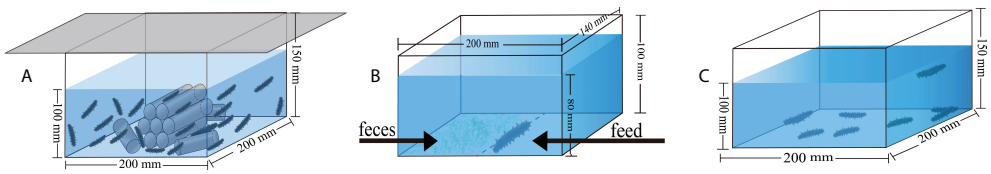

FIGURE 1
The conceptual diagrams show the devices for culture **(A)**, for food preference experiment **(B)**, and for the acute salinity decrease treatments **(C)**.

was calculated according to the following formula (Wang et al., 2016) WGR (%)=(W_t–W_0)/W_0×100.

W_t is terminal wet weight of sea cucumbers (g); W_0 is initial wet weight of sea cucumbers (g).

Acute salinity decrease treatments

Thirty-two sea cucumbers were randomly selected from each group in seawater at both 15°C and 5°C. The 32 sea cucumbers were equally put into four plastic boxes (length × width × height: 20 × 20 × 15 cm, Figure 1C) for each group at both temperatures (N = 4). Generally, the lethal salinity for *A. japonicus* is ~15‰ (Sui, 1988; Zhang et al., 2004). Thus, the salinity of acute salinity decrease treatments was decreased from 32.77 ± 0.16‰ to 15.19 ± 0.37‰ within 18 hours at a rate of 1‰ h^{-1} at 15°C and decreased from 32.53 ± 0.16‰ to 15.05 ± 0.43‰ within 18 hours at 5°C. The number of dead *A. japonicus* was recorded within 24 hours. Evisceration and autolysis were considered as death. Survival rate was calculated as the number of survived individuals divided by the number of all involved sea cucumbers.

Protease activity

To evaluate the usability of fecal diet in the aquaculture of *A. japonicus* and understand the effects of fecal diet on digestion ability, we tested the protease activity between sea cucumbers fed with fecal diet and fed with common food in aquaculture. Aseptic instruments were used to dissect the intestines of sea cucumbers. Intestines of two sea cucumbers were pooled for each replicate at 5°C (N = 3), while intestines of three sea cucumbers were pooled for each replicate at 15°C because of the weight requirement of the samples (N = 3) (Wang et al., 2018). The protease activity was determined by using the Protease ELISA Kit (Mlbio, ml560431) (Günay et al., 2020; Zeng et al., 2021). The specific determination method was used according to the instructions of the reagent provided by Bioengineering (Shanghai) Co., LTD.

Intestinal microbiological 16S rRNA gene sequencing

MiSeq high-throughput sequencing technology was used to investigate the intestinal bacterial community structure of *A. japonicus* fed with prepared feed (group S) and with sea urchin feces (group F) in seawater at both 5°C and 15°C. Sea cucumbers were starved for 24 hours before sampling. Aseptic instruments were used to dissect the intestines of sea cucumbers. For the preparation of 1 mL of intestine samples, the intestines of two sea cucumbers were pooled and mixed as a sample for each of the three replicates for groups F and S at 5°C (N = 3). The intestines of three sea cucumbers were pooled as a mixed sample for each of the three replicates for the two groups at 15°C (N = 3). Then, these pooling samples were thoroughly grounded in a sterile mortar. Genomic DNA was extracted using bacterial DNA extraction kit (Bioengineering (Shanghai) Co., LTD.). High-throughput sequencing was performed using the Illumina MiSeq platform to determine the composition of species of each sample (Yang et al., 2015). The random forest analysis was used to find out which bacteria were responsible for the differences between groups. The *post hoc* analysis was preformed to compare the abundances in different groups within a species classification. Principal component analysis (PCA) was performed to reveal the relationships among the different samples.

Statistical analysis

Normal distribution and homogeneity of variance were assessed using the Kolmogorov-Smirnov test and Levene test for the WGR, survival rate, the number of grasping times, the staying time in the feces side and the feed side, and the protease activity, respectively.

The number of grasping times of both sides, the staying time in both sides at both 15°C and 5°C were tested by the independent-sample t-test for the three groups, except the grasping times of group C at 5°C. Kruskal-Wallis U test was carried out to compare the survival rate during the whole culturing period among the three groups at both 15°C and 5°C. Mann-Whitney U test was carried out to compare the grasping times of *A. japonicus* in the two sides of the group C at 5°C and the differences of the WGR between every two groups at both 15°C and 5°C, because the data was non-normal and/or lacked homogeneity in the variance. The protease activity, the OTUs, Chao, ACE, Shannon index, Simpson index, and Coverage for all the groups at both 15°C and 5°C were tested by the independent-sample t-test. Welsh's t-test corrected with Benjamini-Hochberg FDR for *post-hoc* multiple comparisons was used to compare the proportion (a possible abundance) of Bacteroidetes among different groups. All data analyses were performed using SPSS 22.0 statistical software. A probability level of $P< 0.05$ was considered significant.

Results

Food preference

At the water temperature of 5°C, no significant difference between the grasping times of *A. japonicus* in the two sides was found in sea cucumbers fed with prepared feed ($F = 0.040$, $t = -1.174$, $P = 0.268$). However, sea cucumbers fed with feces had significantly more grasping times when they were in the feces side than the times

when they were in the feed side ($F = 12.985$, $t = 2.936$, $P = 0.022$). Sea cucumbers that were not fed had significantly more grasping times when they were in the feed side than the times when they were in the feces side (Mann-Whitney $U = 5.000$, $Z = 2.089$, $P = 0.037$). The sea cucumbers of group F stayed significantly longer in the feces side than the time they stayed in the feed side ($F = 0.000$, $t = 3.234$, $P = 0.009$). The sea cucumbers of groups S and C stayed significantly shorter in the feces side than the time they stayed in the feed side ($F = 0.000$, $t = 3.746$, $P = 0.004$ for group S; $F = 0.000$, $t = 6.543$, $P < 0.001$ for group C).

At the water temperature of 15°C, no significant difference between the grasping times of the two sides was found in group C ($F = 0.262$, $t = 0.525$, $P = 0.611$). Sea cucumbers of group F had significantly more grasping times when they were in the feces side than the times when they were the feed side ($F = 0.493$, $t = 3.673$, $P = 0.004$). Sea cucumbers of group S had significantly more grasping times when they were in the feed side than the times when they were in the feces side ($F = 0.800$, $t = 3.094$, $P = 0.011$). The sea cucumbers of group F stayed significantly longer in the feces side than the time they stayed in the feed side ($F = 0.000$, $t = 3.692$, $P = 0.004$). Sea cucumbers of groups S and C stayed significantly shorter in the feces side than the time they stayed in the feed side ($F = 0.000$, $t = 5.560$, $P< 0.001$ for group S; $F = 0.000$, $t = 5.089$, $P< 0.001$ for group C; Figure 2).

Survival rate

The sea cucumbers of group C (92.50 ± 6.89%) had significantly lower survival rate than that of sea cucumbers in both group S (100 ± 0.00%, $P = 0.007$) and group F at the water temperature of 5°C (100 ± 0.00%, $P = 0.007$). The sea cucumbers of group C (79.17 ± 6.65%) had significantly lower survival rate than that of sea cucumbers in both group S (93.33 ± 5.16%, $P = 0.027$) and group F at the water temperature of 15°C (98.33 ± 2.58%, $P< 0.000$; Figure 3).

Growth

The WGR of group F (111.15 ± 9.14%) was significantly higher than that in group S (50.62 ± 3.92%, $P = 0.002$) and that in group C at 5°C (6.23 ± 1.72%, $P = 0.002$; Figure 4). The sea cucumbers of group S had significantly higher WGR than that of

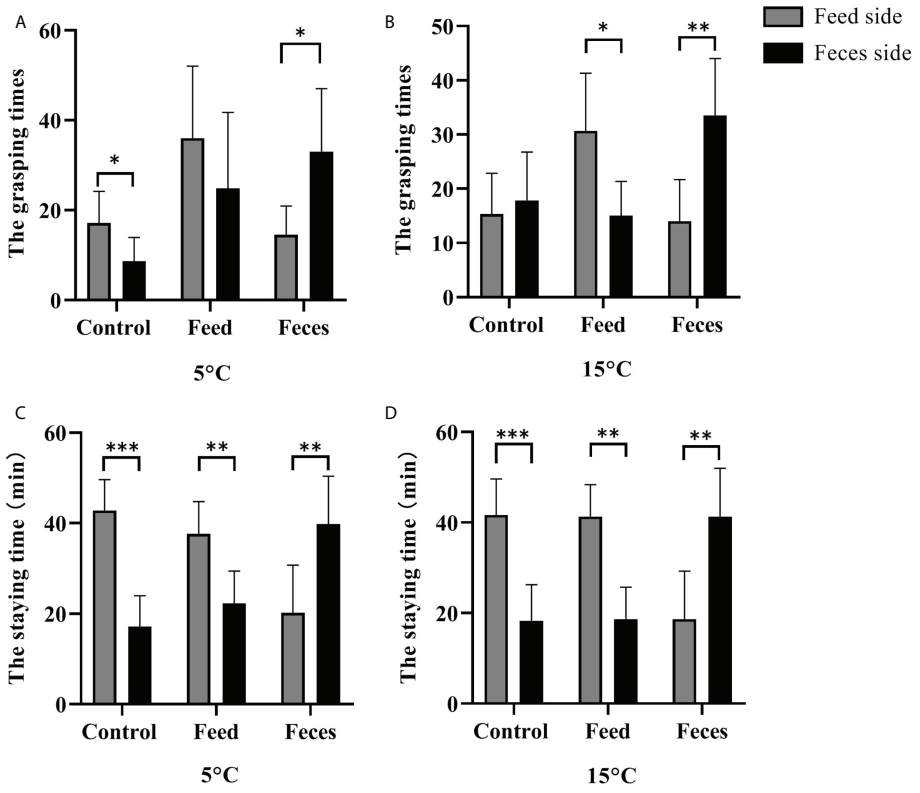

FIGURE 2
The grasping times of sea cucumbers in the feed side and the feces side at 5°C and at 15°C (mean ± SD, N = 6). The staying time of sea cucumbers in the feces side and the feed side at 5°C and at 15°C (mean ± SD, N = 6). Control, feed, and feces refer to groups C, S, and F, respectively. The asterisks *, ** and ***mean $P< 0.05$ and $P< 0.01$ and $P< 0.001$, respectively.

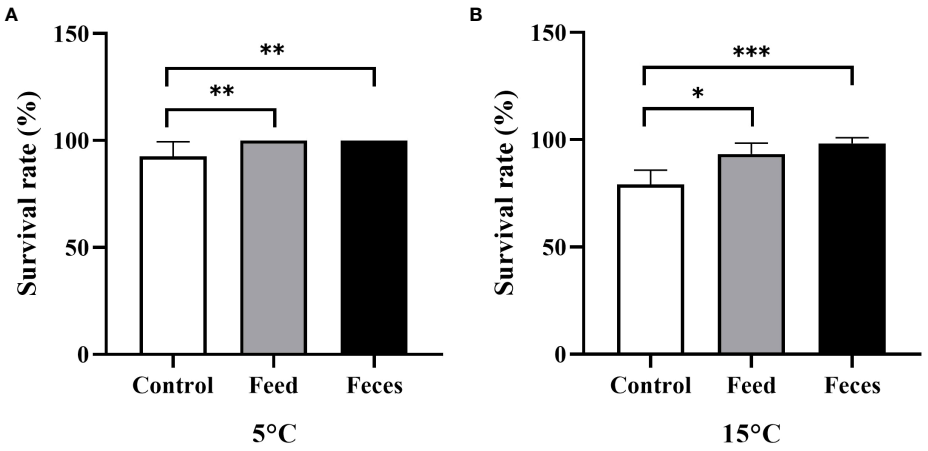

FIGURE 3
The survival rate of *Apostichopus japonicus* in the three groups at 5°C **(A)** and at 15°C **(B)** (mean ± SD, N = 6). Control, feed, and feces refer to groups C, S, and F, respectively. The asterisks *, ** and *** mean $P< 0.05$, $P< 0.01$ and $P< 0.001$, respectively.

sea cucumbers in group C at 5°C ($P = 0.002$). The WGR of group F (204.10 ± 33.99%) was significantly higher than that of group S (89.13 ± 15.50%, $P = 0.002$) and group C at 15°C (-15.28 ± 9.92%, $P = 0.002$; Figure 4). The WGR of group S was significantly higher than that of group C at 15°C ($P = 0.002$).

Microbial composition

At the water temperature of 15°C, small *A. japonicus* fed with feces had significantly higher OTUs ($P = 0.0495$) ACE estimator than those fed with feed ($P = 0.003$, $P = 0.024$). The sea cucumbers of group F had significantly lower Simpson index and significantly higher Shannon index ($P = 0.019$, $P = 0.025$) than those of sea cucumbers in group S. No significant difference of the Simpson index was found between groups S at 5°C and group F at 15°C ($P = 0.154$; Table. 1). No significant difference of the Good' s coverage was found between the two groups at 15°C ($P = 1.000$).

At the water temperature of 5°C, the sea cucumbers fed with feces had significantly higher OTUs ($P = 0.003$), and ACE estimator than those fed with feed ($P = 0.003$, $P = 0.002$). A significantly lower Shannon index and a significantly higher Simpson index were found in group S at 5°C ($P = 0.009$, $P = 0.012$) compared with group F at the same temperature (Table. 1). No significant difference of the Good' s coverage was found between the two groups at 5°C ($P = 1.000$; Table. 1).

Proteobacteria, Firmicutes, and Actinobacteria predominated in bacterial communities in the groups (Figure 5). Bacteroidetes,

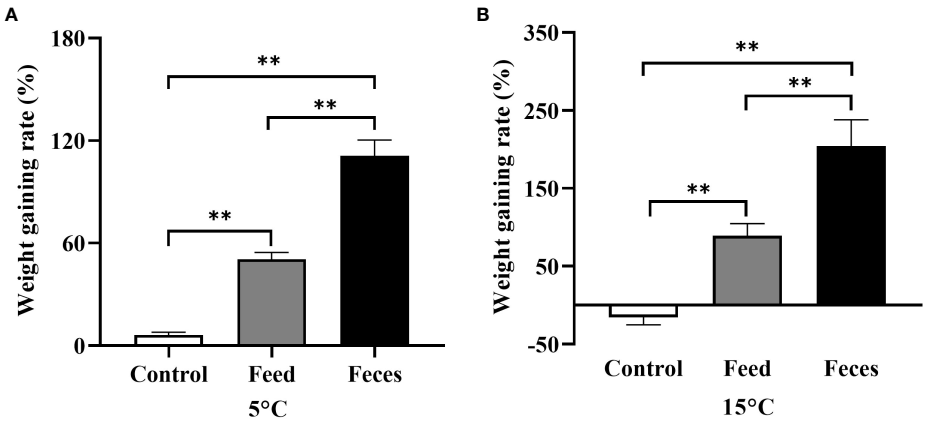

FIGURE 4
The weight gaining rate (WGR) of *Apostichopus japonicus* in the three groups at 5°C **(A)** and at 15°C **(B)** (mean ± SD, N = 6). Control, feed, and feces refer to groups C, S, and F, respectively. The asterisk ** means $P< 0.01$.

TABLE 1 Alpha diversity analysis based on operational taxonomic units (OTU) index for groups F and S at 15 and 5°C.

Sample	Operational Taxonomic Units	Community richness		Community diversity		Coverage
		Chao	Ace	Simpson	Shannon	
Group F at 15°C	774 ± 76.83^{a}	792.64 ± 77.74^{a}	784.43 ± 76.23^{a}	0.05 ± 0.02^{c}	4.49 ± 0.27^{a}	0.99
Group S at 15°C	609 ± 15.72^{b}	608.83 ± 22.54^{b}	611.14 ± 18.22^{b}	0.14 ± 0.00^{b}	3.12 ± 0.02^{bc}	0.99
Group F at 5°C	504 ± 28.62^{b}	506.16 ± 32.01^{bc}	503.35 ± 29.83^{b}	0.09 ± 0.03^{bc}	3.72 ± 0.52^{ab}	0.99
Group S at 5°C	346 ± 30.37^{c}	357.71 ± 34.39^{c}	348.82 ± 30.72^{c}	0.21 ± 0.02^{a}	2.63 ± 0.12^{c}	0.99

Different letters indicates significant differences among the four groups ($P< 0.05$).

Planctomycetes, Gemmatimonadetes, Parcubacteria, and Latescibacteria were the main phylum causing significant differences in between-group variance (Figure 6). Group F at 15°C had significantly higher Bacteroidetes count than group S at both 15°C and 5°C ($P = 0.028$, $P = 0.026$), and had no significant difference in *Bacteroidetes* count from group F at 5°C ($P = 0.114$; Figure 7).

PCA was performed to reveal the relationships among the different samples. Four groups were distinguished as follows: all the samples of group F and group S at 5°C, all the samples of group F and group S at 15°C (Figure 8). Group F and group S at the water temperature of 5°C were separated distinctly by the first principal component axis (PC1) ($P = 0.015$), which accounted for 12.24% of the total variations. Consistently, samples of group F and group S at 15°C were also separated distinctly by PC1 ($P = 0.002$). Furthermore, the second principal component axis (PC2) were accounted for 13.50% of the variance in the bacterial communities. Both the group F samples at 5°C and 15°C ($P = 0.049$) and both the group S samples at 5°C and 15°C were separated distinctly by PC2 ($P = 0.006$). Overall, the PC1 and PC2 axes explained 25.74% of the variations between the different bacterial communities.

Protease activity

Water temperature and diet significantly affected the protease activity ($F = 6.105$, $P< 0.001$; $F = 4.159$, $P< 0.001$). Sea cucumbers of group S had significantly lower intestine protease activity (511.53 ± 98.03 U mL protein) than those of group F (902.25 ± 36.70 U mL protein) at the water temperature of 5°C ($F = 9.232$, $t = 10.558$, $P< 0.001$; Figure 9A). The protease

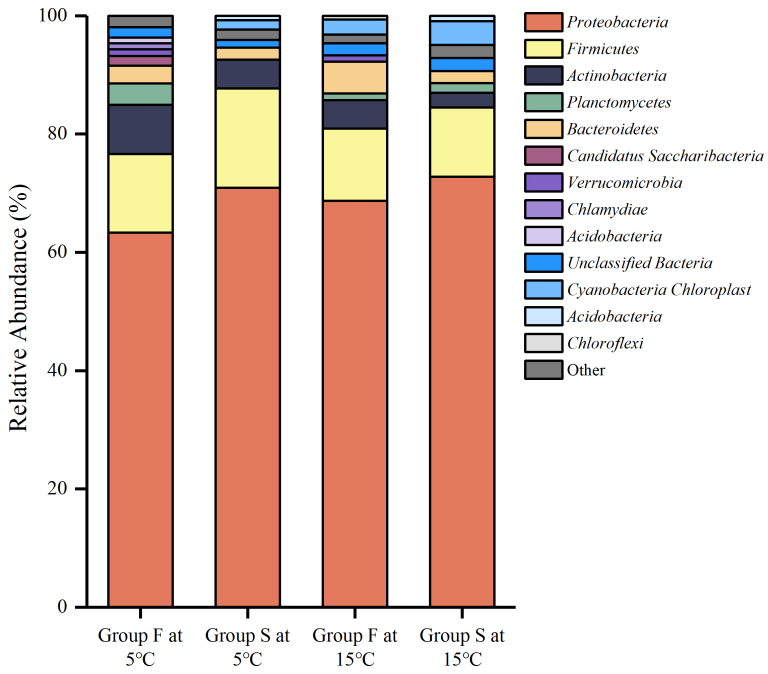

FIGURE 5
Relative abundance of phylum level bacterial communities in different samples.

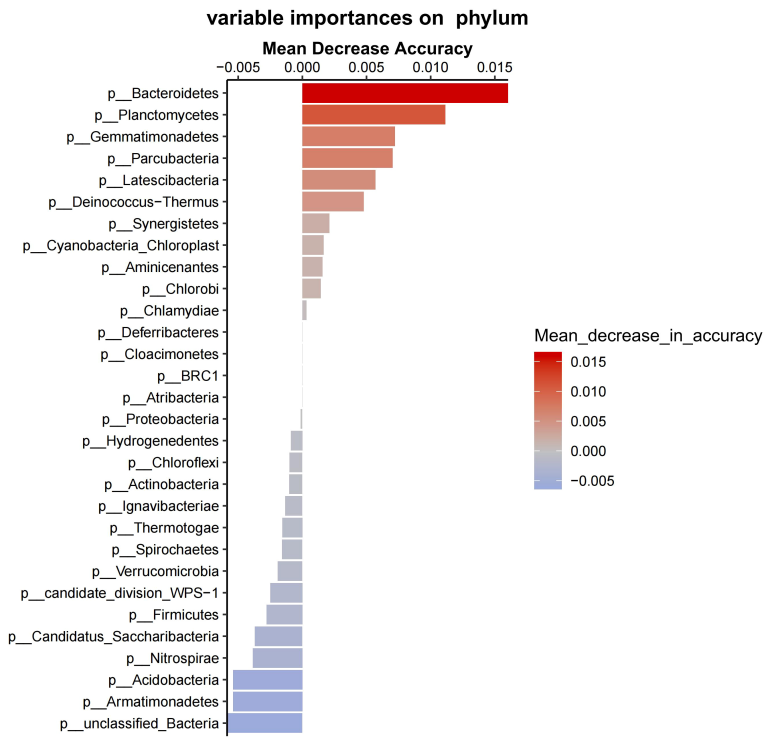

FIGURE 6
The contribution values of bacterial species to differences between groups. The left side shows the names of different phylum (p means phylum). The accuracy decreases from red to blue (see the right side).

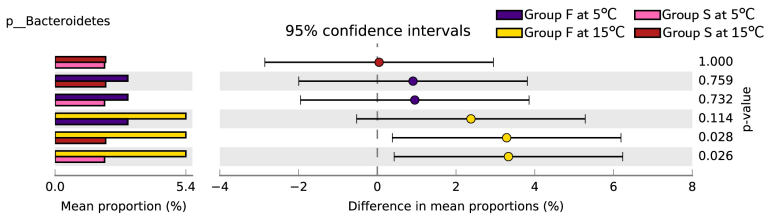

FIGURE 7
The *Post Hoc* analysis results of the abundance ratio of Bacteroidetes (phylum) in different groups. Different colors represent different groups (purple for group F at 5°C, pink for group S at 5°C; yellow for group F at 15°C, red for group S at 15°C). Proportion (left side) means a possible abundance of Bacteroidetes. Difference between proportions for each group is indicated by a dot (right side). The q-values are based on Welsh's t-test and corrected with Benjamini-Hochberg FDR (Phylum).

activity of sea cucumbers of group F (1199.82 ± 101.97 U mL protein) was significantly higher than that of sea cucumbers in group S (997.92 ± 64.76 U mL protein) at the water temperature of 15°C (F = 1.900, t = 4.728, P< 0.001; Figure 9B).

Acute salinity treatments

At the water temperature of 5°C, the survival rate of group F (84.38 ± 11.98%) was significantly higher than that of group C (34.38 ± 25.77%, P = 0.001) and that of group S (40.63 ± 6.25%, P = 0.001). No significant difference in survival rate was found between group S and group C (P = 0.742).

At the water temperature of 15°C, the survival rate of group F (87.50 ± 17.68%) was significantly higher than that of group S (43.75 ± 12.50%, P = 0.002) and that of group C (40.63 ± 6.25%, P = 0.005). No significant difference in survival rate was found between group S and group F (P = 0.611; Figure 10).

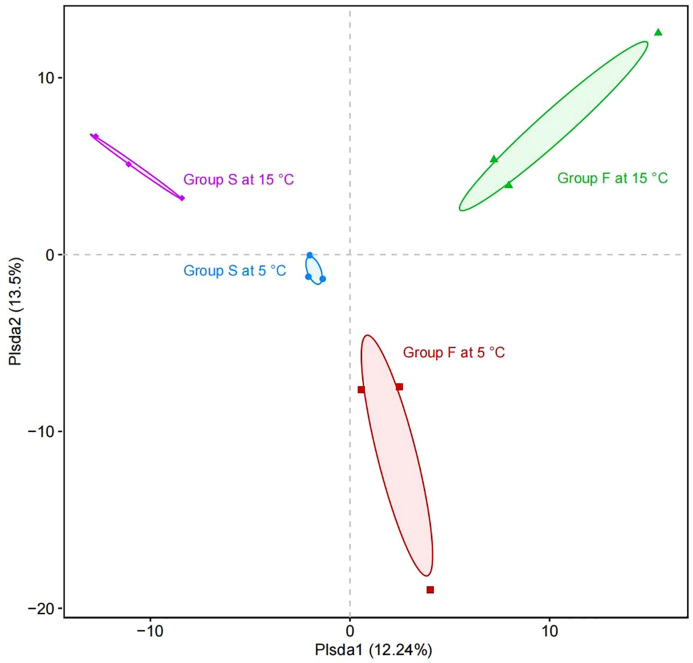

FIGURE 8
Principal coordinate analysis of the composition of microbial communities. The horizontal axis (PC1) and the vertical axis (PC2) represent the two selected principal component axes. The percentage represents the explanation value of the principal component to the difference in sample composition. Horizontal axis and vertical axis of the scale is the relative distance. Points with different colors or shapes represent the samples of different groups.

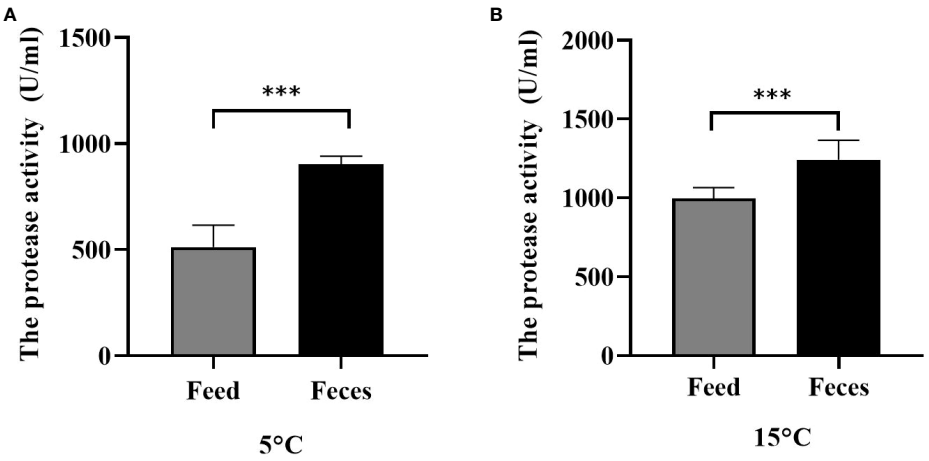

FIGURE 9
The enteral protease activity of *Apostichopus japonicus* at 5°C **(A)** and at 15°C **(B)** (mean ± SD, N = 3). Feed and feces refer to groups S and F, respectively. The asterisk *** means $P < 0.001$.

Discussion

Sea urchin feces is more attractive

Food preference experiment is a useful tool for assessing food usability (Roa, 1992). In the present study, sea cucumbers of group F significantly preferred the feces to the prepared feed at both 5°C and 15°C. However, the sea cucumbers not exposed to feces showed the preference to prepared feed than feces or had no significant preference to feed and feces. Food preference is affected by the nutritional and physiological requirements (Lyons & Scheibling, 2007) and digestive capabilities (Lowe & Lawrence, 1976) of echinoderms. With regular ingestion of natural fresh sea urchin feces that contains readily available live microorganisms, the sea cucumbers intestines possibly became colonized with customized microbial communities to further utilize the remaining nutrients in sea urchin feces (Jensen et al., 2018). Therefore, the feces probably better meets the requirements of digestion and thus is more attractive to small *A. japonicus* after a short period of aquaculture.

Sea urchin feces improves the survival and growth of *A. japonicus*

As an ectotherm, *A. japonicus* have low feeding efficiency, growth rate, and metabolism in winter (Chen, 2004). Sea cucumbers that were not fed had significant lower survival rate than those in groups F and S at 5°C. The present study suggests that failure to feed in winter is associated with the decreased survival rate. Sea cucumbers fed with food (feces or feed) had higher survival rate than that of sea cucumbers in group C at 15°C, which further proves that the potential relationship between death and long-term starvation of small sea cucumbers.

The sea cucumbers fed with the fecal diet had better growth performance than those fed with commercial feed at 15°C. A substantial portion of sea urchin feces is relatively unprocessed vegetative materials colonized by the microbial community (Peduzzi and Herndl, 1986; Yoon et al., 1996; Povero et al., 2003). The nutritional value of these highly digestible feces is probably higher than that of the original diets (Sauchyn and Scheibling, 2009). Consistently, more rapid growth was found in an epibenthic copepod *Tigriopus californicus* population fed with fecal diet (feces of sea urchins *Mesocentrotus franciscanus* and *Strongylocentrotus droebachiensis* who fed with bull kelp) than those fed with bull kelp (*Nereocystis luetkeana*) (Dethier et al., 2019).

Low water temperature greatly limits the physiological activities of *A. japonicus* (Yang et al., 2005; Yang et al., 2006; Liu et al., 2013). Hence, the aquaculture of small sea cucumbers suffers a great challenge in winter. *Apostichopus japonicus* generally starts dormancy at 5°C (Chen, 2004), resulting in feeding cessation, intestine atrophy, decrease of enzyme activity (Tanaka, 1958; Günay et al., 2020) and consequent poor growth (Sui, 1988). The present study found that fecal diet provided ~110% of weight gaining rate for *A. japonicus* (as twice as the feed diet). Therefore, as an environmentally friendly and cost-effective alternative food, the fecal diet is an efficient approach to improving the production efficiency of sea cucumbers at both the optimal growth temperature and low temperature.

Sea urchin feces enhances the intestinal microbial composition of *A. japonicus* (α-diversity and β-diversity)

Sea cucumbers do not have specialized physical grinding and chemical digestive organs (Massin, 1982), resulting in poor digestion ability (Yuan et al., 2006). Hence, their digestion and absorption ability highly depend on the intestinal microbiota

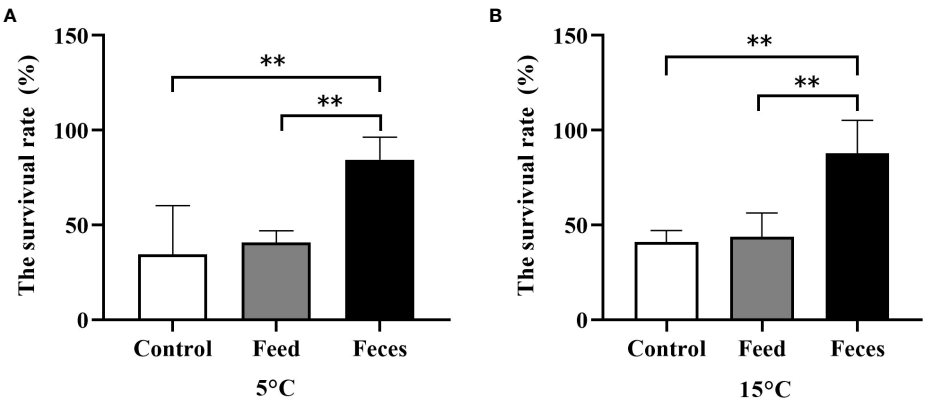

FIGURE 10
Survival rate of *Apostichopus japonicus* in three groups exposed to the acute salinity decrease treatments at 5°C **(A)** and at 15°C **(B)** (mean ± SD, N = 4). Control, feed, and feces refer to groups C, S, and F, respectively. The asterisk **means $P < 0.01$.

(Chang et al., 2004; Yang et al., 2004). Whether the diet enhances the intestinal microbial composition is thus important for consideration. In the present study, small *A. japonicus* fed with feces had significantly higher intestinal bacterial count than those in group S at 15°C, suggesting the fecal diet provides extra microbiota for small sea cucumbers. Since microbiota provides over 70% of energy requirement for *A. japonicus* (Yang et al., 2004), fecal diet probably provides a high energy supply for small sea cucumbers. Moreover, the intestinal samples of sea cucumbers fed with sea urchin feces showed significantly better community richness (Chao, ACE) and more community diversity (Shannon, Simpson) in intestinal bacteria than that of those that were fed with feed at the optimum temperature. This signifies that fecal diet enhances the intestinal microbial composition of *A. japonicus*, and thus has the potential to allow small sea cucumbers to achieve the optimal digestibility of nutrients (Wang et al., 2016) and enhance the resilience ability of small sea cucumbers (Li et al., 2009; Thompson et al., 2010).

Since probiotics in food would alter or enhance the digestive ability (Liu et al., 2009; Thompson et al., 2010; Jensen et al., 2018), probiotics is commonly used in aquaculture (Wang et al., 2016). Nevertheless, probiotics serving as allochthonous species showed no significant impact on the composition of fecal microbial community in humans (Bjerg et al., 2014; Hanifi et al., 2014; Laursen et al., 2017). In present study, however, α-diversity analysis of group F showed more OTUs, better community richness (Chao, ACE), and more community diversity (Shannon, Simpson) than that of group S at 5°C. A reasonable explanation is that fecal diet provides a complex microbial ecosystem rather than one or few probiotics. Our results indicate that the fecal diet significantly affects the function composition of the entire microbial community at both 15°C and 5°C. This is a promising method for colonization and regulation of intestinal bacteria. Therefore, the feces of sea urchins is a promising food to provide higher intestinal bacterial count for small *A. japonicus* and thus enhance the digestion ability of small *A. japonicus* at both the optimum and low water temperatures. In this way, the aquaculture efficiency is consequently improved.

The two groups fed with different diets at 5°C and two groups fed with different diets at 15°C were both separated by PC1. This suggests that the diet is the main factor leading to the separation of PC1, further proving the ability of transforming microbiome in the fecal diet. Moreover, the sea cucumbers fed with the same diet at different water temperatures were both separated by PC2, suggesting that water temperature is the main factor causing the separation of PC2 due to the reason that different temperatures create different bacterial predominance (Feng et al., 2021). The results of the PCA are consistent with the results of the community richness and community diversity analyses. These analyses indicate that the samples of different diets and water temperatures have different characteristic bacterial communities. The present study clearly indicates that fecal diet significantly influences the intestinal bacteria of sea cucumbers. Similar phenomenon has been documented in a variety of species, indicating that intestinal bacteria shaping mechanisms are evolutionarily conserved (Wilson et al., 2020; Haditomo et al., 2021).

The majority of isolates were affiliated to the phyla Proteobacteria and Firmicutes, according to the molecular identification using 16S rRNA gene sequences. Proteobacteria is the keystone microbe phylum and the main metabolically active microbial populations in the intestine of *A. japonicus* (Zhang et al., 2012). Allochthonous species could not take dominance in the microbial community (Bjerg et al., 2014; Laursen et al., 2017; Toscano et al., 2017), suggesting that the fecal diet did not enhance the intestinal microbial composition by changing the main dominant colonizing bacteria.

Furthermore, random forest predicted that Bacteroidetes, Planctomycetes, Gemmatimonadetes, Parcubacteria, and Latescibacteria contribute to the uniquely separated microbial ecology in the intestine ecosystem of *A. japonicus*, which were the main phylum causing significant differences between group variance. Bacteroidetes was the keystone microbe phylum in the intestines of sea urchins, while Planctomycetes was identified in sea urchins fed with macroalgae (Masasa et al., 2021). The finding that Bacteroidetes has significant higher proportion in group F at 15°C than group S at both 15°C and 5°C directly shows that sea cucumbers of group F inherited the intestinal bacteria of sea urchins. Therefore, the fecal diet enhances the intestinal microbial composition of *A. japonicus* through additional supply of bacteria.

Sea urchin feces improves the protease activity of *A. japonicus*

Digestion activity is an important indicator for reflecting the nutritional requirements, dietary preference (Boetius & Felbeck, 1995), and digestive physiology of *A. japonicus* (Yang et al., 2004; Wang et al., 2016). Digestive enzyme activity is closely related to the quality and quantity of nutrients in food (Lee et al., 1984; Wu et al., 2003; Wen et al., 2016). Protease is the most active digestive enzyme in intestine of *A. japonicus* (Fu, 2004; Jiang et al., 2007). The seasonal pattern of protease activity is that the lowest concentration levels occur in winter, while the highest concentration levels occur at ~15°C (Fu, 2004; Günay et al., 2020). The present study surprisingly found a significantly higher protease activity in sea cucumbers fed with sea urchin feces than that in sea cucumbers in the group S at 5°C. Consistently, the feces significantly improved the growth rate

of sea cucumbers at 5°C. This suggests that the feces is not only a valuable food for small sea cucumbers at low temperature, but also an appropriate diet to enhance the enzyme activity and consequently enhance the digestion ability of sea cucumbers in winter. We here encourage aqua-farmers to use the feces as the diet for small *A. japonicus* without heating the water to achieve appropriate growth, which can reduce economic and environmental costs in winter.

Furthermore, the present study found that sea cucumbers fed with feces had significantly higher intestine protease activity than those of group S at 15°C. It is probably because of the presence of intestinal enzymes of sea urchin feces, which enhances the intestine enzyme activity of sea cucumbers (Mamelona & E´milien, 2005). It can be further explained by the entry of viable bacteria from feces to the intestine of small sea cucumbers, which improves digestive enzyme activities (Sauchyn and Scheibling; 2009); Wang et al., 2016). The opinion is well supported by the result that the better protease activity and the better intestinal microbial composition of *A. japonicus* (α-diversity and β-diversity) were found in the samples of group F. A higher protease activity reflects a better digestion ability of *A. japonicus* (Yang et al., 2004; Li, 2013), further proving the feasibility and high developing value of the fecal diet in sea cucumber aquaculture. Considering that enzyme activity is the highest at the optimum temperature for growth and that fecal diet would further increase the growth advantage in this period, we recommend feeding small sea cucumbers with the feces of sea urchins to provide extra digestive benefits at the optimum temperature. Consistently, sea cucumbers had significantly higher growth rate in group F than those of group S at 15°C. This suggests that sea urchin feces probably better meets the need of *A. japonicus* and results in direct growth benefits for sea cucumbers. Therefore, we recommend that aqua-farmers feed small sea cucumbers with fecal diet to achieve better digestion and growth at the optimal temperature.

Sea urchin feces is an appropriate diet for better resistance to low salinity

Intestinal microbiota plays an important role in the host health because an external organ partakes in nutritional metabolism and affects immunity development of the host (O'Hara and Shanahan, 2006; Wang et al., 2019). Bacterial composition can be affected by environmental and dietary factors (Marques et al., 2010; Zhang et al., 2019). Accordingly, regulating intestinal microbiota is an effective method to improve the health of farmed animals (Chauhan and Singh, 2018). Fecal diet has the potential in aquaculture due to its benefit on homeostasis of intestinal microbiota. Sea cucumber aquaculture continuously expands with the increase of market demands and the decrease of natural resources (Jiang et al., 2017; Li & Hu, 2017; Ciji & Akhtar, 2021). However, the expansion is greatly limited because of the salinity requirements for the survival of *A. japonicus* (Zhang et al., 2004; Su et al., 2014). In the present study, we found that sea cucumbers fed with sea urchin feces had the highest survival rate among the three groups in exposure to acute salinity decrease at both 15°C and 5°C, indicating a better resistance to low salinity. This novel finding provides a new perspective for the geographical expansion of *A. japonicus* aquaculture to low salinity areas.

Data availability statement

The datasets presented in this study can be found in online repositories. The data presented in the study are deposited in the NCBI repository, accession number PRJNA859421.

Author contributions

CZ and YY did the investigation, conceived and designed the experiment. YY, YQ, PD, RT, FH, GW performed the experiment. YY, JS performed statistical analysis and visualization. YY, CZ wrote the first draft of the manuscript. CZ reviewed and edited the manuscript. YC provided resources for this study. All authors have read and agreed to the published version of the manuscript.

Funding

This work was funded by the National Natural Science Foundation of China (41506177), a research project for marine economy development in Liaoning province (for Jun Ding), High-level talent support grant for innovation in Dalian (2020RD03), and Liaoning Province "Xingliao Talents Plan" project (XLYC2002107).

Acknowledgments

We appreciate Wei Tang for editorial suggestions.

Conflict of interest

The authors declare that the research was conducted in the absence of any commercial or financial relationships that could be construed as a potential conflict of interest.

Publisher's note

References

An, Z., Dong, Y., and Dong, S. (2007). Temperature effects on growth-ration relationships of juvenile sea cucumber *Apostichopus japonicus* (Selenka). *Aquaculture* 27 (2), 644–648. doi: 10.1016/j.aquaculture.2007.08.038

Bjerg, A. T., Sørensen, M., Krych, L., Hansen, L. H., Astrup, A., Kristensen, M., et al. (2014). The effect of *Lactobacillus paracasei* subsp. *paracasei* L. casei W8® on blood levels of triacylglycerol is independent of colonisation. *Benef. Microbes* 6, 263–269. doi: 10.3920/BM2014.0033

Boetius, A., and Felbeck, H. (1995). Digestive enzymes in marine-invertebrates from hydrothermal vents and other reducing environments. *Mar. Biol.* 122 (1), 105–113. doi: 10.1007/BF00349283

Chang, Y., Yu, C., and Song, X. (2004). "Pond culture of sea cucumbers, apostichopus japonicus, in dalian," in *Advances in Sea cucumber aquaculture and management*. Eds. A. Lovatelli, C. Conand, S. Purcell, S. Uthicke, J. Hamel and A. Mercier (Rome: FAO), 269–272. (In Chinese)

Chauhan, A., and Singh, R. (2018). Probiotics in aquaculture: A promising emerging alternative approach. *Symbiosis* 77, 99–113. doi: 10.1007/s13199-018-0580-1

Chen, J. (2003). Overview of sea cucumber farming and sea ranching practices in China. *SPC beche-de-mer Inf. Bull.* 18, 18–23.

Chen, J. (2004). "Present status and prospects of sea cucumber industry in China," in *Advances in Sea cucumber aquaculture and management*. Eds. A. Lovatelli, C. Conand, S. Purcell, S. Uthicke, J. Hamel and A. Mercier (Rome: FAO), 25–38.

Ciji, A., and Akhtar, M. (2021). Stress management in aquaculture: A review of dietary interventions. *Rev. Aquacult.* 13 (4), 2190–2247. doi: 10.1111/raq.12565

Dethier, M., Hoins, G., Kobelt, J., Lowed, A., Gallowaye, A., Schrame, J., et al. (2019). Feces as food: The nutritional value of urchin feces and implications for benthic food webs. *J. Exp. Mar. Biol. Ecol.* 514, 95–102. doi: 10.1016/j.jembe.2019.03.016

Feng, J., Zhang, L., Tang, X., Xia, X., Hu, W., and Zhou, P. (2021). Season and geography induced variation in sea cucumber (*Stichopus japonicus*) nutritional composition and gut microbiota. *J. Food Composit. Anal.* 101, 103838. doi: 10.1016/j.jfca.2021.103838

Frankenberg, D., and Smith, K. (1967). Coprophagy in marine animals. *Limnol. Oceanogr.* 12, 443–450. doi: 10.4319/lo.1967.12.3.0443

Fu, X. (2004). *Study of protease from digestive tract of sea cucumber (*Stichopus japonicus*). [Master's thesis]* (Qingdao: Ocean Univ. of China).

Gao, F., Yang, H., Xu, Q., Wang, F., and Wu, G. (2009). Effect of water temperature on digestive enzyme activity and intestine mass in sea cucumber *Apostichopus japonicus* (Selenka), with special reference to aestivation. *Chin. J. Ocean. Limnol.* 27 (4), 714–722. doi: 10.1007/s00343-009-9202-3

González, H., and Biddanda, B. (1990). Microbial transformation of metazoan (*Idotea granulosa*) feces. *Mar. Biol.* 106, 285–295. doi: 10.1007/bf01314812

Günay, D., Emiroğlu, D., and Suzer, C. (2020). Seasonal variations of digestive enzymes in sea cucumbers (*Holothuria tubulosa*, G) under culture conditions. *J. Exp. Zool. Part A.* 333 (3), 144–150. doi: 10.1002/jez.2336

Haditomo, A. H. C., Yonezawa, M., Yu, J., Mino, S., Sakai, Y., and Sawabe, T. (2021). The structure and function of gut microbiomes of two species of sea urchins, *Mesocentrotus nudus* and *Strongylocentrotus intermedius*, in japan. front. *Mar. Sci.* 8. doi: 10.3389/fmars.2021.802754

Hair, C., Pickering, T., and Mill, D. (2012). *Asia-Pacific tropical sea cucumber aquaculture, proceedings of an international symposium held in noumea, new Caledonia, 15–17 februar* (Noumea, New Caledonia: Australian centre for international agricultural research), 209 pp.

Hanifi, A., Culpepper, T., Mai, V., Anand, A., Ford, A., Ukhanova, M., et al. (2014). Evaluation of *Bacillus subtilis* R0179 on gastrointestinal viability and general wellness: A randomised, double-blind, placebo-controlled trial in healthy adults. *Benefic. Microbes* 6, 19–27. doi: 10.3920/BM2014.0031

Han, Q., Keesing, J., and Liu, D. (2016). A review of sea cucumber aquaculture, ranching, and stock enhancement in China. *Rev. Fish. Sci. Aquac.* 24 (4), 326–341. doi: 10.1080/23308249.2016.1193472

Jensen, K. E., Taylor, J. C., Barry, R. J., D'Abramo, L., Davis, D., and Watts, S. (2018). The value of sea urchin, *Lytechinus variegatus*, egesta consumed by shrimp, *Litopenaeus vannamei*. *J. World Aquacult. Soc.* 50 (3), 614–621. doi: 10.1111/jwas.12578

Jiang, S., Ren, Y., Tang, B., Li, C., and Jiang, C. (2017). Development status and countermeasures of *Apostichopus japonicus* culture industry in China. *J. Agr. Sci. Tech-Iran* 19 (9), 15–23. doi: 10.13304/j.nykjdb.2017.0202

Jiang, L., Yang, N., Wang, W., Wang, R., and Lu, J. (2007). Effects of temperature and pH on the activities of digestive enzyme in *Apostichopus japonicus*. *Oceanol. Limnol. Sin.* 38 (5), 476–480. (In Chinese with an English abtract)

Laursen, M. F., Laursen, R. P., Larnkjær, A., Michaelsen, K. F., Bahl, M. I., and Licht, T. R. (2017). Administration of two probiotic strains during early childhood does not affect the endogenous gut microbiota composition despite probiotic proliferation. *BMC Microbiol.* 17, 175. doi: 10.1186/s12866-017-1090-7

Lee, P., Smith, L., and Lawrence, A. (1984). Digestive proteases of *Penaeus vannamei* Boone, relationship between enzyme activity, size and diet. *Aquaculture.* 42 (3–4), 225–239. doi: 10.1016/0044-8486(84)90103-0

Li, X. (2013). *Researches on selecting feedstuff and dietary protein requirement of juvenile Apostichopus japonicus. [Master's thesis]* (Yangzhou: Yangzhou University).

Li, C., and Hu, W. (2017). Status, trend and countermeasure in development of sea cucumber *Apostichopus japonicus* selenka industry in China. *Mar. Econo. China* 3, 3–20. (In Chinese with an English abstract)

Li, J., Tan, B., and Mai, K. (2009). Dietary probiotic *Bacillus* OJ and isomaltooligosaccharides influence the intestine microbial populations, immune responses and resistance to white spot syndrome virus in shrimp (*Litopenaeus vannamei*). *Aquaculture* 291, 35–40. doi: 10.1016/j.aquaculture.2009.03.005

Liu, Q. (2015). Characteristics and controlling of water quality during sea cucumber cultivation in the yellow river delta. *Hebei Fisheries* 3, 11–13. (In Chinese with an English abstract)

Liu, C., Chiu, C., Ho, P., and Wang, S. (2009). Improvement in the growth performance of white shrimp *Litopenaeus vannamei*, by a protease-producing probiotic, *Bacillus subtilis E20*, from natto. *J. Appl. Microbiol.* 107, 1031–1041. doi: 10.1111/j.1365-2672.2009.04284.x

Liu, L., Wang, A., Wang, Y., Du, R., and Yang, X. (2013). Influence of temperature and body weight on the emptying time of digestive duct and feces quantity of *Apostichopus japonicus* (Selenka). *Mar. Sci.* 37 (9), 43–48. (In Chinese with an English abstract)

Lowe, E., and Lawrence, J. (1976). Absorption efficiencies of *Lytechinus variegatus* (Lamarch) (Echinadermata, echinoidea) for selected marine plants. *J. Exp. Mar. Biol. Ecol.* 21, 223–234. doi: 10.1016/0022-0981(76)90117-9

Lyons, D., and Scheibling, R. (2007). Effect of dietary history and algal traits on feeding rate and food preference in the green sea urchin *Strongylocentrotus droebachiensis*. *J. Exp. Mar. Biol. Ecol.* 349, 194–204. doi: 10.1016/j.jembe.2007.05.012

Mamelona, J., and E´milien, P. (2005). Green urchin as a significant source of fecal particulate organic matter within nearshore benthic ecosystems. *Exp. Mar. Biol. Ecol.* 314 (2), 163–174. doi: 10.1016/j.jembe.2004.08.026

Marques, T. M., Wall, R., Ross, R. P., Fitzgerald, G. F., Ryan, C. A., and Stanton, C. (2010). Programming infant gut microbiota: Influence of dietary and environmental factors. *Curr. Opin. Biotech.* 21, 149–156. doi: 10.1016/j.copbio.2010.03.020

Masasa, M., Kushmaro, A., Kramarsky-Winter, E., Shpigel, M., Barkan, R., Golberg, A., et al. (2021). Mono-specific algal diets shape microbial networking in the gut of the sea urchin *Tripneustes gratilla elatensis*. *Anim. microbiome* 3 (1), 1–21. doi: 10.1186/s42523-021-00140-1

Massin, C. (1982). "Echinoderm nutrition," in *Food and feeding mechanisms: Holothuroidea*. Eds. M. Jangou and J. Lawrence(Rotterdam: Balkema Publ), 43–53.

Moss, S., Divakaran, S., and Kim, B. (2001). Stimulating effects of pond water on digestive enzyme activity in the pacific white shrimp *Litopenaeus vannamei* (Boone). *Aquac. Res.* 32, 125–131. doi: 10.1046/j.1365-2109.2001.00540.x

Newell, R. (1965). The role of detritus in the nutrition of two marine deposit feeders, the prosobranch *Hydrobia ulvae* and the bivalve *Macoma balthica*. *Proc. Zool. Soc Lond* 144, 25–45. doi: 10.1111/j.1469-7998.1965.tb05164.x

O'Hara, A. M., and Shanahan, F. (2006). The gut flora as a forgotten organ. *EMBO Rep.* 7, 688–693. doi: 10.1038/sj.embor.7400731

Peduzzi, P., and Herndl, G. (1986). Role of bacteria in decomposition of fecal pellets egested by the epiphyte grazing gastropod *Gibbula umbilicaris*. *Mar. Biol.* 92, 417–424. doi: 10.1007/BF00392682

Povero, P., Misic, C., Ossola, C., Castellano, M., and Fabiano, M. (2003). The trophic role and ecological implications of oval faecal pellets in Terra Nova bay (Ross Sea). *Polar. Biol.* 26, 302–310. doi: 10.1007/s00300-003-0485-0

Roa, R. (1992). Design and analysis of multiple-choice feeding-preference experiments. *Oecologia* 89, 509–515. doi: 10.1007/BF00317157

Robertson, D. (1982). Fish feces as fish food on a pacific coral reef. *Mar. Ecol. Prog. Ser.* 7, 253–265. doi: 10.3354/meps007253

Sauchyn, L., and Scheibling, R. (2009). Degradation of sea urchin feces in a rocky subtidal ecosystem: Implications for nutrient cycling and energy flow. *Aquac. Biol.* 6 (3), 99–108. doi: 10.3354/ab00171

Sui, X. (1988). *Culture and enhance of sea cucumber* (Beijing: China agriculture publishing house), 14–56. (In Chinese)

Su, L., Zhou, C., Hu, L., and Xu, J. (2014). Development status and sustainable development of *Apostichopus japonicus* industry in South China. *Fish. Sci. Tech. Info.* 41 (2), 57–60. (In Chinese with an English abstract)

Tanaka, Y. (1958). Feeding and digestive processes of *Stichopus japonicus*. *Bull. Faculty Fisheries Hokkaido Univ.* 9, 14–28.

Thompson, J., Gregory, S., Plummer, S., Shields, R. J., and Rowley, A. F. (2010). An *in vitro* and *in vivo* assessment of the potential of *Vibrio* spp. as probiotics for the pacific white shrimp, *Litopenaeus vannamei*. *J. Appl. Microbiol.* 109 (4), 1177–1187. doi: 10.1111/j.1365-2672.2010.04743.x

Thor, P., Dam, H., and Rogers, D. (2003). Fate of organic carbon released from decomposing copepod fecal pellets in relation to bacterial production and ectoenzymatic activity. *Aquat. Microb. Ecol.* 33, 279–288. doi: 10.3354/ame033279

Toscano, M., De Grandi, R., Stronati, L., De Vecchi, E., and Drago, L. (2017). Effect of *Lactobacillus rhamnosus* HN001 and *Bifidobacterium longum* BB536 on the healthy gut microbiota composition at phyla and species level: A preliminary study. *World J. Gastroenterol.* 23, 2696. doi: 10.3748/wjg.v23.i15.2696

Wang, X. (2015). *The effect of microorganism-treated laminaria japonica feedstuff on the growth and immunity of* Apostichopus japonicus. *[Doctor thesis]* (Dalian: Dalian University of Technology).

Wang, J., Guo, H., Zhang, T., Wang, H., Liu, B., and Xiao, S. (2016). Growth performance and digestion improvement of juvenile sea cucumber *Apostichopus japonicus* fed by solid-state fermentation diet. *Aquac. Nutr.* 23 (6), 1312–1318. doi: 10.1111/anu.12506

Wang, Q., Zhang, X., Chen, M., and Zhang, P. (2018). Comparison of intestinal microbiota and activities of digestive and immune-related enzymes of sea cucumber *Apostichopus japonicus* in two habitats. *Chin. J. Oceanol. Limn.* 36 (3), 990–1001. doi: 10.1007/s00343-018-7075-z

Wang, C., Zhou, Y., Lv, D., Ge, Y., Li, H., and You, Y. (2019). Change in the intestinal bacterial community structure associated with environmental microorganisms during the growth of eriocheir sinensis. *Microbiol. Open* 8, e727. doi: 10.1002/mbo3.727

Wen, B., Gao, Q., Dong, S., Hou, Y., Yu, H., and Li, W. (2016). Effect of dietary inclusion of benthic matter on feed utilization, digestive and immune enzyme activities of sea cucumber *Apostichopus japonicus* (Selenka). *Aquaculture* 458 (1), 1–7. doi: 10.1016/j.aquaculture.2016.01.028

Wilson, A., Koller, K. R., Ramaboli, M. C., Nesengani, L. T., Ocvirk, S., Chen, C., et al. (2020). Diet and the human gut microbiome: An international review. *Dig. Dis. Sci.* 65, 723–740. doi: 10.1007/s10620-020-06112-w

Wu, Y., Sun, J., Zhou, Z., and Gui, Y. (2003). The effects of dietary protein levels on the growth and activities of digestive enzymes in shrimp, *Penaeus chinensis*. *J. Dalian Ocean Univ.* 18 (4), 258–262. doi: 10.16535/j.cnki.dlhyxb.2003.04.005

Yang, G., Tian, X., Dong, S., Peng, M., and Wang, D. (2015). Effects of dietary *Bacillus cereus* G19, *B. cereus* BC-01 and *Paracoccus marcusii* DB11 supplementation on the growth, immune response, and expression of immune-related genes in coelomocytes and intestine of the sea cucumber (*Apostichopus japonicus selenka*). *Fish shellfish Immun.* 45, 800–807. doi: 10.1016/j.fsi.2015.05.032

Yang, H., Yuan, X., Zhou, Y., Mao, Y., Zhang, T., and Liu, Y. (2005). Effects of body size and water temperature on food consumption and growth in the sea cucumber *Apostichopus japonicus* (Selenka) with special reference to aestivation. *Aquac. Res.* 36 (11), 1085–1092. doi: 10.1111/j.1365-2109.2005.01325.x

Yang, H., Zhou, Y., and Zhang, T. (2004). "Biology of *Stichopus japonicus*--Theory and practice," (Beijing: Science Press). (in Chinese).

Yang, H., Zhou, Y., Zhang, T., Yuan, X., Li, X., Liu, Y., et al. (2006). Metabolic characteristics of sea cucumber *Apostichopus japonicus* (Selenka) during aestivation. *J. Exp. Mar. Biol. Ecol.* 330, 505–510. doi: 10.1016/j.jembe.2005.09.010

Yoon, W., Marty, C., Sylvain, D., and Nival, P. (1996). Degradation of faecal pellets in *Pegea confoederata* (Salpidae, thaliacea) and its implication in the vertical flux of organic matter. *Exp. Mar. Biol. Ecol.* 203, 147–177. doi: 10.1016/0022-0981(95)02521-9

Yuan, X., Yang, H., Wang, L., Zhou, Y., and Gabr, H. (2010). Effects of salinity on energy budget in pond cultured sea cucumber *Apostichopus japonicus* (Selenka) (Echinodermata: Holothuroidea). *Aquaculture* 306, 348–351. doi: 10.1016/S1872-2032(07)60070-5

Yuan, X., Yang, H., Zhou, Y., Mao, Y., Zhang, T., and Liu, Y. (2006). The influence of diets containing dried bivalve feces and/or powdered algae on growth and energy distribution in sea cucumber *Apostichopus japonicus* (Selenka) (Echinodermata: Holothuroidea). *Aquaculture* 256, 457–467. doi: 10.1016/j.aquaculture.2006.01.029

Yu, Y., Sun, J., Zhao, Z., Ding, P., Yang, M., Qiao, Y., et al. (2022). Effects of water temperature, age of feces, light intensity and shelter on the consumption of sea urchin feces by the sea cucumber *Apostichopus japonicus*. *Aquaculture* 554, 738134. doi: 10.1016/j.aquaculture.2022.738134

Zeng, F., Rabbi, M., Hu, Y., Li, Z., Ren, X., Han, Y., et al. (2021). Synergistic effects of dietary selenomethionine and vitamin c on the immunity, antioxidant status, and intestinal microbiota in sea cucumber (Apostichopus japonicus). *Biol. Trace Elem. Res.* 199 (10), 3905–3917. doi: 10.1007/s12011-020-02483-3Figurelegends

Zhang, X., Nakahara, T., Miyazaki, M., Nogi, Y., Taniyama, S., Arakawa, O., et al. (2012). Diversity and function of aerobic culturable bacteria in the intestine of the sea cucumber *Holothuria leucospilota*. *J. Gen. Appl. Microbiol.* 58 (6), 447–456. doi: 10.1080/09583157.2012.735223

Zhang, L., Song, X., Hamel, J., Mercier, A., et al. (2015). "Aquaculture, stock enhancement, and restocking," in *The Sea cucumber* Apostichopus japonicus. *history, biology and aquaculture*. Eds. (Salt Lake City, UT: Academic Press (Elsevier), 289–322.

Zhang, Z., Zhang, W., Hu, Z., Li, C., Shao, Y., Zhao, X., et al. (2019). Environmental factors promote pathogen-induced skin ulceration syndrome outbreak by readjusting the hindgut microbiome of *Apostichopus japonicus*. *Aquaculture* 507, 155–163. doi: 10.1016/j.aquaculture.2019.03.054

Zhang, S., Zhang, X., Liu, Z., and Sun, A. (2004). The test on the range of adaptation of the sea cucumbers *Apostichopus japonicus* to salinity. *Shandong Fish* 21 (12), 9–10. (In Chinese)

frontiers | Frontiers in Marine Science

TYPE Original Research
PUBLISHED 26 October 2022
DOI 10.3389/fmars.2022.1029147

OPEN ACCESS

EDITED BY
Chenghua Li,
Ningbo University, China

REVIEWED BY
Qiang Xu,
Hainan University, China
Carlos Rosas,
National Autonomous University of Mexico, Mexico

*CORRESPONDENCE
Viviana Pasquini
viviana.pasquini@unica.it

†These authors have contributed equally to this work

SPECIALTY SECTION
This article was submitted to Marine Biology, a section of the journal Frontiers in Marine Science

RECEIVED 26 August 2022
ACCEPTED 06 October 2022
PUBLISHED 26 October 2022

CITATION
Pasquini V, Porcu C, Marongiu MF, Follesa MC, Giglioli AA and Addis P (2022) New insights upon the reproductive biology of the sea cucumber *Holothuria tubulosa* (Echinodermata, Holothuroidea) in the Mediterranean: Implications for management and domestication. *Front. Mar. Sci.* 9:1029147. doi: 10.3389/fmars.2022.1029147

New insights upon the reproductive biology of the sea cucumber *Holothuria tubulosa* (Echinodermata, Holothuroidea) in the Mediterranean: Implications for management and domestication

Viviana Pasquini*†, Cristina Porcu†, Martina Francesca Marongiu, Maria Cristina Follesa, Ambra Angelica Giglioli and Pierantonio Addis

Department of Life and Environmental Sciences, University of Cagliari, Cagliari, Italy

Holothuria tubulosa is one of the most common sea cucumber species inhabiting the Mediterranean Sea. Due to its commercial interest for the international market, it has been harvested without proper management causing the overexploitation of its stocks. Inadequate management is also caused by lack of information on basic biology and ecology not allowing the estimating of the species vulnerability and resilience to growing anthropogenic pressures. In this paper, we have investigated basic life-history traits of *H. tubulosa* (population structure and reproductive cycle) in a population of Central-Western Mediterranean (Sardinia, Italy). A macroscopic maturity scale for both sexes was defined through an instrumental colorimetric analysis of the gonads and the ramification level of the gonad's tubules, subsequently confirmed by histological analysis. The seasonal trend of the Gonado-Somatic Index, the changes in color of the gonads and tubules ramification indicated that the spawning period of *H. tubulosa* was concentrated in summer with a peak in late August, closely related to the increase in water temperature. A synchronous development of the gonads, with a unique and short reproductive event during the year, was also detected. In conclusion, this study provides new evidence on the biological and ecological features of *H. tubulosa*, essential data for developing a scientifically-based stock assessment as well as conservative management at a local scale. Finally, we provided basic information for the domestication of broodstock in a conservative hatchery.

KEYWORDS

sea cucumber, *Holothuria tubulosa*, maturity scale, histology, spawning cycle, Mediterranean Sea

1 Introduction

Holothurians, known as sea cucumbers, are common benthic marine invertebrates belonging to the Phylum Echinodermata, Class Holothurioidea, represented by more than 1500 species worldwide (Horton et al., 2018). Most sea cucumbers are strong deposit-feeder bioturbators and, as such, are thought to play a key ecological role in benthic biogeochemistry (Roberts et al., 2000; Uthicke, 2001; Mangion et al., 2004; Amaro et al., 2010; Purcell et al., 2016; Neofitou et al., 2019).

Sea cucumbers are part of the culinary culture of Eastern Asian countries and are largely used in traditional Chinese medicine (Yang and Bai, 2015; Yang et al., 2015). They are a valuable source of bioactive compounds used in the pharmaceutical and cosmetic industry and are also considered a gourmet seafood called *trepang* or *bèche de mer* (Kinch et al., 2008; Bordbar et al., 2011; Purcell et al., 2012; Janakiram et al., 2015; Yang and Bai, 2015; Hame at al., 2022). The high cost of *trepang* (generally between 50 to 600 US$ dry kg^{-1}) (Purcell et al., 2012; Ram et al., 2014; Purcell, 2014), and the numerous medical applications of sea cucumbers, led to the overexploitation of most of the Indo-Pacific species (Lovatelli et al., 2004; Conand, 2006; Choo, 2008; Purcell et al., 2011; Conand et al., 2014). In response to the market demand, the fishery of sea cucumbers have shifted to new target species as the Mediterranean ones (González-Wangüemert et al., 2014; González-Wangüemert et al., 2018). In many cases, the sea cucumber harvesting increased without an adequate management, which, coupled with the illegal catches, caused the collapse of several stocks (Toral-Granda et al., 2008; Anderson et al., 2011; Purcell, 2014, González-Wangüemert et al., 2018; Ramírez-González et al., 2020a). One of the main causes of the failure of sea cucumber management can also be a reflection of severe knowledge gaps on basic biological and ecological attributes, and their reproductive biology. Then again, the current lack of information about the sea cucumbers population dynamics depends also upon their peculiar body morphology. Indeed, the lack of a rigid skeleton and the high plasticity of the body wall, that can vary in response to environmental conditions (Bulteel et al., 1992; Kinch et al., 2008; Zang et al., 2012; Prescott et al., 2015; Tolon et al., 2017; Ramírez-González et al., 2020b), limit practically the possibility to estimate appropriately their age/size relationship and growth rates. Moreover, such peculiarity led to different approaches when measuring these organisms with authors reporting the gutted weight, the drained weight or wet weight to build the morphometric relationships producing different reference data (Kazanidis et al., 2010; Aydin, 2020).

Since an accurate knowledge of the reproductive cycle is a crucial step for breeding practices in captivity, more insights about the biology and ecology of sea cucumbers are needed to ultimately produce valuable biomass and reduce the fishing pressure on wild stocks (Morgan, 2000; Agudo, 2006; Purcell et al., 2012; Dominguez-Godino and Gonzàlez-Wangüemert, 2018; Rakaj et al., 2018; Rakaj et al., 2019).

Sea cucumber species are generally gonochoric, only sporadically hermaphrodites, and are mainly broadcast spawners (e.g. Hyman, 1955; Smiley et al., 1988; Smiley, 1990; Smiley et al., 1991; Mohsen and Yang, 2021). The maturation process of gametes seems to be controlled by either exogenous or endogenous factors. Temperature, light intensity, photoperiod, lunar cycle, tidal flux, food quality and its availability are among the most influential exogenous factors (Conand, 1981; Ramofafia et al., 2000; Tan and Zulfigar, 2001; Hamel and Mercier, 2004; Mercier and Hamel 2009; Lee et al., 2018), but their different role in modulating the reproduction is still far to be fully accomplished.

In the Mediterranean Sea, one of the most common sea cucumber species is *Holothuria tubulosa* Gmelin 1791, which inhabits organic matter-rich soft bottoms and *Posidonia oceanica* meadows, where it plays a prominent role in recycling sedimentary organic detritus (Bulteel et al., 1992; Mezali et al., 2006; Mezali and Soualili, 2013; Costa et al., 2014; Boncagni et al., 2019; Pasquini et al., 2021). In the last few years, this species has been one of the most commercially exploited in the whole Mediterranean basin (Gonzàlez-Wangüemert et al., 2014; Gonzàlez-Wangüemert et al., 2015; Gonzàlez-Wangüemert et al., 2018; Dereli and Aydin, 2021) leading the Italian Ministry of Agriculture, Food and Forestry (MIPAAF) to ban sea cucumber fishing along the entire national coastline (Ministerial decree 156/2018), as a precaution for their conservation (Pasquini et al., 2021). Considering its growing economic interest, appropriate biological information is required. Currently, fragmentary data are available about the population structure and reproductive cycle in the Eastern (Bulteel et al., 1992; Despalatović et al., 2004; Dereli et al., 2016; Ocaña and Sanchez Tocino, 2005) and the Western (Tahri et al., 2019) Mediterranean Sea. Nevertheless, no information is reported about the spawning period of *H. tubulosa* in the Central-Western Mediterranean Sea.

In particular, studies about the reproductive period of *H. tubulosa* have mainly been focused on the histological observation of the gonads and yet the macroscopic characteristics and their correspondence with the microscopic features have been almost entirely ignored, resulting in a knowledge gap, in contrast to what has been done for other species (e.g., *H. fuscogilva*; Ramofafia et al., 2000). Furthermore, studies on the reproductive cycle and population dynamics conducted so far on *H. tubulosa* are related to limited temporal and spatial scales and, as such are not exhaustive.

In order to promote the scientific management of *H. tubulosa*, it is essential to acquire a baseline knowledge about its ecology, population dynamics, and reproduction. Therefore, the objectives of the present study are: (1) to provide a detailed description of the morphology of reproductive structures in relation to the

reproductive cycle; (2) to obtain an insight of the seasonal and inter-population variability of the reproductive cycle.

2 Materials and methods

2.1 Study area and sampling

Specimens of *H. tubulosa* were collected in three different sites (Gulf of Oristano, Gulf of Teulada, and Tortolì) (Figure 1) of the coastal area of Sardinia Island (Italy, Central-Western Mediterranean Sea).

A total of 214 specimens were collected by divers (3 – 10 meters depth) in 21 different sample occasions from 2018 to 2022. At each sampling date, sea surface temperature was recorded using a multiparametric probe (*In-Situ* SmarTROLL Multiparameter Handheld). After collection, specimens were placed into a 3L plastic bag and transported to the laboratory inside a cooler box (at *in situ* temperature). In the lab, in order to reduce the intra-specimen variability, sea cucumbers were gently squeezed to remove the excess water from the respiratory tree following the protocol of Costa et al. (2014) and then were weighted (WW, g, ± 0.01 g). The total length (TL, cm, ± 0.1 cm), was recorded using an ichthyometer considering the extended length of the sea cucumber, and the width (TW, cm, ± 0.1 cm) was recorded by caliper. After gutting (the removal of gonads and gut), the cucumbers were also weighted (GW, g, 0.01 g).

2.2 Population structure

Specimens were ordinated according to different size (length) classes and the length-frequency distribution was defined. To analyze relative changes in sea cucumbers morphology, allometric relationships were assessed using the allometric equation established by Keys (1928):

$$Y = aX^b$$

where b is the allometric coefficient and a is the intercept, estimated from least-squares fitting method of the $\log_{10}$ -transformed variables:

$$logY = loga + blogX$$

This equation was used to assess five different relationships (WW- TL; GW- TL; WW- TW; GW-TW; GW-WW). Since *H.*

FIGURE 1
Map of the study area. Sampled sites of Oristano (Or), Teulada (Te), and Tortolì (To) are indicated.

tubulosa lacks in sexual dimorphism, specimens were sexed after dissection, observing the gonads' color, and were divided into four categories: F, females; M, males; I, undetermined, and U, unsexed (that occurred when was not possible to dissect the specimens). The sex-ratio (SR; females:males) was, also, estimated for the entire population.

2.3 Macroscopic and colorimetric analyses of the gonads

2.3.1 Macroscopic observation of the gonads

The macroscopic gonadal stage was assigned considering the following parameters: Gonado-Somatic index (GSI), color and the number of ramifications of the gonadal tubules. The gonad was separated from the gut and the respiratory tree and weighted (GoW, g, ± 0.01 g) and the GSI was calculated as follows:

$$GSI = \left(\frac{GoW}{WW}\right) \times 100$$

whenever possible, the sex of the specimens was assigned by observing the gonads' color according to Despalatović et al. (2004): white for males and pink for females. The number of the gonad tubules ramifications (from 1 to 5, used as a descriptor of the gonad maturation stage; the high the number of ramifications, the more developed the gonad; Ramofafia et al., 2000) was considered as reported in Figure S1, and the highest ramification level recorded.

2.3.2 Colorimetric analysis of the gonads

The gonad color is the most common macroscopic clues to identifying sea cucumbers sex and maturity (Ramofafia et al., 2000; Ramofafia et al., 2003; Despalatović et al., 2004). The color was defined using a reference palette with 10 main colors and the respective RGB scores and Pantones® codes (Pantone Inc. USA) in natural daylight (Table S1) (Prato et al., 2018). However, the capacity to assign colors may vary between observers, hence, an analytical method to assign the color to the gonads was used (Addis et al., 2014). The gonads' colorimetric analyses were conducted using a digital colorimeter (Chroma meter CR-400, Konica Minolta, Tokyo, Japan), which specified the color according to the Commission Internationale de l'Eclairage (CIE, Commission Internationale de l'Eclairage (2008) Vienna, Austria) as lightness (L*), redness (a*), yellowness (b*) color space (CIELAB).

2.4 Histological analysis

Gonads were processed for histological analysis. For each sample, a piece of gonad tissue (0.5 to 1 cm long) was immediately fixed in a buffered 5% formalin solution (0.1 mol L^{-1}, pH 7.4) for 48 h. The tissues were then dehydrated and embedded in a synthetic resin (GMA, Technovit 7100, Bio-Optica, Milan, Italy) following routine protocols and sectioned at 3.5 µm with a rotating microtome (ARM3750, Histo-Line Laboratories, Pantigliate, Italy). Slides were stained with Gill hematoxylin followed by eosin counterstain (H&E) for standard histology and with periodic acid–Schiff (PAS) and Alcian blue (AB) in combination to assess the production of neutral and sulfated acid mucins (Cerri and Sasso-Cerri, 2003). Subsequently, sections were dehydrated in graded ethanol (96–100%), cleared in Histolemon (Carlo Erba Reagents, Cornaredo, Italy) and mounted in resin (Eukitt, Bio-Optica).

Female histological samples were examined to determine the developmental stage of oocytes. The microscopic maturity stages of females were determined based on the ovarian wall thickness, the position of the oocytes in the gonad section and the oocyte size (following the description used by Ramofafia et al., 2000 and modified *ad hoc* for *H. tubulosa*.). The size composition of oocytes was obtained measuring only oocytes where the nucleus was clear, and given that these oocytes are rarely perfectly spherical in shape, in order to reduce the variance, the diameter of each oocyte was taken using Tps.dig v. 2.12 software (Rohlf, 2009) and calculated as average of the major and minor axis.

As in females, to assess the maturity stage of males' gonad, the following clues were considered: the thickness of the testis, the extension of the germinal layers and its folds and the abundance (by rank) of spermatozoa filling the gonad lumen. For each individual, the average thickness was determined by measuring the thickness at five different points.

2.5 Reproductive period and maturity

The seasonality of spawning of *H. tubulosa* was estimated through an analysis of the monthly distribution of the percentage of maturity stages of females and males and the evolution of the mean GSI (see above). A range of mature individuals TL (males and females separately, and total population) was also reported.

2.6 Statistical analyses

To test the adequacy of the model used to assess the TL-WW, TW-WW, TL-GW, WW-GW relationships, an ANOVA test, using the P value for Lack-of-Fit, was performed on previously transformed (ln) data.

The significance of deviation of sex-ratio from the 1:1 null hypothesis was tested using the Chi-Square test (χ^2) (Zar, 1999), while to assess differences among length-frequency distributions, the Kolmogorov-Smirnov test was used.

To evaluate differences between the GSI of the specimens and season, a univariate permutational analysis of variance

(PERMANOVA) was applied using maturity stages, season and month as fixed factor. Prior to the statistical analysis, the GSI data were arcsin transformed ($x' = \arcsin\sqrt{x}$). The PERMANOVA was also performed to test differences in the gonad colors spaces L*, a*, b* (using sex and maturity stages as fixed and orthogonal factors) and in the oocytes' diameters (using season as fixed factor). Principal-components analysis (PCA) was carried out using the PRIMER 7 software (Clarke and Gorley, 2015), to visualize the relationship between GSI and temperature with months considering the whole population and by sex, showing the importance of the contribution of each variable to the PC axes. All PERMANOVA tests were based on Euclidean distances of previously normalized data, using 999 random permutations of the appropriate units. When significant differences were observed, pairwise tests were also performed. P values in the PERMANOVA and pairwise tests were obtained from Monte Carlo asymptotic distributions (Anderson and Robinson, 2003) using the routines included in the PRIMER 7 software (Clarke and Gorley, 2006).

3 Results

3.1 Population structure

Among 214 sea cucumber collected, 170 specimens of *H. tubulosa* were dissected to define the sex. Males (n=47) and females (n=57) are equally distributed (SR= 0.82) showing no significant differences among them (χ^2 = 0.4825; p =0.4876).

Considering the whole population, the WW of sea cucumbers ranges between 52.78 and 989.10 g (278.76g ± 160.85 s.d.), the GW ranges between 33.54 and 296.43 g (133.17g± 97.99 s.d.), the TW ranges between 2.5 and 9.7cm (5.3cm ± 1.2 s.d.), the TL ranges between 9 to 37 cm (20.5cm ± 5.7 s.d.). In detail, in females, the TL ranges from 14 to 37 cm (22.66cm ± 5.56 s.d.), while in males the TL ranges from 11 to 35.5 cm (22.38cm ± 6.03 s.d.) (Figure 2) with both females and males attaining substantially the same size. The results from Kolmogorov–Smirnov two-sample test do not indicate a statistically significant difference in length-frequency distribution among sexes (K–S test = 0.62; p = 0.832).

The allometric equations ($y = ax^b$) between all taken parameters (TL, TW, WW and GW) and estimates are present in Figure 3. The relationships between weights and lengths (Figures 3A–D) show a b value always lower than 3, highlighting a negative allometric growth, with significant power curves. Among them, the best relationship is WW-TL with a slope of 1.725 and R^2 of 0.739. The results of the Analysis of Variance with Lack-of-Fit of the four relationships ($p>0.05$) indicate that the models used to describe the relationships fit with the observed data. A negative allometric growth ($b<1$) is observed also between WW and GW (Figure 3E).

3.2 Macroscopic maturity stages

The reproductive apparatus of *H. tubulosa* consists in a single gonad ramified in several tubules and a gonoduct that lead to the gonopore situated in the anterior part of the organism. All sea cucumbers collected in the present study had a visible and recognizable gonad, leading us to identify these sea cucumbers as adults. Juveniles (i.e. immature specimens) and recruits were not

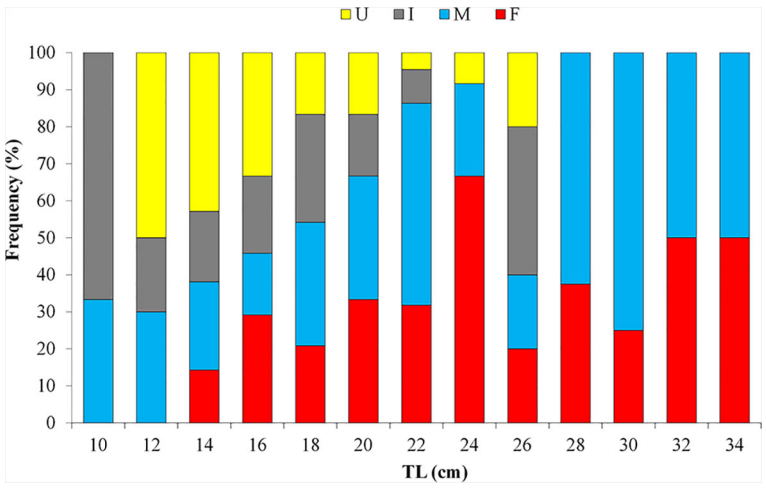

FIGURE 2
Length – frequency distribution in different size classes of female (F), male (M), undetermined sexes (I) and unsexed (U) specimens of *Holothuria tubulosa*.

recorded in the present study. Based on the GSI, the number of gonad ramifications and their color, five macroscopic gonadal stages can be identified for *H. tubulosa*:

3.2.1 Recovery

The gonad is very small, and its weight (GoW) is generally<2 g. The color is pale and translucent (Table S1, ID 454; 461) and is not possible to distinguish between females and males. In this stage, the number of ramifications cannot be assigned macroscopically (Figures 4A, M). The GSI varies between 0 and 1 (Figure 5). The TL of sea cucumbers in this stage is 15.92cm ± 3.4 s.d.

3.2.2 Growing

The weight of the gonad is greatly variable, ranging between 2 and 25g (8.39g ± 9.35 s.d.), with female gonads (9.84g ± 8.90 s.d.) bigger than male ones (8.52g ± 10.02 s.d.). In both sexes, the gonad occupies up to one third of the coelomic cavity (Figures 4B, M). Males have a matt pale yellow gonad (Figure 4M; Table S1, ID 461; 454), whereas females have a translucent red–coral gonad (Figure 4B, Table S1, ID 151; 157). The number of ramifications varies between 2 and 3. The GSI increases and varies between 1 and 10, in detail in females 2.97 ± 1.86 s.d. and males 2.38 ± 2.16 s.d. (Figure 5). The TL of sea cucumbers in this stage is 20.63cm ± 5.949 s.d.

3.2.3 Mature

The gonad reaches the maximum weight (43.13g ± 28.03 s.d.), with female gonad (51.84g ± 33.40 s.d.) bigger than males one (31.27g ± 10.61 s.d.), up to occupy the whole coelomic cavity. Males have a matt pale yellow gonad (Figure 4O; Table S1, ID 157; 461), whereas females have a translucent red-coral and red gonad (Figure 4C; Table S1, ID 172, 485). The number of ramifications varies between 3 and 5 and the GSI is comprised between 3 and 35 (12.93 ± 7.66 s.d.) (Figure 5). In particular, in females, GSI shows values 2 times higher than males, 16.18 ± 8.12 s.d. and 8.52 ± 4.02 s.d. respectively. The mean TL of sea cucumbers in this stage is 23.80cm ± 5.48 s.d.

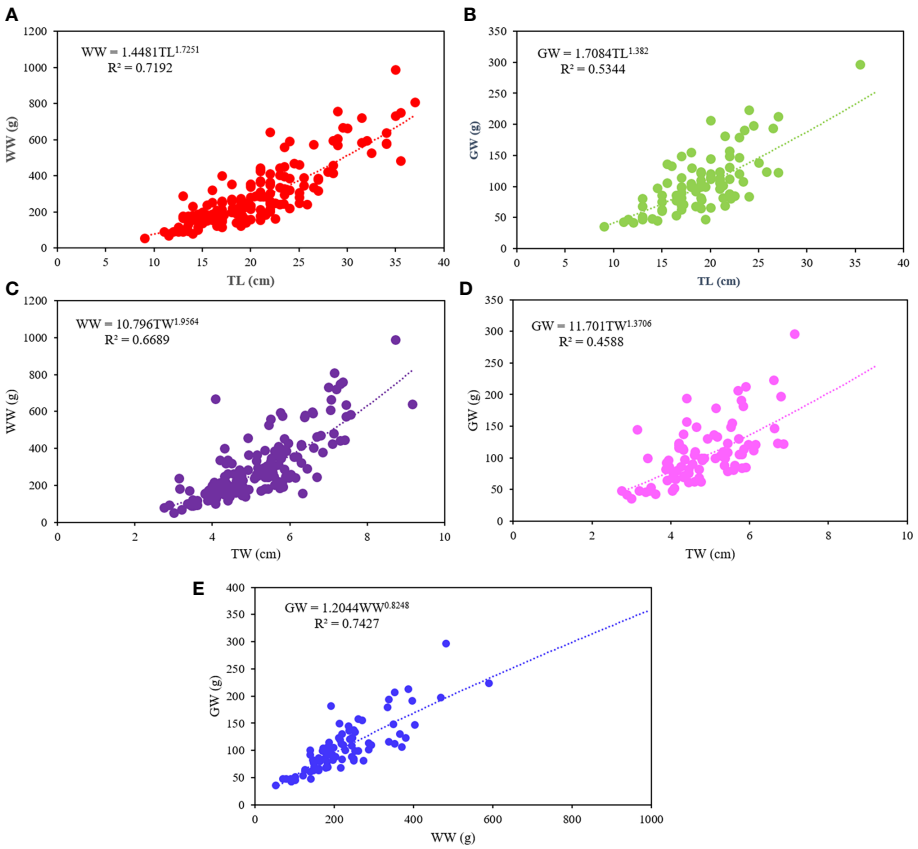

FIGURE 3
Allometric relationships for *Holothuria tubulosa*. **(A)** WW-TL relationship; **(B)** GW-TL relationship; **(C)** WW-TW relationship; **(D)** GW-TW relationship; **(E)** GW-WW relationship. TL, total length; WW, wet weight; GW, gutted weight; TW, total width.

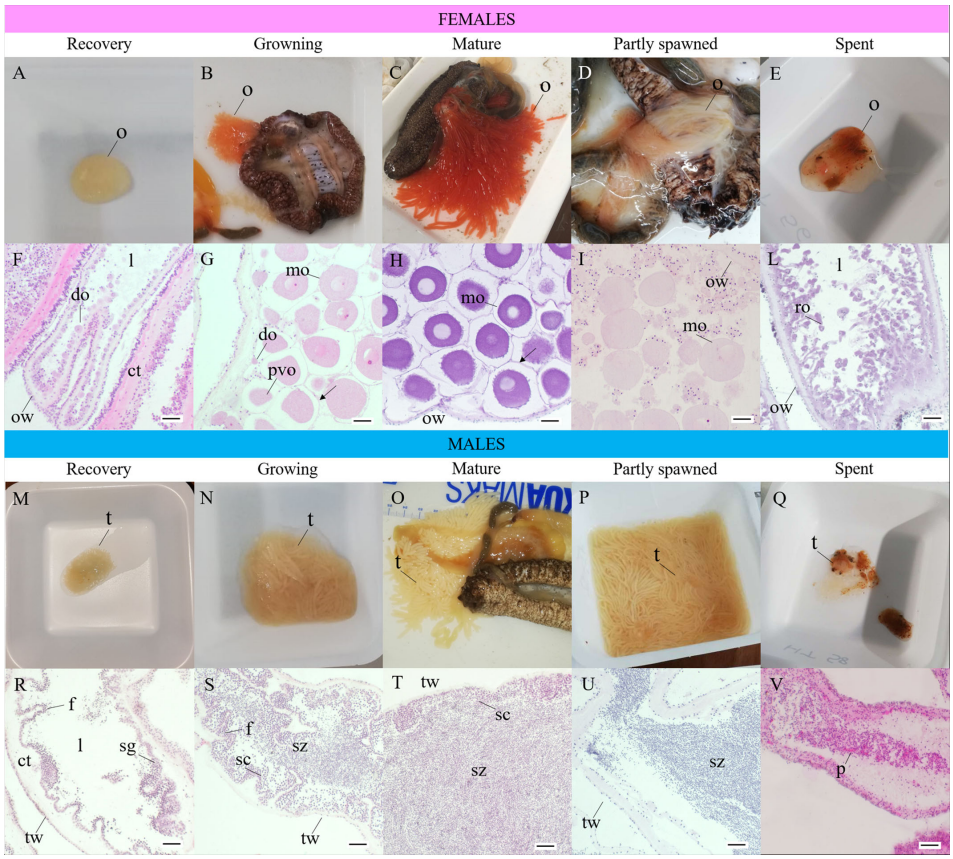

FIGURE 4
Macroscopic and histological maturity stages of *Holothuria tubulosa* females **(A–L)** and males **(M–V)**. **(A)**, ovary at recovery stage (GSI<2, observed in autumn and winter); **(B)**, female in growing stage (TL: 21.3 ± 1.2 s.d.; GSI: 4.0 ± 1.4 s.d.; observed in spring and summer); **(C)**, female in mature stage (TL: 22.8 ± 5.2 s.d.; GSI: 15.8 ± 8.2 s.d.; observed mainly in summer); **(D)**, female in partly spawned stage (TL: 20.1 ± 1.2 s.d.; GSI: 2.29 ± 2.1 s.d.; observed in summer and autumn); **(E)**, ovary in spent stage (GSI<1; observed in autumn and winter); **(F)**, longitudinal section of ovary in recovery stage with small developing oocytes arranged in a single layer, thick ovarian wall **(E–H)**; **(G)**, ovary in growing stage with developing and mature oocytes arranged in multiple layers **(E–H)**; **(H)** ovary in mature stage characterized by fully-grown mature oocytes densely packed; thin ovarian wall (AB/PAS); **(I)**, ovary in partly spawned stage with mature oocytes less abundant and empty spaces in the lumen **(E–H)**; **(L)** ovary in spent stage with thick ovarian wall and unspawned relict oocytes **(E–H)**; **(M)**, testis at recovery stage (GSI< 2, observed in winter); **(N)**, testis in growing stage (TL 20.6 ± 5.3 s.d., GSI 2.3 ± 2.1 s.d., observed in spring and summer); **(O)**, male in mature stage (TL 25.1 ± 5.5 s.d., month of sample GSI 8.5 ± 4.0 s.d. observed in spring and summer); **(P)**, testis in partly spawned stage (TL 17.3 ± 3.1 s.d.; GSI 7.4 ± 4.9 s.d., observed in summer); **(Q)**, testis in spent stage (GSI<1, observed in winter and autumn); **(R)**, testis in recovery stage with spermatogonia on the germinal layer, thick testicular wall **(E-H)**; **(S)**, testis in growing stage with spermatocytes extending towards the lumen and spermatozoa start to fill the lumen **(E–H)**; **(T)**, testis in mature stage with densely packed spermatozoa in the lumen **(E–H)**; **(U)**, testis in partly spawned stage with spermatozoa less densely packed **(E–H)**; **(V)**, testis in spent stage with unspawned spermatozoa and phagocytes visible **(E–H)**. ct, connective tissue; do, developing oocyte; l, lumen; mo, mature oocyte; o, ovary; ow, ovarian wall; p, phagocyte; ro, relicted oocyte; sc, spermatocyte; sg, spermatogonium; sz, spermatozoa; t, testis; tw, testicular wall. (H-E, Hematoxylin and eosin, AB/PAS, Alcian Blu/ Periodic Acid Schiff.

3.2.4 Partly spawned

The gonad is reduced in size, and its weight is 11.42g ± 8.35 s.d., with males' gonad (13.74g ± 8.55 s.d.) bigger than females one (5.61g ± 5.59 s.d.). Males have a matt pale yellow gonad (Figure 4P; Table S1, ID 461), whereas female gonad loses its translucency and appears dull coral-red (Figure 4D; Table S1, ID 157). The gonads are emptied, the tubules are elongated and thin, and the number of ramifications varies between 3 and 4. The GSI is between 1 and 15 (Figure 5), in particular in females is 2.29 ± 2.16 s.d. and in males is 7.47 ± 4.92 s.d. The mean TL of sea cucumbers in this stage is 17.90cm ± 3.00 s.d.

3.2.5 Spent

The gonad is much reduced and the weight is <2g. It shows segments with different colors and is not possible to distinguish between females and males (Figures 4Q, E). Branches ramifications are not visible or recognizable. The GSI is between 0 and 1 (Figure 5). The mean TL of sea cucumbers in this stage is 19.16cm ± 4.65 s.d.

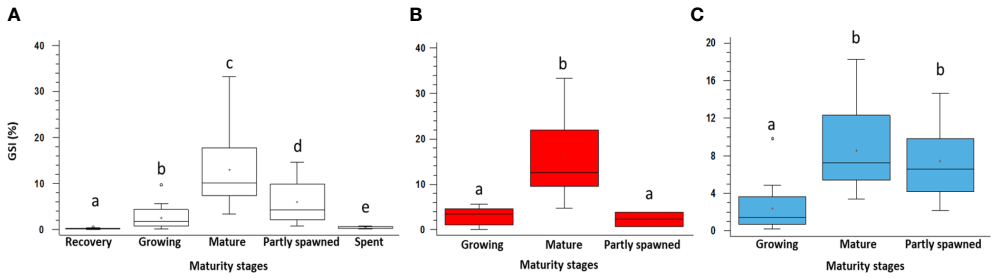

FIGURE 5
GSI variation among different maturity stages of the gonads in *Holothuria tubulosa* specimens. In **(A)** whole sample showing all the maturity stages; **(B)** females; **(C)** males. Lowercase letters indicate the results of the *post-hoc* tests. The boxes show the interquartile range, with the median value indicated by the horizontal line and the '+' sign indicating the mean; whiskers show the range. Individual symbols show outliers.

The statistical analyses reveal significant differences in the GSI among all the maturity stages described above (Table S2, S3; Figure 5). Females and males show a similar trend (Figures 5A, B) despite females have a higher GSI value in Mature (2 times) and males in Partly spawned (3 times), whereas the lowest value is observed in recovery and spent specimens when they could not be sexed with the macroscopic approach.

The color of the gonads differs significantly between Growing and Mature stages in both females and males. The pairwise comparison shows that in Mature females, when compared to the Growing ones, the L* (lightness) component decreases, the a* (redness) one increases, and the b* (yellowness) one does not change (Figures 6A–C). Males' gonad color is much less variable and significant differences occur between Growing

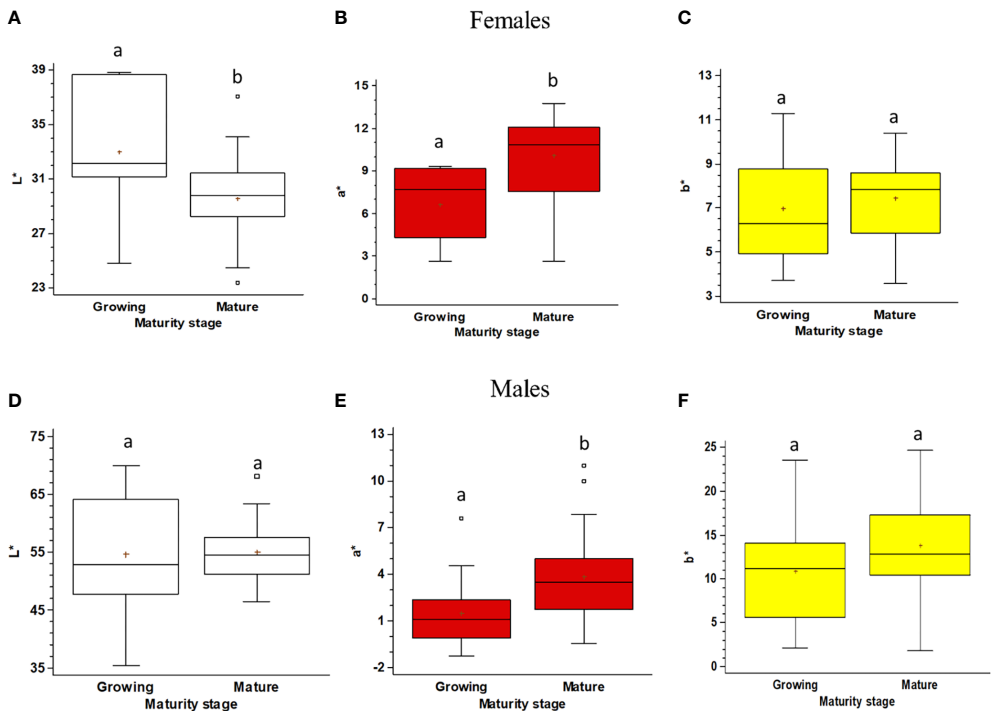

FIGURE 6
Boxplot of the color space (lightness, L*; redness, a*; yellowness, b*) of the gonads of Holothuria tubulosa, for females **(A–C)** and males **(D–F)** at Growing and Mature maturity stages. The boxes show the interquartile range, with the median value indicated by the horizontal line and the '+' sign indicating the mean; whiskers show the range. Individual symbols show outliers. Lowercase letters indicate the results of the pairwise comparison of the L*a*b* value between Maturity stages.

and Mature males only for the a* (redness) component (Figures 6D–F).

3.3 Microscopic maturity stages

Based on the histology of the gonads of males and females (Figure 4) and the diameter distribution of oocytes (Figure 7A) in females, five female gonadal stages are recognized (Figures 4F–M, R–V) and described in Table 1. The oocyte size varies significantly among all the identified maturity stages (Tables S4, S5), except for Mature and Partly spawned, where oocytes show similar diameter (Figure 7A). Moreover, in Mature stage, the oocyte population shows a unimodal distribution with a peak at 110 µm, indicating that *H. tubulosa* females have a synchronized development of the ovaries (Figure 7B).

The cross-inspection of the gonadal stages as determined using separately macroscopical and histological cues provides evidence of a validation of the two different approaches, summarized in Table S6.

3.4 Reproductive period and maturity

The GSI, in both sexes, varies significantly among seasons and months (Figures 8A, B; Table S3), increasing progressively

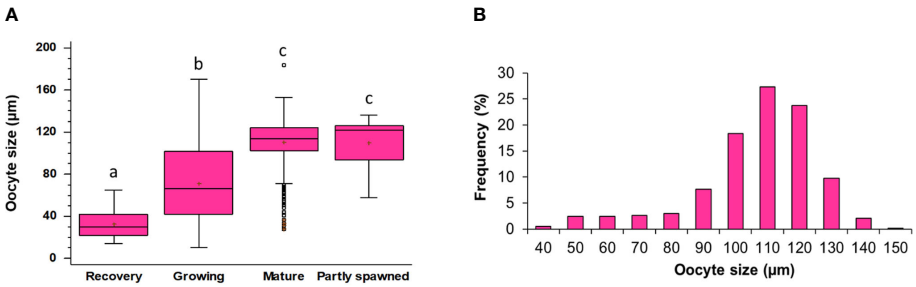

FIGURE 7
(A) Oocytes size in different maturity stages. Lowercase letters indicate the results of the pairwise comparison between Maturity stages. The boxes show the interquartile range, with the median value indicated by the horizontal line and the '+' sign indicating the mean; whiskers show the range. Individual symbols show outliers. Lowercase letters indicate the results of the pairwise comparison of the maturity stages. **(B)** Detail of the size-frequency distribution of oocytes in Mature ovaries.

TABLE 1 Description of the microscopic gonadal stages in female and male of *Holothuria tubulosa* specimens.

Stage	Microscopic description	
	Females	**Males**
Recovery	Ovaries contain only small developing oocytes arranged in a single layer, thick ovarian wall show thickened walls (68.6 ± 25.2 µm).	Testes with thick gonadal wall (85.5 ± 25.5 µm). The germinal epithelium presented numerous folds that increased the surface area for spermatogenesis. Only spermatogonia are visible.
Growing	Ovaries show mainly previtellogenic oocytes in the germinal layer and oocytes at different vitellogenesis levels arranged in multiple layers. As vitellogenesis progressed, fully-grown oocytes, surrounded by small follicular cells, begin to take up a central position in the lumen. The ovarian wall is less thick (39.4 ± 14.4 µm).	Testes characterized by active spermatogenesis. Spermatocytes extend towards the lumen and spermatozoa start to fill the lumen. The testicular wall is less thick (58.0 ± 13.8 µm), and the folds of the epithelium begin to straighten.
Mature	Mature oocytes, surrounded by the follicle membrane, reach their maximum size in all of the gonad layers, including the lumen. Very narrow ovarian wall (15.8 ± 5.4 µm).	Densely-packed spermatozoa completely fill the lumen of the tubule. Spermatogenesis continues and spermatocytes are present in the germinal layer. Narrow gonadal wall (22.2 ± 6.8 µm).
Partly spawned	Ovaries with fewer mature oocytes inside the tubules with empty spaces due to the partial gametes spawn visible. Mature oocytes with evident signals of degradation (without the follicular membrane and without a visible germinal vesicle) are present. The gonad has a thinned wall (16.4 ± 6. µm).	After the partial emission of the gametes, the density of spermatozoa in the testes decreases, living empty areas in the lumen. The gonadal wall continues to be narrow (27.4 ± 8.8 µm).
Spent	Ovaries has traces of unspawned relicted oocytes. Thick ovarian wall with abundant connective tissue that fills the lumen.	Testes with residual unspawned spermatozoa and phagocytes visible. Thick gonadal wall with a large amount of connective tissue.

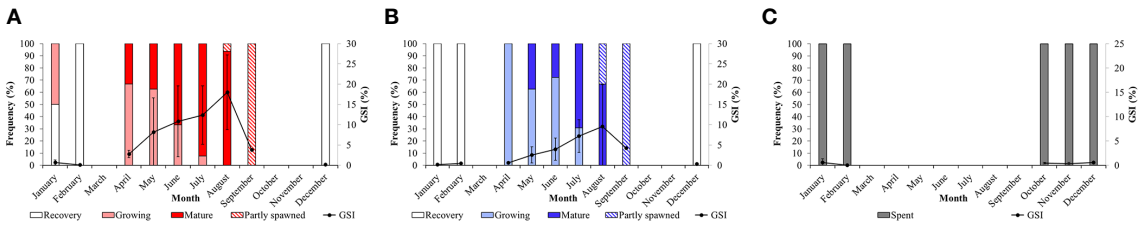

FIGURE 8
Monthly distribution of Holothuria tubulosa females **(A)**, males **(B)** and unassigned specimens **(C)** at each gonadal stages during the sampling months. Gonado-Somatic Index (± s.d.) evolution along months is also reported.

from late autmn (December) to summer, when it reaches the highest value in August, then dropping in September. In general, in spring (April, May and June) and summer (July and August), the GSI in female specimens reaches higher values than that observed in males (Figures 8A, B). Based on the maturity scale of female and male gonads reported above, monthly variations in the frequency of the different gonadal stages are also investigated (Figure 8). As far as the females are concerned, in winter, in correspondence of the lowest surface temperature (14.52°C ± 0.75 s.d.) only the Recovery (December and February) and the Growing stages (January 50% each) are observed (Figure 8A). In spring (April), when the sea surface temperature begins to rise (17.99°C ± 1.90 s.d.), we observe a dominance of the Growing stage (ca. 66%) that progressively gives way to the Mature stage in May and June. During the summer season, the frequency distribution of mature females increases up to 93% when maximum sea surface temperature are recorded (25.45°C ± 1.29 s.d.). Moreover, in August the first Partly spawned females are observed (ca. 6%). Mature and Growing stages disappear in September, when only the Partly spawned stage is observed. No females are observed in October and November. A similar trend is observed in males, characterized by a peak of mature individuals in July and August (Figure 8B). Unassigned specimens (I) in the Spent stage appear only from October to February (Figure 8C). The relationship between temperature and GSI with months and sexes are clearly visualized, Figure 9, S2 respectively, showed by the PCA ordination.

Observing the female sea cucumbers length at different maturity stages, the results reveal that the range of matures is 15-37 cm (22.75 ± 5.15 cm TL), while the TL range of males is 14-35.5 cm TL (23.34 ± 7.15 cm TL). Since *H. tubulosa* does not show any sexual dimorphism, the interval of mature population is 14-37 cm TL (23.01 ± 5.15 cm TL).

The ovary is characterized by different oocyte diameters along the different gonadal stages (Figure 7A). Such variation is also reflected in their size when considering different seasons. Oocyte's diameter varies significantly among seasons, with minimum values in winter, and much higher values in all other seasons. Values increase progressively in spring and summer, while in autumn, the oocyte diameter is greatly variable due to the presence of both female in Recovery and in Growing stages (Tables S5; Figure 10).

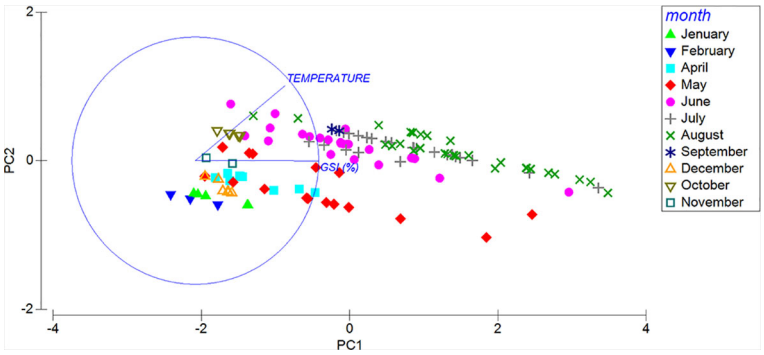

FIGURE 9
Two-dimensional PCA ordination of the pattern of GSI and temperature in different months.

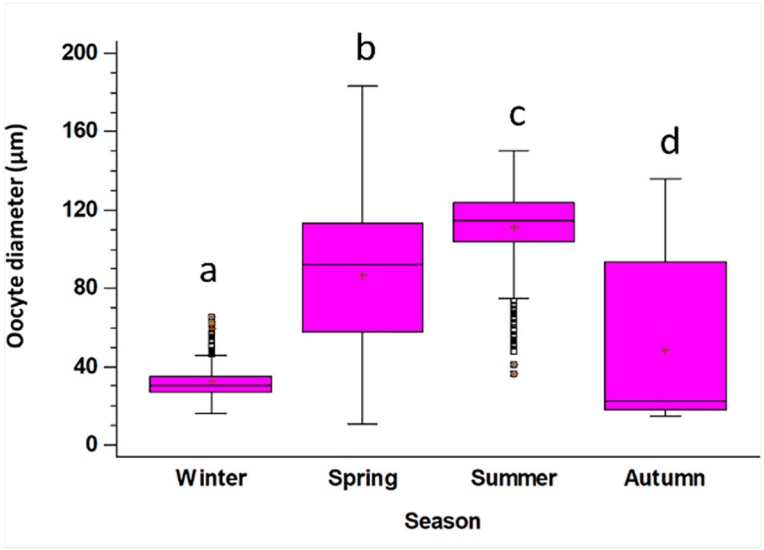

FIGURE 10
Oocyte diameters in the different seasons (Winter, January - March; Spring: April - June; Summer: July - September; Autumn: October - December). The boxes show the interquartile range, with the median value indicated by the horizontal line and the '+' sign indicating the mean; whiskers show the range. Individual symbols show outliers. Lowercase letters indicate the results of the pairwise comparison between the oocytes size in different season.

4 Discussion

Several field and modelling studies have been conducted so far on the population structure of historically exploited sea cucumbers such as *Apostichopus japonicus*, *Cucumaria frondosa*, and *Isostichopus fuscus* (e.g., Herrero-Pérezrul et al., 1999; Reyes-Bonilla and Herrero-Pérezrul, 2003; Hamel and Mercier, 2008; Purcell et al., 2011; Glockner-Fagetti et al., 2016; Ramírez–González et al., 2020b). However, Gonzalez-Wangüemert et al. (2016) put the baseline for the study of population dynamics of the new target species including *Holothuria polii*, *H. mammata*, *H. arguinensis* and *H. tubulosa*. The analysis of sea cucumbers population structure and monitoring, based on common tagging methods, is typically biased by the high morphological plasticity of the body wall (Prescott et al., 2015), which makes poorly effective the use of tags (Kinch et al., 2008). At the same time, body size of holothurians can vary in response to environmental conditions, food availability and stress level of the organism (including the evisceration of the internal organs) (Bulteel et al., 1992; Wilkie, 2001; Zang et al., 2012; Tolon et al., 2017). Consequently, different authors considered the gutted weight and the gutted length to reduce the intraspecific variability (Kazanidis et al., 2010; González-Wangüemert et al., 2014; Prescott et al., 2015; Dereli et al., 2016; Marquet et al., 2017; Aydin, 2020). This approach can be used in fish-dependent data (González-Wangüemert et al., 2014). On the other hand, for restocking and sea ranching activities, where it is necessary to follow the growth of sea cucumbers, this option is not applicable. Another way to reduce the intraspecific variability, avoiding the death of the sea cucumbers, is to gently squeeze the specimens to remove the excess water from the respiratory tree (Sewell, 1990; Costa et al., 2014), the same approach used in the present study to record data of alive specimens. We reported here that, whatever the morphometrical relationship considered, sea cucumber *H. tubulosa* shows a negative allometric growth, indicating that it would preferably invest its resources in increasing the length rather than its wall thickness. This result is corroborated by previous studies on this species (Kazanidis et al., 2010; Aydin, 2020), and for other species belonging to the same genus (e.g. González-Wangüemert at al., 2014; Marquet et al., 2017; Azevedo et al., 2021). Moreover, our data indicate that among the relationships considered here, the Wet Weight (WW)-Total length (TL) relationship represents the most reliable and can be used as proxy for investigating the size structure of *H. tubulosa* and comparing different populations. The use of the WW and the TL parameters, which can be easily taken on alive specimens, has the advantage, not negligible, to avoid the sacrifice of sea cucumbers, representing a useful tool for their monitoring and management (e.g., restocking and/or sea ranching actions).

The sea cucumbers collected in the present study show bigger sizes (max 35 cm TL) and weights (max 989.10 g WW) than those collected in the Dardanelles Strait (max TL 30.3; Dereli et al., 2016), the south Aegean Sea (max 19.7 cm TL and 350g WW, Antoniadou and Vafidis, 2011) and Turkish coasts (max TL 23 cm, max GW 130 g; González-Wangüemert et al., 2014). Such differences could be related to the local different trophic settings of the environment occupied by sea cucumbers combined also with the effect of the local fishery, which can lead

to lose the larger individuals in the exploited populations (Vafeiadou et al., 2010, González-Wangüemert et al., 2014).

The sex-ratio of *H. tubulosa* reveals that males and females are equally represented in the studied population as also reported by Kazanidis et al. (2014) and Despalatović et al. (2004) in the Adriatic Sea, and Dereli et al. (2016) in the Dardanelles Strait on the same species, and by Mezali et al. (2014) on *H. sanctori* in Algerian coasts. However, several studies on the reproductive biology of sea cucumbers such as *H. mammata* in the Atlantic Ocean (Santos et al., 2017; Venâncio et al., 2022), *H. whitmaei* in the Pacific Ocean (Shiell and Uthike, 2006), and *H. leucospilota* in the Western Indian Ocean (Gaudron et al., 2008) highlighted an imbalanced sex ratio with females outnumbered males. Our study was carried out in areas where the population is unexploited, suggesting that this ratio is a natural trait for these non-fissiparous sea cucumbers, while unbalanced sex-ratio described above could be due to evisceration events, association in same-sex groups, unsexed reproduction (i.e. fission), as well as fishing pressure as a possible causes (Shiell and Uthike, 2006; Muthiga et al., 2009; Santos et al., 2017).

Population structure is characterized mainly by adult individuals (TL > 9 cm), which reach the same range in sizes in both sexes, as also reported for the same species in the Aegean (Kazanidis et al., 2010) and Adriatic Sea (Despalotović et al., 2004). However, the failure to detect a separate mode for juveniles and immature holothurians, a common pattern observed also in other species (e.g. Venâncio et al., 2022), may be due to the sampling method used in this study, which is size-selective because the small specimens show cryptic behavior, or even could occupy different environment (Mercier et al., 2000; Hamel et al., 2001; Kazanidis et al., 2010; Aydin, 2019). On the other hand, a very fast growth during the first age of the species (Massin and Jangoux, 1976), a different habitat preference or, most likely, a cryptic or diel behaviour, as observed for other sea cucumber species (e.g., Sloan, 1979; Shiell, 2004; Purcell, 2010; Soliman et al., 2019; Félix et al., 2021) could also explain the few (or absent) juveniles and recruits in Sardinian populations.

Regarding the macroscopic observation of the gonads, it allowed us to identify five different gonadal stages, similarly as observed by Ramofafia et al. (2000, 2003) for the tropical *H. fuscogilva* and *H. scabra*. In detail, the RGB color palette enabled us to distinguish clearly the sex of the developed individuals, but it was almost ineffective in the determination of the sex of undeveloped specimens (Recovery and Spent maturity stages) with gonads characterized by a pale-white color or a heterogeneous color with rust blotches (Marquet et al., 2017). In addition, the discrimination between the Growing and Mature stages within the sexes is not always clear because of the numerous nuances of the gonads color and the observer's sensitivity, which can lead to different color assignments. Thus, the innovative colorimetric method using the CIELAB color space, here used for the first time in holothurians, allowed us to overpass such subjective assignment of the gonad color avoiding misinterpretations of a certain reproductive stage, analysing the different coordinates, lightness, redness and yellowness.

A good correspondence between the maturity stages based on tubule appearance (e.g. color, dimension, ramification degree), and those based on histology is observed. Thus, the tubule morphology in alive specimens, which is possible to observe after a dorsal incision in the body wall near the gonopore, can be used to detect the release of gametes in the breeding programs when the sea cucumbers cannot be sacrificed, as also reported for *H. fuscogilva* (Ramofafia et al., 2000). However, this is an invasive practice which can cause pathogen infection and stress in the sea cucumbers (Becker et al., 2004).

H. tubulosa shows a synchronic gonad development at level of tubules and oocyte size distribution in females, revealed by the histological observation of gonads. This reproductive strategy is widespread among holothurians such as *Holothuria atra*, *H. mexicana*, *H. nobilis*, *Actinopyga echinites*, *Stichopus variegatus* and *Thelenota ananas* (Sewell et al., 1997). The results indicate that *H. tubulosa* does not fit the tubule recruitment model which involves several stages of gonad development in the same gonad, observed in other holothurians as *Isostichopus badionotus* (Foglietta et al., 2004), *H. scabra* (Ramofafia et al., 2003) and *H. floridiana* (Ramos-Miranda et al., 2017).

Both macroscopic and histological approaches have proven to be reliable in identifying the reproductive period of *H. tubulosa* in the study sites. Monthly changes in GSI and the frequency distribution of the maturity stages clearly depict the restricted reproductive season, which is concentrated, in the Sardinian population, at the end of the summer season. Our result is in good agreement with those reported earlier for the same species by Despalatović et al. (2004) in the Adriatic Sea, Kazanidis et al. (2014) in the Aegean Sea, Dereli et al. (2016) in the Dardanelles Strait, and Tahri et al. (2019) in Oran coast (Algeria).

The clear association between the peak of *H. tubulosa* spawning and the maximum values of sea surface temperature recorded in the sampled sites is a common pattern of sea cucumber species (e.g. Bulteel et al., 1992; Despalatović et al., 2004; Kazanidis et al., 2010; Antoniadou and Vafidis 2011; Acosta et al., 2021; Venâncio et al., 2022). Moreover, the seasonal variation of temperature is accompanied by the increase of the day-length and the availability of phytoplankton in the water-column (Venâncio et al., 2022). The increasing of temperature can also modify the metabolism of sea cucumbers (Kühnhold et al., 2019) that use their energy to develop the gonads as observed in other holothurian species such as *A. japonicas* (Yang et al., 2006) and *Australostichopus mollis* (Slater et al., 2011). Furthermore, the seasonality may have an indirect effect on reproduction by increasing food availability

for broodstock through increased benthic productivity (Muthiga, 2006), and fostering the phytoplankton abundance for larval development (Boidron-Metairon, 1995; Cameron and Frankboner, 1989; Rakaj et al., 2018). Another environmental factor that can influence the gametogenesis and spawning in holothurians is the rainfall (e.g. Asha and Muthiah, 2008; Benítez-Villalobos et al., 2013; Leite-Castro et al., 2016; Acosta et al., 2021). Indeed, during the rainy season, there is a significant increase in phytoplankton, related to the contribution of nutrients from runoff and rivers (Acosta et al., 2021). However, in our investigated areas, it does not seem to be a determinant factor, because the pluvial precipitations do not follow a clear seasonal pattern as observed in the tropical regions to determine and characterize the spawning cycle of this species.

Among the life history traits of new target species, the size at maturity represents one of the most common and useful information for the estimation of the minimum fishing size (Navarro et al., 2012) ensuring spawning of mature sea cucumbers and protecting their natural stocks (Abdel-Razek et al., 2005). The absence of immature sea cucumbers did not allow us to define the size at maturity, but here we report that the smallest mature female is observed at 15 cm TL and the smallest mature male measured 14 cm TL. Few information about the size at maturity of the *Holothuria* genus are available in literature. Indeed, the only information about the maturity of *H. tubulosa* comes from the Adriatic Sea (Kazanidis et al., 2014), where it was estimated only in terms of the drained weight of the individuals (approximately 220 g). Beside this, our range of maturity is in agreement with that reported for the congeneric species *H. mammata* showing the size at first maturity in males TL=14.2 cm and females TL=16.7 cm (Venâncio et al., 2022), with which *H. tubulosa* shares a similar geographical distribution (Tortonese, 1965; Borrero-Pérez et al., 2009; González-Wangüemert et al., 2014; González-Wangüemert et al., 2018; Dereli and Aydin, 2021). Hence, our data should be considered as a preliminary evaluation of the adult size-structure, requiring the investigation of lower size classes, not included in this study, to have an exhaustive description of the whole population.

Conclusion

The results of this study provided evidence that the sea cucumber *H. tubulosa* has a synchronous development of the gonads, with an apparently unique reproductive event during the year, corresponding to the end of the summer season. Our results provides a first insight on size-range of matures of this valuable species, giving useful information for the management policy.

This study also shows that either the macroscopic or microscopic approach used to identify the different gonadal stages provide overlapping information. Nevertheless, the macroscopic proxy is faster than, and similarly reliable to, the microscopic one. Additionally, the macroscopic approach can be used in the field following the maturity scale here provided, allowing even not-expert observers such as fishermen to expeditiously determine sex and maturity stage of natural populations of sea cucumbers.

Given our results, this study is essential to increase the biological and ecological knowledge of the populations of *H. tubulosa*, create conditions for the domestication of broodstock in captivity and precise measures for the conservation of biodiversity.

Data availability statement

The raw data supporting the conclusions of this article will be made available by the authors, without undue reservation.

Author contributions

VP and PA conceived and planned the experiments. VP and AG carried out the sampling. VP, CP and MM laboratory analyses. VP, CP, AG carried out the statistical analyses. All authors contributed to the interpretation of the results. VP and CP took the lead in writing the manuscript followed by extensive revision by PA and MF to achieve the final version. All authors provided critical feedback and helped shape the research, analysis and manuscript. VP and CP contributed equally to the study. All authors contributed to the article and approved the submitted version.

Funding

This study has been carried out in the framework of the projects "Innovative species of commercial interest for Sardinian aquaculture: development of experimental protocols for the breeding of sea cucumbers, (project n.1/INA/2.47/2017; cUP: F26C19000000006)" funded by the EuropeanMaritime and Fisheries Fund (EMFF) Programme 2014/2020, Measure:2.47 – Innovation; and co-founded by the "lnEVal: lncreasing Echinoderm Value Chains" (grant n. ID 101 InEVal; CUP: F24I20000160006) funded by ERA-NET BlueBio programme.

Acknowledgments

The authors wish to express their gratitude to the Marine Protected Area Penisola del Sinis – Isola di Mal di Ventre in the people of the director Ing. Massimo Marras and Dr. Roberto Brundu; Dr. Gaspare Barbera technical manager of the L.P.A.

Group fish farm and the Marina di Teulada in the person of Mrs. Barbara Lai, for the logistic support in the field sampling. We are thankful to Dr. Marco Secci and Mr. Marco Maxia (Agris Sardinia Agency) for their help in the field and sampling activities. The collection of sea cucumbers was carried out under the authorization released by Regione Autonoma della Sardegna (Prot. N. 1845, 06/02/2019; Prot. N. 20735, 28/11/2019; Prot. N. 810, 13/01/2021; Prot. N. 0023738, 03/02/2022).

Conflict of interest

The authors declare that the research was conducted in the absence of any commercial or financial relationships that could be construed as a potential conflict of interest.

Publisher's note

Supplementary material

The Supplementary Material for this article can be found online at: https://www.frontiersin.org/articles/10.3389/fmars.2022.1029147/full#supplementary-material

References

Abdel-Razek, F. A., Abdel-Rahmen, S. H., El-Shumy, N. A., and Omar, H. A. (2005). Reproductive biology of the tropical sea cucumber *Holothuria atra* (Echinodermata: Holothuroidea) in the red Sea coast of Egypt. *Egypt. J. Aquat. Res.* 31, 383–402.

Acosta, E. J., Rodríguez-Forero, A., Werding, B., and Kunzmann, A. (2021). Ecological and reproductive characteristics of holothuroids *Isostichopus badionotus* and *Isostichopus sp*. in Colombia. *PloS One* 16 (2), e0247158. doi: 10.1371/journal.pone.0247158

Addis, P., Moccia, D., and Secci, M. (2014). Effect of two different habitats on spine and gonad colour in the purple sea urchin *Paracentrotus lividus*. *Mar. Ecol.* 36 (2), 178–184. doi: 10.1111/maec.12133

Agudo, N. (2006). "Sandfish hatchery techniques," in *Australian Centre for international agricultural research* (Noumea, New Caledonia: Secretariat of the Pacific Community and WorldFish Center), 45.

Amaro, T., Bianchelli, S., Billett, D. S. M., Cunha, M. R., Pusceddu, A., and Danovaro, R. (2010). The trophic biology of the holothurian *Molpadia musculus*: Implications for organic matter cycling and ecosystem functioning in a deep submarine canyon. *Biogeosciences* 7, 2419–2432. doi: 10.5194/bg-7-2419-2010

Anderson, S. C., Flemming, J. M., Watson, R., and Lotze, H. K. (2011). Serial exploitation of global sea cucumber fisheries. *Fish. Fish.* 12, 317–339. doi: 10.1111/1467-842X.00285

Anderson, M. J., and Robinson, J. (2003). Generalised discriminant analysis based on distances. *Aust. N. Z. J. Stat.* 45, 301–318. doi: 10.1111/1467-842X.00285

Antoniadou, C., and Vafidis, D. (2011). Population structure of the traditionally exploited holothurian *Holothuria tubulosa* in the south Aegean Sea. *Cah. Biol. Mar.* 52, 171–175.

Asha, P. S., and Muthiah, P. (2008). Reproductive biology of the commercial sea cucumber *Holothuria spinifera* (Echinodermata: Holothuroidea) from tuticorin, Tamil nadu, India. *Aquacult. Int.* 16, 231–242. doi: 10.1007/s10499-007-9140-z

Aydin, M. (2020). Length – weight relationships and condition factor of four different sea cucumber species in the Aegean Sea. *J. Anatol. Environ. Anim. Sci.* 1, 80–85. doi: 10.35229/jaes.677940

Aydin, M. (2019). Density and biomass of commercial sea Cucumber species relative to Depth in the Northern Aegean Sea. *Thalassas* 35, 541–550. doi: 10.1007/s41208-019-00144-4

Azevedo e Silva, F., Brito, A. C., Simões, T., Pombo, A., Marques, T. A., Rocha, C., et al. (2021). Allometric relationships to assess ontogenetic adaptative changes in three NE Atlantic commercial sea cucumbers (Echinodermata, Holothuroidea). *Aquat Ecol.* 55, 711–720. doi: 10. 1007/ s10452- 021- 09856-3

Becker, P., Gillan, D., Lanterbecq, D., Jangoux, M., Rasolofonirina, R., Rakotovao, J., et al. (2004). The skin ulceration disease in cultivated juveniles of *Holothuria scabra* (Holothuroidea, Echinodermata). *Aquaculture* 242 (1 – 4), 13–30. doi: 10.1016/j.aquaculture.2003.11.018

Benítez-Villalobos, F., Avila-Poveda, O. H., and Gutiérrez-Méndez, I. S. (2013). Reproductive biology of *Holothuria fuscocinerea* (Echinodermata: Holothuroidea) from Oaxaca, Mexico. *Sex Early Dev. Aquat. Org.* 1, 13–24. doi: 10.3354/sedao00003

Boidron-Métairon, I. F. (1995). "Larval nutrition," in *Ecology of marine invertebrate larvae*. Ed. L. McEdward (Boca Raton, FL, USA: CRC Press), 223–248.

Boncagni, P., Rakaj, A., Fianchini, A., and Vizzini, S. (2019). Preferential assimilation of seagrass detritus by two coexisting Mediterranean sea cucumbers: *Holothuria polii* and holothuria tubulosa. *Estuar. Coast.* 231, 106464. doi: 10.1016/j.ecss.2019.106464

Bordbar, S., Anwar, F., and Saari, N. (2011). High – value components and bioactives from sea cucumbers for functional food – a review. *Mar. Drugs* 9 (10), 1761–1805. doi: 10.3390/md9101761

Borrero-Pérez, G., Pérez-Ruzafa, A., Marcos, C., and González-Wangüemert, M. (2009). The taxonomic status of some Atlanto-Mediterranean species in the subgenus *Holothuria* (Echinodermata: Holothuroidea: Holothuriidae) based on molecular evidence. *Zool. J. Lin. Soc* 157, 51–69. doi: 10.1111/j.1096-3642.2009.00529.x

Bulteel, P., Jangoux, M., and Coulon, P. (1992). Biometry, bathymetric distribution, and reproductive cycle of the holothuroid *Holothuria tubulosa* (Echinodermata) from Mediterranean Sea grass beds. *Mar. Ecol.* 13, 53–62. doi: 10.1111/j.1439-0485.1992.tb00339.x

Cameron, J. L., and Fankboner, P. V. (1989). Reproductive biology of the commercial sea cucumber *Parastichopus californicus* (Stimpson) (Echinodermata: Holothuroidea). II. Observations on the ecology of development, recruitment, and the juvenile life stage. *J. Exp. Mar. Biol. Ecol.* 127, 43–67. doi: 10.1016/0022-0981(89)90208-6

Cerri, P. S., and Sasso-Cerri, E. (2003). Staining methods applied to glycol methacrylate embedded tissue sections. *Micron* 34, 365–372. doi: 10.1016/S0968-4328(03)00098-2

Choo, P. S. (2008). "Population status, fisheries and trade of sea cucumbers in Asia," In: *Sea Cucumbers: a Global Review on Fisheries and Trade. FAO Fisheries and Aquaculture Technical Paper.No.516*. Eds. V. Toral – Granda, A. Lovatelli and M. Vasconcellos (Rome: FAO), 81–118. Available at: http://www.fao.org/docrep/011/i0375e/i0375e00.htm.

CIE, Commission Internationale de l'Eclairage (2008). *Colorimetry – part 4: CIE 1976 l*a*b* color spaces* (Vienna: Publication CIE), 12.

Clarke, K. R., and Gorley, R. N. (2015). PRIMER v7: User Manual/Tutorial. PRIMER-EPlymouth..

Conand, C. (1981). Sexual cycle of three commercially important holothurian species (Echinodermata) from the lagoon of new Caledonia. *Bull. Mar. Sci.* 31 (3), 523–543.

Conand, C. (2006). Sea Cucumber Biology, Taxonomy, Distribution and Conservation Status. In: *Proceedings of the CITES workshop on the conservation of sea cucumbers in the families Holothuriidae and Stichopodidae*. A.W. Bruckner (editor). NOAA Technical Memorandum NMFS- OPR 34 , Silver Spring, MD, 244 pp.

Conand, C., Polidoro, B., Mercier, A., Gamboa, R., Hamel, J. F., and Purcell, S. (2014). The IUCN red list assessment of aspidochirotid sea cucumbers and its implications. *SPC Beche-de-mer Inf. Bull.* 34, 3–7.

Costa, V., Mazzola, A., and Vizzini, S. (2014). *Holothuria tubulosa* Gmelin 1791 (Holothuroidea, Echinodermata) enhances organic matter recycling in *Posidonia oceanica* meadows. *J. Exp. Mar. Bio. Ecol.* 461, 226–232. doi: 10.1016/j.jembe.2014.08.008

Dereli, H., and Aydin, M. (2021). Sea Cucumber fishery in Turkey: Management regulations and their efficiency. *Reg. Stud. Mar. Sci.* 41, 101551. doi: 10.1016/j.rsma.2020.101551

Dereli, H., Culha, S. T., Culha, M., Ozalp, B. H., and Tekinay, A. A. (2016). Reproduction and population structure of the sea cucumber *Holothuria tubulosa* in the dardanelles strait, Turkey. *Med. Mar. Sci.* 17, 47–55. doi: 10.12681/mms.1360

Despalatović, M., Grubelić, I., Šimunović, A., Antolić, B., and Žuljević, A. (2004). Reproductive biology of the holothurian *Holothuria tubulosa* (Echinodermata) in the Adriatic Sea. *J. Mar. Biol. Assoc. UK.* 84, 409–414. doi: 10.1017/S0025315404009361h

Domínguez-Godino, J., and Gonzàlez-Wangüemert, M. (2018). Breeding and larval development of *Holothuria mammata*, a new target species for aquaculture. *Aqua. Res.* 49, 1430–1440. doi: 10.1111/are.13597

Félix, P. M., Pombo, A., Azevedo Silva, F., Simões, T., Marques, T. A., Melo, R., et al (2021). Modelling the Distribution of a Commercial NE-Atlantic Sea Cucumber, *Holothuria mammata*: Demographic and Abundance Spatio-Temporal Patterns. *Front. Mar. Sci.* 8, 675330. doi: 10.3389/fmars.2021.675330

Foglietta, L. M., Camejo, M. I., Gallardo, L., and Herrera, F. C. (2004). A maturity index for holothurians exhibiting asynchronous development ofgonad tubules. *J. Exp. Mar. Biol. Ecol.* 303, 19–30. doi: 10.1016/j.jembe.2003.10.019

Gaudron, S. M., Kohler, S. A., and Conand, C. (2008). Reproduction of the sea cucumber *Holothuria leucospilota* in the Western Indian Ocean: biological and ecological aspects. *Invertebr. Reprod. Dev.* 51, 19–31.

Glockner-Fagetti, A., Calderon – Aguilera, L. E., and Herrero – Pérezrul, M. D. (2016). Density decrease in an exploited population of brown sea cucumber *Isostichopus fuscus* in a biosphere reserve from the Baja California peninsula, Mexico. *Ocean Coast. Manage.* 121, 49–59. doi: 10.1016/j.ocecoaman.2015.12.009

González-Wangüemert, M., Aydin, M., and Conand, C. (2014). Assessment of sea cucumber populations from the Aegean Sea (Turkey): first insights to sustainable management of new fisheries. *Ocean Coast. Manage.* 92, 87–94. doi: 10.1016/j.ocecoaman.2014.02.014

González-Wangüemert, M., Domínguez – Godino, J. A., and Cánovas, F. (2018). The fast development of sea cucumber fisheries in the Mediterranean and NE Atlantic waters: from a new marine resource to its over – exploitation. *Ocean Coast. Manage.* 151, 165–177. doi: 10.1016/J.OCECOAMAN.2017.10.002

González – Wangüemert, M., Valente, S., and Aydin, M. (2015). Effects of fishery protection on biometry and genetic structure of two target sea cucumber species from the Mediterranean Sea. *Hydrobiologia* 743, 65–74. doi: 10.1007/s10750-014-2006-2

González-Wangüemert, M., Valente, S., Henriques, F., Domínguez – Godino, J. A., and Serrão, E. A. (2016). Setting preliminary biometric baselines for new target sea cucumbers species of the NE Atlantic and Mediterranean fisherie. *Fish. Res.* 17957, 66. doi: 10.1016/j.fishres.2016.02.008

Hamel, J.-F., Conand, C., Pawson, D. L., and Mercier, A. (2001). Biology of the sea cucumber *Holothuria scabra* (Holothuroidea: Echinodermata) and its exploitation as beche-de-mer. *Adv. Mar. Biol.* 41, 129–223.

Hamel, J., Eeckhaut, I., Conand, C., Sun, J., Caulier, G., and Mercier, A. (2022). Global knowledge on the commercial sea cucumber *Holothuria scabra*. *Adv. Mar. Biol.* 91, 1–286. doi: 10.1016/bs.amb.2022.04.001

Hamel, J.–F., and Mercier, A. (2004). "Synchronous gamete maturation and reliable spawning induction method in holothurians," in *Advances in Sea cucumber aquaculture and management*. Eds. A. Lovatelli, C. Conand, S. Purcell, S. Uthicke, J.–F. Hamel and A. Mercier (Rome: FAO), 359–371. Fisheries Technical Paper. No. 463.

Hamel, J., and Mercier, A. (2008). "Population status, fisheries and trade of sea cucumbers in temperate areas of the northern hemisphere," in *Sea Cucumbers. a global review of fisheries and trade*. Eds. V. Toral – Granda, A. Lovatelli and M. Vasconcellos (Rome: FAO), 257–291. FAO Fisheries and Aquaculture Technical Paper. No. 516.

Herrero-Pérezrul, D., Reyes-Bonilla, H., Garcia-Dominguez, F., and Cintra-Buenrostro, C. E. (1999). Reproduction and growth of *Isostichopus fuscus* in the southern gulf of California, Mexico. *Mar. Biol.* 135, 521–532. doi: 10.1007/s002270050653

Horton, T., Kroh, A., Ahyong, S., Bailly, N., Boyko, C. B., Brandão, S. N., et al. (2018). World register of marine species (WoRMS). Available at: https://www.marinespecies.org/imis.php?module=ref&refid=291592.

Hyman, L. H. (1955). *The invertebrates, vol. 4, Echinodermata* (New York, USA: McGraw – Hill).

Janakiram, N. B., Mohammed, A., and Rao, C. V. (2015). Sea Cucumbers metabolites as potent anti – cancer agents. *Mar. Drugs* 13 (5), 2909–2923. doi: 10.3390/md13052909

Kazanidis, G., Lolas, A., and Vafidis, D. (2014). Reproductive cycle of the traditionally exploited sea cucumber *Holothuria tubulosa* (Holothuroidea: Aspidochirotida) in Pagasitikos Gulf, western Aegean Sea. Greece. *Turk. J. Zool.* 38, 306–315. doi: 10.3906/zoo-1302-31

Kazanidis, G., Antoniadou, C., Lolas, A. P., Neofitou, N., Vafidis, D., Chintiroglou, C., et al. (2010). Population dynamics and reproduction of holothuria tubulosa (Holothuroidea: Echinodermata) in the Aegean Sea. *J. Mar. Biol. Assoc. UK* 90 (5), 895–901. doi: 10.1017/S0025315410000251

Keys, A. B. (1928). The weight-length relationship in fishes. in *Proceedings of the National Academy of Science*, Vol. XIV. 12, 922–925(Washington, DC).

Kinch, J., Purcell, S., Uthicke, S., and Friederich, K. (2008). "Population status, fisheries and trade of sea cucumbers in the Western central pacific," in *Sea Cucumbers: A global review of fisheries and trade*. Eds. M. V. Toral – Granda, A. Lovatelli and M. Vasconcellos (Rome: FAO), 7–55. FAO Fisheries and Aquaculture Technical Paper 516.

Kühnhold, H., Novais, S. C., Alves, L. M. F., Kamyab, E., Lemos, M. F. L., Slater, M. J., et al. (2019). Acclimation capability inferred by metabolic performance in two sea cucumber species from different latitudes. *J. Therm. Biol.* 84, 407–413. doi: 10.1016/j.jtherbio.2019.07.019

Lee, S., Ford, A. K., Mangubhai, S., Wild, C., and Ferse, S. C. A. (2018). Length – weight relationship, movement rates, and *in situ* spawning observations of *Holothuria scabra* (sandfish) in Fiji. *SPC Beche – de – mer Inf. Bull.* 38, 11–14.

Leite-Castro, L. V., Souza, J., Salmito-Vanderley, C. S., Nunes, J. F., Hamel, J. F., and Mercier, A. (2016). Reproductive biology of the sea cucumber *Holothuria grisea* in Brazil: importance of social and environmental factors in breeding coordination. *Mar. Biol.* 163, 67. doi: 10.1007/s00227-016-2842-x

Lovatelli, A., Conand, C., Purcell, S., Uthicke, S., Hamel, J., and Mercier, A. (eds). (2004). Advances in sea cucumber aquaculture and management.

Mangion, P., Taddei, D., Conand, C., and Frouin, P. (2004). "Feeding rate and impact of sediment reworking by two deposit feeders *Holothuria leucospilota* and *Holothuria atra* on fringing reef (Reunion island, Indian ocean)," in *Echinoderms: München*. Eds. T. Heinzeller and J. H. Nebelsick (London: Taylor and Francis), 311–317.

Marquet, M., Conand, C., Power, D. M., Canàrio, A. V. M., and González – Wangüemert, M. (2017). Sea Cucumbers, *Holothuria arguinensis* and *H. mammata*, from the southern Iberian peninsula: Variation in reproductive activity between populations from different habitats. *Fish. Res.* 191, 120–130. doi: 10.1016/S0065-2881(09)55001-8

Massin, C., and Jangoux, M. (1976). Observations ecologiques sur *Holothuria tubulosa*, *H. poli* et *H. forskali* (Echinodermata- Holothuroidea) et comportement alimentaire de *H. tubulosa*. *Cah. Biol. Mar.* 17, 45–59.

Mercier, A., and Hamel, J.-F. (2009). Endogenous and exogenous control of gametogenesis and spawning in echinoderms. *Adv. Mar. Biol.* 55, 1–302.

Mercier, A., Battaglene, S. C., and Hamel, J. (2000). Settlement preferences and early migration of the tropical sea cucumber *Holothuria scabra*. *J. Exp. Mar. Biol. Ecol.* 249, 89–110. doi: 10.1016/S0022-0981(00)00187-8

Mezali, K., and Soualili, D. L. (2013). The ability of holothurians to select sediment particles and organic matter. *SPC Beche-de-mer Inf. Bull.* 33, 38–43.

Mezali, K., Zupo, V., and Francour, P. (2006). Population dynamics of *Holothuria (holothuria) tubulosa* and *Holothuria (lessonothuria) polii* of an Algerian *Posidonia oceanica* meadow. *Biol. Mar. Medit.* 13 (4), 158–161.

Mezali, K., Soualili, D. L., Neghli, L., and Conand, C. (2014). Reproductive cycle of the sea cucumber *Holothuria* (Platyperona) *sanctori* (Holothuroidea: Echinodermata) in the southwestern Mediterranean Sea: interpopulation variability. *Invertebr. Reprod. Dev.* 58, 179–189. doi: 10.1080/ 07924259.2014.883337

Mohsen, M., and Yang, H. (2021). "Sea Cucumbers research in the Mediterranean and the red seas," in *Sea Cucumbers aquaculture, biology and ecology*. Eds. M. Mohsen and H. Yang (Academic Press), 61–101. doi: 10.1016/B978-0-12-824377-0.00002-5

Morgan, A. D. (2000). Induction of spawning in the sea cucumber *Holothuria scabra* (Echinodermata: Holothuroidea). *J. World Aqua. Soci.* 31, 186–194. doi: 10.1111/j.1749-7345.2000.tb00352.x

Muthiga, N. A. (2006). The reproductive biology of a new species of sea cucumber, *Holothuria* (Mertensiothuria) *arenacava* in a Kenyan marine protected area: The possible role of light and temperature on gametogenesis and spawning. *Mar. Biol.* 149, 585–593. doi: 10.1007/s00227-005-0224-x

Muthiga, N., Kawaka, J., and Ndirangu, S. (2009). The timing and reproductive output of the commercial sea cucumber *Holothuria scabra* on the Kenyan coast. *Estuar. Coast. Shelf Sci.* 84, 353–360. doi: 10.1016/j.ecss.2009.04.011

Navarro, P. G., García-Sanz, S., and Tuya, F. (2012). Reproductive biology of the sea cucumber *Holothuria sanctori* (Echinodermata: Holothuroidea). *Sci. Mar.* 76, 741–752. doi: 10.3989/scimar.03543.15

Neofitou, N., Lolas, A., Ballios, I., Skordas, K., Tziantziou, L., and Vafidis, D. (2019). Contribution of sea cucumber *Holothuria tubulosa* on organic load

reduction from fish farming operation. *Aquaculture* 501, 97–103. doi: 10.1016/j.aquaculture.2018.10.071

Ocaña, A., and Sanchez Tocino, L. (2005). Spawning of *Holothuria tubulosa* (Holothurioidea, Echinodermata) in the Alboran Sea (Mediterranean Sea). *Zool. Baetica* 16, 147–150.

Pasquini, V., Giglioli, A. A., Pusceddu, A., and Addisp, P.. (2021). Biology, ecology and management perspectives of overexploited deposit-feeders sea cucumbers, with focus on *Holothuria tubulosa* (Gmelin, 1788). *Adv. Oceanogr. Limnol.* 12, 9995. doi: 10.4081/aiol.2021.9995

Prato, E., Fanelli, G., Biandolino, F., Chiantore, M., Secci, M., Angioni, A., et al. (2018). Influence of a prepared diet and a macroalga (*Ulva* sp.) on the growth, nutritional and sensory qualities of gonads of the sea urchin *Paracentrotus lividus*. *Aquaculture* 493, 240–250. doi: 10.1016/j.aquaculture.2018.05.010

Prescott, J., Zhou, S., and Prasetyo, A. P. (2015). Soft bodies make estimation hard: correlations among body dimensions and weights of multiple species of sea cucumbers. *Mar. Freshw. Res.* 66, 857–865. doi: 10.1071/MF14146

Purcell, S. W. (2014). Value, market preferences and trade of beche – de – mer from pacific island Sea cucumbers. *PloS One* 9 (4), 95075. doi: 10.1371/journal.pone.0095075

Purcell, S. W., Conand, C., Uthicke, S., and Byrne, M. (2016). Ecological roles of exploited sea cucumbers. Oceanography and Marine Biology. *An Annual Review* 54, 367–386. doi: 10.1201/9781315368597-8

Purcell, S. W., Hair, C. A., and Mills, D. J. (2012). Sea Cucumber culture, farming and sea ranching in the tropics: Progress, problems and opportunities. *Aquaculture* 368 – 369, 68–81. doi: 10.1016/j.aquaculture.2012.08.053

Purcell, S. W., Mercier, A., Conand, S., Hamel, J. F., Toral – Granda, M. V., Lovatelli, A., et al. (2011). Sea Cucumber fisheries: global analysis of stocks, management measures and drivers of overfishing. *Fish. Fish.* 14, 34–59. doi: 10.1111/j.1467-2979.2011.00443.x

Purcell, S. W. (2010). *Managing sea cucumber fisheries with an ecosystem approach*. Eds. A. Lovatelli, M. Vasconcellos and Y. Yimin (Rome: FAO Fisheries and Aquaculture Technical Paper), 520, 157.

Rakaj, A., Fianchini, A., Boncagni, P., Lovatelli, A., Scardi, M., and Cataudella, S. (2018). Spawning and rearing of *Holothuria tubulosa*: a new candidate for aquaculture in the Mediterranean region. *Aquacult. Res.* 49, 557–568. doi: 10.1111/are.13487

Rakaj, A., Fianchini, A., Boncagni, P., Scardi, M., and Cataudella, S. (2019). Artificial reproduction of *Holothuria polii*: a new candidate for aquaculture. *Aquaculture* 498, 444–453. doi: 10.1016/j.aquaculture.2018.08.060

Ram, R., Chand, R. V., and Southgate, P. (2014). Effects of processing methods on the value of bêche – de – mer from the Fiji islands. *J. Mar. Sci. Res. Dev.* 4 (3), 1–7. doi: 10.4172/2155-9910.1000152

Ramírez-González, J., Moity, N., Andrade – Vera, S., and Mackliff, H. R. (2020b). Estimation of age and growth and mortality parameters of the sea cucumber *Isostichopus fuscus* (Ludwig 1875) and implications for the management of its fishery in the Galapagos marine reserve. *Aquac. Fish.* 5 (5), 245–252. doi: 10.1016/j.aaf.2020.01.002

Ramírez-González, J., Moity, N., Andrade – Vera, S., and Reyes, H. (2020a). Overexploitation and more than a decade of failed management leads to no recovery of the galápagos sea cucumber fishery. *Front. Mar. Sci.* 7. doi: 10.3389/fmars.2020.554314

Ramofafia, C., Battaglene, S. C., Bell, J. D., and Byrne, M. (2000). Reproductive biology of the commercial sea cucumber *Holothuria fuscogilva* in the Solomon islands. *Mar. Biol.* 136, 1045–1056. doi: 10.1007/s002270000310

Ramofafia, C., Byrne, M., and Battaglene, C. (2003). Reproduction of the commercial sea cucumber *Holothuria scabra* (Echinodermata: Holothuroidea) in the Solomon islands. *Mar. Biol.* 142, 281–288. doi: 10.1007/s00227-002-0947-x

Ramos-Miranda, J., del Río-Rodríguez, R., Flores-Hernández, D., Rojas-González, R. I., Gómez-Solano, M., Cu-Escamilla, A.d., et al (2017). Reproductive cycle of the sea cucumber Holothuria floridana in the littorals of Campeche, Mexico. *Fish. Sci.* 83, 699–714. doi: 10.1007/s12562-017-1100-6

Reyes-Bonilla, H., and Herrero – Pérezrul, M. D. (2003). Population parameters of an exploited population of *Isostichopus fuscus* (Holothuroidea) in the southern gulf of California, Mexico. *Fish. Res.* 59 (3), 423–430. doi: 10.1016/S0165-7836(02)00023-1

Roberts, D., Gebruk, A. V., Levin, V., and Manship, B. A. D. (2000). Feeding and digestive strategies in deposit – feeding holothurians. *Oceanogr. Mar. Biol. Ann. Rev.* 38, 257–310.

Rohlf, F. J. (2009). *TpsDig Version 2.14*.

Santos, R., Dias, S., Tecelão, C., Pedrosa, R., and Pombo, A. (2017). Reproductive biological characteristics and fatty acid profile of Holothuria mammata (Grube, 1840). *SPC Beche-de-mer Inf. Bull.* 37, 57–64.

Sewell, M. A. (1990). Aspects of the ecology of *Stichopus mollis* (Echinodermata: Holothuroidea) in north-eastern New Zealand. *New Zeal. J. Mar. Freshw. Res.* 24, 97–103.

Sewell, M. A., Tyler, P. A., Young, C. M., and Conand, C. (1997). Ovarian development in the class Holothuroidea: a reassessment of the "tubule recruitment model". Biological Bulletin. *Mar. Biol. Laboratory,Woods Hole* 192, 17–26.

Shiell, G. (2004). "Density of Holothuria nobilis and distribution patterns of common holothurians on coral reefs of Northwestern Australia," in *Advances in Sea Cucumber Aquaculture and Management*. Eds. A. Lovateli, C. Conand, S. Purcell, S. Uthicke, J.-F. Hamel and A. Mercier (Rome: FAO), 231–237.

Shiell, G. R., and Uticke, S. (2006). Reproduction of the commercial sea cucumber *Holothuria whitmaei* (Holothuroidea: Aspidochirotida) in the Indian and Pacific Ocean regions of Australia. *Mar. Biol.* 148, 973–986.

Slater, M. J., Lassudrie, M., and Jeffs, A. G. (2011). Method for determining apparent digestibility of carbohydrate and protein sources for artificial diets for juvenile sea cucumber, *Australostichopus mollis*. *J. World Aquacult. Soc.* 42 (5), 714–725. doi: 10.1111/j.1749-7345.2011.00510.x

Sloan, N. A. (1979). Microhabitat and resource utilization in cryptic rocky intertidal echinoderms at Aldabra Atoll, Seychelles. *Mar. Biol.* 54, 269–279. doi: 10.1007/ BF00395789

Smiley, S. (1990). A review of echinoderm oogenesis. *J. Electron Microsc.* 16, 96–114. doi: 10.1002/jemt.1060160203

Smiley, S. (1988). The dynamics of oogenesis and the annual ovarian cycle of Stichopus californicus (Echinodermata: Holothuroidea). *Biological Bulletin. Marine Biological Laboratory, Woods Hole* 175, 79–93.

Smiley, S., McEuen, F. S., Chaffee, C., and Krishnan, S. (1991). "Echinodermata: Holothuroidea," in *Reproduction of marine invertebrates, echinoderms and iophophorates, vol. VI*. Eds. A. C. Giese, J. S. Pearse and V. B. Pearse (Pacific Grove, California, USA: Boxwood Press), 663–750.

Soliman, T., Reimer, J. D., Kawamura, I., van der Meij, S. E. T., Reijnen, B. T., and Paulay, G. (2019). Description of the juvenile form of the sea cucumber *Thelenota anax* H. L. Clar. *Mar. Biodivers.* 49, 547–554. doi: 10.1007/ s12526-017-0820-2

Tahri, Y., Dermeche, S., Chahrour, F., and Bouderbala, M. (2019). The reproduction cycle of the sea cucumber *Holothuria* (Holothuria) *tubulosa* Gmelin 1791 (Echinodermata Hlothuroidea Holothuriidae) in Oran coast, Algeria. *Biodivers. J.* 10, 159–172. doi: 10.31396/Biodiv.Jour.2019.10.2.159.172

Tan, S. H., and Zulfigar, Y. (2001). "Reproductive cycle of stichopus chloronotus (Brand) in the straits of malacca," in *Echinoderms* (Lisse: Swets & Zeitlinger)2000.

Tolon, T., Emiroglu, D., Guinai, D., and Hanci, B. (2017). Effect of stocking density on growth performance of juvenile sea cucumber *Holothuria tubulosa* (Gmelin 1788). *Aquac. Res.* 48 (8), 4124–4131. doi: 10.1111/are.13232

Toral-Granda, V., Lovatelli, A., and Vasconcellos, M. (2008). *Sea Cucumbers. A global review of fisheries and trade* (Rome: FAO), 231–253. FAO Fisheries and Aquaculture Technical Paper. No. 516.

Tortonese, E. (1965). *Echinodermata* (Bologna: Fauna d'Italia. Ed. Calderini).

Uthicke, S. (2001). Nutrient regeneration by abundant coral reef holothurians. *J. Exp. Mar. Bio. Ecol.* 265 (2), 153–170. doi: 10.1016/S0022-0981(01)00329-X

Vafeiadou, A. M., Antoniadou, C., Vafidis, D., Fryganiotis, K., and Chintiroglou, C. (2010). Density and biometry of the exploited holothurian *Holothuria tubulosa* at the Dodecanese, south Aegean Sea. *Rapp. Commun. Int. Mer. Médit* 9, 661.

Venâncio, E., Félix, P. M., Brito, A. C., Azevedo e Silva, F., Simões, T., Sousa, J., et al. (2022). Reproductive biology of the Sea cucumber *Holothuria mammata* (Echinodermata: Holothuroidea). *Biology* 11, 622. doi: 10.3390/biology11050622

Wilkie, I. C. (2001). Autotomy as a prelude to regeneration in echinoderms. *Microsc. Res. Tech.* 55 (6), 369–396. doi: 10.1002/jemt.1185

Yang, H., and Bai, Y. (2015). "*Apostichopus japonicus* in the life of Chinese people". in *The Sea cucumber Apostichopus japonicus. history, biology, and aquaculture*. Eds. H. Yang, J. F. Hamel and A. Mercier (Academic Press), 1–24.

Yang, H., Hamel, J., and Mercier, A. (2015). *The Sea cucumber Apostichopus japonicus: History, biology and aquaculture* (London, UK: Elsevier), 454.

Yang, H., Zhou, Y., Zhang, T., Yuan, X., Li, X., Liu, Y., et al. (2006). Metabolic characteristics of sea cucumber, *Apostichopus japonicus* (Selenka) during aestivation. *J. Exp. Mar. Biol. Ecol.* 330, 505–510. doi: 10.1016/j.jembe.2005.09.010

Zang, Y., Tian, X., Dong, S., and Dong, Y. (2012). Growth, metabolism and immune responses to evisceration and the regeneration of viscera in sea cucumber, *Apostichopus japonicus*. *Aquaculture* 358 – 359, 50–60. doi: 10.1016/j.aquaculture.2012.06.007

Zar, J. H. (1999). *Biostatistical analysis. 4th ed* (Upper Saddle River, NJ: Prentice Hall), 663.

frontiers | Frontiers in Marine Science

TYPE Original Research
PUBLISHED 03 November 2022
DOI 10.3389/fmars.2022.953388

OPEN ACCESS

EDITED BY
Wei Huang,
Ministry of Natural Resources, China

REVIEWED BY
Li Li,
Ocean University of China, China
Chenghua Li,
Ningbo University, China

*CORRESPONDENCE
Songchong Lu
luschvip@outlook.com
Libin Zhang
zhanglibin@qdio.ac.cn

SPECIALTY SECTION
This article was submitted to Marine Fisheries, Aquaculture and Living Resources, a section of the journal Frontiers in Marine Science

RECEIVED 26 May 2022
ACCEPTED 20 October 2022
PUBLISHED 03 November 2022

CITATION
Deng B, Ru X, Wang T, Zhang C, Sun W, Lu S and Zhang L (2022) Seasonal variations in microbial diversity and metabolite profiles of the gut of sea cucumber (*Apostichopus japonicus*). *Front. Mar. Sci.* 9:953388. doi: 10.3389/fmars.2022.953388

Seasonal variations in microbial diversity and metabolite profiles of the gut of sea cucumber (*Apostichopus japonicus*)

Beini Deng[1,2,3], Xiaoshang Ru[2,3,4,5,6], Ting Wang[2,3], Chenxi Zhang[2,3], Wanhui Sun[7], Songchong Lu[1]* and Libin Zhang[2,3,4,5,6]*

[1]College of Life Sciences, Qingdao Agricultural University, Qingdao, China, [2]CAS Key Laboratory of Marine Ecology and Environmental Sciences, Institute of Oceanology, Chinese Academy of Sciences, Qingdao, China, [3]CAS Engineering Laboratory for Marine Ranching, Institute of Oceanology, Chinese Academy of Sciences, Qingdao, China, [4]Laboratory for Marine Ecology and Environmental Science, Qingdao National Laboratory for Marine Science and Technology, Qingdao, China, [5]Center for Ocean Mega-Sciences, Chinese Academy of Sciences, Qingdao, China, [6]Shandong Province Key Laboratory of Experimental Marine Biology, Qingdao, China, [7]Laizhou Municipal Bureau of Marine Development And Fisheries, Yantai, China

The sea cucumber (*Apostichopus japonicus*) is the main economic species in China and has a significant role in aquaculture. Gut microbiome composition is closely related to external environments. In this study, we identified the effects of seasonal changes on the composition and main metabolites of symbiotic microorganisms in the intestine of *A. japonicus*. We used 16S rRNA sequencing to identify the composition of symbiotic microorganisms in different seasons. Intestinal metabolites were determined using liquid chromatography with tandem mass spectrometry, which linked symbiotic microorganisms to intestinal metabolites. Analyzing changes in intestinal microbial composition across different seasons. The results showed that seasonal changes of intestinal microorganisms were significant, *A. japonicus* were infected by *Vibrio* easily in summer, Stigmasterol and sitosterol could affect the growth of body wall of *A. japonicus*. It is vital importance for *A. japonicus* that the results benefit for the growth, immunity and aquaculture.

KEYWORDS

16S rRNA, gut microbiome, metabolomics, sea cucumber (*Apostichopus japonicus*), seasonal variations

Introduction

The sea cucumber (*Apostichopus japonicus*) is highly favored by Asian and Chinese populations due to its unique flavor and taste. The aquaculture of sea cucumbers has significantly increased in recent years, and has become a major aquaculture species in China, generating huge revenues for the aquaculture industry (Ru et al., 2019). Sea cucumbers mainly ingest sediment to extract organic matter and microorganisms (Xu et al., 2015; Mohsen et al., 2018) and are colloquially known as "Ocean scavengers", therefore, they have crucial roles in marine ecosystems. The diet of sea cucumber is closely related to the variation of environment, so, the intestinal contents of sea cucumbers can reflect ecosystem characteristics and environmental changes.

Sea cucumber activities are closely related to the seasons. As a temperate species, spring and autumn are fast-growing seasons when the water temperature is 10–20°C. Thus, feeding rates increase and are concomitant with increased body weight. Aestivation begins when the water temperature reaches 20.0–24.5°C. During aestivation, sea cucumbers stop eating and intestinal degeneration occurs and activities slow down (Mitsukuri, 1903; Tanaka, 1958a; Tanaka, 1958b; Yang et al., 2015). In autumn, water temperatures are decreased and feeding activity returns to normal. In winter, water temperatures are very low and activity, growth, and metabolism of sea cucumber are decreased.

Intestinal microbiotas are associated with all aspects of host health, including metabolism and digestion, the immune system, and even behavior, while disorders or abnormal intestinal microbiota development are related to different gastrointestinal and metabolic diseases (Spor et al., 2011). The gut houses an enormous variety of microbial communities with important roles in host metabolism and immunity (Egerton et al., 2018). The gut microbiome is essential for host health and physiological functions and has important roles enhancing host digestion, regulating gut endocrine functions and neurological signaling, and maintaining host reproductive capacity (Lynch and Pedersen, 2016; Fan and Pedersen, 2021). In particular, the microbiome performs functions that the host cannot perform, including the production and regulation of metabolites which are used as metabolic substrates and signaling molecules, with major impact on host metabolism and health (Schoeler and Caesar, 2019). Thus, gut microbiome variations may lead to metabolite alterations, such as metabolites are the end products of many cell regulatory processes, significant microbiome alterations can impact responses to the external environment (Fiehn, 2020; Xing et al., 2021). Thus, joint microbiome and metabolome studies are required to evaluate and characterize host-microbiome interactions (Turnbaugh and Gordon, 2008; Visconti et al., 2019).

The gut microbiome is highly plastic and is altered throughout life by environmental factors (Goodrich et al., 2014; Goodrich et al., 2016; Xie et al., 2016; Visconti et al., 2019). Microorganisms in organism have critical roles; however, relatively few studies have focused on intestinal microorganism and metabolite links and their relationship with seasonal changes, therefore, we investigated sea cucumber microbiota and metabolism across different seasons using 16S rRNA and liquid chromatography with tandem mass spectrometry (LC-MS/MS). Additionally, using Kyoto Encyclopedia of Genes and Genomes (KEGG) resources, we analyzed different molecular pathways to explore metabolic differences. Our aims were to; (1) identify seasonal variations of intestinal microorganisms, (2) examine the effects of seasonal variations of sea cucumber microbiota and metabolite on immune of sea cucumbers, (3) explore the effects of seasonal variations of sea cucumber microbiota and metabolite on growth of sea cucumbers.

Materials and method

Experimental animals

Sea cucumbers were collected from Rongcheng Swan Lake (Weihai City, Shandong Province, China, 122°59'E, 37°36'N) in November, 2019 (autumn, the seawater temperature was 16.8° C); January, 2020 (winter, the seawater temperature was 1.6°C); April, 2020 (spring, the seawater temperature was 14.1°C); and June, 2020 (summer, the seawater temperature was 23.2°C). Sea cucumbers were weighed approximately 150–200 g. Sea cucumbers were euthanized by decollation, the whole sampling process was aseptic. The intestinal contents from ten individuals, during each season, (40 individuals in total), were used for sampling, 16S rRNA sequencing, and metabolomic analysis. Animals were frozen in liquid nitrogen and stored at −80°C.

Microbial *16S rRNA* sequencing and analysis

Microbial DNA was extracted using HiPure Stool DNA Kits (Magen, Guangzhou, China) according to manufacturer's protocols. The *16S rDNA* hypervariable V3–V4 region was amplified by polymerase chain reaction (PCR) (95°C for 2 min, followed by 35 cycles of 95°C for 30 s, 60°C for 45 s, and 72°C for 90 s, with a final extension of 72°C for 10 min) using primers 341F (5'-CCTACGGGNGGCWGCAG-3') and 806 R (5'-GGACTACHVGGGTATCTAAT-3'). PCR was performed in 50 μL reaction volumes and contained TransGen High-Fidelity PCR SuperMix (TransGen Biotech, Beijing, China), 0.2 μM forward and reverse primers, and 5 ng template DNA.

Clean tags were clustered into operational taxonomic units (OTUs) at ≥ 97% similarity using the UPARSE pipeline (version 9.2.64). Chimeric tags were removed using the UCHIME algorithm to generate effective tags for further analysis. Tag

sequences with the highest abundance were selected. Taxonomic classifications were performed in BLAST (version 2.6.0) (Altschul et al., 1990) and representative OTU sequences were searched against the National Center for Biotechnology Information 16S ribosomal RNA database (http://www.ncbi.nlm.nih.gov) (version 202101) for cluster analysis.

Metabolite profiling

Approximately 50 mg intestinal contents were weighed into a clean microtube. After, 1000 μL extract solvent (acetonitrile-methanol-water in a 2:2:1) was added, the sample was vortexed for 30 s, homogenized at 45 Hz for 4 min, and sonicated for 5 min in an ice-water bath. The homogenate and sonicate circle were repeated three times, followed by incubation for 1 hour at −20°C, and centrifugation at 12000 rpm for 15 min at 4°C. The supernatant was transferred to LC-MS/MS vials and stored at −80°C until MS analysis.

LC-MS/MS analyses were performed using an UHPLC system (1290, Agilent Technologies) on a UPLC HSS T3 column (2.1 mm × 100 mm, 1.8 μm) coupled to a Q Exactive system (Orbitrap MS, Thermo). Mobile phase A comprised 0.1% formic acid in water for positive, and 5 mmol/L ammonium acetate in water for negative. Mobile phase B was acetonitrile. MS raw data (.raw) files were converted to mzML format using ProteoWizard, processed in R package XCMS (version 3.2), and included retention time alignment, peak detection, and peak matching. Data were then filtered using the following criterion: sample numbers contain a metabolite was less than 50% all sample numbers in a group. Normalization to an internal standard (Roberts et al., 2012) for each sample was also performed.

Statistical analysis

Microbiota analyses incorporated abundance, species, α-diversity indices and LEFSe. The abundance statistics of each taxonomy was visualized using Krona (Cheung et al., 2010) (version 2.6). Chao1 and Shannon indices were calculated in QIIME (Caporaso et al., 2010) (version 1.9.1). Species comparison between groups was calculated by welch's t-test in R project Vegan package (version 2.5.3). Biomarker features in each group were screened by LEFSe software (version 1.0), taking Linear Discriminant Analysis (LDA)>3 as a threshold.

For metabolomic analyses, we performed principal component analysis (PCA), analyzed KEGG pathways. T-tests were used as a univariate analysis for screening differential metabolites. P values from t-tests < 0.05 and VIP ≥ 1 were considered differential metabolites between two groups. Metabolites were mapped to KEGG pathways for pathway and enrichment analysis. The calculated *p*-value was gone through FDR correction, taking FDR ≤ 0.05 as a threshold. Pathways meeting these conditions were defined as significantly enriched for differential metabolites.

Results

Gut microbial profiles of *A. japonicus* across different seasons

Gut microbiota composition varied greatly with seasons. The dominant phyla were Planctomycetes and Proteobacteria, as the results shown, these phyla are complementary (Figures 1A, B). It's worth noting that it is higher than other seasons that the relative abundance of Cyanobacteria, Verrucomicrobia and Bacteroidetes in spring (Figure 1B). According to the PCA which revealed the relationship of intestinal microbes among different seasons, the results showed that the compositions of autumn and winter are similar, however, the compositions among spring, summer and autumn are different significantly (Figure 1C).

The statistics results showed that four phyla of intestinal microbiota were significantly different in spring and summer, and four phyla were significantly different in autumn and summer (Figures 2A, B). Notably, the mean abundance of Proteobacteria was higher in summer than in autumn. Thus, LEFSe analysis further on this phenomenon between summer and autumn. Then, we found that *Vibrio* populations spike in summer, significantly higher than in autumn (Figure 3).

Gut microbial diversity in different seasons

Alpha-diversity indices reflected the diversity and richness of symbiotic microbiota in each season, incorporated Chao1 and Shannon indices. Chao1 indices reflect species abundance in samples; thus, symbiotic microbiota abundance was poor in summer, (Figure 4A). Simpson indices reflect species richness, we can learn that the highest richness was in autumn, but the richness was relatively low in spring (Figure 4B). The phenomenon of richness has significant seasonal trends. It rises from spring to autumn, and then falls until the following spring.

Metabolite variations across different seasons

To further understand gut microbe metabolic interactions, LC-MS/MS was used for metabolic profiling. Among the 26,136 identified metabolites, 13,116 were tested in positive ion mode (POS) and 13,020 in negative ion mode (NEG). From PCA, we could learn that the relationships among seasons (Figure 5). It is

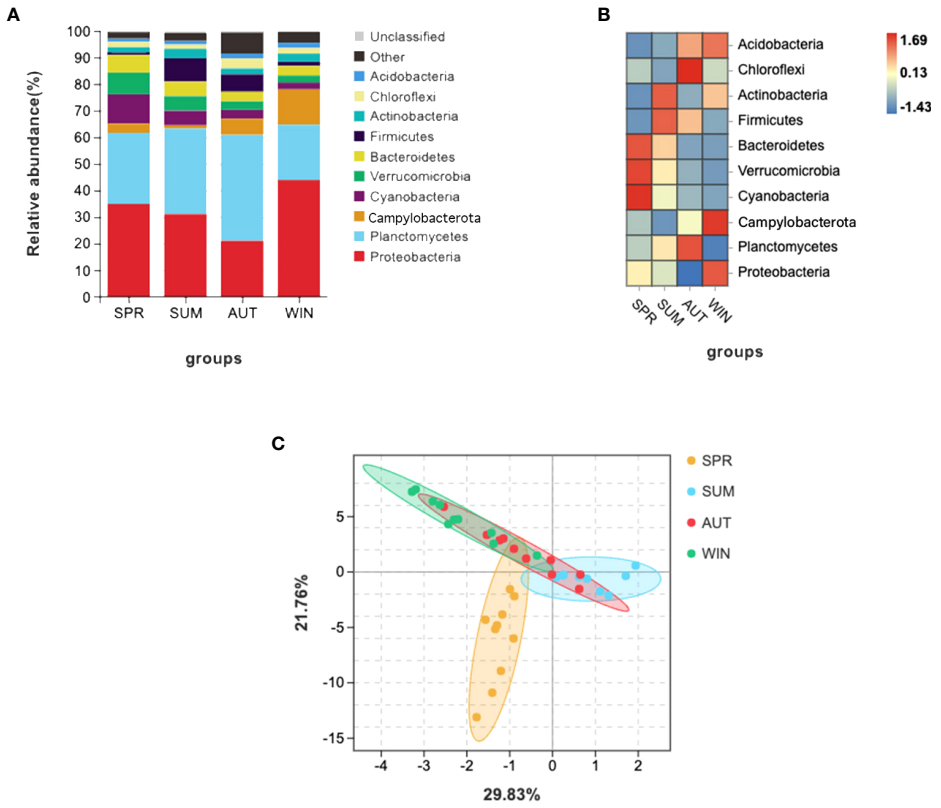

FIGURE 1
16S RNA summary and principal component analysis (PCA) of gut microbiota in *A. japonicus*. **(A)** Relative abundance (%) of the main phyla in the gut microbiota. **(B)** Heatmap showing the dynamic abundance of gut microbiota from *A. japonicus* across different seasons. **(C)** PCA of OTU levels.

interesting that these PCA results are similar with the PCA analysis of microbiota. The principal component of metabolites of autumn and winter are similar, however, the principal component of metabolites among spring, summer and autumn are different significantly.

Differential metabolites were further analyzed using KEGG annotations (VIP > 1, $P < 0.05$). We analyzed three secondary metabolic pathways: amino acid, carbohydrate, and lipid metabolism between summer and spring, and these pathway between summer and autumn (Figure 6). Our results showed that protein digestion and absorption exhibited the most significant differences between summer and autumn (Figure 6). Pathways of biosynthesis of unsaturated fat acids, primary bile acid biosynthesis, and mineral absorption were more significant, while sulfur metabolism exhibited the most significant differences between summer and spring (Figure 7). We also analyzed differences in metabolites among summer, spring, and autumn. Metabolites in summer were significantly higher than those in spring and autumn and mainly included benzene and substituted derivatives (phenylacetaldehyde, L-formylkynurenine, and phenylethylamine), steroids and steroid derivatives (cholesterol sulfate), carboxylic acids and derivatives (L-isoleucine), and glycerophospholipids (lysoPC).

Discussion

Variations in gut microbiota in *A. japonicus* across different seasons

According to the results, we find that the microbiota has seasonal variations in the gut of *A. japonicus*, and traits are significant. Variations of spring, summer and autumn are obviously different. According to Chao1 index, the richness in samples of species is lowest in summer and increased gradually from autumn. It is closely that this phenomenon related to the life history of *A. japonicus*. The reason is that *A. japonicus* entered aestivation in summer, the intestine degenerated, stop feeding, thus, the microbial contents in intestinal tract decrease sharply (Mitsukuri, 1903; Tanaka, 1958a; Tanaka, 1958b; Yang et al., 2015). In autumn, *A. japonicus* recovered feeding, thus, the abundance of gut microbiota increased. According to the

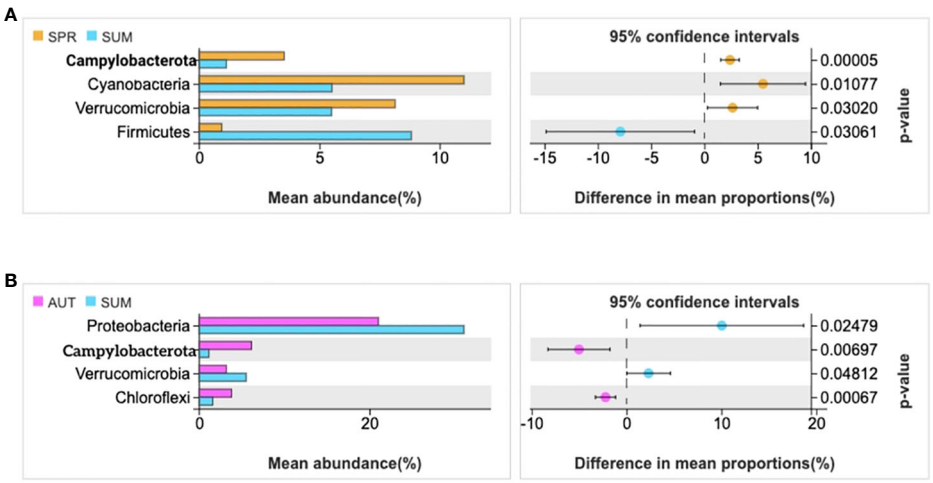

FIGURE 2
Statistical examination of intestinal microbial diversity of A. japonicus across different seasons ($P \leq 0.05$). **(A)** the statistical examination between spring and summer. **(B)** the statistical examination between summer and autumn.

Shannon index, the seasonal variations of intestinal microbial richness were more obvious, it gradually increased from spring to autumn and began to decrease after reaching its maximum in autumn. The change trend of Shannon index is opposite to Chao1, this is the same as the change trend of microorganisms in the environment. This trend maybe relates to the change of sea water nutrient. According to previous research in Weihai sea area (Shandong Province, China), the content of inorganic nitrogen (DIN) in summer is lower than in spring and autumn, DIN changes were positively correlated with Chao1 changes, the N/P of nutrients in autumn is higher than summer and spring (Fang et al., 2012), which is positively correlated with Shannon index. The change trend of microbe in the intestine of *A. japonicus* is consistent with the change of nutrient in the environment. Microbial richness in the gut of the sea cucumber was highest in the autumn, due to the high nutrient composition in seawater in autumn, which promoted the growth of a variety of microbiota (Bunse and Pinhassi, 2017).

From our analysis of intestinal microbial diversity across different seasons, we observed Proteobacteria maintained dominant positions. Proteobacteria is the largest bacterial flora population in aquaculture systems, and the most abundant phylum in the trench sediment and water samples (Herlambang et al., 2021). Thus, Proteobacteria of gut of *A. japonicus* may come from environment. Previous studies have shown that, Proteobacteria is also dominant bacteria in sea urchin (Hakim et al., 2016), and this bacterium has major roles in nitrogen and carbon cycles in aquaculture environments (Wiegand et al., 2018). According to previous research on the rice-fish farming system which investigated the effects of several classes of Proteobacteria in nutrient cycle, such as, Alphaproteobacteria members are involved in the nitrogen cycle (Newton et al., 2011), Gammaproteobacteria help modulate excess nitrate (Fernandes et al., 2014; Herlambang et al., 2021). At the same time, this bacterium is related to sulfur-related processes, from the study of metabolites, it can be found that the sulfur metabolism pathway is indeed subjected to some changes.

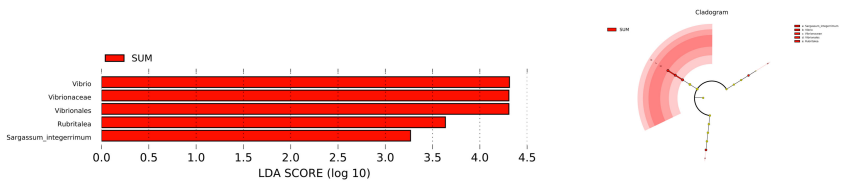

FIGURE 3
LEFSe analyzed the species of gut microbiota of A. japonicus between summer and autumn (LDA>3).

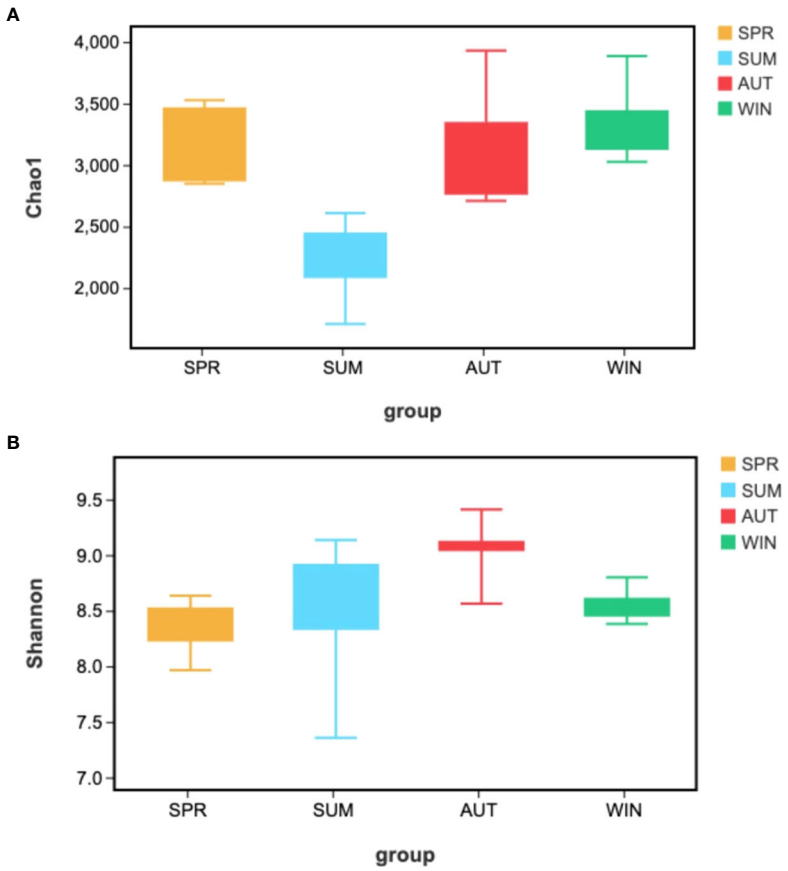

FIGURE 4
Kruskal-Walli's rank sum test analyzed Alpha-diversity difference analysis of gut microbiota from A. japonicus across different seasons by **(A)** Chao1, **(B)** Shannon.

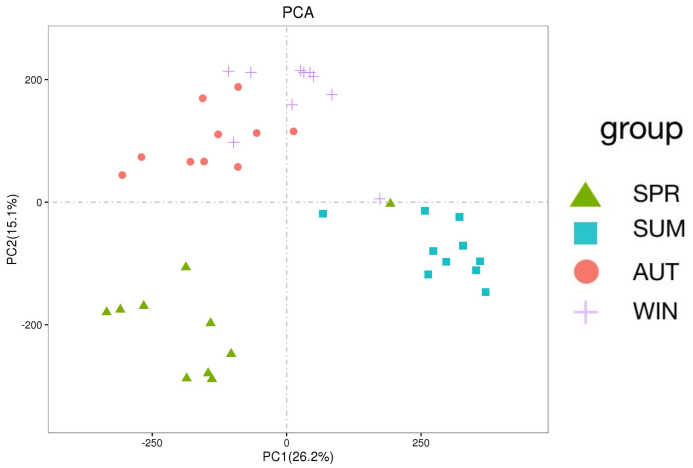

FIGURE 5
PCA shows the diversity analyses of metabolites across different seasons.

10.3389/fmars.2022.953388

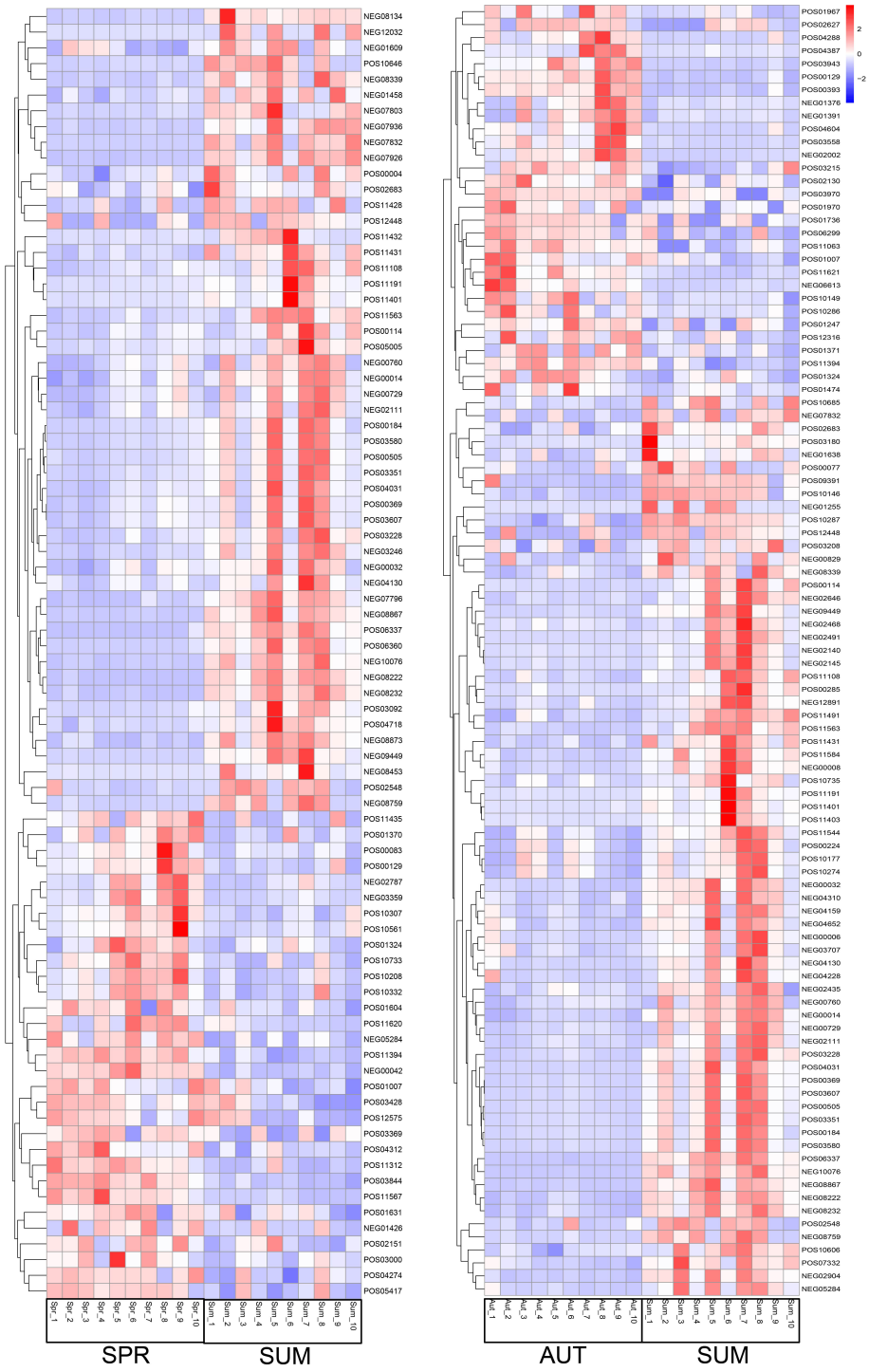

FIGURE 6
Partial metabolite heatmap of *A. japonicus* across different seasons between spring and summer (left), between autumn and summer (right).

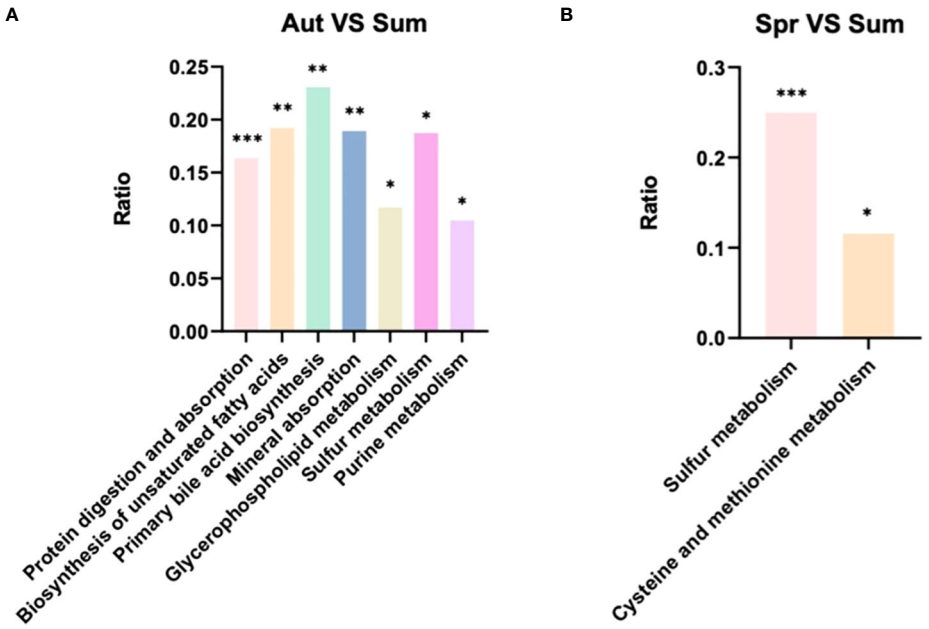

FIGURE 7
KEGG pathway analysis of level 3 differential metabolic pathways **(A)** between autumn and summer and **(B)** spring and summer.

These phenomena indicate that *A. japonicus* participate in biogeochemical cycles through microbial changes.

The effects of *Vibrio* infection on *A. japonicus*

At the species level, *Vibrio* ratios were significantly higher in summer than the other seasons, it may have been due to accelerated growth levels of aquatic *Vibrio* induced by increased temperatures. Importantly, *Vibrio* infection can lead to skin ulcer syndrome (SUS) in sea cucumbers (Yan et al., 2014). It makes us pay attention to prevent bacterial diseases caused by environmental factors in summer. The immune function of *A. japonicus* is mainly controlled by the innate immune system, which is divided into two: cellular and humoral immunity (Gross et al., 2000; Eliseikina and Magarlamov, 2002). Coelomic fluid has im portant roles in the immune processes of *A.japonicus*, the fluid contains immune cells, lysozyme, lectin and other immune active substances, it is an important medium for *A. japonicus* immune cells and immune factors. Analysis of related metabolites which had increased in summer; L-isoleucine, 3-ketosphinganine, lysoPC ((20:4 (5z, 8z, 11z, 14z)), (22:6 (4z, 7z, 10z, 13z, 16z, 19z)), (22:4 (7z, 10z, 13z, 16z)), and cholesterol sulfate. Alterations in these metabolites may be directly related to vibriosis. Isoleucine is an essential metabolite of the immune system; it provides energy for new molecule and cell biosynthesis (Calder, 2006; Nguyen et al., 2018). These observations suggest a correlation possibly exists between isoleucine and immune responses in *A. japonicus*. 3-Ketosphinganine is involved in sphingolipid metabolism. Studies have shown that sphingolipids regulate cell-cell interactions, cell adhesion, cell proliferation and migration, cell death, and other processes partly regulated by sphingolipids. It is also an inflammatory and metabolic disease, Lysosomal storage disorders and other key signaling molecules in many pathophysiological processes (Ponnusamy et al., 2012; Orsini et al., 2019; Dai et al., 2020; Quinville et al., 2021).

In previous studies, after *A. japonicus* infected by *Vibrio*, isoleucine levels are elevated and energy demands increased (Shao et al., 2013). Also, *Vibrio* infection causes oxidative stress (Nguyen et al., 2018). In our study, L-isoleucine levels in summer were significantly higher than in autumn, concomitant with increased *Vibrio* levels in summer. To ensure survival, isoleucine metabolism in *A. japonicus* may have been increased to resist *Vibrio* infection. Also, lysoPC-related metabolites increased as oxidative stress was previously shown to increase lysoPC levels (Balboa and Balsinde, 2006; Oresic et al., 2008; Ru et al., 2017; Ding et al., 2020). Immune system activation produces reactive oxygen species which directly increases oxidative damage, potentially affecting reproduction processes (Faivre et al., 2003; Alonso-Alvarez et al., 2004; Grether et al., 2004; Torres and Velando, 2007). Therefore, *Vibrio* influences in summer may have indirectly impacted *A. japonicus* reproduction in the autumn.

The effects of diet on *A. japonicus* body wall growth across different seasons

In spring and autumn, metabolism levels were significantly higher than in winter and summer. In a previous study on *Holothuria forskali*, stigmasterol and sitosterol extracts are identified in the digestive tract and body wall and were significantly higher than in other body parts (Telahigue et al., 2020). Interestingly, phytosterols are not synthesized by animals, but enter the body *via* the diet (Özyurt et al., 2013). Due to the high consumption rates of *A. japonicus* in the spring and autumn, stigmasterol and sitosterol from the environment are consumed. However, from shrimp research, sitosterol composition changed during the year, levels in shrimp muscle in spring and autumn were at their highest (Özyurt et al., 2013). Therefore, sitosterol levels altered with the seasons. Sterols in nature typically come from specific biological sources of stigmasterol and sitosterol are the main components in higher plants. Therefore, these sterols are used as markers of terrestrial organic matter input in near-shore environments (Rielley et al., 1991; Nytoft et al., 2000) which provide terrestrial higher plant debris. For marine sedimentary environments, sterols can also come from marine phytoplankton, such as some diatoms, and also Cyanobacteria and golden algae produce sterols (Volkman, 1986; Barrett et al., 1995).

By analyzing lipid content in the *A. japonicus* body wall, spring and autumn levels were higher than winter and summer (Gao et al., 2011). This phenomenon may be related to seasonal stigmasterol and sitosterol levels in the body. Also, in fish muscle, stigmasterol was confirmed as a secondary component while sitosterol was a main sterol (Özyurt et al., 2013). Phytosterols also regulate the expression of lipid regulatory genes and new fat formation (Rideout et al., 2010). Therefore, phytosterols may impact body wall growth, and the specific way of nutrition remains to be solved.

Conclusions

We showed that seasonal changes exerted a significant impact on intestinal microorganisms and metabolites in *A. japonicus*. Our research reveals the relationship between the changes of individual metabolic function of sea cucumbers caused by the changes of microorganisms in the intestine, found *A. japonicus* participated in the process of carbon, nitrogen and sulfur cycle in the ocean. The increase of *Vibrio* in summer is a serious threat to the reproduction of *A. japonicus* potentially, which should be paid more attention in aquaculture. Stigmasterol and sitosterol has a potential impact on the growth of *A. japonicus*. These materials can increase the growth of the body wall of *A. japonicus*, which is very important for aquaculture. It provides support for the intestinal immune regulation, self-metabolism, energy absorption, and body growth of sea cucumber in the future.

In this research, we have some deficiency as following, in future, we will (1) subdivide the gut microbiota in different parts of *A. japonicus*; (2) survey seasonal variations of environmental microbiota in experimental sea area; (3) design an experiment to validate effects of *Vibrio*; (4) design an experiment to verify effects of stigmasterol and sitosterol on the body wall of *A. japonicus*.

Data availability statement

The datasets presented in this study can be found in online repositories. The names of the repository/repositories and accession number(s) can be found in the article/Supplementary Material.

Author contributions

BD performed the research and wrote the manuscript. XR conceived and designed the research. TW and CZ acquired the data, WS collected sea cucumbers, SL revised the manuscript for important intellectual content. LZ supervised this study. All authors contributed to the article and approved the submitted version.

Funding

This study was supported by the National Natural Science Foundation of China (41906079), the Scientific Research and Technological Development Program of Fangchenggang (AB20014021), and the International Partners Program of the Chinese Academy of Sciences (133137KYSB20180069).

Conflict of interest

The reviewer CL is currently organizing a Research Topic with the author LZ.

The remaining authors declare that the research was conducted in the absence of any commercial or financial relationships that could be construed as a potential conflict of interest.

Publisher's note

References

Alonso-Alvarez, C., Bertrand, S., Devevey, G., Gaillard, M., Prost, J., Faivre, B., et al. (2004). An experimental test of the dose-dependent effect of carotenoids and immune activation on sexual signals and antioxidant activity. *Am. Naturalist* 164, 651–659. doi: 10.1086/424971

Altschul, S., Gish, W., Miller, W., Myers, E., and Lipman, D. (1990). Basic local alignment search tool. *J. Mol. Biol.* 15 (3), 403–410. doi: 10.1016/S0022-2836(05)80360-2

Balboa, M., and Balsinde, J. (2006). Oxidative stress and arachidonic acid mobilization. *Biochim. Biophys. Acta (BBA)-Molecular Cell Biol. Lipids.* 1761, 385–391. doi: 10.1016/j.bbalip.2006.03.014

Barrett, S. M., Volkman, J. K., Dunstan, G. A., and LeRoi, J. M. (1995). Sterols of 14 species of marine diatoms (bacillariophyta). *J. Phycol.* 31 (3), 360–369. doi: 10.1111/j.0022-3646.1995.00360.x

Bunse, C., and Pinhassi, J. (2017). Marine bacterioplankton seasonal succession dynamics. *Trends Microbiol.* 25 (6), 494–505. doi: 10.1016/j.tim.2016.12.013

Calder, P. C. (2006). Branched-chain amino acids and immunity. *J. Nutr.* 136 (1), 288S–293S. doi: 10.1093/jn/136.1.288S

Caporaso, J., Kuczynski, J., Stombaugh, J., Bittinger, K., Bushman, F. D., Costello, E. K., et al. (2010). QIIME allows analysis of high-throughput community sequencing data. *Nat. Methods* 7, 335–336. doi: 10.1038/nmeth.f.303

Cheung, M. K., Au, C. H., Chu, K. H., Kwan, H., and Wong, C. (2010). Composition and genetic diversity of picoeukaryotes in subtropical coastal waters as revealed by 454 pyrosequencing. *ISME J.* 4 (8), 1053–1059. doi: 10.1038/ismej.2010.26

Dai, Y., Zhang, M., Shi, X., Wang, K., Gao, G., Shen, L., et al. (2020). Kinetic study of aβ (1-42) amyloidosis in the presence of ganglioside-containing vesicles. *Colloids Surfaces B: Biointerfaces.* 185, 110615. doi: 10.1016/j.colsurfb.2019.110615

Ding, K., Zhang, L., Fan, X., Guo, X., Liu, X., and Yang, H. (2020). The effect of pedal peptide-type neuropeptide on locomotor behavior and muscle physiology in the sea cucumber *Apostichopus japonicus*. *Front. Physiol.* 11. doi: 10.3389/fphys.2020.559348

Egerton, S., Culloty, S., Whooley, J., Stanton, C., and Ross, R. P. (2018). The gut microbiota of marine fish. *Front. Microbiol.* 9. doi: 10.3389/fmicb.2018.00873

Eliseikina, M. G., and Magarlamov, T. Y. (2002). Coelomocyte morphoogy in the holothurians *Apostichopus japonicus* (Aspidochirota: Stichopodidae) and *Cucumaria japonica* (Dendrochirota: Cucumariidae). *J. Mar. Biol.* 28, 197–202. doi: 10.1023/A:1016801521216

Faivre, B., Grégoire, A., Préault, M., Cézilly, F., and Sorci, G. (2003). Immune activation rapidly mirrored in a secondary trait. *Science* 300, 103. doi: 10.1126/science.1081802

Fang, Y., Lv, Z., Zhang, H., Li, F., and Xu, B. (2012). "Distribution and variation characteristics of nutrients in rongcheng bay," in *Marine limnology bulletin* (Shandong, China: Transactions of Oceanology and Limnology), vol. 3. , 9.

Fan, Y., and Pedersen, O. (2021). Gut microbiota in human metabolic health and disease. *Nat. Rev. Microbiol.* 19, 55–71. doi: 10.1038/s41579-020-0433-9

Fernandes, S. O., Kirchman, D. L., Michotey, V. D., Bonin, P. C., and Lokabharathi, P. A. (2014). Bacterial diversity in relatively pristine and anthropogenically-influenced mangrove ecosystems (Goa, India). *Braz. J. Microbiol.* 45 (4), 1161–1171. doi: 10.1590/S1517-83822014000400006

Fiehn, O. (2020). Metabolomics — the link between genotypes and phenotypes. *Plant Mol. Biol.* 48 (1), 155–171. doi: 10.1023/A:1013713905833

Gao, F., Xu, Q., and Yang, H. (2011). Seasonal biochemical changes in composition of body wall tissues of sea cucumber *Apostichopus japonicus*. *Chin. J. Oceanol. Limnol.* 29 (2), 252–260. doi: 10.1007/s00343-011-0041-7

Goodrich, J. K., Davenport, E. R., Beaumont, M., Jackson, M. A., Knight, R., Ober, C., et al. (2016). Genetic determinants of the gut microbiome in UK twins. *Cell Host Microbe* 19, 731–743. doi: 10.1016/j.chom.2016.04.017

Goodrich, J. K., Waters, J. L., Poole, A. C., Sutter., J. L., Koren, O., Blekhman, R., et al. (2014). Human genetics shape the gut microbiome. *Cell* 159, 789–799. doi: 10.1016/j.cell.2014.09.053

Grether, G. F., Kasahara, S., Kolluru, G. R., and Cooper, E. L. (2004). Sex-specific effects of carotenoid intake on the immunological response to allografts in guppies (Poecilia reticulata). *Proc. R. Soc. London Ser. B* 271, 45–49. doi: 10.1098/rspb.2003.2526

Gross, P. S., Clow, L. A., and Smith, L. C. (2000). SpC3, the complement homologue from the purple sea urchin, strongylocentrotus purpuratus, is expressed in two subpopulations of the phagocytic coelomocytes. *Immunogenetics* 51, 1034–1044. doi: 10.1007/s002510000234

Hakim, J. A., Koo, H., Kumar, R., Lefkowitz, E. J., Morrow, C. D., Powell, M. L., et al. (2016). The gut microbiome of the sea urchin, lytechinus variegatus, from its natural habitat demonstrates selective attributes of microbial taxa and predictive metabolic profiles. *FEMS Microbiol. Ecol.* 92, 9. doi: 10.1093/femsec/fiw146

Herlambang, A., Murwantoko, M., and Istiqomah, I. (2021). Dynamic change in bacterial communities in the integrated rice–fish farming system in sleman, yogyakarta, Indonesia. *Aquaculture Res.* 52 (11), 5566–5578. doi: 10.1111/are.15432

Lynch, S. V., and Pedersen, O. (2016). The human intestinal microbiome in health and disease. *New Engl. J. Med.* 375, 2369–2379. doi: 10.1056/NEJMra1600266

Mitsukuri, K. (1903). Notes on the habits and life history of *Stichopus japonicus* selenka. *Annotation Zool. Japan* 5, 1–21.

Mohsen, M., Wang, Q., Zhang, L., Sun, L., Lin, C., and Yang, H. (2018). Microplastic ingestion by the farmed sea cucumber *Apostichopus japonicus* in China. *Environ. Pollution* 245, 1071–1078. doi: 10.1016/j.envpol.2018.11.083

Newton, R. J., Jones, S. E., Eiler, A., Mcmahon, K. D., and Bertilsson, S. A. (2011). Guide to the natural history of freshwater lake bacteria. *Microbiol. Mol. Biol. Rev.* 75 (1), 14–49. doi: 10.1128/MMBR.00028-10

Nguyen, T. V., Alfaro, A. C., Young, T., Ravi, S., and Merien, F. (2018). Metabolomics study of immune responses of new Zealand greenshell™ mussels (Perna canaliculus) infected with pathogenic vibrio sp. *Mar. Biotechnol.* 20 (3), 396–409. doi: 10.1007/s10126-018-9804-x

Nytoft, H. P., Bojesen-Koefoed, J. A., and Christiansen, F. G. (2000). C26 and C28-C34 28-norhopanes in sediments and petroleum. *Organic Geochem.* 31 (1), 25–39. doi: 10.1016/S0146-6380(99)00150-3

Oresic, M., Simell, S., Sysi-Aho, M., Nanto-Salonen, K., Seppanen-Laakso, T., Parikka, V., et al. (2008). Dysregulation of lipid and amino acid metabolism precedes islet autoimmunity in children who later progress to type 1 diabetes. *J. Exp. Med.* 205, 2975–2984. doi: 10.1084/jem.20081800

Orsini, M., Chateauvieux, S., Rhim, J., Gaigneaux, A., Cheillan, D., Christov, C., et al. (2019). Sphingolipid-mediated inflammatory signaling leading to autophagy inhibition converts erythropoiesis to myelopoiesis in human hematopoietic Stem/Progenitor cells. *Cell Death Differ.* 26, 1796–1812. doi: 10.1038/s41418-018-0245-x

Özyurt, G., Kuley, E., Etyemez, M., and Özoğul, F. (2013). Comparative seasonal sterol profiles in edible parts of Mediterranean fish and shellfish species. *Int. J. Food Sci. Nutr.* 64 (4), 476–483. doi: 10.3109/09637486.2012.749836

Ponnusamy, S., Selvam, S. P., Mehrotra, S., Kawamori, T., Snider, A. J., Obeid, L. M., et al. (2012). Communication between host organism and cancer cells is transduced by systemic sphingosine kinase 1/Sphingosine 1-phosphate signalling to regulate tumour metastasis. *EMBO Mol. Med.* 4, 761–775. doi: 10.1002/emmm.201200244

Quinville, B. M., Deschenes, N. M., Ryckman, A. E., and Walia, J. S. (2021). A comprehensive review: Sphingolipid metabolism and implications of disruption in sphingolipid homeostasis. *Int. J. Mol. Sci.* 22 (11), 5793. doi: 10.3390/ijms22115793

Rideout, T. C., Harding, S. V., and Jones, P. J. H. (2010). Consumption of plant sterols reduces plasma and hepatic triglycerides and modulates the expression of lipid regulatory genes and *de novo* lipogenesis in C57BL/6J mice. *Mol. Nutr. Food Res.* 54, S7–S13. doi: 10.1002/mnfr.201000027

Rielley, G., Collier, R. J., Jones, D. M., and Eglinton, G. (1991). The biogeochemistry of Ellesmere lake, UK–I: source correlation of leaf wax inputs to the sedimentary lipid record. *Organic Geochem.* 17 (6), 901–912. doi: 10.1016/0146-6380(91)90031-E

Roberts, L. D., Souza, A. L., Gerszten, R. E., and Clish, C. E. (2012). Targeted metabolomics. *Curr. Protoc. Mol. Biol.* 98 (1), 30.2.1–30.2.24. doi: 10.1002/0471142727.mb3002s98

Ru, X., Zhang, L., Li, X., Liu, S., and Yang, H. (2019). Development strategies for the sea cucumber industry in China. *J. Oceanol. Limnol.* 37, 300–312. doi: 10.1007/s00343-019-7344-5

Ru, X., Zhang, L., Liu, S., and Yang, H. (2017). Reproduction affects locomotor behaviour and muscle physiology in the sea cucumber, *Apostichopus japonicus*. *Anim. Behaviour* 133, 223–228. doi: 10.1016/j.anbehav.2017.09.024

Schoeler, M., and Caesar, R. (2019). Dietary lipids, gut microbiota and lipid metabolism. *Rev. Endocrine Metab. Disorder* 20 (4), 461–472. doi: 10.1007/s11154-019-09512-0

Shao, Y., Li, C., Ou, C., Zhang, P., Liu, Y., Su, X., et al. (2013). Divergent metabolic responses of *Apostichopus japonicus* suffered from skin ulceration syndrome and pathogen challenge. *J. Agric. Food Chem.* 61 (45), 10766–10771. doi: 10.1021/jf4038776

Spor, A., Koren, O., and Ley, R. (2011). Unravelling the effects of the environment and host genotype on the gut microbiome. *Nat. Rev. Microbiol.* 9 (4), 279–2290. doi: 10.1038/nrmicro2540

Tanaka, Y. (1958a). Seasonal changes occurring in the gonad of *Stichopus japonicus*. *Bull. Faculty Fisheries* 9, 29–36.

Tanaka, Y. (1958b). Feeding and digestive processes of *Stichopus japonicus*. *Bull. Faculty Fisheries* 9 (1), 14–28.

Telahigue, K., Ghali, R., Nouiri, E., Labidi, A., and Hajji, T. (2020). Antibacterial activities and bioactive compounds of the ethyl acetate extract of the sea cucumber *Holothuria forskali* from Tunisian coasts. *J. Mar. Biol. Assoc. UK.* 100 (2), 1–9. doi: 10.1017/S0025315420000016

Torres, R., and Velando, A. (2007). Male Reproductive senescence: the price of immune-induced oxidative damage on sexual attractiveness in the blue-footed booby. *J. Anim. Ecol.* 76 (6), 1161–1168. doi: 10.1111/j.1365-2656.2007.01282.x

Turnbaugh, P. J., and Gordon, J. I. (2008). An invitation to the marriage of metagenomics and metabolomics. *Cell* 134, 708–713. doi: 10.1016/j.cell.2008.08.025

Visconti, A., Roy, C., Rosa, F., Rossi, F., Martin, T. C., Mohney, R. P., et al. (2019). Interplay between the human gut microbiome and host metabolism. *Nat. Commun.* 10, 1. doi: 10.1038/s41467-019-12476-z

Volkman, J. K. (1986). A review of sterol markers for marine and terrigenous organic matter. *Organic Geochem.* 9 (2), 83–99. doi: 10.1016/0146-6380(86)90089-6

Wiegand, S., Jogler, M., and Jogler, C. (2018). On the maverick planctomycetes. *FEMS Microbiol. Rev.* 42, 739–760. doi: 10.1093/femsre/fuy029

Xie, H., Guo, R., Zhong, H., Feng, Q., Lan, Z., Qin, B., et al. (2016). Shotgun metagenomics of 250 adult twins reveals genetic and environmental impacts on the gut microbiome. *Cell Systems* 3 (6), 572–584. doi: 10.1016/j.cels.2016.10.004

Xing, L., Sun, L., Liu, S., Zhang, L., and Yang, H. (2021). Comparative metabolomic analysis of the body wall from four varieties of the sea cucumber *Apostichopus japonicus*. *Food Chem.* 352, 10. doi: 10.1016/j.foodchem.2021.129339

Xu, Q., Hamel, J. F., and Mercier, A. (2015). Feeding, digestion, nutritional physiology, and bioenergetics - ScienceDirect. *Developments Aquaculture Fisheries Sci.* 39, 153–175. doi: 10.1016/B978-0-12-799953-1.00010-6

Yang, H., Yuan, X., Zhou, Y., Mao, Y. Z., Zhang, T., Liu, Y., et al. (2015). Effects of body size and water temperature on food consumption and growth in the sea cucumber *Apostichopus japonicus* (Selenka) with special reference to aestivation. *Aquaculture Res.* 36 (11), 1085–1092. doi: 10.1111/j.1365-2109.2005.01325.x

Yan, F., Tian, X., Dong, S., Fang, Z., and Yang, G. (2014). Growth performance, immune response, and disease resistance against vibrio splendidus infection in juvenile sea cucumber *Apostichopus japonicus* fed a supplementary diet of the potential probiotic paracoccus marcusii DB11. *Aquaculture* 420, 105–111. doi: 10.1016/j.aquaculture.2013.10.045

frontiers | Frontiers in Marine Science

TYPE Original Research
PUBLISHED 02 December 2022
DOI 10.3389/fmars.2022.992753

OPEN ACCESS

EDITED BY
Chenghua Li,
Ningbo University, China

REVIEWED BY
Xueqiang Lu,
Nankai University, China
Dongxue Xu,
Qingdao Agricultural University, China

*CORRESPONDENCE
Guohua Sun
sgh_smile@163.com
Jianmin Yang
ladderup@126.com
Zan Li
lizanlxm@163.com

SPECIALTY SECTION
This article was submitted to Marine Biology, a section of the journal Frontiers in Marine Science

RECEIVED 13 July 2022
ACCEPTED 09 November 2022
PUBLISHED 02 December 2022

CITATION
Lu L, Ren L, Jiang L, Xu X, Wang W, Feng Y, Li Z, Yang J and Sun G (2022) Integrative proteomics and metabolomics reveal the stress response of semicarbazide in the sea cucumber *Apostichopus japonicus*. *Front. Mar. Sci.* 9:992753. doi: 10.3389/fmars.2022.992753

Integrative proteomics and metabolomics reveal the stress response of semicarbazide in the sea cucumber *Apostichopus japonicus*

Lixin Lu[1], Lihua Ren[2], Lisheng Jiang[2], Xiaohui Xu[1], Weijun Wang[1], Yanwei Feng[1], Zan Li[1]*, Jianmin Yang[1]* and Guohua Sun[1]*

[1]School of Agriculture, Ludong University, Yantai, China, [2]Shandong Marine Resources and Environment Research Institute, Yantai, China

Semicarbazide (SMC), also known as carbamoyl hydrazide, is a key intermediate for the organic synthesis of drugs, pesticides, and a panoply of other applications. It is also regarded as a landmark metabolite of nitrofurazone, a banned veterinary drug. SMC produced in different ways will eventually enter the ocean and become an emerging marine pollutant, affecting the physiological metabolism, behavioral activities, and even survival of aquatic organisms. Sea cucumbers are sediment-feeding organisms, and their risk of exposure to pollutants has attracted increasing attention. In this study, an integrated proteomic and metabolomic approach was used to investigate the responses of *Apostichopus japonicus* treated with SMC (3.72 g/L) for 72 h. After SMC treatment, the proteins and metabolites of *A. japonicus* intestine changed significantly. The results showed that 342 differentially expressed proteins were identified, of which 174 were upregulated, 168 were downregulated, and 74 differentially expressed metabolites, of which 62 were upregulated and 12 were downregulated. These differential proteins and metabolites were primarily involved in energy metabolism, lipid metabolism, signal transduction, immune regulation, autophagy, and apoptosis. On the basis of a combination of proteomic and metabolomic data, a hypothetical network of proteins, metabolites, and pathways in sea cucumbers was also described; the resulting network indicated several significant biological activities in response to SMC. This work offers a thorough analysis of the intricate mechanisms by which sea cucumbers respond to SMC stress and indicates numerous possible indicators for further research on creatures exposed to SMC. Further, our results provide scientific guidance for pollution control of *Apostichopus japonicus* culture to ensure healthy breeding.

KEYWORDS

sea cucumber, semicarbazide, proteomics, metabolomics, iTRAQ, UHPLC-Q-TOF-MS, stress response

Introduction

Semicarbazide (SMC) is a highly water-soluble compound [100.0 g/L (20°C)] that is mainly derived from azodicarbonamide's thermal decomposition and nitrofurazone's breakdown (Tarek et al., 1987; Maingot et al., 2013; Raja et al., 2017). The chemical structure of SMC is very stable, which facilitates its persistence in the environment (Dhandapani et al., 2014). At present, SMC accumulates in aquatic organisms as a new type of water environmental pollutant. According to earlier research, SMC caused male zebrafish (*Danio rerio*) to had lower plasma estrogen levels, thus demonstrating the stress of SMC on the nervous system (Yu et al., 2017). Additionally, a study revealed that SMC can change the morphological structures of important tissues and organs in Sprague-Dawley rats and that it has a certain degree of influence on the male and female reproductive system (Maranghi et al., 2009). Yue et al. (2017) demonstrated that SMC had an endocrine disrupting effect on the thyroid of *Paralichthys olivaceus*. SMC also interfered with neural signaling by antagonizing N-methyl-D-aspartate receptors (NMDARs) and inhibiting glutamate decarboxylase (GAD) (Santos et al., 2008). According to these results, SMC caused specific stress in aquatic creatures.

Apostichopus japonicus is a sediment-feeding organism that inhabits the shallow temperate coasts of the Pacific Northwest (Zhao et al., 2016). In China, it is an economically important food species, and sea cucumber culture has become an important part of the marine aquaculture industry (Xue et al., 2015). Due to the economic importance and ecological value of *A. japonicus*, research on the stress of sea cucumbers by marine pollutants has received increasing attention. In previous research, it was found that SMC was widely distributed in aquatic ecosystems, and the concentration of this compound in *A. japonicus* was very high (Zhao et al., 2016). However, no studies have focused on the stress response of *A. japonicus* to SMC or on its underlying molecular mechanisms.

The omics method in systems biology is a technology based on high-throughput analysis and includes transcriptomics, proteomics, and metabolomics. These methods can be used to analyze organisms' responses to changes in their environment; in particular, the methods can provide richer transcript, protein, and metabolite level information for biological stress studies, thereby revealing biological stress responses to pollutants (Wu et al., 2013; Rossi et al., 2018; Sun et al., 2021). Proteomics involves the study of proteins, and it can identify significant differences between pollutant stress conditions and control conditions (Sun et al., 2016; Yu et al., 2016; Ji et al., 2019). This allows understanding of the complexity of cell functions and provides a direct explanation for the stress response of organisms following exposure to pollution. Metabolomics can accurately track the changes of metabolites in cells, tissues, and biological fluids (Zhao and Lin, 2014). Numerous metabolomic studies have been conducted to examine an organism's stress response to toxic compounds (Ji et al., 2015; Yang et al., 2018; Cao et al., 2021). The production and metabolism of metabolites are the final results of a series of regulatory events, and the functional changes caused by the proteome will be amplified at the metabolic level. Combining proteomics and metabolomics can help us better understand the biological impacts of stresses on organisms since they both have the ability to quantify the disruption of proteins and metabolites engaged in the same metabolic pathway. (Ji et al., 2020). Therefore, in this study, isobaric relative and absolute quantification (iTRAQ) and liquid chromatography-tandem mass spectrometry (LC-MS/MS) were adopted to study the proteome and metabolome of *A. japonicus* after treatment with SMC in order to analyze the protein and metabolic changes, determine the molecular events and pathways that may be related to SMC stress, and ultimately decipher the relevant molecular and metabolic response mechanisms.

Abbreviations: ANT, adenine nucleotide translocator; CALM, calmodulin; CI, complex I; CIII, complex III; C IV, complex IV; CV, complex; CTS, cathepsin; DAG, diacylglycerol DGAT, diacylglycerol O-acyltransferase; D-Gly, D-Glycerate; DGP, D-Glycerate 2-phosphate; ER/SR, endoplasmic/sarcoplasmic reticulum; Gly, Glycerate; GLXK, glycerate2-kinase; GPAT, glycerol-3-phosphate acyltransferase; MGLL, acylglycerol lipase; GPC, glycerol choline phosphate; LPA, lysophosphatidic acids; MAG, monoacylglycerol; PC, phosphatidylcholine; MLCK, myosin-light-chain kinase; NADH, nicotinamide adenine dinucleotide; PA, phosphatidic acid; PARP, poly[ADP-ribose]polymerase; P-ADP-R, poly-ADP-ribose; PLPP, phosphatidate phosphatase; RyR, ryanodine receptor.

Materials and methods

Animals and SMC treatment

Forty *A. japonicus* (weight 100 ± 18 g) used in this experiment were obtained from Penglai Anyuan Aquatic Products Co., Ltd (Shandong Province, China). and were adapted for 10 days in the laboratory (18–20°C). After adapting to the environment, *A. japonicus* were divided into a control group (n = 20) and an SMC exposure group (n = 20). For treatment, 0.322 L of SMC hydrochloride solution (350 g/L) was added to the exposure group to control the concentration of SMC hydrochloride per tank to 3.72 g/L (LC_{50}). The same amount of blank sea water was added to each tank of the control group. After 72 h of exposure, at least 15 A. *japonicus* were taken from each group, and their intestines were sampled, quickly frozen in liquid nitrogen, and then kept at −80°C until subsequent experiments. For proteomics analysis, three sets of biological replicates were performed in each group (the control groups were C1, C2, and C3, and the treatment groups were T1, T2, and T3). For metabolomics analysis, 10 samples were used for each group (C1–C10 for the control groups and T1–T10 for the treatment groups).

iTRAQ-based proteomic analysis

Samples were extracted by the lysis buffer (4% (w/v) SDS, 100 mM Tris/HCl pH 7.6, 0.1 M DDT) lysis method to extract a protein, and the BCA method was used to quantify the protein. Each sample's protein was extracted in the proper quantity, and trypsin digestion was carried out using the filter-aided proteome preparation (FASP) technique. Then, we used a C_{18} Cartridge to desalt the enzymatically hydrolyzed peptides, after which the peptides were freeze-dried. Then, 40 μL of dissolution buffer was added for reconstitution, and the peptides were quantified (OD280) using isobaric tags for relative and absolute quantification (iTRAQ) technology. According to the manufacturer's protocol, 100 μg peptide samples were labeled using iTRAQ 8-plex reagent (AB SCIEX). The labeled peptides of each group were mixed and graded with AKTA Purifier 100. Each fractionation sample was separated by an HPLC liquid system (Easy nLC) with a nanoliter flow rate. The materials were separated by chromatography and then examined using a Q-Exactive mass spectrometer. Protein identification and quantitative analysis were performed using the software Mascot 2.2, and Proteome Discoverer 1.4. Blast2GO (Version 3.3.5) was used to annotate the target protein set with GO functions. The online Kyoto Encyclopedia of Genes and Genome (KEGG) database (http://geneontology.org) was employed for pathway annotation. The distribution of each GO classification or KEGG pathway in the target protein and the total protein sets were compared using Fisher's exact test, and GO annotation or KEGG pathway annotation enrichment analysis was performed on the target protein set.

The quantitative data of the target protein collection was first adjusted (normalized to the (1, 1) interval) for protein hierarchical clustering analysis. Then, the two dimensions of the sample and protein expression were categorized simultaneously (distance algorithm: Euclidean, connection type: Average linkage) using the Complexheatmap R package (R Version 3.4), which also produced a hierarchical clustering heat map.

The protein interaction network analysis was based on the information in the IntAct (http://www.ebi.ac.uk/intact/main.xhtml) or STRING (http://string-db.org/) databases to identify the relationships between the target proteins. We identified the direct and indirect interaction linkages and generated and analyzed the interaction network using CytoScape software (version 3.2.1).

LC-MS/MS-based metabonomic analysis

The samples underwent full-spectrum analysis using HILIC UHPLC-Q-TOF MS technology and the data-dependent acquisition method to collect primary and secondary mass spectrometry data, and XCMS was utilized for peak extraction and metabolite identification. In short, each tissue sample (60 mg) was homogenized after being combined with 200 μL of ultrapure water. The sample was then mixed with 800 l methanol/acetonitrile (1:1, v/v) by eddy current, and then subjected to low-temperature ultrasonic treatment to induce precipitation. The protein precipitate was centrifuged at 13000 rpm for 15 minutes at 4°C after being incubated at −20°C for 1 hour. The supernatant was then collected for analysis. Throughout the analysis process, the sample was placed in an autosampler at 4°C. The sample was separated using an Agilent 1290 Infinity LC Ultra High Performance Liquid Chromatography (UHPLC) HILIC column; the column temperature was 25°C; the flow rate was 0.3 mL/min, and the injection volume was 2 μL. The mobile phase composition was A: water + 25 mM ammonium acetate + 25 mM ammonia; B: acetonitrile, and the gradient elution procedure was as follows: 0–1 min, 95% acetonitrile; 1–14 min, acetonitrile linearly decreasing from 95% to 65%; 14–16 min, acetonitrile linearly decreasing from 65% to 40%; 16–18 min, acetonitrile maintained at 40%; 18–18.1 min, acetonitrile linearly increasing from 40% to 95%; and 18.1–23 min, acetonitrile maintained at 95%. The QC samples were inserted in the sample queue for monitoring to evaluate the stability of the system and the reliability of the experimental data. Electrospray ionization (ESI) in both positive and negative ion modes was used to examine each sample. The samples were separated using UHPLC and analyzed on a Triple TOF 5600 mass spectrometer (AB SCIEX).

Peak alignment, retention time correction, and peak area extraction were performed using the XCMS program after the original data had been transformed by ProteoWizard to mzXML format. For metabolite structure identification, the laboratory's self-built database was searched, and accurate mass matching (25 ppm) and secondary spectrum matching were utilized. We eliminated ion peaks from the XCMS data whose total was more than 2/3. Integration of the positive and negative ion peaks and application of SIMCA-P14.1 were used for pattern recognition. After the data were normalized and preprocessed, multi-dimensional statistical analysis was performed, including unsupervised principal component analysis (PCA), supervised partial least squares discriminant analysis (PLS-DA), and orthogonal partial least squares discriminant analysis (OPLS-DA). Single-dimensional statistical analysis included Student's *t*-test. R software was used to draw a volcano map.

Results

Proteomic response of *A. japonicus* to SMC

iTRAQ quantitative proteomics technology was used to screen the differentially expressed proteins (DEPs) between the control group and the SMC treatment group. A total of 3953

proteins were identified in the SMC-treated and untreated control samples. The statistics of protein quantification results are displayed in the form of volcano plots (Figure 1). Differentially expressed proteins were screened according to the standard of expression fold change (FC) ≥ 1.2 (FC upregulation ≥ 1.2 or downregulation ≤ 0.83) and a p value < 0.05. Differential expression analysis showed that 342 proteins were significantly differentially expressed between the two groups. Among these, 168 proteins were downregulated and 174 proteins were upregulated. Full details of DEPs are presented in Table 1. In the GO enrichment analysis (Figure 2), dynactin complex was the most enriched cellular component, while the most enriched biological processes were nitrate assimilation, aminoglycan metabolic process, and nitrate metabolic process. The differentially expressed proteins were involved in molecular functions such as cation channel activity, oxygen carrier activity, molecular carrier activity, and oxygen binding. KEGG pathway enrichment analysis showed that DEPs were involved in glycerolipid metabolism, oxytocin signaling pathway, RNA degradation, myocardial contraction, and other important pathways (Figure 3).

Metabolic response of *A. japonicus* to SMC

Through the UPLC-Q-TOF-HDMS method, a total of 4450 ion signals were recorded in the positive ion mode, and 3916 ion signals were detected in the negative ion mode. Figure 4 shows the PCA score chart that represents the distributions between the control group and the treatment group in the positive and negative ion modes (Figures 4A, B). A clear separation between the control and treatment groups was observed, suggesting that SMC treatment significantly affected the metabolism of *A. japonicus*. As shown in Figure 5, the O-PLS-DA model demonstrated a significant (p < 0.05) metabolic difference between the control and SMC-treated groups, with Q2 values of 0.905 and 0.911 in the positive/negative ion mode, respectively (Figures 5A, B), indicating their robustness and reliability. According to the volcano plots (Figures 6A, B), there were significant differences in metabolites between the SMC-treated and control samples. In addition, high-resolution MS and MS/MS fragments and database analysis were used for metabolite identification. According to the above scheme, many different metabolites were identified; these are listed in Table 2, with VIP > 1.0 and p < 0.1 as the screening criteria. A total of 74 metabolites were identified in the SMC-treated *A. japonicus* samples, of which 62 were upregulated and 12 were downregulated. Several types of metabolites were identified, including amino acids (threonine, leucine, valine, tyrosine, aspartate, isoleucine), fatty acids (α-linolenic acid, stearic acid, oleic acid, palmitic acid), energy metabolites (inosine, phosphorylcholine), neurotransmitters (acetylcholine, dopamine), intermediates in the tricarboxylic acid cycle (succinic acid), and permeates (taurine). The pathways related to differential metabolites were identified *via* the KEGG pathway enrichment analysis. As shown in Figure 7, SMC treatment significantly affected a set of pathways in *A. japonicus*. Specifically, the ABC transporters, central carbon metabolism in cancer, protein digestion and absorption, aminoacyl-tRNA biosynthesis, and biosynthesis of unsaturated fatty acids were important pathways showing significant changes. According to these findings, *A. japonicus* was negatively affected by SMC stress, and several pathways were dysregulated.

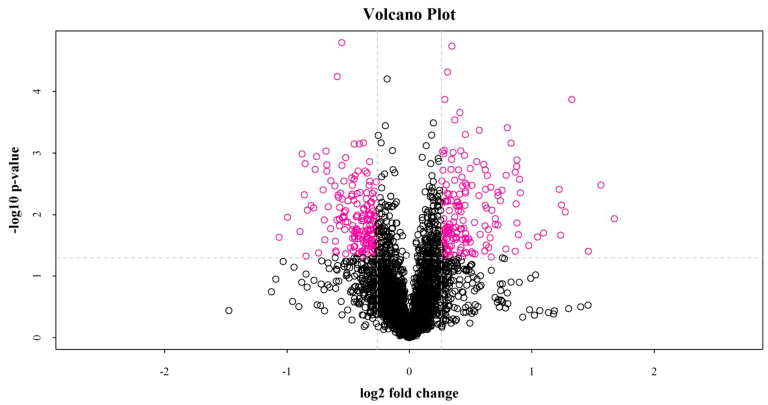

FIGURE 1
The fold change of protein expression between the two groups of samples and the p value obtained by the T test were used to draw a volcano plot to show the significant difference between the two groups of sample data. The abscissa is the difference fold (the logarithmic change with the base of 2), the ordinate is the significant p value of the difference (the logarithmic transformation with the base of 10), and the red dots in the figure are the significantly differentially expressed proteins, and the black dots are the proteins with no difference.

10.3389/fmars.2022.992753

TABLE 1 Details of differentially expressed proteins (DEPs) in *A. japonicus* in response to SMC treatment.

Protein accession	Protein description	Fold change	P value
Energy metabolism			
A0A2G8KBU0	Cytochrome c oxidase subunit	0.7494	0.0433
C3W4X1	Cytochrome c oxidase subunit 2	0.7377	0.0179
A0A2G8LGC5	NADH dehydrogenase	0.7162	0.0346
A0A2G8JQD0	Isocitrate dehydrogenase [NAD] subunit, mitochondrial	0.6673	0.0048
A0A2G8K9N8	Ubiquinone biosynthesis monooxygenase COQ6, mitochondrial	0.7849	0.0369
A0A2G8K5R8	2-oxoisovalerate dehydrogenase subunit alpha	0.6824	0.0016
A0A2G8L542	Delta-1-pyrroline-5-carboxylate dehydrogenase, mitochondrial	0.7823	0.0123
A0A2G8K828	Short/branched chain specific acyl-CoA dehydrogenase, mitochondrial	0.7703	0.0125
A0A2G8L6B2	Dihydropyrimidine dehydrogenase [NADP(+)]	0.5379	0.0189
Lipid metabolism			
A0A2G8KP95	Glycerate kinase	1.3162	0.0255
A0A2G8LRB2	Phosphoinositide phospholipase C	1.3402	0.0061
A0A2G8JB67	Tyrosine-protein phosphatase corkscrew	1.5709	0.0042
A0A2G8LQV1	Receptor-type tyrosine-protein phosphatase T isoform X2	0.7903	0.0174
A0A2G8L4V5	Phosphatidate phosphatase LPIN2	0.7646	0.0116
A0A2G8JP51	Lipid phosphate phosphohydrolase 3	0.7231	0.0174
A0A2G8JXM3	Glycerol-3-phosphate acyltransferase 1	0.5009	0.0110
Signal Transduction			
A0A2G8L6K5	Tyrosine-protein phosphatase corkscrew	1.4066	0.0194
A0A2G8KYA0	Non-specific serine/threonine protein kinase	1.4143	0.0010
A0A2G8JHD5	ATP-binding cassette sub-family D member 3 isoform X2	1.4478	0.0147
A0A142DS44	Heat shock factor binding protein 1	1.3162	0.0423
P21251	Calmodulin	0.8118	0.0402
A0A2G8L0R0	Myosin light chain kinase	0.7915	0.0100
A0A2G8L782	Ryanodine receptor 2	0.7420	0.0193
H2ETN1	Epidermal growth factor receptor	0.6558	0.0034
A0A2G8LH01	Low-density lipoprotein receptor-related protein 2	0.7867	0.0021
A0A2G8K3G5	Anthrax toxin receptor 1	0.7452	0.0101
A0A2G8JYN2	Tubulointerstitial nephritis antigen-like	0.7210	0.0050
A0A2G8LIX4	Scavenger receptor cysteine-rich domain-containing group B protein	0.7399	0.0205
A0A2G8JTD8	Trimeric intracellular cation channel type A	0.6831	0.0056
A0A2G8LG86	Acid-sensing ion channel 1-like	0.7327	0.0228
A0A2G8JV85	Apolipophorins-like	0.6267	0.0015
A0A2G8LEG7	Sideroflexin-2	0.6809	0.0000
A0A2G8KBS9	V-type proton ATPase subunit a	0.7720	0.0184
A0A2G8LDD9	Inactive tyrosine-protein kinase 7	0.7242	0.0239
A0A2G8L0Y9	Eukaryotic elongation factor 2 kinase-like	0.5613	0.0084
A0A2G8LHE4	Leucine carboxyl methyltransferase 1	0.6915	0.0107
Oxidative stress and immunity			
A0A2G8LIZ2	Heat shock protein 70	2.3528	0.0215
A0A2G8JND6	Retinol dehydrogenase 8	2.9528	0.0033
F1JTA0	Complement factor B	1.2210	0.0435
A0A2G8KPN5	Superoxide dismutase [Cu-Zn]	0.6392	0.0170
A0A2G8LQQ1	Cystathionine gamma-lyase	0.8313	0.0250
Autophagy and apoptosis			
A0A1C9UNC6	Caspase-6	1.6578	0.0271
A0A2G8KUS1	Poly [ADP-ribose] polymerase	1.4631	0.0014

(Continued)

10.3389/fmars.2022.992753

TABLE 1 Continued

Protein accession	Protein description	Fold change	P value
A0A2G8L795	Poly(ADP-ribose) polymerase pme-5 isoform X2	1.4086	0.0018
A0A2G8K567	Vacuolar protein sorting-associated protein 13A-like	0.8330	0.0159
A0A2G8KR16	Cathepsin L	0.7963	0.0097
A0A2G8KM37	Cathepsin D	0.7532	0.0424
A0A2G8JRR0	Cathepsin B	0.5860	0.0018
Other functions			
A0A2G8JUX8	Ste20-like protein kinase	1.3226	0.0070
A0A2G8JYA3	Pollen-specific leucine-rich repeat extensin-like protein 1	1.3198	0.0085
A0A2G8JWD2	Transmembrane protein	1.3184	0.0019
A0A2G8LMJ9	Neuroblast differentiation-associate d protein AHNAK	1.3150	0.0073
A0A2G8JX38	B-cell receptor-associated protein 31	1.3128	0.0062
A0A2G8JVJ5	Voltage-dependent calcium channel subunit alpha-2/delta-3 isoform X1	1.3080	0.0063
A0A2G8KQP7	Alpha-crystallin B chain-like isoform X2	1.5840	0.0036
A0A2G8JEW3	Secreted protein	1.5791	0.0238
A0A2G8KSR7	Adipocyte plasma membrane-associated protein-like	1.4823	0.0049
A0A2G8LH06	IgGFc-binding protein	1.4491	0.0433
A0A2G8KSK3	Heterogeneous nuclear ribonucleoprotein U-like protein 1 isoform X2	1.4209	0.0402
A0A2G8JHQ8	Eukaryotic peptide chain release factor GTP-binding subunit ERF3A	1.3794	0.0415
A0A2G8JJ17	Serine/threonine-protein kinase 25 isoform X4	1.3758	0.0206
A0A2G8K113	Protein kinase C	1.3392	0.0090
A0A2G8K7H6	Ran-binding protein 3	1.3335	0.0378
A0A2G8KF70	Non-specific serine/threonine protein kinase	1.3288	0.0073
A0A2G8K8A8	Rregulator of chromatin subfamily A member 5 isoform X4	1.3027	0.0160
A0A2G8KZ85	YTH domain-containing family protein 3	1.3015	0.0236
A0A2G8LP15	E3 ubiquitin-protein ligase UBR4 isoform X5	1.2998	0.0231
A0A2G8JLN5	Heterogeneous nuclear ribonucleoprotein A1-like 3	1.2922	0.0110
A0A2G8JZF1	Putative UPF0505 protein C16orf62	1.2918	0.0003
A0A2G8JYR6	Putative ras-related GTP-binding protein A-like	1.2843	0.0130
A0A2G8JBN0	Eukaryotic translation initiation factor 1A, X-chromosomal	1.2825	0.0166
A0A2G8LDC9	Cysteine sulfinic acid decarboxylase	1.2823	0.0244
A0A2G8JW91	Kinesin-like protein	1.2698	0.0013
A0A2G8LI32	Putative enhancer of mRNA-decapping protein 4	1.2573	0.0329
A0A2G8LGG8	Acid-sensing ion channel 1-like	0.8187	0.0276
A0A2G8K2J1	Peptidylprolyl isomerase	0.8182	0.0126
A0A2G8JPU5	Carbohydrate sulfotransferase 1-like	0.8134	0.0488
A0A2G8K131	Dynamin-1-like protein isoform X2	0.8111	0.0045
A0A2G8KLQ0	Peptidylprolyl isomerase	0.8090	0.0079
A0A2G8LLQ5	Vesicle-associated membrane protein 7 isoform X2	0.8072	0.0326
A0A2G8LPE6	COP9 signalosome complex subunit 4	0.8041	0.0287
A0A2G8JTI2	GRIP and coiled-coil domain-containing protein 2-like	0.7840	0.0256
A0A2G8JZV6	Alcohol dehydrogenase	0.7834	0.0151
A0A2G8JBH7	Lysosomal Pro-X carboxypeptidase	0.7801	0.0250
A0A2G8JGF7	Dystrophin-like protein	0.7788	0.0191
A0A2G8KK99	Maleylacetoacetate isomerase isoform X2	0.7716	0.0078
A0A2G8L8B4	Glutathione S-transferase theta-1	0.7223	0.0047
A0A2G8L161	Cell division cycle protein 23-like isoform X2	0.6912	0.0092
A0A2G8KU36	Quinone oxidoreductase PIG3	0.6867	0.0113
A0A2G8LMT2	C-1-tetrahydrofolate synthase, cytoplasmic-like	0.6857	0.0109

(Continued)

TABLE 1 Continued

Protein accession	Protein description	Fold change	P value
A0A2G8K4U6	Alpha-ketoglutarate-dependent dioxygenase alkB-like 7, mitochondrial	0.6774	0.0044
A0A2G8JM08	Sorbitol dehydrogenase isoform X1	0.6727	0.0118
A0A2G8L9S6	Mmall ubiquitin-related modifier 1-like	0.6692	0.0052
A0A2G8L0G9	UPF0420 protein C16orf58-like isoform X2	0.6585	0.0390
A0A2G8LMU2	Pregnancy zone protein	0.6412	0.0028
A0A2G8L834	DnaJ-like subfamily C member 3	0.7705	0.0007
A0A2G8JX80	Prolyl 4-hydroxylase subunit alpha-1	0.7699	0.0488
C3S1H6	Beta-actin	0.7684	0.0395
A0A2G8KY65	GTP-binding protein SAR1b-like isoform X2	0.7634	0.0126
A0A2G8JWN8	RNA-binding protein with serine-rich domain 1	0.7619	0.0465
A0A2G8LP79	40S ribosomal protein S5-like	0.7614	0.0392

Discussion

Overview of proteomics and metabolomics reactions

iTRAQ as an emerging omics combined with LC-MS can quantitatively screen the entire proteome within a detectable dynamic range to determine the differences in protein expression between individuals and groups under different physiological conditions (Xia et al., 2016). By seeking to capture whole metabolic networks rather than just a small number of individual metabolic pathways, metabolomics marks a paradigm change in metabolic research (Song et al., 2018). Briefly, metabolomics is the thorough analysis of endogenous metabolites in biological systems in relation to their total environment.

Currently, researchers have begun to use a combination of metabolomics and proteomics to identify biological stress responses to environmental pollutants. For example, combined metabolomic and proteomic methods confirmed that exposure to *tetrabromobisphenol A* (TBBPA) affected the growth, development, material metabolism, and energy metabolism of *Mytilus galloprovincialis* (Ji et al., 2016). Chen et al. (2016) studied *P. martensii* exposed to different concentrations of

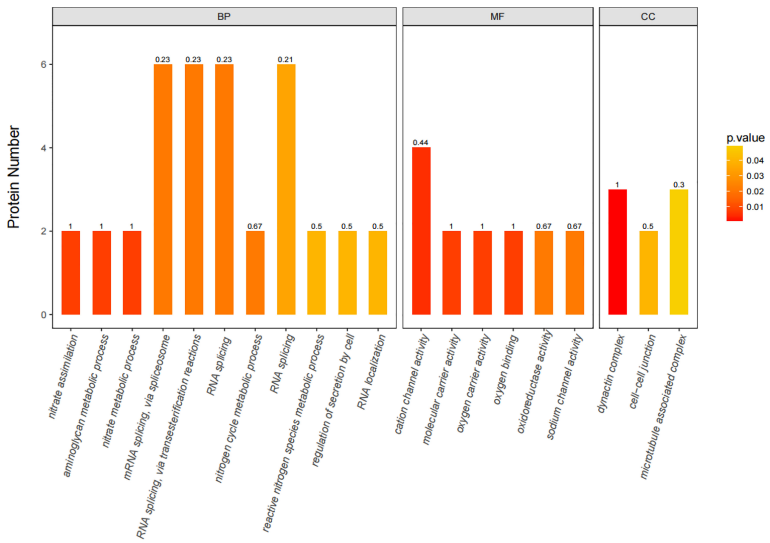

FIGURE 2
The 20 most significantly ($p < 0.05$) enriched GO terms based on differentially expressed proteins (DEPs) in SMC-treated sea cucumbers. GO enrichment for three ontologies (BP, biological process; MF, molecular function; CC, cellular component). The color bar shows the adjusted *p*-value calculated using Fisher's exact test combined with Benjamini Hochberg's correction. Rich Factor represents the ratio of the number of DEPs to the number of all annotated genes in this GO term, marked at the top of the bar graph.

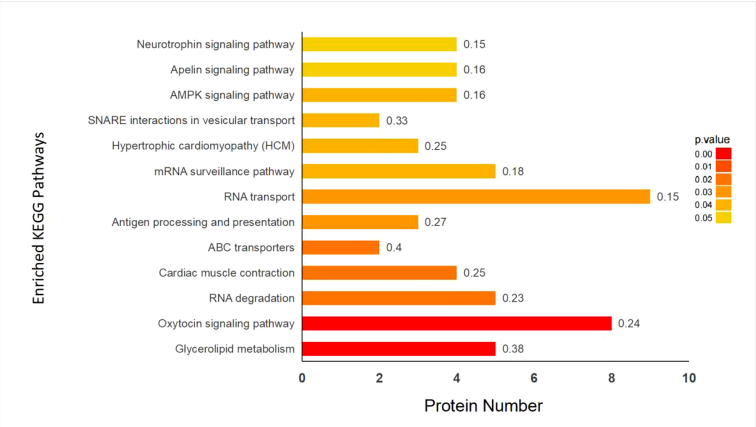

FIGURE 3
Enrichment analysis of KEGG pathway in control (C) and SMC-treated (T) group. The color bar displayed the corrected *p*-value, which was determined using the Fisher's exact test and Benjamini-Hochberg adjustment. Rich Factor that means the ratio of the DEPs number and the number of all annotated genes in this KEGG pathway was labeled on the top of bar diagram.

Benzo[a]pyrene (BaP) and observed severe disturbances in osmoregulation, energy metabolism, and signal transduction.

As an important component of marine ecosystems, *A. japonicus* is an echinoderm suitable for studying stress responses (Xue et ., 2015). The combination of metabolomic and proteomic analyses enables a deeper comprehension of molecular responses to SMC. Considering the important differential proteins and metabolites discovered from the aforementioned investigation, a hypothetical network of *A. japonicus* responses to SMC was summarized (Figure 8). Overall, SMC treatment significantly affected multiple biological pathways at the molecular level, including energy production, lipid synthesis, signal transduction, immune regulation, autophagy, and apoptosis. Possible detailed regulatory processes will be developed in the following discussion.

Changes in energy metabolism related to SMC

In this study, one of the most striking energy-related changes following SMC stress was the downregulation of oxidative phosphorylation and ATP synthesis-related proteins. It is well known that mitochondria are the main site of aerobic respiration in cells, as they participate in the regulation of energy metabolism through oxidative phosphorylation to produce adenosine triphosphate (ATP) (Papa et al., 2012). The primary

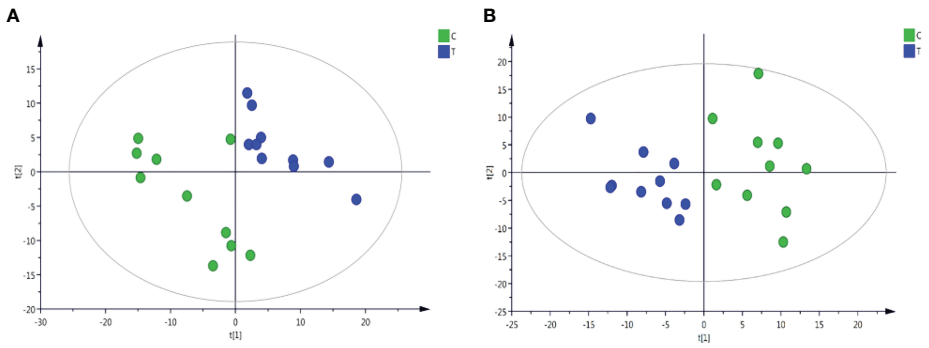

FIGURE 4
Plots of PCA scores of sea cucumber samples from control (C) and SMC-treated (T) samples in the positive and negative ion modes. **(A)**, positive ion mode; **(B)**, negative ion mode. t[1] represents the first principal component PC1, and t[2] represents the second principal component PC2.

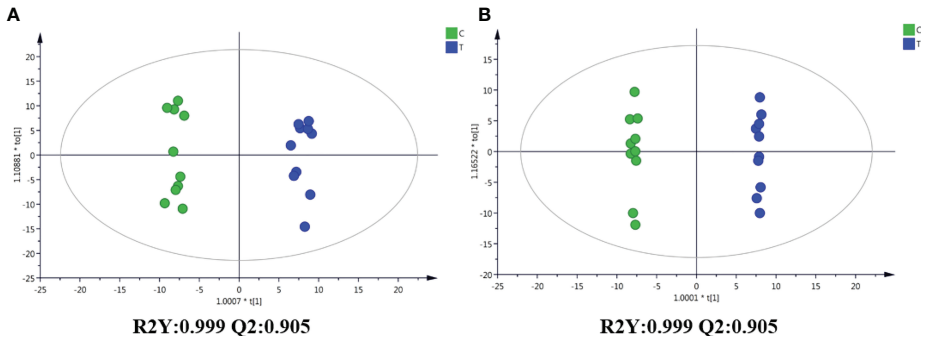

FIGURE 5
OPLS-DA score graphs of the control and SMC-treated (T) sea cucumber samples in the positive and negative ion modes. **(A)**, positive ion mode; **(B)**, negative ion mode.

source of oxidative phosphorylation and ATP generation, the mitochondrial respiratory chain, supplies around 95% of the energy needed for cell survival. The respiratory chain is located in the inner mitochondrial membrane and consists of four functional complexes (I–IV), NADH ubiquinone oxidoreductase (Complex I), succinate ubiquinone oxidoreductase (SQR) (Complex II), ubiquinone oxidoreductase (Complex II), quinone-cytochrome c reductase

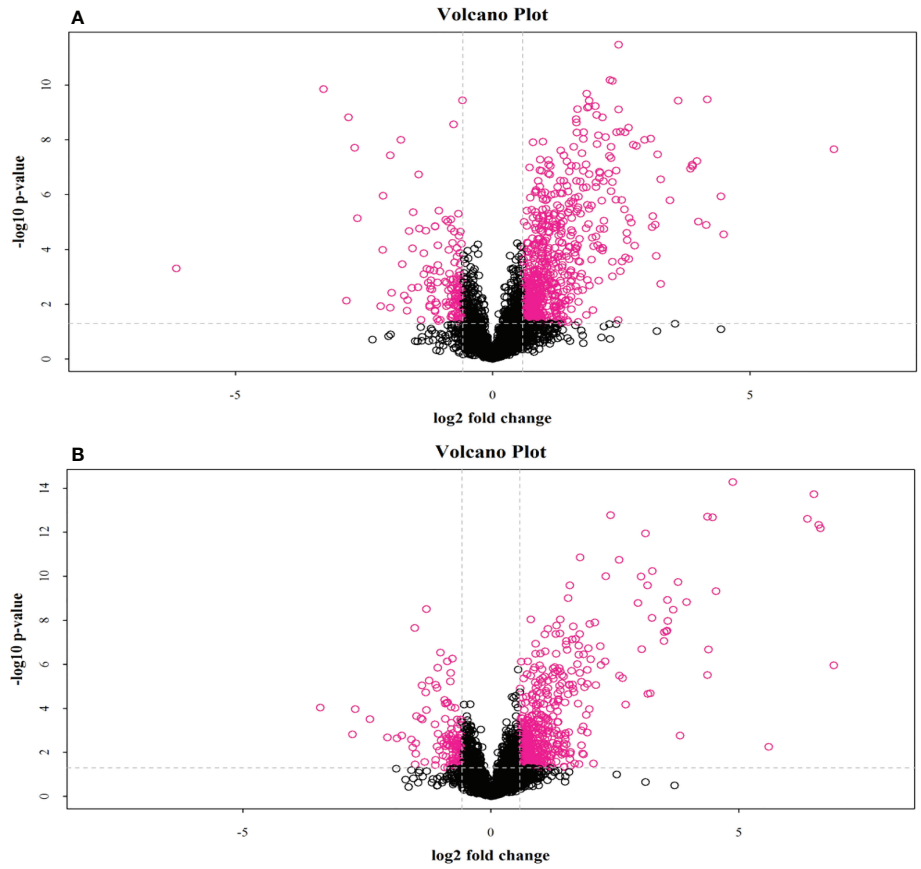

FIGURE 6
Volcano plot of positive and negative ion mode data. The red dots in the figure are metabolites with FC > 1.5 and *P* value < 0.05, **(A)**, positive ion mode; **(B)**, negative ion mode, i.e., the differential metabolites screened by univariate statistical analysis.

10.3389/fmars.2022.992753

TABLE 2 The details of some differential metabolites in A. japonicus after SMC treatment.

Metabolites accession	Metabolites description	Fold change	p-value
Amino acid			
M132T462	Leucine	1.5732	0.0945878
M118T649	Threonine	1.7212	6.86E-06
M116T529	Valine	1.8550	5.70E-05
M182T530	Tyrosine	1.9851	6.85E-05
M148T717	Glutamate	0.7823	0.000511788
M132T738	Aspartate	1.7356	0.000571896
M130T455	Isoleucine	1.9345	0.001292413
M383T717	Cysteine	3.8935	7.67E-05
Fatty acid			
M296T172	alpha-Linolenic acid	2.2786	0.00207822
M362T68	20-Hydroxya ra-chidonic acid	1.4313	0.0017793
M281T69_2	Oleic acid	1.2823	0.001928974
M241T72_2	Pentadecanoic Acid	1.5202	0.003739824
M199T74	Dodecanoic acid	0.7745	0.016345587
M157T77	Pelargonic acid	0.8345	0.017256928
M297T76_3	Nname,cis-9,10-Epoxystearic acid	0.7534	0.070186037
M301T69_2	Eicosapentaenoic acid	1.1745	0.094951041
Energy metabolites			
M258T699	Glycerophosphocholine	0.7378	0.09366439
M506T324	Phosphocholine	1.4653	0.09979502
M249T217	Inosine	5.4545	7.76E-10
M117T703_2	Succinate	0.5976	2.69E-09
Neurotransmitter			
M146T305_2	Acetylcholine	1.4334	0.02043245
M136T531	Dopamine	1.8745	3.11E-05
Other metabolites			
M232T396	N1-Acetylspermidine	12.7714	3.30E-09
M251T217	Inosine	3.9781	1.45543E-08
M162T740	DL-2-Aminoadipic acid	2.4934	1.71697E-08
M300T216	Phytosphingosine	4.6020	1.4888E-07
M298T151	S-Methyl-5'-thioadenosine	3.6522	3.56749E-07
M250T164	Adenosine	3.1360	8.19256E-06
M230T578	Ergothioneine	1.3756	3.28526E-05
M428T262	Stearoylcarnitine	2.5642	4.19356E-05
M152T387	2-Hydroxyadenine	1.7713	0.000205599
M130T717	L-Pyroglutamic acid	0.7200	0.000342016
M379T40	Vitamin D2 (Ergocalciferol)	1.6052	0.001334576
M137T306	Hypoxanthine	1.4872	0.00193461
M360T300	Sphingosine	1.7989	0.002362769
M102T717	1-Aminocyclopropanecarboxylic acid	0.7462	0.002437015
M317T77	15-Deoxy-delta-12,14-PGJ2	0.4993	0.00285459
M869T82	PC(20:5(5Z,8Z,11Z,14Z,17Z)/20:5(5Z,8Z,11Z,14Z,17Z))	0.7187	0.002878113
M400T272	L-Palmitoylcarnitine	2.0490	0.003991729
M104T416	Choline	1.3247	0.006405996
M345T77_1	Retinene	0.5879	0.022496004
M138T497	Anthranilic acid (Vitamin L1)	1.4820	0.031229
M126T517_2	Taurine	1.1014	0.032144836

(Continued)

TABLE 2 Continued

Metabolites accession	Metabolites description	Fold change	p-value
M118T467_2	Betaine	1.0878	0.044871677
M184T82	Phosphorylcholine	0.8147	0.055524807
M554T315	1-O-Octadecyl-sn-glyceryl-3-phosphorylcholine	1.8648	0.063942809
M237T66_2	Phe-Ala	2.1471	0.072509611
M204T538	Acetylcarnitine	1.1321	0.082245277
M123T109	Nicotinamide	0.8443	0.097966808
M189T76_1	Val-Ala	2.0813	0.098723381
M281T245	2'-O-methylinosine	5.9525	5.33569E-09
M142T242	5-Amino-4-carbamoylimidazole (AICA)	14.7897	9.12311E-08
M160T741_2	DL-2-Aminoadipic acid	2.8017	1.41601E-07
M227T191_1	2'-Deoxyuridine	3.1831	1.19342E-06
M356T172	S-Methyl-5'-thioadenosine	3.7894	2.49949E-06
M181T525	D-Sorbitol	2.4867	6.34808E-06
M255T187	Palmitic acid	1.8663	1.72084E-05
M125T112	Thymine	3.2190	4.16774E-05
M130T525	L-Leucine	1.5919	5.64283E-05
M180T532	L-Tyrosine	1.9852	6.85307E-05
M283T186	Stearic acid	1.7626	6.85813E-05
M253T71	cis-9-Palmitoleic acid	2.3058	8.60702E-05
M225T73	Myristoleic acid	4.3993	8.92268E-05
M111T143	Uracil	3.0844	9.22862E-05
M251T305	Deoxyinosine	1.6709	9.48503E-05
M303T67_4	Arachidonic Acid (peroxide free)	1.2636	0.000168795
M135T286	Hypoxanthine	1.3682	0.000238828
M146T717	L-Glutamate	0.7816	0.000511788
M351T60	PGF3a	3.3160	0.000769106
M102T718	(S)-2-aminobutyric acid	0.7413	0.000818827
M257T240	Ribothymidine	5.0191	0.000946338
M119T190	Purine	2.5946	0.003457822
M138T464_3	3-Aminopropanesulphonic Acid	1.4511	0.003577674
M411T73	Grayanotoxin I	1.9272	0.005195049
M243T271_1	Uridine	1.3285	0.007598538
M124T517_2	Taurine	1.0860	0.022698784
M367T105	Perindopril	1.5961	0.0389509
M464T333	Glycocholic acid	1.6780	0.050821061
M227T73	Myristic acid	1.6856	0.05478768
M337T64_3	Erucic acid	1.2606	0.054950855
M165T207	3-Methylxanthine	2.5673	0.084715075

(QCR) (Complex III), cytochrome oxidase (Complex IV), and coenzyme Q and cytochrome C composition (Kim et al., 2015). In the present study, NADH dehydrogenase (ubiquinone) Fe-S protein 7 (NDUFS7), cytochrome C oxidase subunit 2 (COX2), and cytochrome C oxidase subunit 6b (COX6B) were significantly downregulated in the treatment group. NDUFS7 is an important part of mitochondrial complex I, and its mutation may lead to the degeneration of dopaminergic neurons (Shen et al., 2020). Studies have shown that COX6B1 is involved in various processes such as COX assembly, mitochondrial function, and oxidative phosphorylation (Faxén et al., 2005; Björck and Brzezinski, 2018; Björck et al., 2019). Both of these enzymes were significantly downregulated (Figure 8), indicating that SMC inhibited the function of *A. japonicus* mitochondria and reduced energy output. In the metabolomic analysis, the metabolite succinate involved in energy metabolism was significantly downregulated. Succinate is the end result of the anaerobic breakdown of glucose and is a crucial intermediate product in the energy metabolism pathway of invertebrates (Skorokhodova et al., 2013). This indicates that

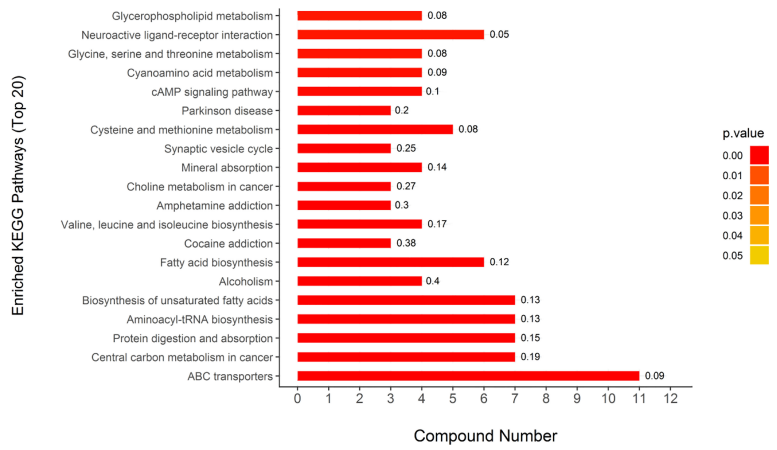

FIGURE 7
KEGG pathway enrichment analysis results of different metabolites. The color bars represent the adjusted *p*-values calculated using Fisher's exact test in conjunction with Benjamini-Hochberg correction. Rich Factor means the ratio of the number of DEPs to the number of all annotated genes in this KEGG pathway; this is labeled at the top of the bar diagram.

the energy metabolism dysfunction was caused by SMC in sea cucumbers.

In the KEGG pathway enrichment analysis of the proteome, we found that eight differentially expressed proteins were significantly enriched in the oxytocin signaling pathway. Studies have shown that prolactin maintains energy balance by promoting the catabolism of fat and glucose in peripheral tissues (Florian et al., 2010; Eckertova et al., 2011). In addition, prolactin can increase the level of glucose in the plasma and increase the utilization of glucose by the body (Skowronski et al., 2017; Khant et al., 2021). Hypothermia, loss of thermoregulation, and altered expression of adrenergic receptor genes were observed in oxytocin receptor-deficient mice (Farland et al., 2017). These results suggest that under SMC stress, *A. japonicus* may

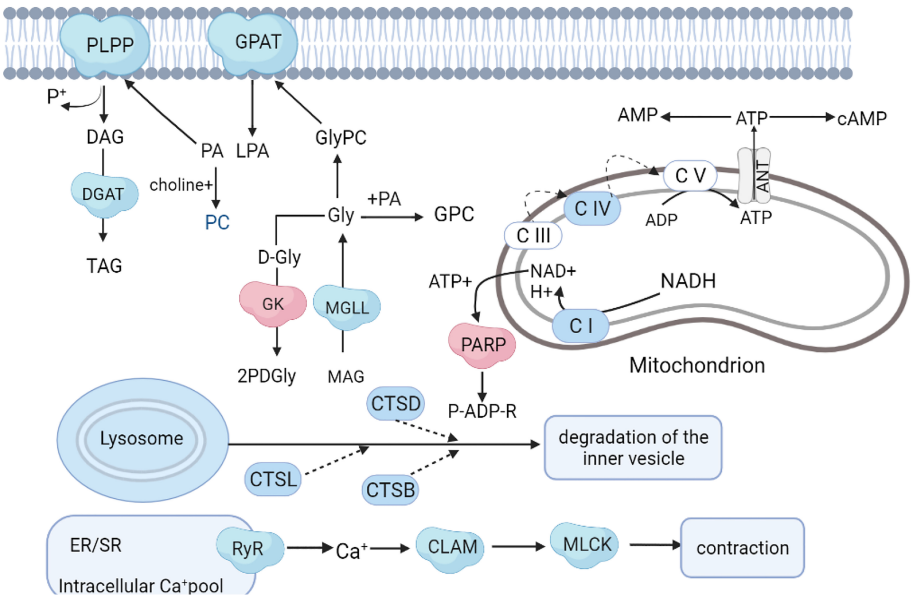

FIGURE 8
Hypothetical network of proteins, metabolites, and pathways in *A. japonicus* affected by SMC treatment. The colors red and blue represent up- and down-regulation, respectively.

decompose fat and glucose through the oxytocin signal transduction pathway to cope with the effects of impaired mitochondrial function and maintain energy balance.

Changes in lipid metabolism associated with SMC

Lipid metabolism is a process in which most of the ingested fat is emulsified into small particles by bile, and then the fatty acids are hydrolyzed to monoglycerides by lipase (Niot et al., 2009). Marine organisms are usually rich in polyunsaturated fatty acids (Ridzwan et al., 2014; Zhang et al., 2020). In this study, four distinct proteins involved in lipid metabolism were identified, namely, glycerol-3-phosphate O-acyltransferase (GPAT), glycerate 2-kinase (GLXK), monoacylglycerol lipase (MGLL), and phosphatidate phosphatase (PLPP). Only GK was upregulated in SMC-treated *A. japonicus*. GLXK is a key protein in glycerolipid metabolism that catalyzes the conversion of D-glycerate to 2-phospho-D-glyceride (Luzarowski et al., 2021). The hydrolysis of monoacylglycerols into glycerol and fatty acids is catalyzed in large part by MGLL (Jing et al., 2021). PLPP belongs to the phosphatidic acid phosphatase family and is a membrane protein that catalyzes the dephosphorylation of various phosphatidic acids (Carman and Han, 2009). Phosphatidic acid forms diglyceride under the catalysis of phosphatidic acid phosphatase and then generates triglyceride (TAG) under the catalysis of diacylglycerol acyltransferase (DGAT). TAG can regulate intracellular fat metabolism and lipid metabolism precipitation (Norbeck et al., 1996). The changes in these common proteins indicated that the lipid metabolism process of *A. japonicus* was disturbed due to the exposure to SMC. The changes in fatty acids such as the significant increases in oleic acid, α-linolenic acid, and palmitic acid, as well as the downregulation of lauric acid, also demonstrated the disturbance to normal lipid metabolism.

GPAT is distributed in the membranes of cells and is involved in various lipid biosynthesis processes such as dephosphorylation, phosphatidic acid, and long-chain fatty acid synthesis (Gimeno and Cao, 2008). In addition, studies have shown the importance of GPAT in regulating energy, glucose, and lipid homeostasis (Wang et al., 2007). GPAT is also a key protein that catalyzes the synthesis of glycerophospholipids (Cao et al., 2006). The majority of phospholipids in the body are glycerophospholipids. In addition to constituting biological membranes, they participate in the identification and signal transduction of proteins by cell membranes and are a component of bile and membrane surfactants. (Zheng and Zou, 2001). Downregulation of GPAT indicated that glycerophospholipid synthesis was inhibited; coincidentally, the significant downregulation of phosphatidylcholine, a common glycerophospholipid in metabolomics, also confirmed the inhibition of glycerophospholipid synthesis (Figure 8).

Changes in signal transduction associated with SMC

A major source of Ca signaling is the internal store primarily located in the endoplasmic/sarcoplasmic reticulum (ER/SR), with cyclic ADP-ribose (cADPR) regulated Ca^{2+} release *via* ryanodine receptors (RyRs) (Otsu et al., 1990). Studies have shown that in mice in which the expression of ryanodine receptor 2 (RyR2) is inhibited, the calcium ion concentration and the expression of calcium ion pathway-related proteins are reduced (Tunwell et al., 1996). In this work, RYRs were significantly downregulated in SMC-treated *A. japonicus*, indicating that their intracellular Ca^{2+} release was inhibited.

Calmodulin is a multifunctional protein that is ubiquitously present in various eukaryotic cells and can bind to calcium ions (Sengupta et al., 1987). Calmodulin participates in a variety of intracellular signaling pathways and is essential for Ca^{2+}-dependent signaling pathways. (Wawrzynczak and Perham, 1984). It is a dynamic Ca^{2+} sensor that can respond to a wide range of Ca^{2+} concentrations and transmit signals downstream (Chin and Means, 2000). Furthermore, Thibodeau et al. demonstrated that calmodulin is a partner of NCX4, an important mediator of Ca^{2+} efflux, especially in neurons associated with sensory conduction (Thibodeau et al., 2020). Calmodulin was downregulated in this study, indicating that calcium ion transport was inhibited. Myosin light chain kinase (MLCK) is a calmodulin-dependent protein kinase that promotes muscle contraction by mediating the phosphorylation of myosin-regulated light chain (Kazuhiro et al., 1996). In this study, the downregulation of MLCK indicated that SMC inhibited the contraction of *A. japonicus* intestinal muscles (Figure 8), which may be attributed to downregulated calmodulin. In metabolomics, two common neurotransmitters, acetylcholine and dopamine, with fold changes of 1.43 and 1.87, respectively, were significantly elevated. Choline acetyltransferase (CHAT) catalyzes the synthesis of the neurotransmitter acetylcholine from choline and acetyl-CoA. Dopamine is also an important chemical in the transmission of neural impulses (Chambers et al., 2019). Changes in these two metabolites support our hypothesis.

In addition, the neurotrophin signaling pathway was significantly enriched. This was manifested by upregulation of tyrosine protein phosphatase, phosphatidyl phospholipaseC (PI-PLC), and serine/threonine protein phosphatase. Neurotrophin signaling pathways control many aspects of neuronal survival, development, and function (Reichardt, 2006). Serine/threonine protein phosphatases and tyrosine protein phosphatases belong to the family of protein phosphatases, which control many physiological activities *via* diverse signaling pathways. (Zhang et al., 2011). PI-PLC regulates an increase in free Ca levels in the cytoplasm,

a decrease in intercellular pH, and an oxidative burst (Abd-El-Haliem and Joosten, 2017). Moreover, other significantly enriched signaling pathways such as the NOD-like receptor signaling pathway, the Apelin signaling pathway, the cAMP signaling pathway, the AMPK signaling pathway, and the Ras signaling pathway were affected to varying degrees by SMC exposure.

Oxidative stress and immune response associated with SMC

Heat shock proteins (HSPs) are a family of stress-response proteins that have been shown to play important roles in surviving external environmental stressors by participating in oxidative stress and immune processes (Kregel, 2002; Liu et al., 2015). Recent studies have indicated that HSPs reduce the levels of reactive oxygen species (ROS) to protect the normal function of the body under stressful conditions (Heckathorn et al., 2002; Rahman et al., 2015). L-glutamate is an important neurotransmitter involved in immune regulation and anti-oxidative stress responses (Long et al., 2015). The significant upregulation of HSPs and the significant reduction of L-glutamate indicated that *A. japonicus* suffered significant oxidative stress on SMC exposure.

Retinoic acid (RA) is an intermediate metabolite of vitamin A. Retinol dehydrogenase (RDH) is the main enzyme in the synthesis of RA. It plays a biological role through the RA signaling pathway and can promote epithelial differentiation and growth of cells involved in the regulation of the immune system (Pino-Lagos et al., 2008). The significant upregulation of RDH, as well as the increase of RA, suggested that *A. japonicus* may counteract the effects of SMC by accumulating RA and reducing ROS levels. Studies have linked cysteine to metals and oxidative stress. Cysteine is normally present at low levels in the body and can be upregulated when the organism is exposed to toxins (Takemoto, 2014). Similar results were obtained in our study, with a significant (3.89-fold) increase in cysteine after SMC exposure.

Hydrogen sulfide (H_2S) molecules are present in the nervous system and smooth muscle cells, and H_2S plays an important physiological regulatory role by participating in inflammation and anti-inflammatory responses (Kimura et al., 2005). Endogenous H_2S is produced by cysteine as a substrate and is catalyzed by the rate-limiting enzymes cystathionine-β synthase (CBS) and cystathionine γ-lyase (CSE) (Chen et al., 2010). In this study, we found that CSE was significantly downregulated in SMC-treated *A. japonicus*, suggesting that it may affect the synthesis of H_2S, leading to the occurrence of inflammatory reactions.

Autophagy and apoptosis associated with SMC

A cellular catabolic mechanism known as autophagy includes non-selective cytoplasmic component breakdown, organelle turnover, and protein degradation (van der Lienden et al., 2018; Fang et al., 2019). The autophagy process is controlled by a variety of proteins. Among the lysosomal proteins, cathepsin (CTS) is the most abundant protease required to activate autophagy, and it plays an important role in degrading proteins in lysosomes (Meijer and Codogno, 2004). In this work, three cathepsins (CTSB, CTSD, and CTSL) were identified as being reduced due to SMC treatment (Figure 8). Studies have shown that autophagy-lysosomal protein degradation was impaired in a CTS knockout mouse model, and mitochondrial clearance was defective, resulting in increased ROS (Lee et al., 2021). Furthermore, in this study, we initially found that the vacuolar protein sorting-associated protein 13A (VPS13A) was significantly downregulated in SMC-treated *A. japonicus*. Studies have shown that members of the VPS13 family are closely involved in a variety of neurodegenerative diseases (Seifert et al., 2011; Schormai et al., 2018). The reduction in autophagy seen in the absence of VPS13A may be the result of more general defects in endocytic transport and lysosomal degradation (Muñoz-Braceras et al., 2019). The latter study also discovered a strong relationship between VPS13A and mitochondria, indicating that VPS13A's function in the endolysosomal pathway may be connected to intracellular communication. These results suggest that autophagy can be reduced through the mitochondrial pathway under SMC stress conditions.

Apoptosis, also known as programmed cell death, is a genetically programmed process that eliminates damaged or redundant cells by activating caspases (Savitskaya and Onishchenko, 2015). In this work, two apoptosis-related proteins were altered upon SMC treatment, manifesting as upregulation of poly[ADP-ribose] polymerase 1 (PARP) and caspase 6 (CASP6). PARP is a major molecule in apoptosis, and its overactivation uses a large amount of NAD^+ as a substrate for poly-ADP-ribosylation, resulting in ATP depletion that eventually leads to cell death (Ahel et al., 2008). Caspases are a relatively evolutionarily conserved family of cysteinyl proteases that initiate and execute apoptosis through specific cleavage of a large number of cellular substrates *via* aspartic acid (Lee et al., 2006). Changes in these two proteins indicated increased apoptosis in *A. japonicus* cells after SMC stress.

Conclusion

In this study, proteomic and metabolomic techniques were used to analyze the proteins and metabolites of *A. japonicus* under SMC stress. The results showed that SMC inhibited the energy metabolism, fat metabolism, Ca^{2+} transmission pathway of *A. japonicus*, and was accompanied by severe oxidative stress and inflammation. In conclusion, this study provides a basis for the interpretation of the response mechanism of *A. japonicus* under SMC stress as well as a reference for the screening of molecular indicators for the detection of SMC pollution in *A. japonicus* in aquaculture. The findings are also of significance for the protection and utilization of *A. japonicus* resources in the natural environment.

Data availability statement

The Metabolomics data presented in the study are deposited inthe EMBL-EBI MetaboLights repository, accession number MTBLS5758 (https://www.ebi.ac.uk/metabolights/MTBLS5758). The Proteome data presented in the study are deposited in the iProX repository, accession number 1667637087317CuFi (https://www.iprox.cn/page/PSV023.html;?url=1667637087317CuFi).

Author contributions

GS and JY designed and supervised the study. LL, LR, LJ and XX prepared the samples. LL, LJ, YF, GS, WW and ZL analyzed all sequencing data. LL and GS wrote the manuscript. All authors contributed to the article and approved the submitted version.

Funding

The research was supported by grants from the National Key R&D Program of China (2018YFD0901602), Modern Agriculture Industry System of Shandong Province (SDAIT-22-02), Natural Science Foundation of Shandong Province (ZR2021MC023), and TaiShan Industrial Experts Programme, China (tscy20190114).

Conflict of interest

The authors declare that the research was conducted in the absence of any commercial or financial relationships that could be construed as a potential conflict of interest.

Publisher's note

References

Ahel, I., Matsusaka, T., Clark, A. J., Pines, J., and Boulton, S. J. (2008). Poly (ADP-ribose)-binding zinc finger motifs in DNA repair/checkpoint proteins. *Nature.* 451 (7174), 81–85. doi: 10.1038/nature06420

Abd-El-Haliem, A. M., and Joosten, M. H. (2017). Plant phosphatidylinositol-specific phospholipase c at the center of plant innate immunity. *J. Integr. Plant Biol.* 59 (3), 164–179. doi: 10.1111/jipb.12520

Björck, M. L., and Brzezinski, P. (2018). Control of transmembrane charge transfer in cytochrome c oxidase by the membrane potential. *Nat. Commun.* 9 (1), 3187. doi: 10.1038/s41467-018-05615-5

Björck, M. L., Vilhjálmsdóttir, J., Hartley, A. M., Meunier, B., Näsvik Öjemyr, L., Maréchal, A., et al. (2019). Proton-transfer pathways in the mitochondrial s. cerevisiae cytochrome c oxidase. *Sci. Rep.* 9 (1), 20207. doi: 10.1038/s41598-019-56648-9

Cao, J., Liao, Y., Yang, W., Jiang, X., and Li, M. (2021). Enhanced microalgal toxicity due to polystyrene nanoplastics and cadmium co-exposure: From the perspective of physiological and metabolomic profiles. *J. Hazard Mater.* 427, 127937. doi: 10.1016/j.jhazmat.2021.127937

Cao, J., Li, D., Li, J., Tobin, F., and Gimeno, R. E. (2006). Molecular identification of microsomal acyl-CoA: Glycerol-3-phosphate acyltransferase, a key enzyme in *de novo* triacylglycerol synthesis. *Proc. Natl. Acad. Sci. U S A.* 103 (52), 19695–19700. doi: 10.1073/pnas.0609140103

Carman, G. M., and Han, G. S. (2009). Phosphatidic acid phosphatase, a key enzyme in the regulation of lipid synthesis. *J. Biol. Chem.* 284 (5), 2593–2597. doi: 10.1074/jbc.R800059200

Chambers, N. E., Meadows, S. M., Taylor, A., Sheena, E., Lanza, K., Conti, M., et al. (2019). Effects of muscarinic acetylcholine m1 and m4 receptor blockade on dyskinesia in the hemi-parkinsonian rat. *Neuroscience.* 409, 180–194. doi: 10.1016/j.neuroscience.2019.04.008

Chen, H., Song, Q., Diao, X., and Zhou, H. (2016). Proteomic and metabolomic analysis on the toxicological effects of benzo[a]pyrene in pearl oyster *Pinctada martensii*. *Aquat Toxicol.* 175, 81–89. doi: 10.1016/j.aquatox.2016.03.012

Chen, L., Yang, T., Yang, L., Guo, X., Meng, L., Cui, Y., et al. (2010). Hydrogen sulphide protects H9c2 cells against chemical hypoxia-induced injury. *Clin. Exp. Pharmacol. Physiol.* 37 (3), 316–321. doi: 10.1111/j.1440-1681.2009.05289.x

Chin, D., and Means, A. R. (2000). Calmodulin: a prototypical calcium sensor. *Trends Cell Biol.* 10 (8), 322–28. doi: 10.1016/s0962-8924(00)01800-6

Dhandapani, A., Manivarman, S., and Subashchandrabose, S. (2014). Molecular structure and vibrational analysis on (E)-1-(3-methyl-2,6-diphenyl piperidin-4-ylidene) semicarbazide. *J. Mol. Struct.* 1058, 41–50. doi: 10.1016/j.molstruc.2013.09.052

Eckertova, M., Ondrejcakova, M., Krskova, K., Zorad, S., and Jezova, D. (2011). Subchronic treatment of rats with oxytocin results in improved adipocyte differentiation and increased gene expression of factors involved in adipogenesis. *Br. J. Pharmacol.* 162 (2), 452–463. doi: 10.1111/j.1476-5381.2010.01037.x

Fang, H., Yao, S., Chen, Q., Liu, C., Cai, Y., Geng, S., et al. (2019). *De novo* -designed near-infrared nanoaggregates for super-resolution monitoring of lysosomes in cells, in whole organoids, and in vivo. *ACS Nano.* 13 (12), 14426–14436. doi: 10.1021/acsnano.9b08011

Farland, L. V., Mu, F., Eliassen, A. H., Hankinson, S. E., Tworoger, S. S., Barbieri, R. L., et al (2017). Menstrual cycle characteristics and steroid hormone, prolactin, and growth factor levels in premenopausal women. *Cancer Causes Control.* 28 (12), 1441–1452. doi: 10.1007/s10552-017-0971-2

Faxén, K., Gilderson, G., Ädelroth, P., and Peter, B. (2005). A mechanistic principle for proton pumping by cytochrome c oxidase. *Nature.* 437 (7056), 286–289. doi: 10.1038/nature03921

Florian, M., Jankowski, M., and Gutkowska, J. (2010). Oxytocin increases glucose uptake in neonatal rat cardiomyocytes. *Endocrinology.* 151 (2), 482–491. doi: 10.1210/en.2009-0624

Gimeno, R. E., and Cao, J. (2008). Thematic review series: Glycerolipids. mammalian glycerol-3-phosphate acyltransferases: new genes for an old activity. *J. Lipid Res.* 49 (10), 2079–2088. doi: 10.1194/jlr.R800013-JLR200

Heckathorn, S. A., Ryan, S. L., Baylis, J. A., Wang, D., Cundiff, L., and Luthe, D. S. (2002). *In vivo* evidence from an *Agrostis stolonifera* selection genotype that chloroplast small heat-shock proteins can protect photosystem II during heat stress. *Funct. Plant Biol.* 29 (8), 935–946. doi: 10.1071/PP01191

Ji, C., Cao, L., and Fei, L. (2015). Toxicological evaluation of two pedigrees of clam ruditapes philippinarum as bioindicators of heavy metal contaminants using

metabolomics. *Environ. Toxicol. Pharmacol.* 39 (2), 545–554. doi: 10.1016/j.etap.2015.01.004

Ji, C., Li, F., Wang, Q., Zhao, J., Sun, Z., and Wu, H. (2016). An integrated proteomic and metabolomic study on the gender-specific responses of mussels mytilus galloprovincialis to tetrabromobisphenol a (TBBPA). *Chemosphere.* 144, 527–539. doi: 10.1016/j.chemosphere.2015.08.052

Ji, C., Lu, Z., Xu, L., Li, F., Cong, M., Shan, X., et al (2019). Evaluation of mitochondrial toxicity of cadmium in clam *ruditapes philippinarum* using iTRAQ-based proteomics. *Environ. pollut.* 251, 802–810. doi: 10.1016/j.envpol.2019.05.046

Ji, C., Lu, Z., Xu, L., Li, F., Cong, M., Shan, X., et al (2020). Global responses to tris(1-chloro-2-propyl) phosphate (TCPP) in rockfish *Sebastes schlegeli* using integrated proteomic and metabolomic approach. *Sci. Total Environ.* 724, 138307. doi: 10.1016/j.scitotenv.2020.138307

Jing, Y., Song, Y., Shi, Q., and Fu, L. (2021). Research progress on FASN and MGLL in the regulation of abnormal lipid metabolism and the relationship between tumor invasion and metastasis. *Front. Med.* 15 (5), 649–656. doi: 10.1007/s11684-021-0830-0

Kazuhiro, K., Ye, L. H., Hayakawa, K., and Okagaki, T. (1996). Myosin light chain kinase: an actin-binding protein that regulates an ATP-dependent interaction with myosin-ScienceDirect. *Trends Pharmacol. Sci.* 17 (8), 284–287. doi: 10.1016/0165-6147(96)10033-x

Khant, A. Z., Kokay, I. C., Grattan, D. R., and Ladyman, S. R. (2021). Prolactin-induced adaptation in glucose homeostasis in mouse pregnancy is mediated by the pancreas and not in the forebrain. *Front. Endocrinol.* 12, 765976. doi: 10.3389/fendo.2021.765976

Kim, S. E., Mori, R., Komatsu, T., Chiba, T., Hayashi, H., Park, S., et al. (2015). Upregulation of cytochrome c oxidase subunit 6b1 (Cox6b1) and formation of mitochondrial supercomplexes: implication of Cox6b1 in the effect of calorie restriction. *Age (Dordr).* 37 (3), 9787. doi: 10.1007/s11357-015-9787-8

Kimura, H., Nagai, Y., Umemura, K., and Kimura, Y. (2005). Physiological roles of hydrogen sulfide: synaptic modulation, neuroprotection, and smooth muscle relaxation. *Antioxid Redox Signal.* 7 (5-6), 795–803. doi: 10.1089/ars.2005.7.795

Kregel, K. C. (2002). Invited review: Heat shock proteins: modifying factors in physiological stress responses and acquired thermotolerance. *J. Appl. Physiol.* 92 (5), 2177–2186. doi: 10.1152/japplphysiol.01267.2001

Lee, C., Chan, J., Clement, M., and Pervaiz, S. (2006). Functional proteomics of resveratrol-induced colon cancer cell apoptosis: caspase-6-mediated cleavage of lamin a is a major signaling loop. *Proteomics.* 6 (8), 2386–2394. doi: 10.1002/pmic.200500366

Lee, J., Jang, S., Choi, M., Kang, M., Lim, S. G., Kim, S. Y., et al. (2021). Overexpression of cathepsin s exacerbates lupus pathogenesis through upregulation TLR7 and IFN-alpha in transgenic mice. *Sci. Rep.* 11 (1), 16348. doi: 10.1038/s41598-021-94855-5

Liu, H., and Yang, L. (2021). Application of high performance liquid chromatography-mass spectrometry in protein detection. *J. Chem. Pharm.* 40, 76–80. doi: 10.13506/j.cnki.jpr.2021.07.012

Liu, P., Fu, J., Xu, P., Wang, X., and Li, S. (2015). The role of heat shock proteins in oxidative stress damage induced by Se deficiency in chicken livers. *Biometals* 28, 163–73. doi: 10.1007/s10534-014-9812-x

Long, S. M., Tull, D. L., Jeppe, K. J., De Souza, D. P, Dayalan, S., Pettigrove, V. J., et al. (2015). A multi-platform metabolomics approach demonstrates changes in energy metabolism and the transsulfuration pathway in chironomus tepperi following exposure to zinc. *Aquat Toxicol.* 162, 54–65. doi: 10.1016/j.aquatox.2015.03.009

Luzarowski, M., Vicente, R., Kiselev, A., Wagner, M., Schlossarek, D., Erban, A., et al. (2021). Global mapping of protein-metabolite interactions in saccharomyces cerevisiae reveals that ser-leu dipeptide regulates phosphoglycerate kinase activity. *Commun. Biol.* 4 (1), 181. doi: 10.1038/s42003-021-01684-3

Maranghi, F., Tassinari, R., Lagatta, V., Moracci, G., Macrì, C., and Eusepi, A. (2009). Effects of the food contaminant semicarbazide following oral administration in juvenile sprague–dawley rats. *Food Chem. Toxicol.* 47 (2), 472–479. doi: 10.1016/j.fct.2008.12.003

Maingot, L., Elbakali, J., Dumont, J., Bosc, D., Cousaert, N., Urban, A., et al (2013). Aggrecanase-2 inhibitors based on the acylthiosemicarbazide zinc-binding group. *Eur. J. Med. Chem.* 69, 244–261. doi: 10.1016/j.ejmech.2013.08.027

Meijer, A. J., and Codogno, P. (2004). Regulation and role of autophagy in mammalian cells. *Int. J. Biochem. Cell Biol.* 36, 45–62. doi: 10.1016/j.biocel.2004.02.002

Muñoz-Braceras, S., Tornero-Écija, A., Vincent, O., and Escalante, R. (2019). VPS13A, a closely associated mitochondrial protein, is required for efficient lysosomal degradation. *Dis. Model. Mech.* 12 (2), dmm036681. doi: 10.1242/dmm.036681

Niot, I., Poirier, H., Tran, T., and Besnard, P. (2009). Intestinal absorption of long-chain fatty acids: Evidence and uncertainties. *Prog. Lipid Res.* 48 (2), 101–115. doi: 10.1016/j.plipres.2009.01.001

Norbeck, J., Påhlman, A. K., Akhtar, N., Blomberg, A., and Adler, L. (1996). Purification and characterization of two isoenzymes of DL-Glycerol-3-phosphatase from saccharomyces cerevisiae. *J. Biol. Chem.* 271 (23), 13875–13881. doi: 10.1074/jbc.271.23.13875

Otsu, K., Willard, H. F., Khanna, V. K., Zorzato, F., and Maclennan, D. H. (1990). Molecular cloning of cDNA encoding human and rabbit forms of the Ca^{2+} release channel (ryanodine receptor) of skeletal muscle sarcoplasmic reticulum. *J. Biol. Chem.* 265 (4), 2244–2256. doi: 10.1016/00086215(90)80036-3

Papa, S., Martino, P. L., Capitanio, G., Gaballo, A., and Petruzzella, V. (2012). The oxidative phosphorylation system in mammalian mitochondria. *Adv. Exp. Med. Biol.* 942, 3–37. doi: 10.1007/978-94-007-2869-1_1

Pino-Lagos, K., Benson, M. J., and Noelle, R. J. (2008). Retinoic acid in the immune system. *Ann. N. Y. Acad. Sci.* 1143, 170–187. doi: 10.1196/annals.1443.017

Rahman, M. A., Ren, L., Wu, W., and Yan, Y. (2015). Proteomic analysis of PEG-induced drought stress responsive protein in TERF1 overexpressed sugarcane (*Saccharum officinarum*) leaves. *Plant Mol. Biol.* 33, 16–30. doi: 10.1007/s11105-014-0784-3

Raja, R., Seshadri, S., Santhanam, V., and Vedhavalli, D. (2017). Growth and characterization of nonlinear optical crystal semicarbazide picrate. *J. Mol. Struct.* 1147, 515–519. doi: 10.1016/j.molstruc.2017.06.035

Reichardt, L. F. (2006). Neurotrophin-regulated signalling pathways. *Philos. Trans. R Soc. Lond B Biol. Sci.* 361 (1473), 1545–1564. doi: 10.1098/rstb.2006.1894

Ridzwan, H., Nurzafirah, N., Hanis, K., and Hanis, Z. F. (2014). Free fatty acids composition in lipid extracts of several Sea cucumbers species from Malaysia. *J. Biochem. Mol. Biol.* 4, 204–207. doi: 10.7763/ijbbb.2014.v4.340

Rossi, C., Marzano, V., Consalvo, A., Zucchelli, M., Mortera, S., Casagrande, V., et al. (2018). Proteomic and metabolomic characterization of streptozotocin-induced diabetic nephropathy in TIMP3-deficient mice. *Acta Diabetol.* 55 (2), 121–29. doi: 10.1007/s00592-017-1074-y

Santos, J. M., Macedo, C. E., and Brandão, M. L. (2008). Gabaergic mechanisms of hypothalamic nuclei in the expression of conditioned fear. *Neurobiol. Learn Mem.* 90 (3), 560–568. doi: 10.1016/j.nlm.2008.06.007

Savitskaya, M. A., and Onishchenko, G. E. (2015). Mechanisms of apoptosis. *Biochemistry.* 80 (11), 1393–1405. doi: 10.1134/S0006297915110012

Schormai, B., Kemlin, D., Mollenhauer, B., Fiala, O., Machetanz, G., Rot, J., et al. (2018). Diagnostic exome sequencing in early-onset parkinson's disease confirms VPS13C as a rare cause of autosomal-recessive parkinson's disease. *Clin. Genet.* 93 (3), 603–612. doi: 10.1111/cge.13124

Seifert, W., Kuhnisch, J., Maritzen, T., Horn, D., Haucke, V., and Hennies, H. C. (2011). Cohen Syndrome-associated protein, COH1, is a novel, giant golgi matrix protein required for golgi integrity. *J. Biol. Chem.* 286 (43), 37665–37675. doi: 10.1074/jbc.M111.267971

Sengupta, B., Friedberg, F., and Detera-Wadleigh, S. D. (1987). Molecular analysis of human and rat calmodulin complementary DNA clones. evidence for additional active genes in these species. *J. Biol. Chem.* 262 (34), 16663–16670. doi: 10.1016/S0021-9258(18)49306-4

Shen, J., Zha, Q., Gao, X., and Cheng, S. (2020). Construction of mutant NDUFS7 plasmid and its effects on neural cells. *J. Chem. Pharm.* 51, 599–606. doi: 10.11665/j.issn.1000-5048.20200512

Skorokhodova, A. Y., Gulevich, A. Y., Morzhakova, A. A., Shakulov, R. S., and Debabov, V. G. (2013). Metabolic engineering of *Escherichia coli* for the production of succinic acid from glucose. *Appl. Biochem. Microbiol.* 49, 29–37. doi: 10.1134/S0003683813070053

Skowronski, M. T., Mlotkowska, P., Tanski, D., Lepiarczyk, E., Oklinski, M. K., Nielsen, S., et al. (2017). Pituitary gonadotropins, prolactin and growth hormone differentially regulate AQP1 expression in the porcine ovarian follicular cells. *Int. J. Mol. Sci.* 19 (1), 5. doi: 10.3390/ijms19010005

Song, Y., Chai, T., Yin, Z., Zhang, X., Zhang, W., Qian, Y., et al. (2018). Stereoselective effects of ibuprofen in adult zebrafish (Danio rerio) using UPLC-TOF/MS-based metabolomics. *Environ. pollut.* 241, 730–739. doi: 10.1016/j.envpol.2018.06.009

Sun, Q., Liu, C., Jiang, K., Fang, Y., Kong, C., Fu, J., et al (2021). A preliminary study on the neurotoxic mechanism of harmine in *Caenorhabditis elegans*. *Comp. Biochem. Physiol. C Toxicol. Pharmacol.* 245, 109038. doi: 10.1016/j.cbpc.2021.109038

Sun, J., Tang, S., Peng, H., Saunders, D. M., Doering, J. A., Hecker, M., et al. (2016). Combined transcriptomic and proteomic approach to identify toxicity pathways in early life stages of Japanese medaka (*Oryzias latipes*) exposed to 1,2,5,6-*tetrabromocyclooctane* (TBCO). *Environ. Sci. Technol.* 50 (14), 7781–7790. doi: 10.1021/acs.est.6b01249

Takemoto, Y. (2014). Cardiovascular actions of l-cysteine and l-cysteine sulfinic acid in the nucleus tractus solitarius of the rat. *Amino Acids* 46 (7), 1707–1713. doi: 10.1007/s00726-014-1733-z

Tarek, M., Zaki, M., Fawzy, M. H., and Mokhtar, M. A. (1987). Application of rhodanine, fluorene and semicarbazide hydrochloride as new spectrophotometric reagents for quinones. *Microchimica Acta*. 90 (5), 321–328. doi: 10.1007/BF01199274

Thibodeau, S., Yang, W., Sharma, S., and Lytton, J. (2020). Calmodulin binds and modulates k^+ dependent Na^+/Ca^{2+} exchanger isoform 4, NCKX4. *J. Biol. Chem.* 296, 100092. doi: 10.1074/jbc.RA120.015037

Tunwell, R. E., Wickenden, C., Bertrand, B. M., Shevchenko, V. I., Walsh, M. B., Allen, P. D., et al (1996). The human cardiac muscle ryanodine receptor-calcium release channel: identification, primary structure and topological analysis. *Biochem. J.* 318 (Pt 2), 477–487. doi: 10.1042/bj3180477

van der Lienden, M. J. C., Gaspar, P., Boot, R., Aerts, J. M. F. G., and Eijk, M. (2018). Glycoprotein non-metastatic protein b: An emerging biomarker for lysosomal dysfunction in macrophages. *Int. J. Mol. Sci.* 20 (1), 66. doi: 10.3390/ijms20010066

Wang, S., Lee, D. P., Gong, N., Schwerbrock, N. M., Mashek, D. G., Gonzalez-Baró, M. R., et al. (2007). Cloning and functional characterization of a novel mitochondrial n-ethylmaleimide-sensitive glycerol-3-phosphate acyltransferase (GPAT2). *Arch. Biochem. Biophys.* 465 (2), 347–358. doi: 10.1016/j.abb.2007.06.033

Wawrzynczak, E. J., and Perham, R. N. (1984). Isolation and nucleotide sequence of a cDNA encoding human calmodulin. *Biochem. Int.* 9 (2), 177–185. doi: 10.1021/bi00321a602

Wu, H., Liu, X., Zhang, X., Ji, C., Zhao, J., and Yu, J. (2013). Proteomic and metabolomic responses of clam Ruditapes philippinarum to arsenic exposure under different salinities. *Aquat. Toxicol.* 136, 91–100. doi: 10.1016/j.aquatox.2013.03.020

Xia, G., Zhang, D., Ma, C., Zhou, J., and Su, R. (2016). Characterization and comparison of proteomes of albino sea cucumber *Apostichopus japonicus* (*Selenka*) by iTRAQ analysis. *Fish Shellfish Immunol.* 51, 229–239. doi: 10.1016/j.fsi.2015.12.027

Xue, Z., Li, H., Wang, X., Li, X., Liu, Y., Sun, J., et al (2015). A review of the immune molecules in the sea cucumber. *Fish Shellfish Immunol.* 44 (1), 1–11. doi: 10.1016/j.fsi.2015.01.026

Yang, W., Zhao, F., Fang, Y., Li, L., Li, C., and Ta, N. (2018). H-1-nuclear magnetic resonance metabolomics revealing the intrinsic relationships between neurochemical alterations and neurobehavioral and neuropathological abnormalities in rats exposed to tris(2-chloroethyl) phosphate. *Chemosphere.* 200, 649–659. doi: 10.1016/j.chemosphere.2018.02.056

Yue, Z., Yu, M., Zhang, X., Dong, Y., Tian, H., Wang, W., et al. (2017). Semicarbazide-induced thyroid disruption in Japanese flounder (*Paralichthys olivaceus*) and its potential mechanisms. *Ecotoxicol Environ. Saf.* 140, 31–40. doi: 10.1016/j.ecoenv.2017.02.043

Yu, M., Feng, Y., Zhang, X., Wang, J., Tian, H., Wang, W., et al. (2017). Semicarbazide disturbs the reproductive system of male zebrafish (Danio rerio) through the GABAergic system. *Reprod. Toxicol.* 73, 149–157. doi: 10.1016/j.reprotox.2017.08.007

Yu, D., Ji, C., Zhao, J., and Wu, H. (2016). Proteomic and metabolomic analysis on the toxicological effects of as (III) and as (V) in juvenile mussel *Mytilus galloprovincialis*. *Chemosphere.* 150, 194–201. doi: 10.1016/j.chemosphere.2016.01.113

Zhao, Y., and Lin, C. (2014). UPLC-MSE application in disease biomarker discovery: The discoveries in proteomics to metabolomics. *Chem. Biol. Interact.* 215, 7–16. doi: 10.1016/j.cbi.2014.02.014

Zhang, J., Zhang, Y., Du, Y., Chen, S., and Tang, H. (2011). Dynamic metabonomic responses of tobacco (*Nicotiana tabacum*) plants to salt stress. *J. Proteome Res.* 10 (4), 1904–1914. doi: 10.1021/pr101140n

Zhang, X., Ning, X., He, X., Sun, X., Yu, X., Cheng, Y., et al. (2020). Fatty acid composition analyses of commercially important fish species from the pearl river estuary, China. *PloS One* 15 (1), e0228276. doi: 10.1371/journal.pone.0228276

Zhao, H., Guo, W., Quan, W., Jiang, J., and Qu, B. (2016). Occurrence and levels of nitrofuran metabolites in sea cucumber from dalian, China. *Food Addit Contam Part A Chem. Anal. Control Expo Risk Assess.* 33 (11), 1672–1677. doi: 10.1080/19440049.2016.1217069

Zheng, Z., and Zou, Y. (2001). The initial step of the glycerolipid pathway: Identification of glycerol 3-phosphate/dihydroxyacetone phosphate dual substrate acyltransferases in saccharomyces cerevisiae. *J. Biol. Chem.* 276 (45), 41710–41716. doi: 10.1074/jbc.M104749200

frontiers | Frontiers in Marine Science

TYPE Original Research
PUBLISHED 09 December 2022
DOI 10.3389/fmars.2022.1036914

OPEN ACCESS

EDITED BY
Marie Antonette Juinio-Meñez,
University of the Philippines Diliman, Philippines

REVIEWED BY
Francisco Solís,
Institute of Marine Science and Limnology, National Autonomous University of Mexico, Mexico
Owen Anderson,
National Institute of Water and Atmospheric Research (NIWA), New Zealand

*CORRESPONDENCE
Ning Xiao
xiaoning@qdio.ac.cn

†These authors have contributed equally to this work and share first authorship

SPECIALTY SECTION
This article was submitted to Marine Biology, a section of the journal Frontiers in Marine Science

RECEIVED 05 September 2022
ACCEPTED 21 October 2022
PUBLISHED 09 December 2022

CITATION
Zheng W, Sun S, Sha Z and Xiao N (2022) Three new species and two new records of Echinothuriidae (Echinodermata: Echinothurioida) from seamounts in the Northwest Pacific Ocean: Diversity, phylogeny and biogeography of deep-sea echinothuriids. *Front. Mar. Sci.* 9:1036914. doi: 10.3389/fmars.2022.1036914

Three new species and two new records of Echinothuriidae (Echinodermata: Echinothurioida) from seamounts in the Northwest Pacific Ocean: Diversity, phylogeny and biogeography of deep-sea echinothuriids

Wanrui Zheng[1†], Shao'e Sun[1,2,34†], Zhongli Sha[1,2,3,4] and Ning Xiao[1,2,3,4*]

[1]Department of Marine Organism Taxonomy and Phylogeny, Institute of Oceanology, Chinese Academy of Sciences, Qingdao, China, [2]Laboratory for Marine Biology and Biotechnology, Qingdao National Laboratory for Marine Science and Technology, Qingdao, China, [3]Shandong Province Key Laboratory of Experimental Marine Biology, Institute of Oceanology, Chinese Academy of Sciences, Qingdao, China, [4]College of Marine Science, University of Chinese Academy of Sciences, Beijing, China

The soft sea urchins Echinothuriidae Thomson, 1872, constitute the most commonly encountered sea urchins in the bathyal environment. The echinothuriids are common and frequently abundant in the Indo-Pacific, but the species diversity is still not completely known yet. Our examination of echinoid specimens collected from seven seamounts in the Northwest Pacific Ocean revealed three new species and two new records. The three new species are described as *Araeosoma cucullatum* sp. nov., *Araeosoma polyporum* sp. nov., and *Hygrosoma involucrum* sp. nov. The two new records included two species from the genus *Araeosoma*. They are distinguished from each other and from congeners by the following characteristics: coloring, ambulacrum, interambulacrum, apical system, spines, and pedicellariae. The identities of the five species are well supported by genetic distance and phylogenetic analyses based on the mitochondrial *cytochrome oxidase subunit I* (*COI*) and *16S rRNA* genes. Based on the distribution data, we explored the distribution patterns of *Araeosoma*, *Calveriosoma*, *Hapalosoma*, *Sperosoma*, *Tromikosoma*, and *Hygrosoma*, the six echinothuriid genera occurring in deep sea, and delineated 10 isolated deep-sea biogeographic provinces all over the world. The Western Pacific harbors higher species diversity of deep-sea echinothuriids than other sea areas worldwide, indicating that the Western Pacific may play an important part in the dispersal and speciation of deep-sea echinothuriids.

KEYWORDS

Echinothuriidae, new species, deep sea, biodiversity, biogeography, new records

Introduction

The order Echinothurioida Claus, 1880, includes the families Echinothuriidae Thomson, 1872a; Kamptosomatidae Mortensen, 1934; and Phormosomatidae Mortensen, 1934. As the largest family, Echinothuriidae includes 53 accepted species, which belong to seven genera (*Araeosoma* Mortensen, 1903; *Asthenosoma* Grube, 1868; *Calveriosoma* Mortensen, 1934; *Hapalosoma* Mortensen, 1903; *Hygrosoma* Mortensen, 1903; *Sperosoma* Koehler, 1897; and *Tromikosoma* Mortensen, 1903) (Kroh and Mooi, 2022). The distinctive hoof-like tip of the oral spines is the most characteristic feature of this family (Thomson, 1872a; Mortensen, 1935). The family Echinothuriidae is the most commonly encountered sea urchin in the deep ocean. They are primarily deep-sea inhabitants, with most species observed at bathyal depths. Only the members of the Indo-Pacific genus *Asthenosoma* Grube, 1868 are observed in shallow depths (Mortensen, 1927; David and Sibuet, 1985; Stevenson and Kroh, 2020).

Araeosoma is the largest genus in Echinothuriidae. Currently, 19 species are included in this genus. Dactylous pedicellariae is a special characteristic of this genus, with nothing similar being known to occur in any other echinothurid or in other echinoids (Mortensen, 1935). The genus *Hygrosoma* is characterized by having ambulacral pores on the oral surface arranged in a single series near the adradial margin, as well as oral primary spines with conspicuously large flaring hoofs (Anderson, 2016). This genus is currently composed of three species: *Hygrosoma hoplacantha* (Thomson, 1877), *Hygrosoma luculentum* (Agassiz, 1879), and *Hygrosoma petersii* (Agassiz, 1880).

Mooi et al. (2004) studied the phylogenetic relationship of the echinothurioids and confirmed that they are monophyletic and basal to most other extant echinoid groups. Anderson (2013; 2016) examined a large collection of echinothurioid echinoids from museum collections in New Zealand and Australia and described eight species in the genus *Araeosoma* and one in the genus *Hygrosoma*. Thereafter, *Araeosoma* and *Hygrosoma* have seldom been reported or investigated in the world oceans.

During surveys of the benthos in the Northwest Pacific Ocean from 2014 to 2019, we collected 11 specimens of *Araeosoma* and seven specimens of *Hygrosoma* from seven seamounts. These new materials provide an opportunity to present: i) descriptions of three new species and two new records; ii) assessment of the intraspecific divergence between the new species and all other known species; iii) evaluation of the systematic status of Echinothuriidae; and iv) discussion of the diversity and distribution and the biogeography of deep-sea echinothuriids. Our study provides new insights into the diversity, phylogeny, and distribution of deep-sea echinothuriids.

Materials and methods

Sampling and preservation

Specimens were collected from the Magellan (Kocebu Guyot), Yap (Y3), Mariana, and Caroline (M4, M5, M7, and M8) seamount areas (207–1,605 m) (Figure 1) using the Remotely Operated Vehicle submersible (ROV) FaXian (Discovery) on board the R/V *KEXUE* (Science) from 2014 to 2019. Subsequently, the specimens were immediately preserved in 75% ethanol and deposited at the Marine Biological Museum of Chinese Academy of Sciences (MBMCAS), Institute of Oceanology, Chinese Academy of Sciences (IOCAS).

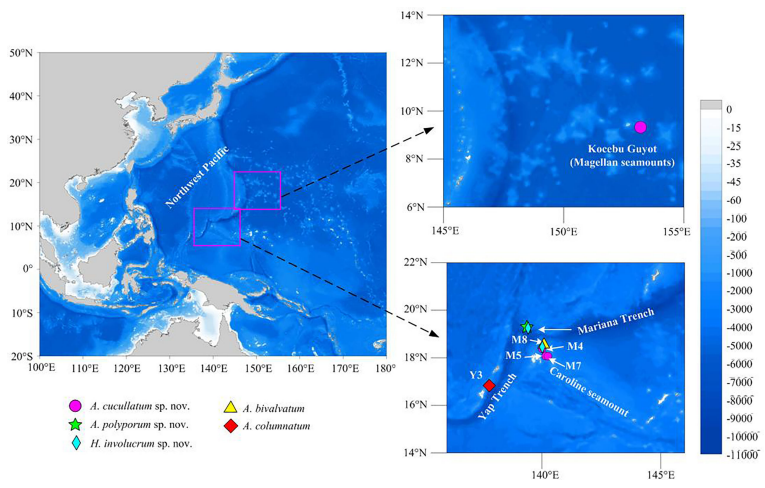

FIGURE 1
Sampling sites in the seamounts of the tropical Western Pacific Ocean.

Morphology observation

The morphological characteristics of the outer test of Echinothuriidae urchins were observed under a stereomicroscope (ZEISS Stemi 2000-C, Wetzlar, Germany). Several pedicellariae of each type that could be found on the type specimens were removed using fine forceps. The pedicellariae were digested in 10% solution of sodium hypochlorite to separate and remove the soft tissue from the individual valves (Anderson, 2013). To avoid over exposure to hydrogen peroxide, which might damage the ossicles, this digestion process was observed under a stereomicroscope. The pedicellaria ossicles were then washed three times in distilled water and dried in absolute ethanol (Coppard and Schultz, 2006). The individual valves and whole pedicellariae were then examined with a scanning electron microscope (Hitachi S-3400N, Tokyo, Japan) and the images recorded in digital format.

DNA extraction and sequencing

One specimen each of *Araeosoma alternatum*, *Araeosoma polyporum* sp. nov., and *Araeosoma bidentatum*; four specimens of *Araeosoma cucullatum* sp. nov.; and seven specimens of *Hygrosoma involucrum* sp. nov. were collected for gene sequencing. Total genomic DNA was extracted from the muscle tissue (<30 mg) from the base of the primary spines of each specimen using the E.Z.N.A.® Tissue DNA Kit (Omega Bio-Tek, Norcross, GA, USA) following the manufacturer's instructions. The DNA was eluted in 50 µl of sterile distilled H_2O (RNase free) and stored at −20°C. Mitochondrial cytochrome oxidase subunit I (*COI*) (~650 bp) and 16S rRNA (*16S*) (~600 bp) genes were amplified by polymerase chain reaction (PCR), which was carried out in a reaction mix containing 1 µl of template DNA, 15 µl of Premix Taq™ (Takara, Otsu, Shiga, Japan), 1 µl of positive and negative primers (10 mM), and 12 µl of sterile distilled H_2O to a total volume of 30 µl.

The primer sequences for each gene region are listed in Supplementary Table S1. The PCR conditions consisted of an initial denaturation at 94°C for 5 min, followed by 35 cycles of denaturation at 94°C for 30 s, annealing at 52°C for 30 s, extension at 72°C for 1 min, and a final extension at 72°C for 7 min. The PCR products were examined with 1.5% agarose gel electrophoresis and purified using the EZ-10 Spin Column DNA Gel Extraction Kit (Sangon Biotech, Shanghai, China) before sequencing. The purified PCR products were bidirectionally sequenced using an ABI PRISM 3730 (Applied Biosystems, Foster City, CA, USA) automatic DNA sequencer with the same primer sets used for PCR amplification.

Barcoding and phylogenetic analyses

The sequencing data were visualized and edited with the Seqman program from DNASTAR (http://www.DNASTAR.com). Manual examination was applied to ensure correct assembly. The assembled sequences were checked using BLAST searches (ncbi.nlm.nih.gov) to ensure that the sequences were not contaminated. The new sequences were then deposited in GenBank under the accession numbers listed in Supplementary Table S2.

Two sequencing datasets were analyzed. The first dataset contained the barcoding sequences of *COI* from all available Echinothuriidae urchins, downloaded from BOLD (https://www.boldsystems.org/) and NCBI (https://www.ncbi.nlm.nih.gov/) databases, which was used to examine species delimitation (Supplementary Table S2). To determine the systematic status of the new Echinothuriidae species, the second dataset contained concatenated sequences of the *COI* and *16S* fragments of 94 species from Echinoidea and three outgroups from Holothuroidea (Supplementary Table S2). The sequences of *16S* were aligned using MAFFT version 5 (Katoh et al., 2005) with default parameters. For the protein-coding gene *COI*, alignment was conducted with MEGA v.6 (Tamura et al., 2013) based on codon positions. The Kimura two-parameter (K2P) genetic distances of *COI* among the Echinothuriidae species were calculated with MEGA v.6. Neighbor-joining (NJ) analysis of the Echinothuriidae species was conducted using MEGA v.6 based on the K2P model. Branch supports were estimated by bootstrapping with 1,000 replicates.

Phylogenetic trees were inferred from the concatenated sequences using the maximum likelihood (ML) and Bayesian inference (BI) methods. The best-fit partitioning schemes and substitution models were selected using PartitionFinder 2.1.1 (Lanfear et al., 2017) (Supplementary Table S3). ML analysis was carried out using the best-fit partition schemes and models in the IQ-TREE web server (Trifinopoulos et al., 2016). The branch support was assessed with 5,000 ultrafast bootstrap replicates (Minh et al., 2013). BI analysis was conducted with MrBayes 3.1 software (Ronquist and Huelsenbeck, 2003) using partition models. The Markov chain Monte Carlo (MCMC) was run for 50,000,000 generations, with sampling every 1,000 generation to allow adequate time for convergence. The first 25% of the sampled trees were discarded as burn-in, with the remaining trees used to estimate the 50% majority rule consensus tree and the Bayesian posterior probabilities (PPs). At the end of the run, the average standard deviation of split frequencies decreased to 0.01. The effective sample size (ESS) values for all sampled parameters were checked using Tracer v1.7 (Rambaut et al., 2018) to make sure convergence was reached.

Biogeographic analysis

Existing distribution data of the echinothuriid species of *Araeosoma*, *Calveriosoma*, *Hapalosoma*, *Sperosoma*, *Tromikosoma*, and *Hygrosoma* were extracted (Supplementary Table S4) from the Ocean Biodiversity Information System (https://obis.org/). The distribution maps of these genera were illustrated with the software Surfer 16. A database of presence (coded 1) and absence (coded 0) for 44 echinothuriid species was established for 29 deep-sea regions (Supplementary Table S5). Statistical analyses were conducted using the software PRIMER v6 (Plymouth Marine Laboratory, Plymouth, UK). The deep-sea biogeographic provinces were delineated based on the unweighted pair group method with arithmetic mean (UPGMA) cluster analysis (Bray–Curtis distance) of all the echinothuriid species.

Results

Taxonomy

Order Echinothurioida Claus, 1880
Family Echinothuriidae Thomson, 1872a
Subfamily Hygrosomatinae Smith and Wright, 1990

Genus Hygrosoma Mortensen, 1903

Type species

Phormosoma petersii A. Agassiz, 1880**, by original designation**

Hygrosoma involucrum sp. nov.

Diagnosis

Adults of large size. Color of ethanol-preserved test and spines, dark brown; tube feet, black. Primary tubercles limited to the outer half of the oral side. Pore pairs of the aboral arranged into three to two series. The hoof of the primary oral spines is white and large (about 8 mm), widely flared. Adapical spines invested in a dark brown skin sheath. Large involute tridentate pedicellariae with long, narrow blades, tip un-serrated; small involute tridentate pedicellariae with short, narrow blades, tip finely serrated. Triphyllous pedicellariae of the usual form. Ophicephalous pedicellariae not found (Figures 2–4).

Holotype

MBM286941, M4 seamount, station FX-Dive 136 (10°28′ N, 140°05′ E), depth 1,469 m, 20 August 2017.

Paratypes

MBM286947, a seamount near the Mariana Trench, station FX-Dive 70 (11°16′ N, 139°25′ E), depth 1,372 m, March 27, 2016. MBM286954, a seamount near the Mariana Trench, station FX-

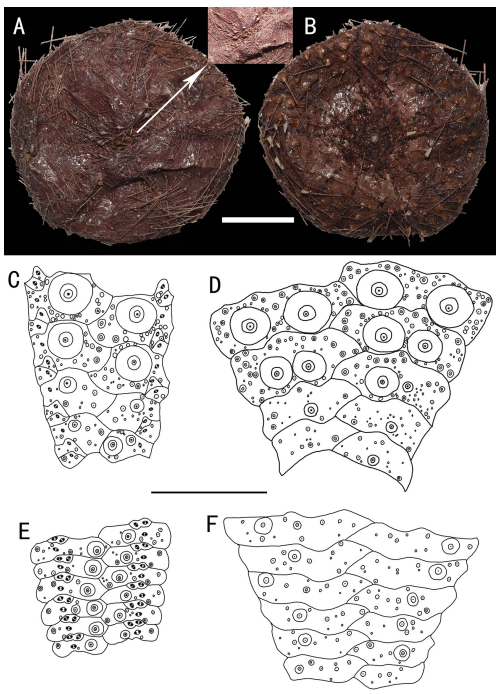

FIGURE 2
Hygrosoma involucrum sp. nov., holotype, MBM286941 (test diameter, 161 mm). **(A)** Aboral view. **(B)** Oral view. **(C–F)** Details of the coronal plates: **(C)**, oral ambulacra **(D)**, oral interambulacral **(E)**, aboral ambulacra **(F)**, aboral interambulacral. *Scale bars*, 50 mm **(A, B)** and 20 mm **(C–F)**.

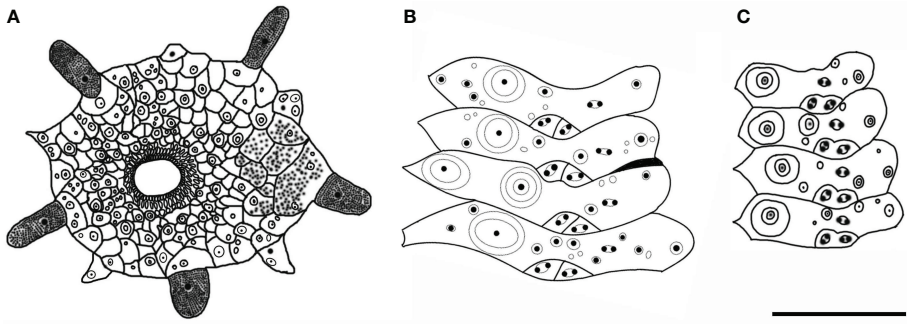

FIGURE 3
Hygrosoma involucrum sp. nov. **(A)** Paratype, MBM286940. Apical system. **(B, C)** Ambulacral plates from the aboral side: **(B)** from the paratype, MBM286970 **(C)**. from the holotype, MBM286941. *Scale bar*, 10 mm.

Dive 62 (11°16′ N, 139°22′ E), depth 1,606 m, March 19, 2016. MBM286973, M4 seamount, station FX-Dive 137 (10°35′ N, 140° 07′ E), depth 1,309 m, August 21, 2017. MBM286972, M4 seamount, station FX-Dive 137 (10°35′ N, 140°07′ E), depth 1,545 m, August 21, 2017. MBM286940, M4 seamount, station FX-Dive 136 (10°28′ N, 140°05′ E), depth 1,281 m, August 20, 2017. MBM286970, M4 seamount, station FX-Dive 138 (10°33′ N, 140° 07′ E), depth 1,103 m, August 22, 2017.

Etymology

Named *involucrum*, from the Latin word *involucrum* (sheath), after spines near the apical system invested in a skin sheath.

Description

Test of holotype (Figures 2A, B): Approximately 161 mm test diameter (TD), flexible, flattened, and pentagonal in outline. Color of ethanol-preserved test and spines, dark brown; tube feet, black. Ratio of ambulacrum to interambulacrum width at ambitus, 1:2.

There are 51–58 plates in each column of the interambulacral, with about 16–18 of these plates on the oral surface. There are 62–65 plates in each column of the ambulacral, with about 18–19 of these plates on the oral surface.

Oral test plating (Figures 2C, D): A primary tubercle occurs on every interambulacral plate from the ambitus to about half of the test, forming a regular adradial series. The other primary tubercles occur on every plate from the ambitus to about half of the test, forming a regular interradius series. In other specimens, e.g., MBM286973, primary tubercles also presented between these two series on a few of the plates. Numerous secondary and miliary tubercles are scattered over these plates. In the ambulacra, a primary tubercle occurs on every plate from the ambitus to about half of the test, forming a regular perradial series. Numerous secondary and miliary tubercles are scattered over these plates.

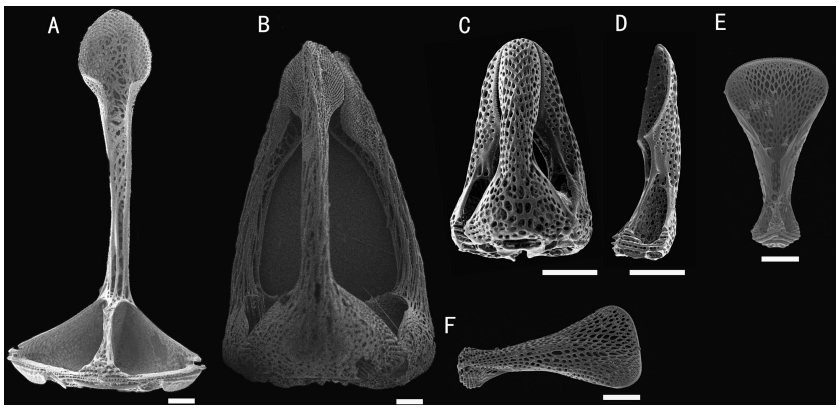

FIGURE 4
Hygrosoma involucrum sp. nov.; holotype, MBM286973. SEM images of pedicellariae. **(A, B)** Large involute tridentate pedicellaria: **(A)** individual valve **(B)** head. **(C, D)** Small involute tridentate pedicellaria: **(C)** head **(D)** individual valve. **(E, F)** Valves of triphyllous pedicellariae. *Scale bar*, 100 µm.

The peristome is approximately 41 mm in diameter, with about four to five boomerang-shaped plates in each column. Each plate has a row of four to eight tubercles. The pore pairs are arranged in a single series. Peristomial spines and tube feet are dark brown colored. Gills moderate.

Aboral test plating (Figures 2E, F): Primary tubercles on the aboral side smaller than those of the oral side. A primary tubercle occurs on every interambulacral plate from the edge of the apical system to the ambitus, forming a regular adradial series. In other specimens, e.g., MBM286940, this differs in that the other primary tubercles occur on a few plates near to the ambitus, forming an irregular interradius series. In the ambulacra, a primary tubercle occurs on every plate, forming a regular perradial series. A few smaller primary tubercles parallel to those of the larger tubercles occur on a few plates. Numerous secondary and miliary tubercles are scattered over these plates. Pore pairs are arranged into two or three discrete columns in series (Figures 3B, C).

The apical system measures 24 mm in diameter, pentagonal. The genital pore is large, opening in the membranous gaps. What is more interesting is that, in one specimen observed, the genital plate is a long strip (Figure 3A). Madreporite distinct, slightly raised, split clearly into three to six sections. Ocular plate large, with one to three small tubercles.

Spines: Hollow and cylindrical, with the longest approximately 52 mm long, 1.5 mm in diameter. Primary spines of the oral surface are smooth, slightly curved, and with about 32 fine longitudinal striations. The hoof of the primary oral spines is white and large (about 8 mm), widely flared. Spines near the apical system invested in a dark brown skin sheath.

Pedicellariae (Figure 4): Two kinds of tridentate pedicellariae are present. One is a large involute form (head length about 1.4 mm) with long, narrow blades; the un-serrated tips about a third of the base width; and the blades in contact for only a small area. The other is an involute form (about 0.4 mm long) with short, narrow blades; the finely serrated tips about a third of the base width. The valves are in contact for nearly half of their length. Triphyllous pedicellariae (about 0.5–0.6 mm) the typical echinothurioid form.

Size range

The median TD of the seven specimens measured was 100 mm, with the largest specimen being 181 mm.

Distribution

Found on a seamount (M4) near the Caroline Ridge and a seamount near the Mariana Trench in the Northwest Pacific Ocean, where the water depth is about 1,103–1,606 m.

Remarks

The most obvious differences between *H. involucrum* sp. nov. and the other three known species of *Hygrosoma* are the characteristics of their pedicellariae. In *H. hoplacantha* (known from the Indo-Pacific), the large tridentate pedicellariae have a broad, strongly involute blade with a distinctly serrated edge (see Figure 21 in Anderson, 2016). In *H. luculentum* (known from the Indo-Pacific), the short, broad-bladed with un-serrated edge tridentate pedicellariae usually present in great numbers (see Plate XIII, Figure 16 in Mortensen, 1903). None of these pedicellariae were found in the specimens examined.

The Atlantic *H. petersii* differs from the new species in terms of the absence of obvious membranous gaps in the apical system and adapical spines without skin sheath. In addition, the pore pairs of *H. petersii* are arranged into two close vertical series on the aboral side (Mortensen, 1935), while those of *H. involucrum* sp. nov. are arranged into two or three series.

Subfamily Echinothuriinae Thomson, 1872

Genus *Araeosoma* Mortensen, 1903

Type species

***Calveria fenestrata* Wyville Thomson, 1872, by original designation**

Araeosoma cucullatum sp. nov.

Diagnosis

Adults of moderate size. The color of the ethanol-preserved test and spines is light brown, darker on the tissue surrounding the tubercles and tube feet, and the membranous gaps white. Membranous spaces widest in the median area between the plates of the interambulacra. A primary tubercle occurs on every interambulacral plate on the oral surface, forming a regular adradial series. The hoof of the primary oral spines is white, moderately long (about 1 mm), slightly flared, and slightly flattened distally. Three kinds of tridentate pedicellariae are present; large tridentate pedicellariae with spoon-shaped valves (Figures 5, 6).

Holotype

MBM286942, Kocebu Guyot, station FX-Dive 175 (17°20′ N, 153°12′ E), depth 1,314 m, April 9, 2018.

Paratypes

MBM286963, M4 seamount, station FX-Dive 132 (10°23′ N, 140°09′ E), depth 1,368 m, August 14, 2017. MBM286971, M7, station FX-Dive 223 (10°04′ N, 140°15′ E), depth 1,363 m, June 11, 2019. MBM286975, M5 seamount, station FX-Dive 214 (10° 05′ N, 140°10′ E), depth 1,497 m, June 1, 2019.

Etymology

Named *cucullatum*, from the Latin word *cucullatus* (spoon-shaped), after the spoon-shaped valves of large tridentate pedicellariae.

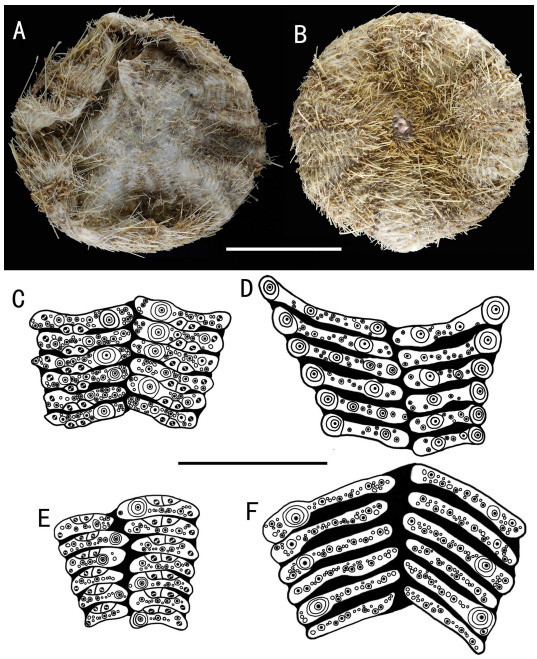

FIGURE 5
Araeosoma cucullatum sp. nov.; holotype, MBM286942 (test diameter, 105 mm). **(A)** Aboral view. **(B)** Oral view. **(C–F)** Details of the coronal plates: **(C)**, oral ambulacra **(D)**, oral interambulacral **(E)**, aboral ambulacra **(F)** aboral interambulacral. *Scale bars*, 50 mm **(A, B)** and 20 mm **(C–F)**.

Description

Test of holotype (Figures 5A, B): Approximately 105 mm TD, flexible, flattened, and circular in outline. The color of the ethanol-preserved test and spines is light brown, darker on the tissue surrounding the tubercles and tube feet, and the membranous gaps white. Ratio of ambulacrum to interambulacrum width at ambitus, 3:4.

There are 34–41 plates in each column of the interambulacral, with about 17–19 of these plates on the oral surface. There are 43–51 plates in each column of the ambulacral, with about 21–25 of

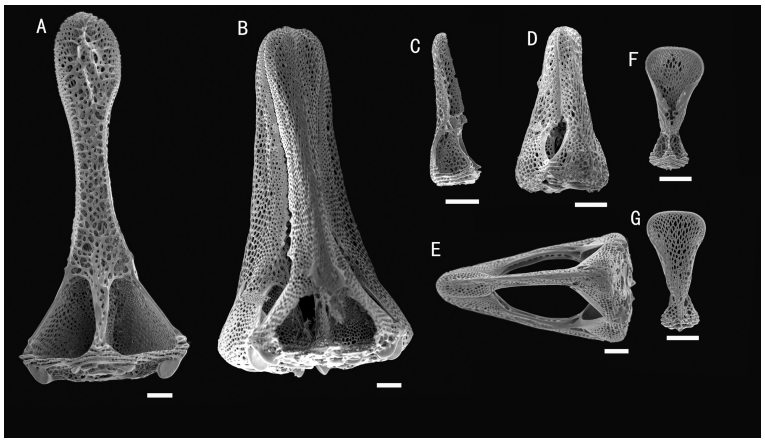

FIGURE 6
Araeosoma cucullatum sp. nov.; holotype, MBM286942. SEM images of pedicellariae. **(A, B)** Large tridentate pedicellaria: **(A)** individual valve **(B)** head. **(C, D)** Rostrate tridentate pedicellaria: **(C)** individual valve **(D)** head. **(E)** Involute tridentate pedicellaria. **(F, G)** Valves of triphyllous pedicellariae. *Scale bar*, 100 µm.

these plates on the oral surface. Membranous spaces widest in the median area between interambulacral plates on the aboral surface. Adapical-most interambulacral plates angled slightly.

Oral test plating (Figures 5C, D): A primary tubercle occurs on every interambulacral plate from the edge of the peristome to the ambitus, forming a regular adradial series. The other primary tubercles occur on every plate or every second plate from the ambitus to about two-thirds of the test. These tubercles form an irregular series adjacent to the interradius. One or two secondary tubercles occur on a few plates. Numerous miliary tubercles scattered over on interambulacral plates. In the ambulacra, a primary tubercle occurs on every plate or every second plate, forming an irregular perradial series. Secondary tubercles are arranged irregularly on the adradial side and perradial side of the pore pairs. Numerous miliary tubercles are scattered over on ambulacra plates.

The peristome is approximately 23 mm in diameter, with about 10 boomerang-shaped plates in each column. Each plate has a row of two to three tubercles. The pore pairs are arranged in a single series. Peristomial spines and tube feet brown colored, the same color as that in the test. Gills large.

Aboral test plating (Figures 5E, F): A primary tubercle occurs on every second interambulacral plate from the ambitus to about four-fifths of the test, forming a regular adradial series. Numerous miliary tubercles scattered over these plates. In the ambulacra, a primary tubercle occurs between every plate to the fifth plate, forming an irregular perradial series. Numerous miliary tubercles are scattered over these plates.

The apical system measures 21 mm in diameter, pentagonal. Genital pores large, opening in the membranous gaps within the disaggregated genital plates. Madreporite distinct, slightly raised, kidney-shaped, and split clearly into one to two sections. Ocular plate large, with three to five small tubercles.

Spines: Hollow and cylindrical, with the longest approximately 14 mm long, 0.5 mm in diameter. The primary spines of the oral surface are smooth, slightly curved, and with about 20 fine, longitudinal striations. The hoof of the primary oral spines is white, moderately long (about 1.8 mm), slightly flared, and slightly flattened distally.

Pedicellariae (Figure 6): Three kinds of tridentate pedicellariae are present. A large kind (head length about 1.5 mm) with distinctly spoon-shaped valves, narrowest in the middle and widened distally, un-serrated tip. The valves are in contact for most of their length, and a base about two times the width of the tip. Two smaller types are also present: one rostrate form (about 0.4–0.6 mm long) with straight-sided, narrow, and un-serrated blades with a rounded tip; the other an involute form (about 1–1.5 mm long) with narrow, un-serrated blade, tips about one-fifth the valve length, and base about four times the width of the tip. Triphyllous pedicellariae (about 0.3–0.4 mm) of the typical echinothurioid form. Dactylous pedicellariae not found.

Size range

The median TD of the four specimens measured was 98.5 mm, with the largest specimen being 118 mm.

Distributions

Found on a seamount (Kocebu Guyot) near the Magellan seamount and three seamounts (M4, M7, and M5) near the Caroline Ridge in the Northwest Pacific Ocean, where the water depth is about 1,314–1,497 m.

Remarks

The new species mostly resembles *Araeosoma coriaceum* (Agassiz, 1879) (known from the Indo-Pacific) in terms of test plate morphology and tuberculation. However, the two species differ in aspects of their tridentate pedicellariae, hoof of primary oral spines, and color. The distinct spoon-shaped valves of the tridentate pedicellariae in *A. cucullatum* sp. nov. are not present in *A. coriaceum*. In addition, in *A. coriaceum*, the rostrate form of the tridentate pedicellariae has a coarsely serrated blade (see Plate LXXIX, Figures 10–15 in Mortensen, 1935). The hoof of the primary oral spines in *A. coriaceum* is smaller than that in *A. cucullatum* sp. nov. The coloration of *A. coriaceum* (greenish black or blackish brown) is quite distinct from that of *A. cucullatum* sp. nov. (light brown) (Agassiz, 1879).

Araeosoma polyporum sp. nov.

Diagnosis

Color of test is translucent, the tubercles and apical system red, oral tube feet and peristome buff, and the membranous gaps and spines white. Membranous spaces widest in the median area between the plates of the column. A primary tubercle occurs on every interambulacral plate on the oral surface, forming a regular adradial series. Some aboral plates have four pore pairs. The hoof of the primary oral spines is white, relatively short (about 0.5 mm), and only slightly flared. Involute tridentate pedicellariae with long, narrow blades, the tip round (Figures 7, 8).

Holotype

MBM286949, a seamount near the Mariana Trench, station FX-Dive 64 (11°18′ N, 139°21′ E), depth 207 m, June 22, 2016.

Etymology

Named *polyporum*, from the Greek word *poly* (many) and *porus* (pore), after the four pore pairs present in aboral plates.

Description

Test of holotype (Figures 7A, B): Approximately 46.4 mm TD, flexible, flattened, and pentagonal in outline. Color of test is translucent, tubercles and apical system red, oral tube feet and peristome buff, and the membranous gaps and spines white. Ratio of ambulacrum to interambulacrum width at ambitus, 1:2.

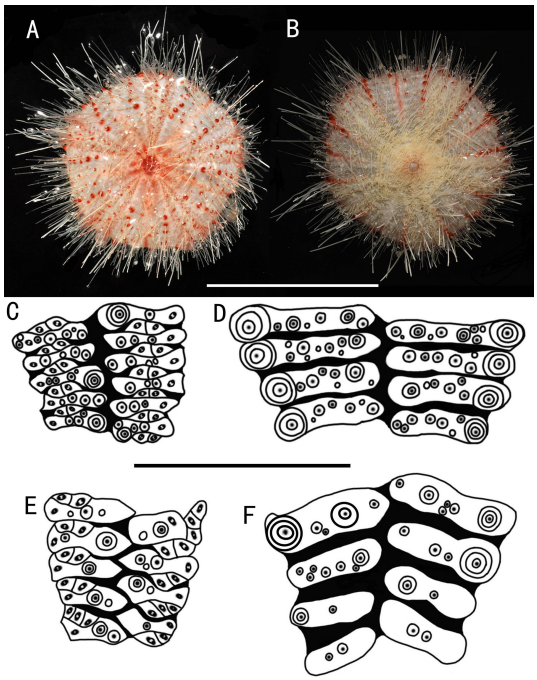

FIGURE 7
Araeosoma polyporum sp. nov.; holotype, MBM286949 (test diameter, 46.4 mm). **(A)** Aboral view. **(B)** Oral view. **(C–F)** Details of the coronal plates: **(C)**, oral ambulacra **(D)**, oral interambulacral **(E)**, aboral ambulacra **(F)** aboral interambulacral. *Scale bars*, 50 mm **(A, B)** and 10 mm **(C–F)**.

There are 41–45 plates in each column of the interambulacral, with about 20–22 of these plates on the oral surface. There are 61–64 plates in each column of the ambulacral, with about 30–32 of these plates on the oral surface. Membranous spaces widest in the median area between the plates of the column. Adapical-most interambulacral plates angled slightly.

Oral test plating (Figures 7C, D): A primary tubercle occurs on every interambulacral plate from the edge of the peristome to the ambitus, forming a regular adradial series. A smaller primary tubercle occurs on a few plates. These tubercles form an irregular series adjacent to the interradius. Numerous secondary and miliary tubercles scattered over these plates. In the ambulacra, a primary tubercle occurs on a few plates, forming an irregular perradial series. Numerous secondary and miliary tubercles are scattered over these plates.

The peristome is approximately 17 mm in diameter, with about 10 boomerang-shaped plates in each column. Each plate has a row of two to three tubercles. The pore pairs are arranged in a single series. Peristomial spines and tube feet buff. Gills small.

Aboral test plating (Figures 7E, F): A primary tubercle occurs on each or every second interambulacral plate from the ambitus to about half of the test, forming an irregular adradial series. One secondary tubercle occurs on a few plates. Numerous miliary tubercles are scattered over these plates. In the ambulacra, a primary tubercle occurs on every plate or every second or every third plate, forming an irregular perradial series. Numerous secondary and miliary tubercles are scattered over these plates. The pore pairs are arranged into three discrete columns in series, gradually curved near the apical system. Some plates have four pore pairs.

The apical system measures 9 mm in diameter, sub-pentagonal. Genital pores are large, opening in the membranous space at the genital plates. Madreporite distinct, slightly raised, and kidney-shaped. Ocular plates are small, with two to three small tubercles.

Spines: Hollow and cylindrical, with the longest approximately 25 mm long, 0.3 mm in diameter. The primary spines of the oral surface are smooth, slightly curved, and with about 20 fine, longitudinal striations. The hoof of the primary oral spines is white and relatively short (about 0.5 mm) and only slightly flared.

Pedicellariae (Figure 8): Two kinds of tridentate pedicellariae are present. One an involute form (head length about 1.8 mm) with long, narrow, and un-serrated blades, tip rounded, and almost the same width of the base; the valves touch only at the widened tip. The other a rostrate form (about 1.5 mm long) with straight-sided blades and an un-serrated tip only slightly narrowing toward the base. The valves are in contact for most of their length. Triphyllous pedicellariae (about 0.3–0.4 mm) of the typical echinothurioid form. Dactylous pedicellariae not found.

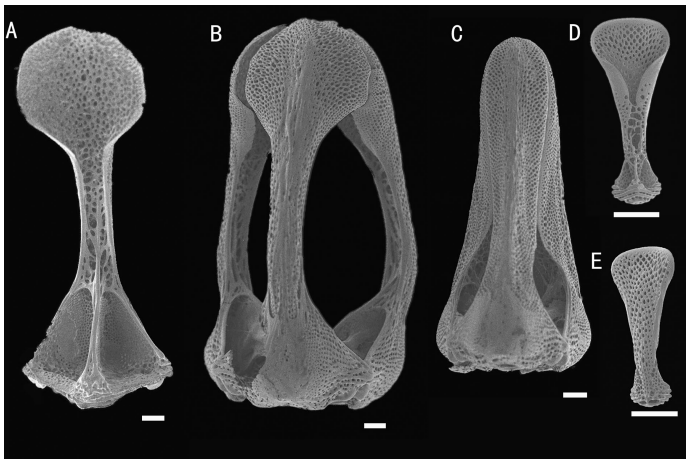

FIGURE 8
Araeosoma polyporum sp. nov.; holotype, MBM286949. SEM images of pedicellariae. **(A, B)** Involute tridentate pedicellaria: **(A)** individual valve **(B)** head. **(C)** Rostrate tridentate pedicellaria. **(D, E)** Valves of triphyllous pedicellariae. *Scale bar*, 100 μm.

Size range

The TD of the single known specimen is 46.4 mm.

Distribution

Found only on a seamount near the Mariana Trench in the Northwest Pacific Ocean, where the water depth is about 207 m.

Remarks

The pore pairs of *A. polyporum* sp. nov. reach up to four in some aboral plates, making it most similar to *Araeosoma owstoni* Mortensen, 1904 (known from the Western Pacific Ocean). *A. polyporum* sp. nov. differs from *A. owstoni* in terms of the presence of the involute form of tridentate pedicellariae and the hoof of the primary oral spines being relatively shorter than that in *A. owstoni*. The coloration of the holotype of *A. owstoni* (flesh colored, aboral spines greenish) is quite distinct from that of *A. polyporum* sp. nov. (red, spines white). However, the Hawaiian specimens showed a wide range of color (the small individuals are white, medium-sized specimens are reddish or brick red, and the larger specimens are dull pale purplish and the spines pinkish) (Agassiz and Clark, 1909).

Araeosoma alternatum Mortensen, 1934

Araeosoma coriaceum Döderlein, 1906: 122. *Araeosoma alternatum* Mortensen, 1934:165; 1935:270; Anderson, 2013:556–559 (Figures 9, 10).

Material examined

MBM286966, Y3 seamount, station FX-Dive 21 (8°51′ N, 137°47′ E), depth 307–381 m, December 24, 2014.

Description

Test (MBM286966) (Figures 9A, B): Approximately 135.4 mm TD, flexible, flattened, and pentagonal in outline. Color of ethanol-preserved test and appendages, nude. Ratio of ambulacrum to interambulacrum width at ambitus, 9:10.

There are 81 plates in each column of the interambulacral, with about 40 of these plates on the oral surface. There are 147 in each column of the ambulacral, with about 58 of these plates on the oral surface. Membranous spaces widest in the median area between interambulacral plates on the aboral surface. These gaps are relatively narrow compared with other *Araeosoma* species. Adapical-most interambulacral plates angled slightly.

Oral test plating (Figures 9C, D): A primary tubercle occurs on every second interambulacral plate (a few occur on every plate) from the edge of the peristome to the ambitus, forming a regular adradial series. The other primary tubercles occur on every plate or every second plate, forming an irregular interradius series. Numerous secondary and miliary tubercles are scattered over these plates. In the ambulacra, a primary tubercle occurs on every plate or every second or third plate, forming an irregular perradial series. Secondary tubercles are arranged irregularly on the adradial and perradial sides of the pore pairs. Numerous miliary tubercles are scattered over these plates. The peristome is approximately 38 mm in diameter, with about 11 boomerang-shaped plates in each column. Each plate has a row of two to three tubercles. The pore pairs are arranged in a single series. The peristomial spines and tube feet are nude colored, the same color as that of the test. Gills small.

Aboral test plating (Figures 9E, F): A primary tubercle occurs on a few interambulacral plates from the ambitus to about half of the test, forming an irregular adradial series. The other primary tubercles occur on a few interambulacral plates from the ambitus to

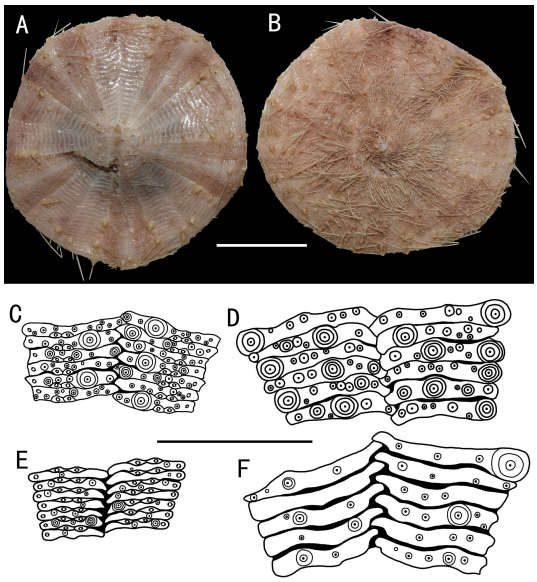

FIGURE 9
Araeosoma alternatum, MBM286966 (test diameter, 135.4 mm). **(A)** Aboral view. **(B)** Oral view. **(C–F)** Details of the coronal plates: **(C)**,oral ambulacra **(D)**, oral interambulacral **(E)**, aboral ambulacra **(F)** aboral interambulacral. *Scale bars*, 50 mm **(A, B)** and 20 mm **(C–F)**.

about half of the test, forming an irregular interradius series. In the ambulacra, a primary tubercle occurs on a few plates, forming an irregular perradial series. There are one to two secondary tubercles in a column of the ambulacra near the apical system. Numerous miliary tubercles are scattered over these plates.

The apical system measures 20 mm in diameter, circle. Genital pores are small, opening in the membranous space at the genital plates. Madreporite oval, not much raised. The ocular plate is large, with one to three small tubercles.

Spines: Hollow and cylindrical, with the longest approximately 32 mm long, 0.6 mm in diameter. The primary spines of the oral surface are smooth, slightly curved, and with about 20 fine, longitudinal striations. The hoof of the primary oral spines is short and widely flaring (about 0.8 mm).

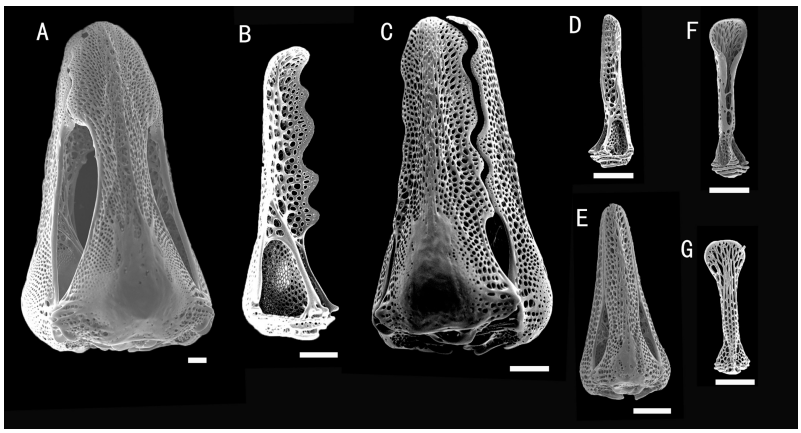

FIGURE 10
Araeosoma alternatum, MBM286966. SEM images of pedicellariae. **(A)** Large involute tridentate pedicellaria. **(B, C)** Large rostrate tridentate pedicellaria: **(B)** individual valve **(C)** head. **(D, E)** Small tridentate pedicellaria: **(D)** individual valve **(E)** head. **(F, G)** Valves of triphyllous pedicellariae. *Scale bar*, 100 μm.

Pedicellariae (Figure 10): Three kinds of tridentate pedicellariae are present. One is a large (head length about 1.8 mm) involute form, coarsely serrated, and the tip widening to half the width of the base. The valves are in contact for most of the tip length. The other is a large rostrate form (head length about 0.8 mm, base about 0.35 mm wide), with a coarsely serrated blade widening toward the base. The valves are in contact for most of their length. Another is a small tridentate rostrate form (about 0.5 mm long) with straight-sided, narrow, and un-serrated blades. The valves are in contact for most of their length, with a base about two times the width of the tip. Triphyllous pedicellariae (about 0.38 mm long) with a cylindrical middle, the blades involute and particularly elongated, the base about as wide as the tip, on a long neck and stalk. These unusual triphyllous pedicellariae are readily found on the specimens examined. Dactylous pedicellariae not found.

Distribution

Depth of 307–1,289 m, in the western Indian Ocean, New Caledonia, New Zealand, Southeast Australia, and the Yap Trench area in the Northwest Pacific Ocean.

Remarks

The specimen was clearly a new record for the Northwest Pacific Ocean, as the species was previously known only from the western Indian Ocean and the South Pacific Ocean. The rostrate tridentate pedicellariae and triphyllous pedicellariae in the specimen examined look remarkably similar to Döderlein's figures of *A. alternatum* (see Tafel XXXVIII in Döderlein, 1906). We noticed some differences, including: 1) the absence of ophicephalous pedicellariae compared to the Auckland Island specimens (see Figure 31 in Anderson, 2013); however, the ophicephalous forms are quite rare and very small, and they have not been found on the holotype either; 2) the middle section of the involute tridentate pedicellariae in the specimen examined is relatively wider than that in the type specimen.

Araeosoma bidentatum Anderson, 2013

Araeosoma bidentatum Anderson, 2013:523–529 (Figures 11, 12).

Material examined

MBM286957, M8 seamount, station FX-Dive 224 (10°36′ N, 140°04′ E), depth 1,314 m, June 12, 2019.

Description

Test (MBM286957) (Figures 11A, B): Approximately 61.5 mm TD, flexible, flattened, and pentagonal in outline. The color of the oral test is buff, sucking disks and peristome orange, and aboral test beige. The membranous connective tissue between the plates is white. Ratio of ambulacrum to interambulacrum width at ambitus, 2:3.

There are 48–52 plates in each column of the interambulacral, with about 19–21 of these plates on the oral surface. There are 51–58 plates in each column of the ambulacral, with about 21–25 of these plates on the oral surface. Membranous spaces widest in the plates of the interambulacral.

Oral test plating (Figures 11C, D): A primary tubercle occurs on every interambulacral plate from the edge of the peristome to the ambitus, forming a regular adradial series. The other primary tubercles occur on every plate from the edge of the peristome to the ambitus, forming a regular interradius series. Numerous secondary and miliary tubercles are scattered over these plates. In the ambulacra, a primary tubercle occurs on every plate to every third plate, forming an irregular perradial series. One secondary tubercle occurs on a few plates. Numerous miliary tubercles are scattered over these plates.

The peristome is approximately 18 mm in diameter, with about eight boomerang-shaped plates in each column. Each plate has a row of tubercles. The pore pairs are arranged in a single series. The peristomial spines are curved, slightly expanded distally. Gills small.

Aboral test plating (Figures 11E, F): A primary tubercle occurs on every second interambulacral plate from the ambitus to about half of the test, forming a regular adradial series. Numerous secondary and miliary tubercles are scattered over these plates. In the ambulacra, a primary tubercle occurs on a few ambulacra plates from the ambitus to about half of the test, forming an irregular perradial series. Numerous miliary tubercles are scattered over these plates.

The apical system measures 12 mm in diameter, circular. Genital pores are large, opening in the membranous space at the genital plates. Madreporite distinct, slightly raised, and subtriangular. The ocular plate is small, with two to five small tubercles.

Spines: Hollow and cylindrical, with the longest approximately 53 mm long, 0.5 mm in diameter. The primary spines of the oral surface are smooth, slightly curved, and with about 24 fine, longitudinal striations. The hoof of the primary oral spines is white and relatively short (about 0.8 mm), only slightly flared. Primary aboral spines invested in a translucent skin sheath.

Pedicellariae (Figure 12): Three kinds of tridentate pedicellariae are present. One a large (about 1.8 mm long) involute form with serrated tips in contact for most of the tip length, with the tip about two-thirds of the width of the base. Two bidentate types are also present. One is straight-sided (about 1.1 mm long) with no involute blades, with the base slightly wider than the blade and the tip slightly serrated. The valves are in contact for most of their length. The other is a rostrate form (about 0.3 mm long) with wide un-serrated blades, only slightly narrowing toward the base. The valves are in contact for most of their length. Triphyllous pedicellariae (about 0.3–0.4 mm) is the typical echinothurioid form. Dactylous (about 2.1 mm): form typical of the genus, with six valves, the blade edges finely "crimped."

Distribution

Depth of 760–1,314 m, in New Zealand, Australia, and the Caroline Ridge area in the Northwest Pacific Ocean.

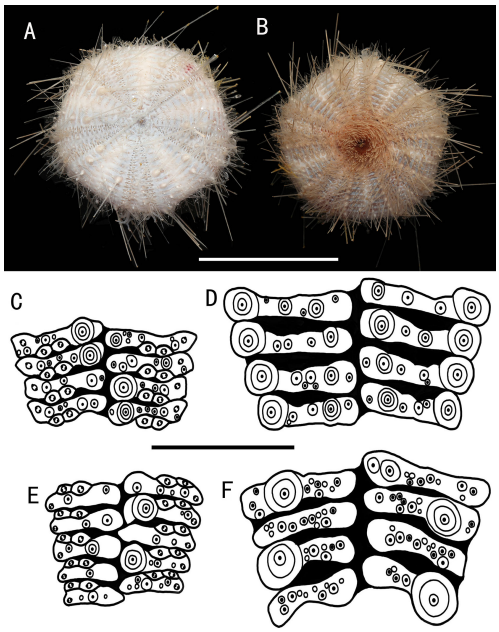

FIGURE 11
Araeosoma bidentatum, MBM286957 (test diameter, 61.5 mm). **(A)** Aboral view. **(B)** Oral view. **(C–F)** Details of the coronal plates: **(C)**, oral ambulacra **(D)**, oral interambulacral **(E)**, aboral ambulacra **(F)** aboral ambulacra. *Scale bars*, 50 mm **(A, B)** and 10 mm **(C–F)**.

Remarks

The specimen was clearly a new record for the Northwest Pacific Ocean, as the species was previously known only from the South Pacific Ocean.

The bidentate pedicellariae are known only from *A. bidentatum*, and this characteristic pedicellaria is common on the single specimen examined. The specimen from the Caroline Ridge area differs from the type specimens regarding the presence of two types of bidentate pedicellariae and the dactylous pedicellariae with six valves. The type specimens only have one type of bidentate pedicellariae and dactylous pedicellariae with five valves (see Figure 5 in Anderson, 2013). Additionally, the coloration of the type specimens (deep red) is quite distinct from that of the specimen examined (buff). We believe that these differences are individual differences, and barcoding and the phylogenetic relationships supported this view (see analysis for details; Figure 13).

Barcoding and phylogenetic relationships

In total, 27 new sequences (14 for *COI* and 13 for *16S*) were obtained (Supplementary Table S2) for *A. alternatum*, *A. polyporum* sp. nov., *A. bidentatum*, *A. cucullatum* sp. nov., and *H. involucrum* sp. nov. For *A. cucullatum* sp. nov. and *H. involucrum* sp. nov., multiple specimens (four and seven specimens per species, respectively) were analyzed to document the intraspecific variability. We observed a hierarchical increase in divergence (K2P distance) according to the different taxonomic levels, within species (from 0% to 0.8%), within congeners (from 1.5% to 12.6%), and within family (16.9%) (Figure 13A). There was a clear barcoding gap for the family Echinothuriidae, which supported the identification of the three new species. The NJ tree showed that the sequencing records for 53 queries representing 12 species formed distinct barcode clusters (Figure 13B), also indicating their successful identification.

In order to explore the phylogenetic position of Echinothuriidae, BI and ML analyses were conducted. The phylogenetic trees resulting from both BI and ML analyses were congruent and generally well supported (Figure 13C). Tree topologies supported the closed relationship of Echinothuriidae and Phormosomatidae. The order Echinothurioida grouped with the lineage Aspidodiadematoida + Pedinoida. Within the family Echinothuriidae, different specimens of *A. cucullatum* sp. nov. and *H. involucrum* sp. nov. were grouped together with high support (BP= 99%–100%, PP = 1.00). The monophyly of the genus *Araeosoma* was well supported (BP = 100%, PP = 1.00). The monophyly of *Hygrosoma* could not be verified because only *H. involucrum* sp. nov. was included in our study; however, it was supported to be a sister to *Araeosoma* (BP = 99%, PP = 1.00).

Biogeographic analyses

The UPGMA cluster analysis found 10 main groups among the 29 deep-sea fields (Figure 14): East Pacific Rise and Northern Atlantic Boreal (1–3), Yap Trench and Indian Ocean (4–5),

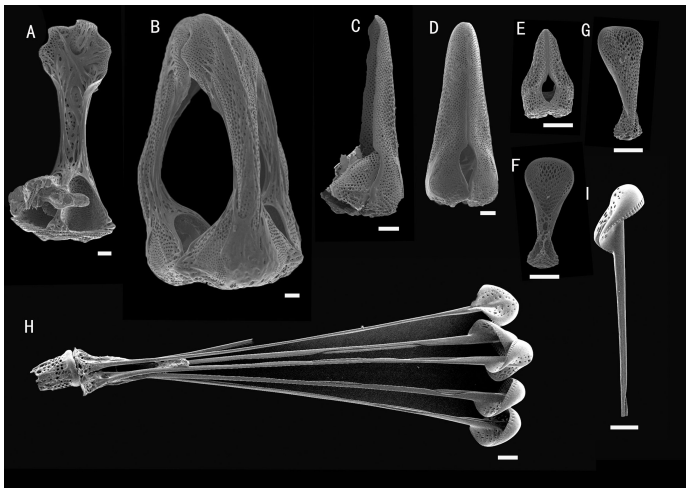

FIGURE 12
Araeosoma bidentatum, MBM286957. SEM images of pedicellariae. **(A, B)** Large tridentate pedicellaria: **(A)** individual valve **(B)** head. **(C, D)** Straight side bidentate pedicellaria: **(C)** individual valve **(D)** head. **(E)** Rostrate bidentate pedicellaria. **(F, G)** Valves of triphyllous pedicellariae. **(H, I)** Dactylous pedicellaria. *Scale bar*, 100 μm.

Western and Central Pacific (6–7), Northern Pacific Boreal (8), North Indian Ocean (9–10), Southwest Pacific (11–13), Indo-Pacific (14–18), Atlantic (19–24), Mariana Trench (25), and Caroline Ridge and the Magellan seamount (26–29). The Mariana Trough, Yap Trench, and Caroline Ridge formed separated groups from each other. The Kocebu Guyot of the Magellan seamount clustered together with Caroline Ridge M4, M5, and M7. However, only one shared species was found in these seamounts, suggesting the low connectivity between seamount populations.

Discussion

Diversity and distribution of echinothuriids

Echinothuriids comprise an abundant echinoderm group widely distributed in deep water. Among the echinothuriid genera inhabiting deep water, *Araeosoma* Mortensen, 1903 was observed in the highest abundance, with a total of 21 valid species including the four newly described species here (Figure 15). To date, 20 species of *Araeosoma* have been discovered in Pacific Ocean deep water, except for *Araeosoma belli* Mortensen, 1903, which was reported from the Gulf of Mexico and the Caribbean Sea (Felder and Camp, 2009; Alvarado, 2010). Among these 20 species, 18 occurred in the Western Pacific. Compared to the abundance of *Araeosoma*, only nine species of *Sperosoma* Koehler, 1897, seven species of *Tromikosoma* Mortensen, 1903, four species of *Hygrosoma* Mortensen, 1903, three species of *Hapalosoma* Mortensen, 1903, and two species of *Calveriosoma* Mortensen, 1934, have been described to date (Figure 14). Like *Araeosoma*, the members of *Sperosoma* and *Calveriosoma* are mainly found in the Western Pacific, which hosts about 55.6% and 50.0% of their total numbers, respectively. All members of *Hygrosoma* and *Hapalosoma* are distributed in the Western Pacific, while the members of *Hygrosoma*, *Sperosoma*, and *Calveriosoma* are recorded in the North Atlantic. The members of *Tromikosoma* are likely to be rarer in the West Pacific than in the East Pacific and North Atlantic.

Biogeography of deep-sea echinothuriids

Based on the water temperature, dissolved oxygen, the particulate organic flux to the seafloor, and salinity, Watling et al. (2013) delineated 14 deep-sea benthic provinces in the world ocean: Arctic Bathyal, North Pacific Boreal, West Pacific Bathyal, Southeast Pacific Ridges, North Pacific Bathyal, Antarctic Bathyal, North Atlantic Boreal, North Atlantic Bathyal, Cocos Plate, Subantarctic, Nazca Plate, New Zealand Kermadec, Indian Ocean Bathyal, and South Atlantic. This model needs to be examined with documented locations of select benthic marine species.

Based on the distribution data of *Araeosoma*, *Sperosoma*, *Tromikosoma*, *Hygrosoma*, *Hapalosoma*, and *Calveriosoma* in deep water, we delineated 10 isolated deep-sea provinces: East Pacific Rise and Northern Atlantic Boreal, Yap Trench and Indian Ocean, Western and Central Pacific, Northern Pacific Boreal, North Indian Ocean, Southwest Pacific, Indo-Pacific, Atlantic, Mariana Trench, and Caroline Ridge and the Magellan seamount (Figure 14). In our analysis, the North and South Indian Oceans likely represent two independent deep-sea

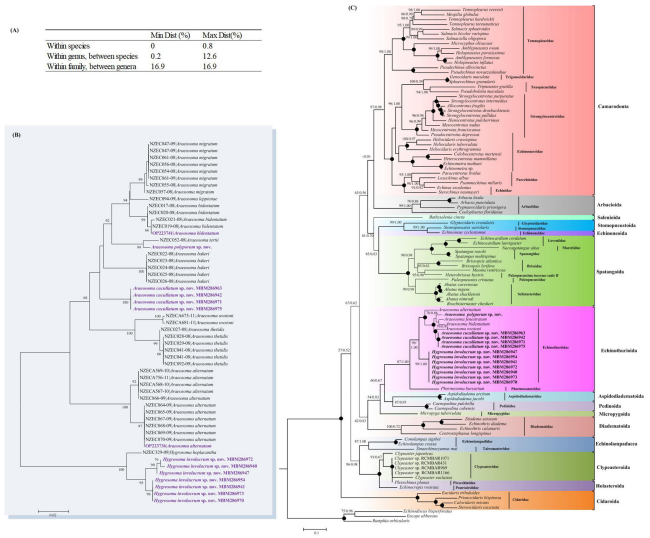

FIGURE 13
(A) *Cytochrome oxidase subunit I* (*COI*) genetic divergence within echinothuriid species. **(B)** Neighbor-joining (NJ) tree inferred from the COI sequences showing the relationships of the echinothuriid species based on the Kimura two-parameter (K2P) model. **(C)** Maximum likelihood (ML) and Bayesian inference (BI) trees of Echinoidea based on the combined sequences of *COI* and *16S*. *Numbers at the nodes* represent the ML (*left*) and BI (*right*) support values. Only values higher than 0.50 are shown. Newly sequenced echinothuriids are in *bold*.

provinces, while the East Pacific Rise and Northern Atlantic Boreal appear to represent a combined province rather than independent ones, which did not coincide with the model provided by Watling et al. (2013). In the present study, the Western Pacific likely included six provinces. Similar to the models proposed in previous studies (Bachraty et al., 2009; Rogers et al., 2012; Watling et al., 2013; Wu et al., 2019), the Western Pacific was geographically more complex than initially thought. In the study of Bachraty et al. (2009), the Western Pacific represented two provinces. Similarly, the Western Pacific was regarded as three provinces in Watling et al. (2013) and Wu et al. (2019) and four provinces in Rogers et al. (2012). Previous

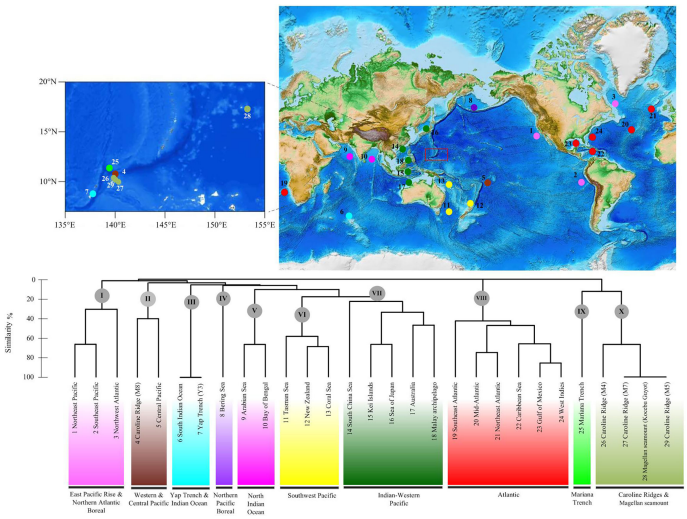

FIGURE 14
Geographical clustering of the 29 deep-sea fields studied based on the unweighted pair group method with arithmetic mean (UPGMA) cluster analysis (Bray–Curtis distance) and an 10-province model based on the data of deep-sea echinothuriid species.

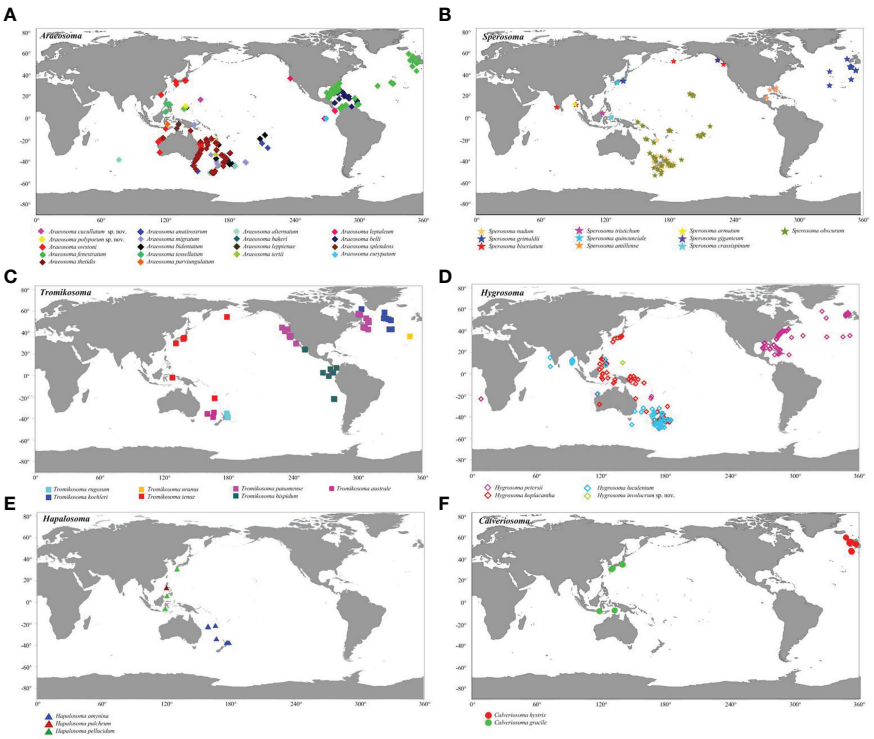

FIGURE 15
Distribution of deep-sea echinothuriid species based on the records of the Ocean Biodiversity Information System (https://obis.org/). **(A)** *Araeosoma* Mortensen, 1903. **(B)** *Sperosoma* Koehler, 1897. **(C)** *Tromikosoma* Mortensen, 1903. **(D)** *Hygrosoma* Mortensen, 1903. **(E)** *Hapalosoma* Mortensen, 1903. **(F)** *Calveriosoma* Mortensen, 1934. *Colors* denote different echinothuriid species.

studies have proposed the East Pacific Rise as the biogeographic center of deep-sea hydrothermal vent fauna (Van Dover and Hessler, 1990; Bachraty et al., 2009). The distribution of echinothuriids showed that the Western Pacific harbored the highest species diversity. This result supported the "possible ancestral position of the Western Pacific" (Moalic et al., 2012; Sun et al., 2018).

The Mariana Trough, Yap Trench, and Caroline Ridge formed separated clusters, although their positions are in close proximity. This is consistent with the estimated low connectivity between the seamount populations (de Forges et al., 2000). However, the Kocebu Guyot of the Magellan seamount, which was far away from Caroline Ridge, clustered together with M4, M5, and M7. The Mariana Trough, as an independent province, is in accordance with the partition scheme of the Northwest Pacific suggested by Kojima and Watanabe (2015) and Wu et al. (2019). Due to the lack of data regarding echinothuriids from these seamounts, we were unable to further delineate the deep-sea provinces, especially those in the Magellan seamount and Caroline Ridge. The 10-province model still needs to be examined by complementary data on other seamounts and other animals.

Conclusion

Based on the examination of specimens of Echinothuriidae collected from seamount areas [Magellan (Kocebu Guyot), Yap (Y3), and Mariana and Caroline (M4, M5, M7, and M8)] in the Northwest Pacific Ocean from 2014 to 2019, we identified three new species—*Araeosoma cucullatum* sp. nov., *Araeosoma polyporum* sp. nov., and *Hygrosoma involucrum* sp. nov.—and two new records including two species from the genus *Araeosoma*. The characteristics of the coloring, ambulacrum, interambulacrum, apical system, spines, and pedicellariae of these species were different from each other and their congeners. There was a clear barcoding gap (K2P genetic distance) for the family Echinothuriidae, and the NJ tree showed distinct barcode clusters for these species, which supported the identification of the five new species. The BI and ML analyses revealed the monophyly of Echinothuriidae. Moreover, UPGMA cluster analysis revealed 10 deep-sea provinces: East Pacific Rise and Northern Atlantic Boreal, Yap Trench and Indian Ocean, Western and Central Pacific, Northern Pacific Boreal, North Indian Ocean, Southwest Pacific, Indo-Pacific, Atlantic, Mariana Trench, and Caroline Ridge and Magellan seamount. Our analysis revealed low connectivity between

the seamount populations. The Western Pacific is geographically complex and harbors a higher species diversity of deep-sea echinothuriids than other sea areas, suggesting the pivotal role of the Western Pacific in the dispersal and speciation of deep-sea echinothuriids.

Data availability statement

The datasets presented in this study can be found in online repositories. The names of the repository/repositories and accession number(s) can be found in the article/Supplementary Material.

Author contributions

WZ, SS, ZS, and NX conceived and designed the research. WZ and NX studied the morphology. SS performed the barcoding, phylogenetic relationship, and biogeographic analyses. WZ, SS, ZS, and NX contributed to the writing and editing of the final manuscript. All authors contributed to the article and approved the submitted version.

Funding

This work was supported by the Strategic Priority Research Program of the Chinese Academy of Sciences (XDA22050302 and XDB42000000), the Key Program of National Natural Science Foundation of China (no. 41930533), the National Key Research and Development Program of China (2021YFE0193700), and the National Science Foundation for Distinguished Young Scholars (42025603).

Acknowledgments

We thank the assistance of the crew of R/V *KEXUE* and ROV FaXian for sample collection and Dr. Kunxuan Li for photographing freshly collected specimens. We also appreciate the reviewers for their constructive comments on an earlier version of the manuscript.

Conflict of interest

The authors declare that the research was conducted in the absence of any commercial or financial relationships that could be construed as a potential conflict of interest.

Publisher's note

Supplementary material

The Supplementary Material for this article can be found online at: https://www.frontiersin.org/articles/10.3389/fmars.2022.1036914/full#supplementary-material

SUPPLEMENTARY TABLE 1
The primer sequences for COI and 16S genes.

SUPPLEMENTARY TABLE 2
The Echinoidea species used in the barcoding and phylogenetic analyses.

SUPPLEMENTARY TABLE 3
The best-fit partitioning schemes and substitution models.

SUPPLEMENTARY TABLE 4
The distribution data of echinothuriid species.

SUPPLEMENTARY TABLE 5
Raw presence-absence (0-1) data for echinothuriid species used in the statistical analyses.

References

Agassiz, A. (1879). "Preliminary report of the echini of the exploring expedition of H.M.S challenger," American Academy of Arts And Sciences in *Proceedings of the American Academy of Arts and Sciences. new series*, (Cambridge: American Academy of Arts & Sciences) 6. 190–212. doi: 10.2307/25138537

Agassiz, A. (1880). Reports of the dredging by the *Blake*-Preliminary report on the echini. *Bull. Museum. Comp. Zool. Harvard.* 8, 69–84.

Agassiz, A., and Clark, H. L. (1909). Hawaiian And other pacific echini. the echinothuridae. *Memoirs. Museum. Comp. Zool.* 34 (3), 192.

Alvarado, J. J. (2010). Echinoderm diversity in the Caribbean Sea. *Mar. Biodivers.* 41 (2), 261–285. doi: 10.1007/s12526-010-0053-0

Anderson, O. F. (2013). A review of new zealand and southeast australian echinothuriinids (echinodermata: echinothuriidae) with descriptions of seven new species. *Zootaxa* 3609 (6), 521. doi: 10.11646/zootaxa.3609.6.1

Anderson, O. F. (2016). A review of new zealand and southeast australian echinothurioids (echinodermata: echinothurioida)–excluding the subfamily echinothuriinae–with a description of a new species of tromikosoma. *Zootaxa* 4092 (4), 451. doi: 10.11646/zootaxa.4092.4.1

Bachraty, C., Legendre, P., and Desbruyeres, D. (2009). Biogeographical relationships among deep-sea hydrothermal vent faunas at global scale. *Deep-Sea. Res. I.* 56, 13711378. doi: 10.1016/j.dsr.2009.01.009

Claus, C. F. W. (1880). *Grundzuge der zoologie. 4th Edition* Vol. 821 (Marburg and Leipzig: N. G. Elwertsche Universitatsbuchhandlung), 522 pp.

Coppard, S. E., and Schultz, H. A. G. (2006). A new species of coelopleurus (Echinodermata: Echinoidea: Arbaciidae) from new Caledonia. *Zootaxa* 1281, 1–19. doi: 10.11646/zootaxa.1281.1.1

David, B., and Sibuet, M. (1985). "Distribution et diversité des échinides," in *Peuplements profonds du golfe de gascogne*. Eds. L. Laubier and C. Monniot (France: IFREMER), 509534.

de Forges, B. R., Koslow, J. A., and Poore, G. C. B. (2000). Diversity and endemism of the benthic seamount fauna in the southwest pacific. *Nature* 405, 944–947. doi: 10.1038/35016066

Döderlein, L. (1906). "Die echinoiden der deutschen tiefsee-expedition," in *Wissenschaftliche ergebnisse der deutschen tiefsee-expedition auf dem dampfer "Valdivia" 1898–1899*, (Jena: VERLAG VON GUSTAV FISCHER) 5. , 61–290.

Felder, D. L., and Camp, D. K. (Eds.) (2009). *Gulf of Mexico: origin, waters, and biota. volume 1, biodiversity* (Bizzell St, College Station; Texas A&M University Press) 1393 pp.

Grube, A. E. (1868). Asthenosoma varium. *Jahresbericht. und. Abhandlungen. der. Schlesischen. Gesellschaft. für. Vaterländische. Cultur.* 45 (1867), 42–44.

Hoareau, T. B., and Boissin, E. (2010). Design of phylum:pecific hybrid primers for dna barcoding: addressing the need for efficient coi amplification in the echinodermata. *Mol. Ecol. Resour.* 10 (6), 960–967. doi: 10.1111/j.1755-0998.2010.02848.x

Jeffery, C. H., Emlet, R. B., and Littlewood, D. (2003). Phylogeny and evolution of developmental mode in temnopleurid echinoids. *Mol. Phylogenet. Evol.* 28 (1), 99–118. doi: 10.1016/S1055-7903(03)00030-7

Katoh, K., Kuma, K., Toh, H., and Miyata, T. (2005). MAFFT version 5: improvement in accuracy of multiple sequence alignment. *Nucleic Acids Res.* 33, 511518. doi: 10.1093/nar/gki198

Koehler, R. (1897). Nouveau genre d'Echinothuride. *Zoologischer. Anzeiger.* 20, 302–307.

Kojima, S., and Watanabe, H. (2015). *Vent fauna in the Mariana Trough*. In: Subseafloor Biosphere Linked to Hydrothermal Systems: TAIGA Concept. Eds. J.-i. Ishibashi, K. Okino and M. Sunamura Springer, Tokyo, Japan, pp. 313–323.

Kroh, A., and Mooi, R. (2022). World echinoidea database. *Sperosoma*. Accessed through: World Register of Marine Species Available at: https://www.marinespecies.org/aphia.php?p=taxdetails&id=123402.

Lanfear, R., Frandsen, P. B., Wright, A. M., Senfeld, T., and Calcott, B. (2016). Partitionfinder 2: new methods for selecting partitioned models of evolution for molecular and morphological phylogenetic analyses. *Mol. Biol. Evol.* 34, 772773. doi: 10.1093/molbev/msw260

Minh, B. Q., Nguyen, M. A. T., and von Haeseler, A. (2013). Ultrafast approximation for phylogenetic bootstrap. *Mol. Biol. Evol.* 30, 1188–1195. doi: 10.1093/molbev/mst024

Moalic, Y., Desbruyeres, D., Duarte, C. M., Rozenfeld, A. F., Bachraty, C., and Arnaud-Haond, S. (2012). Biogeography revisited with network theory: retracing the history of hydrothermal vent communities. *Syst. Biol.* 61, 127137. doi: 10.1093/sysbio/syr088

Mooi, R., Constable, H., Lockhart, S., and Pearse, J. (2004). Echinothurioid phylogeny and the phylogenetic significance of *Kamptosoma* (Echinoidea: Echinodermata). *Deep. Sea. Res. Part II.* 51 (14/16), 1903–1919. doi: 10.1016/j.dsr2.2004.07.020

Mortensen, T. (1903). Echinoidea (Part i.). *Danish. Ingolf-Expedition.* 4 (1), 1–198.

Mortensen, T. (1904). On some echinothurids from Japan and the Indian ocean. *Ann. Magazine. Natural History. Seventh. Ser.* (Oxford University Press) 14, 81–93. doi: 10.1080/03745480409442975

Mortensen, T. (1927). *Handbook of the echinoderms of the British isles* (Oxford, UK: Oxford University Press), 471 pp.

Mortensen, T. (1934). New echinoidea. preliminary notice. *Videnskabelige. Meddelelser. Dansk. Naturhistorisk. Forening. i. København.* 98, 161–167.

Mortensen, T. (1935). *A monograph of the echinoidea II. bothriocidaroida, melonechinoida, lepidocentroida and stirodonta*. Ed. C. A. Reitzel (Copenhagen: Oxford University Press) 647 pp.

Rambaut, A., Drummond, A. J., Xie, D., Baele, G., and Suchard, M. A. (2018). Posterior summarization in bayesian phylogenetics using tracer 1.7. *Syst. Biol.* 67, 901904. doi: 10.1093/sysbio/syy032

Rogers, A. D., Tyler, P. A., Connelly, D. P., Copley, J. T., James, R., Larter, T. D., et al. (2012). The discovery of new deep-Sea hydrothermal vent communities in the southern ocean and implications for biogeography. *PloS Biol.* 10 (1), e1001234. doi: 10.1371/journal.pbio.1001234

Ronquist, F., and Huelsenbeck, J. P. (2003). MrBayes 3: Bayesian phylogenetic inference under mixed models. *Bioinformatics* 19, 1572–1574. doi: 10.1093/bioinformatics/btg180

Smith, A. B., and Wright, C. W. (1990). British Cretaceous Echinoids. part 2, echinothurioida, diadematoida, and stirodonta (1, calycina). *Monograph. Palaeontol. Soc.* 143, 101–198. doi: 10.1080/25761900.2022.12131767

Stevenson, A., and Kroh, A. (2020). "Deep-sea sea urchins," in *Sea Urchins: Biology and ecology* (Amsterdam: Elsevier). *fourth edition*, vol. 43. doi: 10.1016/B978-0-12-819570-3.00014-7

Sun, S., Sha, Z. L., and Wang, Y. R. (2018). Phylogenetic position of alvinocarididae (Crustacea: Decapoda: Caridea): new insights into the origin and evolutionary history of the hydrothermal vent alvinocarid shrimps. *Deep. Sea. Res. Oceanogr. Res. Pap.* 141, 93105. doi: 10.1016/j.dsr.2018.10.001

Tamura, K., Stecher, G., Peterson, D., Filipski, A., and Kumar, S. (2013). MEGA6: molecular evolutionary genetics analysis version 6.0. *Mol. Biol. Evol.* 30, 2725–2729. doi: 10.1093/molbev/mst197

Thomson, C. W. (1872a). Notice of a new family of the Echinodermata. *Proc. R. Soc. Edinburgh.* 7, 615–617. doi: 10.1017/S0370164600042759

Thomson, W. (1872b). On the echinidea of the 'Porcupine' deep-Sea dredging-expeditions. *Proc. R. Soc. London.* 20, 491–497. doi: 10.1098/rspl.1871.0095

Thomson, W. (1877). "The voyage of the "Challenger": the Atlantic: a preliminary account of the general results of the exploring voyage of H.M.S," in *"Challenger" during the year 1873 and the early part of the year 1876* (New York: Harper), 148–149.

Trifinopoulos, J., Nguyen, L. T., Von Haeseler, A., and Minh, B. Q. (2016). W-IQ-TREE: a fast online phylogenetic tool for maximum likelihood analysis. *Nucleic Acids Res.* 44, W232–W235. doi: 10.1093/nar/gkw256

Van Dover, C. L., and Hessler, R. R. (1990). "Spatial variation in faunal composition of hydrothermal vent communities on the East pacific rise and Galapagos rift," in *Gorda ridge: A seafloor spreading center in the united states exclusive economic zone* (New-York: Springer-Verlag).

Watling, L., Guinotte, J., Clark, M. R., and Smith, C. R. (2013). A proposed biogeography of the deep ocean floor. *Prog. Oceanogr.* 111 (apr.), 91–112. doi: 10.1016/j.pocean.2012.11.003

Wu, X., Zhan, Z., and Xu, K. (2019). Two new and two rarely known species of branchinotogluma (annelida: polynoidae) from deep-sea hydrothermal vents of the manus back-arc basin, with remarks on the diversity and biogeography of vent polynoids. *Deep-Sea. Res.* (JUL.) 149. doi: 10.1016/j.dsr.2019.05.011

frontiers | Frontiers in Marine Science

TYPE Original Research
PUBLISHED 12 January 2023
DOI 10.3389/fmars.2022.1052968

OPEN ACCESS

EDITED BY
Libin Zhang,
Institute of Oceanology (CAS), China

REVIEWED BY
Georgina Robinson,
Scottish Association For Marine Science, United Kingdom
Ingrid Lupatsch,
AB Agri Ltd, United Kingdom

*CORRESPONDENCE
Gyda Christophersen
gyda.christophersen@moreforsking.no

SPECIALTY SECTION
This article was submitted to Marine Fisheries, Aquaculture and Living Resources, a section of the journal Frontiers in Marine Science

RECEIVED 24 September 2022
ACCEPTED 23 December 2022
PUBLISHED 12 January 2023

CITATION
Sunde J and Christophersen G (2023) Appetite in captivity - feeding studies of the red sea cucumber *Parastichopus tremulus*. *Front. Mar. Sci.* 9:1052968. doi: 10.3389/fmars.2022.1052968

Appetite in captivity - feeding studies of the red sea cucumber *Parastichopus tremulus*

Jan Sunde and Gyda Christophersen*

Møreforsking AS, Ålesund, Norway

The deposit feeding sea cucumber *Parastichopus tremulus* is an underutilised resource in North Atlantic waters. Geographically it is distributed from the Barents Sea in the north to the Canary Islands in the south. At present performance of *P. tremulus* in aquaculture is largely unknown. Species and stage specific biological knowledge gaps need to be filled for a potential industry to develop, and feeds that support growth needs special attention. Particulate matter (sludge) from fish farms is an unutilised resource that has potential as ingredient in feeds for sea cucumbers, which would help to reduce the environmental footprint of *P. tremulus* aquaculture production. The suitability of salmon sludge as a feed ingredient is unknown. Feeds using dried salmon freshwater sludge (50% and 75% volume ratios) or seaweed powder (*Sargassum* spp. 25%, 50% and 75% volume ratios) were compared in this study. Feed mixes with different ratios of ingredients and sand (0.6-1 mm) were given in excess (50% wet weight/wet weight animal/week) to adult *P. tremulus*. Daily feed intake was estimated by measuring daily faeces production rate. Each animal was given all feeds sequentially, and faeces collected for a ten-day period. Absorption efficiencies were estimated based on analysis of organic matter content in feed and faeces. Large variations were found in feed intake, both between individuals and between days. Our results indicated that *P. tremulus* showed a higher intake of feeds containing seaweed, with a trend of higher intake with increasing seaweed content. Absorption efficiency estimates of seaweed-based feeds ranged from -337 to 73.7%. *P. tremulus* showed a preferential selection of organic particles in the feed with lowest content of seaweed. Absorption efficiency of feeds containing sludge (2.5 – 58.3%) was comparable to that of feeds containing seaweed, however, feed intake of sludge-based feeds was significantly lower than that of the seaweed-based feeds and resulted in large variation in estimates. The results suggest that salmon freshwater sludge could have a potential future use as an ingredient in sustainable feeds for *P. tremulus*, but that optimisation of feed formulations need to be studied further.

KEYWORDS

aquaculture, feed intake, IMTA, *parastichopus tremulus*, *sargassum*, sea cucumber, sludge, absorption efficiency

1 Introduction

Knowledge gaps regarding species specific biology of cold-water sea cucumbers are current obstacles to the development of an aquaculture industry of emerging species from the North Atlantic. Especially feeding in captivity that support growth and development during the entire life cycle is a field that needs substantial attention for achieving successful and healthy production. The red sea cucumber, *Parastichopus tremulus*, is a species which has drawn increased attention from fishers, farmers, manufacturers, product developers, and trade actors during the last decade (Kjerstad et al., 2015; Landes et al., 2019; Schagerström et al., 2022). Being a cold-water species, *P. tremulus* could physiologically be suited for cultivation all along the Norwegian coast as it inhabits the entire geographical range from south to north. The wider distribution of this species in the Eastern Atlantic is from the Barents Sea in the north to the Canary Islands in the south, and west to Iceland and off the western coast of Ireland (Madsen and Hansen, 1994; Christophersen et al., 2021). There is currently no regulated fishery of *P. tremulus*, meaning the sea cucumbers are only available as bycatch from European trawl (shrimp and fish) and pot (Norway lobster) fisheries. Aquaculture has therefore been proposed as an alternative way to produce the species, but at present performance of *P. tremulus* in aquaculture is unknown.

Feeding behaviour of sea cucumbers (holothuroids) differ according to habitat and nutrient availability. Suspension-feeding species, such as e.g. *Cucumaria frondosa* ingest mainly phytoplankton and particles from the surrounding water, whereas deposit-feeding species, to which *P. tremulus* belongs, extract nutrients from the sediment and live on a diet that includes microorganisms, organic detritus, silica fragments and faeces (Yingst, 1976; Hauksson, 1979; Moriarty, 1982; Hudson et al., 2004). Sea cucumbers inhabit all oceans and live in a wide range of depths and on a variety of substrates including gravel, corals, and rocks, but mainly on softer bottoms (Purcell et al., 2012), which is also the case for *P. tremulus* (Christophersen et al., 2021). Most commercial species are deposit feeders having peltate tentacles that extends to acquire mainly particulate matter (Roberts et al., 2000; Purcell et al., 2012). The mouth is directed ventrally, and nutrients are extracted from organic matter within the upper benthic sediment layer, thus contributing to oxygenating and nutrient upcycling through the food chain. Holothurians are also shown to play important ecological roles in coral reef nutrient cycles (Uthicke and Klumpp, 1998). Several species of deposit-feeding sea cucumbers show active selection of organic matter from sediment, such as *Apostichopus californicus* (Paltzat et al., 2008) and *Australostichopus mollis* (Slater and Carton, 2009; Slater and Carton, 2010). In the studies of Hauksson (1977); Hauksson (1979) it was also found that *P. tremulus* has the ability to be selective in its feeding, and select faecal pellets and other sediment particles, which are richer in organic material than the general surface sediment. In nature the feeding pattern may be seasonal and related to availability of food items (David and MacDonald, 2002; Dar and Ahmad, 2006; Xu et al., 2015).

Growth relates to availability of nutritional food, and the dietary needs of sea cucumbers differ between species and the different life stages (Yang et al., 2015). Adult specimens of deposit-feeding sea cucumbers are benthic, but similar to other echinoderms they develop through several pelagic larval stages before metamorphosis and settlement. Depending on the species, the larvae exhibit different nutritional strategies (McEdward and Miner, 2001): either planktotrophic (external feeding) or lecithotrophic (relying on internal energy stores). During the post-larval and settlement phase, dietary requirements change to be more similar to that of the adults (Cameron and Fankboner, 1984). Successful gonad maturation most likely is influenced by both nutritional and environmental conditions (Whitefield et al., 2018) and thus broodstock feed for aquaculture may require optimised diets designed for this purpose. It has been shown that when given a choice of diets, *Apostichopus japonicus* show selective behaviour and that preference may change over time (Xia et al., 2012). Jespersen and Lützen (1971) suggested that *P. tremulus* in Norwegian waters cease to feed from late autumn and during winter, which is the period of low primary production. Understanding the feeding habit of sea cucumbers is thus of great importance when developing relevant aquaculture technology and artificial feeds.

Feeding studies on sea cucumbers in culture indicate that well-balanced diets need to be rich in lipids, essential fatty acids and carotenoids, especially if vitellogenesis and reproduction are to be promoted (Giraspy and Ivy, 2008; Gianasi et al., 2017; Whitefield et al., 2018). Many of these compounds are common ingredients in aquaculture feeds developed for other species, and it has therefore been postulated that particulate waste from fed fish aquaculture could be repurposed as feed or feed ingredients for deposit-feeding species such as sea cucumbers and polychaetes and thus improve the overall sustainability of current aquaculture practice. As an example, the land-based salmon smolt production industry in Norway alone generated more than 10 000 tonnes of sludge (dry matter) in 2017 (Aas and Åsgård, 2017). This nutrient-rich side stream consists of uneaten feed and faeces, of which only a minor fraction is collected and used for low-value applications. There is an increased interest in valorising this side stream for e.g. sustainable energy or feed production. Since deposit feeding species such as *P. tremulus* are able to ingest and utilize nutrients in particulate organic matter, they have been suggested as candidate species for inclusion in integrated multi-trophic aquaculture (IMTA) systems. At present no information exists on the feed preference and nutritional metabolism of *P. tremulus* in culture, and only a few studies have investigated the efficiency of *P. tremulus* in extracting and utilizing organic matter from marine sediments (Hauksson, 1977; Hauksson, 1979).

Macroalgae are among the most common feed ingredients used in Chinese sea cucumber aquaculture (Song et al., 2017), and brown algae are generally regarded as high-quality food sources for temperate sea cucumber species (Liu et al., 2010; Song et al., 2017). Green and red algae most probably are not ingested by sea cucumbers as shown in e.g. *Holothuria forskali* (David et al., 2020). In farming of the sea cucumber *A. japonicus* the commercially available seaweed *Sargassum* spp. is commonly used as an ingredient in feed. There are, few, if any, data published on the suitability of *Sargassum* spp. in feeds for cold-water species, and this study is to our knowledge the first to provide data on the use of *Sargassum* spp. as feed for *P. tremulus*.

The goal of this study was to obtain new information about *P. tremulus* feeding to further the aquaculture development of this species. With this in mind, we wanted to evaluate the feasibility of using either *Sargassum* spp. or dried sludge originating from Atlantic salmon (*Salmo salar* L.) aquaculture as feed ingredients for *P. tremulus*. By composing a series of feeds that ranged in organic content from values close to that of natural sediment to that of high-energy feeds used in aquaculture of other sea cucumber species, we aimed at assessing whether there was an upper limit to the content of organic matter that could be utilized by the sea cucumber. Feed intake and absorption efficiency were measured using faeces production as an indirect indicator of feed consumption. Based on the responses, the two feed sources were compared to evaluate attractivity and suitability of sludge and *Sargassum* as ingredients for *P. tremulus* feed purposes.

2 Materials and methods

2.1 Sea cucumbers and holding conditions

Sea cucumbers were selected from a larger batch of adult *P. tremulus* caught in shrimp trawls during autumn-winter 2019-2020 in the Vigra fjord outside of Ålesund in western Norway (62°N-6°E) and kept in flow-through holding tanks supplied with untreated seawater from 40 m depth until experimental start in May 2020. Length and total wet weight (WW) of the sea cucumbers ranged from 118 to 220 mm and from 39 to 288 g, respectively. Two feeding experiments (Experiment 1 and Experiment 2) were performed, with the first starting in May and the second in October. During the experimental periods, the sea cucumbers were held individually in flow-through 25 L glass aquaria (40 x 25 x 25 cm) supplied with filtrated (1 µm) and UV-treated seawater at a rate of 23.0 ± 0.3 L h^{-1}. Water temperature ranged between ~ 9-13°C and was logged every 15 min in all aquaria using HOBO TidBit v2 UTBI-001 loggers (Onset Computer Corporation, Bourne, MA, USA).

Length and weight were measured at the start and at the end of each feeding experiment. Before each measurement, sea cucumbers were starved for at least 72 hours to ensure emptying of the gut. Body length (mouth to anus) was measured to the nearest 1 mm using a measuring board and total WW to the nearest 0.1 g using an electronic scale (SKX2202, Ohaus GmbH, Nänikon, Switzerland).

2.2 Feed ingredients and composition

Commercially available powdered *Sargassum thunbergii* (Fuzhou Wonderful Biological Technology Co., Ltd., Fujian, China) was acquired and subsequently stored under dry conditions at ambient temperature until feed preparation. Aquaculture sludge was obtained from a freshwater land-based RAS facility (MOWI Steinsvik, Volda, Norway) producing Atlantic salmon (*Salmo salar* L.) smolts. The sludge had been dewatered using a drum filter and dried using an oil-heated drum dryer (Scanship AS, Tønsberg, Norge) to a final dry matter content of 85-90% and was stored at ambient temperature until receipt. Sludge particle size was standardized to <1 mm by sifting through a 1-mm stainless steel sieve (wired mesh) and was subsequently stored at -20°C until feed preparation. The organic feed ingredients, *Sargassum* powder and sludge, were analysed for macronutrient composition and energy content calculated (Table 1). Protein was determined as nitrogen (N) in ground freeze-dried samples using a CHNS–O elemental combustion system (Costech Instruments ECS 4010) at a temperature of approximately 1000°C, where the sample N is converted to N gas/oxides. Results were expressed in g N per 100 g of dried sample and a N-to-protein conversion factor of 6.25 was used. Fatty acids (lipid) were analysed according to ISO 12966-2 and ISO 5509, and carbohydrate content was calculated as the difference between total weight subtracted water, protein, lipid, and ash. For each feed formulation, macronutrient content in Table 2 was calculated from the known composition of each separate feed ingredient (Table 1).

To prepare the experimental feeds, each organic substrate was mixed with sand of grain size 0.6-1 mm. To achieve this range in grain size, commercially dried sand with a grain size 0-2 mm (Adda Byggkjemi AS, Drammen, Norway) was sifted through stainless steel sieves with 1 mm and 0.6 mm wired mesh size and the fraction retained on the 0.6 mm mesh was used. Each feed ingredient was mixed with sand and added filtered fresh water until they had a low moisture mash consistency suitable for deployment in water. Water content thus varied between the experimental feeds depending on the proportion of ingredients used. Due to the physical properties of the sludge and its high water solubility observed when submerged in seawater, feeds that contained sludge were added guar gum as a binder at 1% of feed dry weight (DW) to maintain their integrity (based on Won et al., 2018).

TABLE 1 Macronutrient composition, dry matter, ash and energy content of the experimental feed ingredients (n=3, sd=standard deviation).

Component	*Sargassum* powder		Sludge	
	mean	sd	mean	sd
Dry matter (% WW)	92.0	0.1	87.6	0.1
Ash (% DW)	42.0	0.2	22.2	0.2
Energy (kJ/100 g)	530.7	18.8	902.3	43.9
Protein content (% DW)	10.1	0.1	27.6	0.3
Lipid content (% DW)	0.3	0.1	2.9	1.3
Carbohydrate content (% DW)	39.6	0.1	34.9	1.5

2.3 Experimental setup

Each feeding experiment was carried out using a 3x3 setup, where three individuals were given the same feed in triplicate, hence a total of 9 individually held sea cucumbers were used. During each of two experimental periods (May and October 2020) the sea cucumbers were given three experimental feeds in a rotating experimental design that presented all individuals with all feeds (Table 3). In Experiment 1, sea cucumbers were fed experimental feeds with three different ratios (volume:volume) of seaweed powder and sand: 25:75 (low), 50:50 (medium) and 75:25 (high). The lower range of *Sargassum* content in the experimental feeds was selected based on organic content reported in sediment samples from natural habitats of *P. tremulus* in Norway (Hauksson, 1979; Sargent et al., 1983), and the upper range was based on Liu et al. (2010), who used a mixture of 80% *Sargassum thunbergii* powder and 20% yellow soil in culture of *A. japonicus*.

In Experiment 2, the *Sargassum*:sand feed (50:50) was repeated as a reference feed and compared to two additional feeds that were formulated from dried aquaculture sludge in medium (50:50) and high (75:25) volume ratios. The composition of the individual feed ingredients is given in Table 1, and for the experimental feeds in Table 2. To make sure feed intake was not limited by the amount of feed available, a high feeding rate (50% WW of feed per WW body weight per rotational period) was chosen. Feed was deposited in one portion at the centre of the floor of each aquarium at the start of each feeding period.

Each animal was presented with each feed for 7 days, after which the remaining feed was removed from the tank, and the

TABLE 2 Ash, dry matter (DM), macronutrient composition and energy content of the experimental feeds (n=3, sd=standard deviation) used in Experiment 1 and Experiment 2.

Component	Sargassum low		Sargassum medium		Sargassum high		Sludge medium		Sludge high	
	mean	sd	mean	sd	mean	sd	mean	sd	mean	sd
Ash (%)	94.6	0.2	86.6	0.5	73.0	0.7	75.4	0.3	55.9	0.5
DM (%)	99.2	0.1	98.0	0.1	96.0	0.1	95.7	0.1	92.5	0.1
Protein (% of DM)	1.0	0.1	2.5	0.1	4.8	0.1	9.1	0.1	16.2	0.2
Lipid (% of DM)	0.03	0.0	0.07	0.0	0.14	0.01	0.95	0.30	1.70	0.8
Carbohydrates (% of DM)	3.9	0.1	9.7	0.1	19.0	0.1	11.5	0.5	19.7	0.9
Energy (kJ/kg DM)	52.6	1.9	130.0	4.6	254.7	9	297.1	14.5	510.3	24.9

TABLE 3 Rotational feeding regime used in the experiments.

Rotation period	Individual 1-3	Individual 4-6	Individual 7-9
1	Feed 1	Feed 2	Feed 3
2	Feed 3	Feed 1	Feed 2
3	Feed 2	Feed 3	Feed 1

animals starved for 72 h before the entire sequence was repeated with a new feed. Faeces was collected daily from each tank using a pipette throughout the entire 10-day period. Only particles that could visually be identified as faecal pellets were collected. Samples of faeces and feed were immediately frozen and stored at -20°C until processing. Particulate matter of faeces and feed was retained by filtering the samples through pre-weighed Whatman GF/C RTU glass microfiber filter of 1.2 µm particle retention size (47 mm, GE Healthcare Life Sciences, Buckinghamshire, UK). Any remaining salt was removed by rinsing the filter with 50 mL distilled water. All samples of feed and faeces were analysed for organic matter in terms of ash-free dry weight (AFDW), which was determined as the difference between DW after drying at 60°C for 48 h, and ash weight after combustion at 490°C for 6 hours.

2.4 Calculations and statistical analyses

To standardize measurements, daily faeces production rates were corrected for WW of each animal at the start of the experiment and converted to DW feed per WW initial body weight (mg g^{-1} day^{-1}), according to Zamora and Jeffs (2011). Faeces production was used as an indirect indicator of feed consumption, and daily feed intake was estimated from faeces production rate by relating the ash weight in the faeces collected to the ash content in each respective feed, assuming that mineral absorption from ash was minimal and negligible during the time it passed through the intestine.

The performance of each feed was evaluated by calculating the absorption efficiency (AE), as the difference in organic content (AFDW) of the feed and the collected faeces (Conover, 1966):

AE (%) = $[(AFDW_{feed} - AFDW_{faeces}/(1 - AFDW_{faeces}) \times AFDW_{feed}] \times 100$, where $AFDW_{feed}$ and $AFDW_{faeces}$ is the ash-free dry weight of feed and faeces, respectively.

Both feed intake and AE calculations assumed that the inorganic (ash) fraction was indigestible and unaffected by passage through the digestive tract of *P. tremulus*.

Weight gain (% per 34 days) and specific growth rate (SGR) were calculated for pooled WW data of the 9 individuals over the period of each experiment to investigate the capacity to grow in captivity:

Weight gain (%) = (final weight–initial weight)/initial weight) x 100

SGR (% d^{-1}) = $100 \times (\ln (WW_{final}) - \ln (WW_{initial}))$/# days of experimental period x 100

For statistical analysis, the R package version 4.1.3 (R Core Team, 2022) was used. Data were tested for normality using the Shapiro-Wilks test and for heterogeneity of variance using the Levene's test. For data that were normally distributed, one- or two-way analysis of variance (ANOVA) was used, followed by a *post hoc* Tukey HSD test. For non-normal data that showed homogenous variance, a non-parametric Kruskal-Wallis test was used.

3 Results

The average seawater temperature in the aquaria (n=9) was 9.5 ± 0.2°C for Experiment 1 in May-June and 12.5 ± 0.5°C for Experiment 2 in October. The maximum daily difference in temperature between aquaria never exceeded 0.5°C. There was a slight temperature increase registered (0.5°C) during both experimental periods, but halfway in Experiment 2 a temperature peak (13.5°C) was registered. The sea cucumbers showed a net positive weight gain (5.9% and 6.8%) from start to end of both the experimental periods after being fed the three different diets. WW increased from 127 g to 134 g, and from 98 g to 104 g in Experiment 1 and 2, respectively, corresponding to daily specific growth rates (SGR) of 0.17 and 0.19% d^{-1}.

3.1 Feed intake

The feeding ratio used (50% WW) was found to be sufficient for the animals to feed to satiation in both experiments, as none of the animals were found to have consumed their given feed ration at the end of each rotational period. Faecal production was intermittent, as not all animals produced faeces every day, and was in general found to be highly variable, both between individuals and between days. The average feed intake for each rotational period (10 days) was used to compare attractivity of each of the feeds. There was a significant linear relationship between feed intake and initial WW of the animal for both the *Sargassum* medium ($p<0.0001$) and *Sargassum* high feeds ($p=0.0035$) in Experiment 1, whereas in Experiment 2, no such relationship was found.

In Experiment 1, feed intake was found to be significantly affected by feed type ($p < 0.005$) and there was a trend of higher feed intake with increasing proportion of *Sargassum* powder inclusion in the feed. The feed with the lowest content of *Sargassum*, was associated with a significantly lower feed intake ($p < 0.001$), whereas no significant difference was found in feed intake between animals given feeds with either medium or high content of *Sargassum* (Figure 1).

Overall, the average daily feed intake was lower in Experiment 2 than in Experiment 1. In Experiment 2 (Figure 2), the sea cucumbers showed a higher daily feed intake when the *Sargassum* reference feed was given ($p < 0.00001$), whereas feed intake was similar ($p > 0.05$) and close to zero for both sludge feeds. When comparing feed intake of the reference feed in both experiments, intake was significantly higher in Experiment 2 than in Experiment 1 ($p < 0.002$).

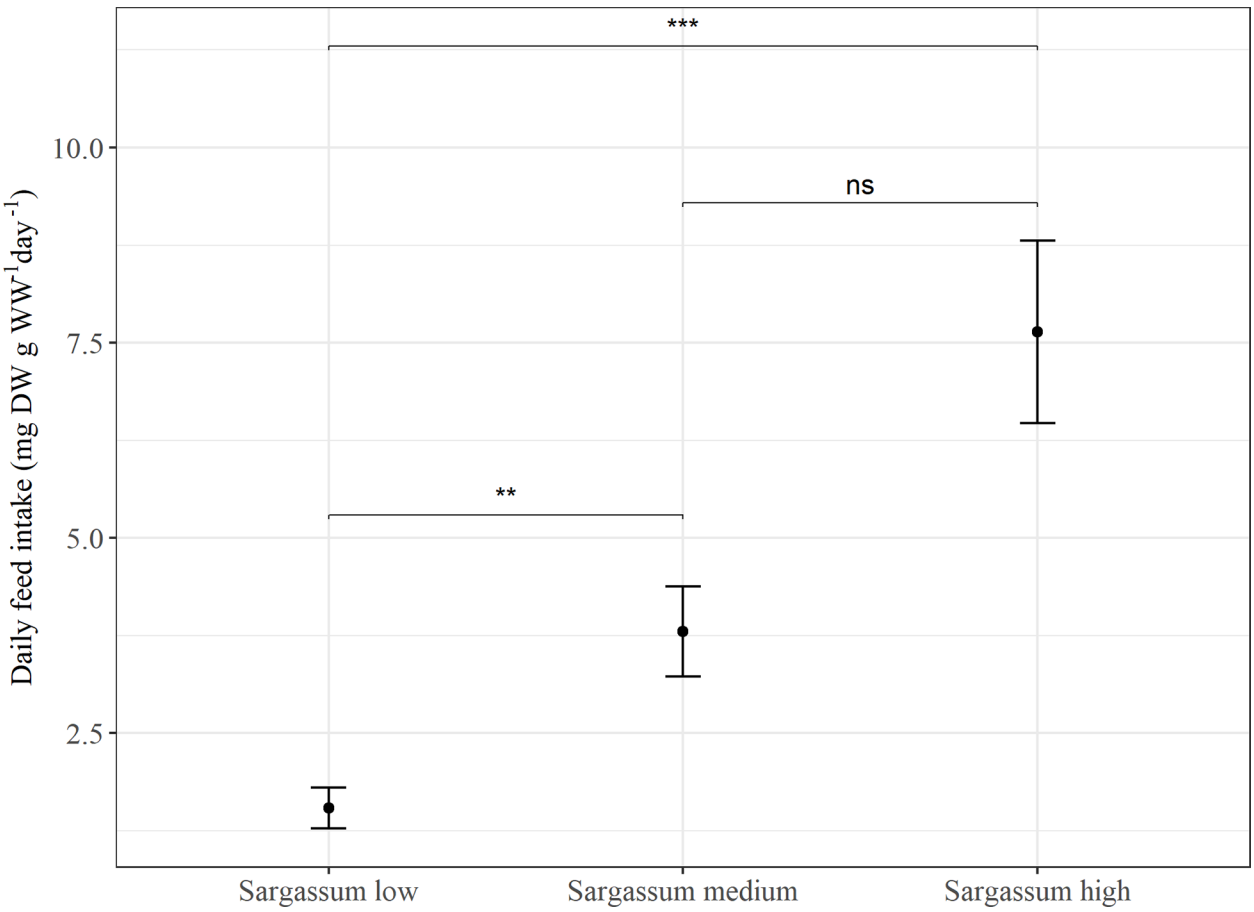

FIGURE 1
Average daily feed intake (mg DW g WW^{-1} day^{-1}) in Experiment 1. P. *tremulus* (n=9) given feeds with three different levels of *Sargassum* powder (low: 25%, medium: 50% and high: 75% v:v) over a 10-day period. Error bars show standard error and significant differences between feeds are indicated with asterisks (ns, not significant; **: p≤0.01; ***: p≤0.001).

3.2 Absorption efficiency

The organic content of each experimental feed and that of the respective collected faeces is given in Table 4. In Experiment 1, there was a strong inverse relationship between organic content in the feed given and that of the resulting faeces (r=0.90), whereas this was not the case in Experiment 2. The variation in faeces organic matter was high, both between individuals and between days.

Absorption efficiency (AE) estimates from feeding the *Sargassum* based feeds in Experiment 1 (Figure 3) found significant differences between all three feed types ($p < 0.0001$), and there was a trend of increasing AE with increasing *Sargassum* content. However, whereas estimates were consistently low or negative for the feed with the lowest *Sargassum* content (-337 ± 194%), they were on average positive for the feeds containing 50% and 75% of *Sargassum* powder (medium: 18.2 ± 52.7% and high: 73.7 ± 27.1%). The negative absorption efficiency for the *Sargassum* low feed is the result of a higher content of organic matter in faeces than in the feed given. On average, the faeces collected showed a more than 4 times higher organic content than the feed (23.6 ± 10.4% vs 5.4 ± 0.2%, see Table 4). For all other feeds, organic content in faeces was lower than that of the feed (Table 4).

In Experiment 2 (Figure 4), the feed with 50% aquaculture sludge on average showed a significantly lower AE than both the reference feed ($p < 0.05$) and the feed with 75% sludge ($p < 0.00001$). However, this estimate showed a large standard deviation (2.5 ± 64.7%), with several measurements of negative AE values. There was no significant difference in AE between the reference *Sargassum* feed (39.0 ± 48.2%) and the feed containing 75% sludge (58.3 ± 28.3%).

4 Discussion

4.1 Feed intake

All individuals consumed all the diets offered in Experiment 1. On the other hand, not all individuals consumed all the diets

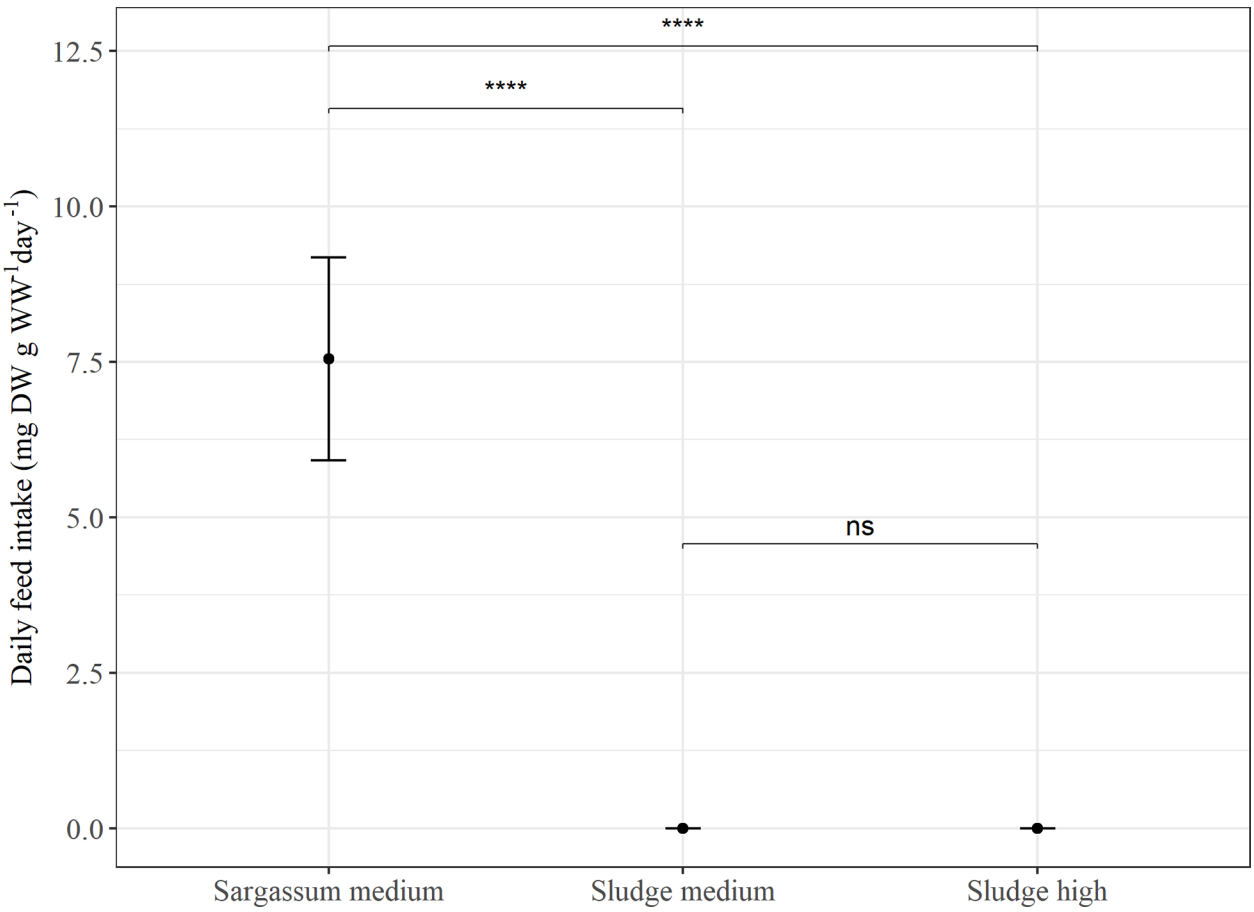

FIGURE 2
Average daily feed intake (mg DW g WW^{-1} day^{-1}) in Experiment 2. P. *tremulus* (n=9) given feeds with either *Sargassum* powder (Sargassum medium: 50% v:v) or aquaculture sludge (Sludge medium: 50% and Sludge high: 75% v:v) over a 10-day period. Error bars show standard error and significant differences between feeds are indicated with asterisks (ns, not significant; ****: p≤0.0001).

offered in Experiment 2. This was particularly apparent for the sludge-based feeds, indicating a degree of aversion in most individuals towards these feed formulations. The assumption of increased feed intake with increasing body size was only partly supported by our results as significant relationships between feed intake and sea cucumber WW was found for the *Sargassum* medium and high feeds in Experiment 1 only. The wide size range of experimental sea cucumbers used (39-288 g) and the intermittent faeces production, may have influenced the results. Previous studies found increased food consumption rates in *A.*

TABLE 4 Content of organic matter (% ash-free dry weight, AFDW) in experimental feeds and faeces from *Parastichopus tremulus* (sd, standard deviation).

Experiment	Feed	Feed (% AFDW)		Faeces (% AFDW)	
		mean	sd	mean	sd
1	Sargassum low	5.4	0.2	23.6	10.4
	Sargassum medium	13.4	0.5	11.0	7.1
	Sargassum high	27.0	0.7	7.1	7.3
2	Sargassum medium	13.4	0.5	8.2	6.5
	Sludge medium	24.6	0.3	24.8	16.1
	Sludge high	44.1	0.5	18.4	12.5

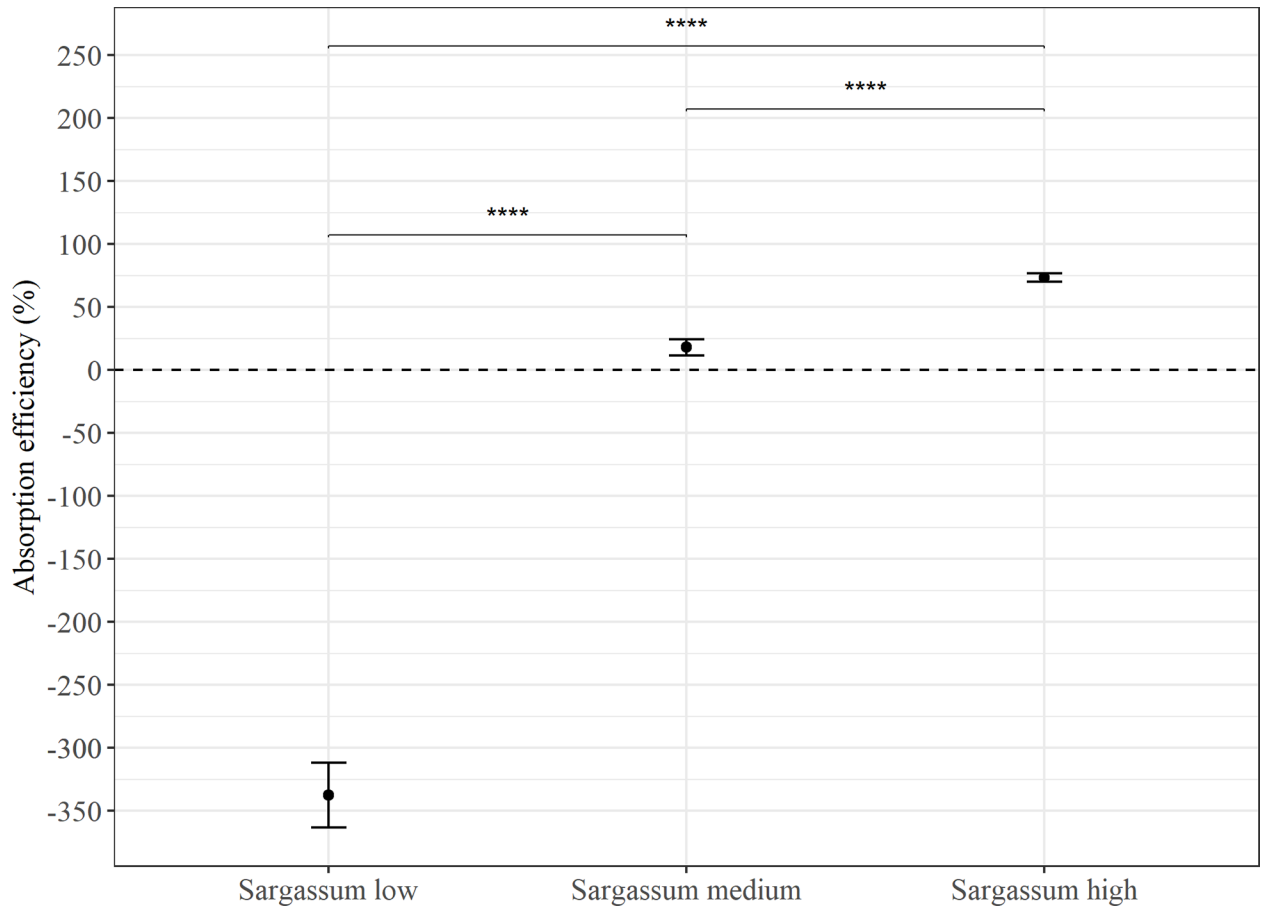

FIGURE 3
Average absorption efficiency (%) in *P. tremulus* (n=9) given feeds with three different levels of *Sargassum* powder (low: 25%, medium: 50% and high: 75% v:v) over a 10-day period in Experiment 1. Error bars show standard error (se) and significant differences between feeds are indicated with asterisks (****: p≤0.0001).

japonicus with increasing body weights of 43, 84 and 147 g as well as with increasing temperatures of 10, 15 and 20°C (Yang et al., 2005). Sun et al. (2015) found significantly lower faeces production rate in small *A. japonicus* (18 g) than in sea cucumbers of 40 g and 89 g, explained by less developed tentacles in the smallest size group. Yang et al. (2005) also observed day-to-day variation in consumption by the different sea cucumbers and that some individuals ceased feeding during the experimental period. This is in line with our findings, where certain individuals showed several days without faeces production. We found indications of increased feed intake with higher water temperature for some individuals when comparing intake of the *Sargassum* reference feed between May-June (Experiment 1, 9.5°C) and Oct-Nov (Experiment 2, 12.5°C), although this difference was not significant overall (p=0.62). Jespersen and Lützen (1971) observed a seasonal feeding pattern in nature, with a higher incidence of *P. tremulus* specimens lacking intestines from the end of October to January in the Oslo fjord in southern Norway, postulating that animals could cease feeding due to a naturally lower nutrient availability during winter months.

Whereas species such as *A. japonicus* show distinct nocturnal feeding behaviour, with higher ingestion and faeces production at night, observed by Sun et al. (2015) in different size groups of *A. japonicus* (18, 40 and 89 g), this seems not to be the case for *P. tremulus* (Jespersen and Lützen, 1971; Hauksson, 1977; Hauksson, 1979). During our experiments, the sea cucumbers were mainly kept under dark conditions and light was only switched on during faeces collection and feeding. Since no video monitoring was employed, we can neither confirm nor refute this hypothesis, but considering that *P. tremulus* inhabits deeper waters than *A. japonicus* (our specimens were collected at about 150 m depth), diurnal light cycles may not be important in influencing feeding behaviour in this species. Jespersen and Lützen (1971) indicated that *P. tremulus* in the Oslo fjord continually fed through night and day and that for animals dredged in deep water, no seasonal variation in feeding was indicated. Based on the irregular frequency of production of

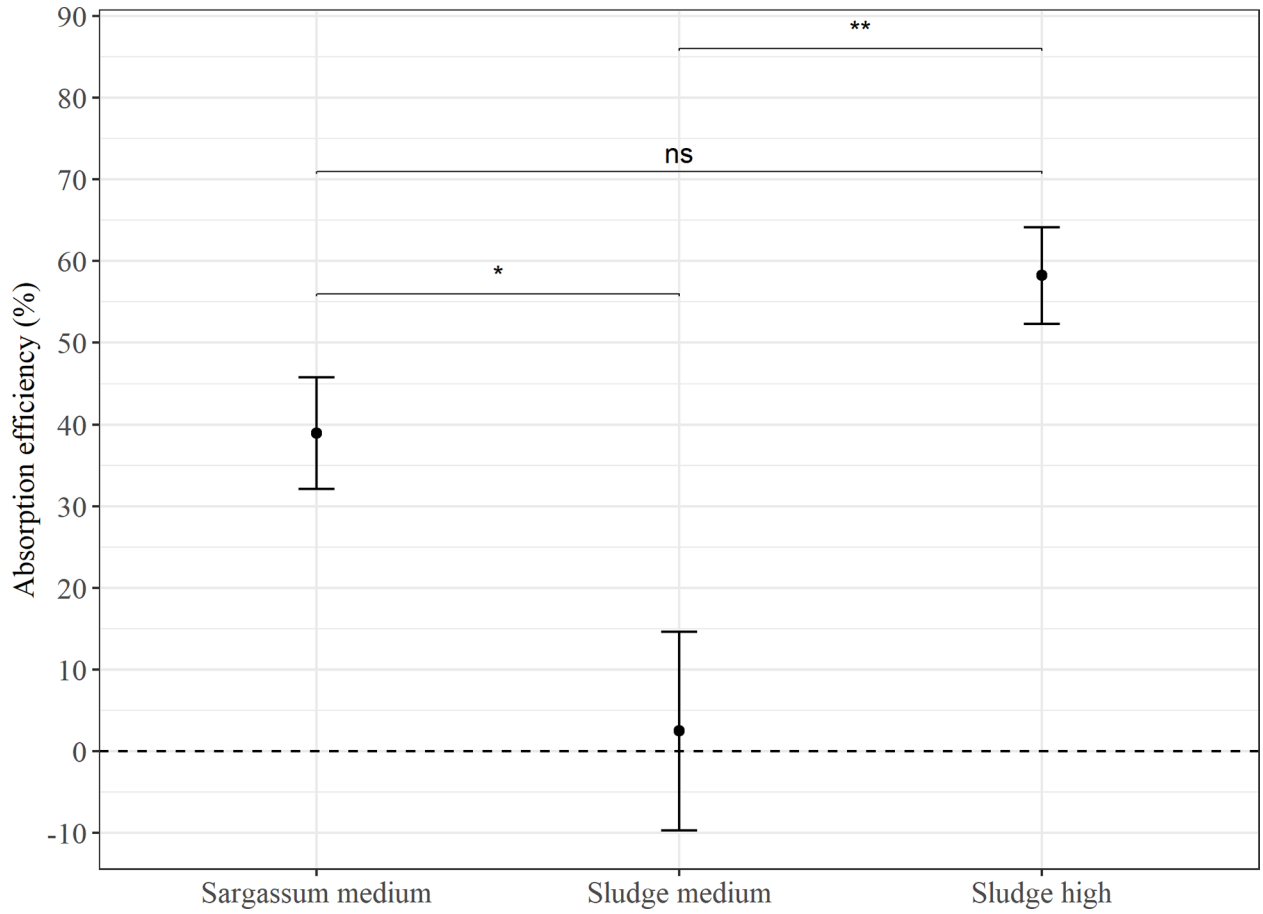

FIGURE 4
Average absorption efficiency (%) in *P. tremulus* (n=9) given feeds with either *Sargassum* powder (Sargassum medium: 50% v:v) or aquaculture sludge (Sludge medium: 50% and Sludge high: 75% v:v) over a 10-day period in Experiment 2. Error bars show standard error and significant differences between feeds are indicated with asterisks (ns, not significant; *: $p \leq 0.05$; **: $p \leq 0.01$).

faecal pellets, the sea cucumbers in our aquaria did not seem to show continuous feeding, but rather large individual and day-to-day variation. Discontinuous defaecation suggests an irregular feeding pattern. Hauksson (1979) estimated that 50% of the gut content is voided at each defaecation event and indicated that the time between each defaecation may vary depending on season or experimental conditions.

The amount of faeces production measured in our study was only partly related to the size of the individual. We also observed large differences in feed intake between the sea cucumbers given the same feed. This is difficult to explain without more detailed investigation of metabolic parameters, which was outside the scope of this study. Other factors related to holding conditions may have an effect on both growth and feed uptake, such as the use of bottom substrate in the tank and the ratio of mud to sand in the feed (Hou et al., 2017).

Feed intake and the absorption efficiency measured in our experiments may have been influenced by the particle size of the organic as well as the inorganic particles (sand). In analyses of intestinal content from *P. tremulus* feeding at 374-505 m depth, about 80% of the particles ingested were <200 µm in size, whereas very few particles were >1 mm (Hudson et al., 2004). We reasoned that the use of sand of grain size 0.6-1 mm as filler in our diets was adequate due to the relatively large size of our sea cucumbers (mean initial WW 127 g) and the upper limit of grain size of 1 mm for the sand and the sludge ingredients was justified by Hudson et al. (2004). As long as grain size was similar (< 0.15 mm), the origin of particles (sea mud vs yellow soil) did not seem to affect growth in *A. japonicus* (Liu et al., 2010).

P. tremulus are reported to be fully exposed on the substratum in nature and do not bury themselves into the sediment (Jespersen and Lützen, 1971). This has been confirmed in aquarium and cage studies (Hauksson, 1977), indicating that feeding in tanks and aquaria can be similar to feeding on the upper sediment layer in nature. Fine branched tentacles that extend from the oral crown are used for ingestion of food particles. From videos recorded by underwater Remote

Operated Vehicles (ROV), Hudson et al. (2004) observed that about half of the 20 tentacles were in contact with the seafloor and actively feeding at any one time. The assumption by Jespersen and Lützen (1971) that *P. tremulus* is non-selective in its feeding habits has been contradicted in later studies (Hauksson, 1979; Hudson et al., 2004). Our results seem to suggest that *P. tremulus* exhibits a selective feeding behaviour when organic matter content of the feed is low. Organic matter content in faeces was more than 400% higher than that of the feed when feeding on the feed with the lowest content of organic matter (*Sargassum* low, 5.4%). Zamora and Jeffs (2011) also found that selection efficiency in *A. mollis* (the accumulation of organic matter in the foregut) increased with decreasing organic matter content (TOM) in the feed and was higher for feeds with 1% and 4% TOM than that of feeds containing 12% and 20% TOM.

The fact that the sea cucumbers gained weight during the time of the experiments, combined with absorption efficiency estimates suggests that *P. tremulus* was able to assimilate at least part of the nutrients from the formulated feeds used in this study. The SGRs measured in this experiment were slightly lower than growth rates of smaller *P. tremulus* of about 15 g fed a diet identical to the *Sargassum* medium diet from May to July (0.2 vs. 0.2-0.3% d^{-1}), but higher than growth rates obtained for the same individuals later in the autumn (Christophersen and Sunde, 2022). These values are in line with SGR reported of juvenile *A. californicus* (0.267% d^{-1}) based on measurements for one year (Hannah et al., 2012). Domínguez-Godino and González-Wangüemert (2019) reported SGR 0.2% $d^{-1}$for adult *Holothuria arguinensis* based on eviscerated body weight. Gianasi et al. (2017) reported SGR based on length and immersed weight within the same range for *C. frondosa*, and SGR 0.4-1.1% d^{-1} are reported for juvenile *A. japonicus* based on dry body weight (Ru et al., 2019). Since we based the SGR on WW, the amount of coelomic fluid and intestines may have influenced the results. However, we have previously documented a high correlation (r = 0.84) between total and body wall WW in *P. tremulus* from western Norway (Christophersen et al., 2021).

The possible aversion for sludge-based feeds observed in Experiment 2, could have partly been due to the short duration of the experiment. Xia et al. (2012) found that *A. japonicus* in a feed selection experiment changed their feed preference for *Sargassum* spp. from rejection to somewhat preferred over a 30-day period, and it is possible feed intake could increase if the animals had been given these feeds over a longer period of time.

4.2 Diet composition and nutritional value

Well balanced diets are prerequisites for capture-based or land-based production of sea cucumbers to maintain physiological properties and enhance growth and nutritional quality of the animals. No information is currently available on what constitutes an optimum diet for *P. tremulus*. In its natural habitat, the deposit feeding *P. tremulus* encounters and ingests substrate of variable quality of which only a small fraction will be assimilated. In general, the digestive physiology of deposit-feeding sea cucumbers is adapted to ingestion of nutrient-poor sediment and only occasionally will they encounter nutrient-rich environments. It is therefore of interest to evaluate to what extent *P. tremulus* is capable of absorbing nutrient-rich feeds.

The experimental diets used in this study ranged from 5.4 – 44.1% in organic content (AFDW, Table 4). For comparison, published values from marine sediments in typical Norwegian fjord systems show a wide range, from 9.3% organic matter in Balsfjord in northern Norway (Sargent et al., 1983), to 0.91-1.36% in the Raune fjord in southwestern Norway (Hauksson, 1979). In areas of intensive aquaculture activity, higher sediment organic matter concentrations could be expected. For instance, Yu et al. (2014) reported 15% organic matter in sediments collected in traps below fish cages in China, 25% higher than that of a reference site, whereas Paltzat et al. (2008) reported 5.9% in sediment samples collected from a suspended culture Pacific oyster farm in Canada. Macronutrient composition of the experimental diets varied from 1 – 16.2% protein, from 3.9 – 19.7% carbohydrates and from 0.03 – 1.70% lipids (Table 3). The capacity and ability of *P. tremulus* to digest these various macronutrients is unknown, but based on studies of other deposit-feeding sea cucumbers fed formulated feeds, it can be elucidated that the majority of nutritional energy that is ingested most likely will be lost through faeces. For instance, Yuan et al. (2006) estimated energy loss through faeces in *A. japonicus* with positive SGR to be between 55.6–67.1% at temperatures of ~13 – 20°C, and that energy deposited in growth was low (5.5–7.9%) when fed diets prepared from dried bivalve faeces and powdered algae. Israel et al. (2019) found that 24.1% of feed energy was digested by the Mediterranean deposit-feeding holothuroid *Actinopyga bannworthi* when fed pellets prepared from particulate gilthead seabream (*Sparus aurata*) waste. In the same study, apparent digestibility coefficients of protein and lipid was 16.6% and 45.9%, respectively, whereas that of organic matter was 26.7%. Formulation of feeds and selecting an appropriate feeding regime is therefore crucial in order to maximise ingestion and absorption of nutrients (Xia et al., 2017). The use of the right kind of sea mud or sand as feed ingredients might be particularly important for improving nutrient absorption by both regulating the residence time of feed in the digestive tract of the sea cucumber and diluting feed nutrients, leading to better growth performance (Shi et al., 2015).

Nutrition research on commercially farmed *A. japonicus* has found that optimal protein content in artificial feeds for this species lies between 16-21% (Sun et al., 2004), with slightly higher optimum dietary protein requirements for juveniles at about 18-24% (Zhu et al., 2005). Similarly, lipid requirements of juvenile *A. japonicus* lie around 5% (Zhu et al., 2005). Seo and

Lee (2011) found that feeds with a protein content of either 20% and 40% and a lipid content of 2% gave the highest growth in juveniles from the same species. Our sludge formulated feeds had a similar protein (9.1-16.2%) and lipid (0.95-1.70%) content, but since feed intake was low during our experiment, AE could not be fully assessed in this study. The experimental feeds were not prepared as extruded pellets, but instead were given as a "wet feed". This allowed the animals to selectively feed on organic particles. We did not add inorganic digestibility markers such as chromic oxide Cr_2O_3 (Liu et al., 2009; Israel et al., 2019), but instead assumed that absorption of minerals from ash were negligible and that the ash content could be considered as a digestibility marker.

Assimilation efficiencies (AE) of the medium and high *Sargassum* feeds as well as the sludge high feed were close to the range of values reported from *A. californicus* feeding on substrate with high organic matter (Ahlgren, 1998; Paltzat et al., 2008). However, these studies utilized a different methodology, where AE was calculated from the difference in organic matter between foregut and hindgut content in dissected animals. Hauksson (1979), using a similar method, found an average AE of around 27% in *P. tremulus* feeding on natural sediment low in organic matter. Ahlgren (1998) estimated an organic matter AE of around 15% for the related cold-water species *A. californicus* feeding on marine sediment low in organic matter. but found a more than 3 times higher AE (50%) when animals fed on salmon net pen fouling debris with a much higher organic matter content. This demonstrated that the animals were able to more efficiently absorb nutrients from a higher energy substrate. Similarly, an absorption of 40.4% of organic matter was found in *A. californicus* feeding on sediments with a high organic content located under Pacific oyster (*Crassostrea gigas*) suspended culture (Paltzat et al., 2008).

Factors that may have influenced our AE estimates include dissolving of the organic fraction of both feed and faecal pellets in the surrounding water. For the feed, leakage of nutrients was attempted minimized by the addition of binder (guar gum, 1%), whereas collection of faeces at 24 h intervals minimized the time the faeces was exposed to water. A defecation rate of ~24 h was reported by Hudson et al. (2004) who studied the movement of trace particles through the intestine of *P. tremulus* held in sea cages, and Hauksson (1979) similarly reported about 20 h for *P. tremulus* fed a typical sediment from a Norwegian fjord. A higher defecation rate was reported by Jespersen and Lützen (1971) who noted that harvested sea cucumbers had emptied their intestines after about 8–10 h when held in aquaria. Higher values of AFDW in faeces than in the feed, as measured when animals were given the *Sargassum* low feed, suggests that nutrient leakage from faeces probably was low, at least for this feed type. However, the low AE measured for the 50% sludge feed could indicate that leakage from feeds prepared from sludge could be higher. Further studies ought to investigate this aspect in more detail if aquaculture sludge is to be used in feed formulation for sea cucumber.

In our study, we offered diets consisting of one organic component mixed with dry sand of grain size 0.6-1 mm in aquaria with no bottom sediment added. In order to ensure only the feed given was ingested, bottom sediment was not used, although some studies suggest this can promote growth. Different types of bottom substrate are recommended for cultivating the species *A. japonicus* (Liu et al., 2010; Hou et al., 2017), and a heterogenous substrate layer may increase the availability for organic matter and facilitate feed intake and enhance growth accordingly. The mean ingestion rate did not differ significantly, but the variability in food intake was lowered between *A. mollis* individuals given feed containing 20% organic matter compared to feed containing 1-12% (Zamora and Jeffs, 2011). We observed very random movements of the different individuals as they were exploring the aquaria side surfaces as well as moving to and from the feed portion during the feeding periods. In a study on the sea cucumber *A. californicus* it was shown that movement was more random on sediment with high level of organic matter than on sediment with a low level of organic matter, but that hard vertical surfaces were favoured independent of organic content in the substrate (van Dam-Bates et al., 2016). This indicates that a high content of organic matter alone is not sufficient to make the sea cucumbers feed continuously in captivity.

Feeds based on single macroalgal ingredients such as *Sargassum* spp. may not be optimal as sea cucumber feed, and are often lacking in specific nutrients, such as omega-3 fatty acids (Feng et al., 2016). For instance, nutrient absorption in *A. japonicus* was improved when macroalgal diets were supplied with benthic microalgae (Gao et al., 2011), and Yuan et al. (2006) found that growth of juvenile *A. japonicus* was improved when powdered fermented algae diets were supplemented with dried bivalve faeces. Fermentation of macroalgal residues with probiotic bacteria also improved growth rates, digestive enzyme activities and intestinal microbiota in *A. japonicus* (Wang et al., 2020). The addition of aquaculture sludge (with a higher lipid content and higher omega-3/omega-6 fatty acid ratios) to sea cucumber feed formulations could help make up for some of the nutritional deficiencies of macroalgae.

These first preliminary results indicate that attractivity and digestibility of *Sargassum* spp. is high in *P. tremulus*, but that long-term studies of growth rates and feed conversion will have to be conducted to evaluate the nutritional and growth-promoting properties of *Sargassum* as an ingredient in formulated feeds for *P. tremulus*. Dried aquaculture sludge from Norwegian freshwater salmon production has a macronutrient composition that could be beneficial for inclusion in sea cucumber formulated feeds, but work remains to increase palatability and optimise incorporation of these ingredients in sea cucumber feeds.

4.3 Aquaculture sustainability

Due to their unique ability to feed on particulate matter and their high value in the seafood market, sea cucumbers have been considered prime candidates for inclusion in integrated multi-trophic aquaculture (IMTA) systems, by adding value and utilizing particulate matter released from finfish aquaculture (Tolon et al., 2017; Zamora et al., 2018; Israel et al., 2019). The Norwegian aquaculture industry which is dominated by Atlantic salmon (*Salmo salar*), releases large amount of valuable nutrients in sludge each year. This represents an underutilized resource that if not used may result in environmental overload. National environmental regulations require that at least 50% of the particulate matter discharged from land-based farms is collected. Attempts have been made at utilizing sludge for biogas (energy) production, but currently most of the collected sludge is sold as a low-valued fertilizer product. Bioconversion of particulate organic matter (sludge) which are residuals from the large Atlantic salmon production in Norway into sea cucumber feed will contribute to the sustainability of both productions. At present, current legislation in the EU/EAA area prohibits the use of waste (faeces) as feed for other food producing organisms.

The potential of *P. tremulus* as an aquaculture species, however, depend on a range of factors such as control of reproduction, growth rate and feed conversion efficiency in culture (Landes et al., 2019). Studies on other sea cucumber species such as *Holothuria scabra* has shown that aquaculture waste products can be used as feed in integrated sea cucumber aquaculture systems (Robinson et al., 2019). To fully evaluate the prospects of *P. tremulus* as an IMTA candidate species for Norway, it would be necessary to evaluate further the performance and growth when fed different feed sources, and also investigate the possibility of further improvement of sludge by microbiological pre-processing to achieve increased digestibility and/or probiotic function (Bao et al., 2017; Wang et al., 2020).

Our study is the first step towards investigating if particular waste (sludge) from the local Atlantic salmon industry could be part of the diet for a potential sea cucumber aquaculture industry in Norway. Our results indicate that sludge could have a use in formulation of sea cucumber feeds, and that it could contribute towards establishing a sustainable value chain. However, the combination of ingredients needs to be optimised through further studies on feed formulation. In China there is also an urgent need to find substitutes for *Sargassum* spp. due to the expansion of semi-intensive sea cucumber farming (Liu et al., 2010; Song et al., 2017), suggesting that re-use of aquaculture waste could have a similar potential in other countries.

Data availability statement

The raw data supporting the conclusions of this article will be made available by the authors, without undue reservation.

Author contributions

GC and JS contributed equally to conception and design of the study, performance of experimental work, data processing and writing of the submitted manuscript. JS performed the statistical analysis. All authors contributed to the article and approved the submitted version.

Funding

The work has been funded by the Research Council of Norway – SANOCEAN (project no. 288536), and the Møre og Romsdal County Municipality - marint miljø og verdiskapingsfond (grant no. 2018-0150).

Acknowledgments

The authors wish to thank MOWI Steinsvik in Volda, Norway for supplying the dried aquaculture sludge used in this experiment.

Conflict of interest

The authors declare that the research was conducted in the absence of any commercial or financial relationships that could be construed as a potential conflict of interest.

Publisher's note

References

Aas, T. S., and Åsgård, T. (2017). Estimated content of nutrients and energy in feed spill and faeces in Norwegian salmon culture. *Nofima Rep.* (in Norwegian). Report no. 18/2017, 8 pages.

Ahlgren, M. O. (1998). Consumption and assimilation of salmon net pen fouling debris by the red sea cucumber *Parastichopus californicus*: implications for polyculture. *J. World Aquaculture Soc.* 29 (2), 133–139. doi: 10.1111/j.1749-7345.1998.tb00972.x

Bao, N., Ren, T., Han, Y., Wang, F., Chen, F., and Jiang, Z. (2017). Alteration of growth, intestinal lactobacillus, selected immune and digestive enzyme activities in juvenile sea cucumber *Apostichopus japonicus*, fed dietary multiple probiotics. *Aquaculture Int.* 25 (5), 1721–1731. doi: 10.1007/s10499-017-0148-8

Cameron, J. L., and Fankboner, P. V. (1984). Tentacle structure and feeding processes in life stages of the commercial sea cucumber *Parastichopus californicus* (Stimpson). *J. Exp. Mar. Biol. Ecol.* 81 (2), 193–209. doi: 10.1016/0022-0981(84)90006-6

Christophersen, G., Bakke, S., and Sunde, J. (2021). Norwegian Red sea cucumber (*Parastichopus tremulus*) fishery and aquaculture north of 60°N latitude: Feasible or fictional? *SPC Beche-de-mer Inf. Bull.* 41, 25–36.

Christophersen, G., and Sunde, J. (2022). The challenge of economically viable aquaculture of the cold-water sea cucumber *Parastichopus tremulus* in Norway. *SPC Beche-de-mer Inf. Bull.* 42, 65–72.

Conover, R. J. (1966). Assimilation of organic matter by zooplankton. *Limnology Oceanography* 11, 338–345. doi: 10.4319/lo.1966.11.3.0338

Dar, M. A., and Ahmad, H. O. (2006). The feeding selectivity and ecological role of shallow water holothurians in the red Sea. *Bêche-de-mer Inf. Bull.* 24, 11–21.

David, F., Hubas, C., Laguerre, H., Badou, A., Herault, G., Bordelet, T., et al. (2020). Food sources, digestive efficiency and resource allocation in the sea cucumber *Holothuria forskali* (Echinodermata: Holothuroidea): Insights from pigments and fatty acids. *Aquaculture Nutr.* 26 (5), 1568–1583. doi: 10.1111/anu.13103

David, V. M. M., and MacDonald, B. A. (2002). Seasonal biochemical composition of tissues from *Cucumaria frondosa* collected in the bay of fundy, Canada: feeding activity and reproduction. *J. Mar. Biol. Assoc. United Kingdom* 82 (1), 141–147. doi: 10.1017/S0025315402005258

Domínguez-Godino, J. A., and González-Wangüemert, M. (2019). Assessment of *Holothuria arguinensis* feeding rate, growth and absorption efficiency under aquaculture conditions. *New Z. J. Mar. Freshw. Res.* 53 (1), 60–76. doi: 10.1080/00288330.2018.1480499

Feng, J., Anisuzzaman, M., U-Cheol, J., Jong-Kuk, C., Hak-Sun, Y., Seung-Wan, K., et al. (2016). Comparison of fatty acid composition of wild and cultured sea cucumber *Apostichopus japonicus*. *Korean J. Fisheries Aquat. Sci.* 49, 474–485. doi: 10.5657/KFAS.2016.0474

Gao, Q.-F., Wang, Y., Dong, S., Sun, Z., and Wang, F. (2011). Absorption of different food sources by sea cucumber Apostichopus japonicus (Selenka) (Echinodermata: Holothuroidea): Evidence from carbon stable isotope. *Aquaculture* 319 (1-2), 272–276. doi: 10.1016/j.aquaculture.2011.06.051

Gianasi, B. L., Parrish, C. C., Hamel, J. F., and Mercier, A. (2017). Influence of diet on growth, reproduction and lipid and fatty acid composition in the sea cucumber *Cucumaria frondosa*. *Aquaculture Res.* 48 (7), 3413–3432. doi: 10.1111/are.13168

Giraspy, D. A. B., and Ivy, G. (2008). The influence of commercial diets on growth and survival in the commercially important sea cucumber *Holothuria scabra* var. versicolor (Conand 1986) (Echinodermata: Holothuroidea). *SPC beche-de-mer Inf. Bull.* 28, 46–52.

Hannah, L., Duprey, N., Blackburn, J., Hand, C. M., and Christopher, M. (2012). Growth rate of the California sea cucumber *Parastichopus californicus*: Measurement accuracy and relationships between size and weight metrics. *North Am. J. Fisheries Manage.* 32, 167–176. doi: 10.1080/02755947.2012.663455

Hauksson, E. (1977). *Ernæringsøkologiske undersøkelser av Stichopus tremulus (Gunnerus), en detritus-etende holothuroid* (Bergen, Norway: University of Bergen). M.Sc. thesis (in Norwegian).

Hauksson, E. (1979). Feeding biology of *Stichopus tremulus*, a deposit-feeding holothurian. *Sarsia* 64 (3), 155–160. doi: 10.1080/00364827.1979.10411376

Hou, Y. R., Sun, Y. J., Gao, Q. F., Dong, S. L., Wen, B., and Yu, H. B. (2017). Optimal mud to sand ratios in sediment for sea cucumber aquaculture as revealed by carbon stable isotopes. *Aquaculture Environ. Interact.* 9, 281–291. doi: 10.3354/aei00228

Hudson, I. R., Wigham, B. D., and Tyler, P. A. (2004). The feeding behaviour of a deep-sea holothurian, *Stichopus tremulus* (Gunnerus) based on *in situ* observations and experiments using a remotely operated vehicle. *J. Exp. Mar. Biol. Ecol.* 301 (1), 75–91. doi: 10.1016/j.jembe.2003.09.015

Israel, D., Lupatsch, I., and Angel, D. L. (2019). Testing the digestibility of seabream wastes in three candidates for integrated multi-trophic aquaculture: Grey mullet, sea urchin and sea cucumber. *Aquaculture* 510, 364–370. doi: 10.1016/j.aquaculture.2019.06.003

Jespersen, A., and Lützen, J. (1971). On the ecology of the aspidochirote sea cucumber *Stichopus tremulus* (Gunnerus). *Norwegian J. Zoology* 19, 117–132.

Kjerstad, M., Ringvold, H., Søvik, G., Knott, K., and Thangstad, T. (2015). "Preliminary study on the utilisation of Norwegian red sea cucumber, *Parastichopus tremulus* (Gunnerus 1767) (Holothuroidea, Echinodermata), from Norwegian waters: resource, biology and market. pp. 109–132," in *Blue bio-resources*. Eds. A. C. Gundersen and L. G. Velle (Norway: Orkana Akademisk).

Landes, A. M., Sunde, J., and Christophersen, G. (2019). "Atlantic Sea cucumber species in the spotlight – prospects for Norwegian aquaculture. pp 19-49," in *International perspectives on regional research and practice*. Eds. L. K. Akslen-Hoel and B. Egilsson (Norway: Orkana Akademisk).

Liu, Y., Dong, S., Tian, X., Wang, F., and Gao, Q. (2010). The effect of different macroalgae on the growth of sea cucumbers (*Apostichopus japonicus* selenka). *Aquaculture Res.* 41 (11), e881–e885. doi: 10.1111/j.1365-2109.2010.02582.x

Liu, Y., Dong, S., Tian, X., Wang, F., and Gao, Q. (2009). Effects of dietary sea mud and yellow soil on growth and energy budget of the sea cucumber Apostichopus japonicus (Selenka). *Aquaculture* 286 (3-4), 266–270. doi: 10.1016/j.aquaculture.2008.09.029

Madsen, F. J., and Hansen, B. (1994). "Echinodermata, Holothurioidea," in *Marine invertebrates of Scandinavia number 9* (Oslo: Scandinavian University press).

McEdward, L. R., and Miner, B. G. (2001). Larval and life-cycle patterns in echinoderms. *Can. J. Zoology* 79 (7), 1125–1170. doi: 10.1139/z00-218

Moriarty, D. J. W. (1982). Feeding of *Holothuria atra* and *Stichopus chloronotus on* bacteria, organic carbon and organic nitrogen in sediments of the great barrier reef. *Mar. Freshw. Res.* 33 (2), 255–263. doi: 10.1071/MF9820255

Paltzat, D. L., Pearce, C. M., Barnes, P. A., and McKinley, R. S. (2008). Growth and production of California sea cucumbers (*Parastichopus californicus* stimpson) co-cultured with suspended pacific oysters (*Crassostrea gigas* thunberg). *Aquaculture* 275 (1-4), 124–137. doi: 10.1016/j.aquaculture.2007.12.014

Purcell, S. W., Samyn, Y., and Conand, C. (2012). *Commercially important sea cucumbers of the world. FAO species catalogue for fishery purposes. no. 6* (Rome: FAO), 150 pp. 30 colour plates.

R Core Team (2022). *R: A language and environment for statistical computing* (Vienna, Austria: R Foundation for Statistical Computing). Available at: https://www.R-project.org/.

Roberts, D., Gebruk, A., Levin, V., and Manship, B. A. D. (2000). Feeding and digestive strategies in deposit-feeding holothurians. *Oceanography Mar. Biology: an Annu. Rev.* 38, 257–310.

Robinson, G., Caldwell, G. S., Jones, C. L. W., and Stead, S. M. (2019). The effect of resource quality on the growth of *Holothuria scabra* during aquaculture waste bioremediation. *Aquaculture* 499, 101–108. doi: 10.1016/j.aquaculture.2018.09.024

Ru, X., Zhang, L., Li, X., Liu, S., and Yang, H. (2019). Development strategies for the sea cucumber industry in China. *J. Oceanology Limnology* 37 (1), 300–312. doi: 10.1007/s00343-019-7344-5

Sargent, J. R., Hopkins, C. C. E., Seiring, J. V., and Youngson, A. (1983). Partial characterization of organic material in surface sediments from Balsfjorden, northern Norway, in relation to its origin and nutritional value for sediment-ingesting animals. *Mar. Biol.* 76 (1), 87–94. doi: 10.1007/BF00393059

Schagerström, E., Christophersen, G., Sunde, J., Bakke, S., Matusse, N. R., Dupont, S., et al. (2022). Controlled spawning and rearing of the sea cucumber, *Parastichopus tremulus*. *J. World Aquaculture Soc.* 53 (1), 224–240. doi: 10.1111/jwas.12816

Seo, J. Y., and Lee, S. M. (2011). Optimum dietary protein and lipid levels for growth of juvenile sea cucumber *Apostichopus japonicus*. *Aquaculture Nutr.* 17, e56–e61. doi: 10.1111/j.1365-2095.2009.00728.x

Shi, C., Dong, S., Wang, F., Gao, Q., and Tian, X. (2015). Effects of the sizes of mud or sand particles in feed on growth and energy budgets of young sea cucumber (*Apostichopus japonicus*). *Aquaculture* 440, 6–11. doi: 10.1016/j.aquaculture.2015.01.028

Slater, M. J., and Carton, A. G. (2009). Effect of sea cucumber (*Australostichopus mollis*) grazing on coastal sediments impacted by mussel farm deposition. *Mar. pollut. Bull.* 58, 1 123–1 129. doi: 10.1016/j.marpolbul.2009.04.008

Slater, M. J., and Carton, A. G. (2010). Sea cucumber habitat differentiation and site retention as determined by intraspecific stable isotope variation. *Aquaculture Res.* 41, e695–e702. doi: 10.1111/j.1365-2109.2010.02607.x

Song, X. Y., Xu, Q., Zhou, Y., Lin, C. G., and Yang, H. S. (2017). Growth, feed utilization and energy budgets of the sea cucumber *Apostichopus japonicus* with different diets containing the green tide macroalgae *Chaetomorpha linum* and the seagrass. *Zostera marina*. *Aquaculture* 470, 157–163. doi: 10.1016/j.aquaculture.2016.12.035

Sun, H., Liang, M., Yan, J., and Chen, B. (2004). "Nutrient requirements and growth of the sea cucumber, *Apostichopus japonicus*," in *Advances in sea cucumber aquaculture and management*, vol. 463 . Eds. A. Lovatelli, C. Conand, S. Purcell, S. Uthicke, J.-F. Hamel and A. Mercier (Rome, Italy: FAO Fisheries Technical Paper), 327–331.

Sun, J., Zhang, L., Pan, Y., Lin, C., Wang, F., Kan, R., et al. (2015). Feeding behavior and digestive physiology in sea cucumber *Apostichopus japonicus*. *Physiol. Behav.* 139, 336–343. doi: 10.1016/j.physbeh.2014.11.051

Tolon, T., Emiroglu, D., Gunay, D., and Ozgul, A. (2017). Sea cucumber (*Holothuria tubulosa* gmelin 1790) culture under marine fish net cages for potential use in integrated multi-trophic aquaculture (IMTA). *Indian J. Geo Mar. Sci.* 46 (4), 749–756.

Uthicke, S., and Klumpp, D. W. (1998). Microphytobenthos community production at a near-shore coral reef: seasonal variation and response to ammonium recycled by holothurians. *Mar. Ecol. Prog. Ser.* 169, 1–11. doi: 10.3354/meps169001

van Dam-Bates, P., Curtis, D. L., Cowen, L. L., Cross, S. F., and Pearce, C. M. (2016). Assessing movement of the California sea cucumber *Parastichopus californicus* in response to organically enriched areas typical of aquaculture sites. *Aquaculture Environ. Interact.* 8, 67–76. doi: 10.3354/aei00156

Wang, G., Meng, Z., Chen, L., Jiang, J., Feng, Y., and Zhang, B. (2020). Effects of kelp residues fermented with probiotics on the culture of sea cucumber, *Apostichopus japonicus*. *Aquaculture Res.* 51 (3), 1133–1142. doi: 10.1111/are.14460

Whitefield, C. R., Oliveira, A. C., and Hardy, S. M. (2018). Composition of phytodetrital food resources affects reproductive success in the deposit-feeding sea cucumber, *Parastichopus californicus* (Stimpson 1857). *J. Exp. Mar. Biol. Ecol.* 500, 1–11. doi: 10.1016/j.jembe.2017.12.004

Won, S., Hamidoghli, A., Lee, J., Bae, J., and Bai, S. C. (2018). Effects of three different dietary binders on juvenile sea cucumber, *Apostichopus japonicus*. *Turkish J. Fisheries Aquat. Sci.* 18 (7), 913–920. doi: 10.4194/1303-2712-v18_7_09

Xia, B., Ren, Y., Wang, J., Sun, Y., and Zhang, Z. (2017). Effects of feeding frequency and density on growth, energy budget and physiological performance of sea cucumber *Apostichopus japonicus* (Selenka). *Aquaculture* 466, 26–32. doi: 10.1016/j.aquaculture.2016.09.039

Xia, S., Zhao, P., Chen, K., Li, Y., Liu, S., Zhang, L., et al. (2012). Feeding preferences of the sea cucumber *Apostichopus japonicus* (Selenka) on various seaweed diets. *Aquaculture* 344, 205–209. doi: 10.1016/j.aquaculture.2012.03.022

Xu, Q., Hamel, J.-F., and Mercier, A. (2015). "Chapter 10. feeding, digestion, nutritional physiology, and bioenergetic," in *The Sea cucumber Apostichopus japonicus. history, biology and aquaculture*. Eds. H. Yang, J.-F. Hamel and A. Mercier (Oxford, UK: Academic Press), 153–176. doi: 10.1016/B978-0-12-799953-1.00010-6

Yang, H., Hamel, J.-F., and Mercier, A. (Eds.) (2015). *The Sea cucumber Apostichopus japonicus. history, biology and aquaculture* (Oxford, UK: Academic Press). doi: 10.1016/B978-0-12-799953-1.00002-7

Yang, H., Yuan, X., Zhou, Y., Mao, Y., Zhang, T., and Liu, Y. (2005). Effects of body size and water temperature on food consumption and growth in the sea cucumber *Apostichopus japonicus* (Selenka) with special reference to aestivation. *Aquaculture Res.* (Oxford: UK) 36 (11), 1085–1092. doi: 10.1111/j.1365-2109.2005.01325.x

Yingst, J. Y. (1976). The utilization of organic matter in shallow marine sediments by an epibenthic deposit-feeding holothurian. *J. Exp. Mar. Biol. Ecol.* 23 (1), 55–69. doi: 10.1016/0022-0981(76)90085-X

Yuan, X., Yang, H., Zhou, Y., Mao, Y., Zhang, T., and Liu, Y. (2006). The influence of diets containing dried bivalve feces and/or powdered algae on growth and energy distribution in sea cucumber *Apostichopus japonicus* (Selenka) (Echinodermata: Holothuroidea). *Aquaculture* 256 (1-4), 457–467. doi: 10.1016/j.aquaculture.2006.01.029

Yu, Z., Zhou, Y., Yang, H., and Hu, C. (2014). Survival, growth, food availability and assimilation efficiency of the sea cucumber *Apostichopus japonicus* bottom-cultured under a fish farm in southern China. *Aquaculture* 426, 238–248. doi: 10.1016/j.aquaculture.2014.02.013

Zamora, L. N., and Jeffs, A. G. (2011). Feeding, selection, digestion and absorption of the organic matter from mussel waste by juveniles of the deposit-feeding sea cucumber, *Australostichopus mollis*. *Aquaculture* 317 (1-4), 223–228. doi: 10.1016/j.aquaculture.2011.04.011

Zamora, L. N., Yuan, X., Carton, A. G., and Slater, M. J. (2018). Role of deposit-feeding sea cucumbers in integrated multitrophic aquaculture: progress, problems, potential and future challenges. *Rev. Aquaculture* 10 (1), 57–74. doi: 10.1111/raq.12147

Zhu, W., Mai, K. S., Zhang, B. G., Wang, F. Z., and Xu, G. Y. (2005). Study on dietary protein and lipid requirement for sea cucumber. *Stichopus japonicus*. *Mar. Sci.* 29, 54–58.

frontiers | Frontiers in Marine Science

TYPE Original Research
PUBLISHED 26 January 2023
DOI 10.3389/fmars.2022.1010014

OPEN ACCESS

EDITED BY
Annie Mercier,
Memorial University of Newfoundland, Canada

REVIEWED BY
Kennedy Wolfe,
The University of Queensland, Australia
Leo Zamora,
Cawthron Institute, New Zealand

*CORRESPONDENCE
Viviana Pasquini
viviana.pasquini@unica.it

†These authors have contributed equally to this work

SPECIALTY SECTION
This article was submitted to Marine Biology, a section of the journal Frontiers in Marine Science

RECEIVED 02 August 2022
ACCEPTED 29 December 2022
PUBLISHED 26 January 2023

CITATION
Pasquini V, Addis P, Giglioli AA, Moccia D and Pusceddu A (2023) Outcomes of feeding activity of the sea cucumber *Holothuria tubulosa* on quantity, biochemical composition, and nutritional quality of sedimentary organic matter. *Front. Mar. Sci.* 9:1010014. doi: 10.3389/fmars.2022.1010014

Outcomes of feeding activity of the sea cucumber *Holothuria tubulosa* on quantity, biochemical composition, and nutritional quality of sedimentary organic matter

Viviana Pasquini*†, Pierantonio Addis†, Ambra Angelica Giglioli, Davide Moccia and Antonio Pusceddu

Department of Life and Environmental Sciences, University of Cagliari, Cagliari, Italy

Introduction: *Holothuria tubulosa* is one of the most common sea cucumbers in the Mediterranean Sea, generally associated with organically enriched coastal sediments and seagrass beds. As a deposit-feeder, it is responsible for strong bioturbation processes and plays a putative key role in sedimentary carbon cycling and benthic trophodynamics. With the aim of exploring the potential use of holothuroids as a tool for remediating eutrophicated sediments, we investigated the effects of *H. tubulosa* on sedimentary organic matter quantity, biochemical composition, and nutritional quality.

Methods: Holothuroids and associated samples of ambient sediments were collected in two sites located in the Central-Western Mediterranean Sea (Sardinia, Italy) and characterized by different trophic status backgrounds: the site of Oristano characterized by sandy-muddy sediments and the presence of mariculture plants (ranked as meso-eutrophic) and the site of Teulada characterized by sandy sediments and *Posidonia oceanica* meadows (ranked as oligo-mesotrophic). We compared the biochemical composition (proteins, carbohydrates, lipids) of ambient sediment *vs* sea cucumbers feces and the sedimentary protein content *vs* protein content in the sediments retrieved in different gut sections (esophagus, mid gut, end gut) of the holothuroid.

Results: Our results reveal that holothuroids feeding on meso-eutrophic sediments can increase protein (1.5 times) and lipid (1.3 times) content through their defecation, thus making these substrates a more labile food source for other benthic organisms. We report here that *H. tubulosa* feeding on meso-eutrophic sediment is most likely able to actively select particles rich in labile organic matter with buccal tentacles, as revealed by the protein content in the esophagus that is up to 2-folds higher than that in the source sediment. According to the inverse relationship between assimilation rates and availability of organic substrates and the optimal foraging theory, *H. tubulosa* feeding on oligo-mesotrophic sediments showed potential assimilation of proteins ca. 25% higher than that of specimens feeding on meso-eutrophic sediments.

10.3389/fmars.2022.1010014

Discussion: Our results reveal that *H. tubulosa* feeding on meso-eutrophic sediments can profoundly influence the benthic trophic status, specifically modifying the biochemical composition and nutritional quality of organic matter, thus paving the way to its possible use in bioremediation actions of eutrophicated sediments and in Integrated Multi-Trophic Aquaculture systems.

KEYWORDS

sea cucumbers, *Holothuria tubulosa*, sediment organic matter, benthic trophodynamics, bioturbation

Introduction

Bioturbation mediated by benthic marine deposit-feeder plays a key role in carbon biogeochemical cycling from coastal to hadal depths (Uthicke and Karez, 1999; Roberts et al., 2000; Lohrer et al., 2004; Slater and Carton, 2009; Amaro et al., 2010; Slater et al., 2011a; Purcell et al., 2016). Bioturbation can indeed influence sediment permeability, chemical gradients in pore waters and sedimentary organic matter (OM) degradation rates (Reise, 2002; Lohrer et al., 2004; Solan et al., 2004; Meysman et al., 2006a; Meysman et al., 2006b; Schenone et al., 2019). Among the most effective bioturbators, sea cucumbers (Phylum Echinodermata), common members of marine benthic communities in world oceans at all depths, count more than 1,500 species (Horton et al., 2018). Deposit-feeding sea cucumbers, ingesting the whole sediment, and feeding on sedimentary OM, can rework large amounts of sediments (5.9 – 12.9 kg dw m^{-2} yr^{-1}) (Coulon and Jangoux, 1993; Uthicke and Karez, 1999; Mangion et al., 2004, Hartati et al., 2020), thus contributing to the redistribution and remineralization of sedimentary organic loads from hadal depth to coastal areas and coral reefs (Amaro et al., 2010; MacTavish et al., 2012; Purcell et al., 2016; Wolfe et al., 2017; Yamazaki et al., 2019).

Bioturbation caused by sea cucumbers extends from the upper layer of the seafloor to several centimeters' depth in the sediment, depending on the variable ability of the different species to dig into the sediment and their borrowing habits (Mercier et al., 1999; Roberts et al., 2000; Amaro et al., 2010; Ramón et al., 2019). During feeding, sediment particles are captured by the sea cucumber with the tentacles and released into the pharynx. Ingested particles are then mixed with the digestive enzymes and, once compressed into a plug that moves along the digestive system are released through the cloaca (Zamora and Jeffs, 2011). Thus, deposit-feeding sea cumbers, with their peculiar feeding activity, can reduce sedimentary OM loads (Slater and Carton, 2009; MacDonald et al., 2013; Neofitou et al., 2019). For this reason, sea cucumbers are considered one of the best candidates for Integrated Multi-Trophic Aquaculture (IMTA) practices (MacDonald et al., 2013; Purcell et al.,2014; Cubillo et al., 2016; Grosso et al., 2021). IMTA, in fact, can transform mariculture potential wastes (e.g., uneaten food and fish feces) into food sources for other reared species positioned at lower trophic levels (Zhou et al., 2006; Slater and Carton, 2007; Slater and Carton, 2009; Slater et al., 2009; Zamora and Jeffs, 2011; Zamora and Jeffs, 2012; Yuan et al., 2013; Lamprianidou et al., 2015; Shpigel et al., 2018). This sort of circular reuse of mariculture waste for producing extra commercial biomass could help mitigate the well-documented impacts of marine aquaculture on the trophic status, biodiversity and functioning of coastal marine ecosystems (Kalantzi and Karakassis, 2006; Pusceddu et al., 2007; Holmer et al., 2008; Holmerm, 2010; Mirto et al., 2010).

So far, sea cucumbers used in IMTA and co-culture trials include high commercially valuable species such as *Apostichopus japonicus* Selenka, 1867 (Zhou et al., 2006; Yuan et al., 2013; Kim et al., 2015), *Australostichopus mollis* Hutton, 1872 (Slater and Carton, 2007; Slater and Carton, 2009; Slater et al., 2009; Zamora and Jeffs, 2011; Zamora and Jeffs, 2012), *Holothuria scabra* Jaeger, 1833 (Mathieu-Resuge et al., 2020), *Parastichopus californicus* Stimpson, 1857 (Paltzat et al., 2008) and *Holothuria tubulosa* Gmelin 1788 (Grosso et al., 2021). Recent experiments have shown that the Mediterranean Sea cucumber *Holothuria tubulosa* grows faster beneath finfish cages than in mariculture-free areas (Tolon et al., 2017). In another study, it was shown that the monthly reduction of organic carbon (OC) caused by *H. tubulosa* (ca. 10 ind m^{-2}) feeding in sediments beneath seabream and seabass cages has been estimated to account up to 62% (Neofitou et al., 2019).

Moreover, sea cucumbers have a high commercial value and are currently overexploited worldwide (Conand, 2006; Anderson et al., 2011a, b; Bordbar et al., 2011; Purcell et al., 2011; Conand et al., 2014; González-Wangüemert et al., 2018). Indeed, holothuroid fisheries have rapidly expanded in the last three decades, because of the increasing demand for food in international markets and biomedical research programs (Bordbar et al., 2011). Holothuroids, in fact, are a traditional food in China and other eastern regions, where they are considered gourmet and luxury seafood (Wen et al., 2010; Yang and Bai, 2015), and sold at prices as high as up to ca. 3000 US$ per dried kg (Purcell et al., 2012; Purcell et al., 2014). The large market demand for these animals has led to overfishing in worldwide oceans and seas, including the Mediterranean. Consequently, 16 species have been classified as threatened with extinction based on standard IUCN methodology (Conand et al., 2014) and 4 species are included in the Convention on International Trade in Endangered Species list (CITES, 2022). In this sense, restocking and stock enhancement practices of holothuroids, eventually also including hatchery production of juveniles could support their protection.

Organic carbon in marine sediments is made of a variable combination of molecules that are differently prone to a rapid utilization by benthic detritivores (Pusceddu et al., 2009). The total organic C content of the sediments is, in this sense, a rather weak descriptor of the potential amount of food for the benthos. Since total

organic C content does not discriminate between refractory vs. labile fractions, its biopolymeric fraction (the sum of protein, carbohydrate and lipid C equivalents, *sensu* Fabiano et al., 1995) is currently used as a more reliable descriptor of the benthic trophic status, namely the availability of food available for the benthos in a variety of wetlands, coastal and even deep-sea sedimentary environments (Pusceddu et al., 2009; Pusceddu et al., 2010; Pusceddu et al., 2011; Dell'Anno et al., 2013). Nonetheless, studies dealing with the role of holothuroids on sedimentary organic matter dynamics have almost exclusively dealt with the mere measurement of total organic C only, with a very few exceptions (Amaro et al., 2010).

With an eye to the potential use of *H. tubulosa* for abating, also in an IMTA perspective, the consequences of benthic eutrophication, we investigated differences in quantity and biochemical composition of sedimentary OM and biochemical composition of *H. tubulosa* feces, along with changes in protein loads of ingested sediment in the different digestive tracts of *H. tubulosa*. More specifically, we posed the following questions: 1) does *H. tubulosa* influence sedimentary OM biochemical composition, and nutritional quality and, thus, the benthic trophic status? 2) does *H. tubulosa* has a specific influence on food availability of sedimentary proteins, supposed to represent the most labile fraction of OM? To answer these questions, we conducted experiments aimed at testing the following null hypotheses: 1) the biochemical composition of sediment OM hosting *H. tubulosa* is not different from that of sea cucumbers feces; 2) the protein loads of the sediment ingested by sea cucumbers do not vary among the digestive tracts and the feces.

Materials and methods

Model species, study sites and sampling strategy

Our study is focused on the sea cucumber *Holothuria tubulosa* Gmelin 1788, one of the most common and most exploited native species across the coastal Mediterranean Sea, where it can be pre-eminently found in organically enriched bottoms and seagrass beds (Tortonese, 1965; Bulteel et al., 1992; Koukouras et al., 2007; Costa et al., 2014; González-Wangüemert et al., 2014; González-Wangüemert et al., 2015; González-Wangüemert et al., 2018; Pasquini et al., 2021; Pasquini et al., 2022). Fishery of *H. tubulosa* is banned by the Italian Government that precautionarily prohibited its harvesting since 2018 (Ministerial decree 156/2018; Pasquini et al., 2021). In other areas of the Mediterranean, such as in Turkey, the fishery of *H. tubulosa* is governed since 2007 (González-Wangüemert et al., 2018; Dereli and Aydın, 2021).

H. tubulosa specimens and sediments were collected from two sites 80 nautical miles apart, in the Gulf of Teulada and the Gulf of Oristano, respectively (Sardinia, W Mediterranean Sea). Sediment grain size was determined by gravimetry after organic matter digestion with H_2O_2 and mesh sieving, using 63, 125, 250, 500, and 1000 µm meshes ICRAM, 2001). The sediments of the Oristano site (39°52'50"N; 8°28'54"E) were characterized by the dominance of sands (63-1000 µm; 75%), followed by mud (<63 µm; 14%) and gravel (>1000 µm; 11%) and by the presence of a nearby offshore mariculture fish farming plant for seabream and shi drum. The Teulada site (38°55'46"N; 8°43'17"E) was characterized by the dominance of sandy sediments (74%), followed by gravel (24%), and mud (1%), and by the presence of wide *Posidonia oceanica* meadows interspersed with unvegetated sediments (Figure 1).

At both sites, holothuroid and sediment samples were collected by SCUBA divers at depths between 3 and 7 m. In order to include environmental conditions spanning from the worst conditions (in winter, January) to the most favorable ones (in spring and, to a lesser extent, in summer: May, June, July), data were collected in April, June, and August 2019 and January, May, and July 2020. At each site and on each sampling date, three metal frames 60x60 cm (sampling unit n=3) were placed on the sea floor having a single sea cucumber in the central sub-square (20x20 cm). From each sampling unit (60x60 frame), three sediment samples were obtained by scraping ca. 50 mL from the top 2 cm of the sea floor with a Falcon-type. One tube was collected from the central sub-square, in which the sea cucumber occurs, and two from other two random sub-squares (n=3 for each sampling unit), resulting in a total of 9 sediment samples per each site at each sampling date (Moccia et al., 2019) (Supplementary Figure 1). All sea cucumbers (one per each 60x60 cm squared frame, n=3) were placed separately into 3-L plastic bag filled with seawater collected *in situ* and maintained in a cooler box (at *in situ* temperature) during transportation to the laboratory (within 1.5 h from sampling). We notice here that the choice of sampling only one specimen per squared frame, despite the official authorization (see the acknowledgments for more details) was dictated by the need of limiting as much as possible the pressure on a locally protected species. Once in the laboratory, sea cucumbers were singularly placed in a tank filled with *in situ* seawater (15-L) kept at *in situ* temperature and salinity, deprived of sediment. The sea cucumbers feces were collected every 6-8 hours and until the complete evacuation of the digestive tract (usually within 3 days). Feces from each specimen were pooled together to ensure the storage of a sufficient amount of feces for the subsequent biochemical analyses. The sediments and the feces were stored at -20°C until the subsequent analyses.

Additional (2-3) sea cucumber specimens were collected at both sites in June 2019 and used for the analysis of the protein content of the sediment within the digestive tract. Sea cucumbers were weighed (± 0.1 g) before dissection and the sediments present in the intestine esophagus (ESO), mid-gut (MID), and end gut (END) were carefully collected to avoid contaminations from the digestive tissue (Amaro et al., 2010) and stored at -20°C until analysis. As for above, we sampled a low number of experimental individuals to limit as much as possible the pressure on a locally protected species.

Biochemical composition of field sediment, holothuroids' feces, and sediment from the holothuroids' digestive tracts

Protein, carbohydrate, and lipid contents were determined spectrophotometrically (Danovaro, 2010). Proteins were determined according to Hartree (1972), as modified by Lowry et al. (1951) and Rice (1982) using the Folin-Ciocalteau reagent in a basic environment and expressed as bovine serum albumin equivalents. The procedure proposed by Gerchakov and Hatcher (1972), based on the phenol and concentrated sulfuric acid reaction with saccharides, was used to

10.3389/fmars.2022.1010014

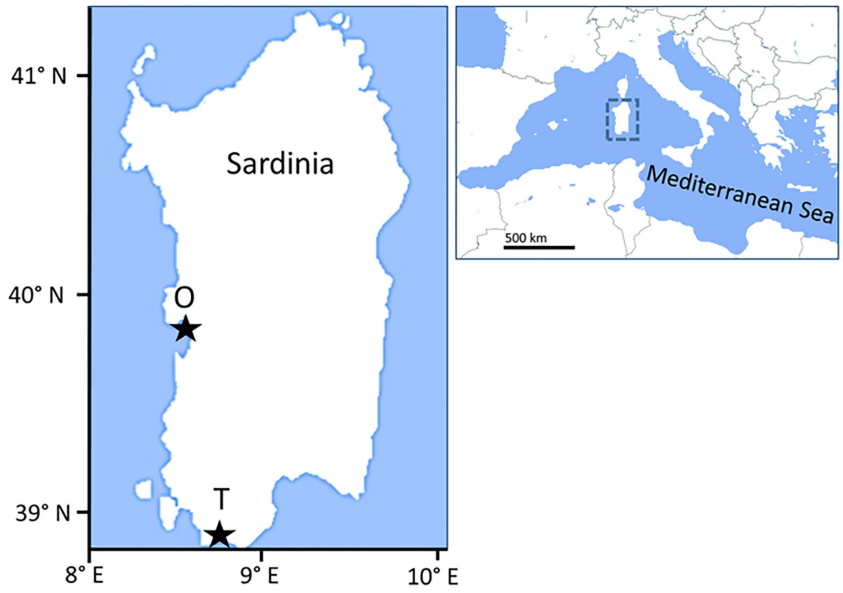

FIGURE 1
Location of the sampling sites in the Oristano (O) and Teulada (T) Gulfs.

determine carbohydrates, then expressed as D (+) Glucose equivalents. Lipids, after extraction in chloroform: methanol (1:1, vol:vol) (Bligh and Dyer, 1959), and evaporation in a dry hot bath at 80 to 100°C for 20 min, were determined after the sulfuric acid carbonization procedure (Marsh and Weinstein, 1966) and expressed as tripalmitin equivalents. For each biochemical assay, blanks were obtained using pre-calcinated sediments (450°C for 4 h). Protein, carbohydrate, and lipid concentrations were converted into C equivalents using the conversion factors 0.49, 0.40, and 0.75 mgC mg^{-1}, respectively, obtained from the C contents of the respective standard molecules (albumin, glucose and tripalmitin, respectively), and their sum was reported as the biopolymeric C (BPC) (Fabiano et al., 1995).

The percentage of proteins potential digestion was calculated as follows:

$$PD = 100 \times \frac{ESO\ \ PRT - END\ \ PRT}{ESO\ \ PRT}$$

where:

PD = potential proteins' digestion

ESO PRT= protein content (mg g^{-1}) in the sediment in the esophagus

END PRT= protein content (mg g^{-1}) in the sediment in the end gut

Chloroplastic pigments (chlorophyll-*a* and phaeopigments) in the ambient sediment were analysed fluorometrically according to Lorenzen and Jeffrey (1980). Pigments were extracted with 90% acetone (24 h in the dark at 4°C). After centrifugation (800 × *g*), the supernatant was used to determine the chlorophyll-*a* and, after acidification with 0.1 N HCl, to estimate the phaeopigments (Danovaro, 2010). The total algal C contribution (sum of chlorophyll-*a* and phaeopigments) to BPC was calculated as the percentage of phytopigment-to-BPC concentrations after converting the total phytopigment concentrations into C equivalents using a mean value of 40 mgC mg^{-1} (Pusceddu et al., 2010). Although the C: Chla can vary from 10 to 100 (on average 35 for phytoplankton) (Cloern et al., 1995), we used the conversion factor proposed in Pusceddu et al. (2010) to allow comparability with other studies carried out in a variety of other shallow coastal aquatic environments (Pusceddu et al., 2009).

Statistical analyses

Differences in quantity and biochemical composition (protein, carbohydrates, lipids, chlorophyll-*a*, phaeopigments) of ambient sediments were investigated using Site (Si; 2 fixed levels: Oristano vs. Teulada) and Month (Mo; 6 fixed levels: April, June, August 2019, and January, May, July 2020) as orthogonal sources of variance, with n=9 for the combination of factors. Differences in OM quantity and biochemical composition in terms of protein, carbohydrates, lipids between sediment and holothuroid feces were investigated separately for the two sites (Oristano and Teulada) using Matrix (Ma; 2 fixed levels: sediment vs. feces) and Month (Mo; 6 fixed levels: April, June, August 2019, and January, May, July 2020) as orthogonal sources of variance. In both designs, as any sampled sediment portion around *H. tubulosa* specimens could have been visited by holothuroids before sampling, we chose to consider as independent replicates of ambient sediments either sediments without or with (in the center of the large frame) holothuroids. This choice generated an unbalanced design, which biases are, however, counterbalanced by the use of PERMANOVA, which is extended to accommodate, apart random effects, hierarchical models, mixed models, quantitative covariates, repeated measures, also unbalanced and/or asymmetrical designs (Anderson, 2017). Differences in protein content among sediment, sediment in the gut (three sectors: esophagus, mid gut, and end gut)

and feces were assessed by means of univariate PERMANOVA tests using the matrix (5 fixed levels: ambient sediment, esophagus, mid gut, end gut and feces) as the sole source of variation.

In all designs, differences were assessed with permutational analyses of variance (PERMANOVA), in both univariate and multivariate contexts. PERMANOVA is a semiparametric method described as a geometric partitioning of multivariate variation in the space of a chosen dissimilarity measure according to a given ANOVA design, with p-values obtained using appropriate distribution-free permutation techniques (Anderson, 2017). PERMANOVA on one response variable using Euclidean distance yields the classical univariate F statistic, so that it can also be used to do univariate ANOVA, but where p values are obtained by permutation (Anderson and Millar, 2004), thus avoiding the assumption of normality (Anderson, 2017). PERMANOVA tests were carried out on Euclidean distance-based resemblance matrixes of normalized data, using 999 random permutations of the appropriate units. When significant differences were observed, pairwise tests were also carried out to ascertain patterns of differences among treatments and/or sampling times.

Multivariate differences in sedimentary OM biochemical composition (in terms of protein, carbohydrate, lipid and phytopigment contents) between sites and months were visualized with a biplot after a canonical analysis of the principal coordinates (CAP) (Anderson and Willis, 2003). CAP allows identifying an axis through the multivariate cloud of points that is best at separating *a priori* groups. The motivation for the CAP routine arose as sometimes there are real differences among *a priori* groups in multivariate space that cannot be easily seen in an unconstrained ordination (e.g., PCA or MDS plots; Anderson and Gorley, 2008). All the statistical analyses were performed using the routines included in the PRIMER 7+ software (Anderson et al., 2008).

Results

Quantity and biochemical composition of organic matter in field sediments

Overall, contents of all organic compounds, but carbohydrates, differed significantly between sites (Supplementary Table 1), with values in the muddy organically enriched sediments at Oristano significantly higher (3-5 times) than those in the sandy poorer sediments at Teulada (Supplementary Figure 2). In both sites, significant temporal variations, though not consistent for the different classes of organic compounds, and significant effects of the Si×Mo interaction occurred only for protein, lipid, and chlorophyll-*a* contents. Results of the pairwise tests conducted to ascertain temporal differences are reported in Supplementary Table 2 and illustrated in Supplementary Figure 2.

In organically enriched sediments at Oristano, seasonal differences in the sedimentary protein contents varied between years: in 2019 values in spring (April) and early summer (June) were generally lower (1.5-2.9 times) than those in all other months, whereas in 2020 values in May were ca. 1.4 times higher than those in July. The lipid contents in this site, were significantly higher (3.5 – 5.4 times) in April 2019 than those in all other months, both in 2019 and 2020. The chlorophyll-*a* content of Oristano sediments in April was 1.7 times higher than those in January 2020 and 1.5 times lower than those in May 2020. Moreover, chlorophyll-*a* contents of Oristano sediments in June 2019 and January 2020 were significantly lower (1.5-3 times) than those in August 2019, May 2020, and July 2020 (Supplementary Figure 2).

In the poorer Teulada sediments, the sedimentary protein contents varied significantly among sampling periods, with values in summer months (June, August) ca. 3-10 times higher than those in spring-winter ones (April, January), respectively of the study year. The lowest sedimentary lipid content was observed in spring 2019 (April), when values were 1.8 times lower than those in January 2020 and 6.5 times lower than those in June 2019. Lipid content in June 2019 was also significantly higher (ca. 3.3 times) than that in August 2019. Temporal variability of the chlorophyll-*a* contents in the poorer Teulada sediments was much less pronounced than in that in the organically enriched sediments in Oristano, with values in Summer 2019 (August) 2.5 times higher than those in Spring (April 2019) and Winter (January 2020). Phaeopigment contents differed significantly only between sites, with values in the richer Oristano sediments up to 7.7 times higher than those in the poorer Teulada ones (Supplementary Figure 2).

The biochemical composition of sediments differed spatially and temporally, as found in sedimentary OM levels (Supplementary Table 3). The pairwise tests revealed that significant differences occurred among sites in all the sampling months, but May and June (Supplementary Table 4A) and that in both sites the biochemical composition of sedimentary OM varied with time. More specifically, in the organically enriched sediments in Oristano proteins (46 – 52%) were the dominant class of organic compounds followed by carbohydrates (34 – 40%) and lipids (9 – 14%) in almost all samplings, with exceptions in April and June 2019, when carbohydrates were dominant class (54-56%) followed by lipids and proteins (April 2019, 32% and 11%, respectively; June 2019, 11% and 35%, respectively) (Supplementary Figure 3).

The biochemical composition of sediments from the poorer Teulada site was more variable (Figure 2) and significant differences among sampling occasions were observed between January 2020 *vs* April, June, and August 2019; and between April *vs* August 2019 (Supplementary Table 4B). Sediments collected in 2019 and in July 2020 were characterized by the dominance of carbohydrates (45 – 61%), followed by proteins (28 – 42%) and lipids (10 -17%); sediments collected in January (2020) showed a dominance of proteins (39%) and similar contributions of lipids and carbohydrates (32 and 29% respectively). The sediments collected in May 2020 were characterized by the dominance of proteins (46%), followed by carbohydrates (41%) and lipids (13%) (Supplementary Figure 3).

Effect of sea cucumbers on quantity and composition of the sedimentary organic matter

The effect of the sea cucumbers' feeding was considered separately for each site. In the organically enriched Oristano site (putatively impacted by mariculture effluents), protein contents were affected by a significant effect of the Mo×Ma interaction (Table 1A). More

10.3389/fmars.2022.1010014

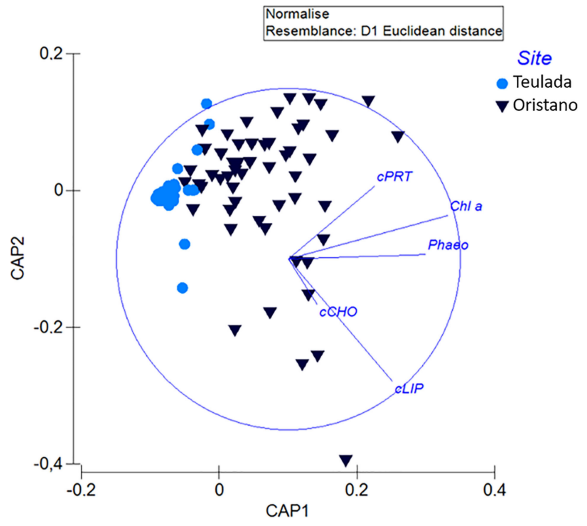

FIGURE 2
The biplot produced after canonical analysis of the principal coordinates (CAP) showing variations in the biochemical composition of sedimentary organic matter (chlorophyll: Chl *a*; phaeopigments: Phaeo; and proteins: cPRT; carbohydrates: cCHO; lipids: cLIP, converted in carbon equivalent) between the organically enriched site of Oristano and the poorer site of Teulada.

specifically, the results of the *post-hoc* tests revealed that the protein content of feces was significantly higher than that in the surrounding sediment in June 2019 (2.4 times) and in July 2020 (1.9 times) (Table 2; Figure 3A). In the poorer Teulada site (mariculture-free sediments) no significant differences between the sediment and the feces were observed (Table 1B; Figure 3B), but differences occurred only among months (Supplementary Table 5). Carbohydrate content of sediment and feces did not vary between the two matrixes in each of the sampling dates in both sites (Tables 1A, B and Figures 3C, D).

In the organically enriched Oristano site the lipid content was affected by a significant Mo×Ma interaction (Table 1A). In more details, the results of the *post-hoc* tests revealed that feces were strongly depleted (-83%) in lipids when compared with the surrounding sediment only in April 2019, whereas in all other sampling months, lipid contents in the feces were significantly higher (by 48 - 67%) than those in the surrounding sediment, with the exception for January 2020, when no significant differences were observed (Table 2 and Figure 3E). In the poorer Teulada site, the lipid content did not vary significantly between the matrices in each of the sampling dates (Table 1B and Figure 3F). The biopolymeric C contents were affected by a significant Mo×Ma interaction only in the organically enriched Oristano site (Table 1A), where the *post-hoc* test revealed that differences in biopolymeric contents between sediments and feces were significant only in summer 2020 (July), with values in feces 2 times higher than those in the sediment (Table 2 and Figure 3G). In the poorer Teulada site biopolymeric C contents did not vary among matrices in any of the sampling periods (Table 1B and Figure 3H).

The biochemical composition of OM was affected by a significant interaction of the factors Mo×Ma only in the organically enriched Oristano site (Table 3A). More in details, differences in OM composition between sediment and feces in Oristano occurred only in April 2019, when carbohydrate and protein contributions to

TABLE 1 Results of univariate PERMANOVA testing for the effects of Months (Mo) and Matrices (Ma) and their interaction on protein, carbohydrate, lipid and BPC contents in sediments and feces from the two sites of Oristano (A) and Teulada (B).

(A) Oristano		Proteins				Carbohydrates				Lipids				Biopolymeric C (BPC)			
Source	DF	MS	Pseudo-F	P (MC)	% EV	MS	Pseudo-F	P (MC)	% EV	MS	Pseudo-F	P (MC)	% EV	MS	Pseudo-F	P (MC)	% EV
Month (Mo)	5	4.813	9.761	***	32	1.047	1.141	ns	2	1.175	2.394	ns	5	0.338	0.396	ns	0
Matrix (Ma)	1	8.915	18.080	***	21	0.002	0.003	ns	0	1.561	3.180	ns	3	1.706	2.000	ns	3
Mo × Ma	5	1.382	2.802	*	13	0.688	0.750	ns	0	4.150	8.454	***	57	2.432	2.850	*	28
Residual	60	0.493			33	0.918			98	0.491			35	0.853			69
(B) Teulada		Proteins				Carbohydrates				Lipids				Biopolymeric C (BPC)			
Source	DF	MS	Pseudo-F	P (MC)	% EV	MS	Pseudo-F	P (MC)	% EV	MS	Pseudo-F	P (MC)	% EV	MS	Pseudo-F	P (MC)	% EV
Month (Mo)	5	2.105	2.509	*	13	1.477	1.484	ns	5	1.746	1.910	ns	9	1.661	1.749	ns	8
Matrix (Ma)	1	1.821	2.170	ns	3	0.913	0.918	ns	0	2.783	3.046	ns	7	1.308	1.377	ns	1
Mo × Ma	5	1.364	1.626	ns	11	0.115	0.116	ns	0	0.801	0.877	ns	0	0.297	0.313	ns	0
Residual	60	0.839			73	0.995			95	0.914			84	0.950			91

DF, degree of freedom; MS , mean squares; Pseudo-F, F; P(MC), probability level after Monte Carlo simulations. *P< 0.05; **P< 0.01; ***P< 0.001; ns, P>0.05; EV, % of explained variance.

10.3389/fmars.2022.1010014

TABLE 2 Results of the pairwise comparisons contrasting proteins and lipid contents between sediment and feces in the meso-eutrophic site (Oristano) in all sampling dates.

		Proteins		Lipids		Biopolymeric C (BPC)	
Site	Month	t	P(MC)	t	P(MC)	t	P(MC)
Oristano	Apr	1.003	ns	3.092	**	1.728	ns
	Jun	6.783	***	3.258	*	0.794	ns
	Aug	0.930	ns	3.282	**	1.962	ns
	Jan	2.150	ns	0.987	ns	1.503	ns
	May	0.178	ns	2.788	*	0.698	ns
	Jul	4.022	**	2.490	*	3.319	**

t, T value, P(MC), probability level after Monte Carlo simulations. *P< 0.05; **P< 0.01; ***P< 0.001; ns, not significant.

biopolymeric C were higher in feces than in the sediments, at the expense of lipids, and in Jul-Aug 2020 because of a higher lipid contribution in feces, at the expenses of proteins (Table 3B; Figure 4A). In the poorer Teulada, the biochemical composition did not vary between sediment and feces in all sampling periods (Table 3B; Figure 4B).

Proteins quantity in food sources, holothuroids' digestive tracts and feces

The results revealed that the protein content differed significantly among the different matrices (ambient sediment, digestive tracts, and feces) only in the organically enriched Oristano site (Table 4A), where

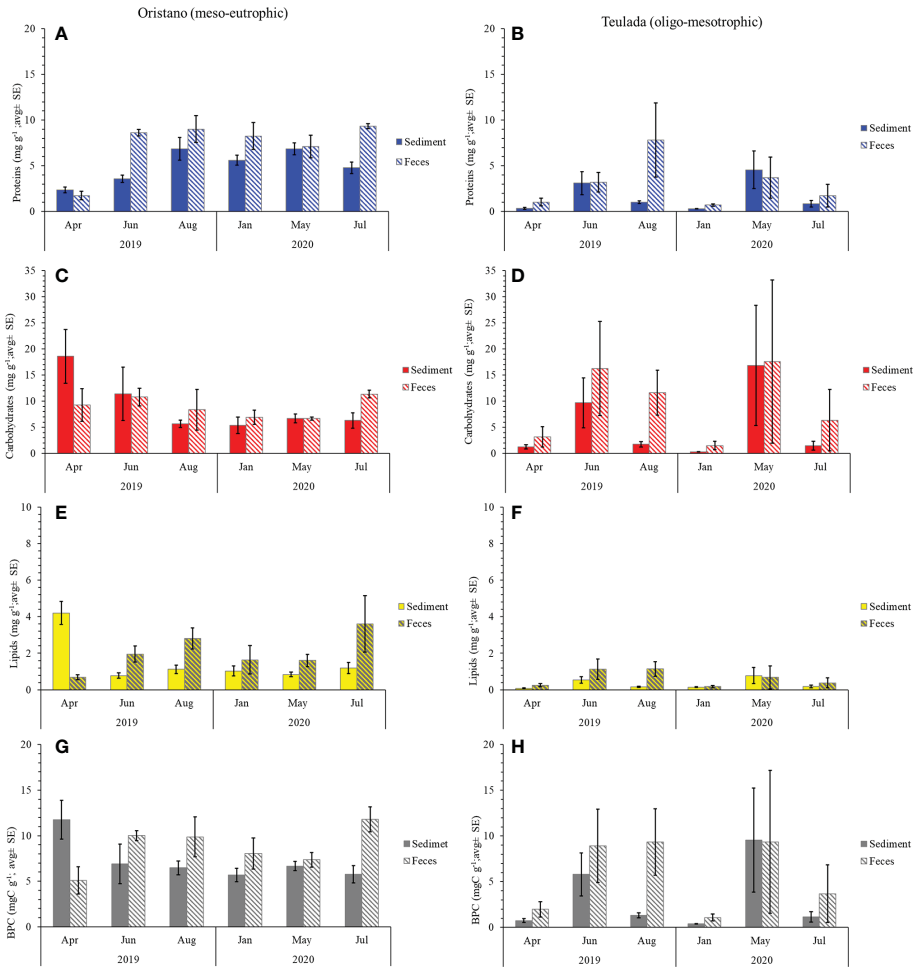

FIGURE 3
Protein **(A, B)**, carbohydrate **(C, D)**, lipid **(E, F)**, and BPC **(G, H)** contents in sediment and feces from Oristano (organically enriched site) and Teulada (poorer site) during the study period. Error bars indicate standard error (sediments n=9; feces n=3).

10.3389/fmars.2022.1010014

TABLE 3 Results of multivariate PERMANOVA testing for the effects of Month, Matrices and their interactions on the biochemical composition of OM in two study sites (A); and results of the pairwise comparisons testing for differences in the biochemical composition of OM between sediment and feces in the meso-eutrophic site (Oristano) during the study period (B).

(A)	Site	Source	DF	MS	Pseudo-F	P(MC)	%EV
	Oristano	**Month (Mo)**	5	7.035	3.699	**	15
		Matrix (Ma)	1	10.478	5.510	**	8
		Mo × Ma	5	6.220	3.271	***	26
		Residual	60	1.902			51
	Teulada	**Month (Mo)**	5	5.327	1.939	ns	9
		Matrix (Ma)	1	5.517	2.008	ns	3
		Mo × Ma	5	2.280	0.830	ns	2
		Residual	60	2.748			87
(B)	Site		Month	t	P(MC)		
	Oristano		**Apr**	1.943	*		
			Jun	1.768	ns		
			Aug	1.492	ns		
			Jan	1.512	ns		
			May	0.959	ns		
			Jul	2.869	**		

DF, degree of freedom; MS, mean squares; Pseudo-F, F; P(MC), probability level after Monte Carlo simulations. *P< 0.05; **P< 0.01; ***P<0.001; ns, P>0.05; EV, % of explained variance, t, T value.

proteins' content of sediment in the esophagus was ca. 2 times higher than that in the ambient sediment, and slightly decreased along the other digestive tracts (Table 4B; Figure 5). The estimated digestion rate of proteins along the digestive tracts of *H. tubulosa* (Figure 5A) was slightly higher (40%) in specimens from the poorer Teulada site than that in specimens from the organically enriched Oristano site (30%). As a result, the amounts of proteins accumulated in the esophagus in specimens from Oristano are so high that feces are enriched in proteins when compared to the ambient sediment, whereas in the poorer Teulada site feces have protein contents similar to those measured in the ambient sediment (Figures 5B, C).

Discussion

Trophic status of ambient sediments

We report here that, as expected, the two investigated sites were characterized by well-delineated differences in benthic trophic status, as assessed in terms of quantity and composition of sedimentary OM. The sandy-mud sediments of the Oristano site, influenced by putative organic inputs released by a close mariculture plant, were in fact characterized by biopolymeric C contents (dominated by proteins) generally > 3 mgC g^{-1} and by a limited temporal variability of either quantity or composition of sedimentary OM. The sandy sediments of the Teulada site were characterized by biopolymeric C contents varying from<1 mgC g^{-1} in Winter and early Spring to 1-3 (or higher) mgCg^{-1} in Summer, and a much wider temporal variability of OM biochemical composition (though generally characterized by the dominance of carbohydrates). Overall, chlorophyll-*a* contents and the algal contribution to biopolymeric C (estimated as the percentage fraction of total phytopigments transformed in C equivalents over biopolymeric C contents) were higher in the Oristano than in the Teulada sediments. Meso-eutrophic sediments are typically characterized by biopolymeric C contents > 3 mgC g^{-1} (Pusceddu et al., 2011) and a general dominance of proteins over carbohydrates (Pusceddu et al., 2009; Pusceddu et al., 2011), which makes them a more labile source of food for benthic (especially deposit-feeders) consumers (Pusceddu et al., 2009). According to this, we can rank the sediments from Oristano as meso-eutrophic, and those from Teulada as oligo-mesotrophic. Moreover, the contribution of total phytopigments (as a proxy of OM of primary origin) to biopolymeric C was slightly higher in Oristano (ca. 14 ± 4%) than in Teulada (ca. 10 ± 4%). Since the higher the algal fraction of biopolymeric C, the higher the lability of sediment OM for benthic consumers (Pusceddu et al., 2003), altogether our results indicate that the two sites offered totally different trophic conditions (i.e., food availability levels) to the holothuroids.

Effects of *H. tubulosa* on the benthic trophic status

Deposit-feeders sea cucumbers are generally associated with soft organic-rich bottoms, where they rework the upper sediment layers feeding on the most readily utilizable OM (Yingst, 1982; Roberts et al.,

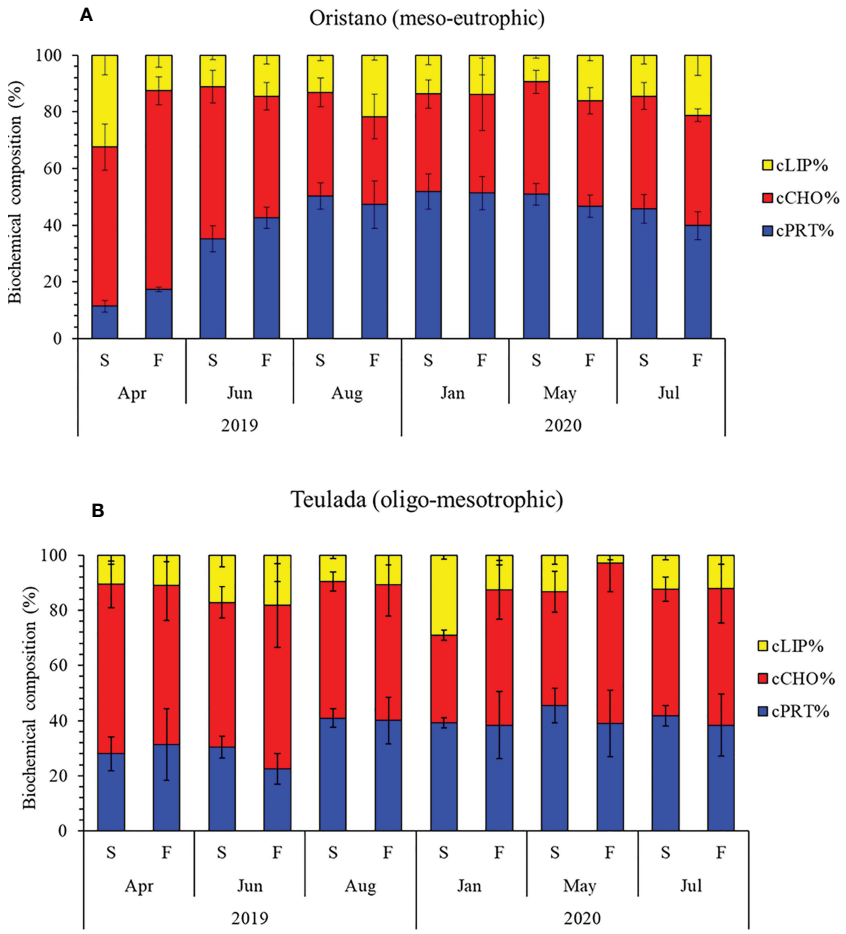

FIGURE 4
Variations in the percentage contribution of proteins, carbohydrates, and lipids to the BPC in sediments (S) and feces (F) in the organically enriched site of Oristano **(A)** and in the poorer site of Teulada **(B)**. Error bars indicate the standard error (sediments n=9; feces n=3). cLIP, lipid; cCHO, carbohydrate; cPRT, protein.

2000; Purcell et al., 2016). The studies conducted so far on the feeding behavior of coastal sea cucumbers investigated the fate of total organic matter (TOM, as obtained by the loss on ignition technique) and/or total organic carbon (TOC), without considering the biochemical composition and the biopolymeric C content of the sediments. Both TOM and TOC include any organic molecule and do not allow a distinction between labile (i.e., nutritionally available) vs. refractory fractions of OM (Pusceddu et al., 2009). In this regard, most recently the biochemical gross composition of sedimentary OM (in terms of protein, carbohydrate, and lipid contents) has been used as a proxy of OM availability for benthic consumers (Danovaro et al., 2001; Gambi et al., 2014; Gambi et al., 2017).

To shed light on the potential role of *H. tubulosa* on the benthic trophic status, we investigated differences in quantity and biochemical composition of ambient sediments and sea cucumbers' feces in two distinct sites characterized by the above-described different background trophic status. Although the analysis refers to a relatively limited number of individuals in each sampling unit, our data suggest that the feces produced by *H. tubulosa* feeding on sediment from the less productive "oligo-mesotrophic" site showed the same OM contents as the ambient sediment. Instead, sea cucumbers feeding on richer (meso-eutrophic) sediments (Oristano) produced, especially in Summer, feces with OM contents significantly higher than those of the surrounding sediment. These results are consistent with previous studies conducted by comparing when OM contents in sediment and feces of other holothuroids (Mercier et al., 1999). These results are apparently in contrast with those from previous studies showing that holothuroids feeding can abate OM sedimentary contents on long time scales (Paltzat et al., 2008; Slater and Carton, 2009; MacDonald et al., 2013; Neofitou et al., 2019). At a first glance, such a discrepancy could be related to the different proxy of OM quantity used in this study (biopolymeric C) and that (TOM) used in previous studies. Although we did not estimate TOM contents in the sediment and the feces, such discrepancy suggests that *H. tubulosa* consumes TOM, but releases feces enriched in biopolymeric compounds. Since biopolymeric C is assumed to represent the most labile fraction of OM, our results suggest that other mechanisms, besides nutrition and assimilation, could be responsible for increasing BPC contents in feces. For instance, based on the results of previous studies which identified

10.3389/fmars.2022.1010014

TABLE 4 Results of the univariate PERMANOVA testing differences in the protein content of the source sediment, digestive tract and feces of *H. tubulosa* in the two study sites (A); and results of the pairwise comparison testing for difference in protein contents in the source sediment (S), digestive tracts (esophagus = ESO; mid gut = MID; end gut = END) and feces (F) in the meso-eutrophic site (Oristano) (B).

(A)	Site	Source	DF	MS	Pseudo-F	P(MC)	%EV
	Oristano	**Matrix (Ma)**	4	3.512	15.458	***	82
		Residual	13	0.227			16
	Teulada	**Matrix (Ma)**	4	1.077	0.269	ns	0
		Residual	13	15.923			100
(B)	Site		Contrast	t	P(MC)		
	Oristano		**S, F**	6.783	***		
			S, ESO	6.860	***		
			S, MID	0.061	ns		
			S, END	3.537	**		
			F, ESO	2.100	ns		
			F, MID	2.862	ns		
			F, END	4.063	*		
			ESO, MID	2.682	ns		
			ESO, END	7.475	*		
			MID, END	1.369	ns		

DF, degrees of freedom; MS, mean square; Pseudo-F, F statistic; P(MC), probability level after Monte Carlo simulations; %EV, percentage of explained variation; ***P< 0.001; ns, not significant; t , t value. *P< 0.05; **P< 0.01.

meiofauna as a food source for holothuroids (Wolfe and Byrne, 2017; Wolfe et al., 2018; Wolfe et al., 2021), we cannot exclude that some of the observed patterns could be also due to the different intake of meiofauna in the two different environmental assets. Moreover, we have to consider that seasonal variations in the intake of organic C by holothuroids, caused, for instance, by aestivation in Summer and hibernation in Winter as observed in other temperate species (e.g., *A. japonicus*; Ji et al., 2008; Yu et al., 2014) could cause variations in their

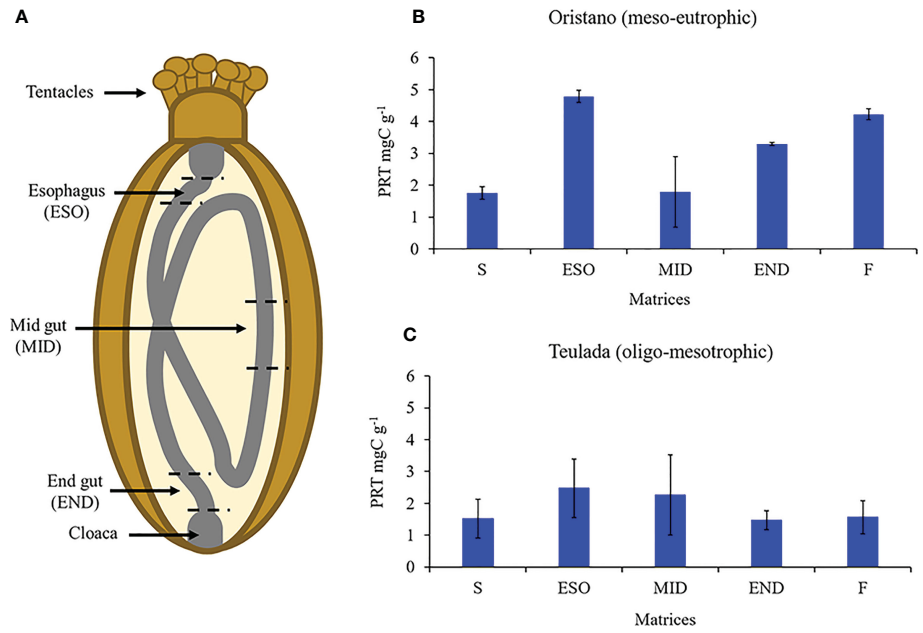

FIGURE 5
Schematic representation of sea cucumbers' digestive tract **(A)**. Protein contents (PRT) of source sediment (S), sediment in the esophagus (ESO), mid gut (MID), and end gut (END) and feces (F) of holothurians from the meso-eutrophic site (Oristano, **B**) and from the oligo-mesotrophic site (Teulada, **C**). Error bars indicate standard error (n=9 S; n=3 ESO; MID; END; F).

behavior and effects on sedimentary OM. Nevertheless, nor previous studies (Günay et al., 2019) nor our study have observed this in *H. tubulosa*.

We notice also that the overall increase in BPC contents of feces produced by holothuroids feeding on OM-rich sediments (Oristano), was accompanied by an increase of the most labile components of OM (i.e., proteins and lipids). Since both proteins and lipids are high-energy compounds putatively used by holothuroids for their somatic growth and gonad development, respectively (Yang et al., 2006; Slater et al., 2011b), their enrichment in the feces appears counterintuitive. Whatever the potential explanations (see below), this result first indicates that feces released by holothuroids during their feeding can enhance locally and temporarily the nutritional quality of the ambient sediment. Since this enrichment process is not detected in the more oligotrophic site, we contend that the efficacy of sea cucumbers as bioreactors (whatever the effect on the sediment trophic status) is most likely modulated by the actual quantity and nutritional quality of the sedimentary OM.

Fate of proteins ingested by *H. tubulosa*: Role of food particle selection and estimate of potential assimilation of proteins

As delineated above, the protein content in *H. tubulosa* feces collected from the meso-eutrophic site (Oristano) is higher than that in the ambient sediment. This apparently counterintuitive result could be caused by the peculiar feeding behavior of the sea cucumbers and, to shed light on the mechanism behind such a phenomenon, we compared protein contents in ambient sediment with those in sediment remains within the holothuroids' gut and feces from the two sites. The protein content in the esophagus of *H. tubulosa* is significantly higher than that in the source sediment only in specimens collected from the meso-eutrophic site (Oristano), suggesting, in this trophic asset, the presence of a possible accumulation or a concentration mechanism of proteins in the esophagus. This result is consistent with the results reported on the protein contents of the deep-sea holothuroid *Molpadia musculus* gut, in which the concentration factor was estimated to be 3.1 (Amaro et al., 2010). Other studies, based on total N or total OM contents reported a similar concentration mechanism in *Australostichopus mollis* (Slater et al., 2011a, b; Zamora and Jeffs, 2011) and *Parastichopus californicus* (Paltzat et al., 2008). The increase in proteins (or total OM) contents in sediment remains retrieved from the esophagus can be explained by the presence of a selection mechanism of protein-rich particles ingested by holothuroids. Several studies have indeed proven that holothuroids, rather than simply packing up sediment particles with mucus and digestive fluids, can select, possibly by chemo-selection mechanisms, food particles with their tentacles (Uthicke and Karez, 1999; Roberts et al., 2000; Dar and Ahmad, 2006; Paltzat et al., 2008; Slater et al., 2011a; Navarro et al., 2013; Ramón et al., 2019; Hartati et al., 2020). However, this hypothesis is not supported everywhere as, in our study, the concentration mechanism was reported only for holothuroids from the OM-enriched sediments (Oristano). Nevertheless, we must notice that the protein and lipid enrichment of gut sediments and feces of holothuroids, when compared to ambient sediments, could be also the result of the presence of mucus coating the feces before their release (Mercier et al., 1999; Slater et al., 2011b). Based on our sampling approach, we cannot exclude this, but we notice here that such enrichment is documented only from OM-enriched sediments, giving room to consider this process the result of mixed effects associated with either the physiology of feces production or with the process of food particles selection.

The apparently different behavior of holothuroids feeding on sediments with different OM contents could be related to the different sediment grain size and organic nutritional quality observed in the two sites. Sediments from the meso-eutrophic site (Oristano) show a fraction of mud and fine sand, including the particles typically selected with buccal tentacles (Mezali and Soualili, 2013), higher than that in the oligo-mesotrophic site (Teulada). Moreover, we report here also that the estimated protein assimilation rate of holothuroids from the oligo-mesotrophic site (ca. 40%) is higher than that (ca. 30%) of holothuroids from the meso-eutrophic one. This result fits the known inverse relationship between assimilation rates and availability of organic substrates (Roberts et al., 2000; Zamora and Jeffs, 2011) and the optimal foraging theory, which foresees that consumers tend to optimize energy intake by means of a trade-off between the quantity of energy necessary for survival and that spent to acquire it (Stephens and Krebs, 1986). Our contention, indeed, corroborated by the finding of higher defecation rates of the holothuroid *Thelenota anax* in sediments with lower organic matter levels (Hammond et al., 2020), suggests that feces produced by holothuroids in oligo-mesotrophic bottoms are poorer in protein contents than those from meso-eutrophic sediments because of their larger needs of accumulating energy from a poorer food source. Although on a merely speculative basis, due to the restricted number of specimens considered here, our results support the hypothesis that the sea cucumber *H. tubulosa* can select food particles from the surrounding sediment and concentrate them in the esophagus, but also that the potential assimilation can be strongly dependent upon the relative amount of available food and its nutritional quality.

Protecting and harnessing sea cucumbers' environmental services

With an eye to the possible use of sea cucumbers as a bioremediation tool of eutrophicated sediments, since proteins are N-rich compounds, and N is the most limiting factor for heterotrophic nutrition (Dell'Anno et al., 2002; Pusceddu et al., 2009), we conclude that the availability of protein-enriched feces could foster and facilitate the transfer of energy towards higher trophic levels, thus limiting benthic eutrophication (i.e., the accumulation of huge amounts of labile organic C in sediments below fish cages; Pusceddu et al., 2007). In this sense, *H. tubulosa*, by accelerating the detritus cycling, especially in OM-enriched sea floors, could be also potentially used to condition the benthic trophic status for additional components (including reared species, such as small scavenging crustaceans) of the 'manipulated' food webs in Integrated Multi-Trophic Aquaculture (IMTA) (Neofitou et al., 2019). Encouraging results from recent studies on breeding Mediterranean holothuroids, including *H. tubulosa*, pave the way for the possibility of using captive-bred specimens as tools for

bioremediation and IMTA purposes, at the same time limiting the exploitation of this protected species (Rakaj et al., 2018; Pasquini, 2022).

Conclusions

H. tubulosa is a "continuous" feeder that can ingest and rework large amounts of sediment and can have a role on the recycling of seagrass detritus in *Posidonia oceanica* meadows (Costa et al., 2014; Boncagni et al., 2019). Here we showed that the sea cucumber *H. tubulosa* can influence the benthic trophic status of marine sediments, specifically by modifying the quantity, biochemical composition, and nutritional quality of sedimentary OM. Our results proved also that *H. tubulosa* influences particularly the sedimentary contents of the most labile molecules (i.e., proteins and lipids) and that, by producing protein- and lipid-enriched feces (especially in meso-eutrophic assets), can contribute making labile substrates more available for higher trophic levels.

Holothuroid fisheries had rapidly grown and expanded in the last three decades and large market demand for these animals has led to overfishing in worldwide oceans and seas, including the Mediterranean. Since our results have shown that holothuroids play an important role in conditioning sediment OM content, possibly interacting with species from different trophic levels, we anticipate that their overfishing, besides posing their populations at risk, might have severe consequences on the structure of benthic communities and ecosystem functioning.

Based on the changes in protein concentration of sediment within the digestive tract we also provided elements in support of the hypothesis of an active selection of labile food particles by holothuroids and that this mechanism could be dependent upon sediment grain size and the actual bioavailability of organic substrates. Finally, based on our results, we conclude that, since the 'bioreactor' efficacy of *H. tubulosa* can vary according to the OM quantity biochemical composition and nutritional quality of the ambient sediment, their use in Integrated Multi-trophic Aquaculture and bioremediation actions should be modulated accordingly.

Data availability statement

The raw data supporting the conclusions of this article will be made available by the authors, without undue reservation.

Author contributions

VP, AP, and PA conceived and planned the experiments. VP, AG and DM carried out the sampling and laboratory analyses, VP and AP carried out the statistical analyses. All authors contributed to the interpretation of the results. VP and PA took the lead in writing the manuscript followed by extensive revision by AP to achieve the final version. All authors provided critical feedback and helped shape the research, analyses, and manuscript. All authors contributed to the article and approved the submitted version.

Funding

This study has been carried out in the framework of the projects "Marine habitats restoration in a climate change-impaired Mediterranean Sea [MAHRES]", funded by the Ministero dell'Università e della Ricerca under the PRIN 2017 call (Protocol: 2017MHHWBN; CUPF74I19001320001), and "Innovative species of commercial interest for Sardinian aquaculture: development of experimental protocols for the breeding of sea cucumbers, (project n.1/INA/2.47/2017)" funded by the European Maritime and Fisheries Fund (EMFF) Programme 2014/2020, Measure:2.47 – Innovation; and the EU co-founded project "InEVal: Increasing Echinoderm Value Chains" (grant n. ID 101 InEVal) funded by ERA-NET BlueBio programme.

Acknowledgments

The authors wish to express their gratitude to the Marine Protected Area Penisola del Sinis – Isola di Mal di Ventre in the people of the director Ing. Massimo Marras and Dr. Roberto Brundu; Dr. Gaspare Barbera technical manager of the L.P.A. Group fish farm and the Marina di Teulada in the person of Mrs. Barbara Lai, for the logistic support in the field sampling. We are thankful to Dr. Marco Secci and Mr. Marco Maxia (Agris Sardinia Agency) for their help in the field and sampling activities. The collection of sea cucumbers was authorized with Scientific Research Permit for echinoderms by Regione Autonoma della Sardegna (Prot. N. 6261, 03/05/2018; Prot. N. 1845, 06/02/2019; Prot. N. 20735, 28/11/2019).

Conflict of interest

The authors declare that the research was conducted in the absence of any commercial or financial relationships that could be construed as a potential conflict of interest.

Publisher's note

Supplementary material

The Supplementary Material for this article can be found online at: https://www.frontiersin.org/articles/10.3389/fmars.2022.1010014/full#supplementary-material

References

Amaro, T., Bianchelli, S., Billett, D. S. M., Cunha, M. R., Pusceddu, A., and Danovaro, R. (2010). The trophic biology of the holothurian *Molpadia musculus*: Implications for organic matter cycling and ecosystem functioning in a deep submarine canyon. *Biogeosciences* 7, 2419–2432. doi: 10.5194/bg-7-2419-2010

Anderson, M. J. (2017). "Permutational multivariate analysis of variance (PERMANOVA)," in *Wiley StatsRef: Statistics reference online*. Eds. N. Balakrishnan, T. Colton, B. Everitt, W. Piegorsch, F. Ruggeri and J. L. Teugels (Wiley), 1–15.

Anderson, S. C., Flemming, J. M., Watson, R., and Lotze, H. K. (2011a). Rapid global expansion of invertebrate fisheries: Trends, drivers, and ecosystem effects. *PloS One* 6 (3), 1–9. doi: 10.1371/journal.pone.0014735

Anderson, S. C., Flemming, J. M., Watson, R., and Lotze, H. K. (2011b). Serial exploitation of global sea cucumber fisheries. *Fish. Fish.* 12, 317–339. doi: 10.1111/j.1467-2979.2010.00397.x

Anderson, M. J., Gorley, R. N., and Clarke, K. R. (2008). *PERMANOVA+ for PRIMER: Guide to software and statistical methods. 1st ed* (Plymouth, UK: PRIMER-E).

Anderson, M. J., and Millar, R. B. (2004). Spatial variation and effects of habitat on temperate reef fish assemblages in northeastern new Zealand. *J. Exp. Mar. Biol. Ecol.* 305, 191–221. doi: 10.1016/j.jembe.2003.12.011

Anderson, M. J., and Willis, T. J. (2003). Canonical analysis of principal coordinates: a useful method of constrained ordination for ecology. *Ecology* 84, 511–525. doi: 10.1890/0012-9658(2003)084[0511:CAOPCA]2.0.CO;2

Bligh, E. G., and Dyer, W. J. (1959). A rapid method of total lipid extraction and purification. *Can. J. Biochem. Physiol.* 37, 911–917. doi: 10.1139/o59-099

Boncagni, P., Rakaj, A., Fianchini, A., and Vizzini, S. (2019). Preferential assimilation of seagrass detritus by two coexisting Mediterranean sea cucumbers: *Holothuria polii* and. *Holothuria tubulosa. Estuar. Coast.* 231, 106464. doi: 10.1016/j.ecss.2019.106464

Bordbar, S., Anwar, F., and Saari, N. (2011). High-value components and bioactives from sea cucumbers for functional food - a review. *Mar. Drugs* 9 (10), 1761–1805. doi: 10.3390/md9101761

Bulteel, P., Jangoux, M., and Coulon, P. (1992). Biometry, bathymetric distribution, and reproductive cycle of the holothuroid *Holothuria tubulosa (Echinodermata)* from Mediterranean Sea grass beds. *Mar. Ecol.* 13, 53–62. doi: 10.1111/j.1439-0485.1992.tb00339.x

CITES (2022) *Checklist of CITES species*. Available at: https://checklist.cites.org (Accessed December 14, 2020).

Cloern, J. E., Grenz, C., and Vidergar-Lucas, L. (1995). An empirical model of the phytoplankton chlorophyll: Carbon ratio-the conversion factor between productivity and growth rate. *Limnol. Oceanogr.* 40, 1313–1321. doi: 10.4319/lo.1995.40.7.1313

Conand, C. (2006). "Sea Cucumber biology, taxonomy, distribution and conservation status," in *Proceedings of the CITES workshop on the conservation of sea cucumbers in the families holothuriidae and stichopodidae*. Ed. A. W. Bruckner (Silver Spring, MD: NOAA Technical Memorandum NMFSOPR 34), 33–50.

Conand, C., Polidoro, B., Mercier, A., Gamboa, R., Hamel, J.-F., and Purcell, S. (2014). The IUCN red list assessment of aspidochirotid sea cucumbers and its implications. *SPC Beche-de-mer Inf. Bull.* 34, 3–7.

Costa, V., Mazzola, A., and Vizzini, S. (2014). *Holothuria tubulosa* gmelin 1791 (Holothuroidea, Echinodermata) enhances organic matter recycling in *Posidonia oceanica* meadows. *J. Exp. Mar. Bio. Ecol.* 461, 226–232. doi: 10.1016/j.jembe.2014.08.008

Coulon, P., and Jangoux, M. (1993). Feeding rate and sediment reworking by the holothuroid *Holothuria tubulosa (Echinodermata)* in a Mediterranean seagrass bed off ischia island, Italy. *Mar. Ecol. Prog. Ser.* 92, 201–204. doi: 10.3354/meps092201

Cubillo, A. M., Ferreira, J. G., Robinson, S. M. C., Pearce, C. M., Corner, R. A., and Johansen, J. (2016). Role of deposit feeders in integrated multi-trophic aquaculture – a model analysis. *Aquaculture* 453, 54–66. doi: 10.1016/j.aquaculture.2015.11.031

Danovaro, R. (2010). *Methods for the study of deep-sea sediments, their functioning and biodiversity* (Boca Raton: CRC Press, Taylor & Francis Group).

Danovaro, R., Dell'Anno, A., and Fabiano, M. (2001). Bioavailability of organic matter in the sediments of the porcupine abyssal plain, northeastern Atlantic. *Mar. Ecol. Prog. Ser.* 220, 25–32. doi: 10.3354/meps220025

Dar, M. A., and Ahmad, H. O. (2006). The feeding selectivity and ecological role of shallow water holothurians in the red Sea. *SPC Beche-de-mer Inf. Bull.* 24, 11–21.

Dell'Anno, A., Mei, M. L., Pusceddu, A., and Danovaro, R. (2002). Assessing the trophic state and eutrophication of coastal marine systems: a new approach based on the biochemical composition of sediment organic matter. *Mar. pollut. Bull.* 44, 611–622. doi: 10.1016/s0025-326x(01)00302-2

Dell'Anno, A., Pusceddu, A., Corinaldesi, C., Canals, M., Heussner, S., Thomsen, L., et al. (2013). Trophic state of benthic deep-sea ecosystems from two different continental margins off Iberia. *Biogeosciences* 10, 2945–2957. doi: 10.5194/bg-10-2945-2013

Dereli, H., and Aydın, M. (2021). Sea Cucumber fishery in Turkey: Management regulations and their efficiency. *Reg. Stud. Mar. Sci.* 41, 101551. doi: 10.1016/j.rsma.2020.101551

Fabiano, M., Danovaro, R., and Fraschetti, S. (1995). A three-year time series of elemental and biochemical composition of organic matter in subtidal sandy sediments of the ligurian Sea (Northwestern Mediterranean). *Cont. Shelf Res.* 15, 1453–1469. doi: 10.1016/0278-4343(94)00088-5

Gambi, C., Corinaldesi, C., Dell'Anno, A., Pusceddu, A., D'Onghia, G., Covazzi-Harriague, A., et al. (2017). Functional response to food limitation can reduce the impact of global change in the deep-sea benthos. *Global. Ecol. Biogeogr.* 26 (9), 1008–1021. doi: 10.1111/geb.12608

Gambi, C., Pusceddu, A., Benedetti-Cecchi, L., and Danovaro, R. (2014). Species richness, species turnover and functional diversity in nematodes of the deep Mediterranean Sea: Searching for drivers at different spatial scales. *Global. Ecol. Biogeogr.* 23 (1), 24–39. doi: 10.1111/geb.12094

Gerchakov, S. M., and Hatcher, P. G. (1972). Improved technique for analysis of carbohydrates in sediments. *Limnol. Oceanogr.* 17, 938–943. doi: 10.4319/lo.1972.17.6.0938

González-Wangüemert, M., Aydin, M., and Conand, C. (2014). Assessment of sea cucumber populations from the Aegean Sea (Turkey): first insights to sustainable management of new fisheries. *Ocean Coast. Manage.* 92, 87–94. doi: 10.1016/j.ocecoaman.2014.02.014

González-Wangüemert, M., Domínguez-Godino, J. A., and Cánovas, F. (2018). The fast development of sea cucumber fisheries in the Mediterranean and NE Atlantic waters: from a new marine resource to its over-exploitation. *Ocean Coast. Manage.* 151, 165–177. doi: 10.1016/J.OCECOAMAN.2017.10.002

González-Wangüemert, M., Valente, S., and Aydin, M. (2015). Effects of fishery protection on biometry and genetic structure of two target sea cucumber species from the Mediterranean Sea. *Hydrobiologia* 743, 65–74. doi: 10.1007/s10750-014-2006-2

Grosso, L., Rakaj, A., Fianchini, A., Morroni, L., Cataudella, S., and Scardi, M. (2021). Integrated multi-trophic aquaculture (IMTA) system combining the sea urchin *Paracentrotus lividus*, as primary species, and the sea cucumber *Holothuria tubulosa* as extractive species. aquaculture. *Aquaculture* 534, 736268. doi: 10.1016/j.aquaculture.2020.736268

Günay, D., Emiroğlu, D., and Suzer, C. (2019). Seasonal variations of digestive enzymes in sea cucumbers (*Holothuria tubulosa*, G. 1788) under culture conditions. *J. Exp. Zool.* 333 (3), 144–150. doi: 10.1002/jez.2336

Hammond, A. R., Meyers, L., and Purcell, S. W. (2020). Not so sluggish: movement and sediment turnover of the world's heaviest holothuroid, *Thelenota anax*. *Mar. Biol.* 167 (5), 1–9. doi: 10.13057/biodiv/d210552

Hartree, E. F. (1972). Determination of proteins: A modification of the lowry method that gives a linear photometric response. *Anal. Biochem.* 48, 422–427. doi: 10.1016/0003-2697(72)90094-2

Hartati, R., Zainuri, M, Ambariyanto, A, and Widianingsih, W (2020). Feeding selectivity of *Holothuria atra* in different micro-habitat in Panjang Island, Jepara (Java, Indonesia). *Biodiversitas* 21, 2233–2239. doi: 10.13057/biodiv/d210552

Holmer, M., Argyrou, M., Dalsgaard, T., Danovaro, R., Diaz-Almela, E., Duarte, C. M., et al. (2008). Effects of fish farm waste on *Posidonia oceanica* meadows: Synthesis and provision of monitoring and management tools. *Mar. Poll. Bull.* 56 (9), 1618–1629. doi: 10.1016/j.marpolbul.2008.05.020

Holmerm, M. (2010). Environmental issues of fish farming in offshore waters: Perspectives, concerns and research needs. *Aquac. Env. Int.* 1, 57–70. doi: 10.3354/aei00007

Horton, T., Kroh, A., Ahyong, S., Bailly, N., Boyko, C. B., Brandão, S. N., et al. (2018). *World register of marine species (WoRMS)*. Available at: https://www.marinespecies.org/imis.php?module=ref&refid=291592.

ICRAM (2001). *Sedimenti, scheda 3: Analisi delle caratteristiche granulometriche* (Roma, Italy: Italian Ministry for Environment), 122.

Ji, T., Dong, Y., and Dong, S. (2008). Growth and physiological responses in the sea cucumber, *Apostichopus japonicus* selenka: Aestivation and temperature. *Aquaculture* 283, 180–187. doi: 10.1016/j.aquaculture.2008.07.006

Kalantzi, I., and Karakassis, I. (2006). Benthic impacts of fish farming: Meta-analysis of community and geochemical data. *Mar. Poll. Bull.* 52, 484–493. doi: 10.1016/j.marpolbul.2005.09.034

Kim, T., Yoon, H. S., Shin, S., Oh., M. H., Kwon, I., Lee, J., et al. (2015). Physical and biological evaluation of co-culture cage systems for grow-out of juvenile abalone, *Haliotis discus hannai*, with juvenile sea cucumber, *Apostichopus japonicus* (Selenka), with CFD analysis and indoor seawater tanks. *Aquaculture* 447, 86–101. doi: 10.1016/j.aquaculture.2014.07.001

Koukouras, A., Sinis, A. I., Bobori, D., Kazantzidis, S., and Kitsos, M. S. (2007). The echinoderm *(Deuterostomia)* fauna of the Aegean Sea, and comparison with those of the neighbouring seas. *J. Biol. Res.* 7, 67–92.

Lamprianidou, F., Telfer, T., and Ross, L. G. (2015). A model for optimization of the productivity and bioremediation efficiency of marine integrated multitrophic aquaculture. estuar. *Coast. Shelf Sci.* 164, 253–264. doi: 10.1016/j.ecss.2015.07.045

Lohrer, A. M., Thrush, S. F., and Gibbs, M. M. (2004). Bioturbators enhance ecosystem function through complex biogeochemical interactions. *Nature* 431 (7012), 1092–1095. doi: 10.1038/nature03042

Lorenzen, C., and Jeffrey, J. (1980). Determination of chlorophyll in sea water. UNESCO. *Tech. Papers Mar. Sci.* 35, 1–20.

Lowry, O. H., Rosebrough, N. J., Farr, A. L., and Randall, R. J. (1951). Protein measurement with the folin phenol reagent. *J. Biol. Chem.* 193, 265–275. doi: 10.1016/S0021-9258(19)52451-6

MacDonald, C. L. E., Stead, S. M., and Slater, M. J. (2013). Consumption and remediation of European seabass (*Dicentrarchus labrax*) waste by the sea cucumber *Holothuria forskali*. *Aquac. Int.* 21, 1279–1290. doi: 10.1007/s10499-013-9629-6

MacTavish, T., Stenton-Dozey, J., Vopel, K., and Savage, C. (2012). Deposit-feeding sea cucumbers enhance mineralization and nutrient cycling in organically enriched coastal sediments. *PloS One* 7 (11), 50031. doi: 10.1371/journal.pone.0050031

Mangion, P., Taddei, D., Conand, C., and Frouin, P. (2004). "Feeding rate and impact of sediment reworking by two deposit feeders holothuria leucospilota and holothuria atra on fringing reef (Reunion island, Indian ocean)," in *Echinoderms: München*. Eds. T. Heinzeller and J. H. Nebelsick (London: Taylor and Francis), 311–317.

Marsh, J. B., and Weinstein, W. J. (1966). A simple charring method for determination of lipids. *J. Lipid Res.* 7, 574–576. doi: 10.1016/S0022-2275(20)39274-9

Mathieu-Resuge, M., Le Grand, F., Schaal, G., Kraffe, E., Lorrain, A., Letourneur, Y., et al. (2020). Assimilation of shrimp farm sediment by *Holothuria scabra*: A coupled fatty acid and stable isotope approach. *Aquat. Living Resour.* 33, 1–12. doi: 10.1051/alr/2020004

Mercier, A., Battaglene, S. C., and Hamel, J.-F. (1999). Daily burrowing cycle and feeding activity of juvenile sea cucumbers *Holothuria scabra* in response to environmental factors. *J. Exp. Mar. Biol. Ecol.* 239, 125–156. doi: 10.1016/S0022-0981(99)00034-9

Meysman, F. J. R., Galaktionov, O. S., Gribsholt, B., and Middelburg, J. J. (2006a). Bioirrigation in permeable sediments: advective pore-water transport induced by burrow ventilation. *Limnol. Oceanogr.* 51, 142–156. doi: 10.4319/lo.2006.51.1.0142

Meysman, F. J. R., Middelburg, J. J., and Heip, C. H. R. (2006b). Bioturbation: a fresh look at darwin's last idea. *Trend. Ecol. Evol.* 21 (12), 688–695. doi: 10.1016/j.tree.2006.08.002

Mezali, K., and Soualili, D. L. (2013). The ability of holothurians to select sediment particles and organic matter. *SPC Beche-de-mer Inf. Bull.* 33, 38–43.

Mirto, S., Bianchelli, S., Gambi, C., Krzelj, M., Pusceddu, A., Scopa, M., et al. (2010). Fish-farm impact on metazoan meiofauna in the Mediterranean Sea: Analysis of regional vs. habitat effects. *Mar. Env. Res.* 69, 38–47. doi: 10.1016/j.marenvres.2009.07.005

Moccia, D., Cau, A., Meloni, M. C., and Pusceddu, A. (2019). Small-scale distribution of metazoan meiofauna and sedimentary organic matter in subtidal sandy sediments (Mediterranean Sea). *Adv. Oceanogr. Limnol.* 10 (1), 57–66. doi: 10.4081/aiol.2019.8169

Navarro, P. G., García-Sanz, S., Barrio, J. M., and Tuya, F. (2013). Feeding and movement patterns of the sea cucumber *Holothuria sanctori*. *Mar. Biol.* 160, 2957–2966. doi: 10.1007/s00227-013-2286-5

Neofitou, N., Lolas, A., Ballios, I., Skordas, K., Tziantziou, L., and Vafidis, D. (2019). Contribution of sea cucumber *Holothuria tubulosa* on organic load reduction from fish farming operation. *Aquaculture* 501, 97–103. doi: 10.1016/j.aquaculture.2018.10.071

Paltzat, D. L., Pearce, C. M., Barnes, P. A., and McKinley, R. S. (2008). Growth and production of California sea cucumbers (*Parastichopus californicus* stimpson) co-cultured with suspended pacific oysters (*Crassostrea gigas* thunberg). *Aquaculture* 275, 124–137. doi: 10.1016/j.aquaculture.2007.12.014

Pasquini, V. (2022). *Reproductive biology and ecology of the sea cucumber holothuria tubulosa gmelin 1788* (Italy: University of Cagliari), 147. PhD thesis.

Pasquini, V., Giglioli, A. A., Pusceddu, A., and Addis, P. (2021). Biology, ecology and management perspectives of overexploited deposit-feeders sea cucumbers, with focus on *Holothuria tubulosa* (Gmelin 1788). *Adv. Oceanogr. Limnol.* 12 (2). doi: 10.4081/aiol.2021.9995

Pasquini, V., Porcu, C., Marongiu, F. M., Follesa, M. C., Giglioli, A. A., and Addis, P. (2022). New insights upon the reproductive biology of the sea cucumber *Holothuria tubulosa* (Echinodermata, holothuroidea) in the Mediterranean: Implications for management and domestication. *Front. Mar. Sci.* 9. doi: 10.3389/fmars.2022.1029147

Purcell, S. W. (2014). Value, market preferences and trade of beche-De-Mer from pacific island Sea cucumbers. *PloS One* 9 (4), 95075. doi: 10.1371/journal.pone.0095075

Purcell, S. W., Conand, C., Uthicke, S., and Byrne, M. (2016). Ecological roles of exploited sea cucumbers. *Oceanogr. Mar. Biol. Annu. Rev.* 54, 367–386. doi: 10.1201/9781315368597-8

Purcell, S. W., Mercier, A., Conand, S., Hamel, J. F., Toral- Granda, M. V., Lovatelli, A., et al. (2011). Sea Cucumber fisheries: Global analysis of stocks, management measures and drivers of overfishing. *Fish. Fish.* 14, 34–59. doi: 10.1111/j.1467-2979.2011.00443.x

Purcell, S. W., Hair, C. A., and Mills, D. J. (2012). Sea Cucumber culture, farming and sea ranching in the tropics: Progress, problems and opportunities. *Aquaculture* 368-369, 68–81. doi: 10.1016/j.aquaculture.2012.08.053

Pusceddu, A., Bianchelli, S., Canals, M., Sanchez-Vidal, A., Durrieu De Madron, X., Heussner, S., et al. (2010). Organic matter in sediments of canyons and open slopes of the Portuguese, Catalan, southern Adriatic and Cretan Sea margins. *Deep Sea Res. Part I Oceanogr. Res.* 57, 441–457. doi: 10.1016/j.dsr.2009.11.008

Pusceddu, A., Bianchelli, S., Gambi, C., and Danovaro, R. (2011). Assessment of benthic trophic status of marine coastal ecosystems: Significance of meiofaunal rare taxa. *Estuar. Coast. Shelf Sci.* 93, 420–430. doi: 10.1016/j.ecss.2011.05.012

Pusceddu, A., Dell'Anno, A., Danovaro, R., Manini, E., Sarà, G., and Fabiano, M. (2003). Enzymatically hydrolyzable protein and carbohydrate sedimentary pools as indicators of the trophic state of 'detritus sink' systems: a case study in a Mediterranean coastal lagoon. *Estuaries* 26, 641–650. doi: 10.1007/BF02711976

Pusceddu, A., Dell'Anno, A., Fabiano, M., and Danovaro, R. (2009). Quantity, biochemical composition and bioavailability of sediment organic matter as complementary signatures of benthic trophic status. *Mar. Ecol. Prog. Ser.* 375, 41–52. doi: 10.3354/meps07735

Pusceddu, A., Fraschetti, S., Mirto, S., Holmer, M., and Danovaro, R. (2007). Effects of intensive mariculture on sediment biochemistry. *Ecol. Appl.* 17 (5), 1366–1378. doi: 10.1890/06-2028.1

Rakaj, A., Fianchini, A., Boncagni, P., Lovatelli, A., Scardi, M., and Cataudella, S. (2018). Spawning and rearing of Holothuria tubulosa: a new candidate for aquaculture in the Mediterranean region. *Aquacult. Res.* 49, 557–568. doi: 10.1111/are.13487

Ramón, M., Simarro, G., Galimany, E., and Lleonart, J. (2019). Evaluation of sediment particle size selection during feeding by the holothurian *Parastichopus regalis* (Cuvier 1817). *Reg. Stud. Mar. Sci.* 31, 100763. doi: 10.1016/j.rsma.2019.100763

Reise, K. (2002). Sediment mediated species interactions in coastal waters. *J. Sea Res.* 48 (2), 127–141. doi: 10.1016/S1385-1101(02)00150-8

Rice, D. L. (1982). The detritus nitrogen problem: New observations and perspectives from organic geochemistry. *Mar. Ecol. Prog. Ser.* 9, 153–162. doi: 10.3354/meps009153

Roberts, D., Gebruk, A. V., Levin, V., and Manship, B. A. D. (2000). Feeding and digestive strategies in deposit-feeding holothurians. *Oceanogr. Mar. Biol. Ann. Rev.* 38, 257–310.

Schenone, S., O'Meara, T., and Thrush, S. F. (2019). Non-linear effects of macrofauna functional trait interactions on biogeochemical fluxes in marine sediments change with environmental stress. *Mar. Ecol. Progr. Ser.* 624, 13–21. doi: 10.3354/meps13041

Shpigel, M., Shauli, L., Odintsov, V., Ben-Ezra, D., Neori, A., and Guttman, L. (2018). The sea urchin, *Paracentrotus lividus*, in an integrated multi-trophic aquaculture (IMTA) system with fish (*Sparus aurata*) and seaweed (*Ulva lactuca*): Nitrogen partitioning and proportional configuration. *Aquaculture* 490, 260–269. doi: 10.1016/j.aquaculture.2018.02.051

Slater, M. J., and Carton, A. G. (2007). Survivorship and growth of the sea cucumber *Australostichopus* (Stichopus) *mollis* (Hutton 1872) in polyculture trials with green-lipped mussel farms. *Aquaculture* 272, 389–398. doi: 10.1016/j.aquaculture.2007.07.230

Slater, M. J., and Carton, A. G. (2009). Effect of sea cucumber (*Australostichopus mollis*) grazing on coastal sediments impacted by mussel farm deposition. *Mar. pollut. Bull.* 58 (8), 1123–1129. doi: 10.1016/j.marpolbul.2009.04.008

Slater, M. J., Jeffs, A. G., and Carton, A. G. (2009). The use of the waste from green-lipped mussels as a food source for juvenile sea cucumber, *Australostichopus mollis*. *Aquaculture* 292 (3–4), 219–224. doi: 10.1016/j.aquaculture.2009.04.027

Slater, M. J., Jeffs, A. G., and Sewell, M. A. (2011a). Selective movement and deposit-feeding in juvenile sea cucumber, *Australostichopus mollis* determined *in situ* and in the laboratory. *J. Exp. Mar. Bio. Ecol.* 409 (1-2), 315–323. doi: 10.1016/j.jembe.2011.09.010

Slater, M. J., Lassudrie, M., and Jeffs, A. G. (2011b). Method for determining apparent digestibility of carbohydrate and protein sources for artificial diets for juvenile sea cucumber, *Australostichopus mollis*. *J. World Aquacult. Soc* 42 (5), 714–725. doi: 10.1111/j.1749-7345.2011.00510.x

Solan, M., Cardinale, B. J., Downing, A. L., Engelhardt, K. A. M., Ruesink, J. L., and Srivastava, D. S. (2004). Extinction and ecosystem function in the marine benthos. *Science* 306 (5699), 1177–1180. doi: 10.1126/science.1103960

Stephens, D. W., and Krebs, J. R. (1986). *Foraging theory* (Princeton, NJ, USA: Princeton University Press).

Tolon, M. T., Emiroglu, D., Gunay, D., and Ozgul, A. (2017). Sea Cucumber (*Holothuria tubulosa* gmelin 1790) culture under marine fish net cages for potential use in integrated multitrophic aquaculture (IMTA). *Indian J. Geo. Mar. Sci.* 46, 749–756.

Tortonese, E. (1965). *Fauna d'Italia, Echinodermata* (Echinodermata. Fauna d'Italia: Ed. Calderini, Bologna.), 419.

Uthicke, S., and Karez, R. (1999). Sediment patch selectivity in tropical sea cucumbers (Holothuroidea: Aspidochirotida) analysed with multiple choice experiments. *J. Exp. Mar. Biol. Ecol.* 236, 69–87. doi: 10.1016/S0022-0981(98)00190-7

Wen, J., Hu, C., and Fan, S. (2010). Chemical composition and nutritional quality of sea cucumbers. *J. Sci. Food Agri.* 90, 2469–2474. doi: 10.1002/jsfa.4108

Wolfe, K., and Byrne, M. (2017). Biology and ecology of the vulnerable holothuroid, *Stichopus herrmanni*, on a high-latitude coral reef on the great barrier reef. *Coral Reefs.* 36 (4), 1143–1156. doi: 10.1007/s00338-017-1606-5

Wolfe, K., Deaker, D. J., Graba-Landry, A., Champion, C., Dove, S., Lee, R., et al. (2021). Current and future trophic interactions in tropical shallow-reef lagoon habitats. *Coral Reefs.* 40 (1), 83–96. doi: 10.1007/s00338-020-02017-2

Wolfe, K., Vidal-Ramirez, F., Dove, S., Deaker, D., and Byrne, M. (2018). Altered sediment biota and lagoon habitat carbonate dynamics due to sea cucumber bioturbation in a high-pCO_2 environment. *Glob. Change Biol.* 24 (1), 465–480. doi: 10.1111/gcb.13826

Yamazaki, Y., Sakai, Y., Mino, S., Suda, W., Hattori, M., Meirelles, P. M., et al. (2019). Repeated selective enrichment process of sediment microbiota occurred in sea cucumber guts. *Environ. Microbiol. Rep.* 11 (6), 797–807. doi: 10.1111/1758-2229.12791

Yang, H., Zhou, Y., Zhang, T., Yuan, X., Li, X., Liu, Y., et al. (2006). Metabolic characteristics of sea cucumber, *Apostichopus japonicus* (Selenka) during aestivation. *J. Exp. Mar. Biol. Ecol.* 330, 505–510. doi: 10.1016/j.jembe.2005.09.010

Yang, H., and Bai, Y. (2015). "Apostichopus japonicus in the life of Chinese people". in *The Sea cucumber Apostichopus japonicus. history, biology, and aquaculture*. Eds. H. Yang, J. F. Hamel and A. Mercier (Academic Press), 1–24.

Yingst, J. Y. (1982). Factors influencing rates of sediment ingestion by *Parastichopus parvimensis* (Clark), an epibenthic deposit-feeding holothurian. *Estuar. Coast. Shelf Sci.* 14, 119–134. doi: 10.1016/S0302-3524(82)80040-6

Yuan, X., Yang, H., Meng, L., Wang, L., and Li, Y. (2013). Impacts of temperature on the scavenging efficiency by the deposit-feeding holothurian *Apostichopus japonicus* on

a simulated organic pollutant in the bivalve-macroalage polyculture from the perspective of nutrient budgets. *Aquaculture* 406–407, 97–104. doi: 10.1016/j.aquaculture.2013.05.009

Yu, Z., Zhou, Y., Yang, H., Ma, Y., and Hu, C. (2014). Survival, growth, food availability and assimilation efficiency of the sea cucumber *Apostichopus japonicus* bottom-cultured under a fish farmin southern China. *Aquaculture*, 426–427, 238–248. doi: 10.1016/j.aquaculture.2014.02.013

Zamora, L. N., and Jeffs, A. G. (2011). Feeding, selection, digestion and absorption of the organic matter from mussel waste by juveniles of the deposit-feeding sea cucumber, *Australostichopus mollis*. *Aquaculture* 317 (1–4), 223–228. doi: 10.1016/j.aquaculture.2011.04.011

Zamora, L. N., and Jeffs, A. G. (2012). The ability of the deposit-feeding sea cucumber *Australostichopus mollis* to use natural variation in the biodeposits beneath mussel farms. *Aquaculture* 326–329, 116–122. doi: 10.1016/j.aquaculture.2011.11.015

Zhou, Y., Yang, H., Liu, S., Yuan, X., Mao, Y., Zhang, T., et al. (2006). Feeding and growth on bivalve biodeposits by the deposit feeder *Stichopus japonicus* selenka Echinodermata: Holothuroidea) co-cultured in lantern nets. *Aquaculture* 256 (1–4), 510–520. doi: 10.1016/j.aquaculture.2006.02.005

frontiers | Frontiers in Marine Science

TYPE Original Research
PUBLISHED 14 February 2023
DOI 10.3389/fmars.2023.1033710

OPEN ACCESS

EDITED BY
Libin Zhang,
Institute of Oceanology (CAS), China

REVIEWED BY
Gianna Innocenti,
University of Florence, Italy
Piero Cossu,
University of Sassari, Italy

*CORRESPONDENCE
Paolo Stara
paolostara@yahoo.it
Maria Cristina Follesa
follesac@unica.it
Rita Cannas
rcannas@unica.it

†These authors share first authorship

SPECIALTY SECTION
This article was submitted to Marine Biology, a section of the journal Frontiers in Marine Science

RECEIVED 31 August 2022
ACCEPTED 12 January 2023
PUBLISHED 14 February 2023

CITATION
Stara P, Melis R, Bellodi A, Follesa MC, Corradini C, Carugati L, Mulas A, Sibiriu M and Cannas R (2023) New insights on the systematics of echinoids belonging to the family Spatangidae Gray, 1825 using a combined approach based on morphology, morphometry, and genetics. *Front. Mar. Sci.* 10:1033710. doi: 10.3389/fmars.2023.1033710

New insights on the systematics of echinoids belonging to the family Spatangidae Gray, 1825 using a combined approach based on morphology, morphometry, and genetics

Paolo Stara[1*†], Riccardo Melis[2†], Andrea Bellodi[2†], Maria Cristina Follesa[2*], Carlo Corradini[3], Laura Carugati[2], Antonello Mulas[2], Michela Sibiriu[2] and Rita Cannas[2*]

[1]Centro Studi di Storia Naturale del Mediterraneo, Geomuseo Monte Arci, Masullas, Italy, [2]Department of Life and Environmental Sciences, University of Cagliari, Cagliari, Italy, [3]Dipartimento di Matematica e Geoscienze, Università di Trieste, Trieste, Italy

Spatangoids are probably the least resolved group within echinoids, with known topological incongruencies between phylogenies derived from molecular (very scarce) and morphological data. The present work, based on the analysis of 270 specimens of Spatangidae (Echinoidea, Spatangoida) trawled in the Sardinian seas (Western Mediterranean), allowed us to verify the constancy of some characters that we consider to be diagnostic at the genus level —such as the path of the subanal fasciole and the relationship between labrum and adjacent ambulacral plates —and to distinguish two distinct forms within the studied material. Based on morphological characters, morphometrics, and molecular analyses (sequencing of two mitochondrial markers: cytochrome *c* oxidase subunit1 (COI) and 16S), most of the individuals were classified as morphotype A and attributed to the species *Spatangus purpureus*, the most common spatangoid in the Mediterranean Sea, while a few corresponded to a different morphotype (B), genetically close to the species *Spatangus raschi*. Preliminary morphological analyses seemed to indicate that morphotype B specimens from Sardinia are slightly different from *S. raschi* and from *Spatangus subinermis* individuals, the second species of the family known to occur in the Mediterranean Sea. On the basis of morpho-structural observations and molecular analyses, comparing Mediterranean living forms with species from other areas (Central Eastern Atlantic, North Sea and neighboring basins, South African Sea, Philippines and Indonesian Archipelago, New Zealand, and Hawaiian Islands), the clear distinction of *S. purpureus* from several other species classified as *Spatangus* was confirmed. Based on the morphological and genetic differences, we propose to maintain the genus *Spatangus* including in it only the type species *S. purpureus* among the living species and to establish the new genus *Propespatagus* nov. gen. to include several other species previously classified as *Spatangus*. The clear distinction among different genera was also detected in fossil forms of *Spatangus*, *Propespatagus* nov. gen., and *Sardospatangus* (†) from the European Oligo-Miocene sedimentary rocks of Germany; the Miocene of Ukraine, Italy, and

North Africa; the Plio-Pleistocene of Italy; and the Mio-Pliocene of Florida (USA). The new data can help in addressing taxonomic ambiguities within echinoids, as well as in improving species identification, and hence biodiversity assessments in the Mediterranean region.

KEYWORDS

echinoids, *Propespatagus*, new genus, Mediterranean, DNA analyses, morphology, morphometrics

1 Introduction

Irregular sea urchins (Irregularia), predominantly infaunal and bilaterally symmetrical forms covered by small and specialized spines (Mongiardino Koch et al., 2022), are subdivided into Atelostomata (heart urchins and allies) and Neognathostomata (sand dollars, sea biscuits, and "cassiduloids") (Mongiardino Koch et al., 2022). Atelostomata are recognized as the most diverse of the clades of echinoids (Kroh, 2020). Thanks to their robust globular skeleton (the test), plenty of morphological data are available for both extant and extinct species (Kroh and Smith, 2010; Mongiardino Koch and Thompson, 2021). Despite this, studies on their systematics and diffusion in different oceans are sparse, apart from some important recent works (Smith and Stockley, 2005; Smith et al., 2006; Kroh and Smith, 2010; Ziegler et al., 2012 and citations therein), but many of them are relatively old (Mortensen, 1907; Clark, 1917; Mortensen, 1948; Mortensen, 1951; Serafy and Fell, 1985; Baker and Rowe, 1990, and citations therein). Furthermore, in addition to the descriptions based on morphological characters (Shin, 2013; Filander and Griffiths, 2017), there are only a few recent studies based on structural analysis (Sumida et al., 2001).

It has been demonstrated that fossil taxa improve phylogenetic analysis of morphological datasets, even when highly fragmentary (Mongiardino Koch, 2021).

Apart from morpho-structural data (from fossils and living species), genetic data could represent complementary resources for unraveling the phylogenetic relationships (Mongiardino Koch et al., 2022).

In general, these two approaches, morphological and molecular, have been developed largely in isolation, with very few studies integrating them. Moreover, conflicts between morphological and molecular evidence often provided unclear results (Smith et al., 2006; Kroh and Smith, 2010; Thompson et al., 2017; Mongiardino Koch et al., 2018). However, the continuous development of new data sets and methods has allowed for important recent advances. For instance, Kroh (2020) proposed a revised classification that incorporates results from morphological as well as phylogenetic and phylogenomic studies, suggesting that this classification could be further modified as taxon sampling of phylogenomic analyses increases, reducing the areas of conflict between morphological and molecular data. Mongiardino Koch and Thompson (2021) demonstrated that combining different data sources increases topological accuracy and helps resolve conflicts between molecular and morphological data. Similarly, Mongiardino Koch et al. (2022), using 18 novel genomes and transcriptomes to build a phylogenomic dataset with a near-complete sampling of major lineages, revised the phylogeny and divergence times of echinoids and place their history within the broader context of echinoderm evolution.

The present study focuses on irregular sea urchins of the family Spatangidae Gray, 1825, according to Smith and Kroh (2011) and Kroh and Mooi (2022), which includes three genera: *Spatangus* Gray, 1825, *Plethotaenia* H.L. Clark, 1917, and *Granopatagus* Lambert, 1915. The first genus is reported to be present all over the world, while the second is restricted to the Caribbean Sea (Mortensen, 1951; Néraudeau et al., 2010; Kroh and Mooi, 2022).

The third, *Granopatagus*, is controversial. According to Smith and Kroh (2011), it includes four species: two are extant species (*Granopatagus inermis* Mortensen, 1913, distributed in the Mediterranean and along the Atlantic-European coasts, and *Granopatagus paucituberculatus* (Agassiz & Clark, 1907) from Hawaii), while the other two are fossil species (*Granopatagus lonchophorus* (Meneghini, in Desor, 1858) and *Granopatagus subinermis* (Pomel, 1883)). On the contrary, according to Kroh and Mooi (2022), *Granopatagus* includes only the fossil species *Granopatagus loncophorus*, while the other three species are moved to the genus *Spatangus*, and the two distinct species *G. inermis* and *G. subinermis* unified as *Spatangus subinermis* (fossil+recent).

The distinctive characters of the genus *Granopatagus* were never fully described. Originally, Lambert (1915) proposed *Granopatagus* as a sub-genus of *Spatangus* on the basis of 1) a very deep sinus, 2) very short petals, and 3) the almost total lack of primary tubercles. However, these characters are not distinctive at a genus level; moreover, the type specimen used for the description, once kept in the Museum of the University of Pisa, is no longer available.

Recently, a further genus, *Sardospatangus* Stara, Charbonnier et Borghi, 2018, has been proposed by Stara et al. (2018). It is an extinct genus of which only fossil species are known in peri-mediterranean sedimentary rocks.

Based on previous reports, there are two extant species of Spatangidae present in the Mediterranean continental shelf and offshore: *Spatangus purpureus* Müller, 1776 (Figure S1), i.e., the type species of the genus *Spatangus*, and *S. subinermis* (*sensu* Kroh and Mooi, 2022).

To date, only a few reports or studies have been published on the Mediterranean populations of these two species (Risso, 1826; Mortensen, 1913; Bonnet, 1926; Tortonese, 1965; Borri et al., 1990).

To solve the numerous taxonomic uncertainties of this and other genera, starting from the middle of the last century, several researchers have been oriented toward the analysis of the pattern (scheme) of the plates composing the test (test plating) and on their fasciole pathways (Kroh, 2005; Smith and Stockley, 2005; Kroh, 2007; Stara et al., 2016; Stara et al., 2018).

Despite the observations on heterochrony previously published by Mc Namara (1982; 1987; 1988; 1989), where the authors reported a wide variability in the relationships between the plates (spatangoids not included in the studies), raising doubts about their use in systematic diagnostics, these characters proved to be valid. Smith and Stockley (2005), analyzing a large number of 89 species belonging to several genera, stated that the fasciole pathways are highly conservative, and therefore, the authors considered them distinctive characters of considerable phylogenetic (and systematic) importance. Similarly, Stara et al. (2018) considered the number of plates adjacent to the labrum and the shape, size, and reciprocal position of the plates that compose the oral face of spatangoids and spatangids as a set of highly diagnostic characters in systematic studies.

On the contrary, in the past, only rare comparative studies based on molecular analysis of spatangids were performed (Littlewood and Smith, 1995; Smith et al., 1995; Stockley et al., 2005; Smith et al., 2006; Kroh and Smith, 2010; Kroh, 2020).

The main goal of this work focused on the family Spatangidae, a group of spatangoids whose phylogenetic relationships are less resolved (Kroh, 2020), is to describe the spatangids collected in the Sardinian seas, to clearly identify the species collected, and to clarify their systematic position. The genus-level diagnostic characters used by Stara et al. (2018), such as the shape and arrangement of certain plates that compose the plastron of the oral face, are primarily used. The Sardinian spatangids are compared with both fossil species (from European and peri-mediterranean locations) and extant species (distributed worldwide).

Morphometric measurements and genetic analyses are used in combination for the first time to complement and support the results of the structural–morphological analyses.

The diagnostic characters, useful to distinguish the different forms under study (genera and/or species), are fully described and discussed. The new data can help in addressing taxonomic ambiguities within echinoids, as well as in improving species identification, and hence biodiversity assessments in the Mediterranean region.

2 Material and methods

2.1 Sampling

The study was primarily based on the analysis of 270 recent spatangids, trawled along the coasts of Sardinia during the experimental Mediterranean International Trawl Surveys (MEDITS; Spedicato et al., 2019) from 2018 to 2019 or available in museum collections (Figure 1 and Table 1). A subset of 21 specimens was preserved in alcohol for the genetic analyses, while the others were preserved as dried tests and were mostly deprived of spines.

To compare the oral schemes of the Sardinian samples and other extant species, fossils of Spatangidae of sedimentary rocks from the Oligocene to Pleistocene were studied from 1) Europe (Germany, Ukraine, and Italy), 2) North Africa (Melilla, Spain), and 3) USA (Florida). Other data, used for comparison in morphometric analyses or the plating reconstruction, were taken from bibliographic or museum sources (Table 1).

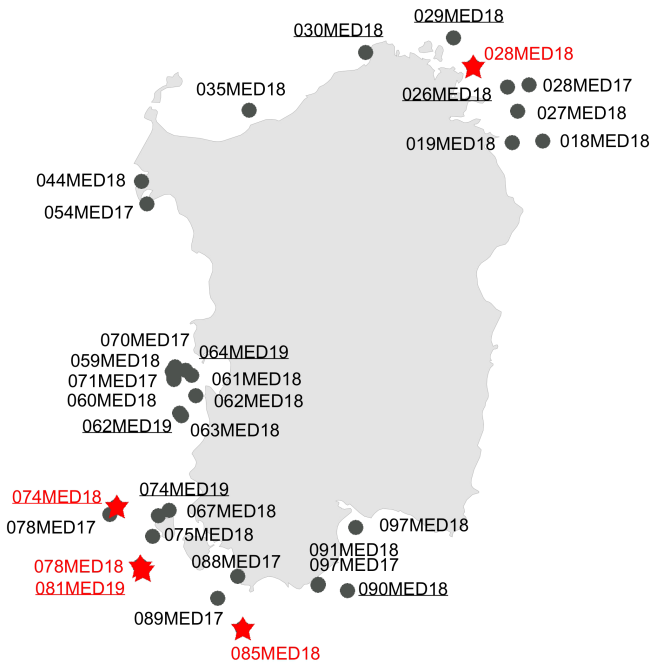

FIGURE 1
Map of the site collection during the MEDITS trawling campaign carried out along the Sardinian coasts. Circles in black = morphotype A (*Spatangus purpureus*); same red = morphotype B (*Propespatagus* sp. 1).

10.3389/fmars.2023.1033710

TABLE 1 Summary information on the spatangids analyzed.

Species	Institution	Acronym	Recent or fossil	Locality	N	Notes	Reference
Spatangus purpureus	Università degli studi di Cagliari, Italia	UNICA	Recent	Sardinia (Western Mediterranean)	230	Morphotype A	Present study
S. purpureus	Museo Aquilegia Masullas, Italia	MAC	Recent	Sardinia (Western Mediterranean)	30	Morphotype A	Present study
***Propespatagus* sp. 1**	Università degli studi di Cagliari	UNICA	Recent	Sardinia (Western Mediterranean)	9	Morphotype B	Present study
***Propespatagus* sp. 1**	Museo Aquilegia Masullas, Italia	MAC	Recent	Sardinia (Western Mediterranean)	1	Morphotype B	Present study
Spatangus* cf. *purpureus	Museo Aquilegia Masullas, Italia	MAC	Fossil	Pliocene Otranto, Puglia, Italy	1	MAC PL.2015 Pliocene	Present study
Spatangus* cf. *purpureus	Museo Aquilegia Masullas, Italia	MAC	Fossil	Terre Rosse, Siena Tuscany, Italy	1	MAC PL.2016 Pliocene	Present study
Spatangus* cf. *purpureus	Museo Aquilegia Masullas, Italia	MAC	Fossil	Ostia, Latium, Italy	1	MAC PL.2017 Pleistocene, Holocene	Present study
Spatangidae ind.	Museo Aquilegia Masullas, Italia	MAC	Fossil	Chesapeake Bay, Florida, USA	1	Cas.003, Caschili Collection Mio-Pliocene	Present study
S.* cf. *purpureus	Museo Aquilegia Masullas, Italia	MAC	Fossil	Otranto, Puglia,	1	F. Ciapelli Collection, Prato, Italy, Pliocene nn	Present study
***Propespatagus* sp.**	Museo Aquilegia Masullas, Italia	CIA.C MAC	Fossi	Otranto, Puglia,	2	F. Ciapelli Collection, Prato, Italy, Pliocene. classified as *Granopatagus* sp.nn	Present study
Sardospatangus caschilii	Museo Aquilegia Masullas, Italia	MAC	Fossil	Isili, Cagliari province, Sardinia	7	Miocene, Burdigalian, PL.344; 1551–1556	Stara et al., 2018
***Propespatagus* sp. 1**	Donné d'Observations pour la Reconnaissance et l'Identification de la faune et la flore Subaquatiques	DORIS	Recent	France, N–W Mediterranean	1	Classified as *Spatangus subinermis*	https://doris.ffessm.fr. n 1253 Foto Frèdéric CHEREAU
Propespatagus* cf. *subinermis	Museo paleontologico il Mare Antico Salsomaggiore Terme	MUMAB	Fossil	Plio-Pleistocene Rio Stirone, Parma	2	Coll. E. Borghi Moden, as *Granopatagus subinermis.* nn	Néraudeau et al., 1998
Propespatagus* cf. *subinermis	Museo paleontologico il Mare Antico Salsomaggiore Terme	MUMAB	Fossil	Plio-Pleistocene Rio Stirone, Parma	1	Coll. E. Borghi Modena, as *G. subinermis.* nn	Néraudeau et al., 1998
Spatangus* cf. *purpureus	Museo paleontologico il Mare Antico Salsomaggiore Terme	MUMAB	Fossil	Plio-Pleistocene Rio Stirone, Parma	1	Coll. E. Borghi Modena nn	Néraudeau et al., 1998
Spatangus inermis Mortensen (1913)	Stazione Zoologica Anton Dorn, Naples, Italy	SZN	Recent	Ischia, gulf of Naples	2	Holotype no. 1097 and 1 Paratype number	Mortensen, 1913

(Continued)

TABLE 1 Continued

Species	Institution	Acronym	Recent or fossil	Locality	N	Notes	Reference
***Spatangus* sp2**	Natural History Museum of Vienna, Geological— Paleontological Department, Austria	NHMW	Fossil	Badenian (Miocene) of Podjarków, bei Kurovice, Ukraine	1	(Sptangus desmaresti) No. 1859.0045.556	Kroh (2005)
***Spatangus desmaresti* Goldfuss, 1829**	Museum d'Histoire Naturelle, Genève, Suisse	MHNG	Fossil	Doberg, Westphalia, Germany.	1	de Loriol collection no. 127-27828	Smith and Kroh, 2011
***Spatangus saheliensis* Pomel, 1887**	Muséum National d'Histoire Naturelle, Paris, France	MNHNF	Fossil	Miocene-Pliocene of Melilla, Spain	1	Coll. Lachkhem no. R62132	Lachkhem and Roman, 1995
***Spatangus californicus* H.L. Clarck**	Muséum National d'Histoire Naturelle, Paris, France	MNHNF	Recent	S. Catalina Island, California, USA Japan	2	A66829 L23322 Stored as *Spatangus luetckeni*	Present study Mortensen, 1951
***Spatangus luetckeni* A, Agassiz, 1872**	–	–	Recent	Hokodate, Japan	1	–	Schultz, 2009, in Kroh and Mooi, 2022
***Propespatagus paucituberculatus* (A. Agassiz & H.L. Clarck, 1902)**	Museum of Comparative Zoologiy at Harvard.	MCZ Harvard	Recent	Hawaiian Islands	1	Plate III	Mortensen, 1951
***Propespatagus multispinus* (Mortensen, 1925)**	Copenaghen Museum Museum of New Zealand	NHMD	Recent	Aukland-Campbell Island New Zealand	2	Cotype Plate II Type n ECH.82	Mortensen, 1951 Collections.tepapa.govt.nz
***Propespatagus capensis* (Döderlein, 1905)**	–	–	Recent	East London S. Africa	1	Plate I	Mortensen, 1951
***Propespatagus raschi* (Lovén, 1896)**	The Swedish Museum of Natural History	SMNH	Recent	Shetland Islands North Atlantic	2	Plate XIII PlateII	Lovén, 1896 Mortensen, 1951
***S. californicus* H.L. Clarck**	–	–	Recent	Baja California, Mexico	1	Plate II	Mortensen, 1951
***Spatangus mathesoni*, McKnight, 1967**	National Institute of Water & Atmospheric Research	NIWA	Recent	New Zealand	2	Paratype P-42 and no. 50049	Present study
***Plethotaenia spatangoides* (A. Agassiz, 1883)**	–	–	Recent	Cuba	1	Plate 39, Figures 1–10	Mortensen, 1951.
***Plethotaenia angularis* Chesher, 1968**	–	–	Recent	Bahama to Barbados, Caribbean	1		Chesher, 1968;Schultz, 2009, in Kroh and Mooi, 2022
***P. angularis* Chesher, 1968**	Smithsonian Institution	NMNH	Recent	Caribbean	1	E10726,	Chesher, 1968;Smith and Kroh, 2011

The institution is responsible for the sampling or the possession of museum collections and related acronyms, the locality of the collection, and the number of specimens, notes, and references. In the first column, the species name corresponds to the new denomination proposed in this study.

2.2 Structural, morphological, and biometric analyses

The biometric measurements taken from the samples analyzed in this work are illustrated in Figures 2A, B. The abbreviations used are those commonly used in specialist literature.

TL = length of the test; TW = width of the test; TH = height of the test; α = angle of divergence between the anterior paired petals; β = angle of divergence between the posterior paired petals; L1 = height of the periproct, detected along the interradial sutures; L2 = width of the periproct, at the widest point, as shown in Figure 2A; L3 = distance between the lower edge of the periproct and the support base of the test; L4 and L5, length and width of the anterior paired petals, respectively; L6 and L7, length and width of the posterior paired petals, respectively; L8 = distance between the frontal genital pores and the posterior margin of the test; L9 = depth of the sinus anterior to the ambitus; L10 = distance between the most advanced point of the front "shoulders" of the test; L11 = distance between the anterior margin of the labrum and the anterior margin of the test; L12 = length of the labrum L13 = length of the sternal plates; L14 = width at the basis of the labrum; L15 = width of the group of plates formed by the sternals and those belonging to the adjacent ambulacra I and V; L16 = maximum width of the sternal plates; L17; distance between the two outermost points, in transverse section, of the sub-anal fasciole; FW = fasciole width (thickness).

Measurements of TL, TH, and TW were performed using a caliper measuring to one-twentieth of a millimeter; TL was reported in mm, while the other measurements were reported in % of TL; the length and

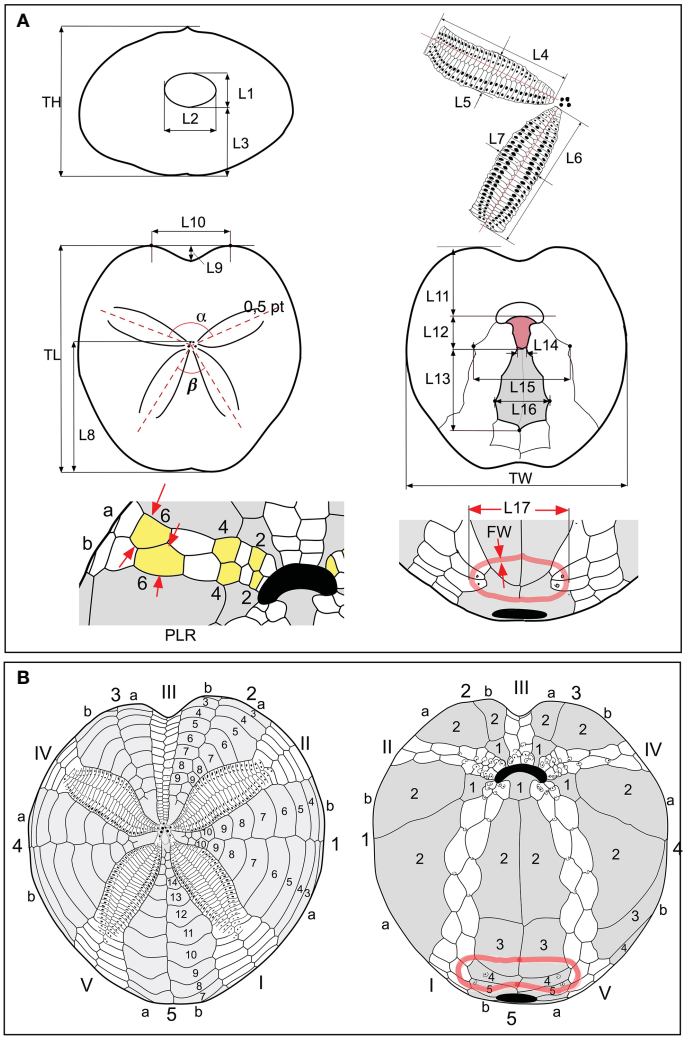

FIGURE 2
(A) Scheme of biometric measurements used in this study. **(B)** Conventional numbering of plates according to Lovén (1874). The ambulacral plates are numbered in Roman numerals; the interambulacral in Arabic numerals. Each area is divided into two columns "a" and "b"; the count occurs counterclockwise in the aboral view and clockwise in the oral view.

width of the front petal (L4 and L5) were measured by a caliper in mm and then converted into % of TL; the same for the measurements concerning the periproct (L1, L2, and L3); the measurement of L1 was taken between the opening point of the periproct along the interradial suture of interambulacrum 5; the other measurements were taken from the photos, as detailed below; the angles are reported in degrees. To obtain these measurements, each specimen included in the database was photographed by a Nikon D 300s camera, equipped with a Zeiss Macro-Planar 2/50 mm lens, in order to minimize distortions. Adoral, posterior, and anterior photographs were taken with the camera perpendicular to the interested faces. Each view is the result of many photos combined using the Helicon Focus program, version 4.2.9, d-STUDIO for Mac OS X, in order to optimize the final depth of field. The other morphometric characters were determined directly in % of TL, from the photos analyzed in the Autodesk Graphic 3.1 program, for Mac.

In addition to the specimens caught in Sardinian seas, the morphological analyses included a further 39 specimens (Table 1) in four genera: *Sardospatangus* Stara, Charbonnier et Borghi, 2018 (†); *Spatangus* Gray, 1825; *Pletothaenia* Clark, 1917; and *Granopatagus* Lambert, 1915.

With the use of a similarity matrix based on the Euclidean distance, multivariate differences in the morphological measurements of the different samples were illustrated by the Canonical Analysis of Principal Coordinates (CAP; Anderson and Willis, 2003), obtained using the PRIMER v7 software. The Primer V7 software also used to verify the statistical significance of the differences between the groups identified by the CAP, through the analysis of similarities (ANOSIM) test, and to identify which measurements contributed to these differences, by means of the SIMPER test (SIMilarity PERcentages) (Clarke and Gorley, 2015).

The test plating in oral and aboral views of all the species analyzed in this work was drawn following Lovén (1874) (Figure 2B).

Boxplots (Figure S2), with interpolation of the quartiles, were obtained using the software PAST 3.11, Paleontological Statistics software package for education (Hammer et al., 2001).

2.3 DNA extraction, amplification, sequencing, and alignment

A subset of the specimens analyzed morphologically were investigated using molecular tools. Genomic DNA was extracted using a PureLink® Genomic DNA Kit, based on the selective binding of DNA to a silica-based membrane, according to the manufacturer's protocol. The genomic DNA was eluted in 50 µl of Elution Buffer (10 mM of Tris-HCl).

Two genes were selected for analysis: the mitochondrial 16S rRNA (16S) and cytochrome *c* oxidase subunit1 (COI). Polymerase chain reaction (PCR) amplification of fragments was performed with 25-µl reaction volume. Each reaction tube contained 3.5 µl of 10× buffer (Dream Taq® buffer, Thermo Fisher Scientific, Waltham, MA, USA), 2.5 µl of 2 mm dNTPs, 0.2 µl of each 20 mm primer, 0.16 µl of Taq polymerase (Dream Taq® Thermo Fisher Scientific), and 2.5 µl of DNA (50–100 ng). COI fragment was amplified using the primer pair EchinoF1 (5′-TTTCAACTAATCATAAGGACATTGG-3′) and EchinoR1 (5′-CTTCAGGGTGTCCAAAAAATCA-3′) (Ward et al., 2008). PCRs started with denaturation at 95°C (5 min) and were followed by 95°C (30 s), 50°C (60 s), and 72°C (60 s) for 35 cycles. The 16S fragment was amplified using the primer pair 16 Sar (5′-CGCC TGTTTATCAAAAACAT-3′) and 16Sbr (5′-CCGGTCTGAAC TCAGATCACGT-3′) (Palumbi et al., 1991). PCR conditions used were denaturation at 94°C (2 min) followed by 94°C (25 s), 47°C (60 s), and 72°C (60 s) for 40 cycles. The PCR products were checked on an agarose gel (1.5%) with SYBR® Safe DNA Gel Stain (10,000×). Purification and sequencing were carried out by Macrogen Europe (Amsterdam, The Netherlands). Alignments were elaborated using the ClustalW method (Thompson et al., 1994) implemented in MEGA v7 (Kumar et al., 2016).

2.4 Genetic analyses and phylogenetic reconstructions

Since the partition homogeneity test implemented in PAUP* v4.0a169 (Swofford, 2003) indicated that the 16S and the COI datasets did not significantly differ in their phylogenetic signal ($p = 0.53$), the two mtDNA markers were analyzed separately and concatenated. The principal indices of genetic diversity (the number of haplotypes [H], haplotype diversity [hd], nucleotide diversity [π] and relative standard deviations, and the average number of nucleotide differences [k]) were estimated in DnaSP, while the p-distance among sequences and between the two *Spatangus* morphotypes were performed in MEGA. In order to evaluate the relationship among the sequences from Sardinian specimens and the homologous sequences deposited for the genus *Spatangus* in GenBank and BOLD public databases, PAUP and MrBayes v3.2.6 (Ronquist et al., 2012) software were also used for the phylogenetic reconstruction. Specifically, four different methods were used to investigate the phylogeny: the neighbor joining (NJ), the maximum parsimony (MP), and the maximum likelihood (ML), performed in PAUP with 1,000 bootstrap replicates, and the Bayesian inference (BI) method obtained using MrBayes with 20 million generations and 25% of burn-in. In the phylogenetic reconstructions, sequences of *Echinocardium laevigaster* A. Agassiz, 1869 (COI: AJ639913; 16S: AJ639813; Stockley et al., 2005) and *Brissus unicolor* (Leske, 1778) (COI: MN683889-91 (Collin et al., 2020); 16S: AJ639822, Stockley et al., unpublished) were used as the outgroup.

The molecular data were also combined into a matrix of 38 morphological characters, since the use of independently evolving characters together may best represent the evolution of the species and improve the accuracy of phylogenetic reconstructions (Chippindale and Wiens, 1994; Huelsenbeck et al., 1996; Bucklin and Frost, 2009). The matrix considers only the 38 characters that can be better applied to spatangids than that by Stockley et al. (2005) and Kroh and Smith (2010), which include 88 characters. The full list of morpho-structural characters and character state definitions used in phylogenetic reconstructions are listed in the Supplementary Material and Table S1.

The combined morphological/molecular dataset was statistically evaluated for incongruence using the partition homogeneity test, and the phylogenetic trees were reconstructed using the same approaches and the same software described for the molecular analysis: weight = 5 and 1 for morphological and molecular characters, respectively, as described in Bucklin and Frost (2009). The same methods were applied using only the morphological character matrix, but in this case, all characters were unordered and unweighted.

3 Results

3.1 Morphology–morphometrics

Considering the whole sample of spatangids collected in Sardinian seas, two different morphotypes were found: the vast majority of specimens (n = 260) corresponded to m orphotype A, i.e., the commonest Mediterranean species S. purpureus, while 10 specimens, provisionally referred to here as morphotype B, showed a similar general shape to morphotype A but a different plastron plating. The observations made on the specimens collected in Sardinian seas are summarized in Table 2. The test size (TL) ranges from 64.5 to 123 mm, but with the largest frequency of medium-large individuals, from 93 to 110 mm. The sample showed a wide variability of the main measurements, but some characters have a lower variability (low SD).

CAP analysis based on a similarity matrix of the Euclidean distances clearly identified two groups (Figure 3) (ANOSIM $p < 0.05$). The SIMPER test (Table S2) highlighted the contribution of the 10 variables in the differentiation of the two morphotypes. The top five variables that provided the greatest contribution to the differentiation in decreasing order are L17 (16.93%), L4 (9.76%), L3 (6.74%), L16 (6.73%), and L6 (6.58%). The difference between morphotypes A and B is clearly visually highlighted in the boxplot of Figure S2 based on L17 and FW measurements.

Considering the plating (Figures 2A, B, 4A, B), the main differences between the two forms were found in the following: 1) the fasciole pathway, which is broad and surrounds two lobes (bilobed) on the episternal plates in morphotype A (mean L17 = 41.67), which is small and surrounds only one lobe (monolobed) in the center between the two episternals in morphotype B (mean L17 = 26.73); 2) ambulacral plates I.6.a, I.7.a, and I.8.a and V.6.b, V.7.b, and V.8.b (see Figure 2B) narrow and protrude toward the center

TABLE 2 Morphometric measurements in recent spatangids.

Measure	Overall				Morphotype A				Morphotype B			
	Min	Max	Mean	SD	Min	Max	Mean	Stand. dev.	Min	Max	Mean	SD
TL	64.50	123.50	123.50	13.98	64.50	123.50	101.67	14.26	96.70	122.70	106	8.37
TW	81.00	102.30	102.30	2.95	81.00	102.30	94.48	2.96	89.70	97.60	92.94	2.44
TH	**45.00**	**60.70**	**60.70**	**2.97**	**46.50**	**60.70**	**53.48**	**2.86**	**45.00**	**54.70**	**51.14**	**3.79**
FW	0.70	3.60	3.60	0.56	0.70	1.90	1.21	0.27	3.00	3.60	3.32	0.21
L1	6.90	19.80	19.80	1.73	6.90	19.80	19.80	1.74	7.60	9.10	9.10	0.43
L2	9.00	20.20	20.20	1.49	9.00	20.20	20.20	1.43	10.96	12.50	12.50	0.60
L3	**9.48**	**27.20**	**27.20**	**3.18**	**11.30**	**27.20**	**27.20**	**2.90**	**9.48**	**26.50**	**26.50**	**6.63**
L4	**29.60**	**49.50**	**49.50**	**3.25**	**34.80**	**49.50**	**41.98**	**2.58**	**29.60**	**36.60**	**33.32**	**2.10**
L5	8.70	18.30	18.30	1.55	10.00	18.30	18.30	1.39	8.70	11.30	11.30	0.94
L6	**32.30**	**47.20**	**47.20**	**2.74**	**36.40**	**47.20**	**41.53**	**2.39**	**32.30**	**38.50**	**35.75**	**2.31**
L7	8.50	17.80	17.80	1.51	9.30	17.80	17.80	1.37	8.50	11.60	11.60	0.96
L8	**41.40**	**65.40**	**65.40**	**2.82**	**41.40**	**65.40**	**65.40**	**2.80**	**57.60**	**63.60**	**63.60**	**2.36**
L9	**4.10**	**11.90**	**11.90**	**1.40**	**4.10**	**7.90**	**5.86**	**0.74**	**9.30**	**11.90**	**10.71**	**0.98**
L10	**14.90**	**29.30**	**29.30**	**2.09**	**18.00**	**29.30**	**22.35**	**1.78**	**14.90**	**21.50**	**17.88**	**2.15**
L11	19.90	31.20	31.20	2.20	19.90	31.20	31.20	2.15	20.60	25.50	25.50	1.69
L12	5.30	14.10	14.10	1.44	5.30	14.10	14.10	1.30	5.60	7.10	7.10	0.59
L13	34.00	44.80	44.80	1.75	34.00	44.80	44.80	1.77	36.00	41.30	41.30	1.44
L14	3.40	11.00	11.00	1.57	3.90	11.00	11.00	1.50	3.40	5.40	5.40	0.85
L15	**29.30**	**47.30**	**47.30**	**2.74**	**29.30**	**47.30**	**47.30**	**2.61**	**32.00**	**37.10**	**37.10**	**1.66**
L16	**22.60**	**37.20**	**37.20**	**2.75**	**24.20**	**37.20**	**37.20**	**2.39**	**22.60**	**26.70**	**26.70**	**1.37**
L17	**25.40**	**48.90**	**48.90**	**4.06**	**36.70**	**48.90**	**41.67**	**2.09**	**25.40**	**27.80**	**26.73**	**0.81**

Acronyms of the measurements are described in the main text and SM. TL is reported in mm, and the other measurements are given as % of TL. The measurements in bold are indicated by the SIMPER test as those contributing to the differentiation between morphotype A and B. Minimum, maximum, and mean values ± standard deviation (SD) are shown for the whole sample and morphotype A/B separately.

of the fasciole occluding (or almost) interambulacrum 5 in morphotype B; 3) the episternal plates' shapes are broad and not very indented by the adjacent ambulacra in morphotype A, while they are narrow, long, and deeply indented by the ambulacral plates in morphotype B.

Furthermore, morphotype B has a narrow and deep anterior sinus, while it is wide and shallow in morphotype A (L9 = 10.71 and 5.86, respectively).

After verification of the number of ambulacral plates in contact with the labrum, no variability was found in the ratio of labrum/number of adjacent ambulacral plates, but growth anomalies only. Of the specimens, 7.69% had labrum deformations, and only 4.23% had at least two plates on one side of the labrum. Other data are summarized in Table S3 and Figures S3, S4.

Concerning the number of primary tubercles (or their presence/absence) in certain interambulacral aboral areas, we observed that their number is very variable but also that they are present in all five interambulacra of all the individuals studied. Moreover, we also observed that these tubercles are always present in the five interambulacra but in a constantly lower number in morphotype B specimens.

3.2 Morphological and morpho-structural comparisons

Both recent and fossil spatangids were compared to morphotypes A and B, examining plating and morpho-structural matrix characters.

Firstly, the schemes (plating) of the oral face of morphotype A and morphotype B were compared with species classified as *Spatangus*. *Spatangus inermis* Mortensen (1913), *Spatangus paucituberculatus* (A. Agassiz & H.L. Clark, 1902), *Spatangus multispinus* (Mortensen, 1925), *Spatangus raschi* Mortensen (Lovén, 1869), and *Spatangus capensis* Döderlein (1905) showed the same scheme as morphotype B (Figure 5, in order: 5b, c, d, e, f). Instead, *Spatangus luetkeni* A. Agassiz, 1872, *Spatangus californicus* Clark, 1917, and *Spatangus mathesoni* McKnight, 1967 have intermediate characters between the two morphotypes under examination.

Furthermore, the study of fossil species (listed in Table 1) highlighted that *G. subinermis* Pomel, 1875 (Figure 5A) had many features in common with morphotype B. *Spatangus desmaresti* (Figure 6C) had the same basic structure as the plastron of morphotype A (Figure 4A). Instead, *Sardospatangus caschilii* and *Sardospatangus saheliensis* (Figures 6A, B) have peculiar plating,

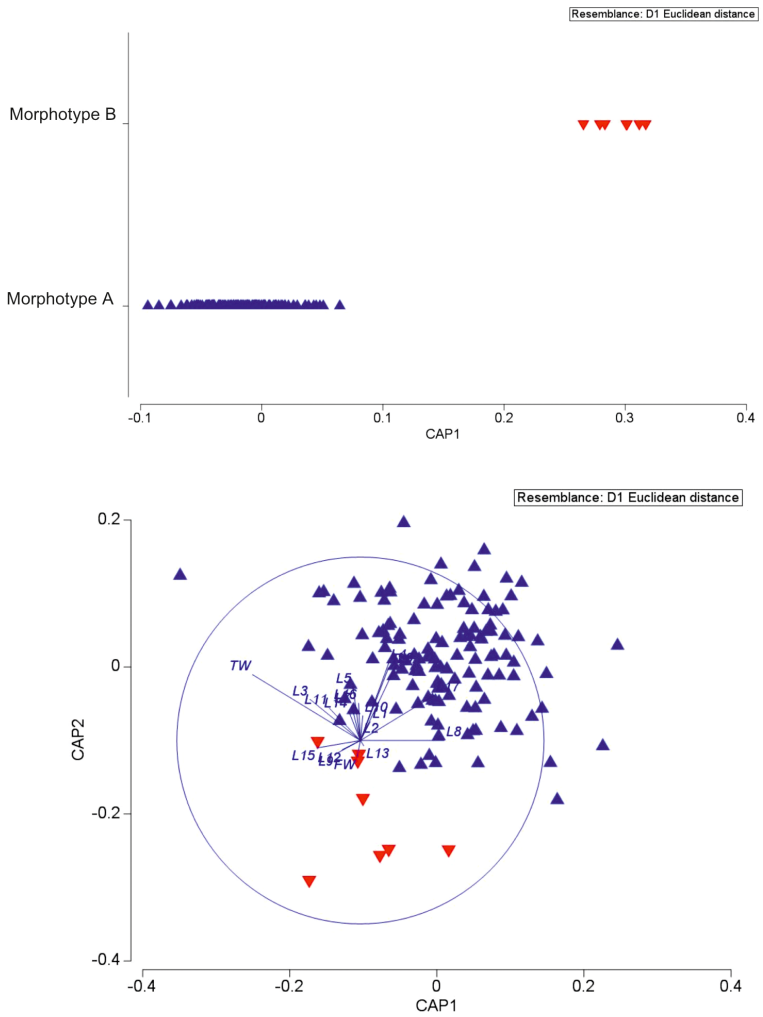

FIGURE 3
Canonical analysis of principal coordinates of biometric data of the two spatangids under study.

different from both morphotypes A and B. *Sa. saheliensis*, which has a very deep groove, small petals (Figure 6B), and few primary tubercles, differs from *Sa. caschilii*, which has a shallow groove and large petals (Figure 6A). At the genus level, however, we can see that *S. paucituberculatus* (Figure 5C), despite its very deep groove, relatively small petals, and rare primary tubercles (as *Sa. saheliensis*), falls into another genus due to the different plastron structure.

S. subinermis (Figure 5A) is superimposable, in terms of the structure of the plastron and length of petals, to the extant morphotype B (Figure 4B); the extant *S. purpureus* (morphotype A) (Figure 4A) has the same basic shape of the plastron (a single ambulacral plate on each side of the labrum and a wide and bilobed fasciole, with wide and not indented episternals) of *S. desmaresti* (Figure 6C). Moreover, *Spatangus* sp. 1 of the Miocene of Ukraine (Figure S5) shows the labrum with only one plate per side of large episternal plates (even if the fasciole is not visible). Finally, also *Spatangus* cf. *purpureus* of the Pleistocene of Italy (Figure S6) share all the characters of the extant *S. purpureus*.

The extant *Plethotaenia angularis* (Figure 6D) shares with morphotype B the main characters of the plastron including the shape of the subanal fasciole, but the presence of pseudofasciole around the petals on the aboral face (Figure 6D up) clearly detaches it from the latter, as, however, it detaches from *Sardospatangus* (fossils) and *Spatangus* (extant and fossils), which have a wide and bilobed fasciole (cf. Figures 6A down, b down; 4A down).

Finally, *S. californicus* (Figure 6E) and *S. mathesoni* (Figure 6F) can be distinguished from all other forms. They first differ in having a wide fasciole (apparently monolobate) and the episternal plates intermediate between those of morphotype A and morphotype B; the latter shows small petals and plastron superimposable to that of morphotype B (Figure 4B with Figures 6E, F), while the anterior sinus is deep and narrow, and the test is low and vaguely discoid (in adult individuals) as in *Plethotaenia* (Figure 6F); the fossil spatangid from the Florida Mio-Pliocene (USA) is very similar to *S. purpureus*, except for the fasciole, which is small and (apparently) monolobed (Figure S7A, B).

3.3 Phylogenetic analyses using molecular and morphological data

To shed light on morphological differences recorded among specimens of spatangoids collected in Sardinian waters in 2018 and

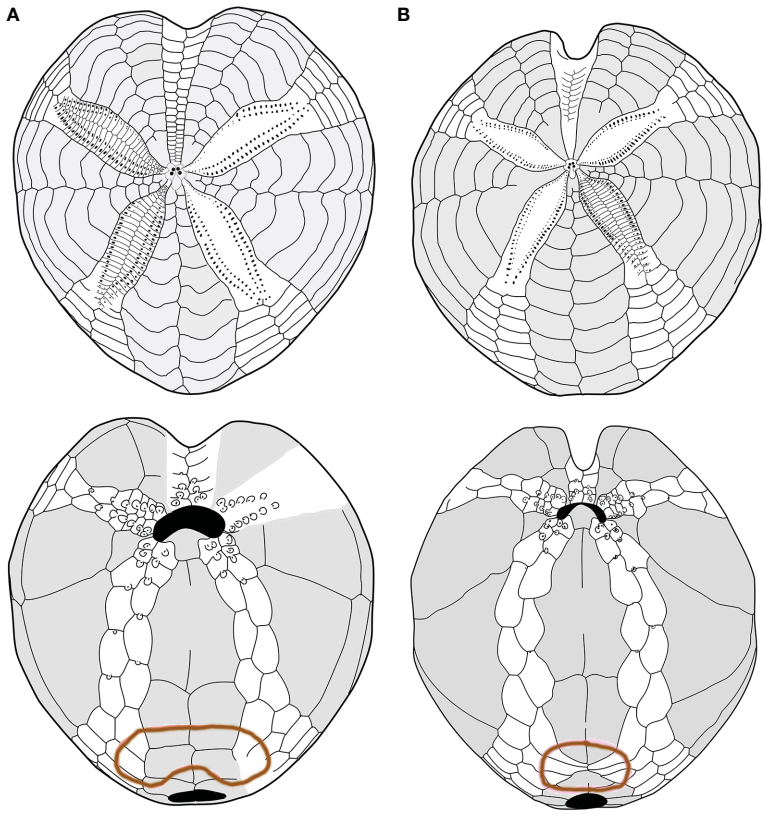

FIGURE 4
(A, B) Comparison between schemes (or pattern): **(A)** *Spatangus purpureus*, aboral (up) and oral view; **(B)** *propespatagus* sp. 1 aboral (up) and oral view.

2019 and to investigate the taxonomical relationships between morphotypes A and B, 16 and 5 specimens form morphotypes A and B, respectively, were investigated using molecular tools.

All specimens were successfully processed for DNA extraction, but some individuals failed to provide PCR products for one or several fragments. A total of 15 individuals were successfully sequenced for one or both markers: 10 individuals for morphotype A and 5 for morphotype B (details of the specimens are provided in Table S4). A final alignment of 646 and 522 bp was obtained for the COI and 16S fragments, respectively. The principal indices of genetic diversity are reported in Table 3. The Sardinian individuals are characterized by a high haplotype diversity ($hed_{COI} = 0.857$; $hd_{16S} = 0.769$; $hd_{conc} = 0.923$) and a low nucleotide diversity ($\pi_{COI} = 0.027$; $\pi_{16S} = 0.014$; $hd_{conc} = 0.022$) for both the markers, while the average number of nucleotide differences results higher for concatenated markers (k = 25.87) and COI (k = 17.55) than for the 16S marker (k = 7.36). Morphotype A showed a higher number of haplotypes than B, which showed only one substitution for COI and no variable sites for the 16S (Table 3).

Concerning the genetic distances between the two morphotypes, pairwise DNA differences ranged between 33 and 37 for COI and between 13 and 15 for 16S. The p-distances between groups were 5.3% and 2.7% for COI and 16S, respectively. The concatenated markers showed a genetic differentiation that ranged between 47 and 52 nucleotides, corresponding to a p-distance of 4.2%.

The Sardinian samples were compared with homologous sequences from the public repositories; a total of 14 sequences for COI (final alignment: 560 bp), 10 sequences for 16S (final alignment: 422 bp), and 3 concatenated sequences (final alignment: 1,108 bp) were added to our alignments (see Table S5 for details).

In all the trees, with the four methods used for both separate and concatenated DNA markers (Figures 7, S8, S9), the Sardinian sequences clustered in two different groups with high statistical support, corresponding to morphotypes A and B. Sequences from morphotype A clustered with the sequences deposited in GenBank as *S. purpureus* (O.F. Muller, 1776), while sequences from morphotype B, which were separated from morphotype A sequences, are placed in a clade with other species (e.g., *S. californicus* H. L. Clark, 1917, *S. multispinus* Mortensen, 1925, and *S. raschi* Lovén, 1869). The closest sequences to morphotype B are those deposited as *S. raschi*. The same findings were obtained also for the trees of combined morphological and molecular characters (Figure 8), confirming the occurrence of two clearly separate groups in the Sardinian waters. Once again, the individuals from morphotype A are attributed to the species *S. purpureus*, while specimens from group B seem different from the currently described species of Spatangidae but are placed together with the species *S. multispinus* and *S. raschi*.

The analysis of the trees obtained from the morphological character matrix (Figure S10) showed several groups within the clade of the family Spatangidae. In particular, once more, the species *S. purpureus*, corresponding to our morphotype A, is placed in a separate clade of the individuals belonging to morphotype B, supporting the differentiation identified from the molecular tool.

Finally, Figure S11 shows the stratigraphic relationship between fossils species analyzed.

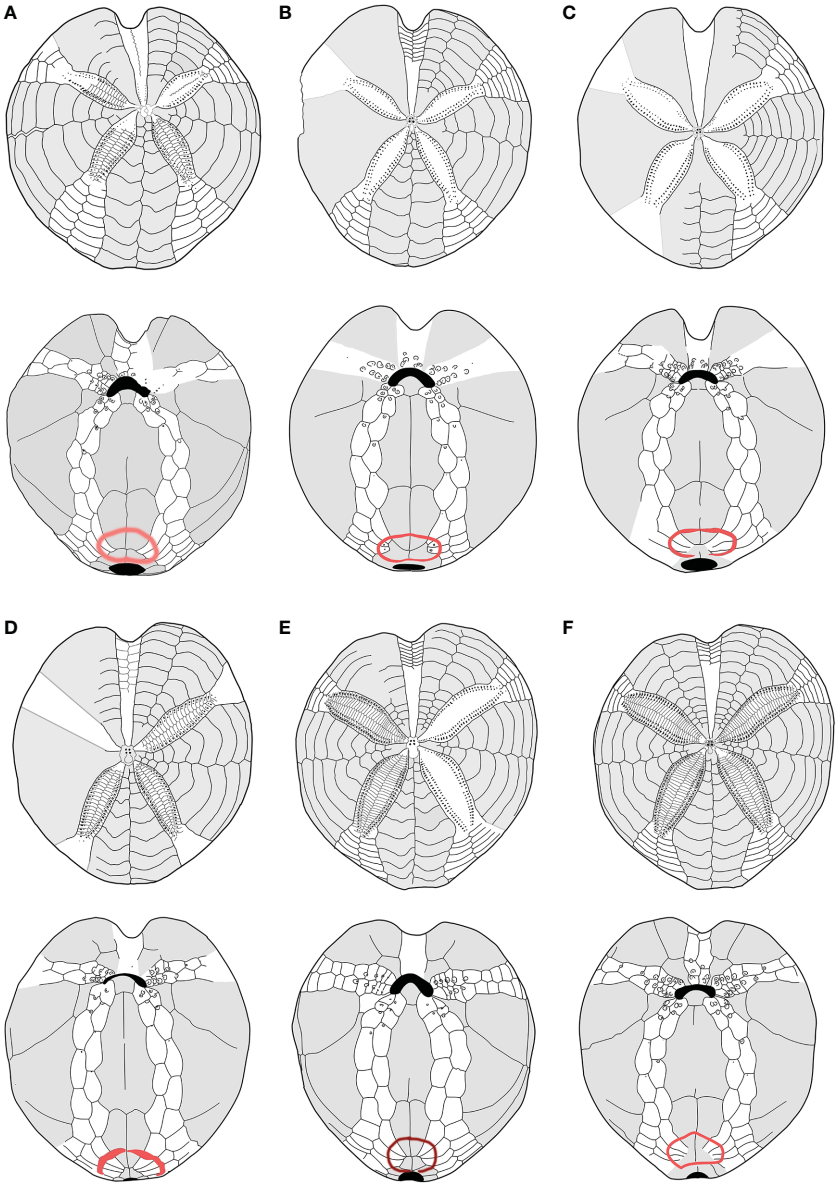

FIGURE 5
(A–F) Structural similarities in aboral (up) oral and oral (down) schemes, between recent and fossil species of *Propespatagus* analyzed in this work: **(A)** *Propespatagus subinermis*, Pliocene di Otranto, Lecce, Puglia (Italy); **(B)** *Propespatagus inermis*, Gulf of Naples, Mediterranean (redrawn from Mortensen, 1913); **(C)** *Propespatagus paucituberculatus*; **(D)** *Propespatagus multispinus*; **(E)** *Propespatagus raschi*, Shetland Islands; **(F)** *Propespatagus capensis*, seas of Cape Town, South Africa. Schemes (platings) c– f were redrawn from Mortensen (1951).

In summary, based on morphological and genetic results for morphotype B, we establish a new genus, named *Propespatagus* gen. nov., where morphotype B specimens are to be hosted. See section 5 for the formal description.

4 Discussion

This article aims to contribute to improving the knowledge of the diversity, distribution, and systematics of the Spatangidae in the Mediterranean Sea, through the study of specimens recently collected in the Western Mediterranean (Sardinia), using, for the first time, a combined approach based on morphometric measurements and genetic and structural–morphological analyses. Furthermore, paleontological data are used to complement the data and support the results of the analyses.

Morphometrics, genetics, and structural morphology converge toward the occurrence of two distinct species in the area under investigation: morphotype A is easily identifiable as *S. purpureus*, and morphotype B largely corresponds to the description of *S. subinermis* (*sensu* Kroh and Mooi, 2022). The observations made on the specimens collected in Sardinian seas showed a wide variability of the main measurements and the difficulty in finding resolutive characters for the identification of taxa (Table 2), confirming what was observed by Bonnet (1926). For instance, focusing on the number of primary tubercles in certain interambulacral aboral areas cannot be regarded as clearly resolutive since we observed in our sample of *S. purpureus* (260 individuals) that, as claimed by Bonnet (1926), this

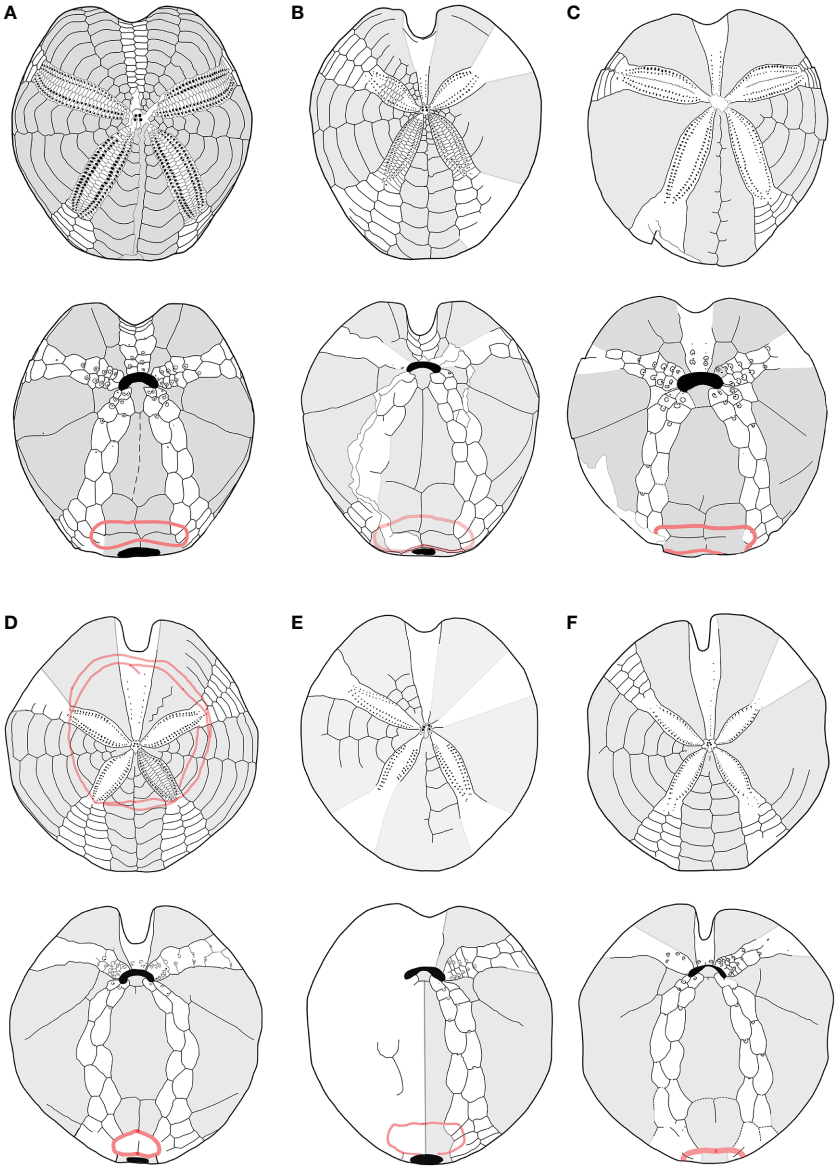

FIGURE 6
(A–F) Structural similarities in aboral (up) oral and oral (down) schemes, between fossil and recent species of Spatangidae analyzed in this work. **(A)** *Sardospatangus caschilii*, Miocene, Burdigalian of Isili, Sardinia, Italy (MAC PL 344); **(B)** *Sardospatangus saheliensis*, Messinian-Pliocene of Melilla, Spain, North African coasts (MNHN no. R62132); **(C)** *Spatangus desmaresti*, Oligocene, Chattian of Doberg, Westphalia, Germany (MHNG no. 127-27828); **(D)** *Plethotaenia angularis*, Recent, Caribbean Sea (Redrawn from Schultz, 2009, in Kroh and Mooi, 2022; **(E)** *Spatangus californicus*, Baia California, Mexico (Redrawn from Mortensen, 1951); **(F)** *Spatangus mathesoni*, New Zealand, Station D0231 (NIWA paratype P42).

character is very variable, with the primary tubercles present in all five interambulacra of all the individuals studied; at the same time, we also observed, in our sample of morphotype B (10 individuals), that these tubercles are always present in the five interambulacra, but in a lower number. However, other structural features of the plastron plating (Figures 4A, B; the fasciole pathway, the ambulacral plates (I.6.a, I.7.a, and I.8.a as well as V.6.b, V.7.b, and V.8.b), the episternal plates' shape, and the shape and depth of the anterior sinus) allowed to clearly distinguish the two forms. Similarly, in our study, both morphometrics and genetics clearly separated the two types.

Despite the fact that the great variability observed by Bonnet (1926) was also present in our sample, it did not prevent the use of various diagnostic characters, appropriately chosen, for the separation between species and genera in the same family.

In this study, we observe that the variability described by McNamara (1982; 1987; 1988; 1989) was not present in the abundant sample of extant spatangid collected in Sardinia, as already seen by Stara et al. (2018) on a large sample of fossil Spatangidae specimens collected in the sedimentary rocks of the Sardinian Miocene.

Based on the peculiar features of morphotype B, here, we establish a new genus, named *Propespatagus* gen. nov., and we name the extant specimens studied *Propespatagus* nov. sp. 1, awaiting to have more material for a formal specific institution according to International Code of Zoological Nomenclature (ICZN) rules.

At the same time, based on the plating of the oral face similar to morphotype B, a number of species thus far attributed to the genus *Spatangus* (i.e., *S. inermis*, *S. subinermis*, *S. paucituberculatus*,

TABLE 3 Indices of genetic diversity for the Sardinian specimens calculated for the two mitochondrial markers and for the concatenated sequences.

	N	H	hd ± SD	π ± SD	k
COI					
Morphotype A	9	4	0.750 ± 0.112	0.0019 ± 0.0006	1.22
Morphotype B	5	2	0.600 ± 0.175	0.0009 ± 0.0003	0.60
Total	14	6	0.857 ± 0.056	0.0272 ± 0.0045	17.55
16S					
Morphotype A	9	4	0.694 ± 0.147	0.0016 ± 0.0005	0.83
Morphotype B	5	1	–	–	–
Total	14	5	0.769 ± 0.076	0.0141 ± 0.0022	7.36
16S+COI					
Morphotype A	8	6	0.929 ± 0.084	0.0019 ± 0.0005	2.25
Morphotype B	5	2	0.600 ± 0.175	0.0005 ± 0.0002	0.60
Total	13	8	0.923 ± 0.050	0.0222 ± 0.0032	25.87

N = number of sequences; H = number of haplotypes, hd = haplotype diversity, π = nucleotide diversity and relative standard deviations (SD), and k = average number of nucleotide differences.

S. multispinus, *S. raschi*, *S. capensis*) are transferred to *Propespatagus* gen. nov.

S. luetkeni, from the Japanese coasts, *S. californicus*, from the Gulf of California, and *S. mathesoni*, from New Zealand, remain in the genus *Spatangus* because their oral patterns show intermediate characters between the two reference genera, or the data in our possession are not sufficient for an in-depth analysis.

Concerning the fossils, the generic attribution of *S. desmaresti* is confirmed, having the same basic structure as the plastron of *S. purpureus*; genus *Sardospatangus*, with the species *Sa. caschilii* and *Sa. saheliensis*, is a valid genus as its features are different from our types A and B. The form previously called *G. subinermis* Pomel, 1875, of the Italian Plio-Pleistocene, is here proposed to be renamed as *Propespatagus subinermis* Pomel (1875) sp.

The subdivision between genera was mainly based on diagnostic characters of the oral face that, among all the districts of the spatangoid dermaskeleton, are the ones where evolution has worked both for plate accretion and for plate addition (Smith, 2005), constituting the "plastron". We also focused on the subanal fasciole, whose characters were considered by Smith and Stockley (2005) to be highly informative and reliable from a phylogenetic point of view.

The division between species within the two resulting genera (*Spatangus* and *Propespatagus*) was made using the same criteria, as well as a number of other characters (in part borrowed from Stockley et al., 2005 and Kroh, 2020), but in this case, tested in their variability. Some uncertainties in the species attributions made in the past remain, and this is for at least two reasons: 1) the choice of poorly diagnosed characters and 2) the scarcity of the material used in the

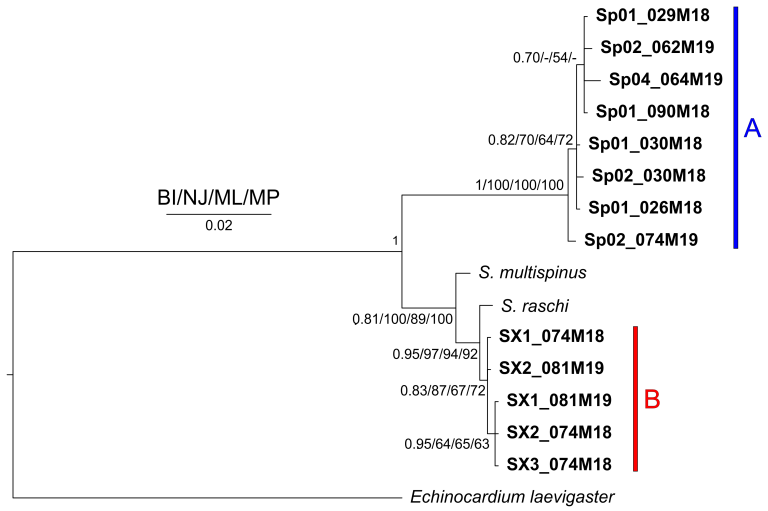

FIGURE 7
Tree obtained with the concatenated 16S and cytochrome c oxidase subunit1 (COI) sequences. Near the nodes are the values for the Bayesian probability (BI) or the bootstrap support (NJ/ML/MP). In bold are the Sardinian spatangids. The bars and capital letters A (blue) and B (red) indicate the sequences of morphotype A and B, respectively.

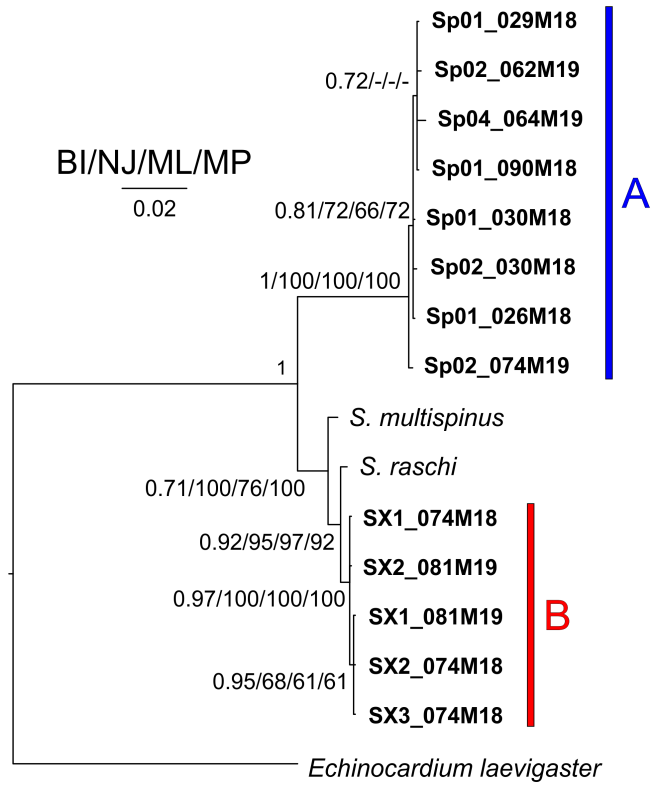

FIGURE 8
Tree obtained combining morphological and molecular characters. Near the nodes are the values for the Bayesian probability (BI) or the bootstrap support (NJ/ML/MP). In bold are the Sardinian spatangoids. The bar and capital letters A (blue) and B (red) indicate the sequences of morphotype A and B, respectively.

oldest studies. In fact, many species have been established based on the description of a single specimen, often poorly described and/or illustrated.

Reviewing the sequence of fossils examined in this work, from a geologic/temporal point of view, the group of *Spatangus* (morphotype A) shows a path partially connected with *Sardospatangus* and probably with the Florida spatangid. The rest of the spatangids seems to form a different and interconnected group, having all the components of a very similar plastron.

In Figure 9, based on plastron schemes, we represent the hypothetical phylogenetic relationship between and within the groups and in Figure 10 their present geographical distribution.

In the present study, *S. purpureus* was found all around the coast of Sardinia at a wider depth ranging (from 22 to 183 m of depth), while *Propespatagus* was rare, found only in a few locations (range 86–181 m), generally coexisting with *S. purpureus* (Figure 1). Unlike in *S. purpureus*, *Propespatagus* shows a very thin and fragile test [observation also made by Mortensen (1913)] both for individuals of *Propespatagus inermis* from the Mediterranean and for specimens caught in different areas of the Pacific Ocean. This also applies to *S. mathesoni* of New Zealand (personal communication by Owen Anderson, NIWA). These details suggest the better adaptation to different environments than that of *S. purpureus*, but also a probable common ancestor in the second group (morphotype B — *Propespatagus*). It could therefore be hypothesized that morphotype B, *Propespatagus*, only partially (and coincidentally) shares the same environment as *S. purpureus*, and this would explain its low frequency in our fishing hauls. However, all these aspects need to be further addressed in dedicated studies in the future.

Concerning the genetic data, the newly generated sequences are the first genetic data for Spatangidae specimens caught in the Mediterranean Sea. In the past, DNA sequencing, in particular the COI DNA barcoding approach, has proved to be highly effective for echinoderm species discrimination, with the vast majority of species easily distinguished by their COI barcodes (Ward et al., 2008; Layton et al., 2016). In our study, nucleotide differences indicated the two morphotypes are molecularly distinct, and their degree of divergence is comparable to that of true valid species. Sequences from individuals of morphotype A can be identified as *S. purpureus*. The identification of specimens of morphotype A is solid, relying on both morphological appearance and sharing of molecular data with several sequences of *S. purpureus* deposited in GenBank/BOLD for multiple individuals and areas of the NE Atlantic Ocean. On the contrary, the identification of morphotype B specimens is more problematic. Molecular data seem to indicate that *Propespatagus* nov. sp. 1 is very close to *Propespatagus raschi*, differing only in a few nucleotide positions, the same degree of divergence that in previous studies was measured as the mean intraspecific value based on COI sequences (Ward et al., 2008; Layton et al., 2016). Special caution is required for the tentative molecular identification of morphotype B in this study since it was based on the only public available sequences for *P. raschi* from a single article (Stockley et al., 2005) and presumably a single individual caught in the NE Atlantic (United Kingdom), while, unfortunately, any sequence from *P. subinermis*, the second species known to occur

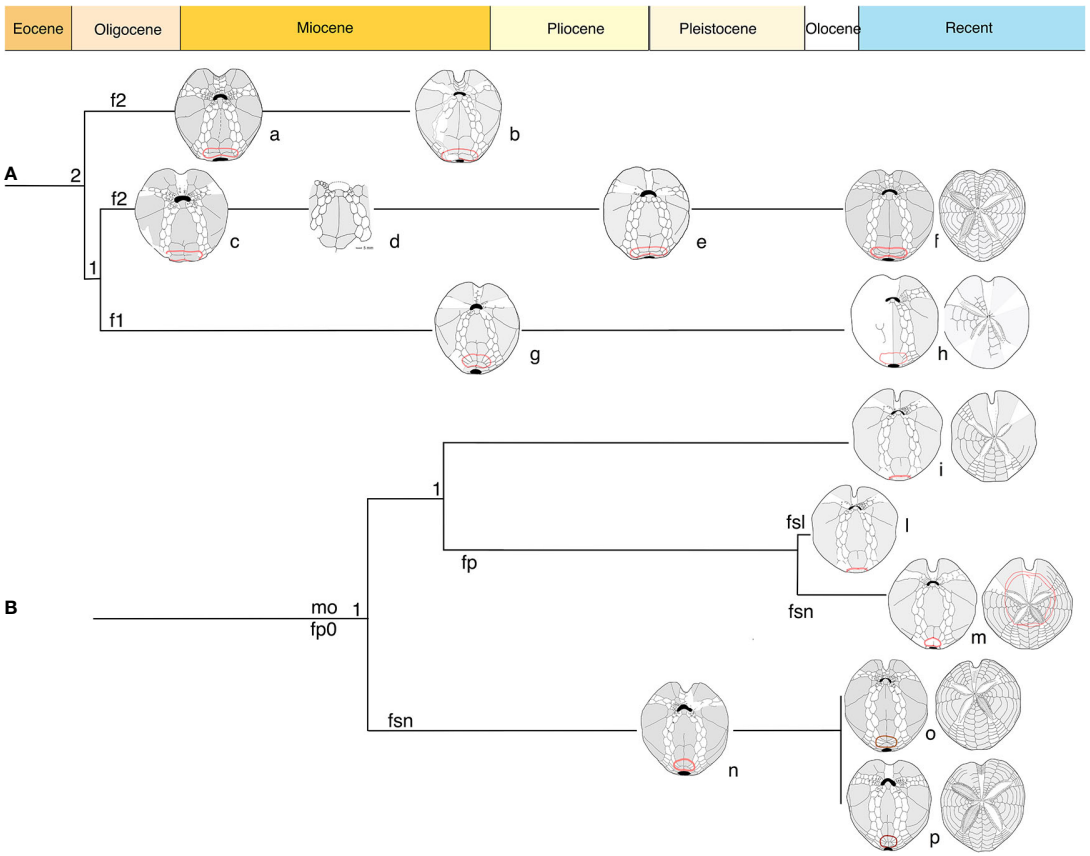

FIGURE 9
Diagram based on structural characters in adoral schemes. **(A)** Clade *Spatangus*/*Sardospatangus*; **(B)** clade *Propespatagus*, *Plethotaenia*, and other spatangids. Numbers: 1 = 1 plate; 2 = 2 plates per side of labrum. Letters: f1, f2 = fasciole with 1 or 2 indicating monolobed or bilobed. Other: fp = peripetal fasciole; fp0 = non- peripetal fasciole; fsl = large subanal fasciole; fsn = normal subanal fasciole. Specimens a– p, in order: *Sardospatangus caschilii*; *Sardospatangus saheliensis*; *Spatangus desmaresti*; *Spatangus* sp. 2 Ukraine; *Spatangus* cf. *purpureus*; *Spatangus purpureus*; Spatangidae sp. Florida; *"Spatangus" californicus*; *"Spatangus" mathesoni*; *Plethotaenia spatangoides*; *Plethotaenia angularis*; *Propespatagus subinermis*; *Propespatagus* sp. 1; *Propespatagus raschi*.

in the Mediterranean Sea, was available. Therefore, additional studies, combining morphological and molecular analyses, with extensive, dedicated sampling in the Atlantic and Mediterranean, are highly suggested to further investigate the differentiation between *Propespatagus* nov. sp. 1 (up to now documented only from the Mediterranean) and *S. raschi* (endemic to the NE Atlantic).

5 Description of the new genus and the species studied

This section is dedicated to the full description of the two species, as well as the diagnostic characters, useful to distinguish the new genus.

5.1 Systematic of Spatangidae

According to Kroh, 2020
Order Spatangoida L. Agassiz, 1840
Suborder Brissidina Kroh and Smith, 2010
Superfamily Spatangoidea Gray, 1825
Family Spatangidae Gray, 1825

5.1.1 Diagnostic characters of Spatangidae

Emended diagnosis (modified after Smith and Kroh, 2011): Spatangoidea with ethmolytic apical disc with four gonopores, flush or slightly depressed petals, pointed and closed distally; reduced pores adapically in the anterior column of the anterior paired petals; labrum, which does not extend beyond the second adjacent ambulacral plate; episternal plates equal and opposite; subanal fasciole present; rudimentary peripetalous fasciole may be present; periproct opening between plates 5.a.4 and 5.b.4 in the rear face; aboral face with scattered primary scrobiculate tubercles, variable in number, with the areolas indented but never very deep.

Genera included:

1) *Spatangus* Gray, 1825
2) *Plethothaenia* Clark, 1917
3) *Sardospatangus* Stara, Charbonnier et Borghi, 2018
4) *Propespatagus* gen. nov.

The diagnostic characters of the two species belonging to *Spatangus* and *Propespatagus* genera, on which this work is based, are described below.

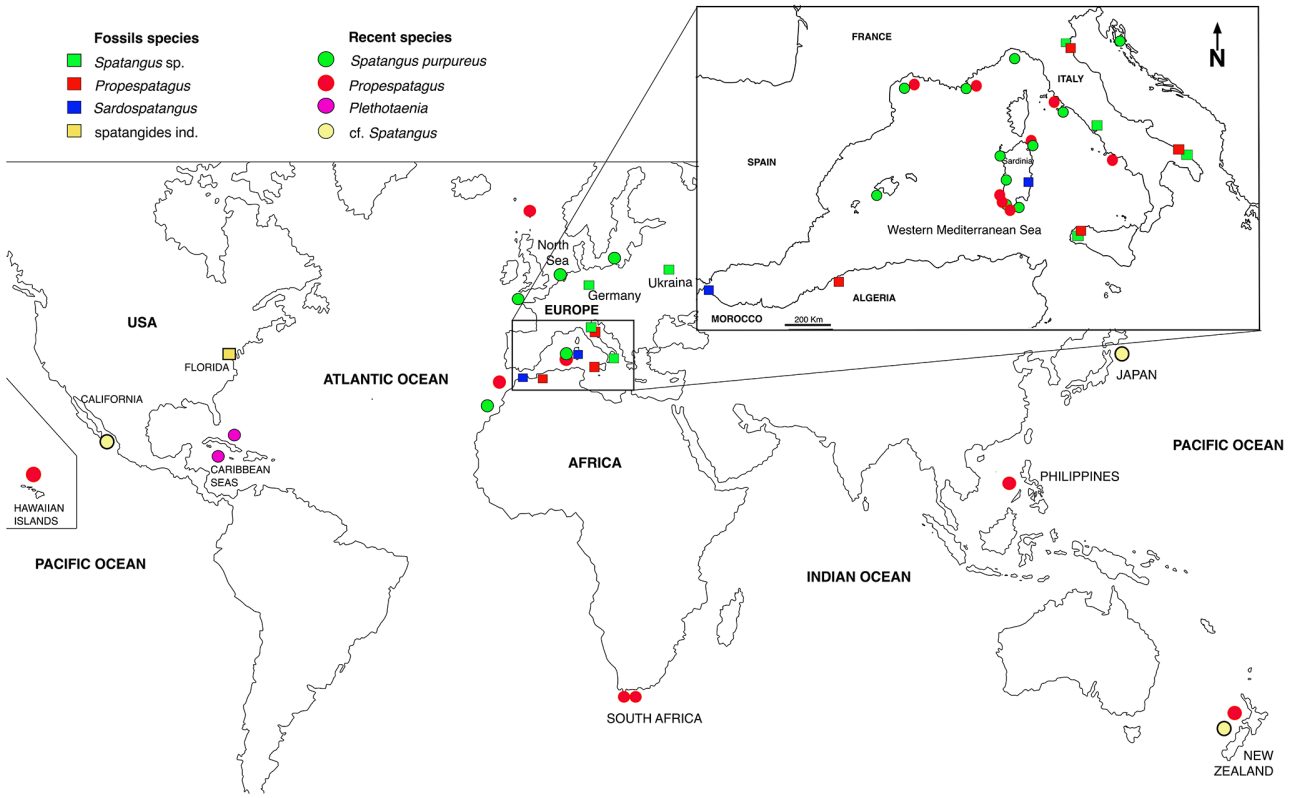

FIGURE 10
Geographical distribution of the analyzed species.

5.1.2 Diagnostic characters of the genus *Spatangus*

5.1.2.1 Description

Cordiform test with anterior groove; aboral surface domed; rounded margin, with slightly raised plastron; small apical disc, with a madreporic plate extending to the center and beyond the two posterior pores, where it tends to widen; narrow anterior ambulacrum with small simple isopores and phyllodes in peribuccal areas; the other ambulacra are petaloid adapically; slightly arched anterior paired petals with the pores of the anterior column adapically rudimentary or atrophied; the other pores large, paired and conjugated; posterior paired petals slightly expanded adapically and narrowing distally; medium- sized periproct, from subcircular to slightly elliptical, with greater horizontal diameter, open at the top on the posterior face, which is low and oblique and visible from below; small and kidney -shaped peristome, mostly covered by the labrum; labrum anvil- shaped, in contact with only one ambulacral plate on each side; finely tuberculated plastron, formed by wide and paired sternals, and wide episternal; heterogeneous aboral tubercles, with the primary ones scattered in the interambulacra in variable numbers, small and with shallow areoles; primary short spines; subanal fasciole, relatively thin and made up of very fine granules; it runs on large ambulacral plates that do not indent interambulacrum 5; the first two (sometime three) of these carry a subanal pore; the fasciole starts from the perradial suture between the two episternal plates, enclosing two large relief (bilobed) covered by tick tuberculation.

5.1.2.2 Species included:

S. purpureus Müller, 1776

S. desmaresti Goldfuss, 1829 (†)

?*Spatangus* sp. 2 Kroh, 2004 (†)

Many species of the European Miocene have been moved to the genus *Sardospatangus* Stara, Charbonnier et Borghi, 2018. Several other species need to undergo a systematic revision.

5.1.2.3 Distribution

Germany (Oligocene, Chattian); Ukraine (Miocene) and Plio-Pleistocene to Recent; Mediterranean and East Atlantic coasts from Senegal to North Sea.

Notably, in this work, the pedicellariae are not described because they are not considered diagnostic in the discrimination of the genera and species of Spatangidae; in the remarks in *Propespatagus* gen. nov. (ex *Spatangus* Auct.), moreover, we report only some characters that we consider diagnostic in this context. For any further information, see Mortensen (1913; 1951) and Néraudeau et al. (1998).

5.1.3 *S. purpureus* Müller, 1776

Figures 4A, 11A–F; Table 2

5.1.3.1 Essential synonymy

The complete list would be extremely wide and superfluous for the purpose of this work. However, for a historical reconstruction, we refer to Mortensen (1951) and, for an updated systematic situation, to WoRMS (World Register of Marine Species).

1776 —*S. purpureus* Müller p. 236, not figured, recent, coll. not indicated.

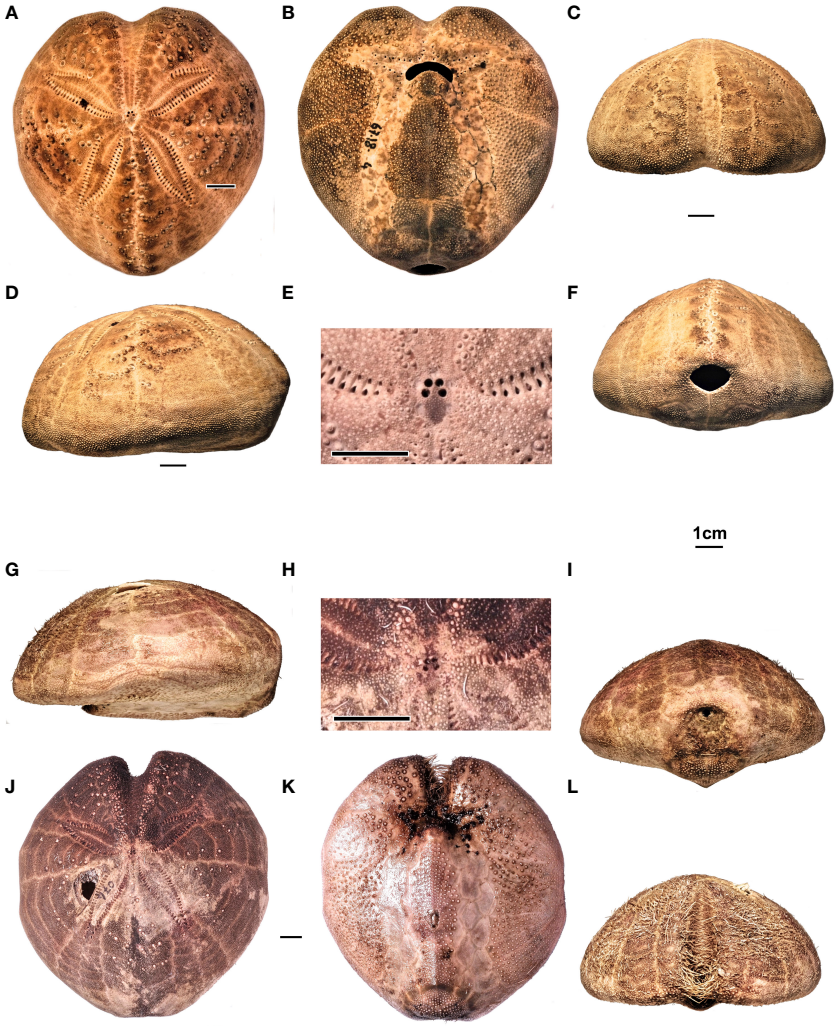

FIGURE 11
(A–F) *Spatangus purpureus*, Sardinia. Specimen MZ UNICA 067-MED18-4. In order, **(A–D)** aboral, adoral, frontal, and lateral views; **(E)** detail of the apical disc; **(F)** posterior view. **(G–L)** *Propespatagus* sp. 1, Sardinia. Specimen 074-MED18-2, holotype: **(G)** lateral, **(I)** posterior, **(K)** adoral, and **(L)** frontal views. Specimen 074-MED 18-1, **(J)** aboral view. Specimen MZ UNICA 085-MED18-1, **(H)** apical disc, detail.

1788— *S. purpureus* Müller p. 5, pl. 6, Figures 3–5, pl. 25, Figure 5.
1834— *S. purpureus* Müller, Blainville, p. 202, pl. 14, Figures 1–3.
1862— *S. purpureus*. Dujardin & Hupé, p. 607.
1862— *Spatangus meridionalis*. Dujardin & Hupé, p. 608.
1871 —*S. meridionalis*. Lütken, p. 138.
1872— *S. meridionalis*. Gray, p. 123.
1872— *S. purpureus*. A. Agassiz, p. 158.
1874— *S. purpureus*. Gauthier, p. 402.
1879— *S. purpureus*. Ludwig, p. 560.
1883— *S. purpureus*. Koehler, p. 127.
1891 —*S. purpureus*. Gregory, p. 42, 46.
1901 —*S. purpureus*. Mortensen, p. 29.
1905— *S. purpureus*. Döderlein, p. 199.
1906— *S. purpureus*. Döderlein, p. 260.
1906— *S. purpureus*. Checchia –Rispoli, p. 95.
1907— *S. purpureus*. Mortensen, p. 123.
1951— *S. purpureus* Müller, Mortensen, p. 10
1998— *S. purpureus* Müller, Néraudeau, Borghi & Roman, p. 6.
2005— *S. purpureus* Müller, Kroh, p. 150.
2018— *S. purpureus* Müller, Vadet & Nicolleau, pp. 106–108.
2018— *S. purpureus* Müller, Stara, Charbonnier & Borghi, p. 310.

5.1.3.2 Distribution

Fossils, from the Italian Plio-Pleistocene (Néraudeau et al., 1998; present study); recent, from Mediterranean to Atlantic European coasts (present study; Smith and Kroh, 2011; Stara et al., 2018; Vadet and Nicolleau, 2018).

5.1.3.3 Material studied

260 specimens fished along the coasts of Sardinia and deposited (30 specimens) at the MAC, inventoried IVM # and (230 specimens) at the MZ UNICA, inventoried MZ #; 2 fossil specimens from the Pliocene of Otranto, Puglia; 1 from Pliocene of Terre Rosse, Siena, Tuscany, and 1 from the Pleistocene-Holocene of Ostia, Lazio, Italy (MACPL 2015-2017).

5.1.3.4 Description

A species of *Spatangus* with the cordiform and domed test, rounded margin, relatively flat oral face, shallow anterior groove, labial plate in contact with a single ambulacral plate on each side, and wide contact with the sternals; thin sub-anal fasciole, laterally extended and bilobed.

In our sample, TL range from 64.5% to 123.5% TL and TW from 81% to 102.3% TL (Table 3).

The apical disc is positioned slightly anterior to the center (L8 average = 59.58% TL); ethmolytic, with the two anterior pores slightly closer together (Figure 7A).

Ambulacrum III is tight, with 27–29 minute and undifferentiated pores, and runs along the anterior groove progressively deepening, as it approaches the margin, where it reaches the maximum width. Other ambulacra petaloids adapically. The petaloids are relatively long and wide, despite their variability (L4 varies from 34.8 to 49.5% TL, an average of 42.4; L5 varies from 10 to 18.3% TL, mean of 13.3), and divergence between them an average of approximately 124 degrees. The pores of the anterior series become smaller or rudimentary (Figure 11A); adorally, each ambulacrum carries two series of five to six well-developed phyllodes that open into the peribuccal dimple (Figure 11B). Near the peristome, the plates are shorter than wide, but they progressively lengthen and then shorten toward the margin, where, however, they widen considerably (Figure 4A). The poriferous areas, in their central petaloid tract, measure approximately one-quarter of the interporiferous ones, which are devoid of tubercles; also the adoral portion carrying phyllodes is naked, while the marginal areas are covered by numerous small secondary tubercles. PLR is highly variable and ranges from 2.5 to 5.1 (average 3.6) in the sample examined (N 20). Paired posterior petaloids do not differ from the anterior by length and width (L6 ranges from 36.4 to 48.8% TL, average 41.9; L7 ranges from 9.3 to 17.8% TL), but the shape is generally less arched than the anterior ones with a divergence between them of approximately 62 degrees; the poriferous and interporiferous areas are similar to those of the paired frontal petals. On the adoral face, ambulacra I and V form a shower of elongated plates devoid of tubercles, which delimits the plastron without indenting it, where L15 measurements on average 38.5% TL (Figure 2). In Plates 6 and 7 there are evident two sub-anal pores, open within the perimeter of the fasciole.

All the interambulacra are amphiplacous, with the first plate extending up to the fourth (sometimes the fifth) plate of the anterior adjacent ambulacra and the third of the posterior paired ambulacra.

The labial plate extends only to the first adjacent ambulacral plate. The labrum protrudes anteriorly to partially cover the peristome, mushroom or anvil- shaped with the relatively wide base in contact with the two sternal plates (in our sample of *Spatangus*, L14 varies from 4% to 11% TL, with an average of 6.6% TL. The ratio between the averages of the length and width of the labrum in our sample is approximately 1.5. The sternal plates are broad (average L16 = approximately 30% TL; average L13 = 38.8% TL), with ratio L13/L16 = approximately 1.3, and do not restrict contact with the episternals, which normally falls at the fifth adjacent ambulacral plate (in our sample (n 128), it falls at the fourth plate of the ambulacrum V only in one case).

On the aboral interambulacra, tuberculation is heterogeneous and very variable; it consists of crenulate and perforate primary tubercles, whose areoles, which rarely exceed 2.4% TL in diameter, are arranged in straight lines or a "V"- shaped series along the plates of all the interambulacra (Figures 11A, D) and increase in size and diameter in the adapical direction.

On the adoral face, tuberculation is much more regular and less variable. All the interambulacra, including the plastron and the labrum, are covered by secondary perforated crenulate and scrobiculate tubercles (Figure 11B), which decrease in size as they approach the edge of the test. All ambulacra, indeed, are free from primary tubercles. Secondary tubercles are widespread especially at the edges of the anterior groove, while miliary tubercles are diffused and dense over the entire surface, except along the ambulacral poriferous areas.

The spines are articulate on the tubercles through thin but robust muscles anchored around the base of the stem and generally have the neck bent toward the posterior and/or lateral part of the body of the echinoid. The primary spines are thicker and longer than the secondaries; very variable in length, but normally are more than 15 mm long; they are found above all on the aboral surface and in a small part of the adoral portion of interambulacra 2 and 3, where they are shorter.

The secondary ones are densely distributed among the primaries and on the oral surface and generally less than 10 mm, mixed with the thin miliary spines, in analogy with the correspondent tubercles, as above described. However, in 110-mm- long individuals, we measured primary spines up to 34.5 mm long, equaling 31% TL (see also Figure S1).

On the adoral surface, there are also spatulate spines and hook-like curved spines, as on the labrum; each type of spine is clearly specialized in a specific function, but for further information, see Mortensen (1951).

In some individuals, 110 mm long, the oral secondary spines are up to 16.5 mm long, equaling approximately 15% TL.

The peristome is transverse and kidney-shaped and positioned approximately 25% TL far from the anterior margin on average (n 180). In living individuals, the stoma is surrounded by imbricated plates that open in the center.

The periproct is transverse and broad elliptic (Figure 11F) (mean L1 approximately 11% TL; mean L2 approximately 14% TL); it opens more or less high on the posterior face (on average 18% TL).

The subanal fasciole is thin and covered by a thick and very fine granulation, which carries very thin specialized spines (clavulae), with FW 1.21% TL on average; the pathway is long, with L17 measuring on average 43.7% TL (n 116), bilobed posteriorly and almost rectilinear anteriorly. The fasciole crosses the plates 5.a.3 and 5.b.3, then it passes in the ambulacrum I in position I.a.6 → 8, and returns to intercept interambulacrum 5 in 5.b.5 → 4 with a slight curve, goes back symmetrically in the other half of the test in 5.a.4 → 5, V.b.8 → 6, and finally rejoins the beginning of the loop (Figures 4A, 11B, F). Inside each lobe, there is a relief, highlighted by tubercles that decrease in size from the center to the periphery.

5.1.3.5 Remarks

The only fossils that should be accepted in the genus *Spatangus* and compared with *S. purpureus*, are *S. desmaresti* from the Oligocene of Germany and *Spatangus* sp. 2 from the Miocene of Ukraine. In the latter species, the labrum is in contact with only one adjacent ambulacral plate per part, but the fasciole is not visible; however,

from the close-up photos provided by Kroh (personal courtesy, August 2019), two distinct lobes, typical of *Spatangus* structure, seem visible. Many Plio-Pleistocene or Quaternary *Spatangus* specimens, which could be compared with living *S. purpureus*, have been recorded from many Mediterranean localities [see Néraudeau et al. (1998); Borghi (2012) and Stara et al. (2018)], but they will be re-evaluated when greater quantities of specimens will be available.

5.1.3.6 Distribution

Mediterranean, East, and North Atlantic from Senegal (GBIF, 2022) to Faroe Island and North seas (Mortensen 1951; Smith and Kroh, 2011). Other marine areas to be verified.

5.1.4 Diagnostic characters of the genus *Propespatagus*

Propespatagus gen. nov. Stara P., Melis R., Bellodi A., Follesa M.C., Corradini C., Carugati L., Mulas A., Sibiriu M., Cannas R.

Etymology: from *Propes* (Latin = close/similar) and *patagus* (name used by Jules Lambert, eminent French echinologist, to indicate some spatangoids).

Type species: MZ UNICA 074-MED18-2.

5.1.4.1 Diagnosis

Cordiform test with anterior groove, which can be very deep; aboral surface domed and pointed forward; rounded margin tending to narrow anteriorly, with keeled plastron; small ethmolytic apical disc, with four gonopores and a madreporic plate extending to the center and beyond the two posterior pores, where it tends to widen; narrow anterior ambulacrum with small simple isopores and phyllodes in peribuccal areas; the other ambulacra have flush petaloids; slightly arched anterior paired petals with the pores of the anterior column adapically rudimentary or atrophied; the other pores large, paired and conjugated; slightly expanded posterior paired petals adapically, narrowing distally; medium- sized periproct, from subcircular to slightly elliptical, with greater horizontal diameter, open at the top on the posterior face; small and kidney -shaped peristome, mostly covered by the labrum; labrum anvil- shaped, small, in contact with only one ambulacral plate on each side; finely tuberculated plastron, formed by long, narrow and paired sternals, and long and strongly posteriorly convergent episternals; heterogeneous aboral tubercles, with primary tubercles scattered in the interambulacra in variable numbers, small and with shallow areoles; primary short spines; small subanal fasciole, from cordiform to circular (slightly wider than long), thick and made up of very fine granules; the fasciole runs on narrow ambulacral plates, which strongly indent interambulacrum 5 at the rear, almost occluding it in some species; the first two of these plates carry a subanal pore; the fasciole starts from the perradial suture (in relief) between the two episternal plates, enclosing a single relief (monolobed) cover by tick tuberculation (see also Smith, 2013).

5.1.4.2 Species included

Propespatagus raschi (Lovén, 1869)
P. subinermis (Pomel, 1883)
P. paucituberculatus (A. Agassiz. & H.L. Clark, 1902)
P. capensis (Döderlein 1905)
P. inermis (Mortensen, 1913)
Propespatagus multispinus (Mortensen, 1925)
Propespatagus sp. 1, this work
Propespatagus sp. 2, this work

Other species, thus far classified as *Spatangus*, could belong to this new genus, but further studies and in particular molecular analysis are necessary to verify their correct taxonomic position.

5.1.4.3 Distribution

Fossil: from the Pliocene to the Holocene of Italy; living: from the Mediterranean and the Eastern Atlantic, the Shetland Islands, Pacific, and Indian Oceans.

5.1.5 *Propespatagus* sp. 1

Propespatagus sp. 1, Figures 4B; 11G–L, Table 2

Holotype: specimen MZ UNICA 074-MED18-2, illustrated in Figure 11.

Paratypes: MZ UNICA 028-MED18-1, 2; other specimens UNICA 074-MED18-1; MZ UNICA 078-MED-18-1 to 4; MZ UNICA 085-MED-18 1; MAC.IVM 350-1.

Diffusion. West Mediterranean, Sardinian coasts, and probable French coasts (Bonnet, 1926; DORIS, 2022).

5.1.5.1 Diagnosis

Species with domed test (thin and fragile), margin from rounded to narrow in the anterolateral region, with the oral face concave in the anterior part and convex in the posterior half, with plastron raised and keeled; very deep and narrow anterior groove; small labral plate in contact with only one ambulacral plate on each side, and with the two sternals longer than wide; thick, cordiform, heart- shaped or circular sub-anal fasciole, which runs on ambulacral plates 6, 7, and 8, which strongly indent inter-ambulacrum 5, forming an evident single central relief within the fasciole (monolobate), in the sub-periproctal region. Primary tubercles are scattered in the aboral part of all five interambulacra.

5.1.5.2 Description

Cordiform test with rounded margins, decidedly pointed anteriorly (Figure 11G), with narrow and close shoulders (L10 varies from 14.9 to 21.5% TL, average = 17.8% TL) and maximum height rear to apex on interambulacrum 5; test truncated posteriorly by an inclined face in an adoral sense, in the upper part of which opens the periproct (Figures 11G, I). Medium-large size (TL varies from 64.5 to 123 mm). The average width of the test (TW) is 92.94% TL.

The aboral face is raised posteriorly, with the maximum height (TH varies from 45 to 54.7% TL, average 51.14% TL) placed behind the apical disc (Figures 11G, J). The anterior groove is narrow and very deep, with the sinus L9 ranging from 9.3% to 11.9% TL (average = 10.71% TL).

The peristomial area is slightly sunken, on the oral face, which is slightly concave anteriorly, but with the labrum and the plastron in relief (Figures 11G, K).

The aboral tuberculation is scarce and heterogeneous, constituted by scrobiculate, crenulated, and perforated tubercles, small and with not very deep areoles; the test is covered with a

thick granulation that supports thin and short spines. The fasciole is small/medium- sized (L17 varies from 26.4 to 27.8, average 26.73% TL), but thick (average FW = 3.32% TL), and forms a subcircular or cordiform loop.

The apical disc is small (width approximately 1.8% TL) and slightly anterior to the center; L8 ranges from 57.6% to 64.4% TL (average approximately 61.8% TL), ethmolytic, with four gonopores; the anterior is slightly closer (Figure 11H).

Ambulacrum III with small and undifferentiated pores; it forms a deeper and wider anterior groove when approaching the margin with L9 that ranges from 9.3 to 11.9 (average of 10.7% TL); L10 approximately 18% TL (Figures 11L, K).

Paired anterior ambulacra petaloid in the aboral tract, mostly straight, slightly arched backward; relatively short and narrow; L4 ranges from 29.6% to 36.6% TL (average L4 = 33.3) and L5 ranges from 8.7% to 11.3% TL (average = 10% TL). The petals diverge on average at approximately 127 degrees; the pores of the anterior series become smaller adapically, and in many cases become rudimentary, but in smaller numbers than in *Spatangus* (Figure 11J); adorally, each ambulacrum carries two sets of five to six well-developed peribuccal phyllodes into the peristomial dimple. Near the peristome, the plates are shorter than wide, and they contain unipores surrounded by large periporal areas and gradually lengthen to then shorten toward the edge, where they widen again; the PLR is high and ranges from 3.7 to 4.5. The poriferous areas, in their central petaloid tract, are large about one-third of the interporiferous ones, which are devoid of tubercles; both the aboral and adoral tracts carrying phyllodes are bare, while the marginal areas are covered by numerous small secondary tubercles. The posterior paired ambulacra are longer (L6 ranges from 32.3% to 38.5% TL, average 35.7% TL) and relatively narrow (L7 ranges from 7.7% to 11.6% TL, average 9.7% TL); normally, they are more straight and slightly sharper than the anterior ones and diverge between them by approximately 60 degrees. The poriferous areas, in their central tract, measure approximately one-third of the interporiferous ones, which are devoid of tubercles. The non-petaloid aboral tract and the periplastronal tracts are devoid of tubercles, while the marginal tracts are covered by a dense secondary tuberculation. On the adoral face, ambulacra I and V form a more or less sub-parallel series of elongated plates that delimit the plastron (Figures 4B, 11K); in correspondence with the posterior part of the plastron, the relative ambulacral plates 6, 7, and 8 strongly indent the episternals (Figures 4B, 11K). In plates 6 and 7, there are evident pores within the perimeter of the fasciole.

The plastron is raised, keeled, and densely tuberculate as well as the labrum. The labrum protrudes anteriorly to cover a large part of the peristome; it is mushroom-shaped, short (average L12 = 6.2% TL) extending halfway through the adjacent ambulacral plates, with the base in short contact with the two sternal plates (average L14 = 4.3% TL). The sternal plates are narrow and long (average L13 = 38.5% TL and average L16 = 24.3% TL, with the ratio between L13/L16 approximately 1.6). The suture between the sternal and episternal plates falls normally at the fifth adjacent ambulacral plate. Posteriorly, the episternals are strongly indented by the ambulacral plates, so much as to occlude, in some specimens, interambulacrum 5; within the perimeter of the subanal fasciole, the episternals form a central tuberculate relief (Figures 11I, K).

The primary tuberculation is heterogeneous and scarce on the aboral interambulacral side (Figure 11J); the primary tubercles are small, crenulated, and perforated, with the shallow areoles, which rarely exceed 2% TL in diameter; they are arranged singly or in short horizontal lines, obliquely on the plates of the interambulacra, more abundant adapically. The primary spines are rather short, not exceeding 15% TL; they are thin and striped; the secondary ones do not exceed 7% TL, are very thin, and cover the entire surface, interspersed with the miliaries.

All the interambulacra, in the oral face, including the plastron and the labrum, are covered by secondary perforated and scrobiculate tubercles, which diminish in size as they approach the edges of the plates and toward the margin of the test (Figure 11K). Also, the adoral tract of the ambulacrum III has secondary tubercles, while the periplastronal tracts of the ambulacra are naked. The fasciole is covered by a very fine granulation that carries very thin clavulae; the rest of the tuberculate surface within the fasciole has spines no longer than 0.7% TL and is very thin.

The peristome is transverse, small, and kidney-shaped, approximately 23% TL far from the anterior border (Figure 11K). In living individuals, the stoma is surrounded by imbricate plates that leave a central opening and is covered for the most part by the labrum.

The periproct is small (L1 measuring on average 8.5% TL) and is slightly elliptical transverse (mean L2 = 11.5% TL) and opens between plates 5.a.4/5 and 5.b.4/5 (Figure 11I).

The fasciole is thick, with a short path that varies from roundish to cordiform, with L17 ranging from 25.4% to 27.7% TL (on average 26.7% TL). The pathway starts from the center of the two episternal plates, which is positioned along their perradial suture. The formula is 5.a.3 and 5.b.3; then it runs on the ambulacra in the I.a.6 → 9 position and then returns to intercept the interambulacrum at 5.b.4, drawing a slight indentation in the presence of a subanal dimple, to continue symmetrically in the other half of the test in 5.a.4, V.b.9 → 6, to then close the path rejoining with the start of the loop (Figures 4B, 11I, K). Inside the loop drawn by the fasciole (monolobate), there is one relief, highlighted by tubercles larger in the center, which decrease in size as they approach the fasciole.

5.1.5.3 Remarks

Propespatagus sp. 1 (Figures 4B, 11J) differs from *P. inermis* (Figure 5B) in having a deeper anterior sinus (mean L9 = 10.7, versus a maximum of 8.7% TL) and primary tubercles widespread in all interambulacra, while *P. inermis* is completely tubercle-free in interambulacra 1 and 4. *Propespatagus paucitubercolatus* (Figure 5C) is very close morphologically to the Sardinian species, since it has a similar anterior sinus, but it differs in the primary tuberculation, absent in the two interambulacra 1 and 4, and in the length of the petals, which are longer [mean L6 = 41% (n 2) against TL 35.7 (n 10)]; however, given the geographical distance and the presumed environmental difference and pending molecular analyses, it is treated here as a distinct species.

P. sp. 1 differs from *P. raschi*, in the lower height (51 against 60% TL), in its shorter petals (average L6 = 35.7 against 42% TL) (Figure 5E), and in the size of the fasciole (average L17 = 26.7 *vs.* 23% TL and FW thicker).

P. sp. 1 differs from *P. capensis* (species very close to *P. raschi*) in the lower test height (TH = 51, against 60% TL), in having a different

number of spines (see raschi), and in the lack of tubercles primary on the aboral extrapetal ambulacral surfaces. *P.* sp. 1 also differs from *P. multispinus*, with shorter spines (15% TL *vs*. 27% TL) and much fewer in number.

Finally, *P.* sp. 1 clearly differs from *P. raschi* and *P. capensis* in having a much deeper sinus (Figures 5E, F) and much smaller petals. The set of characters, as also visible in Figures 5E, F, clearly detaches the two Atlantic species from the Sardinian ones.

For complete descriptions of *P. raschi*, *P. capensis*, *P. paucituberculatus*, and *P. multispinus*, see Mortensen (1951).

6 Conclusion

The availability of a significant number of studied specimens allowed us to clarify the variability limits of some important diagnostic characters, enhancing the possibility to discriminate species and genera among the Spatangidae.

The use of all these characters in the morphometric and morpho-structural analyses, and the appropriate genetic analyses performed, allowed us to clarify the taxonomical relationships within the family Spatangidae, distinguishing four genera. This method aims to lay the foundations also for the specific distinction within this and other spatangoid families.

Data availability statement

The data presented in the study are deposited in the GenBank® repository (Sayers et al., 2022), accession number OP361060-OP361073; OP359422- OP359435. Additional details on DNA sequences are found in the article/Supplementary Material.

Author contributions

PS: Conceptualization, Methodology, Formal Analysis, Data curation, Visualization, Writing- Original draft preparation, Writing - Review & Editing. RM: Investigation, Formal Analysis, Data curation, Visualization, Writing- Original draft preparation. AB: Investigation, Formal Analysis, Writing- Original draft preparation. MCF: Resources, Writing - Review & Editing. CC: Supervision, Writing - Review & Editing. LC: Writing - Review & Editing, AM: Formal Analysis, Writing- Original draft preparation, MS: Investigation, Formal Analysis. RC: Methodology, Formal Analysis, Visualization, Writing- Original draft preparation, Writing - Review & Editing, Resources. All authors contributed to the article and approved the submitted version.

Acknowledgments

We thank all contributors to this research. In particular, we are grateful to all the participants in the scientific surveys, as well as the crew of each research vessel for their sampling effort: Andreas Kroh (the NHMW) Wien, Austria; Sylvain Charbonnier (MNHNF) Paris, France; Claudia di Somma and Andrea Travaglini (SZN) Naples, Italy; Anderson Owen (NIWA), Wellington, New Zealand; and Luigi Sanciu (MAC) Masullas, Oristano, Sardinia, Italy. Also heartfelt thanks to the paleontologist researchers (Fabio Ciappelli (Private collection), Prato, Tuscany; Enrico Borghi (Private Collection), Modena, Emilia Romagna; and Giuseppe Carone (Paleontological Museum of Vibo Valentia), Calabria, Italy), who provided us with precise indications on paleontological localities and their collected specimens.

Conflict of interest

The authors declare that the research was conducted in the absence of any commercial or financial relationships that could be construed as a potential conflict of interest.

Publisher's note

All claims expressed in this article are solely those of the authors and do not necessarily represent those of their affiliated organizations, or those of the publisher, the editors and the reviewers. Any product that may be evaluated in this article, or claim that may be made by its manufacturer, is not guaranteed or endorsed by the publisher.

Supplementary material

The Supplementary Material for this article can be found online at: https://www.frontiersin.org/articles/10.3389/fmars.2023.1033710/full#supplementary-material

References

Anderson, M. J., and Willis, T. J. (2003). Canonical analysis of principal coordinates: a useful method of constrained ordination for ecology. *Ecology* 84 (2), 511–525. doi: 10.1890/0012-9658(2003)084[0511:CAOPCA]2.0.CO;2

Baker, A. N., and Rowe, F. W. E. (1990). Atelostomatid Sea urchins from Australian and new zeland waters (Echinoidea: Cassiduloida, holasteroida, spatangoida, neolampadoida. *Invertebrate. Taxonomy.* 4, 281–316. doi: 10.1071/IT9900281

Bonnet, A. (1926). Document pour servir à l'étude de la variation chez les Échinides. v. variations du test chez le *Spatangus purpureus*. *Bull. l'Institut. Océanographique. Monaco.* 23, 1–27.

Borghi, E. (2012). Il genere Spatangus (Echinoidea) nel Langhiano dell'Appennino reggiano. *Notiziario della Società Reggiana di Scienze Naturali. Reggio Emilia* 2010, 43–61.

Borri, M., Righini, P., and Piras, A. (1990). Fauna echinologica dei fondi molli dell'alto tirreno e note sulle biocenosi relative. *Atti. Della. Società. Italiana. di. Sci. Naturali. e del. Museo. Civico. di. Storia. Naturale. di. Milano.* 131 (26), 377–410.

Bucklin, A., and Frost, B. W. (2009). Morphological and molecular phylogenetic analysis of evolutionary lineages within clausocalanus (Copepoda: Calanoida). *J. Crustacean. Biol.* 29 (1), 111–120. doi: 10.1651/07-2879.1

Chesher, R. H. (1968). The systematics of sympatric species in West Indian spatangoids: A revision of the genera *Brissopsis, Plethotaenia, Paleopneustes*, and *Saviniaster*. *Stud. Trop. Oceanogr.* 7, 1–168, pls 1-35.

Chippindale, P. T., and Wiens, J. J. (1994). Weighting, partitioning, and combining characters in phylogenetic analysis. *Syst. Biol.* 43 (2), 278–287. doi: 10.2307/2413469

Clark, H. L. (1917). Hawaiian And other pacific echini / by Alexander agassiz and Hubert Lyman Clark. *Mem. Mus. Comp. Zool.* 46 (2), 234.

Clarke, K. R., and Gorley, R. N. (2015). *Primer v7: user manual/tutorial* (Plymouth: PRIMER-E Ltd).

Collin, R., Venera-Pontón, D. E., Driskell, A. C., Macdonald, K. S., Geyer, L. B., Lessios, H. A., et al. (2020). DNA Barcoding of echinopluteus larvae uncovers cryptic diversity in neotropical echinoids. *Invertebrate. Biol.* 139 (2), e12292. doi: 10.1111/ivb.12292

DORIS (2022) *Spatangus subinermis*. Available at: https://doris.ffessm.fr/Especes/Spatangus-subinermis-Spatangue-profond-d-Europe-1293/(rOffset)/0. [accessed August 27, 2022]

Filander, Z., and Griffiths, C. (2017). Illustrated guide to the echinoid (Echinodermata: Echinoidea) fauna of south Africa. *Zootaxa* 4296, 1–72. doi: 10.11646/zootaxa.4296.1.1

GBIF (2022). *Spatangus purpureus* O.F.Müller, 1776 in GBIF Secretariat (2022). GBIF Backbone Taxonomy. Checklist dataset. https://doi.org/10.15468/39omei [accessed https://via GBIF.org on August 27, 2022]

Gray, J. E. (1825). An attempt to divide the echinida, or Sea eggs, into natural families. *Ann. Philos. New series.* 10, 423–431.

Hammer, Ø., Harper, H. A. T., and Ryan, P. D. (2001). PAST: Paleontological statistics software package for education and data analysis. *Palaeontol. Electronica.* 4(1), 4. Available at: http://palaeo-electronica.org/2001_1/past/issue1_01.htm.

Huelsenbeck, J. P., Bull, J. J., and Cunningham, C. W. (1996). Combining data in phylogenetic analysis. *Trends Ecol. Evol.* 11 (4), 152–158. doi: 10.1016/0169-5347(96)10006-9

Kroh, A. (2005). *Echinoidea neogenica. catalogus fossilium austriae. band 2* (Wien: Verlag der Österreichischen Akademie der Wissenschaften) Vienna, 210 p., 82

Kroh, A. (2007). Hemipatagus, a misinterpreted loveniid (Echinodermata: Echinoidea). *J. Syst. Palaeontol.* 5 (2), 163–192. doi: 10.1017/S1477201906002021

Kroh, A. (2020). "Phylogeny and classification of echinoids," in *Sea Urchins: Biology and ecology*. Ed. J. Lawrence (Cambridge: Academic Press), 1–17. doi: 10.1016/B978-0-12-819570-3.00001-9

Kroh, A., and Mooi, R. (2022) *World echinoidea database. spatangus Gray*. Available at: https://www.marinespecies.org/aphia.php?p=taxdetails&id=123430 (Accessed 2022-07-26).

Kroh, A., and Smith, A. B. (2010). The phylogeny and classification of post-Palaeozoic echinoids. *J. Syst. Palaeontol.* 8 (2), 147–212. doi: 10.1080/14772011003603556

Kumar, S., Stecher, G., and Tamura, K. (2016). MEGA7: Molecular evolutionary genetics analysis version 7.0 for bigger datasets. *Mol. Biol. Evol.* 33 (7), 1870–1874. doi: 10.1093/molbev/msw054

Lachkhem, L., and Roman, J. (1995). Les échinoïdes irréguliers (néognathostomes et spatangoïdes) du messinien de melilla (Maroc septentrional). *Annales. Paléontol. (Vertébrés-Invertébrés).* fasc. 4, vol. 81, 247–278.

Lambert, J. (1915). Description des échinides des terrains néogènes du bassin du rhône. *Mémoires. la. Société. Paléontol. Suisse.* 41, 155–240.

Layton, K. K. S., Corstorphine, E. A., and Hebert, P. D. N. (2016). Exploring Canadian echinoderm diversity through DNA barcodes. *PloS One* 11 (11), 16. doi: 10.1371/journal.pone.0166118

Littlewood, D. T., and Smith, A. B. (1995). A combined morphological and molecular phylogeny for sea urchins (Echinoidea: Echinodermata). *Philos. Trans. R. Soc. Lond. B. Biol. Sci.* 347 (1320), 213–234. doi: 10.1098/rstb.1995.0023

Lovén, S. (1874). Etudes sur les echinoidees. *Kongelige. Svenska. Vetenskaps-Akademiens. Handlingar.* 11, 1–91.

McNamara, K. J. (1982). Heterochrony and phylogenetic trends. *Paleobiology* 8 (2), 130–142. doi: 10.1017/S0094837300004474

McNamara, K. J. (1987). Plate translocation in spatangoid echinoids: its morphological, functional and phylogenetic significance. *Paleobiology* 13 (3), 312–325. doi: 10.1017/S0094837300008897

McNamara, K. J. (1988). "Heterochrony and the evolution of echinoids," in *Echinoderm phylogeny and evolutionary biology*. Eds. C. R. C. Paul and A. B. Smith. (Oxford: Oxford University Press), 111–119.

McNamara, K. J. (1989). The role of heterochrony in the evolution of spatangoid echinoids. *Geobios* 22, 283–295. doi: 10.1016/s0016-6995(89)80029-4

Mongiardino Koch, N. (2021). Exploring adaptive landscapes across deep time: A case study using echinoid body size. *Evolution* 75(6), 1567–1581. doi: 10.1111/evo.14219.

Mongiardino Koch, N., Coppard, S. E., Lessios, H. A., Briggs, D. E.G., Mooi, R., and Rouse, G. W. (2018). A phylogenomic resolution of the sea urchin tree of life. *BMC Evol Biol* 18(1), 189. doi: 10.1186/s12862-018-1300-4.

Mongiardino Koch, N., and Thompson, J. R. (2021). A total-evidence dated phylogeny of echinoidea combining phylogenomic and paleontological data. *Syst. Biol.* 70(3), 421–439. doi: 10.1093/sysbio/syaa069

Mongiardino Koch, N., Thompson, J. R., Hiley, A. S., McCowin, M. F., Armstrong, A. F., Coppard, S. E., et al. (2022). Phylogenomic analyses of echinoid diversification prompt a re-evaluation of their fossil record. *Elife* 11. doi: 10.7554/eLife.72460.

Mortensen, T. (1907). *The Danish ingolf-expedition 1895–1896. Echinoidea, pt. 1* (Copenhagen: Bianco Luno).

Mortensen, T. (1913). Die echiniden des mittelmeeres. eine revidierte ubersicht der im mittelmeere lebended echiniden, mit bemerkungen uber neue oder weniger bekannte formen. *Zool. Station zu Neapel. zugleich. ein. Repertorium. fur. Mittelmeerkunde.* 21, 1. Berlin, VERLAG VON R. FRIEDLÄNDER & SOHN

Mortensen, T. (1948). Contributions to the Biology of the Philippine Archipelago and adjacent regions. *Report on the Echinoidea collected by the United States Fisheries Steamer "Albatross" during the Philippine Expedition, 1907-1910. Part 3: The Echinoneidae, Echinolampidae, Clypeastridae, Arachnidae, Laganidae, Fibulariidae, Urechinidae, Echinocorythidae, Palaeostomatidae, Micrasteridae, Palaepneustidae, Hemiasteridae, and Spatangidae*. Smithsonian Institution, United States National Museum Bulletin Bulletin. Washington, US. 100, 93–140.

Mortensen, T. (1951). *A monograph of the Echinoidea. V, 2. Spatangoida II. Amphisternata II. Spatangidae, Loveniidae, Pericosmidae, Schizasteridae, Brissidae* (Copenhagen: C. A. Reitzel).

Néraudeau, D., Borghi, E., and Roman, J. (1998). Le genre d'échinide *Spatangus* dans les localités du pliocène et du pléistocène d'Émilie (Italie du nord). *Annales. Paléonol.* 84, 3–4. 243-264.

Néraudeau, D., Dudicourt, J.-C., Boutin, F., Ceulemans, L., and Nicolleau, P. (2010). Les Spatangus du miocène et du pliocène de l'Ouest de la France. *Annales. Paléontol.* 96 (4), 159–170. doi: 10.1016/j.annpal.2011.05.001

Palumbi, S. R., Martin, A., Romano, S., McMillan, W. O., Stice, L., and Grabowski, G. (1991). *The simple fool's guide to PCR, version 2.0* (Honolulu: Department of Zoology and Kewalo Marine Laboratory University of Hawaii).

Risso, (1826). *Histoire naturelle des principales productions de l'Europe mèridionale et particulièrement de celles des environs de nice et des alpes maritimes* (Paris - Strasbourg, G. Levrault).

Ronquist, F., Teslenko, M., van der Mark, P., Ayres, D. L., Darling, A., Höhna, S., et al. (2012). MrBayes 3.2: efficient Bayesian phylogenetic inference and model choice across a large model space. *Syst. Biol.* 61 (3), 539–542. doi: 10.1093/sysbio/sys029

Sayers, E. W., Bolton, E. E., Brister, J. R., Canese, K., Chan, J., Comeau, D. C., et al. (2022). Database resources of the national center for biotechnology information. *Nucleic Acids Res* 50(D1), D20–d26. doi: 10.1093/nar/gkab1112.

Schultz, H. (2009). *Sea Urchins II: Worldwide irregular deep water species* (Hemdingen: Heinke & Peter Schultz Partner Scientific Publications), 501–849, ISBN: .

Serafy, D. K., and Fell, F. J. (1985). *Marine flora and fauna of the northeastern united states. Echinodermata: Echinoidea* (U.S. DEPARTMENT OF COMMERCE: NOAA Technical Report NMFS).

Shin, S. (2013). A newly recorded Sea urchin (Echinoidea: Spatangoida: Spatangidae) from geomundo island, Korea. *Anim. Syst. Evol. Diversity* 29 (4), 308–311. doi: 10.5635/ased.2013.29.4.308

Smith, A. B. (2005). "Growth and form in echinoids. the evolutionary interplay of plate accretion and plate addition," in *Evolving form and function: Fossils and development. proceedings of a symposium honoring Adolf seilacher for his contributions to paleontology, in celebration of his 80th birthday*. Ed. D. E.G. Briggs(New Haven, Connecticut USA, Peabody Museum of Natural History), 181–195.

Smith, A. B. (2013). "Key to genera of spatangidae," in *The echinoid directory*. Eds. A. B. Smith and A. Kroh (World Wide Web Electronic publication.). The Natural History Museum, London. Available at: http://www.nhm.ac.uk/research-curation/research/projects/echinoid-directory/taxa/key.jsp?id=297. [Accessed August 27, 2022].

Smith, A. B., and Kroh, A. (2011). *The echinoid directory* (World Wide Web electronic publication). The Natural History Museum, London. Available at: http://www.nhm.ac.uk/research-curation/projects/echinoid-directory. [Accessed August 27, 2022].

Smith, A. B., Littlewood, D. T. J., and Wray, G. A. (1995). Comparing patterns of evolution: Larval and adult life history stages and ribosomal RNA of post-Palaeozoic echinoids. *Philos. Transactions.: Biol. Sci.* 349 (1327), 11–18.

Smith, A. B., Pisani, D., Mackenzie-Dodds, J. A., Stockley, B., Webster, B. L., and Littlewood, D. T. (2006). Testing the molecular clock: molecular and paleontological estimates of divergence times in the echinoidea (Echinodermata). *Mol. Biol. Evol.* 23 (10), 1832–1851. doi: 10.1093/molbev/msl039

Smith, A. B., and Stockley, B. (2005). Fasciole pathways in spatangoid echinoids: a new source of phylogenetically informative characters. *Zool. J. Linn. Soc.* 144 (1), 15–35. doi: 10.1111/j.1096-3642.2005.00161.x

Spedicato, M. T., Massutí, E., Mérigot, B., Tserpes, G., Jadaud, A., and Relini, G. (2019). The MEDITS trawl survey specifications in an ecosystem approach to fishery management. *Sci. Marina.* 83 (S1), 9–20. doi: 10.3989/scimar.04915.11X

Stara, P., Borghi, E., and Kroh, A. (2016). Revision of the genus mariania (Echinoidea) with the description of two new species from the Miocene of Italy. *Bull. Geosci.* 91 (1), Stara65–88. doi: 10.3140/bull.geosci.1576

Stara, P., Charbonnier, S., and Borghi, E. (2018). Redefinition of prospatangus thieryi Lambert 1909 (Echinoidea, spatangoida), in sardospatangus nov. gen. with two new species from Sardinia, Italy. *Annales. Paleontol.* 104 (4), 309–327. doi: 10.1016/j.annpal.2018.10.001

Stockley, B., Smith, A. B., Littlewood, T., Lessios, H. A., and Mackenzie-Dodds, J. A. (2005). Phylogenetic relationships of spatangoid sea urchins (Echinoidea): taxon sampling density and congruence between morphological and molecular estimates. *Zool. Scripta.* 34 (5), 447–468. doi: 10.1111/j.1463-6409.2005.00201.x

Sumida, P. Y. G., Tyler, P. A., Thurston, M. H., and Gage, J. D. (2001). Early post-metamorphic ontogenesis of deep-sea spatangoids (Echinoidea, spatangoida) of the NE Atlantic ocean. *Invertebrate. Biol.* 120 (4), 378–385. doi: 10.1111/j.1744-7410.2001.tb00046.x

Swofford, D. L. (2003). *PAUP*. phylogenetic analysis using parsimony (* and other methods). version 4* (Sunderland, Massachusetts, Sinauer Associates).

Thompson, J. R., Erkenbrack, E. M., Hinman, V. F., McCauley, B. S., Petsios, E., and Bottjer, D. J. (2017). Paleogenomics of echinoids reveals an ancient origin for the double-

negative specification of micromeres in sea urchins. *Proc Natl Acad Sci U S A* 114(23), 5870–5877. doi: 10.1073/pnas.1610603114.

Thompson, J. D., Higgins, D. G., and Gibson, T. J. (1994). CLUSTAL W: improving the sensitivity of progressive multiple sequence alignment through sequence weighting, position-specific gap penalties and weight matrix choice. *Nucleic Acids Res.* 22 (22), 4673–4680. doi: 10.1093/nar/22.22.4673

Tortonese, E. (1965). *Echinodermata Fauna d'Italia Volume VI*. 186 fig., 424 pp Bologna: Edizioni Calderini.

Vadet, A., and Nicolleau, P. (2018). Evolution des spatangues. *Annales de la Société d'Histoire Naturelle du Boulonnais*. Tome XVII. 1, 4, 128pp.

Ward, R. D., Holmes, B. H., and O'Hara, T. D. (2008). DNA Barcoding discriminates echinoderm species. *Mol. Ecol. Resour.* 8 (6), 1202–1211. doi: 10.1111/j.1755-0998.2008.02332.x

Ziegler, A., Stock, S., Menze, B., and Smith, A. (2012). "Macro- and microstructural diversity of sea urchin teeth revealed by large-scale micro-computed tomography survey," in *Proc. SPIE 8506, Developments in X-Ray Tomography VIII*, 17 October 2012, Vol. 85061G. doi: 10.1117/12.930832

frontiers | Frontiers in Marine Science

TYPE Original Research
PUBLISHED 09 March 2023
DOI 10.3389/fmars.2023.1087339

OPEN ACCESS

EDITED BY
Jinghui Fang,
Chinese Academy of Fishery Sciences (CAFS), China

REVIEWED BY
Chunlin Wang,
Ningbo University, China
Vijaykumar Muley,
National Autonomous University of Mexico, Mexico

*CORRESPONDENCE
Lina Sun
sunlina@qdio.ac.cn

SPECIALTY SECTION
This article was submitted to Marine Biology, a section of the journal Frontiers in Marine Science

RECEIVED 02 November 2022
ACCEPTED 22 February 2023
PUBLISHED 09 March 2023

CITATION
Su F, Liu S, Xing L, Huo D, Yang H and Sun L (2023) Understanding gene regulation during the development of the sea cucumber *Apostichopus japonicus* using comparative transcriptomics. *Front. Mar. Sci.* 10:1087339. doi: 10.3389/fmars.2023.1087339

Understanding gene regulation during the development of the sea cucumber *Apostichopus japonicus* using comparative transcriptomics

Fang Su[1,2,3,4,5], Shilin Liu[1,2,3,4,5], Lili Xing[1,2,3,4,5], Da Huo[1,2,3,4,5], Hongsheng Yang[1,2,3,4,5,6] and Lina Sun[1,2,3,4,5]*

[1]CAS Key Laboratory of Marine Ecology and Environmental Sciences, Institute of Oceanology, Chinese Academy of Sciences, Qingdao, China, [2]Laboratory for Marine Ecology and Environmental Science, Qingdao National Laboratory for Marine Science and Technology, Qingdao, China, [3]CAS Engineering Laboratory for Marine Ranching, Institute of Oceanology, Chinese Academy of Sciences, Qingdao, China, [4]University of Chinese Academy of Sciences, Beijing, China, [5]Shandong Province Key Laboratory of Experimental Marine Biology, Qingdao, China, [6]The Innovation of Seed Design, Chinese Academy of Sciences, Wuhan, China

Embryonic development, especially metamorphosis and settlement, has a major impact on the life history of marine invertebrates. *Apostichopus japonicus* is an economically important species of sea cucumber. In this study, we performed RNA sequencing on six key stages of *A. japonicas* development: fertilized eggs, blastula, gastrula, auricularia, doliolaria, and pentactula. A total of 32,353 genes were identified and annotated as a reference gene set for subsequent pairwise comparison analysis. After filtering out low-quality genes, the dynamic molecular responses to development were revealed by WGCNA. The results showed that of the 20 modules, genes in the blue, yellow, and darkslateblue modules were highly correlated with the gastrula, auricularia, and blastula stages, respectively. GO terms for "RNA" and "proteasome complex" were most significantly enriched in the blue module. In the darkslateblue and yellow module, receptors of signaling pathways and metabolic processes were significantly enriched, respectively. All DEGs were categorized into 34 terms, mainly associated with signal transduction and cellular immunity. The expression pattern of genes associated with adhesion, cell cycle, signal, transcription factor, extracellular matrix (ECM), and cytoskeleton was analyzed according to gene function. The results of this study facilitated a more comprehensive understanding of the molecular characteristics of sea cucumber embryonic development and will provide theoretical guidance for larva rearing in sea cucumber culture.

KEYWORDS

Apostichopus japonicus, development, metamorphosis, RNA-Seq, WGCNA

1 Introduction

Apostichopus japonicus (Selenka) is distributed in shallow temperate and temperate-cold waters along the coasts of China, Japan, Korea, and Russia. This species is considered to be one of the most valuable sea foods, due to its extraordinary nutritional and medicinal properties (Yang et al., 2015). *A. japonicus* also displays some unique biological characteristics, such as evisceration, regeneration, aestivation, and autolysis (Yang et al., 2015). It has been extensively studied from many perspectives, including feeding behavior and movement patterns (Pan et al., 2015; Sun et al., 2015), reproduction and breeding (Kato et al., 2009; Ahmed et al., 2011; Soliman et al., 2013), responses to environmental changes (temperature, salt, light, and dissolved oxygen) (Dong et al., 2010; Meng et al., 2011; Xu et al., 2016; Huo et al., 2017), disease and immunity (Gu et al., 2010; Zhang et al., 2014), and physiology and behavior of regeneration or aestivation (Chen et al., 2015; Miao et al., 2017; Sun et al., 2017a; Sun et al., 2017b). In 2017, we published the *A. japonicus* genome, the first fine sea cucumber genome, making an important contribution to sea cucumber and echinoderm research (Zhang et al., 2017). *A. japonicus*, as a representative species for sea cucumbers, is becoming a good model species for research.

Development is the most important biological process for species. In recent years, there have been a number of studies on sea cucumber development, promoting our understanding of these species. Researchers have elucidated the development and growth morphogenesis patterns of different kinds of sea cucumbers, including *Cucumaria frondose* (Gianasi et al., 2018), *Stichopus* sp. (Curry fish) (Hu et al., 2010), *Isostichopus fuscus* (Hamel et al., 2003), and *A. japonicus* (Yang et al., 2015). *A. japonicus* has received the most attention from researchers due to its high economic value in China and Asia. The life cycle of *A. japonicus* can be divided into eight major developmental stages. Embryonic and larval development before the juvenile phase can be divided into six key stages as follows: fertilization of eggs, blastula, gastrula, auricularia, doliolaria, and pentactula (Yang et al., 2015). To date, there have been numerous studies on the effect of environmental factors (such as density, temperature, salinity, and pH) on the development of *A. japonicus* (Li and Li, 2009; Liu et al., 2010; Yuan et al., 2015), mainly focusing on survival rate and metamorphosis. However, there has been a lack of studies on genetic mechanisms and gene regulation associated with development.

Morphological changes in the development of fertilized eggs to juvenile have been reported in the literature. When the fertilization membrane is lifted, it indicates that the ovum is successfully fertilized. After multiple cell divisions, the number of cells increased and the cell volume became smaller. The blastula is a hollow sphere surrounded by a thin layer of cells, and the egg membrane is clearly visible. The embryo is detachable by rotation and then rotate freely with the oscillation of surface cilia in a finger ring shape. As development proceeds, the vegetal pole invades and forms mesenchymal cells. The digestive tract is not fully differentiated, and morphological distinctions are not obvious. The gastrula further develops into auricular larvae, and the digestive system begins to improve. The food particles enter the mouth with the water flow formed by the oscillation of the cilia. Calcareous ossicle begin to form and continue to elongate towards the posterior end. According to the development morphology of the water cavity, the auricular larvae are divided into three stages: early-auricularia larva, mid-auricularia larva, late-auricularia larva (Qiu, 2013). At the late-auricularia larva stage, five small vesicles grow outward the water cavity, resembling finger-like branches (Wang et al., 2019). The body shrinks to a cylindrical shape and the larvae metamorphose into doliolaria. Most of the cilia fall off, and the movement ability and swimming ability of the larvae decrease. At the pentactula stage, the cilia rings degenerate and disappear completely. The larvae change from planktonic life to benthic life, with five tentacles protruding. The larvae sink to the attachment base and crawl by the first tube foot and tentacles. However, the global gene regulation patterns of *A. japonicus* development and key regulatory gene families are still not well understood.

With the development of high-throughput sequencing techniques, a number of *A. japonicus* transcriptomes have been successfully constructed, including transcriptomes of intestine regeneration (Sun et al., 2011), intestines, respiratory trees and coelomic fluid (Du et al., 2012), response to pathogen infection (Zhou et al., 2014; Gao et al., 2015), and albinism biogenesis (Xing et al., 2018). However, comparative transcriptomes of all key stages of *A. japonicus* development have not yet been constructed, as it is very hard to assemble 18 transcriptomes *de novo* with mega data. Fortunately, the fine *A. japonicus* genome provides a good reference, which makes this possible (Zhang et al., 2017). In the current study, we applied transcriptomic techniques to identify differentially expressed genes (DEGs) of six different developmental stages of *A. japonicus*. The results of this study provided a better understanding of the mechanisms of *A. japonicus* development. Furthermore, these data will increase the amount of genetic information for *A. japonicus*, providing a good foundation for investigating the molecular/genetic mechanisms of sea cucumbers.

2 Materials and methods

2.1 Sample collection

Parent culture, spawning, and larva rearing were performed in our breeding base in Qingdao. The embryos and larvae of *A. japonicus* were cultivated in 2 m×5 m×1.5 m cement pools at 20 ± 1°C. Samples from six major developmental stages were collected: fertilized eggs (F, ~20 min after fertilization), blastula (B, ~10 h), gastrula (G, ~26 h), auricularia (A, ~ 8 d), doliolaria (D, ~ 10 d), and pentactula (P, ~ 12 d). The samples were monitored under a microscope to ensure developmental synchrony. Three samples at each developmental stage were collected as biological replicates. Each sample was washed with ddH_2O, frozen, and stored in liquid nitrogen. Finally, a total of 18 samples were prepared for sequencing to obtain 18 transcriptomes.

2.2 RNA extraction, library preparation, and illumina sequencing

Total RNA was extracted from 18 samples as mentioned above using the RNAeasy mini kit (Qiagen, USA) according to the manufacturer's instructions. The quality and concentration of RNA was measured by NanoDrop 1000 (Thermo). A total of 18 RNA samples were used for isolation, fragmentation, and construction of the cDNA library. Extracted total RNA was treated with DNase I, Oligo (dT) and used for RNA isolation. A total of 3 μg RNA per sample was used as input material for the RNA sample reparations. Fragmentation was carried out using divalent cations under elevated temperatures in NEBNext First Strand Synthesis Reaction Buffer (5×). Then cDNA was synthesized using the mRNA fragments as templates. Short fragments were purified and resolved with EB buffer (10 mM Tris-HCl, pH 8.5) for end reparation and single nucleotide A (adenine) addition. Subsequently, the short fragments were connected with adapters. Suitable fragments were selected for PCR amplification. During the QC steps, an Agilent 2100 Bioanalyzer and an ABI StepOnePlus Real-Time PCR System (Applied Biosystems, Foster City, CA, USA) were used in the quantification and qualification of the sample library. Finally, sequencing was carried out using Illumina HiSeq 4000 by the Beijing Genome Institute (BGI) (Shenzhen, China). Table S1 (supplementary material) gives a brief overview of the condition of the samples and summarizes the key characteristics of the transcriptome sequencing.

2.3 Transcriptome assembly, SNP and indel detection, novel transcript prediction and gene expression analysis

The sequencing reads which were of low quality, adaptor-polluted, or had a high number of unknown base (N) reads, were removed prior to further analyses. Filtering was performed using internal software of BGI. All sequencing data and quality information can be found in Table S1 in the supplementary material. HISAT (v0.1.6-beta) (Kim et al., 2015) was used to map all clean reads to the sea cucumber genome (NCBI accession number: PRJNA354676) (Zhang et al., 2017). After genome mapping, we used GATK to call SNP and INDEL variants for each sample (McKenna et al., 2010). After that, StringTie (v1.0.4) was used to reconstruct novel transcripts (Pertea et al., 2015), cuffcompare (v2.2.1) was used to compare reconstructed transcripts to draft genome annotation, and CPC (v0.9-r2) was used to predict the coding potential of novel transcripts (Kong et al., 2007). After novel transcript detection, we merged novel coding transcripts with reference transcripts to get complete reference, then we mapped clean reads to it using Bowtie2 (V2.25) (Langmead and Salzberg, 2012), then calculated gene expression level for each sample with RSEM (V1.2.12) (Li and Dewey, 2011). The gene expression summary was shown in Table S1 in the supplementary material. With gene expression results, NOIseq based on a noise distribution model was chosen to detect DEGs (Parameters: Fold Change ≥ 2.00 and Probability ≤0.8).

2.4 Gene functional annotation

The obtained genes were annotated according to the sea cucumber genome annotation (Zhang et al., 2017). The novel transcripts were annotated using BLAST programs with SwissProt, NCBI non-redundant (Nr) protein, and NCBI non-redundant nucleotide sequences (Nt) databases. The GO (http://www.geneontology.org/) and KEGG databases (http://www.genome.jp/kegg/) were used to classify and group the identified proteins. A hypergeometric test was used to define significantly enriched GO terms and pathways of differentially expressed genes. The terms which FDR not larger than 0.001 were defined as significant enriched.

2.5 WGCNA analysis

Co-expression networks were constructed using the WGCNA (v1.47) package in R (Langfelder and Horvath, 2008) to identify specific modules associated with larva development at different stages. The fragments per kilobase of transcript per million mapped reads (FPKM) of each gene was calculated as the gene expression level. Genes were filtered out when FPKM < 2 in more than 70% of samples and outlier samples were deleted. The rest genes in the 17 libraries were imported into WGCNA to construct co-expression modules using the automatic network construction function block wise Modules with default settings. To find biologically or clinically significant modules, module eigengenes were used to calculate the correlation coefficient with samples. Intramodular connectivity (K.in) and module correlation degree (MM) of each gene was calculated with the R package WGCNA. Genes with high connectivity tended to be hub genes which might have important functions. To identify modules significantly associated with different developmental stages, correlation analysis was performed using the module eigengene with gene expression levels in different groups (F, B, G, A, D, P). Modules with high gene expression were considered as target modules. To further analyze the biological functions of genes in each target module, GO and KEGG pathway enrichment analysis were performed. GO terms and pathways with p-value corrected by FDR ≤ 0.05 were considered to be significantly enriched.

2.6 Real-time PCR validation

The same RNA as used for Illumina sequencing was used in this experiment. The first strand cDNA was synthesized in a 25-μL reaction system as follows: 1) 4 μL RNA and 1 μL oligodT18 were denatured at 70°C for 5 min; 2) 1 μL M-MLV reverse transcriptase (Promega), 5 μL M-MLV buffer (25 mM KCl, 10 mM Tris-HCl, 0.6 mM $MgCl_2$, and 2 nM DTT, pH 8.3), 5 μL dNTP, 1 μL ribonuclease inhibitor, and 8 μL RNase-free water were added at 42°C for 1 h.

The synthesized cDNA was diluted with RNase-free water and stored at -80°C for subsequent quantitative real-time PCR. All gene mRNA expression levels were determined using the SYBR Green® real-time PCR assay with an Eppendorf Mastercycler® ep realplex (Eppendorf, Hamburg, Germany). The primers were designed using Primer3 (v0.4.0; http://bioinfo.ut.ee/primer3-0.4.0/primer3/) and are listed in Table S2 in the supplementary material. The amplification volume was 25 µL, and it contained 12.5 µL SYBR Green Master Mix (Takara), 0.5 µL (each) forward and reverse primer (10 µM), 1 µL diluted cDNA, and 10.5 µL RNase-free water. Thermal cycling was as follows: 1) 95°C for 5 s and 2) 40 cycles at 95°C for 10 s, 60°C for 20 s, and 72°C for 30 s. Melting curve analysis of the amplification products was performed to demonstrate the specificity of the PCR products. NADH dehydrogenase was used as a housekeeping gene for internal standardization (Sun et al., 2011; Sun et al., 2017b). The $2^{-\Delta\Delta CT}$ method was used to analyze mRNA expression levels. All data are reported as means ± SE (N = 5), and the level of statistical significance was set at $P < 0.05$. Analysis was carried out using SPSS18 software.

3 Results and discussion

3.1 Overview of the transcriptomes

In the current study, 8.25~8.98 Gb × 18 data from sea cucumbers at six key developmental stages were generated by high-throughput sequencing techniques, and have been submitted to NCBI (accession NO. PRJNA889469). After read filtering, 53.20~59.96 Mb× 18 clean reads were obtained to construct 81,146 transcripts with contig N50 of 3910bp, which were further grouped into 32,353 genes. Among all transcripts, 48,098 transcripts were novel transcripts by reconstruction after mapping sequenced reads to the reference genome. Of these, 24,275 were previously unknown splicing events for known genes, 5,494 were novel coding transcripts without any known features, and the remaining 18,329 were long noncoding RNAs. The mRNA expression levels of all genes can be found in Table S3 in the supplementary material.

Thanks to the development of high-throughput sequencing techniques, many transcriptomes have been constructed to understand global gene regulation or response mechanisms to different types of biological processes in sea cucumbers (Sun et al., 2011; Du et al., 2012; Zhang et al., 2013; Gao et al., 2015; Xing et al., 2018). However, the gene expression patterns of development, one of most important biological processes, are still not known. In 2012, Du et al. (Du et al., 2012). constructed the transcriptomes of embryos and larvae. However, these data could only provide relatively complete gene sets and did not reveal the gene regulation patterns of development of sea cucumbers, because the embryo and larva samples were pooled to construct two libraries and the sampling times did not coincide with five key developmental stages. In this study, we revealed the global gene expression patterns of six developmental stages, which detailed all gene regulation patterns during sea cucumber development.

3.2 Construction and analysis of weighted gene co-expression network

To better understand the gene co-expression network during sea cucumber development, WGCNA analysis was carried out to obtain 20 modules based on hierarchical clustering of calculated dissimilarity after filtering low-quality samples and genes (Figure 1A; Supplementary Table S4). Genes with similar

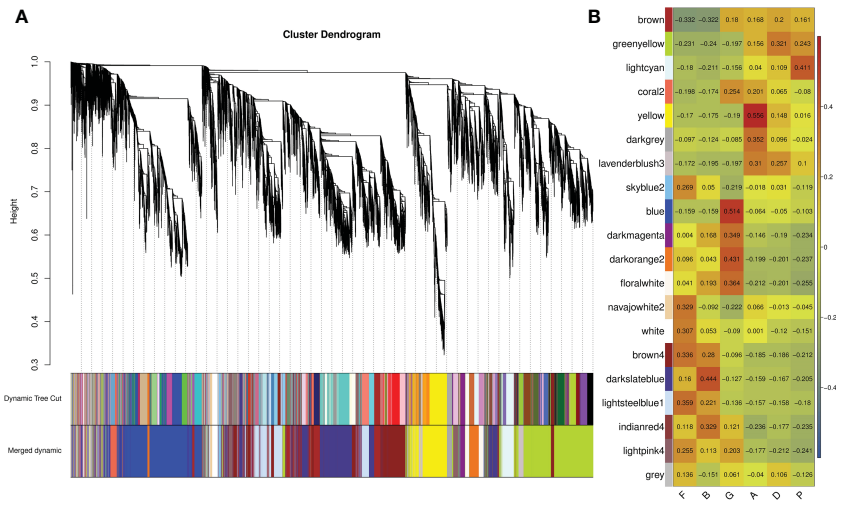

FIGURE 1
Weighted gene correlation network analysis (WGCNA) of all genes in different developmental stages. **(A)** Hierarchical cluster tree showing correlation modules identified by WGCNA. Each leaf in the tree represents one gene and each major tree branch represents one module, labelled with different colors. Modules with similar expression patterns are merged as merged dynamic. **(B)** Correlation matrix between modules and developmental stages. Red represents high expression and blue represents low expression.

expression patterns are represented on the same branch. Each branch represents a co-expression module. According to the similarity of the module eigengene, the modules with similar expression patterns are merged to obtain the final merged dynamic modules. Genes that do not fit into any module are shown in gray. The numbers of genes in modules ranged from 56 to 2,925 (Supplementary Table S5), and a heat map of sample expression patterns based on module eigengene was generated to visualize the correlation matrix between modules and groups (Figure 1B; Supplementary Table S6). Some modules were found to relate to specific developmental stages. The genes in the greenyellow, lightcyan, yellow, and lavenderblush3 modules were highly expressed in the auricularia, doliolaria, and pentactula stages, but were expressed at low levels in fertilized eggs, blastula, and gastrula stages. However, the darkmagenta, darkorange2, floralwhite, indianred4, and lightpink4 modules showed a completely opposite correlation. Furthermore, the results showed that the blue and yellow modules were positively correlated with the gastrula and auricularia stages, respectively. Additionally, the darkslateblue module had the highest correlation coefficient with the blastula stage. Therefore, we treated the three modules that were highly associated with these developmental stages as the target modules.

To further explore the function of module genes, we performed GO and KEGG enrichment analysis for each target module (Figure 2; Supplementary Tables S7, S8). GO terms for "RNA" and "proteasome complex", such as "translation factor activity, RNA binding (GO:0008135)", "RNA binding (GO:0003723)", "RNA processing (GO:0006396)" and "proteasome complex (GO:0000502)", were most significantly enriched in the blue module. In the darkslateblue module, receptors of signaling pathways were significantly enriched. The representatives were "immune response-activating cell surface receptor signaling pathway (GO:0002429)", "immune response-regulating cell surface receptor signaling pathway (GO:0002768)" and "antigen receptor-mediated signaling pathway (GO:0050851)". Additionally, genes grouped in the yellow module were significantly enriched in metabolic processes, such as "neurotransmitter metabolic process (GO:0042133)", "single-organism carbohydrate catabolic process (GO:0044724)", and "carbohydrate catabolic process (GO:0016052)". According to the KEGG pathway enrichment results, "proteasome (ko03050)", "spliceosome (ko03040)", and "protein export (ko03060)" pathways related to gene information processes were enriched in the blue module. In the darkslate and yellow modules, metabolic pathways were significantly enriched. Overall, GO and KEGG enrichment analysis demonstrated the role of modular genes in the larval development of *A. japonicus*.

The correlation network of significantly enriched genes in the three target modules is illustrated in Figure 3. According to the target module size, the top five genes with the highest All.kWithin values were identified as hub genes (Table S9 in the supplementary material). In the correlation network of the blue module, protein mago nashi homolog (MAGOH), zinc finger C4H2 domain-containing protein-like isoform X1(AC4H2), N-acetyltransferase 10 (NAT10), nuclear pore complex protein Nup107 isoform X1 (Nup107 complex), and eukaryotic translation initiation factor 3 subunit F (eIF3f) were identified as hub genes (Figure 3A; Supplementary Table S9). MAGOH is one of the three core proteins of the exon junction complex (EJC), and is essential for the normal development of embryos and nerves (Asthana et al., 2022). AC4H2 plays a vital role in regulating nervous system development, and has already been identified in multiple species

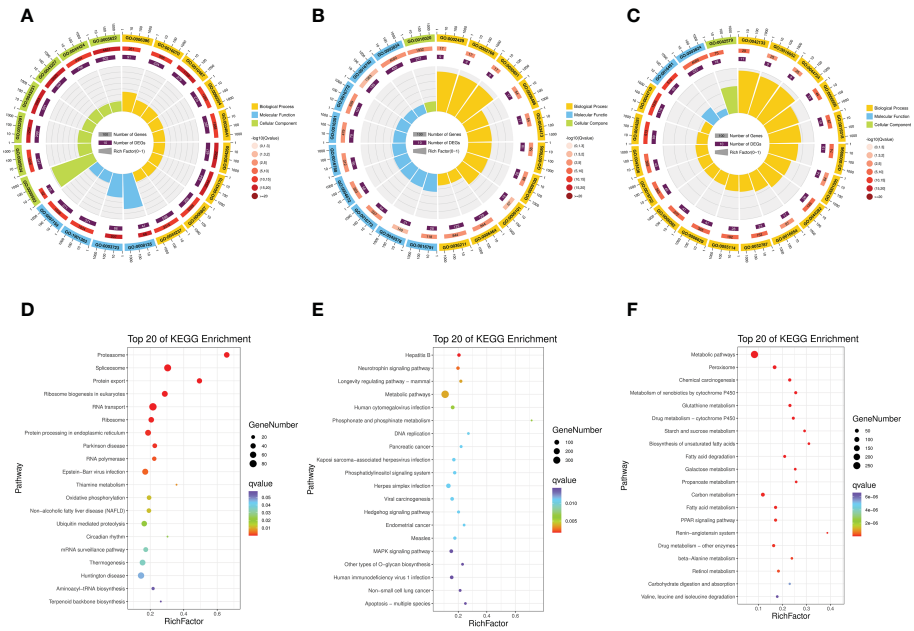

FIGURE 2
Gene Ontology (GO) enrichment analysis of genes in blue module **(A)**, darkslateblue module **(B)** and yellow module **(C)**. Kyoto Encyclopedia of Genes and Genomes (KEGG) enrichment analysis of genes in blue module **(D)**, darkslateblue module **(E)** and yellow module **(F)**.

10.3389/fmars.2023.1087339

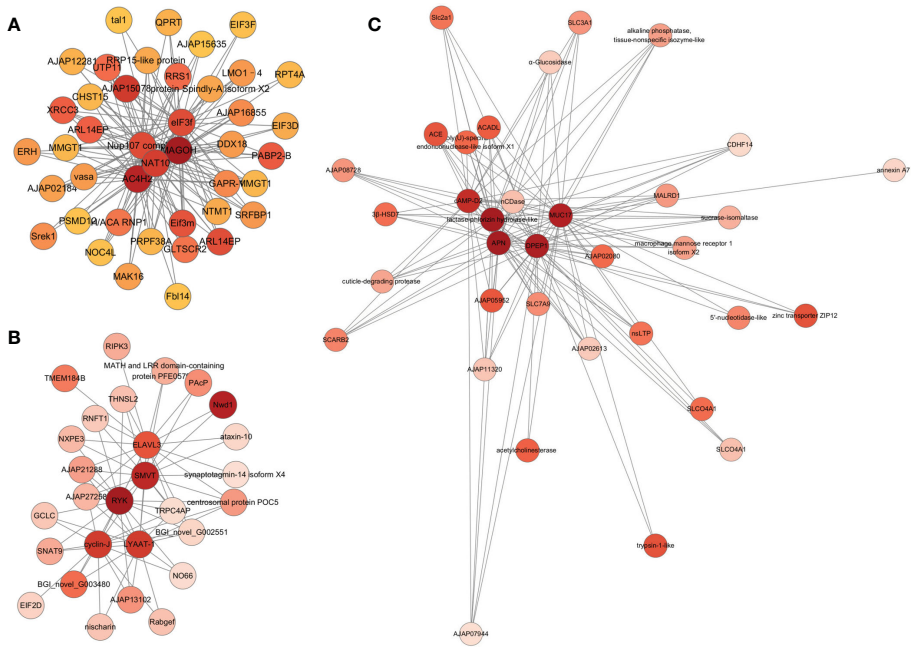

FIGURE 3
Correlation network visualization of the interactions between the top 5 genes with the highest connectivity in three target modules. Each node labelled with the abbreviation of gene name. Node colors represent connectivity, and darker nodes represent higher connectivity. **(A–C)** represent blue, darkslateblue and yellow module, respectively.

(May et al., 2015; Ma et al., 2017). NAT10 promotes cell proliferation and thereby participates in malignant transformation of various cancers. In addition, NAT10 is expressed in the central nervous system of the embryo (Guo et al., 2020). Nup107 complex is part of the Nuclear Pore Complex (NPC) structural scaffold and the role of the Nup107 complex in gene expression is not restricted to nucleo-cytoplasmic transport, but also participates in neural differentiation in vertebrates (Gonzalez-Aguilera and Askjaer, 2012). The first nerve cells were detected in the apical region of the epidermis in the late gastrula stage (Nakano et al., 2006). Thus, the blue module was closely related to neurological genesis. Genes for enzymes associated with digestion and immunity, such as lactase-phlorizin hydrolase-like, aminopeptidase N (APN), dipeptidase 1-like (DPEP1), mucin-17 isoform X2 (MUC17), and cAMP-regulated D2 protein-like (cAMP-D2) were identified as hub genes of the yellow module (Figure 3B, Table S9 in the supplementary material). During the auricularia stage, the digestive system begins to improve. For the darkslateblue module, tyrosine-protein kinase RYK isoform X4 (RYK), sodium-dependent multivitamin transporter (SMVT), lysosomal amino acid transporter 1 (LYAAT-1), cyclin-J, and ELAV-like protein 3 isoform X2 (elavl3) were identified as hub genes (Figure 3C, Table S9 in the supplementary material). RYK may be a co-receptor along with FZD8 of Wnt proteins, such as WNT1, WNT3, WNT3A and WNT5A. LYAAT-1 defines a subgroup of lysosomal transporters in the amino acid/auxin permease family (Sagne et al., 2001). These genes were involved in the transportation of substances and the cell cycle.

3.3 Differential expression genes and real-time PCR validation

Using 32,353 genes as a reference, five comparison groups: F Vs B, B Vs G, G Vs A, A Vs D, and D Vs P, were used to analyze the differential expression of genes during *A. japonicus* development using NOIseq arithmetic (fold-change≥2.0 and probability≥0.8). The number of up-regulated genes and down-regulated genes was 20 and 112, 1,781 and 1,535, 535 and 97, 98 and 272, and 12 and 29, respectively (Figure 4). The highest number of genes showing

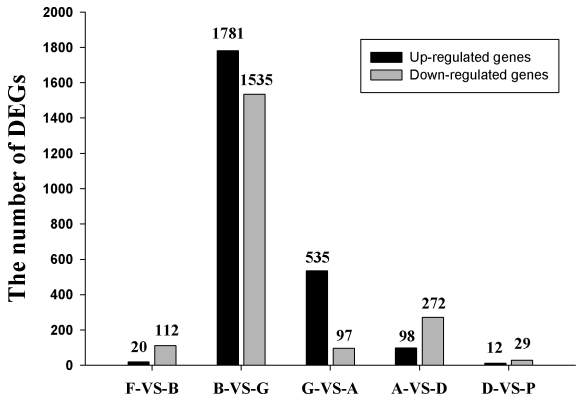

FIGURE 4
The number of differentially expressed genes (DEGs) in five comparison groups.

differential expression were between the blastula to gastrula stage (B Vs G). All DEGs are listed in Supplementary Table S10.

For validation purposes, RT-PCR analysis in four genes including cyclinB, ferritin, SoxB1, and cubilin-like protein was conducted in the six development stages (Figure 5). The results showed that the overall trend and variation of RT-PCR based expression patterns among these selected genes was coincident with those obtained by RNA-Seq based detection.

3.4 Gene function and KEGG pathway enrichment analysis of DEGs

All DEGs could be categorized into 34 terms. "Signal transduction", "Global and overview maps", "Cancers", "Endocrine system", "Transport and catabolism", "Infectious diseases: Viral", "cellular community", "Translation", "Digestive system", and "Signaling molecules and interaction" were the 10 most enriched terms during the entire development process of sea cucumbers (Supplementary Figure S1). Among almost all terms, the number of DEGs in the B Vs G comparison group was the largest, followed by the G Vs A comparison group (Figure 6), thus, there was strong gene expression regulation from blastula to auricularia. Compared with other pathways, the AVsD comparison group had the largest proportion in "cell growth and death".

GO enrichment analysis showed significant enrichment of DEGs in three categories: molecular function (MF), cellular component (CC), and biological process (BP) (Table S11 in the supplementary material). In the MF category, 1, 14, 2, and 1 terms were enriched in the F Vs B, B Vs G, G Vs A, and D Vs P groups, respectively. In the CC category, 3, 23, 1, and 5 terms were enriched in the F Vs B, B Vs G, G Vs A, and A Vs D groups, respectively. In the BP category, 12, 17, 1, and 1 terms were enriched in the F Vs B, B Vs G, G Vs A, and A Vs D groups, respectively.

KEGG pathway enrichment analysis showed two pathways were enriched in F Vs B, including Ribosome and Vibrio cholera infection. Three pathways were enriched in B Vs G, including Ribosome, Protein export and Proteasome, while 16 pathways were enriched in G Vs A, including Protein digestion and absorption, Renin-angiotensin system as well as Pancreatic secretion. Six pathways were enriched in A Vs D, including cell cycle, oocyte meiosis, and p53 signaling pathway. Two pathways were enriched in D Vs P (Figure S2; Supplementary Table S12).

3.5 Gene regulation during the development of fertilized eggs to blastula

The transition from fertilized eggs to blastula is the first stage in sea cucumber development. It involves the expulsion of polar bodies, rapid cell division, and the expansion and break down of the fertilization envelope (Yang et al., 2015). About 1 hour after fertilization, the fertilized egg enters the cleavage stage. The cells gradually decrease in size after division and enter the blastocyst stage at about 7 to 9 h. The whole blastocyst stage lasts for about 13 h and is divided into a stationary stage and a rotational stage. Compared with fertilized eggs, blastocysts are multicellular embryos. We analyzed DEGs and found 20 up-regulated genes and 112 down-regulated genes during this stage. To evaluate the function of DEGs, we conducted GO and KEGG enrichment analysis. The significant GO cellular component terms were related to ribosome components, such as "ribosomal subunit" and "ribosome". The biological process ontology includes terms associated with viral reproduction (Supplementary Table S11).

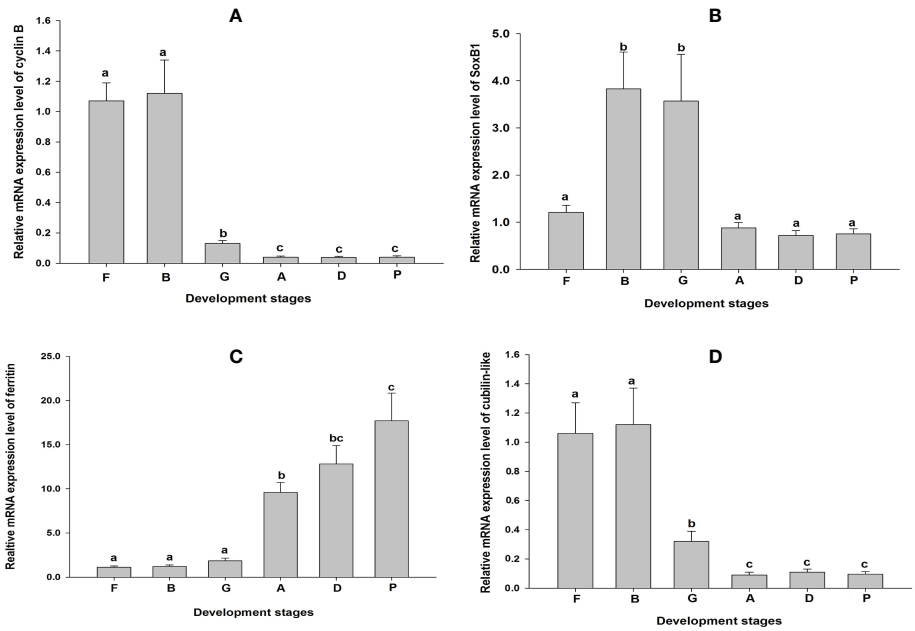

FIGURE 5
Validation of cyclin B **(A)**, SoxB1 **(B)**, ferritin **(C)** and cubilin-like **(D)** using RT-PCR. Data are shown as the mean ± SD. The lowercase letters indicate statistically significant differences ($p < 0.05$).

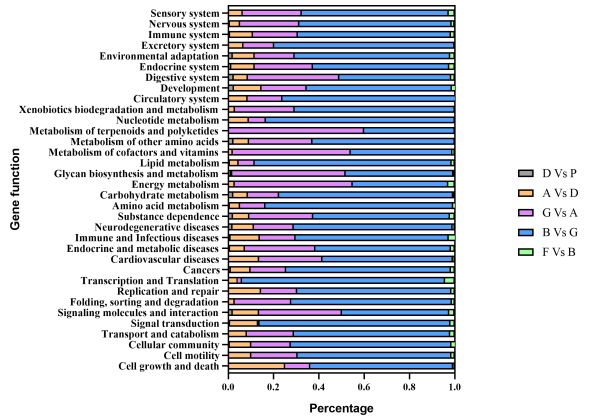

FIGURE 6
The percentage of DEGs enriched in each term at different developmental stages.

The KEGG enrichment analysis results showed that DEGs are enriched in "Ribosome", "Vibrio cholerae infection" and "Amoebiasis" (Figure S2). "Vibrio cholerae infection" and "Amoebiasis" are the common pathways during the comparative transcriptomic analysis of the early development in pacific white shrimp Litopenaeus vannamei (Wei et al., 2014). This suggests that the two pathways are involved in the embryonic development process. The ribosome as a complicated organelle mainly catalyzed the amino acids into peptide chains (translation). "Ribosome" is a basic cellular biology pathway involved in cell division and other cellular activities. Among the DEGs, lamin B receptor (LBR) was the most significantly upregulated gene. LBR is an integral membrane protein of the interphase nuclear envelope involved in mitotic nuclear envelope breakdown (Margalit et al., 2005; Olins et al., 2010), which called open mitosis. Thus, we speculated that LBR promoted NE breakdown to regulate open mitosis of sea cucumber cells. The results implied that two major events in this developmental process were DNA rapid replication for cell proliferation and immune response for protecting organisms from environmental stress.

3.6 Gene regulation during development from blastula to gastrula

The highest number of genes (up-regulated genes: 1,781; down-regulated genes: 1,535) showed differential expression during development from the blastula to gastrula stage (B Vs G), suggesting that this is a key period during sea cucumber development. It is worth noting that of the top 30 known up-regulated DEGs listed in Table S10 according to probability values and mRNA expression, a total of seven DEGs were associated with metalloproteinase, including three genes coding matrix metalloproteinase and four genes coding zinc metalloproteinase. In addition, many transcription factors, key genes in conservative signaling pathways as well as cell cycle regulation genes were significantly up-regulated during this stage, such as FoxQ1 (forkhead box protein Q1-like), FoxA, Wnt-8a, and frizzled 9-10. These results are consistent with the fact that during gastrulation the germ layers of the embryo are formed and the body plan of the organism is established (Tam and Loebel, 2007).

Most DEGs were categorized into "Immune and infectious diseases" (519 DEGs), "Cancers" (434 DEGs), and "Signal transduction" (408 DEGs) (Figure 6). The most enriched pathways in this process were "Ribosome", "Protein export", and "Proteasome", which were responsible for translation and protein folding, sorting, and degradation (Figure S2B).

3.7 Gene regulation during development from gastrula to auricularia

In this process, the digestive tract of sea cucumbers gradually starts to open and they start to feed. A total of 535 up-regulated genes and 97 down-regulated genes were screened during this stage. Among them, Proteinase T/proprotein convertase subtilisin/kexin type 9 preproprotein was up-regulated over 2,000-fold from the gastrula stage to the auricularia stage in sea cucumbers. This gene was the most highly expressed gene in the intestine of healthy *A. japonicus*, However, it was not highly expressed in the body wall or respiratory tree (Yang et al., 2009), indicating that the expression of this gene was very advantageous for intestine digestion.

At this stage, the majority of DEGs were categorized into "Immune and Infectious diseases" (122 DEGs), "Digestive system" (102 DEGs), and "Endocrine system" (94 DEGs) (Figure 6). The most enriched pathways were "Protein digestion and absorption", "Renin-angiotensin system", "Pancreatic secretion", "Carbohydrate digestion and absorption", and "Fat digestion and absorption", which were responsible for both the digestive endocrine systems (Figure S2C). In light of these findings, we speculated that the formation of the digestive tract and the start of feeding were the key events in this process.

3.8 Gene regulation during development from auricularia to doliolaria

During the development of auricularia to doliolaria, the planktotrophic larva, the auricularia, undergoes a dramatic morphological transformation at the onset of metamorphosis (Lacalli and West, 2000). At this stage, 98 up-regulated genes and 272 down-regulated genes were found. The majority of DEGs were categorized into "Immune and Infectious diseases" and "Signal transduction", accounting for 99 and 60 DEGs, respectively (Figure 6). MAP kinase-interacting serine/threonine-protein kinase 1 isoform X1 and PTSP-like peptide neurotransmitter precursor were most significantly up-regulated during the development from auricularia to doliolaria, and have been found to play important roles in the metamorphosis process. As mentioned above, nerve cells begin to form in the late gastrula stage and the adult nervous system develops during the doliolaria stage (Nakano et al., 2006). This indicates that metamorphosis is a multigenic synergistically involved process regulated by endogenous neurotransmitters

(Matsuura et al., 2009). Among all the down-regulated genes, the two genes associated with DNA replication, zinc finger RAD18 domain-containing protein C1orf124 homolog (C1orf124) and spalt-like transcription factor (SALL), were the most significant. C1orf124 is a regulator of translesion synthesis and participates in polymerase switching (Ghosal et al., 2012). SALLs are evolutionarily conserved proteins that participate in embryonic development. In oncology studies, SALLs are involved in cellular apoptosis, angiogenesis, invasion, and metastasis (Ma et al., 2021). This is consistent with the most significantly enriched signaling pathway being the 'cell cycle', suggesting active cellular events during metamorphosis (Figure S2D).

3.9 Gene regulation during development from doliolaria to pentactula

Sea cucumber larva develop from doliolaria to pentactula, and use their tentacles to attach to the substrate at ~ 12 days post-fertilization, which was a key part of substrate detection/selection and settlement 1. By this stage, the morphological structure of most of organs has taken shape. Hence, relatively few genes showed differential expression during this process. Four up-regulated genes and 10 down-regulated genes were screened. "Salivary secretion" and "Prion diseases" were the most enriched pathways (Figure S2E).

3.10 Individual key DEGs

Key genes related to sea cucumber development were classified into seven groups according to gene function: adhesion, cell cycle, signal, transcription factor, extracellular matrix (ECM), and cytoskeleton. The detailed information of gene expression can be seen in Supplementary Table S13.

3.10.1 Adhesion

The expression profiles of 9 cadherin genes and 14 protocadherin Fat genes, as well as 18 integrin genes, are summarized in Figure 7A. Genes from the same family showed different expression patterns. The expression levels of Cadherin Ap showed an increasing trend during the developmental process, especially from doliolaria to pentactula. The expression trend of the remaining 7 cadherin genes was opposite to Cadherin Ap. The expression levels of most protocadherin Fat genes were gradually down-regulated. The integrin genes exhibited low expression levels from doliolaria to pentactula.

3.10.2 Cell cycle

The expression profiles of 8 cell division control protein (Cdc) family genes, 19 cyclin family genes (Cyc), 7 DNA replication licensing factor genes (MCM), and 9 origin recognition complex genes (Orc) are summarized in Figure 7B. Cdc family genes exhibited low expression levels from auricularia to pentactula. Cdc6 is essential for the formation of pre-replication complexes at the origins of DNA replication (Davis et al., 2008). The ORC1 gene, which plays an important role in the initiation of DNA replication, was also highly expressed at the fertilized egg and blastula stages. Cyclin B accumulates and binds to Cdk1 at the G2-phase, playing a vital role in G2-to-M transition (Lemonnier et al., 2020). The expression level of MCM genes were up-regulated from fertilized egg to auricularia. During the development from fertilized eggs to blastula, cells proliferate through the mitotic cell cycle. Therefore, these genes regulate the cell division cycle.

3.10.3 Signal

Two family genes (Notch and Wnt) related to key signal pathways were screened (Figure 7C). There was no obvious pattern in Notch gene expression, and there were high expression genes in each stage. The expression levels of Wnt16 and WntA were up-regulated from auricularia to pentactula. Wnt4 and Wnt5 showed opposite expression levels.

3.10.4 Transcription factor

A total of 23 forkhead transcription factor (Fox) genes were expressed during development. The expression patterns of eight Sox genes, five T-box transcription factors, six Krueppel-like factors, and eight paired box proteins are shown in Figure 7D. SoxB1, a multifunctional gene involved in maintaining stem cell multipotency, was highly expressed from blastula to auricularia stages. Tbx2/3 showed high expression during development from gastrula to pentactula. Interestingly, Pax5 was highly expressed from the fertilized egg to the gastrula stage and Pax9 was highly expressed from the auricularia to pentactula stages. The expression time of these two genes covers the entire larval development process.

3.10.5 ECM

Many genes associated with ECM were expressed during sea cucumber development, including 40 Matrix metalloproteinase (MMPs), 41 collagen, six tenascin, and 24 laminin (Figures 7E–G). The expression levels of most MMPs were up-regulated at doliolaria and pentactula stages. Most collagen genes were up-regulated from the auricularia to pentactula stage. However, laminin genes were highly expressed at the early stages of development.

3.10.6 Cytoskeleton

During sea cucumber development, many cytoskeleton genes were expressed, including 14 actin, 46 myosin, and 30 tubulin (Figures 7H, I). The expression of many actin and tubulin genes were highly expressed from the auricularia to pentactula stages, while many myosin genes exhibited high expression levels at the early stages of development.

It has been clear for many years that matrix metalloproteinase hydrolyze ECM components, play a central role in embryogenesis, normal tissue remodeling, wound healing, and angiogenesis (Dolmatov et al., 2021). Wnt-8 and frizzled 9-10, the key genes of the Wnt signaling pathway, which controls the embryonic processes involved in body axis patterning, cell fate specification, cell proliferation, and cell migration (Clevers, 2006), were up-regulated over 200-fold at gastrula stage. The nervous system is

10.3389/fmars.2023.1087339

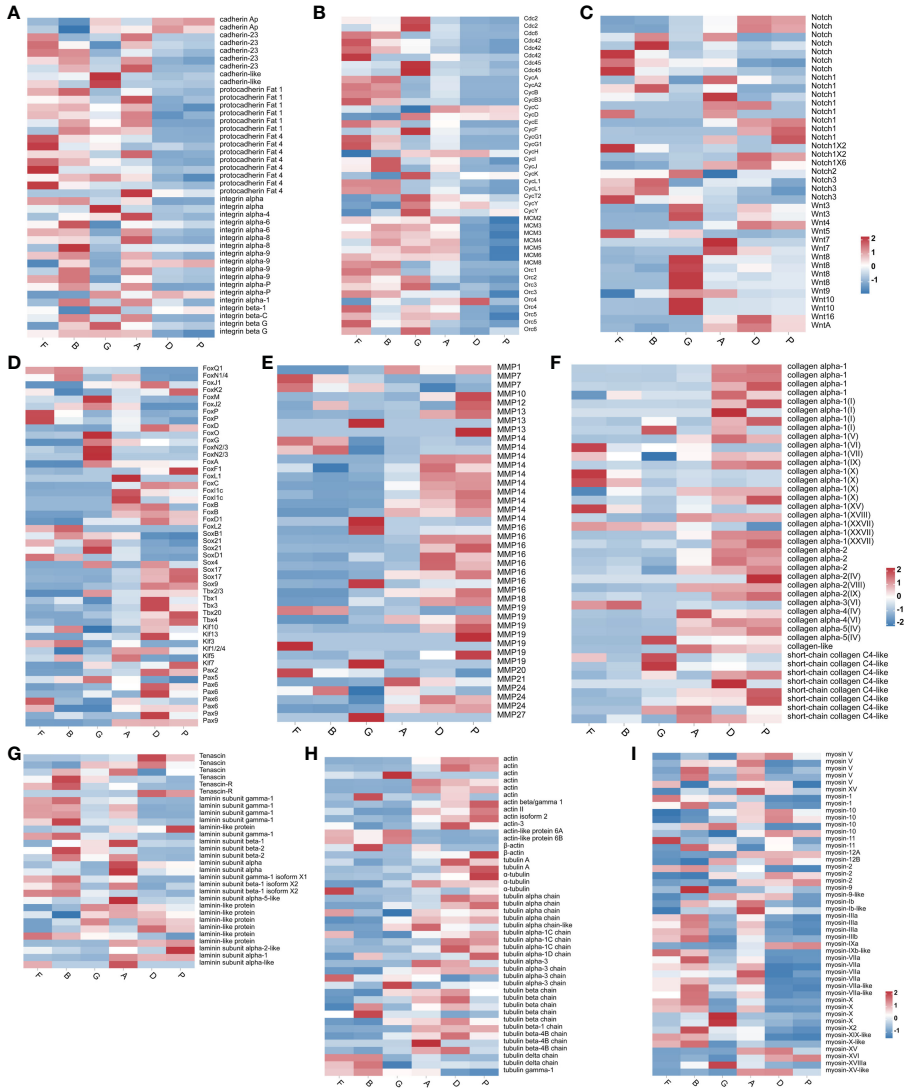

FIGURE 7
Heatmap diagram showing the expression levels of transcripts annotated as adhesion genes **(A)**, cell cycle genes **(B)**, signal genes **(C)**, transcription factor **(D)**, ECM genes **(E–G)** and cytoskeleton genes **(H, I)**.

developed from the ectoderm formed during gastrulation, so key genes, regulating neural development such as dorsal root ganglia, homeobox protein-like was significantly up-regulated. In addition, Cdc20-like expression was up-regulated to regulate cell division from the blastula to the gastrula stage (Yu, 2007), Cdc family genes were also up-regulated during blastula and gastrula stage. It is worth noting that TNF receptor-associated factor 6-like (TRAF6) was down-regulated over 250-fold, which may due to the fact that TRAF6 negatively regulates NF-κB.

4 Conclusion

In the present study, RNA-Seq analysis was conducted on six embryonic and larval stages of sea cucumber development as follows: fertilized eggs, blastula, gastrula, auricularia, doliolaria, and pentactula. A total of 53.20~59.96 Mb× 18 clean reads were obtained, and 32,353 genes were identified and annotated. After filtering out low-quality genes, the dynamic molecular responses to development were revealed by WGCNA. The blue module and the yellow module were positively correlated with the gastrula and auricularia stages, respectively. The darkslateblue module had the highest correlation coefficient with the blastula stage. GO terms for "RNA" and "proteasome complex" were most significantly enriched in the blue module. In the darkslateblue and yellow module, receptors of signaling pathways and metabolic processes were significantly enriched, respectively. Five comparison groups, F Vs B, B Vs G, G Vs A, A Vs D, and D Vs P, were used to analyze differential expression genes during the development of *A. japonicus*. All DEGs could be categorized into 34 terms, with "Immune and Infectious diseases" being the most enriched. There was strong gene expression regulation from blastula to Auricularia. Functional enrichment analysis was performed on DEGs from each comparison group. The behavioral events and molecular features

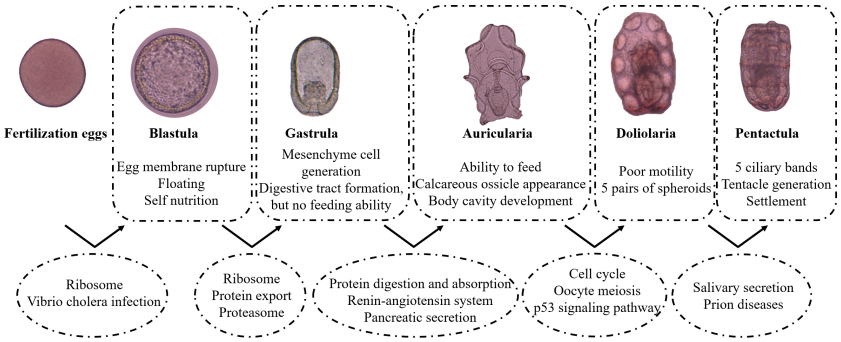

FIGURE 8
The major events during fertilization eggs to pentactula are shown in box. The significantly enriched signal pathways are shown in circle.

are summarized in Figure 8. The expression pattern of genes associated with adhesion, cell cycle, signal, transcription factor, extracellular matrix (ECM) and cytoskeleton was analyzed according to gene function. These results suggested that development and metamorphosis relied on complex molecular mechanisms in which many genes were involved. The present study provided useful transcriptomic resources for further research on *A. japonicus* development.

Data availability statement

The datasets presented in this study can be found in online repositories. The names of the repository/repositories and accession number(s) can be found below: BioProject, PRJNA889469.

Author contributions

LS and HY conceived the study. FS carried out the field and laboratory work, participated in the data analysis, and drafted the manuscript. SL and LX collected the parent sea cucumbers. DH collected the experimental samples. LS, LX, and SL revised the manuscript. All authors approved the manuscript for publication. All authors contributed to the article and approved the submitted version.

Funding

This study was supported by the National Natural Science Foundation of China (No. 42076093, 42276143), the Strategic Priority Research Program of the Chinese Academy of Sciences (No. XDA24030304), Youth Innovation Promotion Association CAS (No. 2019209).

Conflict of interest

The authors declare that the research was conducted in the absence of any commercial or financial relationships that could be construed as a potential conflict of interest.

Publisher's note

All claims expressed in this article are solely those of the authors and do not necessarily represent those of their affiliated organizations, or those of the publisher, the editors and the reviewers. Any product that may be evaluated in this article, or claim that may be made by its manufacturer, is not guaranteed or endorsed by the publisher.

Supplementary material

The Supplementary Material for this article can be found online at: https://www.frontiersin.org/articles/10.3389/fmars.2023.1087339/full#supplementary-material

SUPPLEMENTARY FIGURE 1
Diagram of the gene function in different comparison groups.

SUPPLEMENTARY FIGURE 2
KEGG enrichment analysis of DEGs in F Vs B **(A)**, B Vs G **(B)**, G Vs A **(C)**, A Vs D **(D)** and D Vs P **(E)**.

SUPPLEMENTARY TABLE 4
List of gene-module relationships.

SUPPLEMENTARY TABLE 6
Sample expression pattern.

SUPPLEMENTARY TABLE 7
GO enrichment analysis in three target modules.

SUPPLEMENTARY TABLE 8
KEGG enrichment analysis in three target modules.

SUPPLEMENTARY TABLE 13
The expression profile of key genes.

References

Ahmed, H. O., Katow, T., and Katow, H. (2011). Spatiotemporal expression pattern of gonad-stimulating substance-like peptide of the sea cucumber, *Apostichopus japonicus*. *Dev. Growth Differ* 53 (5), 639–652. doi: 10.1111/j.1440-169X.2011.01277.x

Asthana, S., Martin, H., Rupkey, J., Patel, S., Yoon, J., Keegan, A., et al. (2022). The physiological roles of the exon junction complex in development and diseases. *Cells* 11 (7). doi: 10.3390/cells11071192

Chen, M., Zhu, A., and Storey, K. B. (2015). Comparative phosphoproteomic analysis of intestinal phosphorylated proteins in active versus aestivating sea cucumbers. *J. proteomics.* 135, 141–150. doi: 10.1016/j.jprot.2015.09.016

Clevers, H. (2006). Wnt/beta-catenin signaling in development and disease. *Cell* 127 (3), 469–480. doi: 10.1016/j.cell.2006.10.018

Davis, A. J., Yan, Z., Martinez, B., and Mumby, M. C. (2008). Protein phosphatase 2A is targeted to cell division control protein 6 by a calcium-binding regulatory subunit. *J. Biol. Chem.* 283 (23), 16104–16114. doi: 10.1074/jbc.M710313200

Dolmatov, I. Y., Nizhnichenko, V. A., and Dolmatova, L. S. (2021). Matrix metalloproteinases and tissue inhibitors of metalloproteinases in echinoderms: Structure and possible functions. *Cells* 10 (9), 2331. doi: 10.3390/cells10092331

Dong, G., Dong, S., Wang, F., and Tian, X. (2010). Effects of light intensity on daily activity rhythm of juvenile sea cucumber, *Apostichopus japonicus* (Selenka). *Aquaculture Res.* 41 (11), 1640–1647. doi: 10.1111/j.1365-2109.2010.02534.x

Du, H., Bao, Z., Hou, R., Wang, S., Su, H. , Yan, J., et al. (2012). Transcriptome sequencing and characterization for the sea cucumber *Apostichopus japonicus* (Selenka 1867). *PloS One* 7 (3), e33311. doi: 10.1371/journal.pone.0033311

Gao, Q., Liao, M., Wang, Y., Li, B., Zhang, Z., Rong, X., et al. (2015). Transcriptome analysis and discovery of genes involved in immune pathways from coelomocytes of Sea cucumber (*Apostichopus japonicus*) after vibrio splendidus challenge. *Int. J. Mol. Sci.* 16 (7), 16347–16377. doi: 10.3390/ijms160716347

Ghosal, G., Leung, J. W., Nair, B. C., Fong, K. W., and Chen, J. (2012). Proliferating cell nuclear antigen (PCNA)-binding protein C1orf124 is a regulator of translesion synthesis. *J. Biol. Chem.* 287 (41), 34225–34233. doi: 10.1074/jbc.M112.400135

Gianasi, B. L., Hamel, J.-F., and Mercier, A. (2018). Morphometric and behavioural changes in the early life stages of the sea cucumber *Cucumaria frondosa*. *Aquaculture* 490, 5–18. doi: 10.1016/j.aquaculture.2018.02.017

Gonzalez-Aguilera, C., and Askjaer, P. (2012). Dissecting the NUP107 complex: Multiple components and even more functions. *Nucleus* 3 (4), 340–348. doi: 10.4161/nucl.21135

Gu, M., Ma, H., Mai, K., Zhang, W., Ai, Q., Wang, X., et al. (2010). Immune response of sea cucumber *Apostichopus japonicus* coelomocytes to several immunostimulants *in vitro*. *Aquaculture* 306 (1-4), 49–56. doi: 10.1016/j.aquaculture.2010.05.024

Guo, X., Hao, Y., Zhao, Y., and Shi, H. (2020). Research advances on the function of n-acetyltransferase 10. *Chem. Life* 40 (11), 2014–2019.

Hamel, J.-F., Hidalgo, R. Y., and Mercier, A. (2003). Larval development and juvenile growth of the Galapagos sea cucumber. *Isostichopus fuscus*.

Hu, C., Xu, Y., Wen, J., Zhang, L., Fan, S., and Su, T. (2010). Larval development and juvenile growth of the sea cucumber *Stichopus* sp. (Curry fish). *Aquaculture* 300 (1-4), 73–79. doi: 10.1016/j.aquaculture.2009.09.033

Huo, D. L., Li, X., Ru, X., Liu, S., Zhang, L., et al. (2017). Differential expression of miRNAs in the respiratory tree of the Sea cucumber *Apostichopus japonicus* under hypoxia stress. *G3 (Bethesda)* 7 (11), 3681–3692. doi: 10.1534/g3.117.1129

Kato, S., Tsurumaru, S., Taga, M., Yamane, T., Shibata, Y., Ohno, K., et al. (2009). Neuronal peptides induce oocyte maturation and gamete spawning of sea cucumber, *Apostichopus japonicus*. *Dev. Biol.* 326 (1), 169–176. doi: 10.1016/j.ydbio.2008.11.003

Kim, D., Langmead, B., and Salzberg, S. L. (2015). HISAT: A fast spliced aligner with low memory requirements. *Nat. Methods* 12 (4), 357–360. doi: 10.1038/nmeth.3317

Kong, L., Zhang, Y., Ye, Z. Q., Liu, X. Q., Zhao, S. Q., Wei, L., et al. (2007). CPC: assess the protein-coding potential of transcripts using sequence features and support vector machine. *Nucleic Acids Res.* 35 (Web Server issue), W345–W349. doi: 10.1093/nar/gkm391

Lacalli, T. C., and West, J. E. (2000). The auricularia-to-doliolaria transformation in two aspidochirote holothurians, *Holothuria mexicana* and *Stichopus californicus*. *Invertebrate Biol.* 119 (4), 421–432. doi: 10.1111/j.1744-7410.2000.tb00112.x

Langfelder, P., and Horvath, S. (2008). WGCNA: An r package for weighted correlation network analysis. *BMC Bioinf.* 9, 1–13. doi: 10.1186/1471-2105-9-559

Langmead, B., and Salzberg, S. L. (2012). Fast gapped-read alignment with bowtie 2. *Nat. Methods* 9 (4), 357–359. doi: 10.1038/nmeth.1923

Lemonnier, T., Dupre, A., and Jessus, C. (2020). The G2-to-M transition from a phosphatase perspective: A new vision of the meiotic division. *Cell Div* 15, 9. doi: 10.1186/s13008-020-00065-2

Li, B., and Dewey, C. N. (2011). RSEM: accurate transcript quantification from RNA-seq data with or without a reference genome. *BMC Bioinf.* 12, 1–16. doi: 10.1186/1471-2105-12-323

Li, L., and Li, Q. (2009). Effects of stocking density, temperature, and salinity on larval survival and growth of the red race of the sea cucumber *Apostichopus japonicus* (Selenka). *Aquaculture Int.* 18 (3), 447–460. doi: 10.1007/s10499-009-9256-4

Liu, G., Yang, H., and Liu, S. (2010). Effects of rearing temperature and density on growth, survival and development of sea cucumber larvae, *Apostichopus japonicus* (Selenka). *Chin. J. Oceanology Limnology* 28 (4), 842–848. doi: 10.1007/s00343-010-9092-4

Ma, P., Ren, B., Yang, X., Sun, B., Liu, X., Kong, Q., et al. (2017). ZC4H2 stabilizes smads to enhance BMP signalling, which is involved in neural development in xenopus. *Open Biol.* 7 (8), 170122. doi: 10.1098/rsob.170122

Ma, T., Shi, S., Jiang, H., Chen, X., Xu, D., Ding, X., et al. (2021). A pan-cancer study of spalt-like transcription factors 1/2/3/4 as therapeutic targets. *Arch. Biochem. Biophys.* 711, 109016. doi: 10.1016/j.abb.2021.109016

Margalit, A., Vlcek, S., Gruenbaum, Y., and Foisner, R. (2005). Breaking and making of the nuclear envelope. *J. Cell Biochem.* 95 (3), 454–465. doi: 10.1002/jcb.20433

Matsuura, H., Yazaki, I., and Okino, T. (2009). Induction of larval metamorphosis in the sea cucumber *Apostichopus japonicus* by neurotransmitters. *Fisheries Sci.* 75 (3), 777–783. doi: 10.1007/s12562-009-0098-9

May, M., Hwang, K. S., Miles, J., Williams, C., Niranjan, T., Kahler, S. G., et al. (2015). ZC4H2, an XLID gene, is required for the generation of a specific subset of CNS interneurons. *Hum. Mol. Genet.* 24 (17), 4848–4861. doi: 10.1093/hmg/ddv208

McKenna, A., Hanna, M., Banks, E., Sivachenko, A., Cibulskis, K., Kernytsky, A., et al. (2010). The genome analysis toolkit: A MapReduce framework for analyzing next-generation DNA sequencing data. *Genome Res.* 20 (9), 1297–1303. doi: 10.1101/gr.107524.110

Meng, X.-L., Dong, Y.-W., Dong, S.-L., Yu, S.-S., and Zhou, X. (2011). Mortality of the sea cucumber, apostichopus japonicus selenka, exposed to acute salinity decrease and related physiological responses: Osmoregulation and heat shock protein expression. *Aquaculture* 316 (1-4), 88–92. doi: 10.1016/j.aquaculture.2011.03.003

Miao, T., Wan, Z., Sun, L., Li, X., Xing, L., Bai, Y., et al. (2017). Extracellular matrix remodeling and matrix metalloproteinases (ajMMP-2 like and ajMMP-16 like) characterization during intestine regeneration of sea cucumber *Apostichopus japonicus*. *Comp. Biochem. Physiol. Part B: Biochem. Mol. Biol.* 212, 12–23. doi: 10.1016/j.cbpb.2017.06.011

Nakano, H., Murabe, N., Amemiya, S., and Nakajima, Y. (2006). Nervous system development of the sea cucumber *Stichopus japonicus*. *Dev. Biol.* 292 (1), 205–212. doi: 10.1016/j.ydbio.2005.12.038

Olins, A. L., Rhodes, G., Welch, D. B., Zwerger, M., and Olins, D. E. (2010). Lamin b receptor: Multi-tasking at the nuclear envelope. *Nucleus* 1 (1), 53–70. doi: 10.4161/nucl.1.1.10515

Pan, Y., Zhang, L., Lin, C., Sun, J., Kan, R., and Yang, H. (2015). Influence of flow velocity on motor behavior of sea cucumber *Apostichopus japonicus*. *Physiol. Behav.* 144, 52–59. doi: 10.1016/j.physbeh.2015.02.046

Pertea, M., Pertea, G. M., Antonescu, C. M., Chang, T. C., Mendell, J. T., and Salzberg, S. L. (2015). StringTie enables improved reconstruction of a transcriptome from RNA-seq reads. *Nat. Biotechnol.* 33 (3), 290–295. doi: 10.1038/nbt.3122

Qiu, T. (2013). Research and application of key technical principles of sea cucumber (Apostichopus japonicus Selenka) ecological seed breeding (Doctoral dissertation, Doctoral Thesis. University of Chinese Academy of Sciences).

Sagne, C., Agulhon, C., Ravassard, P., Darmon, M., Hamon, M., El Mestikawy, S., et al. (2001). Identification and characterization of a lysosomal transporter for small neutral amino acids. *Proc. Natl. Acad. Sci. United States America* 98 (13), 7206–7211. doi: 10.1073/pnas.121183498

Soliman, T., Yamazaki, Y., Niiyama, H., and Tsunoda, K. (2013). Spontaneous captive breeding and larval development in the green and red variants of the Japanese sea cucumber *Apostichopus japonicus*(Selenka 1867). *Aquaculture Res.* 44 (5), 738–746. doi: 10.1111/j.1365-2109.2011.03078.x

Sun, L., Chen, M., Yang, H., Wang, T., Liu, B., Shu, C., et al. (2011). Large Scale gene expression profiling during intestine and body wall regeneration in the Sea cucumber *Apostichopus japonicus*. *Comp. Biochem. Physiol. Part D: Genomics Proteomics* 6), 195–205. doi: 10.1016/j.cbd.2011.03.002

Sun, L., Sun, J., Xu, Q., Li, X., Zhang, L., and Yang, H. (2017a). Metabolic responses to intestine regeneration in sea cucumbers *Apostichopus japonicus*. *Comp. Biochem. Physiol. Part D: Genomics Proteomics* 22, 32–38. doi: 10.1016/j.cbd.2017.02.003

Sun, L., Xu, D., Xu, Q., Sun, J., Xing, L., Zhang, L., et al. (2017b). iTRAQ reveals proteomic changes during intestine regeneration in the sea cucumber *Apostichopus japonicus*. *Comp. Biochem. Physiol. Part D: Genomics Proteomics* 22, 39–49. doi: 10.1016/j.cbd.2017.02.004

Sun, J., Zhang, L., Pan, Y., Lin, C., Wang, F., Kan, R., et al. (2015). Feeding behavior and digestive physiology in sea cucumber *Apostichopus japonicus*. *Physiol. Behav.* 139, 336–343. doi: 10.1016/j.physbeh.2014.11.051

Tam, P. P., and Loebel, D. A. (2007). Gene function in mouse embryogenesis: Get set for gastrulation. *Nat. Rev. Genet.* 8 (5), 368–381. doi: 10.1038/nrg2084

Wang, C., Sun, T., Guo, J., Zhang, K., and Yin, L. (2019). Studies on embryonic and larval development of yellow river delta Sea cucumber (*Apostichopus japonicus*). *Fisheries Sci. Technol. Inf.* 46 (04), 196–200+205. doi: 10.16446/j.cnki.1001-1994.2019.04.004

Wei, J., Zhang, X., Yu, Y., Huang, H., Li, F., and Xiang, J. (2014). Comparative transcriptomic characterization of the early development in pacific white shrimp *Litopenaeus vannamei*. *PloS One* 9 (9), e106201. doi: 10.1371/journal.pone.0106201

Xing, L., Sun, L., Liu, S., Li, X., Zhang, L., and Yang, H. (2018). Transcriptome analysis provides insights into the mechanism of albinism during different pigmentation stages of the albino sea cucumber *Apostichopus japonicus*. *Aquaculture* 486, 148–160. doi: 10.1016/j.aquaculture.2017.12.016

Xu, D., Sun, L., Liu, S., Zhang, L., and Yang, H. (2016). Understanding the heat shock response in the Sea cucumber *Apostichopus japonicus*, using iTRAQ-based proteomics. *Int. J. Mol. Sci.* 17 (2), 150–162. doi: 10.3390/ijms17020150

Yang, H., Hamel, J.-F., and Mercier, A. (Eds.). (2015). The sea cucumber Apostichopus japonicus: History, biology and aquaculture. Academic Press.

Yang, A.-F., Zhou, Z.-C., He, C.-B., Hu, J.-J., Chen, Z., Gao, X.-G., et al. (2009). Analysis of expressed sequence tags from body wall, intestine and respiratory tree of sea cucumber (*Apostichopus japonicus*). *Aquaculture* 296 (3-4), 193–199. doi: 10.1016/j.aquaculture.2009.08.016

Yu, H. (2007). Cdc20: A WD40 activator for a cell cycle degradation machine. *Mol. Cell* 27 (1), 3–16. doi: 10.1016/j.molcel.2007.06.009

Yuan, X., Shao, S., Dupont, S., Meng, L., Liu, Y., and Wang, L. (2015). Impact of CO2-driven acidification on the development of the sea cucumber *Apostichopus japonicus* (Selenka) (Echinodermata: Holothuroidea). *Mar. pollut. Bull.* 95 (1), 195–199. doi: 10.1016/j.marpolbul.2015.04.021

Zhang, P., Li, C., Zhang, P., Jin, C., Pan, D., and Bao, Y. (2014). iTRAQ-based proteomics reveals novel members involved in pathogen challenge in sea cucumber *Apostichopus japonicus*. *PloS One* 9 (6), e100492. doi: 10.1371/journal.pone.0100492

Zhang, P., Li, C., Zhu, L., Su, X., Li, Y., Jin, C., et al. (2013). *De novo* assembly of the sea cucumber *Apostichopus japonicus* hemocytes transcriptome to identify miRNA targets associated with skin ulceration syndrome. *PloS One* 8 (9), e73506. doi: 10.1371/journal.pone.0073506

Zhang, X., Sun, L., Yuan, J., Sun, Y., Gao, Y., Zhang, L., et al. (2017). The sea cucumber genome provides insights into morphological evolution and visceral regeneration. *PloS Biol.* 15 (10), e2003790. doi: 10.1371/journal.pbio.2003790

Zhou, Z. C., Dong, Y., Sun, H. J., Yang, A. F., Chen, Z., Gao, S., et al. (2014). Transcriptome sequencing of sea cucumber (*Apostichopus japonicus*) and the identification of gene-associated markers. *Mol. Ecol. Resour* 14 (1), 127–138. doi: 10.1111/1755-0998.12147

Frontiers in Marine Science

Explores ocean-based solutions for emerging global challenges

The third most-cited marine and freshwater biology journal, advancing our understanding of marine systems and addressing global challenges including overfishing, pollution, and climate change.

Discover the latest Research Topics

See more →

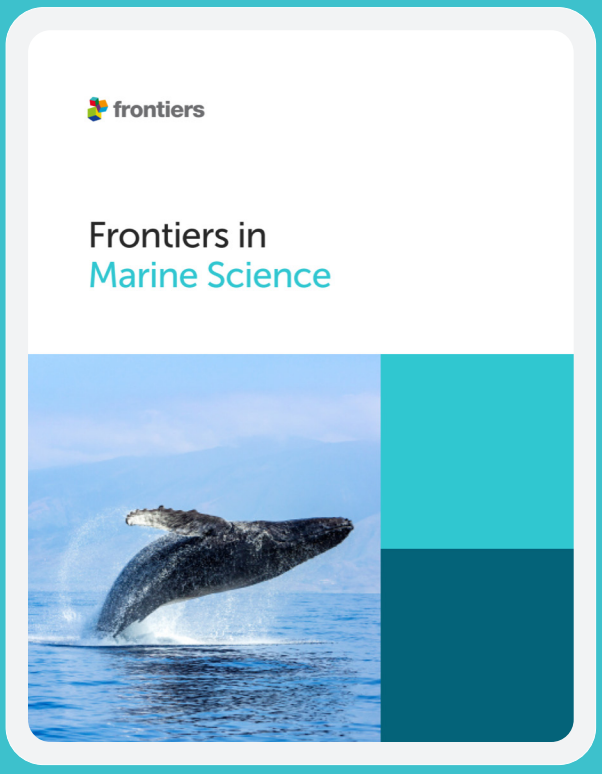

Frontiers

Avenue du Tribunal-Fédéral 34
1005 Lausanne, Switzerland
frontiersin.org

Contact us

+41 (0)21 510 17 00
frontiersin.org/about/contact